The University of Sheffield
The Department of Engineering Materials

Mathematical description of absorbance spectra for Fe and Cu doped soda-lime-silica glasses

Tarja T Volotinen

PhD thesis

31st May 2007

Acknowledgements

First of all I wish to extend my warm gratitude to the Department of Engineering Materials, The University of Sheffield, for the direct financial support, the facilities for this PhD research project and for the opportunity to study engineering materials, glass and ceramics, during Sept. 2002 - May 2007; as well as for the chances to practise teaching and supervision of undergraduates. I wish also to thank WRAP projects (Colorite and its present extension) with GTS for the interesting collaboration and the financial support.

My warmest thanks I wish to extend to my supervisor Dr. John M Parker for his gentle and patient guidance, for his understanding of my diabetes that seriously delayed the completing of this thesis, and in particular for the stimulating and encouraging scientific discussions we had on the topic.

I also thank Dr. Paul A Bingham, Sheffield University and Dr. Robert Klement, Aleksander Dubcek University in Trencin for the interesting and stimulating collaboration; Dr. David Hollis, Paisley University and Dr. Haruki Niida, NSG, Japan, for the stimulating discussions over the iron absorbance spectra and anything else.

Mr. Andrew Wilkinson is acknowledged for the arrangement of the Excel spreadsheets package, called "Colour prediction program", suitable for the manual fitting of the absorbance data, and for the temperature testing of a few of the glasses of this work in his MSc project.

Dr. Lech Wosinski at The Royal Institute of Technology, Stockholm, is thanked for the refractive index measurements and Dr. Jouni Hiltunen at Joensuu University for the scattering and reflection measurements, as well as Prof. A. Roos at Uppsala University, Ångström lab for the diffuse reflectance measurements.

The excellent technicians, Ian Watts and Dean Haylock are warmly acknowledged for the joyful melting of the 256 glasses, and Phil Staton, Barbara Horsfield and Bev Lane for their sympathy at sample preparation and technical support at testing.

My husband Pauli, granddaughter Jade and grandson Hunter are acknowledged for their special love, continuous support and encouragement that made my life enjoyable in spite of the various challenges this work put on me.

On the 31st of May, 2007, in Sheffield, England

Tarja Volotinen

Mathematical description of absorbance spectra for Fe and Cu doped soda-lime-silica glasses

Tarja T Volotinen

Abstract

Absorbance spectra and colour for a coloured soda-lime-silica glass can be predicted from colorant concentrations and melting conditions; and conversely: the concentrations for each colorant ion, valence and site (octahedral, tetrahedral) can be "measured" from an absorbance spectrum.

The necessary accurate mathematical descriptions for the absorbance spectra of the two most common colorants and contaminants, Cu and Fe, have been developed over the wavenumber range extending from UV to Near IR (200 – 3300 nm) in a soda-lime-silica (NCS) glass, singly or doubly doped with Cu and Fe. The effect of melting conditions on the absorbance spectra are studied over a concentration range from contamination level 0,01 to 2 mol % of added colorant. The obtained fitted spectra have been used to analyse the mutual redox ratios and concentrations of the Fe and Cu ions and sites for a number of contaminated, singly and doubly doped glasses at varied concentration levels, melted in reducing and oxidising conditions. The obtained absorbance spectra are in accordance with the known ligand field theory and each fitted absorbance peak has been identified, and the site configurations for each ion identified.

Accurate fitting parameters of the absorbance spectra of Cu and Fe ions have been obtained for summed Gaussian peaks for each valence (Cu^{1+}, Cu^{2+}, Fe^{2+} and Fe^{3+}) and site (Fe^{2+} octahedral and tetrahedral, Fe^{3+} octahedral and tetrahedral) in NCS glasses melted in oxidising and reducing conditions. The fitting parameters (peak heights, i.e. absorbance coefficients in $(cm*mol\ \%)^{-1}$ units, peak positions and peak widths) have been defined and calibrated with known data for all five peaks of Fe^{2+} ions, nine peaks of Fe^{3+} ions, four peaks of Cu^{2+} ions and one peak for Cu^{1+} ions, including the UV peaks of all these ions that define the UV-edge of the absorbance spectra and in most cases extend far into the visible range. Equally accurate fitting parameters and functions are developed also for background loss corrections of absorbance caused by surface reflections, OH-bands and IR-edge.

For the first time the fitted spectra are shown to scale with Fe and Cu concentrations so well that the developed fitting method can be meaningfully used to analyse doubly and singly doped glasses melted under various conditions. Small, of the order of 0,002 mol % changes in site concentrations, e.g. for Fe^{2+} ions in tetrahedral sites, can be repeatedly measured. The melting conditions have a complex effect on the spectrum of Fe^{3+} ions in tetrahedral and octahedral sites, changing the proportion of the concentrations. Fe^{2+} ions cause significant absorbance over the entire wavelength range studied. Several other novel results are also reported.

Mathematical description of absorbance spectra for Fe and Cu doped soda-lime-silica glasses

8. Absorbance spectra of undoped and low iron NCS glasses
9. A copy of the poster presentation, T Volotinen et al (2005), *The coordination environment of Cu^{2+} ions in silicate glasses, studied by optical absorption and EPR spectroscopy: An effect of composition on spectral parameters and structure.*
10. A copy of the conference paper, T Volotinen et al, (2004), *Analysis of absorption peak widths of Cu^{2+}- ions in silicate glasses, Proc. of The XXICG.*
11. Fitting parameters of Cu^{2+} and Cu^{1+} ions in singly and doubly doped NCS glasses

1 Introduction

1.1. The aims

Can the colour of a glass be designed with a computer? I.e. can the absorbance spectrum of a coloured, decolorized or filtering glass be designed with a computer? Furthermore, can the absorbance spectrum be reliably predicted from a given composition of glass? Or can the colorant ions and concentrations be reliably quantified from a measured absorbance spectrum of an unknown coloured glass? This thesis explores the principles that must be addressed to answer these questions.

The principle question is: Can the absorbance spectrum for each valence state of the polyvalent colouring ions of the first row transition metals (TMs: Ti, V, Cr, Mn, Fe, Co, Ni, Cu) and the colouring rare earth ions (Res: Ce, Er, Pr, Nd, etc.) be accurately described as a sum of a few Gaussian peaks? The number of fitted peaks for each valence state should depend on the number of electron d-d transition (for TMs) and f-f (for REs) and charge transfer energies. Each Gaussian peak can be described with three parameters (the position, height and width of the peak), which are shown being related to several factors: those fundamental to the absorption phenomena and dopant concentration, those related to the ligand field (created by the closest neighbouring ions and the host glass composition) and the configuration of the closest surrounding ions of the colourant ions and those dependent on the redox ratio of the present colorant ions. The accuracy of the fitted parameters is expected to be related to several factors: the glass melting and annealing conditions, sample preparation, measurement method, background correction method and fitting procedure.

Distinguishing pure ion absorbance spectra from the background losses and from each other is one of the most challenging tasks solved in this work, by fitting the logical parts of the significant background losses, i.e. surface related losses (mainly reflection loss), water peaks and infra red edge (IR edge) with separate Gaussian peaks or other suitable mathematical functions. Fitting of the contamination losses, mainly caused by iron in the glasses studied and its mutual redox with other colorant ions, is the background correction method. Fitting the ultraviolet edge (UV edge) is also developed. The UV-edge is dominated by the charge transfer absorption peaks of either iron (that appears as contamination in silicate glasses) or the other present dopants.

The meaning of the Gaussian peaks' parameters of the main ion spectra stays as is well-known in the literature. The absorbance peak positions, described the average transition energies, are dependent on the ligand field created by the closest neighbouring anions (oxygen ions in silicate glasses) and the number of the 3d electrons of the TM (4f electrons of the RE). The height of each peak, or more accurately the areas of the peaks, represent the transition

intensities and energy distribution. The intensity of each peak should be dependent on the linear absorption coefficient of the transition and the thickness of the sample, and according to the Beer-Lambert law should scale linearly with the concentration of the transition applying ions in the glass. The widths should depend on the site structure and dimensional variation (i.e. ligand field variation and glass inhomogeneity) for the transition providing dopant ions and on thermal effects (homogeneous) on their sites. Whether the peaks widths correlate to the slope of the transition energy curve as a function of the ligand field applied by the closest anions, should be studied.

One important question is: whether optical basicity can be used as "the measure" of the ligand field for accurate fitting of the effect of various host glasses, as is earlier suggested by Bates (1962), Paul (1982), Burns (1993), Bingham (2000 and 2002).

The transition energies (i.e. the positions of individual transition peaks or combined bands on a wavenumber scale) and their absorption coefficients are quite well known from literature (e.g. Bamford (1978)). However, some adjustments might be needed to these parameters in this work, mainly due to the improved accuracy in measurements, background correction and fitting. In particular, some adjustments may be found necessary to the dependencies of these parameters on the glass material composition, melting conditions, redox etc.

One important question also is: can the absorbance spectrum for a doubly doped glass, including possible mutual cross-reduction reactions between polyvalent dopants, also be described mathematically?

The aims can be summarised: The main goal of this work is to develop such an accurate fitting method for the absorbance spectra that can be reliably used for computerised design of absorbance spectrum of the studied type of glass. It is aimed to increase the scientific understanding on the absorbance spectra of the studied TM ions. The obtained results are also aimed to be used to accurately "measure" by optical absorbance spectroscopy the concentrations and redox ratios of the colourant ions in glasses. Because the quantity of the ion's concentration would correlate to the area of the fitted summed absorbance peaks, not to a sum band height, an improved accuracy is expected. Thus the results shall improve the optical transmission spectroscopy method as an analysis, measurement and research tool for coloured, decolourised and filtering glasses and their site structures.

1.2. Why this study is needed?

The glass industry desires to increase its use of recycled glass and its own cullet as a raw material as they melt with a lower energy consumption compared to melting from powdered batch of base ingredients, such as sand, soda, limestone, etc. Effective design method and approval of new glass colours without an extensive test melting programme is desired,

especially by window glass, machine blown and pressed container and tableware manufactures. In addition to wishing to computerise design of glass colour, the development of the optical spectroscopy method is needed, because the ion concentrations in coloured glasses are so low (0,005 – 1 mol %), that hardly any other common method shows significant signal-to-noise relationships allowing to study of the structure of the glass around the studied ions.

The modifying and complicated factors mentioned above have been studied before in numerous studies, but they need to be re-investigated. Many earlier studies have not provided suitable or accurately enough documented data required for full mathematical description of the spectra.

The kind of complete mathematical description provided win this thesis on the two TM ions (Fe and Cu) has not, to my knowledge, been reported before. Most reported studies on these ions were recorded tens of years before suitable computing and fitting tools became available (Weyl, 1959; Bamford, 1977; Bates, 1962; Duran, 1983 and 1985). Measurement equipment did not earlier either provide enough good resolution, accuracy or suitable digital data for automatic data processing. Usually only one ion has been studied in each work (Xiang, 1988; Bingham 2000). Even very recently published papers consider only the measured raw data for peak heights or top positions of the combined absorbance bands (Kido, 2004; Gödeke, 2001; Parkash, 2004).

The understanding of how the absorbance peak positions should vary according to the ligand field theory has been available for a few tens of years (Tanabe-Sugano by Bates, 1962; Paul, 1982). The mathematical computing tools suitable for accurate fitting of the multiple peaks have, however, become available more recently (Bingham, 2000). Accurate and precise mathematical fitting of the spectra can now be provided. Especially, widths of absorbance peaks that are broad and possibly affected by various factors, have been neglected in most earlier studies.

Many earlier accurate studies (such as Xiang, 1988; Cable et al, 1989; etc.) were made on glasses made from purified chemicals, melted in inert crucibles and taken to equilibrium of the colorant ions in order to avoid several of the complicating factors (background correction, cross-redox with contaminants, effects of melting conditions etc.). The test glasses of this work are melted from usual, commercial, non-purified powder batches either in gas-fired (reducing conditions, in mullite crucibles) or electrically heated (oxidising conditions, in platinum crucibles) furnaces, where the manufacturing method slightly better resembles the commercial glass making processes. Thus the results and the developed analysis method of this work may be relevant and applicable to glass research and industry, even though the test glass compositions used for this work differ slightly from commercial glasses. Some money may be saved in glass design and analysis of coloured, decolourised and filtering glasses, if glass

absorbance spectrum can be designed by a computer, instead of making extensive series of new glass melts.

1.3. The approach of this work

The defined task of this thesis work is extensive (various glasses and various colorant ions, non-pure chemicals, various background losses to be distinguished, etc.) and challenges many earlier not well solved issues, such as taking into account the effect of the contamination of Fe^{2+} and Fe^{3+}-ions' spectra within a wide wavelength range from 200 – 3200 nm. The amount of prepared samples (Annex 1) is actually too great to be analyzed in detail in one thesis. Deep analysis therefore has been only carried out on the spectra of Fe and Cu doped NCS glasses. For all other colorants (Annex 1: glasses containing Cr, Co, Ni, Mn, V, Ce, Ti, Er, Nd, Eu, Sm, Ho, Dy, Pr, Tb) the absorbance spectra were measured and tentatively fitted in some cases (Ce, Cr, Co, Ni, Nd, Er, Se). Some of the results were reported at SGT Glass conferences 2003, 2004 2005 and 2006 by Volotinen et al.

Most effort has been required to find an effective way of fitting of the whole spectrum, because most of these colorants have some charge transfer peaks in the UV-range and several sets of transition peaks due to two or more valences present, and each valence state may appear in two different structural configurations (such as octahedra, tetrahedra, etc.) and each configuration may contain two to seven different absorbance peaks, each one having three fitting parameters. Homogeneity of some samples should have been improved by re-melting to get the most accurate data for the fitting analysis, but it is out of the question due to limited time.

The background correction method used in the beginning of the work (i.e. to subtract the reflection-loss-corrected and thickness-normalized clear glass spectrum from the similarly treated measured spectrum of the doped glass) did not work well enough for accurate fitting. Thus a new, fitting method of the background loss correction needed to be developed (Chap. 3).

The available computer software, SPSS Ver. 12 and 13, did not solve the fitting problem very well, because it could not handle in practice more than six freely varying parameters for overlapping absorbance peaks. Thus an Excel based manual fitting program was developed in this project (Chap. 3.2) with help of the master degree student A. Wilkinson and the supervisor Dr. J. M. Parker and tested in collaboration within the WRAP and COLORITE projects, by various persons at Glass Technology Services in Chapeltown, UK. The Gaussian peaks parameters of the fitted absorbance spectra given in this thesis (Chaps 3 – 6) and the modifications to the software (the background correction, IR-edge, UV-edge-charge transfer peaks and calculation method of ion and structural unit concentrations) given in this report are fitted by myself, or clearly referred to the origin of the data.

1.4. Literature study

1.4.1. Coloured and filtering glasses

Transparent coloured glasses are usually doped either by using absorbing ionic colorants (transition metal and rare earth oxides), or by complex chromophore colorants, absorbing and scattering nano-sized particles (i.e. colloidal, reduced or crystalline metal or semiconductor particles), by fluorescing ions e.g. Nd or Pr, (Weyl, 1959; Bamford, 1977; Parker, 2004) or in special cases by using scattering from transparent particles of a particular size and refractive index (pure scattering filters, i.e. Christiansen filters, also called dispersion filters) (Musikant, 1986). A particular hue is achieved by controlling the redox ratio of the valence states of a colorant ion, or by using several dopants and/or fluorescing dopants. The same methods are used to make filtering glasses that absorb strongly at ultraviolet (UV) and short visible wavelengths (e.g. beer bottle glasses) and/or at near infrared (NIR) wavelengths (special window glasses), or to make glass filters that have a band-pass transmission window or edge filters that absorb strongly at wavelengths shorter than a certain wavelength (Bamford, 1977; Vogel, 1994; Fanderlik, 1983; Bray, 2000 and 2003).

Alternatively, a clear glass may be coloured by using transparent or opaque coating, clear or coloured glass layers, or made to be opaque by growing non- transparent particles of the order of light wavelength size with a particular size and shape distribution (Vogel, 1994). For glass art items several coloured layers may be joined together, such as a clear glass layer, a transparent coloured glass layer and an opaque glass layer (Flygt, 2004; Bray, 2000 and private discussions with various glass artists). Special dichromatic colours are made by combining colours that either only absorb light at specific wavelengths of light sources (e.g. sun light or a certain type of lamp) or by combining a non-fluorescing and fluorescing ions that are sensitive only for a certain part of the light spectrum, or using interference effects of thin layers or a specific surface structure/roughness (Parker, 2004 and private discussions with various glass artists).

Coloured glasses and filters are usually made of silicate, halide or phosphate glasses. Most common ionic colouring agents (Table 1.4.1. and Fig. 1.4.1.) are transition metals of the first row (Ti, V, Cr, Mn, Fr, Co, Ni, Cu) and rare earths (Ce, Pr, Nd, Sm, Eu, Dy, Ho and Er), but also some heavier transition metals (such as U, Pt, Rh, Pd, W, Mo, Ru) are used as colorants. Typical absorbance spectra for sodium silicate glasses doped with the first row TMs and melted under various conditions, are shown in Fig. 1.4.1.

Colloidal metal- or semiconductor particles (such as Au, Ag, Cu, CdS, CdSe, CdSeS, CdZnSe, CdTe, etc.) are also widely used to make yellow and red colours. No single ionic

colorant or their combination is known to give red colour for silicate glasses. Yellows and oranges, and all other colours, can be made with various ionic and chromophore colorants.

Table 1.4.1. Most common colorant ions and colloidal agents in glasses (Bamford, Vogel, Weyl).

Type	Element	Valence	Colour
Transition metals	Fe	2+	Green, sometimes blue
	Fe	3+	Brown- yellow
	Cu	2+	Blue, turquoise
	Cr	3+	Green
	Cr	6+	Amber – yellow
	Ni	2+	Violet (tetrahedral)
	Ni	2+	Yellow (octahedral)
	Co	2+	Blue
	Co	3+	Faint pink
	Mn	2+	Pale yellow
	Mn	3+	Violet
	V	5+	Faint yellow
	V	4+	Blue
	V	3+	Green
	Ti	3+	Violet – purple
Rare earths	Ce	4+	Yellow
	Sm	3+	Yellow
	Pr	3+	Green
	Nd	3+	Violet
	Ho	3+	Yellow
	Er	3+	Pale red
Metals	Ag	Colloid	Yellow
	Cu	Colloid	Red
	Au	Colloid	Red
	P	Colloid	Red
	Te	Colloid	Red
	Se	Colloid	Pink
Semiconductors	CdS	Colloid	Yellow
	CdSe	Colloid	Pink
	CdS_xSe_{1-x}	Colloid	Orange
	CdZnSe, Sb_2Se_3	Colloid	Red
	FeS	Colloid	Amber

Many of the transition metal ions may combine in various ways with the surrounding glass matrix, network-formers and network modifiers resulting in different (e.g. octahedral, tetrahedral etc.) structures of the ion surrounding anions. Some species may form chromophores, i.e. molecules, where another ion, such as S^{-2}, replaces one surrounding oxygen of a colorant ion, such as Fe^{3+} in tetrahedral configuration, resulting in a complex Fe_2SO_2 molecule, called the FeS chromophore, containing an Fe-S bond (Karlsson 1969; Bamford, p. 107; Beerkens, 2003).

Na_2SO_4 is added to glass as a refining agent to remove the bubbles during melting. Fe-S chromophores are formed in highly reducing conditions in melted soda-lime-silica glass and cause an amber colour and absorption spectrum different from the usual spectrum of the Fe^{3+}-ions surrounded only by oxygen ions.

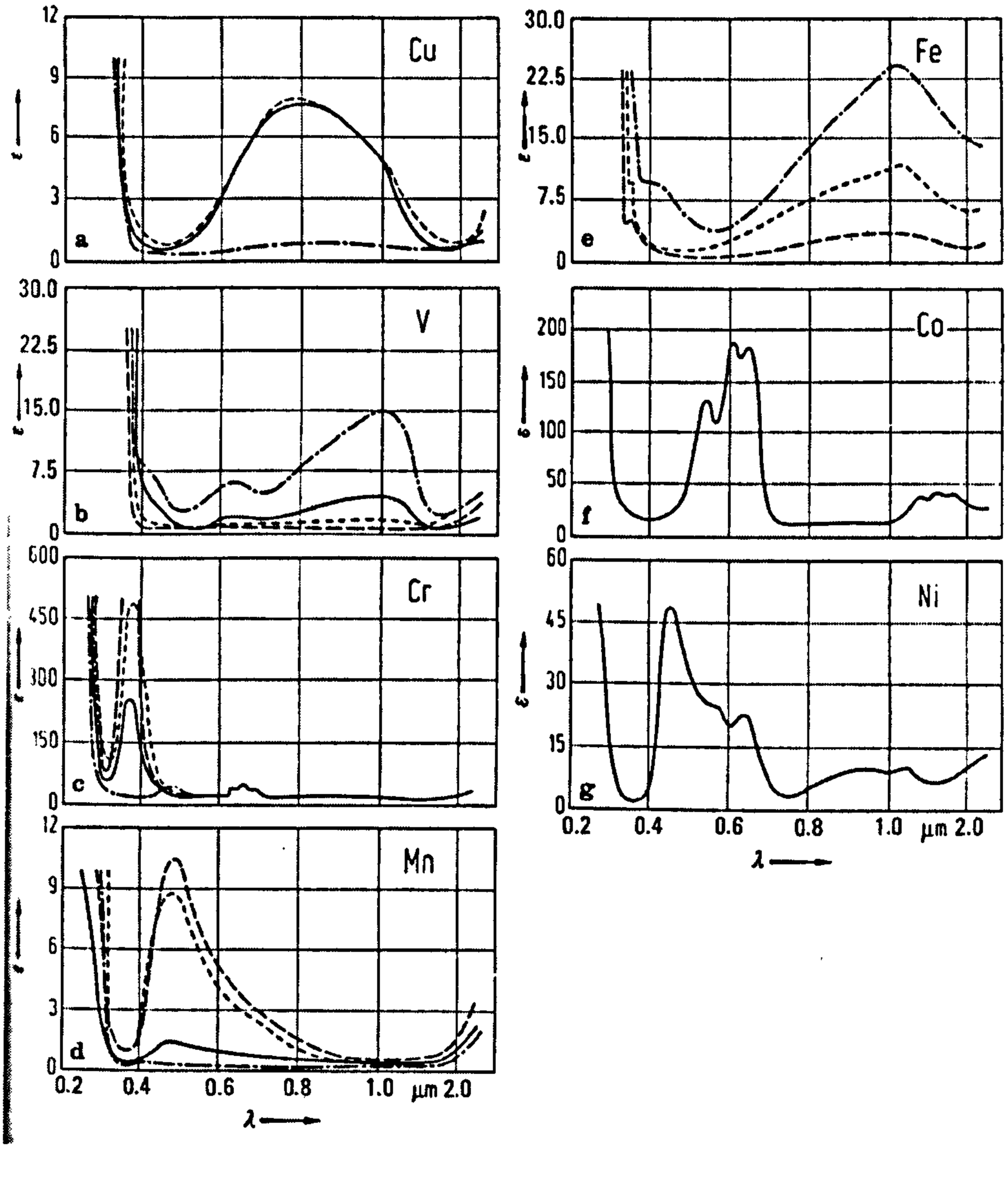

Fig. 1.4.1. Absorption spectrum of sodium silicate glasses doped with the usual TM ion colorants and melted in oxidising (———— Na_2O content about 15 mole % and – – – – Na_2O content about 40 mole %) and reducing (_ . _ . _ . Na_2O content about 15 mole % and ‐ ‐ ‐ ‐ ‐ ‐ ‐ ‐ Na_2O content about 40 mole %) athmosphere. ε = molar normal extinction coefficient in litre/(mole cm) and λ is wavelength in µm. (Scholze, 1990, p. 235).

Ionic colouring agents are usually added as oxide or carbonate powders into a glass batch in concentrations of the order of 0.1 – 2 mol %, or as a liquid solution or colloidal solution painted onto a clear glass surface and imbedded by firing (stained glasses). Ion implantation techniques

can also be used. Edge-filters and red glasses usually contain so called striking agents, which form a second phase, i.e. small colloidal metal or crystallized particles on heat treatment and which shift the UV-edge to longer wavelengths (Vogel, 1994, p. 241 – 250). E.g. CdS, CdSe, CdTe (Fig. 1.4.2.) form colloidal particles in potash-zinc-silica glasses (Vogel, p. 237) and Cu, Ag and Au (Fig. 1.4.3.) are also well-known to form ruby glasses (Doremus, 1994, p. 313 - 317; Bamford, 1977, p.80 – 105 and Vogel, 1994, p. 241 - 250). Various other heavy metal and semiconductor ruby chromophores are known (Vogel, p. 245 – 250). The cut-off edge of UV absorption can be moved within a wide wavelength range by using different heat treatment with a time-temperature profile (Rawson, 1991, p. 25 – 26, 99 – 103).

In striking colours the attenuation is partly caused by electron hopping between the tiny (5 – 50 nm) metal or semiconductor colloidal particles (i.e. nanoparticles, with a 5 – 50 nm diameter) and partly by Mie scattering from the particles and particle clusters (Vogel, p. 248). In edge filters the attenuation at short wavelengths is caused by Rayleigh scattering from controlled size particles. Rayleigh scattering is a special case of Mie's scattering theory holding for particles much smaller than wavelength of light. The narrower the particle size distribution, the sharper is the cut-off edge. The total number of scatterers per unit volume also affects the filtering performance.

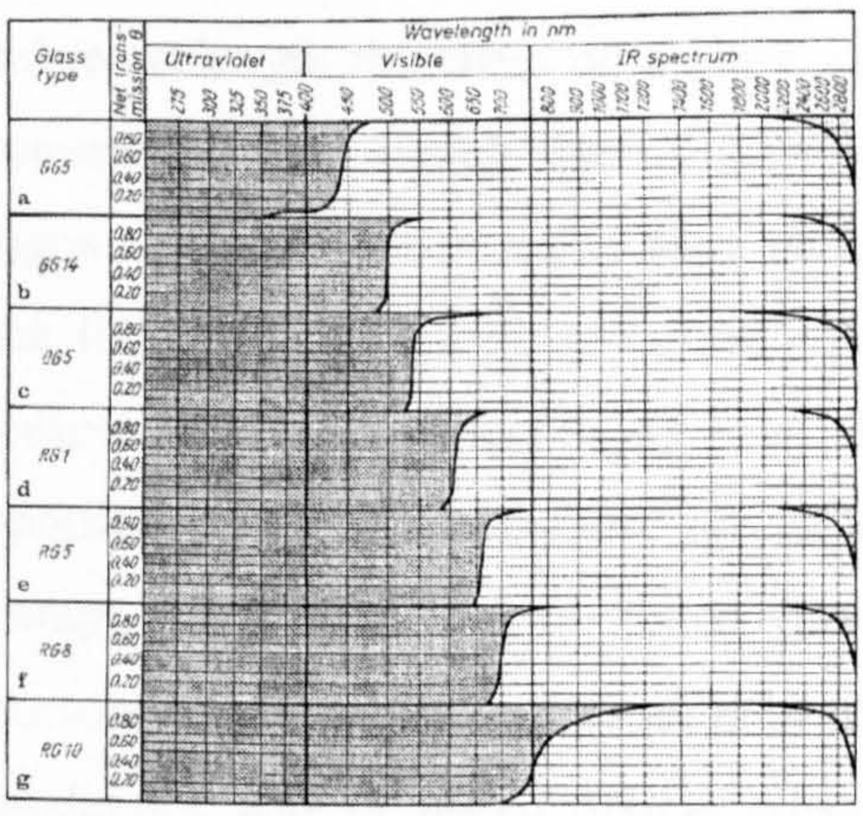

Fig. 1.4.2. Transmission spectra of Schott "striking" color glasses in K-Ca-silicate glass and Zn-K- silicate glasses (Vogel, 1994, p. 237). The white areas represent the transmitted light, and the grey areas are absorbed. These filters are made by a "striking" method using CdS, CdSe or CdTe colorants.

Glass filters doped with ionic transition metal and rare earth colorants (Table 1.4.1) have either a broad band-pass window (FWHM broader than 150 nm, Fig. 1.4.1) or are high - pass type edge filters doped with striking colours (Fig. 1.4.2.). Edge filters have typically a sharp absorption edge, absorbance increasing from 0.1 to 2 - 3 within 50 nm (Fig. 1.4.2.). Interference based Christiansen filters with narrow pass-bands are made of a powder (such as silica) and liquid or glass, which have slightly different refractive index curves, that cross at a certain wavelength. The filter is transparent at the wavelength where the refractive indexes are equal. At

other wavelengths Rayleigh and Mie scattering (depending on the refractive index difference and particle size distribution) cause strong scattering. The transmission wavelength changes with temperature.

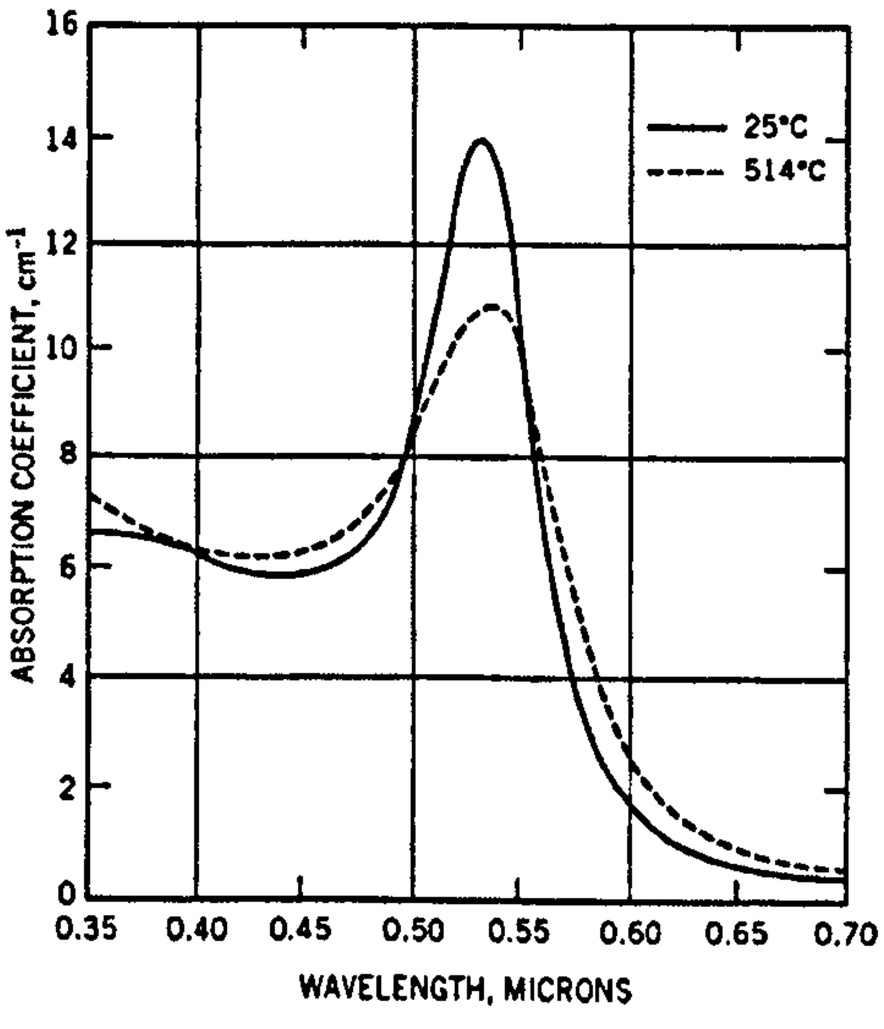

Fig. 1.4.3 Absorption of striking gold particles measured at two temperatures. (Doremus,1994, p. 316).

A thin film layer of a transparent material with a higher (or differing) refractive index and a sub-wavelength thickness on a glass surface behaves like a colouring layer for a reflected and transmitted light signals due to interference between the front and back surface reflected light signals. Which colour can be seen, depends on the incidence angle and wavelength spectrum of the light source as well as on the coating material and layer thickness. During recent years various thin film filters have been developed for a wide range of optical and photonic applications (lenses, cameras, spectacles, lasers, various types of fiberoptic communications components), as well as for tinted, filtering window glasses. They are used to form cavity end mirrors of laser diodes or as an anti-reflecting or wavelength selecting wall before a photonic modulator and in micro optical cross connect mirrors, and as various types of band-pass wavelength filters in wavelength de-multiplexing devices. The transmission window profile can be made to fit almost any shape of spectrum and to any width ranging from sub-nanometer widths to several hundred nm. A symmetric square shape of window (Fig. 1.4.4.) with out-of band blocking by a factor of 10^7 can be achieved. Narrow band pass filters with temperature stability better than 0.02 nm within the service temperature range +10 – +85 °C are available.

Thin film filters are typically made of glassy oxide films (SiO_2, TiO_2, ZrO_2, HfO_2, Nb_2O_5, Ta_2O_5) with a precise refractive index and thickness by vaporizing the film material by heating it electrically and sublimating it on a substrate (membrane or a flat surface of solid material) at -70

– +200 °C in vacuum, depending on the process technology used (physical vapour deposition PVD, ion assisted deposition IAD, ion-beam sputtering IBS or reactive magnetron sputtering technique). In some processes also a suitable gas atmosphere (oxygen, argon, nitrogen etc.) can be used. Thus the material is rapidly solidified from the vapour phase to a solid phase at a high cooling rate resulting in a usable, but not necessarily an optimized, stable structure. Optical thickness of the sublimed layer (= thickness * refractive index) is continuously monitored by measuring the reflected or transmitted wavelength during the sublimation.

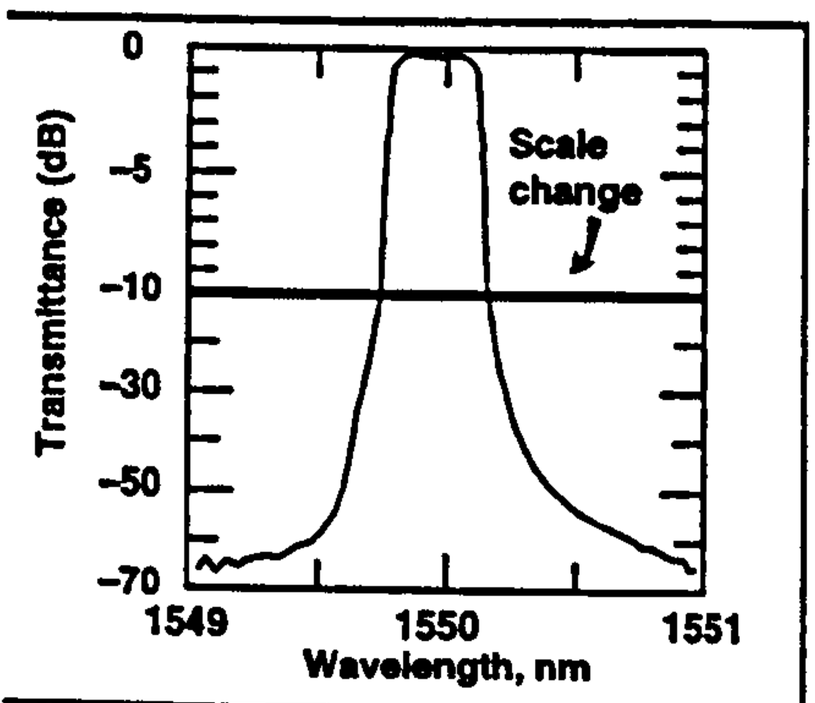

Fig. 1-106 Measured $T(\lambda)$ (on a decibel scale) of a 50 GHz bandpass for WDM. The ordinate changes scale at –10 dB. After Sargent [01].

a)

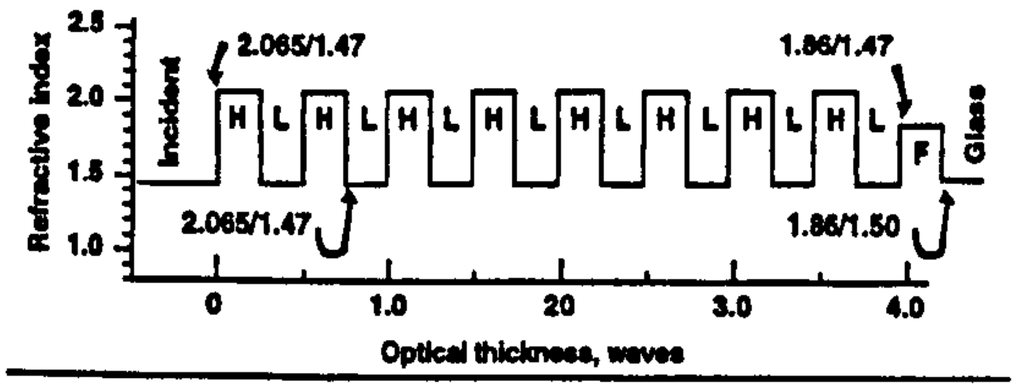

b)

Fig. 1.4.4. a) Transmission spectrum of a stacked thin-film filter and b) the refractive index profile of another thin film filter with a sub nanometre bandpass window (Baumaister (2002)).

Temperature stability of these kinds of stacked thin film filters is achieved by using such layer materials that the factor "temperature expansion coefficient * refractive index changing rate per temperature" for the two layer repeating unit is zero. However, this requirement is such a challenge that only some filter types available in the market are stable over a wide range of service temperatures. Furthermore, the band pass window of these filters shifts with entrance angle due to the change of the effective optical thickness. In addition, radiation stability at high optical power/surface area at any UV-Vis-NIR-wavelength, and in particular, in a UV- or IR-range is also questioned, compared to glass filters and colours. So absorbing metal and rare earth ions (examined in this work) and the well-known metal- and semiconductor particles are most commonly used in coloured and filtering glasses.

1.4.2. Colour of glass and colour coordinates

According to Judd et al (1975, p. 388) and Hunt (1987, p. 17), a human being can distinguish ten million different colours. The colour of glass is "defined" by the light spectrum that is detected by the eyes of an observer. The light is either reflected from the glass item surface, reflected/scattered from its internal material structure or transmitted through it. The detection process of human eyes is logarithmic on received optical power (energy), i.e. it is easier to detect colour nuances, hues and shades at lower optical power level (low brightness) than at high power level.

The colour seen mainly depends on the absorption spectrum of the glass material. On the other hand, the colour seen is dependent on the spectrum of the launching light and on the other wavelength dependent losses caused by the item under consideration. With a monochromatic light source all items appear to have the same colour as the light source, with lighter and/or darker details. Therefore, a colour can be meaningfully defined only with a standard light source of a known spectrum. To determine colour for a glass sample from a transmittance or reflectance spectrum measured with a spectrophotometer (spectrometer), the spectrum must be first normalized to a standard light source by multiplying with a relative spectral power distribution of a relevant standard illuminant (Hunt, 1987). These standard illuminant spectra S(λ), with 1, 2, 5, 10 and 20 nm wavelength steps and normalised to power 100 at 560 nm, are available at website: http://cvision.ucsd.edu/ and from International Commission on Lighting (C.I.E.).

Furthermore, the sensitivity of human eyes is dependent on the wavelength of the light signal, and the sensitivity spectrum of a standard human observer can be described mathematically as a sum of three colour-matching functions of red, green and blue "detectors" (Hunt, 1987, p. 45-47; Bamford, 1977, p. 16 - 33). The colour vision sensitivity varies within human beings. C.I.E. has therefore defined the Standard Calorimetric Observer (CIE1931, CIE1971; CIE 1986b with 2°-vision angle, with 1, 2, 5, 10 and 20 nm steps) and CIE 1964 Supplementary Standard Colorimetric Observer, often referred as the 10° Observer. The tristimulus values X, Y and Z of the observed spectrum are then calculated as the sums over the wavelength range for the terms: the colour-matching value $(x(\lambda), y(\lambda), z(\lambda))$ * the standard illuminant value S(λ)* the measured transmittance T(λ). (Hunt, p.46 – 51; Bamford, p. 18 -19). The new daylight standard Illuminant D6500 is used, if there is no requirement for any other light source, also available from the website: http://cvision.ucsd.edu/.

The colour coordinates i.e. the relative tristimulus values, usually called chromaticity coordinates x, y z of the incident light (from the observed item) are finally calculated as x = X/(X+Y+Z), y = Y/(X+Y+Z) and z = Z/(X+Y+Z). For these holds equation x+y+z=1, and thus usually only x and y are shown and discussed with comparing the distance and direction of the

point (x,y) from the S_E spot at the chromaticity diagram (Fig. 1.4.5). The position of S_E, the equi-energy stimulus (X = Y = Z and x = y = z = 1/3) represents white, grey and black colours because this system in insensitive to the brightness.

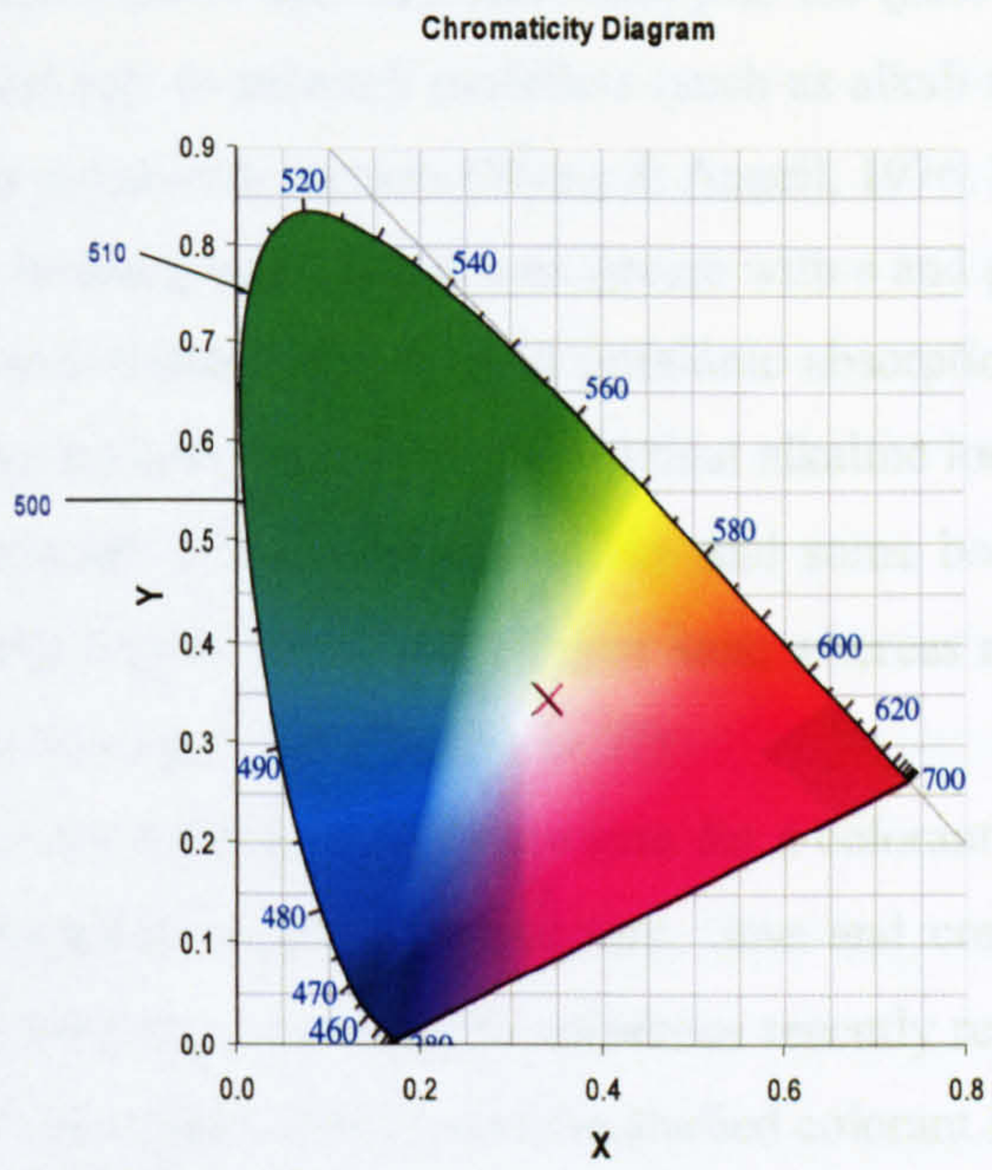

Fig 1.4.5. Chromaticity Diagram with measured and synthesized colour coordinates x and y of a faint reddish glass sample of this work. The synthesized colour coordinates are calculated for a mathematically described spectrum of the glass, by using the method developed in this work. The appearance of the colours in the chart (Ref. http://cvision.ucsd.edu/) is dependent on the computer and printer settings used to produce this graph.

For the glass industry and in particular for faint colours the above presented C.I.E. colour coordinates do not give a suitable resolution to distinguish faint colours or to design decolourising batches. Therefore usually the CIELAB system with coordinates L*, a* and b* calculated from the C.I.E. colour coordinates are prefered. L*, a* and b* are calculated from the C.I.E. coordinate values X, Y and Z, i.e. $L^*=116(Y/Y_n)^{1/3}- 16$, $a^* = 500[(X/X_n)^{1/3}-(Y/Y_n)^{1/3}]$ and $b^* = 200\ [(Y/Y_n)^{1/3}-(Z/Z_n)^{1/3}]$, where n refers to the coordinates of the S_E point defined with the same light source (Hunt, p. 66 and 197). In this system L* correlates to lightness, a* correlates to redness or greenness and b* to yellowness or blueness.

1.4.3. Structure of ion doped coloured glass

The absorption spectra of the studied colorant ions result from the intraionic and interionic electron transitions. The energy levels of the 3d and 4f orbitals, and therefore the absorbed energies of intraionic transitions between the orbitals are defined by the number of electrons in

3d- or 4f-orbitals, the energy state and valence of the ion and the strength of the ligand field defined by the configuration and dimensions of the closest neighbouring anions. The effect of next closest cations is very weak and thus neglected.

The first order transition metal and rare earth ions join the glass network mostly with ionic bonds in similar sites and role to network modifiers (such as alkali metal and alkali earth ions) and in some cases partly as network formers (Wong & Angell, 1976; Sudo, 1999, p.152 -; France 1991, p. 57). Chemical bonding with closest ions occurs with s and p orbital electrons, not with those electrons in 3d- and 4f-shells involved in intraionic absorption transitions. The colorant metal ions typically have a higher valence (2+ - 6+) than alkaline ions (1+). The silicon-oxygen SiO_4-tetrahedral-ring network is therefore opened up and some bonds are broken. Typically transition metal ions have four or six closest oxygen ions, whereas rare earths can have various configurations from 6 to 9 oxygen ions (France, p. 57).

The final structure of the surrounding oxygen ions for a colorant ion in a glass is dependent on the host glass composition, melting temperature, time and conditions, as well as on the cooling and annealing processes. According to numerous recently reported studies, the structure of the closest neighbouring oxygen ions around the studied colorant ions in glasses is close to an equilibrium crystalline structure of the respective metal/rare earth oxides. In the literature (Bamford, 1977; Bates,1962; Paul,1982; Burns, 1993; Rao et al, 1995; Cotton, 1988; etc.) measured, overlapping absorption bands are be found for these TMs in crystalline oxides, glasses and aqueous liquids.

Bamford's (1977), Bates's (1962) and Paul's (1982) data are used in this work as the main guidance to find the starting parameters for the fitting of Gaussian peaks to the measured absorption spectra. The hypothesis of almost crystalline structure is the base of the ligand field theory, developed from crystal field theory, and thoroughly studied by Bates and Paul, and is also used as the base assumption for this work, even though it has not been found in literature to be approved for colorant ions in glasses (See Chapters of Results and Conclusions). Earlier, other ideas were presented, such as random glass structure, but they are not needed to describe the results of this work (Chapters 4 – 9).

According to recently reported structural studies (Burns, 1993; Rao et al, 1995; West, 2004; Cotton, 1988), silicate glasses have a short range order in their structure and a certain three dimensional network matrix, but lack uniformity and long range periodicity of crystalline structure. Typical sites of transition metal ions have octahedral or tetrahedral configuration of the closest oxygen ions in silicate glasses. The most common transition metal crystalline monoxide structure is the rock salt structure, and, for dioxides, the rutile structure (Burns, 1993; Rao et al,

1995; West, 2004; Cotton, 1988). Zinc-blend, olivine and a few other structures are also found within the polyvalent first row transition metal oxides (Burns, Rao et al).

Most of the transition metals, as well as a few rare earths, are polyvalent in glasses, i.e. they appear simultaneously in two or three valence states. The concentration ratio (i.e. the redox ratio) of the ion depends on the host glass composition and its basicity, melting conditions (temperature and concentration of oxygen in the firing atmosphere) and annealing conditions during which the final valences of the colorant ions and the final structure of their neighbourhoods and for the host glass are defined. During melting under reducing melting conditions, i.e. a low O_2-concentration, the concentration of the lower valence ions increases and in oxidizing conditions the concentration of the higher valence ions increases. The chemical bonding with the s- or p-orbital electrons have higher energy than the inner "electrons shells" of d- or f-orbitals, within which the intraionic absorption causing transitions occur.

1.4.4. Absorption spectrum of colouring ions

Most of transition metals, i.e. of elements from Sc to Zn, from Y to Cd, from Ce to Lu and further to Hg, and from Ac to Lr, can colour glass by causing absorption at visible wavelengths. In most cases several absorption peaks, or peak groups, can be found in the range from UV to IR light (200 – 3000 nm). In this work, only the first row transition metal ions are studied.

We can categorise the sources of absorption in glasses to ions, chromophores and colour centres. Transition metal and rare earth ions have two kinds of electron transitions: transitions between the ion and its ligands, called *charge transfers* (p- or s- orbital electrons involved) (Fig. 1.4.6.), and intraionic *electron transitions* within 3d- (for transition metals) (Fig. 1.4.6.) or 4f-orbitals (rare earths). Both types of transitions can occur simultaneously in the same ions, because separate electrons are involved. Charge transfer absorption of the colorant ions cause very intense peaks ca. 1000 – 10 000 times stronger than the intraionic transitions) in the UV range and an UV-edge for a doped or even in clear glasses that are made of normal, non-purified ingredients (Paul, 1982, p. 304). In many cases the UV-edge extends up to the shortest visible wavelengths. The metal to ligand and ligand to metal charge transfers, the electrons involved, energies and their absorption spectra are described in detail by Level (1968, p. 224 – 248) and for the studied ions in glasses also by Paul, (1982, p. 315 – 323). Burns (1993, p. 115 - 132) also describe *intervalence transfers* between 3d orbitals and neighbouring cations in adjacent sites, such as Fe^{2+} and Fe^{3+} in crystalline minerals, and Bingham (2000) has referred to his results to attribute some of the fitted peaks of Fe- absorption spectra in glasses.

The intraionic transitions are actually prohibited by the quantum mechanics rules (i.e. Laporte forbidden), but occur anyway in glasses in the colouring ions at visible light energies within the

partly vacant 3d-and 4f- orbitals with a relatively weak absorption intensity, and weaker absorption energy (at longer wavelengths) than the charge transfers. The energy levels and shapes of d- and f-orbitals are affected by the electric- or magnetic fields of the closest ligands (e.g. oxygen ions), and thus split to several new groups of orbitals compared to free ions with perfectly symmetric ligand fields. Usually two or more overlapping transitions, i.e. overlapping absorption peaks are found. In general, the absorption peaks of d-transitions in silicate glasses are quite weak and broad (FWHM 50 nm to 400 nm, see Fig. 1.4.6. in Chap. 1.4.1., and Bamford, 1977; Paul, 1982; Scholze, 1991). The fitted absorption peak positions has been found to vary by 10 – 30 nm with host glass basicity (Bingham, 2001, 2002; Duran, 1983, 1985) i.e. being dependent on the average ligand field of the host glass.

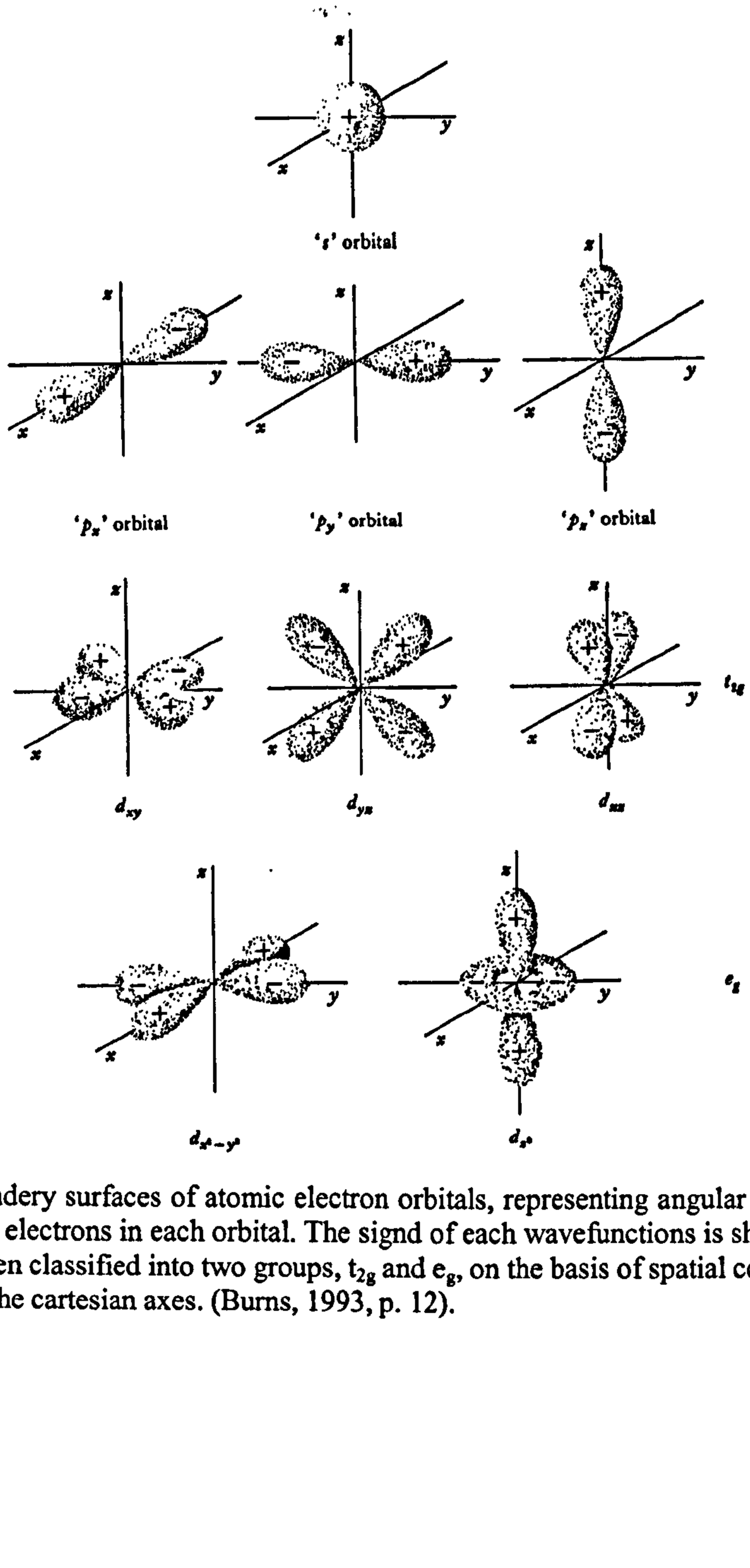

Fig. 1.4.6. Boundery surfaces of atomic electron orbitals, representing angular distribution propabilities for electrons in each orbital. The signd of each wavefunctions is shown. The d orbitals have been classified into two groups, t_{2g} and e_g, on the basis of spatial configuration with respect to the cartesian axes. (Burns, 1993, p. 12).

The transitions within f-orbitals cause similar intense but much narrower absorption peaks (FWHM 10 – 50 nm) compared to d-transitions. The peaks positions move only by a few nanometer with host glass. The absorption peaks are less sensitive to the glass host and ligand fields than for d-transitions.

Absorption caused by colloidal metal particles (Cu, Au, Ag, etc.) is caused by scattering and intra-particle absorption, both dependent on the particle size, i.e. proportional to r^6 (scattering) and to r^3 (intra-particle absorption), r being the particle radius (Bach et al, 1995, p. 364). For colorant semiconductor particles (CdSSe etc.) in silicate glasses an absorption edge can be found at a wavelength typically above 500 nm, below which wavelength all light energy is mainly absorbed by lifting electrons from valence band to conducting band, and above which the glass is transparent (Bach et al, p. 366 – 367).

In chromophores, the electrons transit between intra-molecular orbitals similarly to intraionic transitions, though of different energies causing absorption peaks of similar types or wider than ionic transitions. Colour centres are network- and material defects, where O- or Si- or another glass component-ion is missing. These sites have typically a free electron or vacancy (hole) to attract an extra electron, which can be excited by light and cause absorption. The absorption caused is wide band overall raising of background attenuation at all wavelengths. Typically colour centre types of defects are caused by irradiation, energetic laser light exposure or during high temperature treatments and rapid forming at an unsuitable temperature.

The absorbed energy in the glass is either exchanged to heat or lost by fluorescence, i.e. escaping as photons at longer, specific wavelengths corresponding to the energy levels available or by another type of luminescence (broad wavelength range, low intensity). In some cases absorbed energy causes chemical reactions or extraction of electrons (photosensitivity), in particular, when charge transfer at energetic UV wavelengths is involved. In the infrared region the energy is mainly absorbed by molecular vibrations (heat). Absorption peaks of intraionic transitions at certain frequencies (i.e. wavenumbers, wavelengths) occur, when there is available an electron to be excited and an energy gap between orbitals equal to the energy of the passing light. The peak wavelength λ (in vacuum) corresponds to wavenumber υ (1/wavelength) and is related to the absorbed energy ΔE (the energy difference between the orbitals- or orbital groups of the transition) by the well known equation $\lambda = 1/\upsilon = ch/\Delta E$, where c is light speed in vacuum and h is Planck constant (= $6.62608 * 10^{34}$ Js). Light energy and intensity are related to $(\text{amplitude})^2$. In glass the light velocity and amplitude are decreased compared to velocity and amplitude in vacuum. The energy values should be considered by taking this into account. However, in this work the vacuum wavenumber of the light is used as a relative measure of energy in literature and experienced at visual consideration of coloured glass. Only a systematic

error is caused in structural considerations, which does not disturb the achieving of the goals of this work.

1.4.5. Ligand field theory

Ligand field theory, developed by Tanabe and Sugano was thoroughly studied by Bates (1962) for the colouring transition metals in glasses. It describes how the electron transition energies between the 3d-orbitals (~ absorption peak positions) depend on the number of electrons in 3d-orbitals and the strength of the ligand field in symmetric octahedral and tetrahedral configurations of the closest ligand ions. Detailed summaries of the ligand field theory, that is developed from crystal field theory, are found in various books, such as Lever (1968), Burns (1993), Cotton (1988), Bates (1962), Paul (1982) and a concise summery in Varshneya (1994, p. 463 – 470). In addition, molecular orbital theory is used, in particular, for non-symmetric chemical species in other glasses and other chemical species.

An example of an Fe^{3+} ion spectrum compared with ligand field theory is given in Fig. 1.4.7. This theory gives a mathematical description for the absorption peak positions, transition energies by using a set of 3 – 4 parameters defined from the structure of the ligand field. Fig. 1.4.8. presents $3d^n$ configurations for transition metal ions.

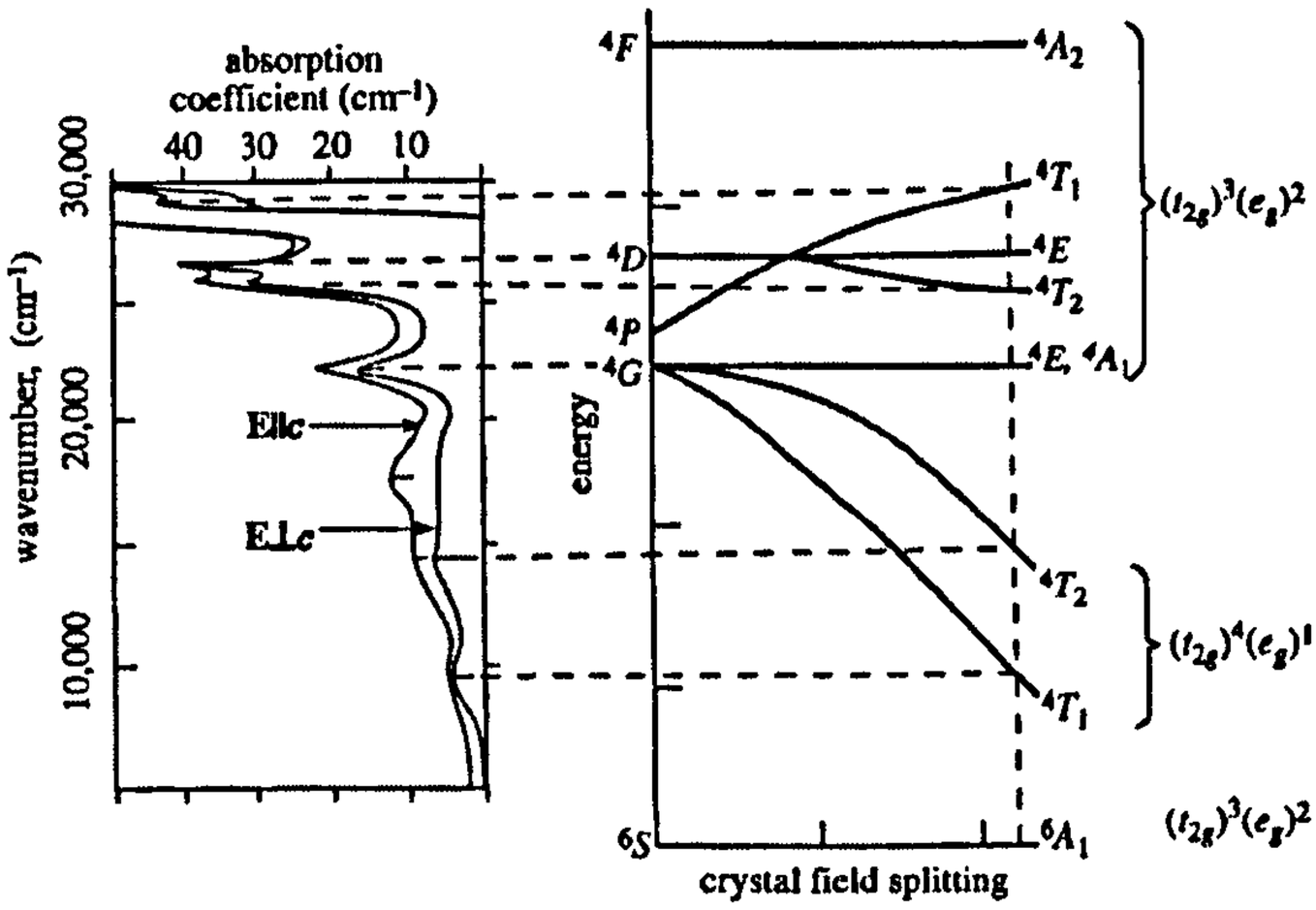

Fig.1.4.7. A measured transition absorption spectrum for Fe^{3+} ions in crystalline form, matched to ligand field theory, $3d^5$ spin-forbidden transitions (Burns, 1993, p. 68).

The ligand field theory describes how the positions of the absorption peaks change, to which direction and how far with increasing symmetric ligand field strength. If the symmetry of the ligand configuration is disturbed (e.g. an octahedral configuration modified with increasing extent of tetragonal distortion by moving away two opposite ligands of the six available), another new energy levels appear and the energy level diagram must be modified according to the case.

An example of, how the distortion changes the energy levels and cause splitting in an octahedral configuration is given in Fig. 1.4.9.

	Atomic number	Element	Electronic configurations: Atom	M(I)	M(II)	M(III)	M(IV)	M(V)	M(VI)
first-series transition elements	19	K	[Ar]$4s^1$	[Ar]					
	20	Ca	[Ar]$4s^2$		[Ar]				
	21	Sc	[Ar]$3d^14s^2$			[Ar]			
	22	Ti	[Ar]$3d^24s^2$		[Ar]$3d^2$	[Ar]$3d^1$	[Ar]		
	23	V	[Ar]$3d^34s^2$		[Ar]$3d^3$	[Ar]$3d^2$	[Ar]$3d^1$	[Ar]	
	24	Cr	[Ar]$3d^54s^1$		[Ar]$3d^4$	[Ar]$3d^3$	[Ar]$3d^2$	[Ar]$3d^1$	[Ar]
	25	Mn	[Ar]$3d^54s^2$		[Ar]$3d^5$	[Ar]$3d^4$	[Ar]$3d^3$		
	26	Fe	[Ar]$3d^64s^2$		[Ar]$3d^6$	[Ar]$3d^5$			
	27	Co	[Ar]$3d^74s^2$		[Ar]$3d^7$	[Ar]$3d^6$			
	28	Ni	[Ar]$3d^84s^2$		[Ar]$3d^8$	[Ar]$3d^7$			
	29	Cu	[Ar]$3d^{10}4s^1$	[Ar]$3d^{10}$	[Ar]$3d^9$				
	30	Zn	[Ar]$3d^{10}4s^2$		[Ar]$3d^{10}$				
	31	Ga	[Ar]$3d^{10}4s^24p^1$			[Ar]$3d^{10}$			
	32	Ge	[Ar]$3d^{10}4s^24p^2$				[Ar]$3d^{10}$		

[Ar] = Argon core, $1s^22s^22p^63s^23p^6$

Fig. 1.4.8, Electronic configuration and spectroscopic terms (ground term for each electronic configuration is listed first) arising from each $3d^n$ configuration for transition metal ions (Burns, 1993, p. 53). Notation M(I), M(II), ... means M^+, M^{2+},... ions, respectively.

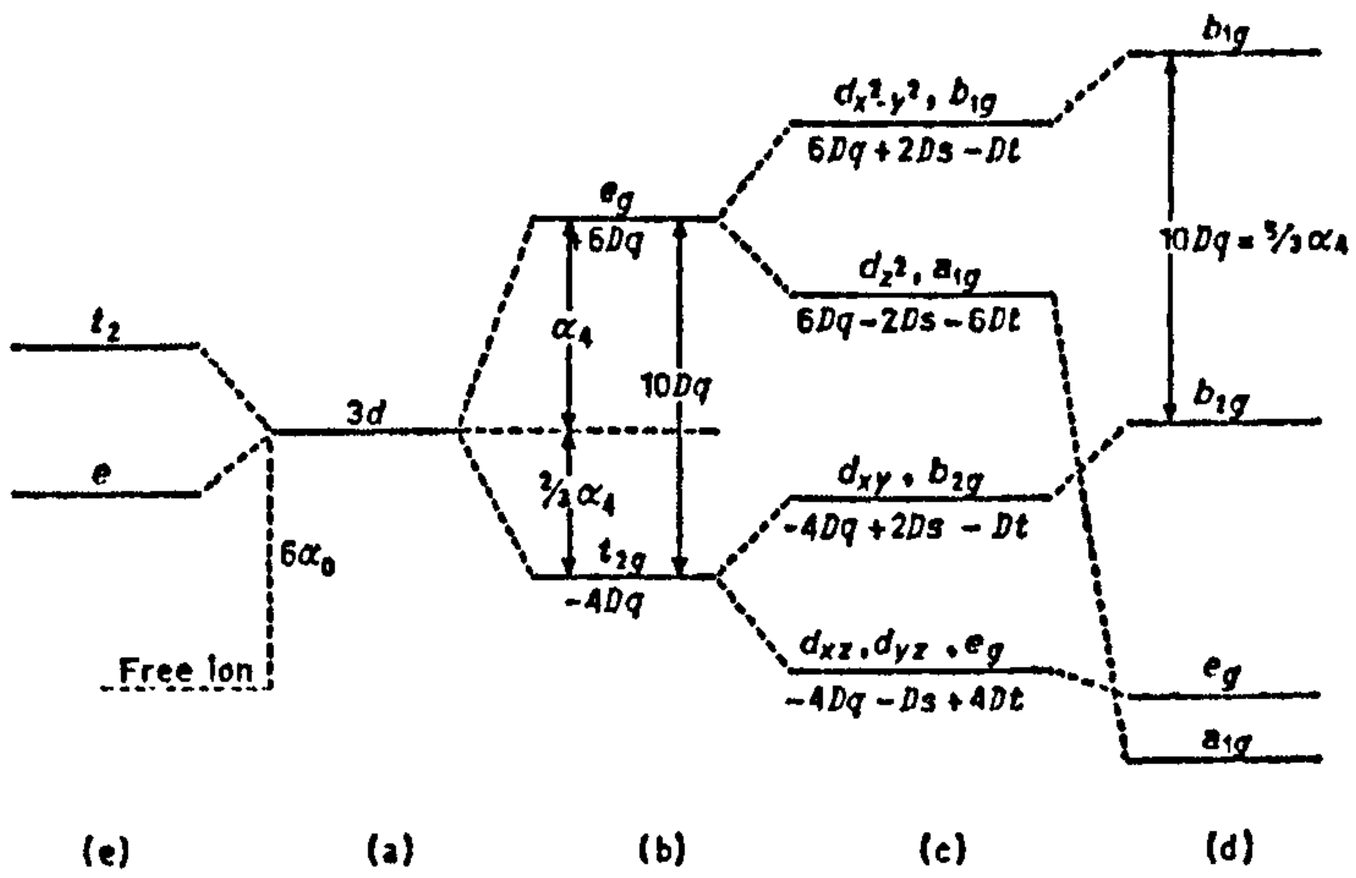

Fig. 1.4.9 Energy levels in the point charge approximation. A) spherically perturbed d shell, b) octahedral peturbation, c) octahedron with weak tetragonal distortion (elongation along z-axis), d) strong tetragonal distortion or square planar environment, e) tetrahedral perturbation, (Lever, 1968, p.76).

Each valence state of each TM has a number of electrons in $3d^n$ orbitals, where n = 0 to 10 = the number of electrons. Several transition metals have the same number of electrons in 3d orbitals, such as Cr^{3+} and Mn^{4+} have $3d^3$ (Fig. 1.4.8), and thus also similar ligand field structure and similar "finger print" system of absorption energy levels (peak positions). The average

strength of the ligand field is usually different for each TM in the same glass due to different ionic radius and other factors, and the absorption peaks are thus not overlapping.

It has been found by various researchers that this theory is applicable to describe most of the pure ionic absorption peaks of transition metals as Gaussian peaks (three parameters: height, position and width) in glasses. However, it is difficult to compare the theory to the published data or to the measured spectra or to use the theory for a glass colour design program without making own experiments. Reason to this is that the reported tests does not seem to be made systematically, and it is not often recorded in detail what the glass compositions were, how they were melted and annealed/heat-treated. Thus the key questions to be answered by this work are: a) whether the ion sites in glasses are adequately similar and sufficiently equal to the crystal types of ligand fields assumed by the theory, b) whether different transition metal ions with a similar number of electrons are affected in the same way by a ligand field in similar glass hosts and ion sites; c) trends in peak widths; d) trends in peak heights; consequences of more than one transition metal doping; e) enough wide scaling range with concentration needed to consider practical absorption levels and f) consequences of charge transfer absorption at UV wavelengths and complex chromophores.

The ligand field theory does not describe the effect of the host glass on the heights of the absorption peaks. The heights depend on the redox ratio of the ion valence states, on the "popularity" (i.e. frequency, intensity) the individual transitions and the structural uniformity of the sites (height versus width variation). The "popularity" of transitions depend on the filling of the energy levels, i.e. energy state of the ion. At a high energy state (high spin state) single electrons with similar spins, fill all 3d energy levels and only as few as possible of the levels have electron pairs with opposite spins, and in low energy states the lowest energy levels are fully occupied with electron pairs of opposite spins, and the upper levels are empty. The detailed analysis of the various energy states for each d^n configuration is found in Paul's book Chemistry of Glasses, 2nd Ed. (1990) on p.284 – 289. Splitting of energy states D, P and F, that have been found to match certain TM ions absorption spectra by Paul, are found in Fig. 1.4.10. (Paul. p. 288). The "popularity" of transitions can be assumed to depend on the amount of electrons at each energy level, and on all the factors that may change it. Certain ions, such as Fe^{2+} can in theory have six different occupation sets of energy states (Burns, 1993, p. 55), depending on the strength of ligand field.

The widths of the absorption peaks are not considered by the ligand field theory either. They are thought to be related to a random variation of glass structure (variation of the distances and angles to the ligands within the similar sites of the ions). It is known that the peak widths decrease by decreasing temperature and by crystallising.

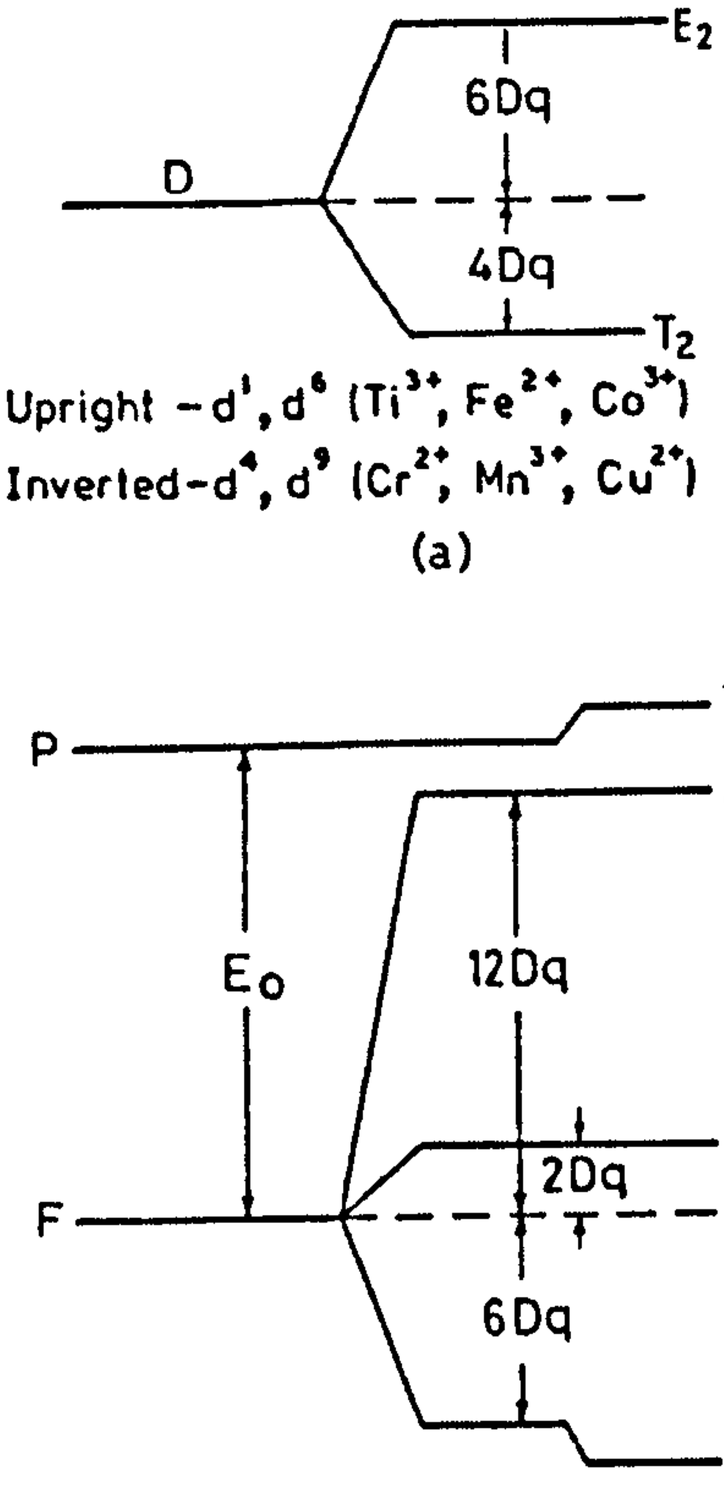

Fig. 1.4.10. The splitting of d orbitals, a) for D-state, b) and c) for P and F states. The diagrams are appropriate for octahedral fields and when inverted apply to tetrahedral or cubic fields (Paul, 1990, p. 288).

1.4.6. Parameters Dq, C and B

The strength, intensity of the ligand field, experienced by an ion in a surrounding configuration of the closest ions is dominantly dependent on the nearest ions and their charges, their spatial positions and distances to the ion. It is described with the parameter 10Dq, the energy difference between the t_{2g} and e_g orbitals (also called as crystal field splitting = Δ_0), of the ligand field theory, and its magnitude is related to the surrounding configuration of charged ions in an octahedral configuration of the six closest ions by equation (Burns, 1990, p. 8 - 26) :

$$\Delta_0 = 10Dq = \frac{Z_L e^2}{6R^5}\langle r^4 \rangle = \frac{Q\langle r^4 \rangle}{R^5},$$

where ($Z_L e$) is the charge on the ligands separated by a distance R from the cation, r is the radial distance of the electron from the nucleus (referring to the polar coordinates of an electron in space) and Q is a constant. Thus 10Dq $\propto R^{-5}$. Thus the effect of the closest ligands dominates

the splitting of the energy orbitals. The parameter $<r^4>$ is the mean value of the fourth power of the radial distance of a 3d orbital from the nucleus. Its value is assumed to be approximately constant for cations of similar valence in the same transition series.

In practise, in order to demonstrate the effects of dimensional distortions, state of covalency of the bonding and the effect of the base glass on the energy levels or their differences, the Tanabe-Sugano diagrams are calculated using semiempirical Racah parameters C and B. The detailed information can be found in Bates (1962, p. 206 – 207); Burns (1993) and Paul, (1990) for the calculation of the peak positions as a function of Dq for each $3d^x$ ion in each environment. The third Racah parameter A is a product of C and B. The parameters C and B are usually known for free ions. E.g. for Fe^{2+} and Fe^{3+} ions in glass, various different parameters are quoted in the literature depending on the glass composition and preparation, the ion valence and surrounding configuration of the ligands, as was reported by Bingham (2000, p. 55), and a few examples are given in Chap. 5. In particular, it is important to be aware of the parameters used to calculate a Tanabe-Sugano diagram given in the literature, because the positions and assigning of the peaks obtained in an optical absorption spectra can be seriously affected by using a non-relevant diagram (i.e. a non-relevant B and C).

1.4.7. Effect of host glass, optical basicity

The composition and structure (fictive temperature, homogeneity, etc.) of the host glass as well as the bonding to the host glass create the ligand field for a dopant ion in a glass. The final structure is dependent on the thermal history of the glass (melting temperature and conditions, annealing conditions, cooling rate etc.). Furthermore, the optical absorption spectrum of a metal ion dissolved into a host glass is dependent on the site configuration, where it is located. In this work only oxide glasses are studied, and the studied metal ion dopants are assumed mainly to be sited as separate dissolved ions, as network modifiers, surrounded by oxygen ions that in turn are linked to alkaline ions or alkaline earth ions and silicon ions. It is possible, especially for Fe ions to behave like glass formers, i.e. get linked to each other with oxygen ions in between, forming a glass network. Clustering of iron oxides and or iron silicates inside the glass have been reported. However, the detailed structural studies are excluded from this work.

One practical parameter to describe the average effect of the host glass composition, i.e. the ligand field, on the dopant ions is optical basicity (Duffy, 2000, 2002, 2004 A and B, and many other of his previous papers). E.g. Bingham et al (2001, 2002) showed that the fitted peak positions of Fe^{2+} show a linear relationship with optical basicity of the host glass. Its meaning can be understood as an inverse average magnitude of bonding force of the oxygen ions, thus being a kind of inverse value for the ligand field, by which the oxygen ions affect the electron

orbitals of the dopant ions. The optical basicity values are calculated by using Duffy's (2002) experimental Λ(oxide) values for individual oxides, and the equation:

$$\Lambda_{glass} = X(AO_{a/2}) * \Lambda(AO_{a/2}) + X(BO_{b/2}) * \Lambda(BO_{b/2}) + \ldots,$$

where $X(AO_{a/2})$, $X(BO_{b/2})$, …, are the proportions of oxide (O^{-2}) atoms contributed by each of the oxides, and $\Lambda(AO_{a/2})$, $\Lambda(BO_{b/2})$, …, are the optical basicities of the individual oxides.

In 2000, Duffy et al demonstrated a linear relationship between optical basicity (~ average donated charge by oxygens in %) and some absorption peaks of Mn^{2+} and Fe^{3+} ions in phosphate, borate and silicate glasses. Duffy et al (2002) also showed that there is a linear relationship between the log of redox ratios and optical basicity of the host glass for Fe, Ce, Cr, Sn, and As dopants in silicate oxide glasses, and gave equations, such as $\log\{[Fe^{2+}]/[Fe^{3+}]\} = 3.2 - 6.5*\Lambda_{glass}$. The relationship is demonstrated within the optical basicity range 0.52 – 0.67 in lithium, sodium and potassium silicate glasses.

2. Experimental methods

2.1. Introduction, glass samples

The main goal of this thesis is to develop a mathematical description for the absorption spectra of the dopant TM and RE ions in silicate glasses. All together 250 glass samples were prepared, varying melting conditions, glass composition and dopants. The glass compositions tested are typical three to five component silicate glasses (Annex 1 and 3) with various optical basicities (0,53 – 0,63) and resemble compositions used for clear and coloured flat and container glasses. The melting temperature and time were kept constant (1450 °C, 5 h), but the melting atmosphere (oxygen concentration) was varied between gas-fired furnace or electric furnace and by adding either none or some reducing or oxidising agent. The examined dopants were added to the batches as pure oxide powders. The dopants, including all main ionic colorants and decolourisers used by glass industry, were varied between, no dopant, a single TM (Ti, V, Cr, Mn, Fe, Co, Ni, Cu), any possible pair of the studied TM's, a single RE (Ce, Pr, Nd, Sm, Eu, Tb, Dy, Ho, Er) and some combinations of REs and TMs, and Se. Nano-particle colorants, such as CdS, CdSeS, rubies of Cu and other metals, were excluded. (See Annex 1).

Glass compositions (Annex 1) were calculated in the normal way (Cable, 1996 b) by using mol % concentrations and designing at first the host glass composition, including the refining agent (Na_2SO_4) and the eventual reducing (carbon as graphite powder) or oxidising agent ($NaNO_3$). The dopant oxides were added on the top, thus actually causing a slight modification to the host glass composition compared to the undoped, non-reduced or non-oxidised base glass samples. The glass compositions, calculated from the batch are given in Annex 1. The final glass compositions achieved differ slightly from the calculated values (Annex 3). Variations to glass compositions are caused during melting due to volatilisation and dissolution of material from wet crucible walls and by eventual weighing errors and humid raw materials. Impurities are also introduced by raw materials of commercial grade, by dissolution from crucibles and by touching the melt with the iron tongs used for moving crucibles in the top – open furnaces.

The compositions for all the glasses made for this project are given in Annex 1, even though a few of them were lost at melting due to a too strong reduction of their colorant ions. In a couple of cases, a replacement sample was needed due to a batch calculation error. All the prepared glass samples (Annex 1) have influenced the analysis and conclusions of this thesis, even though various samples are not specifically mentioned. All samples have been analysed by visual inspection on the received colour, transparency and homogeneity, and by optical spectroscopy for transmission properties. For gas-melted samples also the colour of the quickly quenched glass remaining in the crucible was inspected. A polished glass sample was prepared and a transmission absorbance curve was measured for all received samples. The absorption

spectrum data has been mathematically analysed for almost all of the samples, even though only a selection of the most interesting results are highlighted in this thesis and discussed in detail.

2.2. Batch preparation, glass melting and annealing

The test samples of silicate glasses (Annex 1) contained 60 – 70 mol % silica (sand) and 5 – 15 mol % of three or four of the following glass network modifiers (Li_2O, Na_2O, K_2O, CaO, BaO, MgO, ZnO) and formers (B_2O_3, Al_2O_3). Information of the used chemicals is given in Annex 4. The SiO_2 was added to the batch as LA Sand and to the pure glass samples (marked with "Cle" in Annex 1) as a pure silica powder. Impurities of the raw materials are given in Annex 3 and 4.

The alkali and alkali earths were added as carbonates except that the melts were refined with 0,35 mol % Na_2SO_4 replacing the chemically equivalent amount of Na_2CO_3. For those melts oxidised with $NaNO_3$ the chemically equivalent amount of Na_2CO_3 was also replaced. The calcium carbonate (limestone powder) used in usual samples also contained impurities (Annex 4), and for the ultra pure samples, purified laboratory chemicals (containing less than 0,002 weight % Fe_2O_3) were used. MgO was added together with CaO as dolomite. Purified laboratory chemicals were used for all other host glass ingredients (Annex 4).

The batches were prepared by weighing as accurately as possible (to a ± 0,1 % reproducibility) the ingredients with the same two weighing balances, a coarse and a fine to avoid possible systematic differences between the scales. The batches were mixed roughly and the lumps were crushed with a steel spatula on an even paper sheet. The final mixing was done by manually rotating the batches in closed plastic bags in which the batches also were stored until melting. $BaCO_3$ was added directly to the bag to avoid its special problem, the sticking to the paper and, in particular, to the steel spatula used for mixing on paper.

The samples were melted either in top-filled, natural gas-fired furnaces or in top-filled, electric furnaces at 1450°C for five hours. The temperature was controlled automatically with internal thermocouple sensors of the furnaces, and additionally for the gas furnaces it was checked by an external pyrometer. The accuracy of the temperature setting in gas furnaces is of the order of few degrees, but varies inside of the furnace by ± 5 °C depending on the distance of the crucible from the firing flames, and in the electric furnaces two - three degrees Celcius. The concentration of oxygen gas also varies inside of the gas-fired furnaces, the atmosphere is thus more reducing in those crucibles closest to the flames. Five to seven crucibles were melted in each lot of samples.

Most gas-fired furnace samples were melted in CP1 (300 g glass) mullite crucibles (See Annex 1) made at Sheffield University, The Department of Engineering Materials. These

samples were not homogenised by any other method than waiting for 5 hours. The samples made in electric furnaces were melted in platinum crucibles (containing 2 % Rh, 100 g glass) and homogenised either by casting to frit into pure deionised water after 3 hours and re-melted for two hours, or by continuous stirring with a platinum stirrer for four hours before being cast to the sample. The glass melts were cast as 6 - 10 mm free plates on a warmed iron plate or as 25 mm * 20 mm * 5 cm bars in warmed iron moulds. The cast glass items (plates and bars) were annealed at 540 °C for one hour and subsequently cooled at a rate of 1°C/min to room temperature. Stress levels were not checked, but they are assumed to be low, because the samples could be cut by a diamond saw without cracking.

2.3. Sample preparation

The annealed glass plates and bars were cut by a diamond saw to suitable samples for each measurement method. Glass samples for optical transmission spectroscopy methods (ca. 20 mm × 25 mm × 4 mm) were manually polished in six stages using silicon carbide powders (grit size 240, 400 and 600) and water; using silicon carbide metal polishing papers (800 and 1200) with water, and finished with CeO_2-powder of 2 μm particle size with water. The final thickness of the samples varied 4 - 9 mm, depending on the dopant concentration and measured absorbance. The thickness was adjusted to get the ratio of signal (i.e. the absorbance of the doped ions) to background as high as possible, so that the absorption peaks of the examined dopant ions became as high as possible within the accurately measurable absorbance range, i.e. were as close as possible to absorbance 3. Sample thickness was limited to 7 mm for doped glasses and 9 mm for undoped glasses. The accurate measurement range of the transmission absorbance with Perkin Elmer Launch 900 UV-VIS-IR spectrophotometer was 0,03 – 3,5. Thus for some glasses, two or more samples with different thicknesses were prepared to get acceptable transmission absorbance data. The thinnest samples were 0,6 mm and thickest 10 mm.

The CeO_2-powder finish is a chemical corrosion process, enhanced by mechanically removing the reaction residues against the rotating wheel. It is known to increase the refractive index of the surface by sticking in the surface (Vogel, 1993). The quality of the polished surfaces was visually inspected. The sample thickness and evenness of the parallel surfaces was controlled to be within ± 0,02 mm with a digital calliper.

The same polished samples and surfaces were used for UV-Vis-IR, MidIR and reflection & scattering spectroscopy, as well as for refractive index measurements and photoluminescence spectroscopy. When necessary the surfaces were carefully cleaned with alcohol and drying under hot air.

2.4. Optical transmission spectroscopy

Two kinds of optical transmission spectroscopy measurements were performed on the glass samples, MidIR (on selected samples) and UV-Vis-Near IR (on all samples). The UV-Vis-Near IR transmission absorbance spectra of the prepared doped and undoped samples were measured over a 184 - 3200 nm range with a Perkin-Elmer Launch 900 spectrometer (Fig. 2.4.1) of the Department of Engineering Materials, The University of Sheffield. The measurement was performed with 2 nm scanning steps and with 0,8 – 1,12 nm slit windows at each wavelength. The equipment has two lamps that are switched at 319 nm and two monochromators and detectors that are switched at 860 nm.

The eventual drift of the absorbance response of the equipment was measured without a sample (Fig. 2.4.2) and is better than ± 0,001 during the first hour. However, somewhat higher drift of measured absorbance may have been included to the measured data during a two - three hours measurement series. The resolution of the measurement equipment was checked without moving the sample, to be better than ± 0,001. However, the received reproducibility of the measured absorbance spectra (a few months between the measurements) is of the order of ± 0,002 for the best quality flat samples (Fig. 2.4.3). In some cases a ± 0,1 step has been found at 860 nm in measured absorbance without sample (Fig. 2.4.4). The equipment was checked by the laboratory engineer, and the step was found to disappear when an extra black blanket was placed over the equipment. So there might be a tiny hole for sun light to leak into the equipment. All measurements are done without the extra blanket cover, so a ± 0,001 step at 860 might be included to several of the measured absorbance spectra.

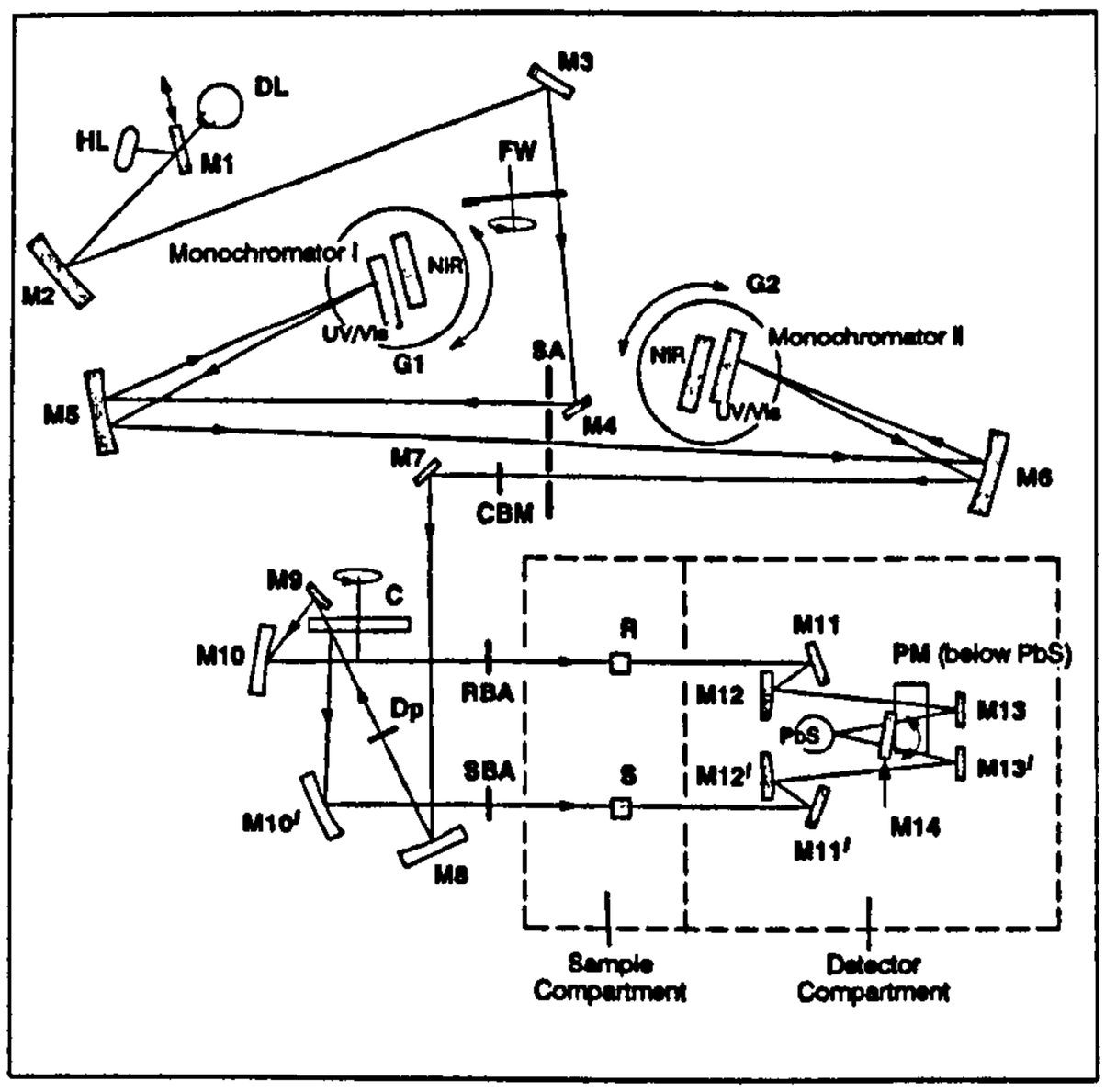

Fig. 2.4.1 Schematics of the optics, Perkin Elmer UV/Vis/NIR Lambda 900 Spectrometer

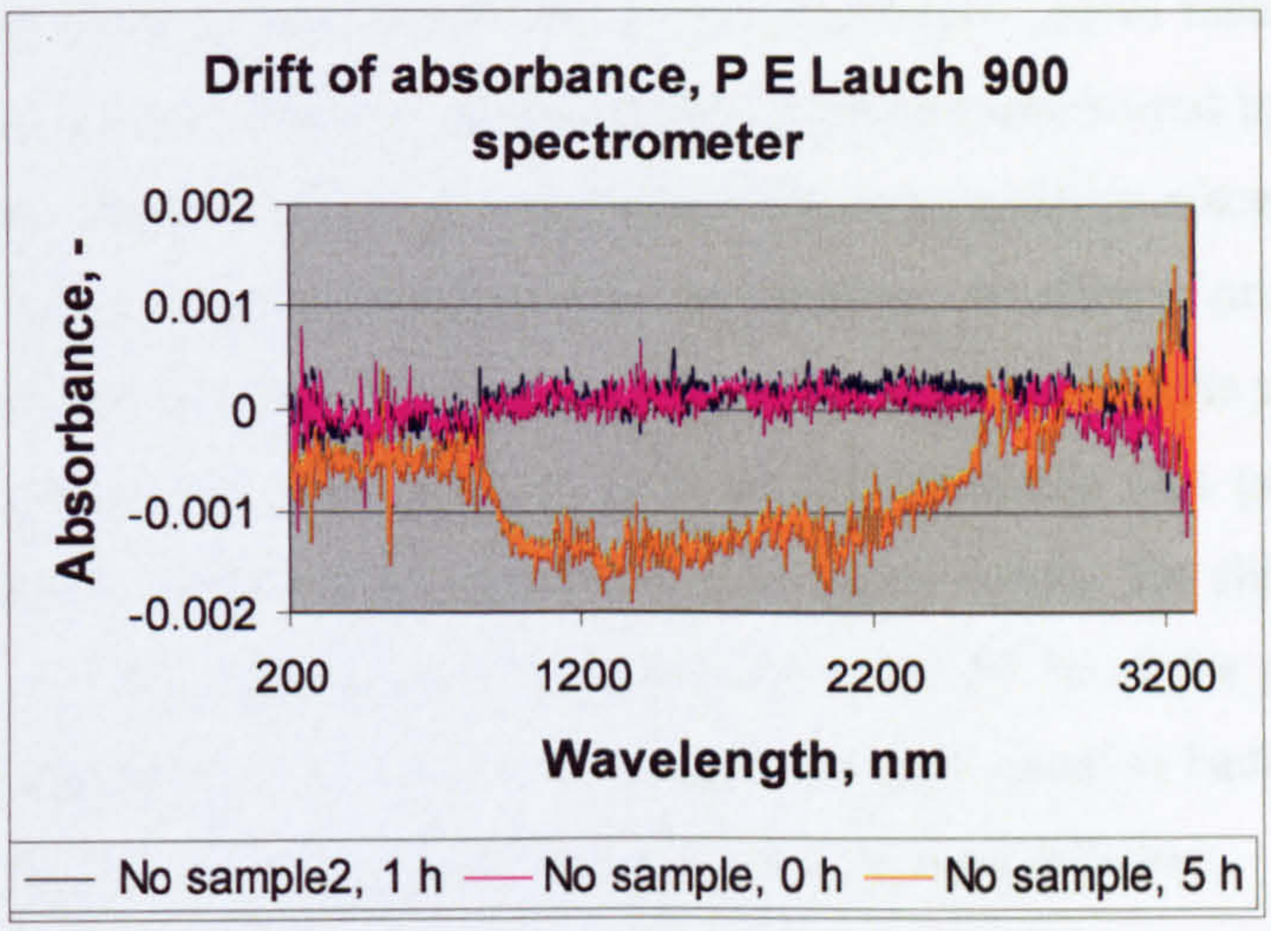

Fig. 2.4.2. The usual repeatability of the measured absorbance for Perkin Elmer Launch 900 UV-Vis-Near IR Spectrophotometer, measured without sample.

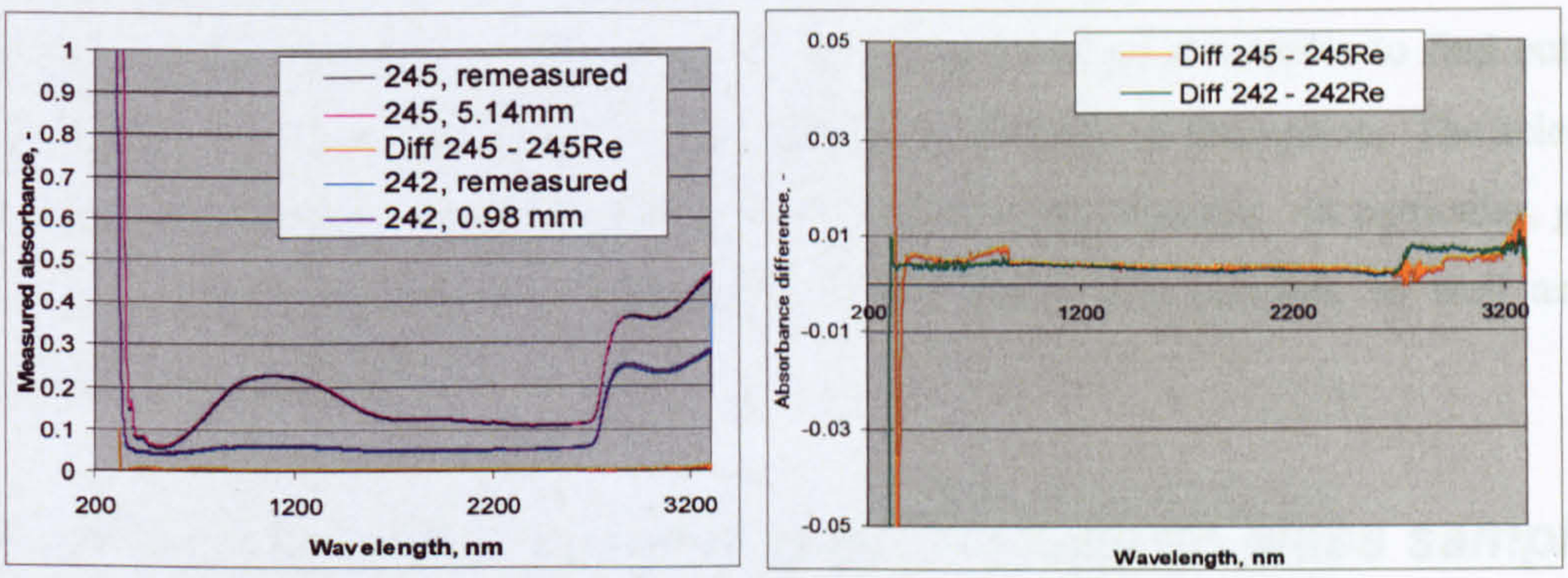

Fig. 2.4.3. The reproducibility of the measured absorbance spectra for two samples, re-measured a few months after the first measurement.

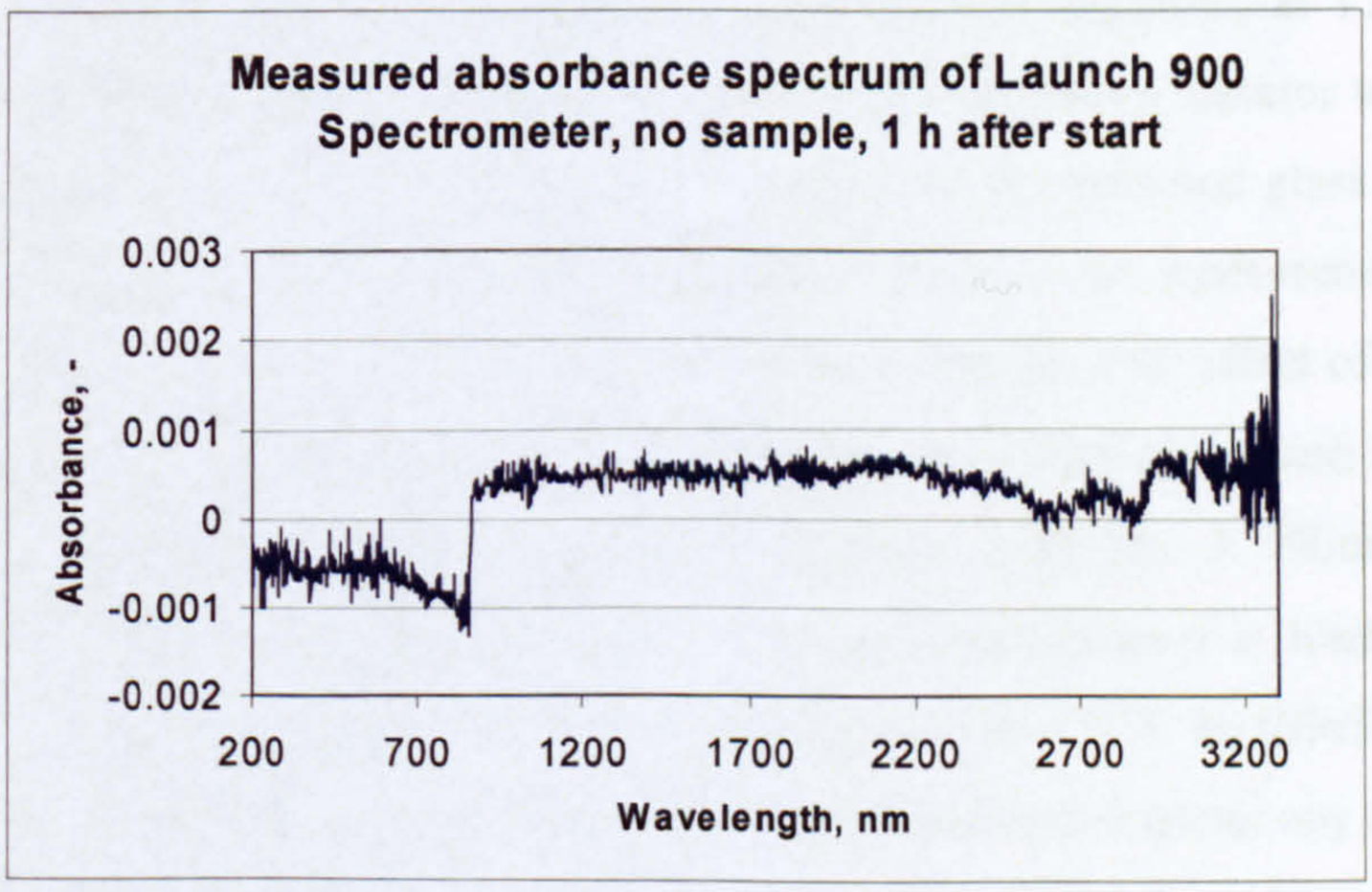

Fig. 2.4.4. Measured absorbance response of the equipment 1 h after the start and calibration.

In particular, a step could be seen at 860 nm in the absorbance curves measured without a sample (Fig. 2.4.2. and 2.3.4.). The two detectors and monochromators used by the equipment are switched at 860 nm. Steps at 860 nm are also caused by non-parallel surfaces of the samples and by the refractive index variation (cords) inside the samples. In order to minimise the steps to below 0,002 many of the samples were re-polished, and/or assembled in the sample holder so that the thickest corner or side was pointing down and the thinnest was pointing up, thus minimising the horizontal spread-out of the transmitted signal before the slit in front of the detector head. Two or more samples were prepared for about 50 % of the glasses, in order either to reach a thin enough sample to give an accurate and high signal to background ratio, or in order to eliminate the step in the spectrum caused by the changed detectors.

The Perkin Elmer 200 FTIR spectrometer in normal, non-interference mode was used for measuring transmission spectra in the Mid-IR, 370 – 7796 cm^{-1} range (27 μm – 1,280 μm). These measurements were done in transmission mode by using step size and slit window 1 cm^{-1}. The Mid-IR transmission spectra were measured for about 50 selected samples to find out the absorption peaks at wavelengths above 3.3 μm causing the IR-edge of absorption. The selected samples represented most of the examined glass compositions and dopants. In particular, good signal-to-noise ratios were measured for lightly doped and/or thin samples, as well as for samples made of pure chemicals.

2.5. Reflection and scattering spectroscopy on glass samples

In order to examine more deeply the quantity and significance of the reflection and scattering losses at UV and visible wavelength ranges, for about 30 selected samples also reflection, backscattering, transmission and forward-scattering spectra were measured at 170 – 850 nm with a Perkin Elmer Spectrometer 9, equipped with an integrating sphere detector with a one nm step size and slit window. These measurements were done on the polished glass samples that were also used for the main absorption measurements. There is no measurement spectrum window limiting slit between the sample and the detector, so the possible effect of fluorescence (photoluminescence) was not filtered out. These measurements were performed at InFotonics research centre of Joensuu University in Finland together with Dr. J. Hiltunen. These measurements were done in transmission mode. The spectrum top level at transmission was calibrated to 1,00 using the reflection spectra of the white standard, NPL certified sample. The level of zero signal was checked by measuring a "reflected" spectrum without any sample, using a black light hole. The transmittance background was found to be of the order of 0,002 in the worse case.

2.6. Diffuse reflection spectroscopy

In order to examine more deeply the absorption peaks at UV-wavelengths below 320 nm especially for Fe-doped samples, diffuse reflection spectra were measured on crushed glass powder samples at wavelength range 200 – 2500 nm by using a Perkin Elmer Launch 900 Spectrometer equipped with a Spectralon integrating sphere detector. The 28 samples measured were prepared from fragments cut by a diamond saw from the cast glasses and crushed in a standard way, using a metal cylinder shaped precision mortar under another hard metal cylinder that was hit repeatedly by a heavy hammer. The particle size was not controlled, but only the finer particles were used. The particles were stuck to a black electrician's tape manually and large particles were wiped off. The finer glass powder remained attached to the tape on its own. The signal area hit by light used was about 20 mm * 5 mm wide. The tape was directly attached on to the edges of the sample holder hole.

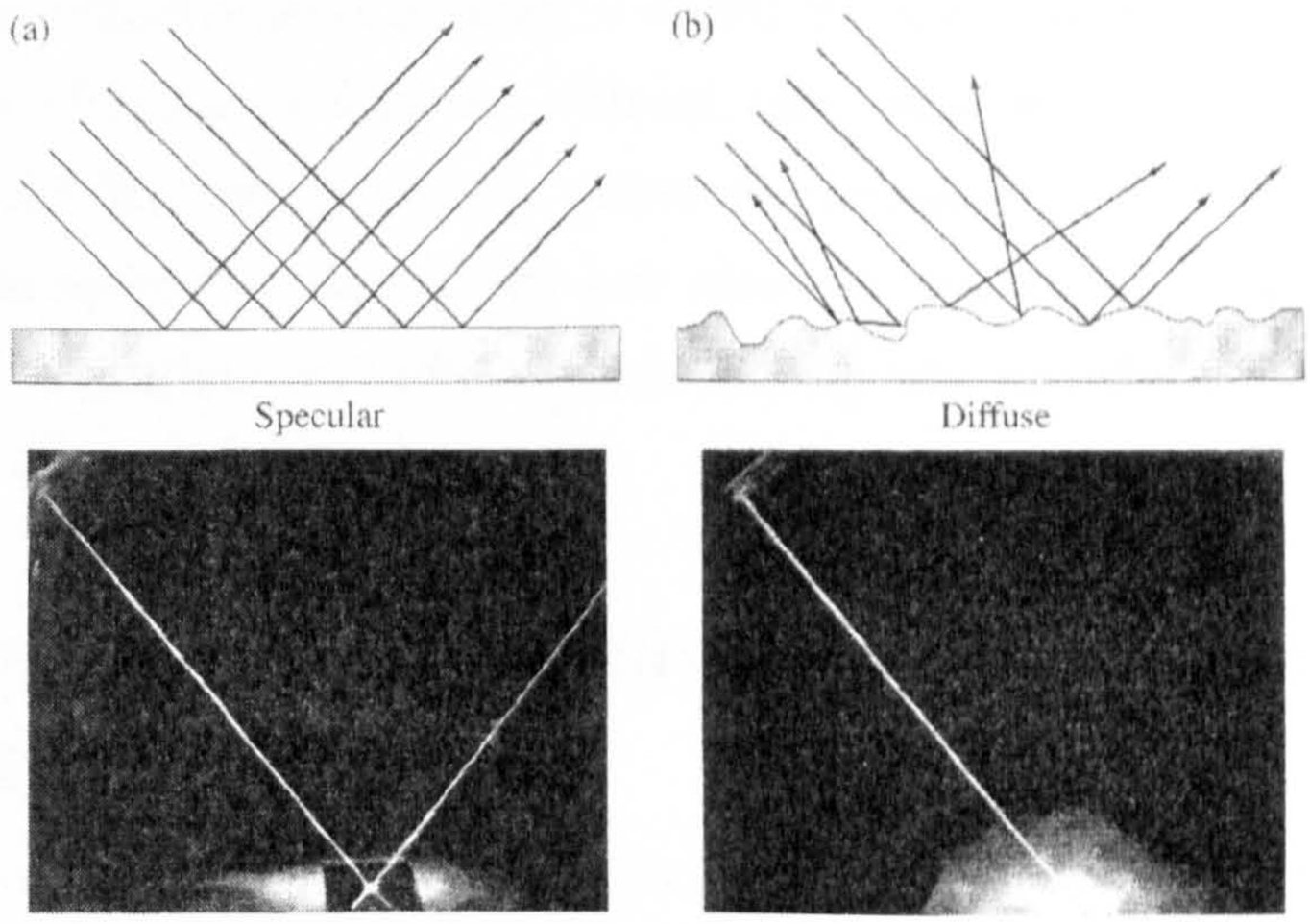

Fig. 2.6.1. a) Specular reflection of a glass sample and b) diffuse reflection of a powdered glass sample or a rough surface (Hecht, 2002, p. 99).

The measurement was done in transmission mode, i.e. the output reflectance was measured as a per cent of the white reference reflectance spectrum. The reference level of 100 % was calibrated using the spectrum of the specially made white Teflon powder sample stacked into a flat frame. It has a lower absorbance at short UV wavelengths than the standard, inorganic white powder sample. The zero-level was checked without any sample by using a black hole. It was on the level of 0,02 % over the measurement range. These measurements were performed at The Ångström Laboratory of The University of Uppsala. For the analysis of the results, see Chaps. 5.4.5 - 5.4.8.

2.7. Refractive index measurement with prism coupler method

The refractive indexes of about 50 samples were measured by using a Metricon Model 2010 Prism Coupler Thin Film Thickness/Refractive Index measurement system. The measurement of the bulk material refractive index of a flat surface is a standard feature of the equipment. The principle of operation resembles closely the operation of the Abbe refractometer. When a material with index n is brought into intimate contact with a prism with index n_p, laser light directed onto the base of the prism will be totally reflected at the prism base until the angle of incidence θ becomes less than the critical angle θ_c, where $\theta_c = \arcsin(n/n_p)$. θ_c is easily measured, since the detector intensity drops abruptly as θ drops below the critical angle and the light starts to leak into the bulk material. Since the n_p is known, n can be determined from the equation given above. For bulk materials thicker than 10 μm, as was the case in these measurements, the refractive index accuracy is ±0,001 and resolution ±0,0005. The equipment had three lasers at 632.8 nm, 1300 nm and 1550 nm, which all were used. The samples were the same ones used for the main absorption spectra measurements of this work. Prior to the measurements, the surfaces of the samples were carefully cleaned by wiping with a soft lens paper wetted with isopropanol and dried by gentle blowing with purified air. For analysis of the results see Chap. 4.2.

2.8. Photoluminescence spectroscopy and analysis methods of the results

Photoluminescence spectra were measured for about 50 soda-lime-silica samples to find out which one of the dopants would show significant photoluminescence at wavelength range 200 – 900 nm, i.e. wavelengths within and around the visible light range. This information was needed to judge whether stable narrow band absorbance filters could be made of silicate glasses doped with the examined TMs and REs. The Hitatchi F-4500 Fluorescence spectrophotometer with an intense Xenon lamp light source at The Department of Chemistry, Sheffield University was used. For many samples an emission spectrum was measured at selected excitation wavelengths, and conversely, keeping emission wavelength and window fixed and scanning the excitation wavelength. A 10 nm window was used for both excitation and emission in most cases. The incident signal and detection signal are separated by 90 ° angle. The polished glass samples (the same ones used for the main absorption measurements) were placed at about a 50 - 60° angle to the excitation beam, in order to prevent the specular reflection (Fig. 2.6.1) reaching

the detector and also to minimise the effect of Rayleigh scattering strongest within the specular reflection cone of ±8° around the principal reflection of the excitation beam.

These measurements were not thoroughly studied, because it was found that all examined TMs showed wide photoluminescence peaks within the visible range, when excited at 200 – 250 nm wavelengths or by wavelengths of the absorption peak tops. Thus one of the goals, to develop narrow band filters was found irrelevant. The results, can however be used for rough checking of most intensive photoluminescence peaks for the examined dopant ions in the examined glasses. See Chap. 3.6. Most of the results will be analysed and reported later.

2.9. Electron paramagnetic resonance spectroscopy

The method is briefly described in Annex 9 and in Chap. 6.5.2.

2.10. Other analysis methods used

In order to find out how much the received soda-lime-silica glass composition differs from the batch calculated compositions, as well as to know the level of the examined colorant ions present in the host glass materials as contaminants (in particular Fe), an X-ray fluorescence analysis of the composition of received glass was purchased for four samples. A Philips PW2440 wavelength dispersive sequential X-ray Spectrometer with UniQuant 4 analytical program was used. The method, calibration and applications are described by West, M (2001), who also prepared these measurements (Annex 3). The accuracy and resolution of the received concentrations are of the order of ± 1 % of the received value or 0,02 weight %, which ever is higher (West, 2001, p. 111 - 112). However, the resolution and accuracy do not take into account the multiple valences of species and the resolution is poorer for the light elements than for heavy and poorer for very low concentrations. Boron and lighter elements can not be detected reliably.

In order to check the glass transformation temperature for annealing purposes, standard DTA (differential temperature analysis) measurements were made on a few samples.

3. Development of fitting analysis method for optical absorbance spectroscopy

3.1 Introduction

The samples were prepared and the transmission absorbance spectra were measured as described in Chaps. 2.1 - 2.4. Measurement accuracies of the equipment and received spectra are also considered there. This chapter describes, how the measured spectra are corrected for background losses and the questions necessary to be addressed for this task.

The aim of this work is to develop accurate mathematical fitting of summed Gaussian peaks to the pure absorption spectra of the colouring ions studied. An equally accurate background loss correction is therefore needed, because a significant portion of the light is lost through several other phenomena at the surfaces and inside the glass sample, e.g. by reflection, scattering, refraction, absorption by host glass and its contaminants, etc.. Each type of loss depends in its own particular way on light wavelength and the sample, i.e. has an absorbance spectrum. Samples for this work were made from normal, non-pure, grade of raw materials, similar to commercial glass making. Examples of measured absorbance spectra for a doped and non-doped glasses are shown in Fig. 3.1.1.

A new accurate fitting of all the significant background loss components is developed to distinguish the pure ion absorption from the background. It is also used to interpret the changes in the mutual cross-redox between the dopant ions and contaminants (such as iron, copper, etc.) in their reduction/oxidation (redox) ratios, as well as to recognise and measure the relative amount and effect of bound OH-ions on the spectra that usually define the IR-edge of the spectrum.

The greatest challenge of this work was to find the right fitting parameters for the UV-edge caused by the UV- peaks of Fe^{3+} and Fe^{2+} ions. It was not known, how strong is the absorbance caused by the Fe^{2+} ions at the UV-edge (at wavenumbers above 15000 cm^{-1}), until finally the glasses codoped with Cu and Fe (containing only Fe^{3+} ions) were successfully fitted very recently (Chap. 6, May 2007), and the glasses codoped with Ce and Fe were tentatively fitted (February 2007, to be reported at ICG conference in July 2007 in Strasbourg). The earlier assumption was that the UV-edge was caused by Fe^{3+} ions and the background losses, i.e. reflection and scattering losses as well as some background loss of the host glass, as had been discussed by many previous researchers, e.g. Bingham, 2000 – 2002.

The contaminant iron spectrum, consisting of d-d transition and charge transfer spectra of Fe^{2+} and Fe^{3+} ions, can be seen as a part of the colorant ion spectra investigated, not as background. Due to the mutual cross-redox of iron with other colouring ions, the UV-edge height and position are dependent on the colorants studied.

The measured host glass absorbance is not zero, nor a constant with wavelength, or negligible (Fig. 3.1.1, Glass 97). The background loss is mainly caused by absorption losses of the contaminants iron and water (in some cases also copper), and by reflection losses at the sample surfaces. Significant absorption by the contaminant iron ions is found over the whole wavelength range (Fig. 3.1.1, and Chaps. 5 and 6). The tails of UV absorbance peaks of both Fe^{2+} and Fe^{3+} ions extend over the visible range. The wide and shallow absorption band at 700 - 2500 nm is caused by the Fe^{2+}-ions, and at wavelengths above 2600 nm the background is caused by OH-molecules bound to the host glass and a peak assigned to Fe^{2+} ions in this work (Chap. 3.6 and Chaps 5 – 6). In addition, there are reflection losses at both glass surfaces, which are partly dependent on the glass refractive index and its variation with wavelength (Chap. 3.5). Some elastic Rayleigh scattering may also occur in inhomogeneous samples from a rough surface and particles there, and from bubbles, cord and unmelted or precipitated particles inside the glass (Chap 4.1).

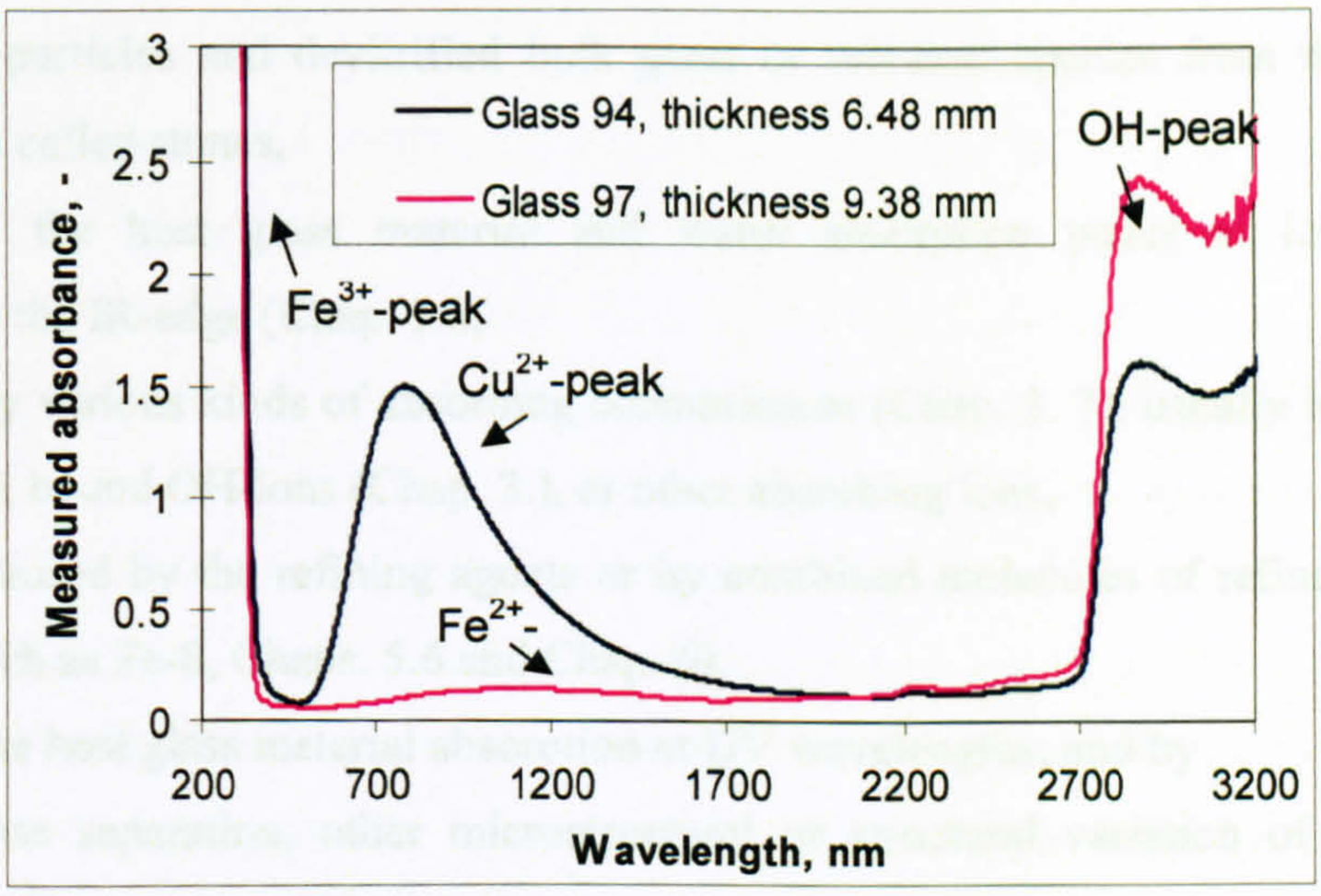

Fig. 3.1.1 Measured absorbance spectra for a Cu-doped (0,5 mol %) soda-lime-silica glass (Glass 94) and the similar undoped host glass (Glass 97). Both glasses were melted in a gas-fired furnace in mullite crucibles at 1450 °C for 5 hours, cast on a heated iron plate, and subsequently annealed at 540 °C for an hour and cooled to room temperature with 1 °C/min rate.

The transmission absorbance spectra for this work are measured over a wide UV-visible-infrared wavelength range from 185 nm to 3300 nm to capture as much data as possible concerning the ion spectra which in many cases extend from the UV well into the IR-range. The redox ratios of the ion valence states and their possible structural states

(octahedral/tetrahedral, etc.) can thus be reliably identified. The key questions addressed here are:

- How to prepare the samples and do the measurements so that the best possible signal-to-background ratio and also an adequate signal-to-noise ratio could be received?
- Which processes cause significant background loss in the studied glasses?
- How to distinguish and appropriately separate the significant background losses from the ion absorbance spectra?

3.2 Background loss causing phenomena

Significant background loss in a measured transmission absorbance spectrum of a glass sample may be caused by one or several of the following phenomena:

-reflection at the surfaces (Chap. 3.5),

-refraction and scattering from non-parallel, non-flat and/or uneven sample surfaces and/or from inhomogeneous glass due to chemical variability, frozen-in stresses; thermal or compositional refractive index variations called cords; bubbles and seeds (small bubbles); unmelted batch particles and devitrified bulk glass or released species from the furnace or melting crucible, called stones,

-the tails of the host glass material and water absorption peaks at longer infrared wavelengths, i.e. the IR-edge (Chap. 3.6,

-absorption by various kinds of absorbing contaminants (Chap. 3. 7): usually iron (Chap. 5), copper (Chap. 6), bound OH-ions (Chap. 3.), or other absorbing ions,

-absorption caused by the refining agents or by combined molecules of refiner species and colorant ions (such as Fe-S, Chaps. 5.6 and Chap. 6),

-the tails of the host glass material absorption at UV wavelengths, and by

-possible phase separation, other microstructural or structural variation of the glass, or attenuation caused by any crystalline particles or reduced, precipitated metal particles, which are not examined in this thesis.

Each of these attenuation processes varies, in its own characteristic way, with the wavelength of the light, i.e. with the frequency of the light ($\propto$ energy, related to wavenumber = 1/wavelength). On a logarithmic absorbance scale, the absorbance spectrum of a silicate glass sample of unit thickness measured by a spectrophotometer (spectrometer) is the sum of the attenuation spectra of all these phenomena (Bamford, 1978, p. 12 - 15 and Bach et al, 1995, p. 82 - 94). If transmission units are used, they multiply. However, those losses that occur at the surfaces (reflection and surface scattering) do not "scale" with thickness, i.e. need to be subtracted first. At wavelengths where the glass is transparent (i.e. total absorbance below 1),

multiple reflections may need to be taken into account for the reflection loss correction (Bamford, 1977, p. 12). The multiple reflections are neglected in this work, because thick (of the order of 1 cm) samples are used for most transparent glasses (e.g. Glass 196).

To determine just the colour of a piece of glass, background loss correction is not necessary. The colour and the known CIE- or CIELAB colour coordinates (Chap. 1.4.2) are determined on a transmittance spectrum T(λ) (where λ is wavelength) measured at normal incidence within the visible wavelength range 400 – 700 nm. If the colour codes are needed for a unit thickness of a glass the transmittance curve should be corrected for the surface (reflection) losses, or the transmission should be measured in an index matching oil arrangement to minimise the surface losses.

3.3 Correction methods used earlier

There is no accurate standard method available in the literature for background correction. In many scientific reports background loss is neglected by using high dopant concentrations, ultra pure host glasses and/or very thin test samples. In practise, the reflection losses can be neglected over a narrow wavelength range, such as the visible range, by using a two beam spectrometer and immersing the sample into refractive index matching oil in a cuvette holder. The influence of the background losses at surfaces could thus be minimised. However, a reflection at the cuvette edges occur anyway. To keep the liquid absolutely clean and to adjust the refractive indexes of all three species (the sample, cuvette and the liquid) to be optimal over the wide wavelength range on this study with various dopants and host glasses with differing refractive indexes would have been messy, and impossible in practise.

Neither absorption spectra of colorant ions, nor background losses usually scale accurately over powers of concentration range, or add up linearly, due to various reasons discussed in the later chapters of this thesis. Sample preparation, i.e. weighing the batch, melting, casting, annealing and sample cutting and surface polishing are all critical for the final accuracy, signal-to-background and signal-to-noise ratios achieved.

Also the understanding about what is causing, or included in a background loss, varies in the literature (Bamford, Weyl, Paul, Cable, Duran, Wong & Angel, Bingham etc.). Either a limited wavelength range, such as 400 – 700 nm is used, or the UV-edge is considered as an Urbach tail of the host material absorption peaks (Si-O, or Na-O bonds), or the effect of OH-contamination and IR-edge are neglected. In many earlier papers the UV-edge has been manually extrapolated from a plotted curve (Weyl, Bamford, Duran etc.), or fitted to an exponential function to subtract the UV-edge at high wavenumbers (Bingham et al 2000), assuming the edge would not be affected by colour dopants or the glass making process. Cable et al (1989 – 1992), and many

others, have used ultra pure ingredients to make their scientific test samples and carefully manufactured and homogenized their test glasses to avoid the many types of background losses and extrapolated the remaining background (including reflection losses at surfaces) to zero thickness from absorbance values plotted as a function of thickness at each wavelength.

Bingham (2000, p. 29), who studied the absorbance of Fe-ions in various silicate glasses subtracted a spectrum of a undoped host glass at all wavelengths to correct for the reflection losses and used a simple exponential function of Urbach-tail type for the UV-edge between at 27000 – 30000 cm^{-1}, $A_{UV}(\nu) = b_0 * EXP (b_1 * \nu)$, where A is absorbance per unit thickness, b_0 and b_1 were the fitted constants and ν is the variable wavenumber in cm^{-1}-units (Bingham, 2000, p.86). He assumed (p. 42) that the edge is created by charge transfer peaks of Fe^{3+} and Fe^{2+}-ions at wavenumbers 43500 and 50000 cm^{-1} respectively, but did not analyse it further. Paul (1990), Jong and Angel (1976) do not reveal their methods and Weyl (1951, reprinted 1999) and Bamford (1977) did not correct for background other than reflection losses (by subtracting a constant value, 0,04 or 0,036, from the measured absorbance at all wavelengths. In particular, I have not yet found any report in the literature, where the background of IR-edge and OH-peaks had been separated from the absorption spectra (See Chap. 3.6).

Another, simple background correction method, i.e. subtraction of reflection loss and normalised absorption spectrum of the non-doped host class, are used in those cases where small changes in the IR- and UV-edge and the effect of contamination Fe on the colourant ion balance can be neglected. However, the undoped sample may differ in Fe^{2+} and Fe^{3+}-concentrations from the coloured sample due to differing dissolved amount of contamination from crucible or a mutual redox between the colorant ions and contamination Fe. In some case even molecule colorant species are formed (such as Fe-S, Fe-Se, etc.).

When Fe-contamination is significant, as it is in the most samples of this work and normally in glass industry, its spectrum must be fitted and its redox taken into account as the Fe would be a colorant. The mutual redox with the other colorants and the contamination Fe ions of concentrations as low as 0,01 weight % have been seen to matter in this work (Chaps 5 and 6).

3.4 Effect of photoluminescence

Fluorescence, i.e. photo-luminescence, may make a significant input to the received, detected optical power spectrum during an absorbance measurement, if the measurement equipment has an un-filtered broadband light source, such as a Xenon-lamp and/or the monochromators are located after the sample. In this work such a spectrometer was only used to measure the photo-luminescence spectra of the ions (Chap. 2.8). The absorption measurements and reflection loss measurements were performed with spectrometers that have broadband

lamps and filters. There was no monochromator after the sample, and the width of the detected wavelength window was so small (0,8 – 1,2 nm) that effect of photoluminescence that mainly emits light at wavelengths longer than the wavelength used for exciting, can be neglected at all other wavelengths except very short ones below 220 nm.

Most of the transition metal- and rare earth ions studied have significant, strong fluorescence bands at UV-, visible- and near infrared wavelengths when illuminated by an UV-light source or at an absorbing wavelength. Such a fluorescence peak occurs typically at a slightly longer wavelength than the excitation and significantly modifies the colour, the appearance of such glasses. Commercial tableware items containing praseodymium and neodymium are available. Strong fluorescence of these ions occurs at certain wavelength bands of visible range. Thus the most accurate spectrophotometers (as used in this work) have monochromators before the sample, and the wavelength scale is scanned from the lowest energy (longest wavelength) to the highest energy (shortest wavelength).

3.5 Reflection loss correction and normalising to 10 mm thickness

3.5.1. Introduction

One significant background loss process in transmission absorbance measurement is reflection at glass surfaces. The difficulty for this work is to know sufficiently accurately, i.e. with the order of the resolution of the absorbance measurements (with a ± 0,0005 accuracy) the level and wavelength dependency of the surface losses over the wide, 185 – 3300 nm wavelength range. Accurate knowledge of the reflection loss curve is needed to distinguish it from other surface-related losses and from the absorption losses that scale with sample thickness, especially for glasses with low absorption or low concentration of dopants (faint colours) and for very thin samples (i.e. below 2 mm thickness), where the reflection losses can be of similar size or greater than the measured ion absorbance for a sample. The usual assumption that the reflection losses are constant in the visible range, e.g. 0,036 absorption (Bamford, 1977, p. 35), can not be used, because the reflection losses at short wavelengths and UV-edge would be strongly underestimated and slightly overestimated above the visible range. The refractive index and thus the reflection loss level also varies with glass composition within the silicate glasses studied in this work.

Surface scattering losses, however, were minimised by polishing the surfaces to a shining optical quality that was checked by visual inspection (Chap. 2.3). The level of these losses is estimated from the same absorbance raw-data, measured as a function of sample thickness that was used to estimate the reflection losses.

The following approach of five steps is used to estimate the average reflection loss curve over the 200 – 3300 nm wavelength range for the doped and undoped soda-lime-silica glasses:

1. The refractive indexes at three wavelengths (632,8 nm, 1300 nm and 1550 nm, Annex 2) for various doped and undoped samples were measured to estimate the effect of glass composition and dopants on the refractive index.
2. The literature data was searched for the refractive index variation over the wavelength range in similar glasses.
3. Reflectance with a spectrometer equipped with an integrating sphere detector for various undoped and doped glasses was measured to estimate the reflection loss magnitude especially at the UV-end of the consideration range, where the absorption of the samples is high due to the charge transfer peaks of iron and other dopant ions.

4. The average reflection loss curve over the range 300 – 3300 nm was calculated for 15soda-15calcia-70 silica glasses (NCS) glasses from the refractive index and reflection loss information obtained over the wavelength range.
5. In order to double-check that the other surface losses would be negligible, the total amount of surface related losses over the wavelength range was also estimated with a second method on the similar samples as was used for the absorbance measurements. It was extrapolated from the absorbance curves measured for a set of samples with various thicknesses, all prepared from the same glass piece melted in one pot. The extrapolated surface absorbances at zero thickness were recorded with ten nanometre steps over the wavelength range.

In addition to finding the background loss correction curve over the wide consideration range of wavenumbers, these supporting measurements gave other valuable information, such as whether reflectance measurements at normal incidence angle on glass samples could be used to determine the colour coordinates of glasses. The effects that the dopants and glass composition has on the refractive index of the glasses are also revealed.

3.5.2. Reflection loss

Incidentally, UV-Visible-IR light does not reflect elastically from a flat glass surface in air, because the reflecting signal partly penetrates into the isotropic glass material to about a depth $0{,}1\lambda - \lambda$ (λ = wavelength) depending on the glass absorption coefficient (Klein and Furtak, 1986, p. 71 and 93 – 95, and Hecht, 2002, p. 96) and reflects from the material atoms, ions, dipoles, molecules and microstructure. Therefore, the reflected and scattered signals also bear information of the absorbance spectrum of the glass, as is obtained in Chap 4.1 and shown with diffuse reflection results (Chap. 5.4.5). The reflection loss of silicate glasses decreases with increasing wavelength in the studied wavelength range.

In general, at a wavelength far away from the resonance wavelengths of electron charge transfer peaks in UV and molecule vibrations in IR, the reflectance $R(\lambda)$ and transmittance $T(\lambda)$ at an interface between a non-absorbing glass and a material with differing refractive index are dependent on the spatial incidence angle and the polarisation of the light according to the well-known Fresnel's theory (Hecht, 2002, p. 113 - 131). At normal incidence the dependence on the polarisation direction disappears (Hecht, p. 121). The reflectance $R(\lambda) = (I_i(\lambda)-I_t(\lambda))/I_i(\lambda)$ can be calculated as $R(\lambda) = [(n_t(\lambda)-n_i(\lambda))/(n_t(\lambda)+n_i(\lambda))]^2$ and the transmittance $T(\lambda) = I_t(\lambda)/I_i(\lambda)$ can be calculated as $T(\lambda) = 4n_t(\lambda)n_i(\lambda)/(n_t(\lambda)+n(\lambda)_i)^2$ for a non-absorbing glass sample. Conversely, the refractive index n (at a wavelength) can be calculated from the reflectance as $n(\lambda) = (\sqrt{R(\lambda)} +$

1)/(1-√R(λ)). Both T(λ) and R(λ) are similar at both surfaces in relation to the respective normal incident optical power to the surface, from air to the glass and from glass to the air.

The reflection loss of two surfaces at normal incidence is thus

$$A_{ref}(\lambda) = -2 * \log_{10}(1 - R(\lambda)),$$

where R(λ) is the reflectance at an air-glass surface at normal angle. The refractive index of air is about $n_1 \approx 1$, a constant within the visible range. The refractive index of soda-lime-silica glass at yellow 589 nm wavelength can be roughly approximated to be constant ($n_2 \approx 1{,}51$), which implies reflection losses $A_{ref}(\lambda) \approx 0{,}04$. Reflectance varies strongly with incidence angle (not addressed in this work) and slightly with wavelength over the 185 – 3300 nm wavelength range.

At such wavelengths, where the sample is transparent or semitransparent, i.e. internal absorption is low, the light beam reflected from the entrance surface travels and reflects several times between the interfaces. For such a case the reflection factor P can be estimated to be P(λ) $\approx (1\text{-}R(\lambda))^2/(1\text{-}R(\lambda)^2) = 2n(\lambda)/(n(\lambda)^2 + 1)$ (Bach et al, 1995, p. 83).

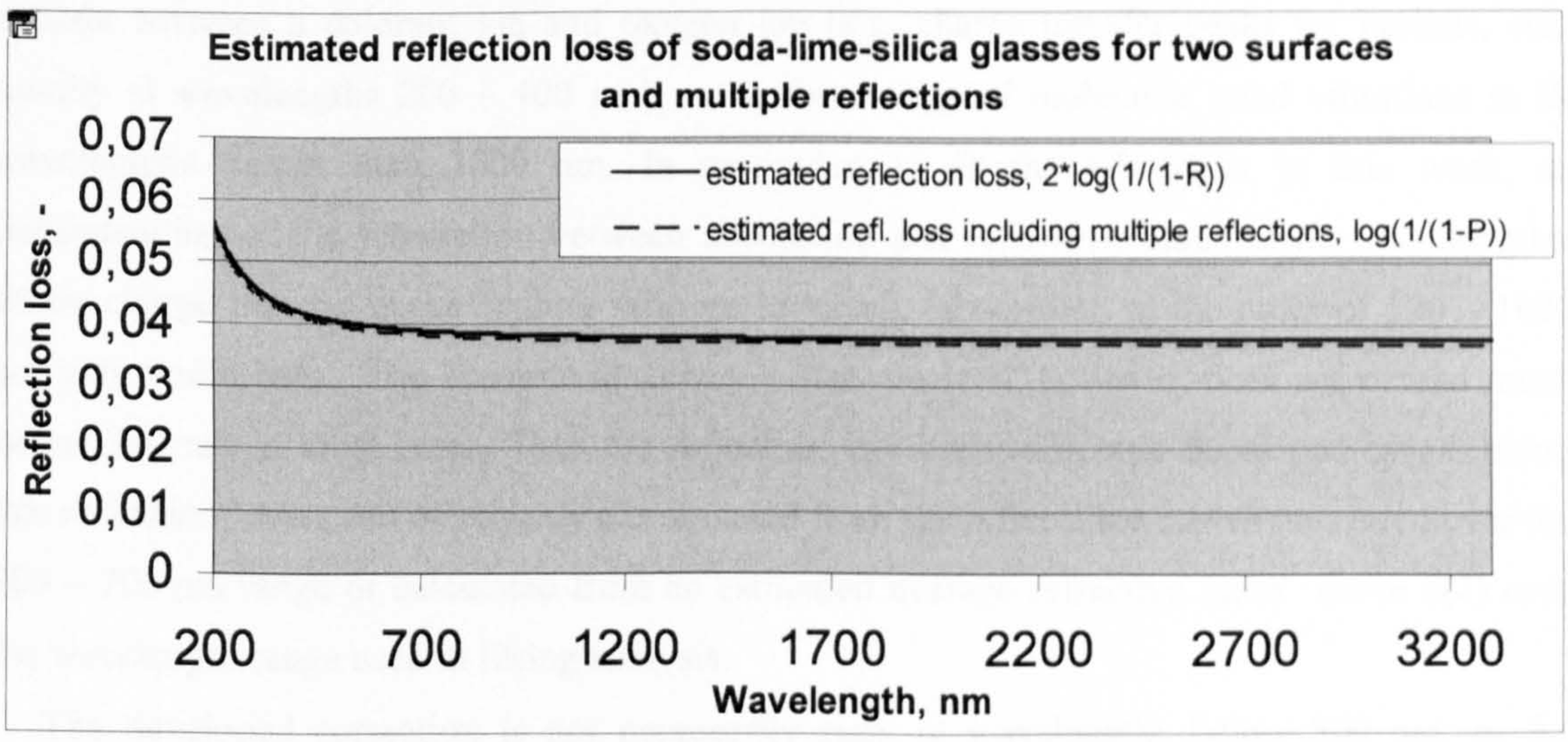

Fig. 3.5.1. Calculated reflection loss of normal two surface case (the blue line) and including the effect of a thin, transparent sample with multiple reflections (the pink - - - line). The difference is small, of the order of 0,0009. The estimated reflection loss is calculated from the fitted refractive index curve, presented in Fig. 3.5.2., p. 43. The curves are for NCS glasses.

The estimated average reflection loss curve (Fig. 3.5.1) is subtracted from the measured absorbance values at each wavelength for the studied glasses, before a measured absorbance is

normalised to 10 mm thickness for a further analysis. For samples with differing refractive index, a possibility to change the "height" of this curve is included in the analysis software.

3.5.3. Estimation of the refractive index and reflection loss curves

The level of refractive index depends on the glass host composition (e.g. density, polarizability etc.), structure (thermal history, i.e. fictive temperature and residual stresses) and the dopants (ionic radius, molar weight etc.) according to Scholze (1991, p. 214-219) and Bach et al (1995, p. 19 - 104). For accurate reflection loss calculation at a wide, 185 – 3300 nm wavelength range used in this work, the effects of composition and dopants on refractive index and its variation with wavelength are necessary to be taken into account.

Wavelength dependency of reflectance and reflection loss originates from the wavelength dependency of the refractive index of the glass n(λ). Both refractive index n and absorption coefficient k (natural logarithm) are both particularly strongly dependent on wavelength at those wavenumbers (= 1/wavelength), at which the energy of the light equals the energy of an electron transfer from a valence band to conduction band in the glass host material ions (Si, Na etc.) at short ultraviolet wavelengths (below 200 nm), or to the energy needed for an electron transfer between a colorant ion and oxygen ion (e.g. charge transfer peaks for Fe-ions, etc., usually at wavelengths 200 – 400 nm), or to the energy of molecular band vibrations at IR wavelengths longer than 3000 nm. In particular, to fit the UV-edges in this work, an understanding of the interaction between absorption and refractive index at the wavelengths, where charge transfer peaks or their tails are involved, (absorption of the order of 100 – 1000 per cm) would help. The accurate absorbance data received, however, does not extend much below 300 nm in most cases. Thus the reflection loss correction was developed by assuming that reflection losses can be roughly extrapolated from the reflectance curves measured over the 300 – 700 nm range or calculated from an estimated average refractive index curve n(λ) over the wavelength range used in fitting analysis.

The developed correction is not necessarily right at wavelengths below 300 nm, or for glasses with very intense charge transfer peaks extending to longer wavelengths. To develop an individual reflection loss correction for every single glass piece is beyond resources available, and would not necessarily improve the results, because there are also other uncertainties involved, due to the sample preparation etc., which is of the order of 0,01 absorption and may be more or less wavelength dependent (Chaps. 2, 4.2, 5 and 6).

The refractive index of the air can be assumed to be constant (= 1,000) over the wavelength range 186 – 3300 nm used in this work and not to vary significantly with temperature or

humidity (Handbook of Chemistry and Physics, 1987, p. E-373) at normal room conditions. All absorbance and refractive index measurements were performed under ambient room conditions, i.e. at a temperature 23 ± 5 °C, relative humidity 40 – 95 %.

The temperature dependence of the refractive index of the studied glasses at temperatures around room temperature is assumed to be negligible, i.e. of the order of pure silica glass, i.e. 9 – 11 * 10^{-6} $°C^{-1}$ (Scholze, 1991, p. 228 and Izawa etal,1987, p.45). For ordinary silicate glasses the refractive index change with temperature at ambient room temperature is less than for pure silica glass, i.e. within the range 1 – 10 * 10^{-6}/°C (Bach et al, 1995, p. 108-109; Scholze, 1991, p. 229). Thus the possible variation of reflection loss due to temperature variation of refractive index at ambient room temperature is assumed to be negligible for this work.

The refractive index variation with wavelength for the examined silicate glasses is assumed to be of similar shape to that of pure silica glass (Fig. 3.5.2), and the added alkali and alkaline earth and metal oxides of the examined compositions will raise the curve from the level of pure silica glass. This assumption is used because it was not possible to directly measure the reflection loss or the refractive index over a wide wavelength range in this work.

Refractive indices (Chap. 4.3, Annex 2) were measured at three wavelengths (at 632.8 nm, 1300 nm and 1550 nm) for various samples in order to estimate the effect and wavelength dependence of the refractive index on the reflection loss in the studied silicate glasses doped with various transition metal- and rare earth oxides. The measured refractive index values (Annex 2, and Fig. 3.5.1) on the samples of this work are probably slightly higher than the bulk refractive index of the glasses, because CeO_2 powder is used at the final stage of the surface polishing. It is known to raise the surface index slightly. However, the refractive indexes are measured for the same surfaces as the absorbance measurements, therefore they are assumed to be relevant for the reflection loss correction for the absorbance curves of this work. A reference pure silica sample, originally calibrated by NPL, were used to check the calibration of the refractive index measurement equipment (Annex 2, and Fig. 3.5.1). Its surfaces had probably been polished with diamond paste or another method that does not increase the surface refractive index.

The known Cauchy formula (Bach et al, 1995, p. 24) with three terms was fitted to the pure silica data and the values were then modified to match the average refractive values measured for the examined soda-lime-silica glasses (NCS–glasses). According to the equation, the refractive index n at wavelengths far from the resonance peaks is $n = a+b/\lambda^2 + c/\lambda^4$. The parameters a = 1,517, b = 6200 and c = -1000000 and wavelength λ as nm, were fitted to the pure silica data. They give a shape to the refractive index curve reminiscent of the refractive data of pure silica glass found from the literature up to 1600 nm (Fig. 3.5.2), and at a level that

matches to the measured average refractive indices of the soda-lime –silica glasses (Fig. 3.5.3, and Chap. 4.3 and Annex 2).

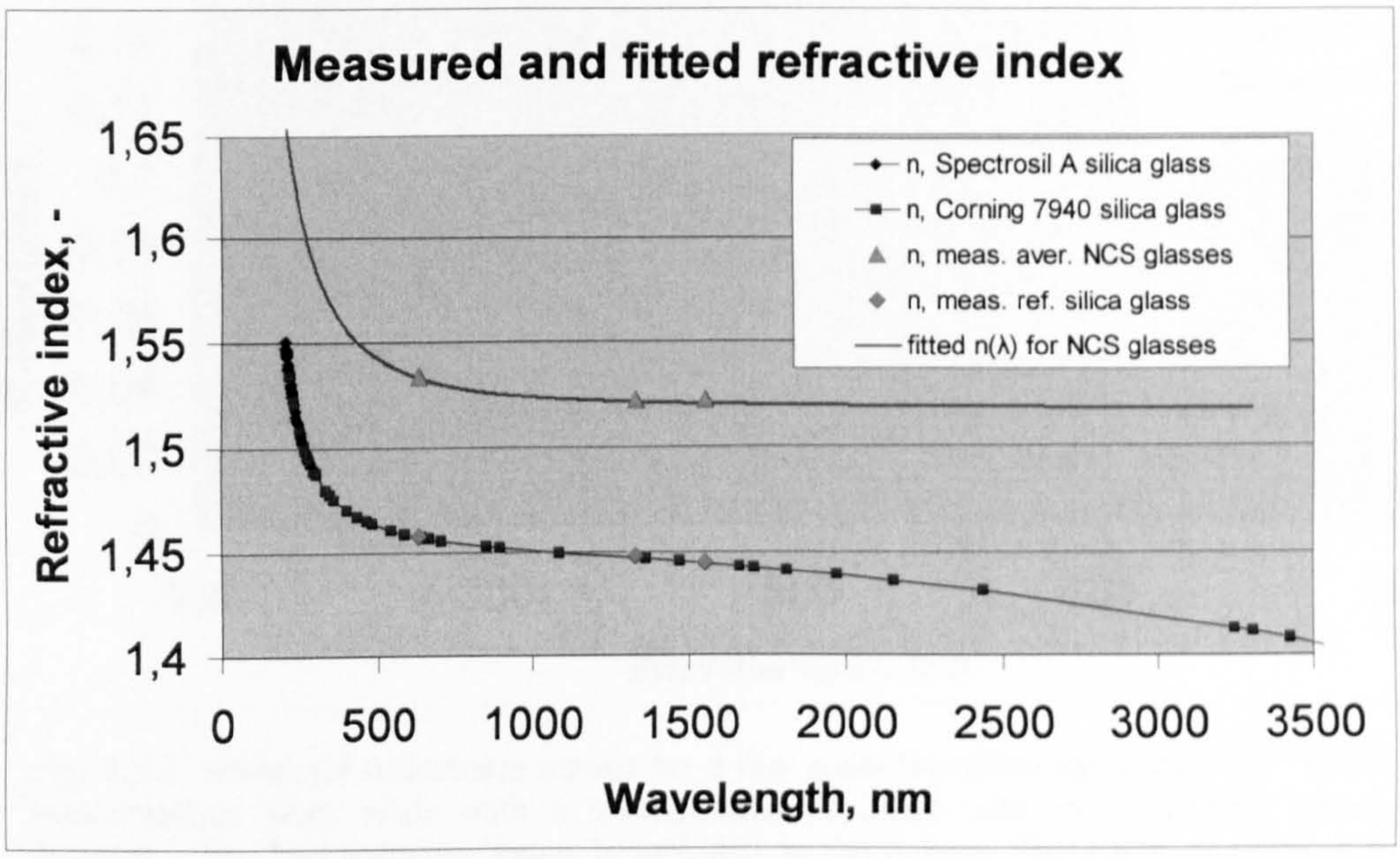

Fig. 3.5.2 Refractive index of two pure silica glasses from literature (Turpin 1965 and Corning 1969), as well as the measured ref. indexes of the reference silica glass and the soda-lime-silica glasses (NCS-glasses) of this work in average. Fitted refractive index vs wavelength (Cauchy equation) used in this work for estimation of reflection losses.

The used variation of Cauchy equation holds from UV-edge to near IR-range and gives an accuracy of the order of 10^{-4} within the visible range (Bach et al, 1995, p. 24). The measured reflectance curve (method Chap. 2.5) for a Cr-Mn doped highly absorbing Glass 216 (the composition is given in Annex 1) was used to calculate the refractive index at wavelengths 250 – 600 nm (Figs. 3.5.3.3, and 4) and that was used as a guidance for the shape of curvature at short wavelengths. The calculated fitted refractive index agree within a ± 0,01 range with the values given at 540 nm for soda-lime-silica glasses (Bach et al, 1995, p. 39 – 40, Musikant, 1985, p. 20). The NCS glasses studied in this report have slightly higher concentration of CaO (15 mol %, high density) and slightly less Na_2O (14 mol %, lower density) than the typical 18soda-12lime-glasses for which the literature numbers are given, and thus a slightly higher refractive index is measured. About 1 mol % of soda is lost at melting according to Annex 3.

The transmitted, backwards reflected, forward-scattered and backward-scattered spectrum were measured for several samples of this work at a large spatial angle distribution at the detection by using a spectrometer equipped with an integrating sphere-detector (Chaps. 2.5 and 4.1). These reflectance results are used here as a guidance to quantify the level of the reflection losses over a wide wavelength scale (Figs 3.5.3 and 3.5.4).

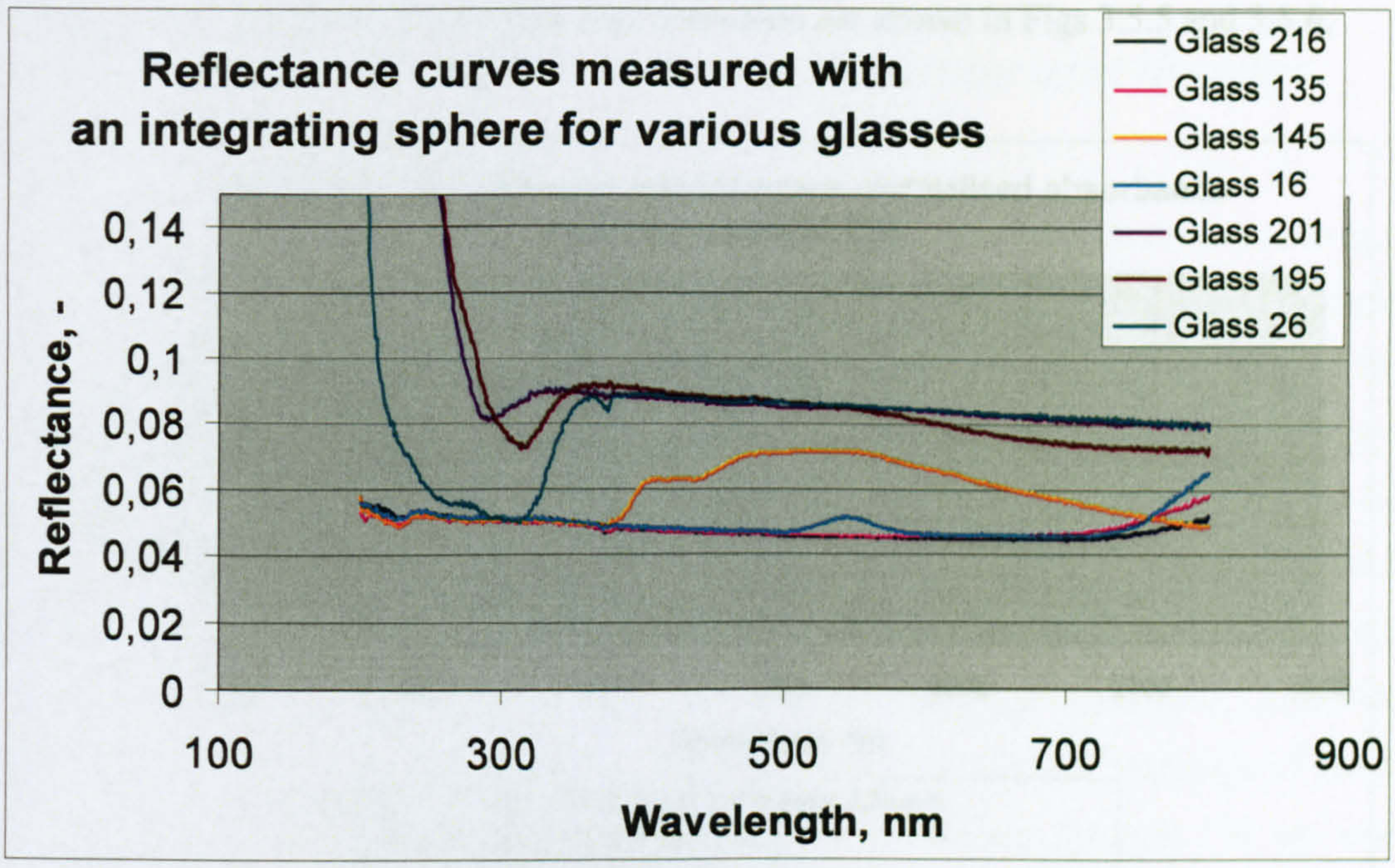

Fig. 3.5.3 Measured reflectance curves for a few soda-lime-silica glass samples. These measurements were made with a spectrometer equipped with an integrating sphere detector. The backscattered signal is included in the curves. The curve of Glass 216 represents mainly the reflection from one surface because the absorbance of this glass is ultra high, >>5, and the curves of Glass 201 and 26 samples at wavelengths 350 - 700 represent reflectance from two surfaces. Their total absorbances in this window is low, below 0,01.

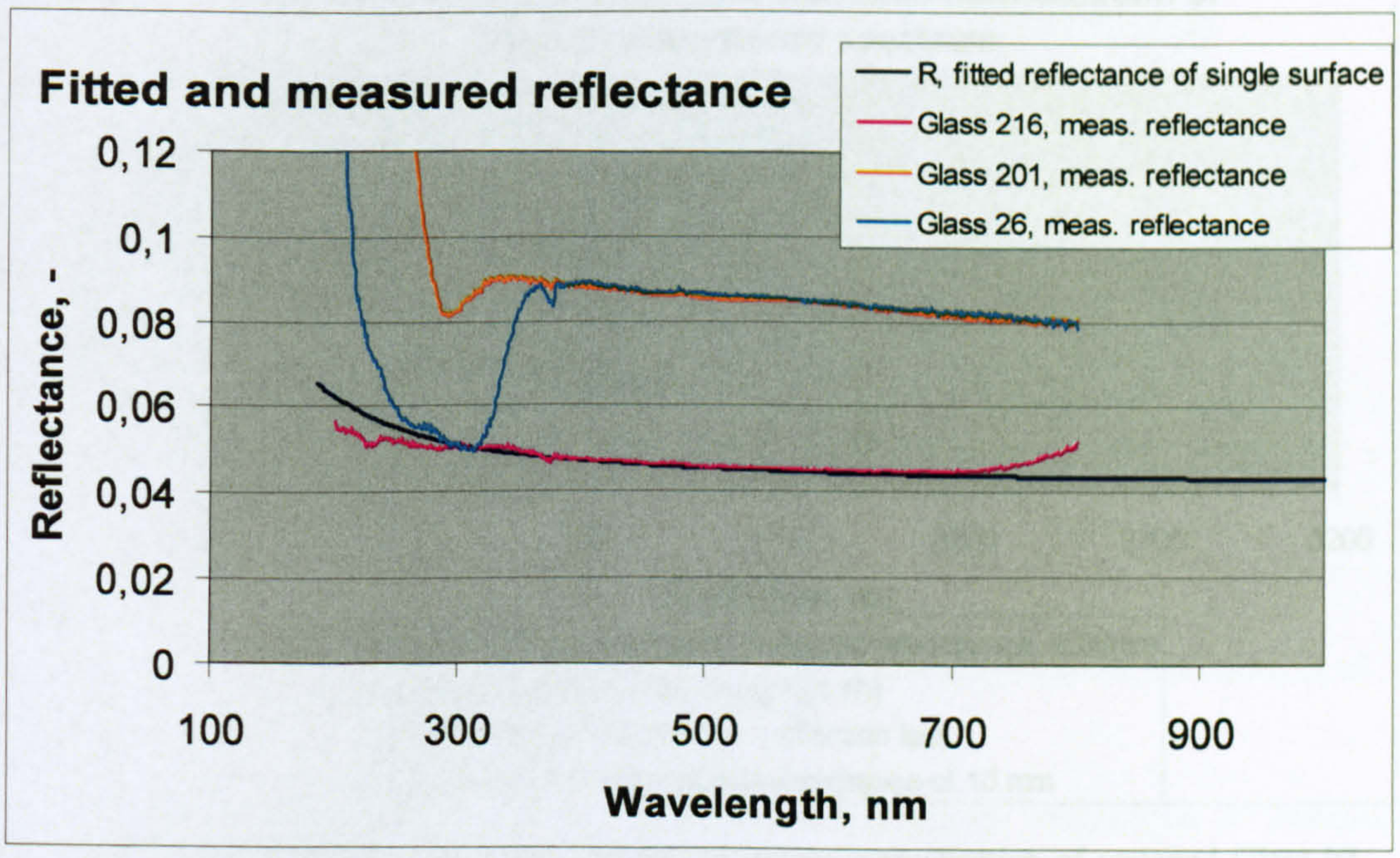

Fig. 3.5.4 Fitted and measured reflectance (R) for soda-lime silica glasses. The measured reflectance of Glass 216 agrees with the calculated reflectance curve above 300 nm.

Finally, two examples of reflection loss correction are shown in Figs 3.5.5 and 3.5.6.

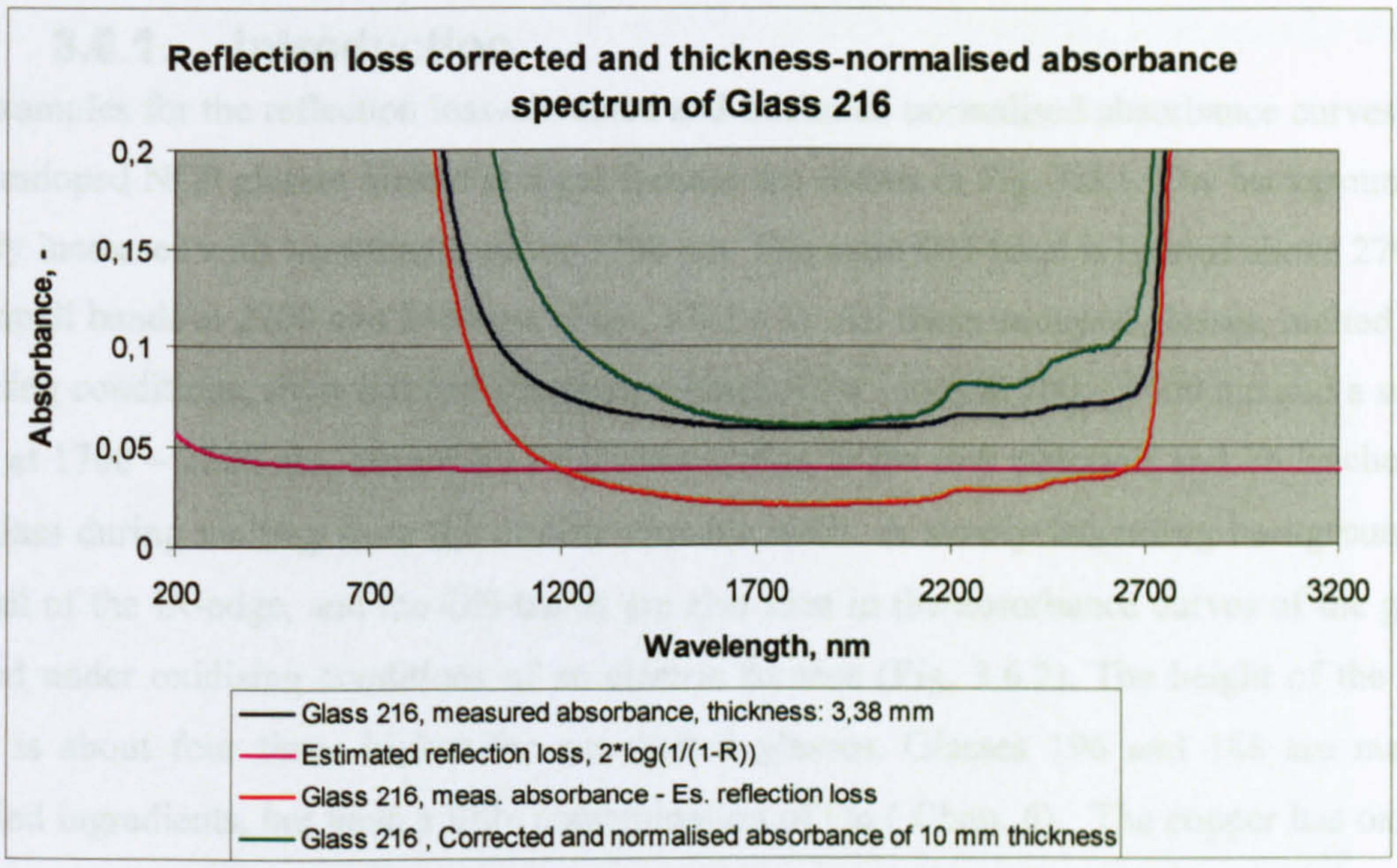

Fig. 3.5.5 Reflection loss correction and thickness normalisation of Glass 216. The glass was melted in an electric furnace in a platinum crucible at 1450 °C for 5 hours.

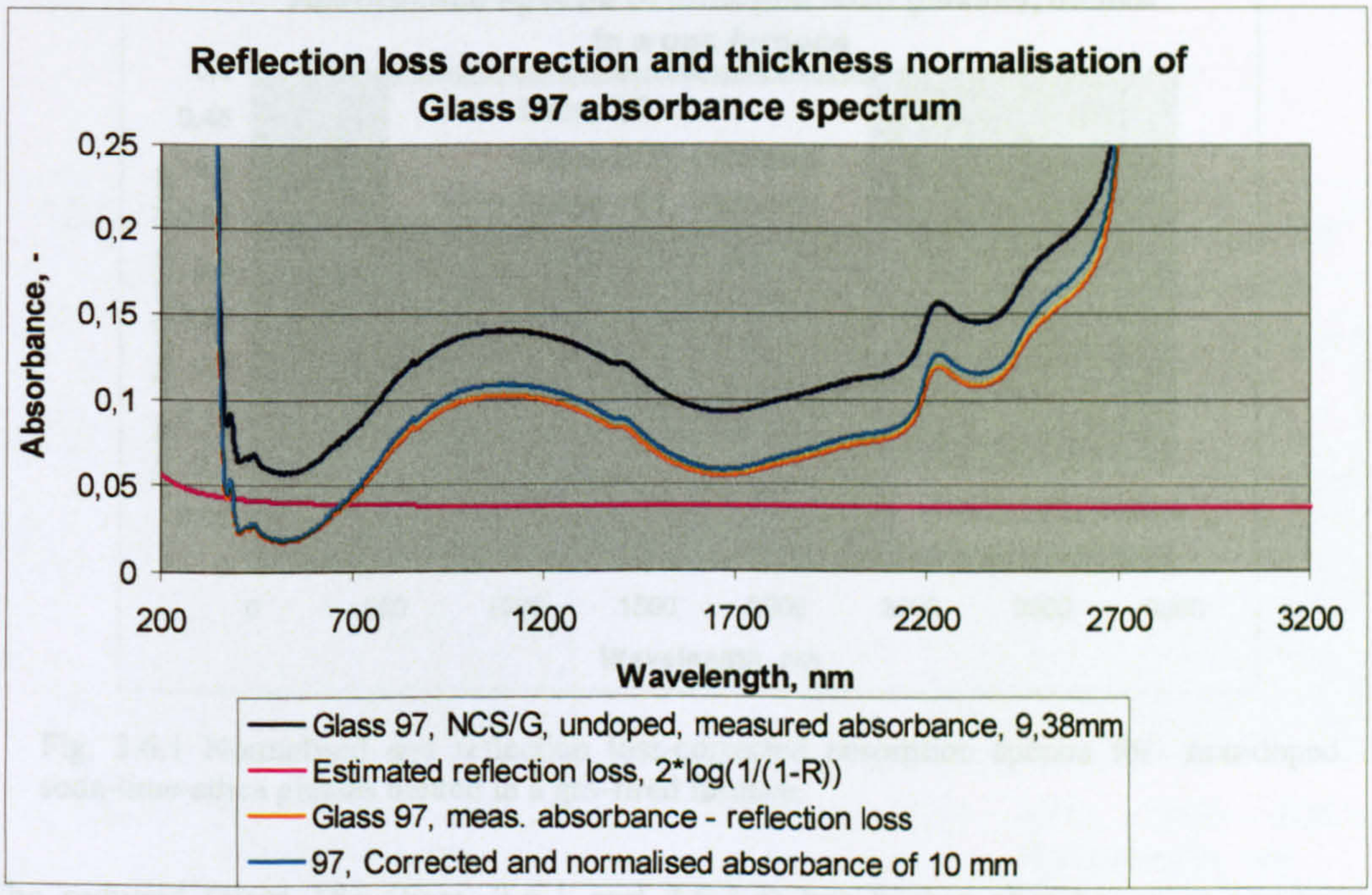

Fig. 3.5.6 Reflection loss correction and thickness normalisation of undoped Glass 97. The glass was melted in a gas-fired furnace in a mullite crucible at 1450 °C for 5 hours.

3.6 Fitting of background caused by water and IR-edge

3.6.1. Introduction

Examples for the reflection loss-corrected and thickness normalised absorbance curves for a few undoped NCS glasses melted in a gas furnace are shown in Fig. 3.6.1. The background loss slowly increases with wavelength above 1700 nm. The main OH-band is located above 2700 nm and small bands at 2200 and 2600 nm (Figs. 3.6.1 - 3). All these undoped glasses, melted under reducing conditions, show a broad absorbance band of Fe^{2+} ions at 700 – 1600 nm and a smaller band at 1700 – 2500 nm, caused by Fe contamination in the raw materials and Fe leached into the glass during melting from the mullite crucible walls. A slowly increasing background, i.e. the tail of the IR-edge, and the OH-bands are also seen in the absorbance curves of the glasses melted under oxidising conditions of an electric furnace (Fig. 3.6.2). The height of the OH – band is about four times higher for gas melted glasses. Glasses 196 and 188 are made of purified ingredients, but have a little contamination of Cu (Chap. 6). The copper has oxidised all iron of Glass 188 to Fe^{3+}, but the slowly increasing background is clearly seen above 1700 nm.

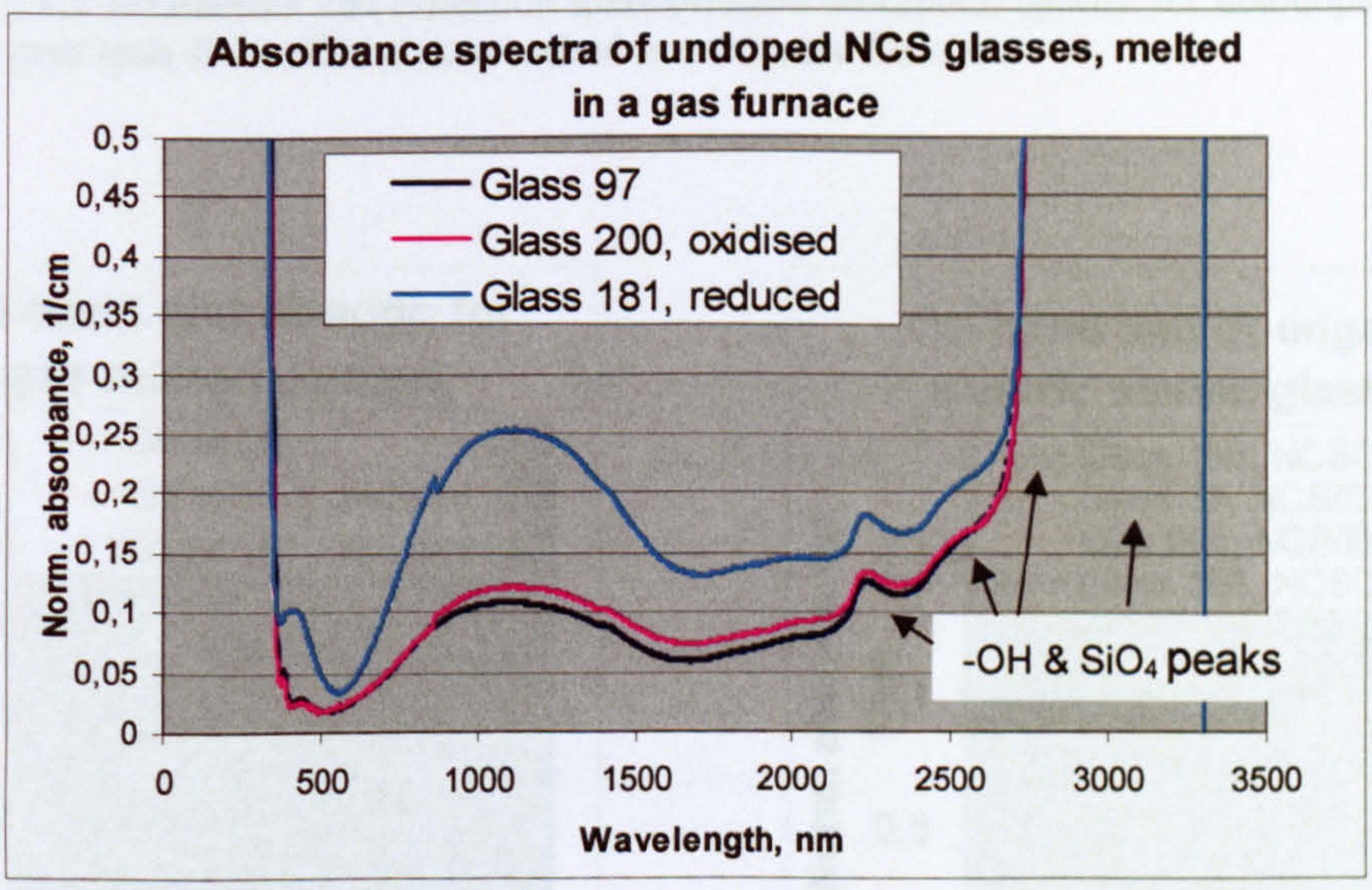

Fig. 3.6.1 Normalised and reflection loss-corrected absorption spectra for non-doped soda-lime-silica glasses melted in a gas-fired furnace.

The reduced Glass 181 (Figs. 3.6.1 and 3.6.3.a) has higher absorbance at wavenumbers above 1700 nm than the oxidised Glass 200 and other glasses melted under oxidising conditions in an electric furnace (Figs. 3.6.2 and 3.6.3 b). The main difference between these glasses is the redox ratio $[Fe^{2+}]/[Fe^{3+}]$ that is greater for Glass 181. The IR-edge tail and OH- related peaks

can be seen also in the electric furnace melted non-doped glasses and even in the glasses melted from ultra pure chemicals (marked with "Cle", Fe-content ≤ 0,01 weight %, Fig. 3.6.2). So the background contains probably both an IR-edge tail and Fe^{2+} absorption, as is actually shown in Chaps. 5 and 6.

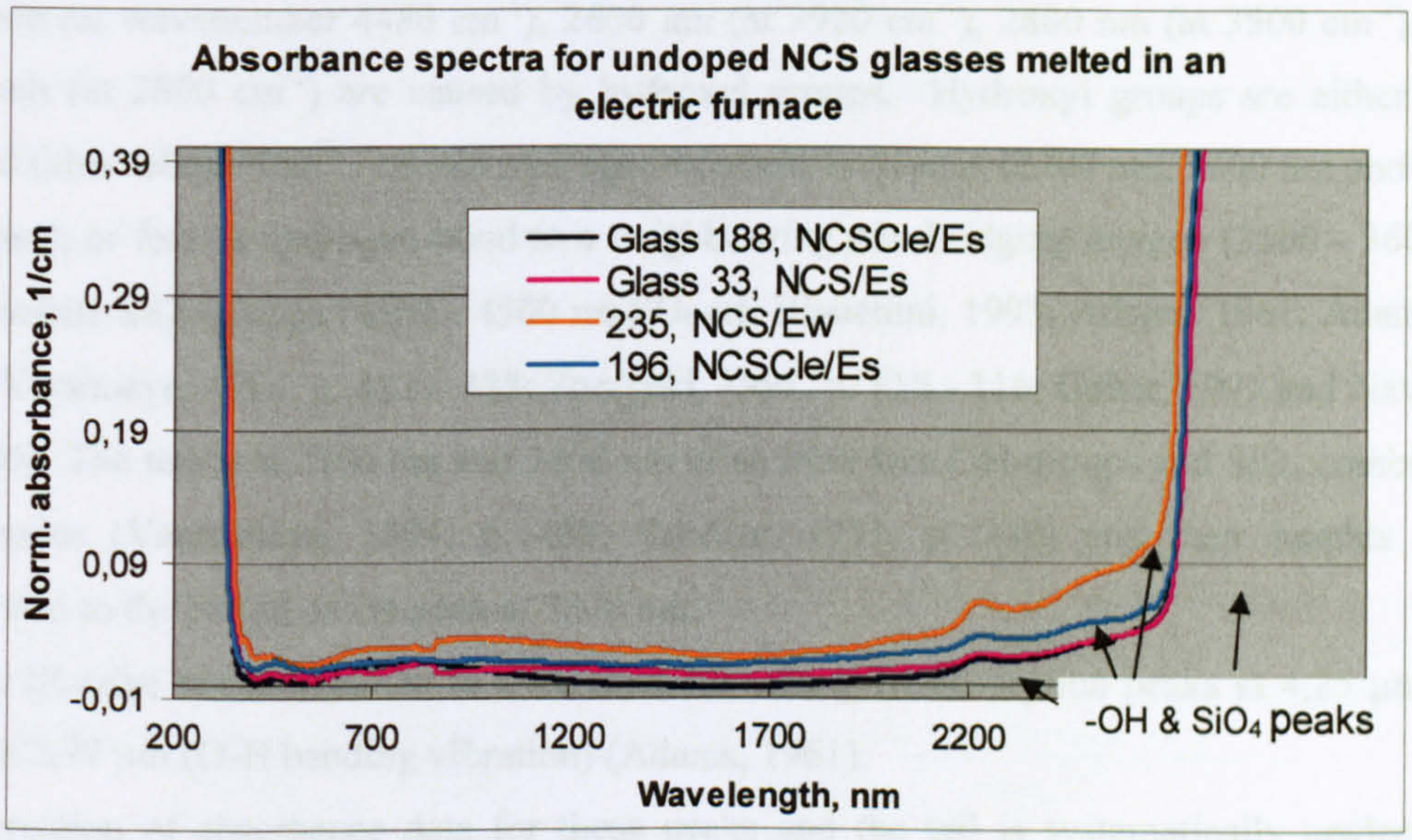

Fig. 3.6.2 Normalised and reflection loss-corrected absorption spectra for non-doped and ultra pure soda-lime-silica glasses melted in an electric furnace.

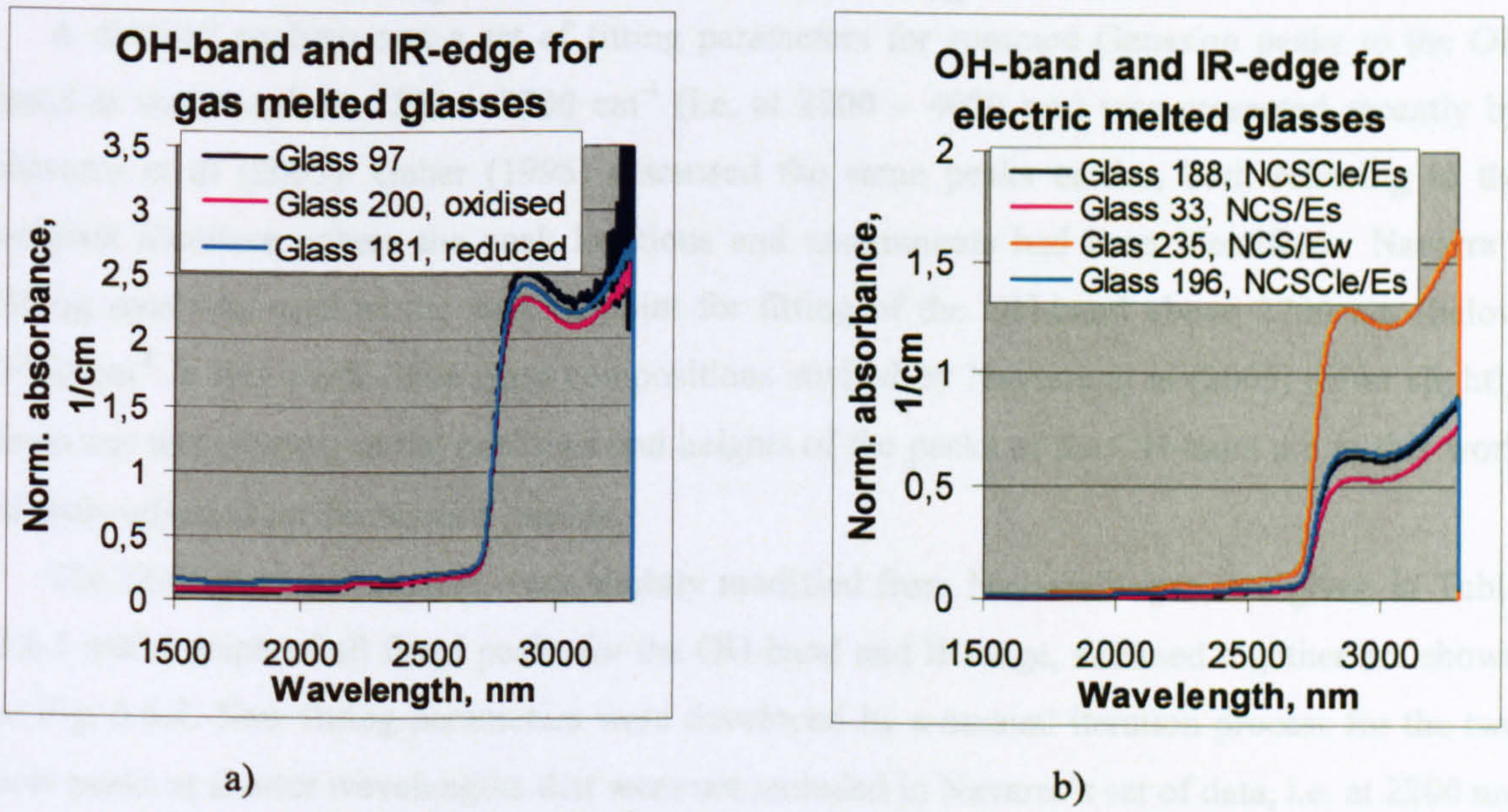

a) b)

Fig 3.6.3 The OH-bands and IR-edges of the absorbance spectra of the undoped glasses shown in a) in Fig. 3.6.1 and b) in Fig.3.6.2.

they are also included in the total summed, fitted OH-band, called "water" in Chaps. 5 and 6 and quoted with a common concentration multiplier in fitting analysis of absorbance curved.

In a few studied glasses an extra OH-related peak has been detected at wavenumber 7052 cm^{-1} and fitted with a 120 nm width and 0,016 height (not included to the Table 3.6.1). A new exponential function was developed to fit the IR-edge tail that extends down to 1600 nm in gas-fired glasses.

The fitted, summed OH-band is multiplied by concentration parameter m_{OH} of the OH, i.e. "water" concentration of the glass. The unit is so far a.u. because no calibration was available within this work. The received concentration corresponds to the area of the whole band including the two new peaks. The multiplier is thus an accurate "measure" of the total concentration of OH-ions in the glass. The obtained water concentrations of the analysed Fe and Cu doped NCS glasses are presented in Chaps. 5 and 6.

Table 3.6.1 The fitting parameters of the OH-band, i.e. " water", obtained by iteration from Navarra's data (Navarra et al, 2005). This set of data apply to the undoped and with Cu and/or Fe doped NCS glasses melted in gas and electric furnaces (Chap. 5 and 6). The heights of Peaks 8 and 9 are 10 times the given values* for Cu-doped glasses.

Peak	*Position, cm^{-1}*	*Width, cm^{-1}*	*Height, a.u.*cm^{-1}*
p1	2685	258	0,63
p2	2861	76	0,04
p3	3143	211	0,41
p4	3396	106	0,266
p5	3497	68	0,243
p6	3570	46	0,213
p7	3624	32	0,098
p8	3920	230	0,016*
p9	4475	95	0,0097*
p10	7052	120	-

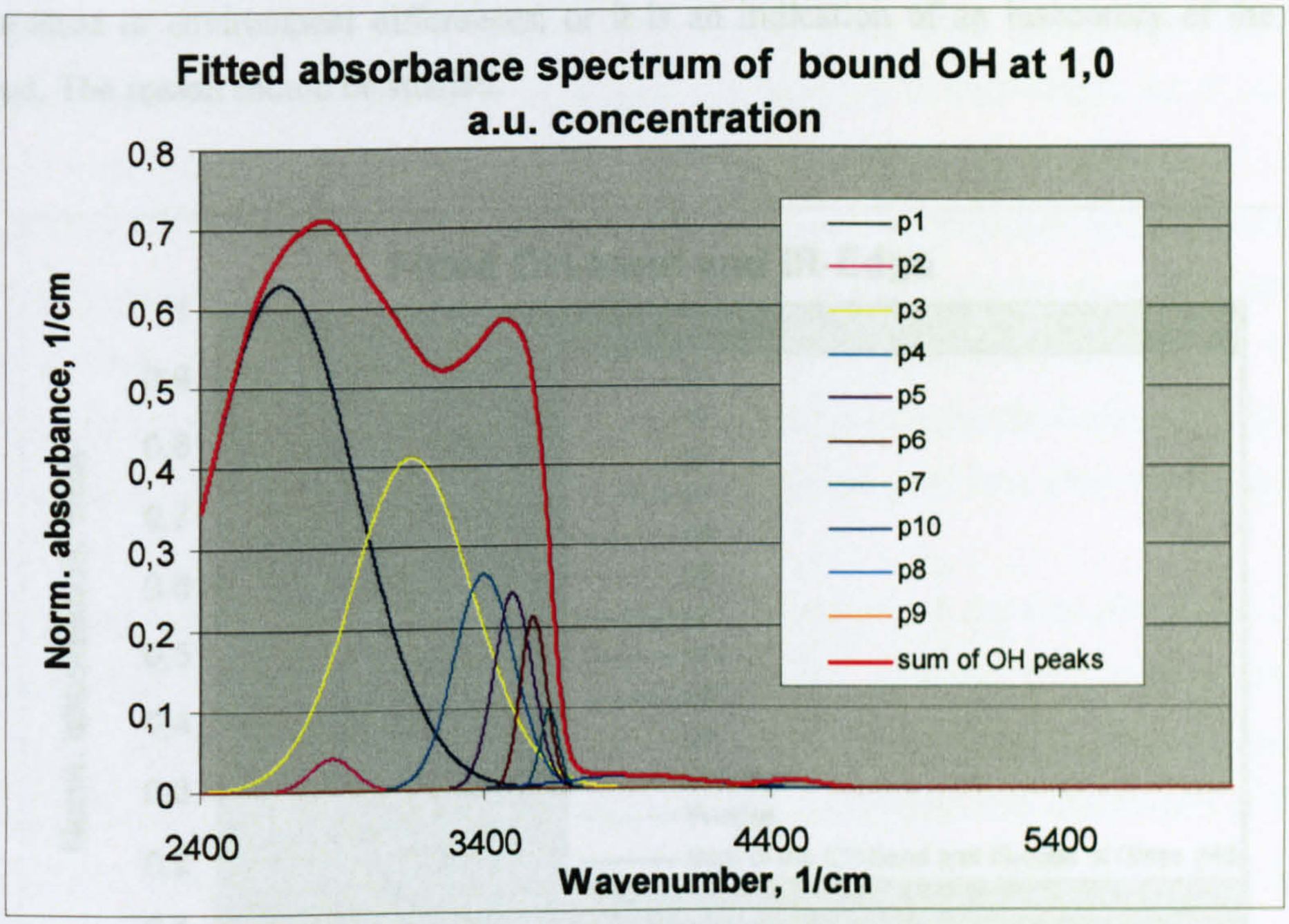

Fig. 3.6.4 The fitted absorbance spectrum of the OH-band (peaks p1 – p10) including the peaks at 3920 and 4475 cm^{-1}. The fitting parameters of Table 3.6.1 are used.

The IR-tail is fitted as an exponential function $y = m_{IR} * A * \lambda^B$, where $A = 1.30 * 10^{-4}$ and $B = 6.800$ and λ, the wavelength insert in micrometers, are the fitted parameters and m_{IR} is the variable multiplier modified at fitting according to the absorbance of the glass under consideration (Fig. 3.6.5). This equation is a pure mathematical fit to the data of this work, i.e. to the residual signal after the OH-band and Fe^{2+} absorbance spectrum were subtracted from the signal. This multiplier, m_{IR}, is also related to the OH-concentration of the glass and to the structure of SiO_4- network.

Both OH- and IR concentrations are determined for the studied Cu and Fe-doped glasses (Chaps. 5 and 6). They seem to mainly depend on the concentration of the water remaining in the glass after melting and annealing. The only systematic difference noticed in fitting analysis was of Cu doped glasses melted in electric furnace. The peak height at 4480 cm^{-1} was about 10 time higher compared to similar glasses doped only with iron. The reason for this has not been studied, yet.

The fitted concentrations of water (m_{OH}) and IR-edge (m_{IR}) have been noticed to vary a little independently of each other, maybe due to compositional and/or structural differences of the glasses (Chaps 5 and 6), caused by the corrosion of mullite crucible material (increases the concentrations of soda silica and alumina of the glass and melting temperature, or annealing

temperature or environment differences; or it is an indication of an inaccuracy of the fitting method. The reason should be studied.

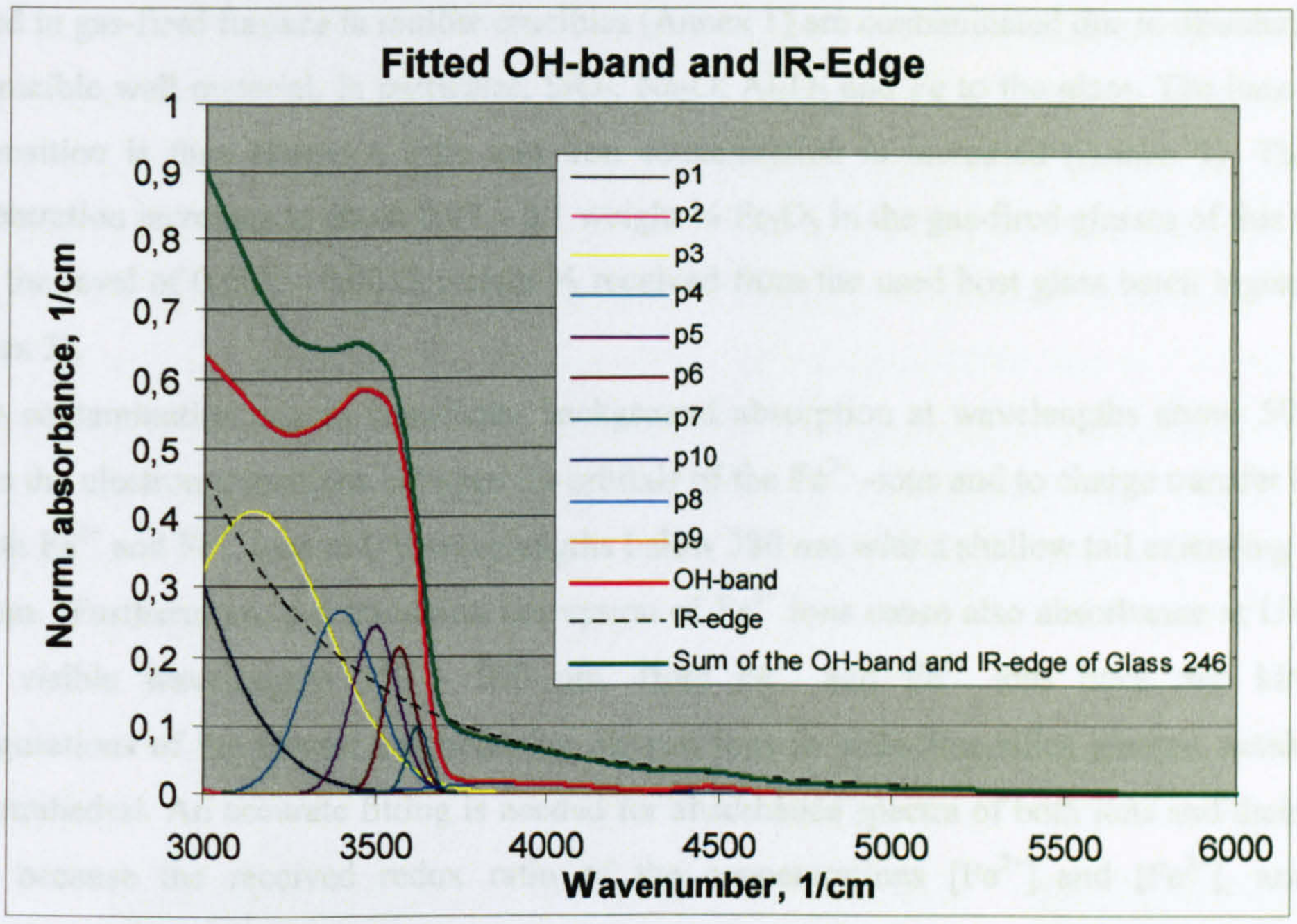

Fig. 3.6.5 Fitted OH-band and IR-edge tail absorbance spectra. The sum is calculated the water concentration multiplier $m_{OH} = 0,89$ and IR multiplier $m_{IR} = 0,72$, typical values for electric melted NCS glasses.

3.7 Fitting of UV-edge and contaminant iron absorption

The base glass ingredients of standard commercial grade used in this work (LA sand, limestone, soda ash, potash, dolomite etc.) contain a little (up to 0.01 weight %) of absorbing colorant ions as contaminations: Fe, Co, Cu, Cr, SO_3, etc. (Annex X). In addition, all samples melted in gas-fired furnace in mullite crucibles (Annex 1) are contaminated due to dissolution of the crucible wall material, in particular, SiO_2, Na_2O, Al_2O_3 and Fe to the glass. The base glass composition is thus altered a little and iron concentration is increased (Annex 3). The Fe-concentration increases to about 0,07 – 0,1 weight % Fe_2O_3 in the gas-fired glasses of this work, from the level of 0,001 – 0,0015 weight % received from the used host glass batch ingredients (Annex 3).

Fe contamination causes significant background absorption at wavelengths above 500 nm due to the electron transitions between 3d-orbitals of the Fe^{2+} -ions and to charge transfer bands of both Fe^{2+} and Fe^{3+} ions at UV wavelengths below 380 nm with a shallow tail extending up to 600 nm. Furthermore, d-d transition absorption of Fe^{3+} ions cause also absorbance at UV and short visible wavelengths 350 - 500 nm. Both Fe^{2+} and Fe^{3+} ions have two kind of configurations of the closest neighbouring oxygen ions in soda-lime-silica glasses, octahedral and tetrahedral. An accurate fitting is needed for absorbance spectra of both ions and their both sites, because the received redox ratio of the concentrations [Fe^{2+}] and [Fe^{3+}], and the proportions of the sites, are dependent on very many factors in glasses.

The fitted spectra for all parts of iron absorbance spectrum are developed and tested by fitting various Fe doped NCS glasses in Chaps. 5.4 – 5.7. The sets of fitting parameters for reducing and oxidising melting conditions, and Fe dopant and contamination concentration levels, given there, are used to fit the iron contamination spectra and the UV-edge of the Fe and/or Cu doped glasses of this work (Chaps. 5 and 6).

4. Supporting results

4.1 Extrapolation of surface losses

To develop a mathematical description of colorant ion absorbance spectra the first questions were: whether the internal absorbance is linearly proportional to sample thickness, whether the surface related loss (that does not scale with thickness) depends on wavelength, and whether significant surface losses other than reflection loss exists on the samples? The answers to these questions were sought by preparing 9 samples of Glass 94 (a NCS melted in gas-fired furnace and doped with 0,5 mol % CuO) with thicknesses ranging from 0,935 mm to 7,22 mm and measuring their spectra (Figs. 4.1.1 and 4.1.2). The Cu^{2+} absorption band is seen around 800 nm and the band caused by OH^--groups is seen at 2700 – 3300 nm. The UV-edge, caused by the UV-bands of Cu^{2+}, Cu^{1+} and contaminant Fe^{3+} ions and weak d-d absorbance of Fe^{3+} is seen at 330 - 420 nm (Fig. 4.1.2).

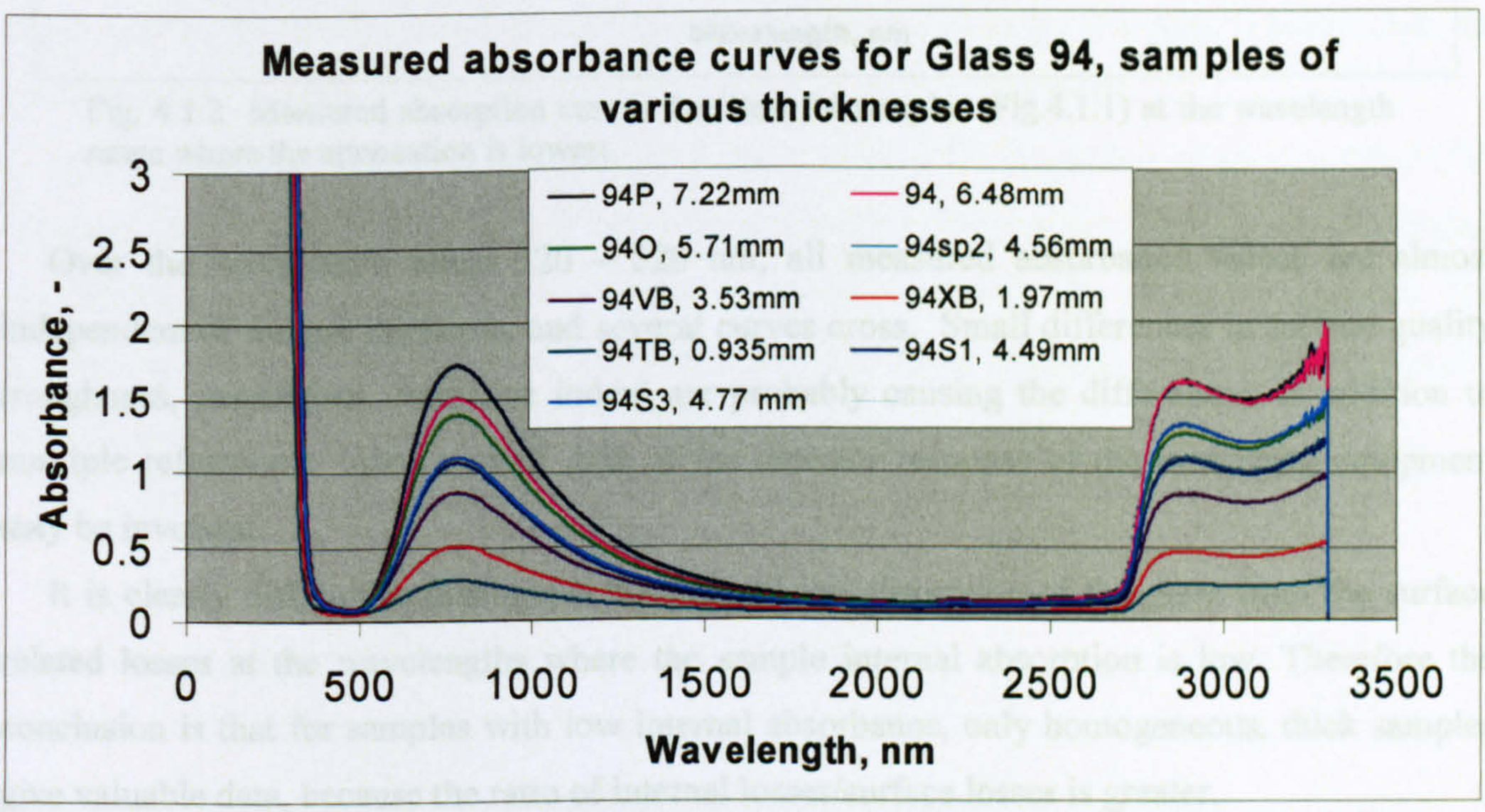

Fig. 4.1.1 Measured absorbance curves of Glass 94, a soda-lime-silica glass doped with 0.5 mol % CuO, melted in gas-fired furnace. The sample thickness was varied from 0.935 mm to 7.22 mm.

The heights of the Cu^{2+} bands at 800 nm are seen to increase with the sample thickness (Fig.4.1.1). However, at the wavelength range from 350 nm to 530 nm (Fig. 4.1.2) the curves do not appear in the logical order of sample thickness. In particular, the samples with thickness below 3 mm have higher absorption than would be expected from the curves of the thicker samples. The reasons for the unusual behaviour of 0.935 mm and 3.53 mm samples were not studied. Possible causes are inhomogeneity of the glass, or inhomogeneity of the $Cu^{2+}/Cu^{1+}/Cu$ concentrations due to their very sensitive redox ratios caused by melting conditions and

annealing (Chap. 6), or inhomogeneity of the mutual redox between Fe contaminant ions and Cu-ion in the glass. The glass had been melted in a large (1 kg) mullite pot, from which some additional iron was leached out into the glass (Chap. 6, Annex 3).

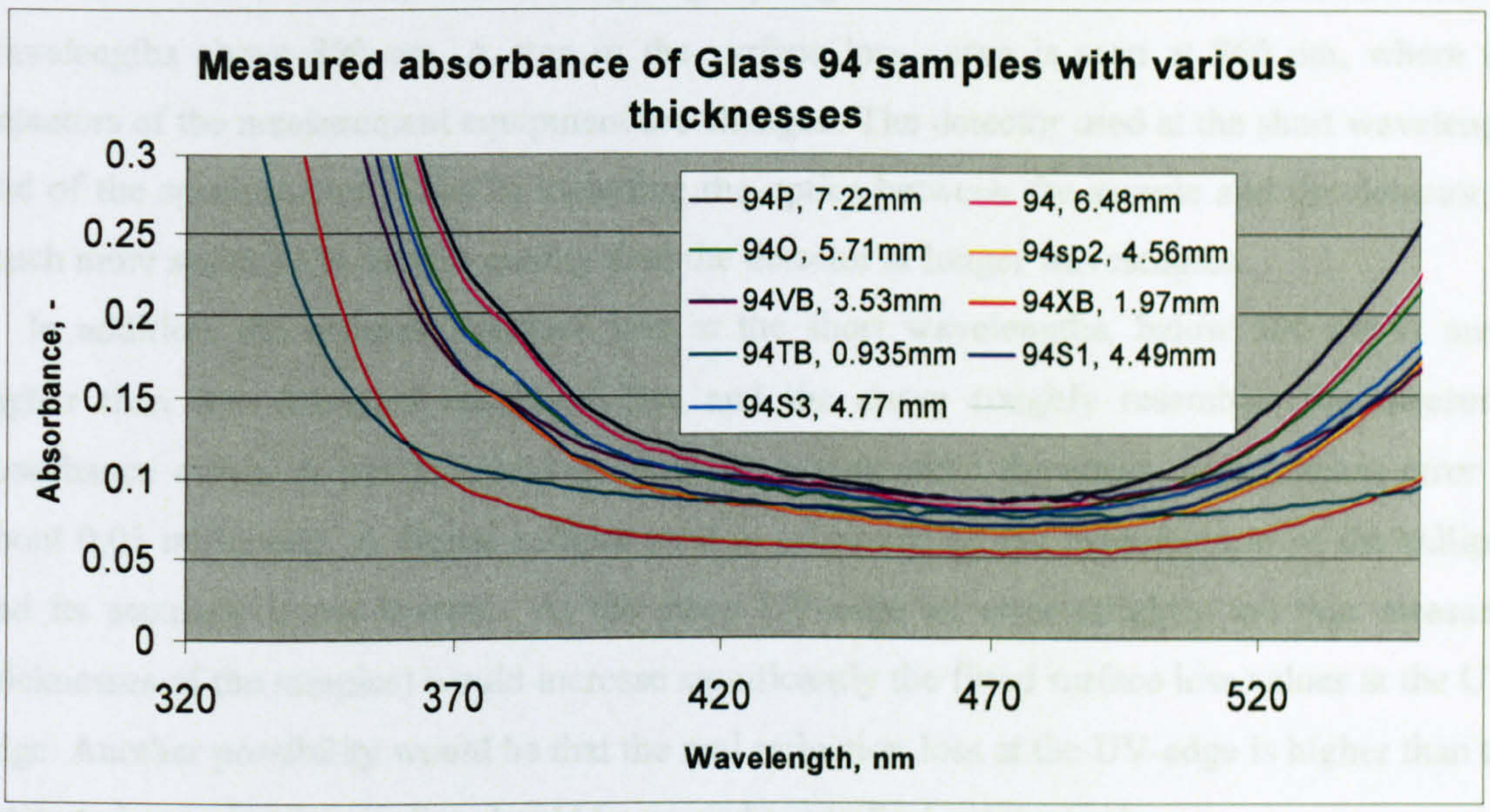

Fig. 4.1.2 Measured absorption curves for Glass 94 samples (Fig.4.1.1) at the wavelength range where the attenuation is lowest.

Over the wavelength range 320 – 520 nm, all measured absorbance values are almost independent of sample thickness, and several curves cross. Small differences in surface quality (roughness, parallelism, refractive index) are probably causing the differences, in addition to multiple reflections. Also a small drift of the detector response of the measuring equipment may be involved.

It is clearly difficult to distinguish the internal ion absorption of the glass from the surface related losses at the wavelengths where the sample internal absorption is low. Therefore the conclusion is that for samples with low internal absorbance, only homogeneous, thick samples give valuable data, because the ratio of internal losses/surface losses is greater.

The measured absorbance values were plotted as a function of sample thickness (Fig. 4.1.3) at several wavelengths, and a line was fitted to each set of data. The fitting residuals, R^{2-} values, were high, around 0,99 , at all those wavelengths, where internal absorption of the sample is high. At the wavelengths where internal absorption is low, i.e. at 320 – 530 nm, the residuals are worse (Fig. 4.1.4).

The fitted parameters were calculated over the entire wavelength range from the UV-edge below 320 nm to the OH^- -peak up to 3200 nm., as shown in Figs. 4.1.4 and 4.1.5. The fitted linear absorption coefficient a, the total surface loss b, and the total absorbance y (for a 1 mm

thick sample) are thus received as a function of wavelength. The data represents Glass 94, which was doped with 0,5 mol % CuO.

The received surface loss is compared with the estimated reflection loss (Chap. 3.5) in Fig. 4.1.5. The received surface loss is only slightly higher than the estimated reflection losses at wavelengths above 860 nm. A step in the surface loss curve is seen at 860 nm, where the detectors of the measurement equipment are changed. The detector used at the short wavelength end of the spectrometer (Chap.2) including the optics between the sample and the detector, is much more sensitive to sample quality than the detector at longer wavelengths.

In addition, the estimated surface loss at the short wavelengths, below 500 nm is much higher than the estimated reflection loss and the curve roughly resembles the measured absorbance curve. A possible reason could be a systematic thickness measurement error of about 0,05 millimeter. A digital calliper used is calibrated by the manufacturer of the calliper, and its accuracy is not known. At the steep UV-edge an error (slightly too thin measured thicknesses of the samples) would increase significantly the fitted surface loss values at the UV-edge. Another possibility would be that the real reflection loss at the UV-edge is higher than the estimated one. Further studies should be carried out to find out the truth.

In this work the estimated reflection loss curve is used for correction of all measured UV-Vis-Near IR absorbance spectra Studied (Chaps 5 and 6). The surface related losses, including the reflection loss, are assumed to be of the similar size and shape for all studied samples. The accuracy of this correction method can be concluded to be of the order of 0,01 at wavelengths away from the UV-edge and worse at the UV-edge (Annex 4, Chap. 3.1.6).

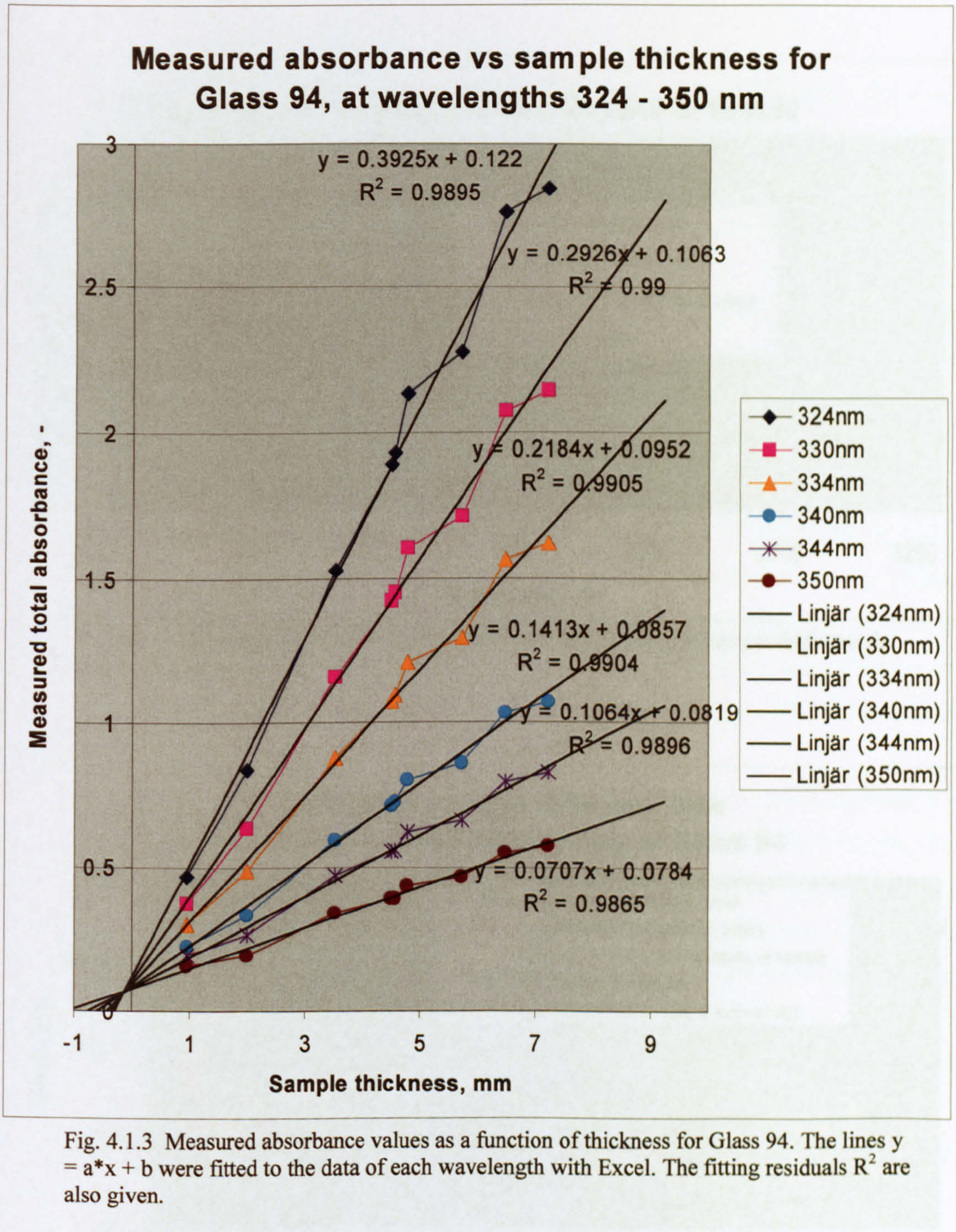

Fig. 4.1.3 Measured absorbance values as a function of thickness for Glass 94. The lines y = a*x + b were fitted to the data of each wavelength with Excel. The fitting residuals R^2 are also given.

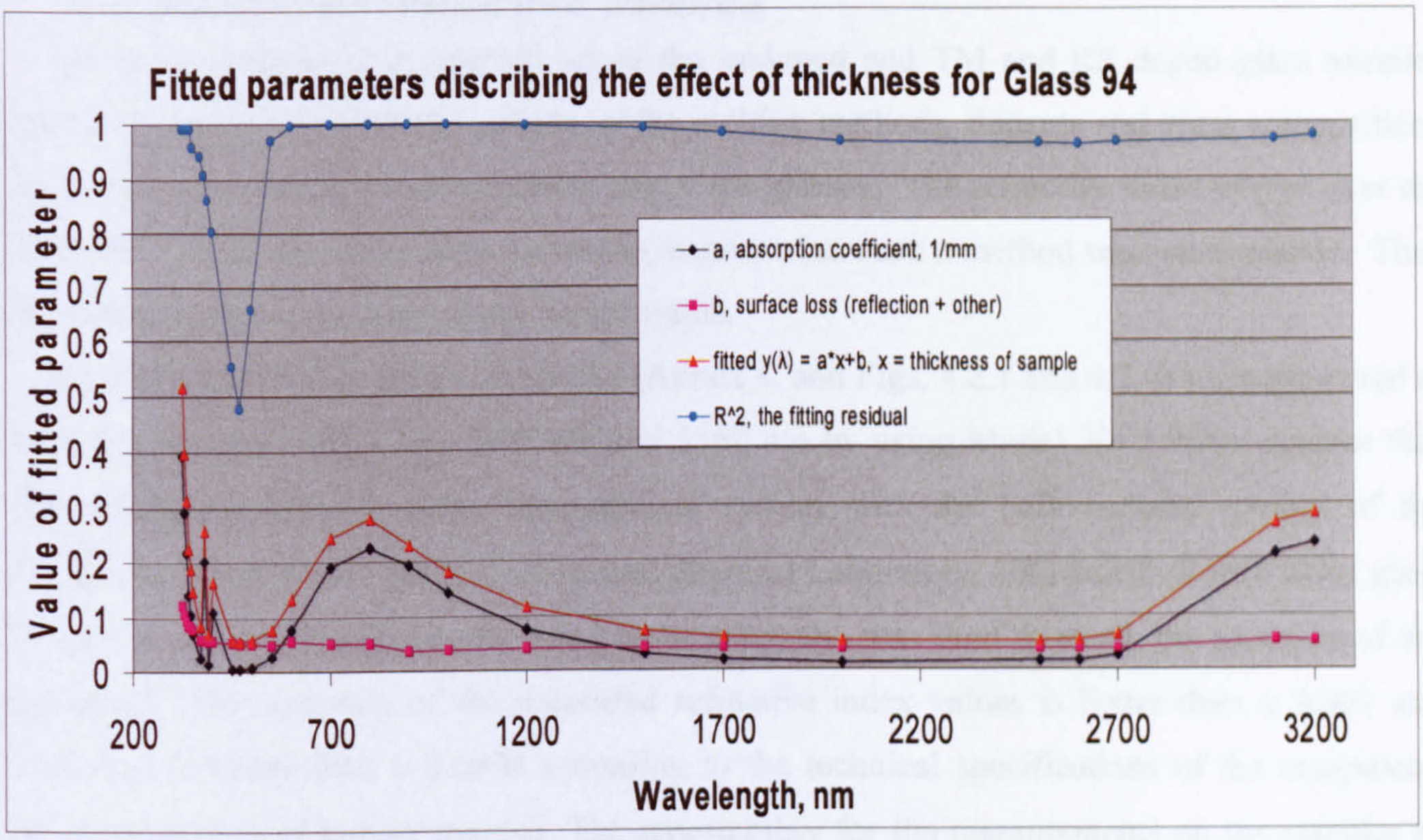

Fig. 4.1.4 The fitted parameters for the absorbance dependency on sample thickness for Glass 94 (Fig. 4.1.1 – 3).

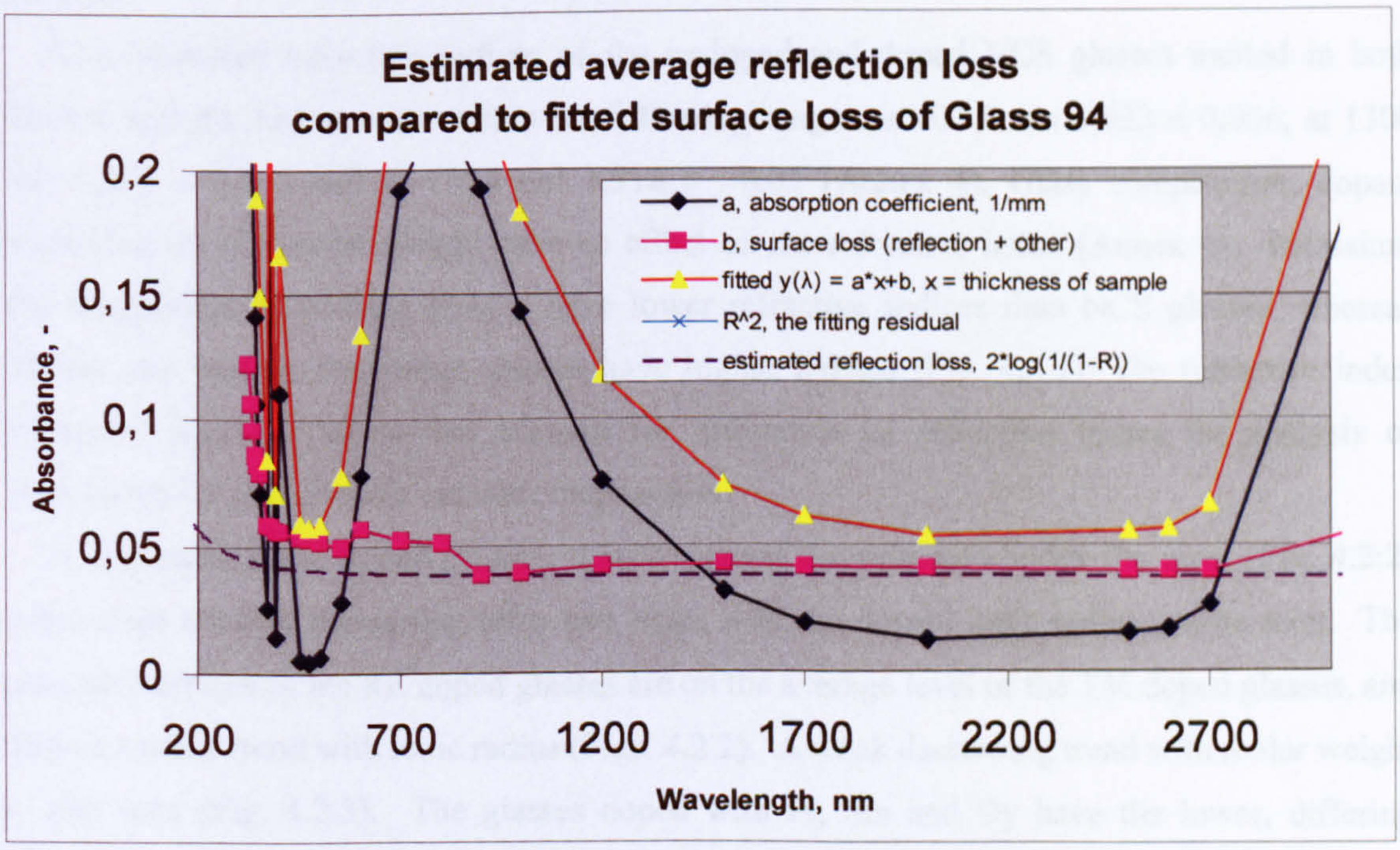

Fig. 4.1.5 Comparison of the estimated reflection loss curve used for reflection loss correction, and the surface loss fitted from the measured absorbance curves of Glass 94.

4.2 Measured refractive indices

Refractive indices of a selected set of the undoped and TM and RE doped glass samples were measured to find out the effects of the melting methods, dopants and glass compositions on the refractive indices and reflection loss of the glasses. The refractive index curves over the wide 200 – 3300 nm range were wanted to measure, but such a method was not available. Thus the measurement was done at three wavelengths.

Refractive indices of about 50 glasses (Annex 4, and Figs. 4.2.1 and 4.2.2) were measured at three wavelengths 628,3 nm, 1300 nm and 1550 nm by using Model 2010 Prism coupler thin film thickness/refractive index measurement system with the bulk material variant of the method from Metricon. An NPL (National Physical Laboratory, UK) certified pure silica glass sample of which refractive index was known precisely, was used to check the accuracy of the equipment. The accuracy of the measured refractive index values is better than ± 0,001 and resolution is better than ± 0,0005 according to the technical specifications of the equipment, Operation and maintenance manual. The repeatability for the measurements on the samples of this work was found to be the same as the given resolution. Small temperature changes around room temperature, < ± 5°C, do not affect the measurement results, within these levels of accuracy.

The measured refractive indices of the undoped and doped NCS glasses melted in both electric and gas furnaces are within the following ranges: at 632,8 nm 1,533 ± 0,006, at 1300 nm 1,521 ± 0,012 and at 1550 nm 1,518 ± 0,07 (Annex 4). Glass composition, dopant concentration and molar weight have an effect on the refractive index (Annex 4). Potassium and magnesium containing glasses have lower refractive indices than NCS glasses, whereas lithium and barium containing glasses have higher indices (Fig. 4.2.1). The refractive index difference must be taken into account for estimation of reflection losses for analysis of absorbance for glasses with various composition.

In the studied TM doped glasses, titanium raises the refractive index the most (Fig. 4.2:2) and a clear trend of decreasing refractive index with the dopant ionic radius can be seen. The refractive indices of the RE doped glasses are on the average level of the TM doped glasses, and show a weaker trend with ionic radius (Figs. 4.2.2). A weak decreasing trend with molar weight is also seen (Fig. 4.2.3). The glasses doped with Pr, Sm and Dy have the lower, differing refractive indices (Fig. 4.2.3). The Pr and Dy dopants may occupy different sites and Sm may have another valence than the usual 3+ of rare earth ions in silicate glasses. Fitting analysis of the measured absorbance spectra might give a more detailed information. It is aimed to be carried out in future.

It can be concluded that the refractive index changes caused by dopants and glass composition variations should be taken into account for accurate reflection loss correction.

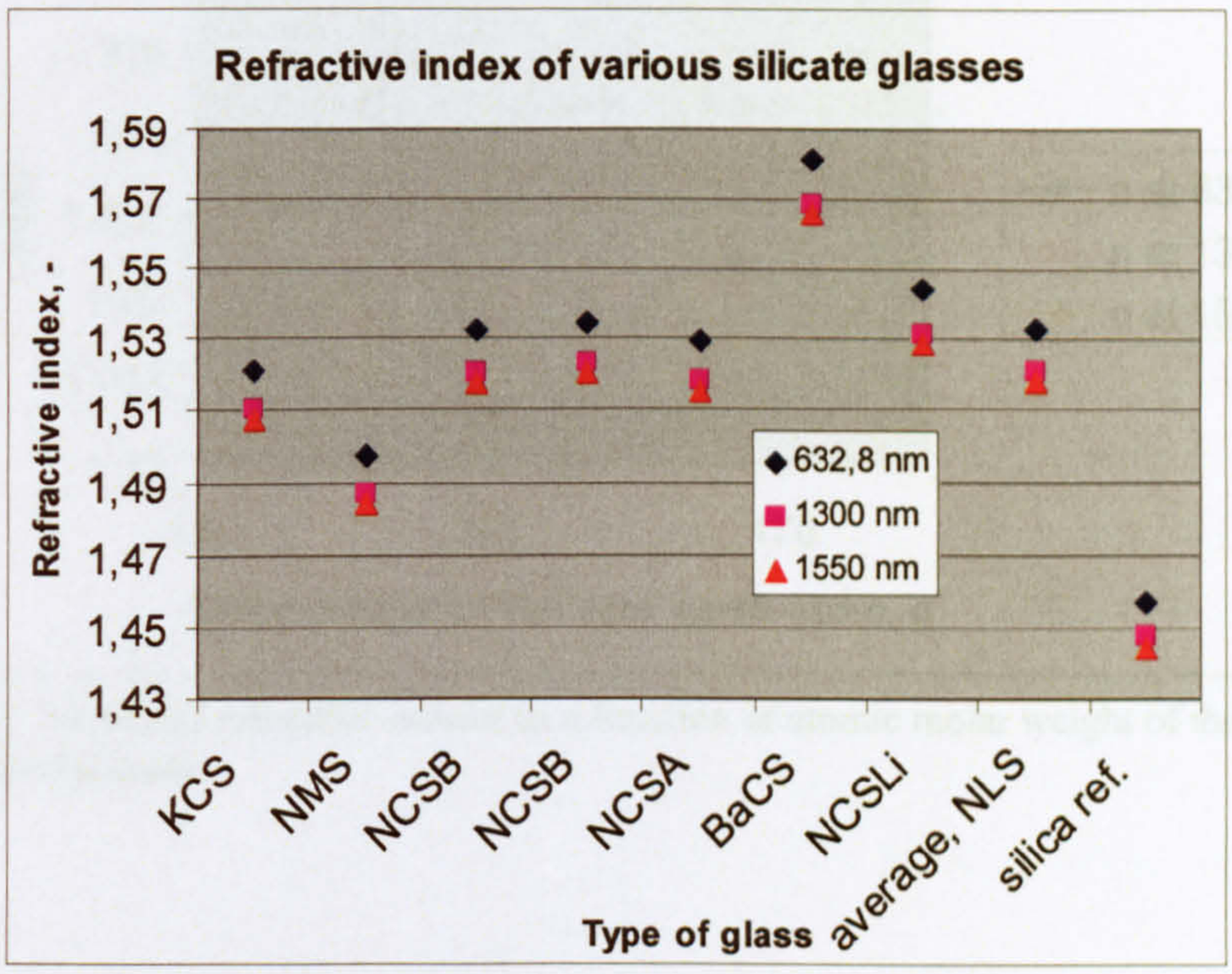

Fig.4.2.1 Measured refractive indices for the various silicate glasses (Annex 4 and compositions given in Annex 1).

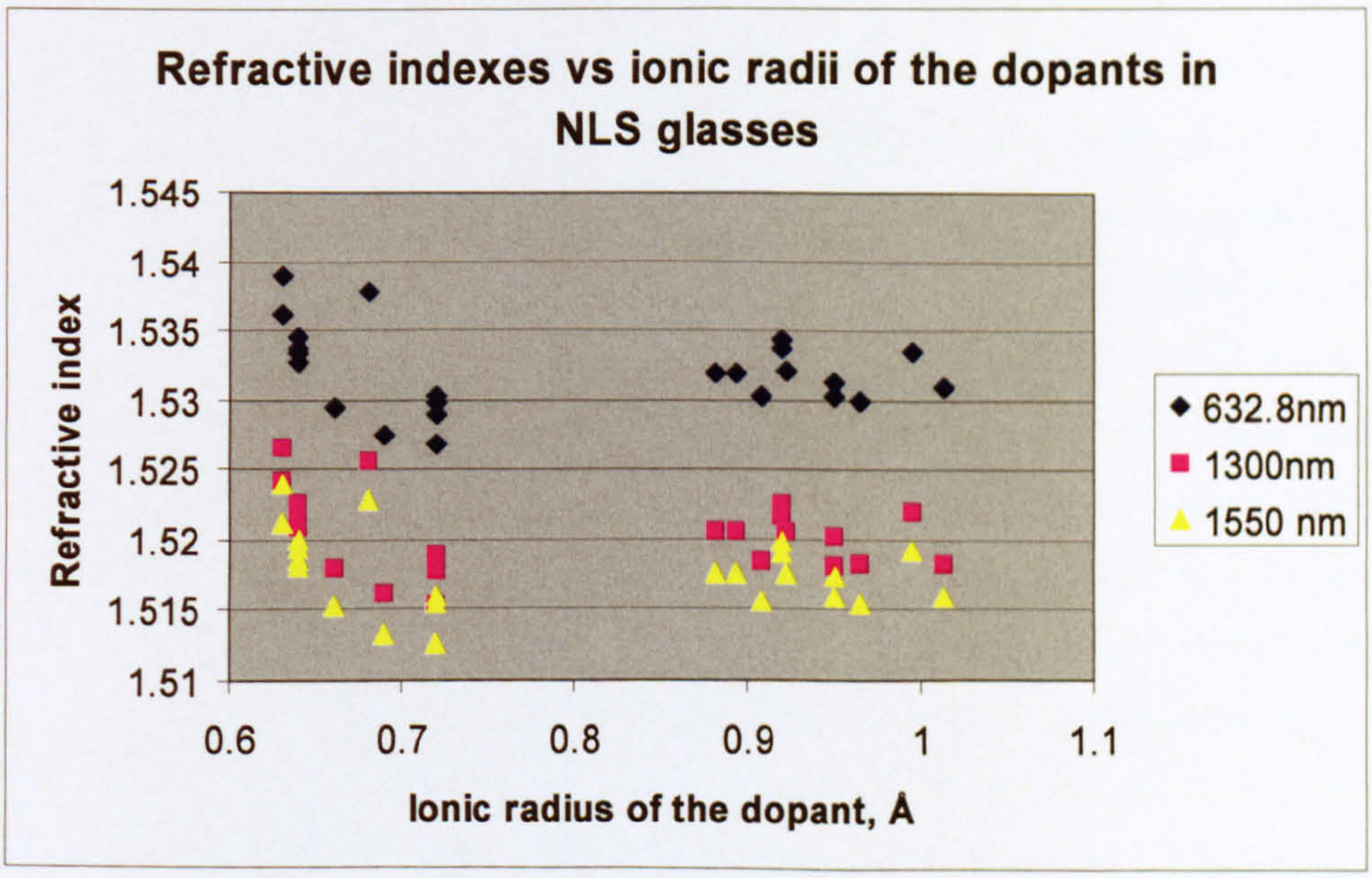

Fig. 4.2.2 Refractive indices of the doped NCS glasses as a function of dopant ionic radius. The TM dopants have ionic radii smaller than 0,8 Å and the Re dopants 0,87 – 1,03 Å. The radii data is taken from Weast et al (1987, p. F-157)

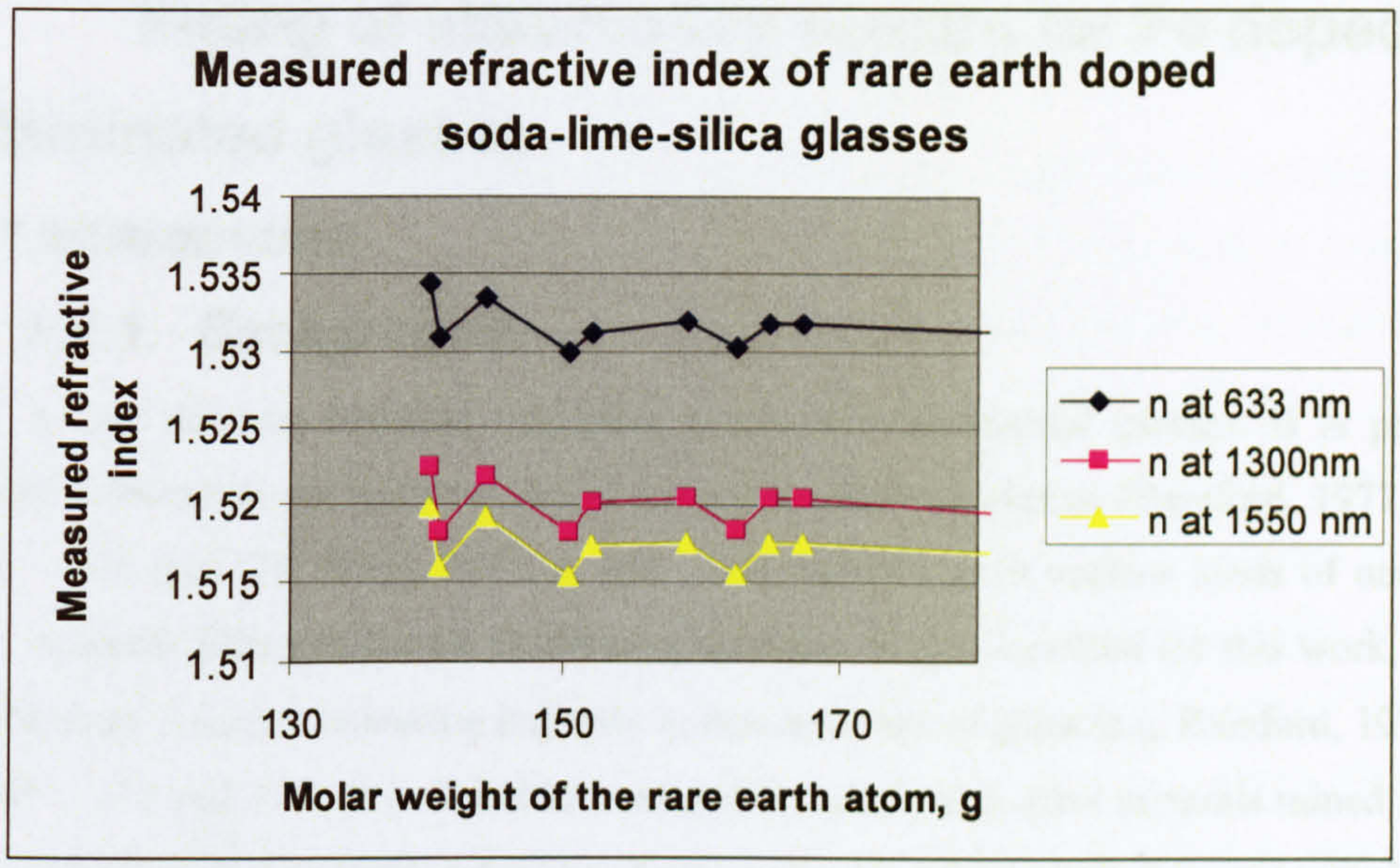

Fig.4.2.3 Measured refractive indices as a function of atomic molar weight of the rare earth doped glasses.

5. Fitting of absorbance spectra for Fe doped and contaminated glasses

5.1 Introduction

5.1.1. Background

Iron is one of most common colouring agents for commercial glasses. It is present in significant concentrations in amber, green and other coloured glasses (Bamford, 1977, p. 35 – 38, 165 – 171 and 176; Weyl, 1951, p. 89 - 120), as well as in various kinds of uncoloured glasses. Accurate fitting of the Fe absorbance spectrum is also essential for this work, because iron is the most common colouring impurity in raw materials of glass (e.g. Bamford, 1977, p. 35 – 38, 165 – 171 and 176). It is found in sand and limestone and other minerals mined from the ground, as well as in chemically synthesized raw materials, such as soda ash, and recycled cullet used for glass making. Some iron also leaches into the glass melt from the refractory materials of industrial glass melting pots and tanks, and from various types of ceramic crucibles and tools used for glass melting and preparation in research.

On the other hand, for flat window glass for solar control, iron is added to the glass in order to increase the absorbance of harmful ultraviolet radiation, and to reduce heat loss and to minimise energy consumption of air conditioning and need for heating of buildings. Iron (actually Fe^{2+}) has high absorption of near infrared radiation emitted by the hot glass melt, which is beneficial for flat glass process. In glass melting in deep tanks and feeders its high Near IR absorption is a problem, because it reduces heat transfer through the molten glass

The high UV absorption of Fe^{3+} and Fe^{2+} ions, even at low iron concentrations of the order of 0,01 mol %, dominates absorption at short wavelengths and moves the cut-off wavelength, the UV edge, to the border of visible wavelengths to around 370 - 400 nm for a glass thicker than 2 mm. Therefore iron is commonly used for filtering out damaging UV radiation in container and window glasses to protect various products and people from solar and lighting UV radiation.

Particularly important for the development of a mathematical description of iron absorbance spectrum is that the spectrum is very sensitive to the host glass composition (e.g. Bingham, 2000, 2001, 2002; Rüssel, 1993; Kurkjian, 1968 and 1970; Steele et al, 1965; Paul et al, 1965), to melting and annealing conditions (e.g. Kukkadapu et al 2005; Rüssel, 1993; Schirmer et al 2003) and to other multivalent ions (refining agents, colorants etc.) in the glass (e.g. Bamford, 1961 and 1977, p. 84). The intensity of the UV-absorption peaks, the redox ratio between the Fe^{2+} and Fe^{3+} ion concentrations, as well as the proportions of octahedral and tetrahedral sites occupied for both ions, may change. Mutual redox reactions occur during melting, cooling and

annealing even at low Fe concentration levels of below 0,02 mol %, according to the above mentioned literature and the results reported here.

The d-d transition absorbance spectrum of iron within the range studied consists of two to four absorption peaks for Fe^{2+} and at least eight peaks for Fe^{3+} due to each valence state appearing in soda-lime-silica glasses in both octahedral and tetrahedral configurations of neighbouring ions, (e.g. Kurkjian et al (1968), Kurkjian (1970), Levy et al (1976), Ades et al (1990), Volotinen et al (2006)). The proportions of Fe ions in these sites cannot currently be measured accurately by any analytical method at iron concentrations below 5 weight %.

Furthermore, both valence states have intense and broad charge transfer peaks in the UV, with linear absorption coefficients of the order of 2000 $(cm*mol\ \%)^{-1}$ (Fe^{3+}) and 1000 $(cm*mol\ \%)^{-1}$ (Fe^{2+}) (Steele et al, 1965, Bamford, 1977, p. 36) . The widths of these peaks are shown in this work to be 3000 cm^{-1} and 6000 cm^{-1} (Chap. 5.2). A ferric peak is centred at approximately 225 nm and ferrous at 200 nm according to Bamford (1977, p. 36) in a silicate glass, whereas Traverse et al (1992) found them at 250 and 220 nm in a soda-lime-magnesia-silica glass. The tails of these peaks may cross each other and reach into visible wavelengths (as shown in this work), dominating the UV edge of the glass. The tails affect the absorbance spectra up to wavelengths of about 500 nm in silicate glasses, depending on the iron content, redox and various other factors.

A literature study (Chap. 5.2) on the peak positions, heights, widths and numbers for each valence state and site configuration produced various sets of data for iron in silicate glasses. Data from Bingham (2000), Ades et al (1990), Traverse et al (1992) and Shirmer et al (2003) were fitted to the spectra of this work, but did not give sufficiently good accuracy, and particularly did not scale with iron concentration without major changes to the parameters. The background correction methods used by previous researchers vary and are only mentioned briefly, not described in sufficient detail for accurate comparison with each other or to the data of this work. The measurement equipment and methods used in the earlier studies are not described in detail either. Furthermore, it is well known that optical measurement technology and understanding have developed hugely during the past 50 years, in particular since 1980. The advanced computerised data analysis software suitable for the fitting of complex spectra have been available only for a few years.

Precise parameters for the positions, heights and widths of all these sets of absorbance peaks must be developed for an accurate mathematical description of the Fe absorbance spectra in the glasses of this work. The Fe ion spectra are therefore re-examined in detail for similar host glasses to this work. In order to better understand and for comparison of this work with Bingham's work (200, 2001, 2002), a selected set of his glasses spectra have also been re-fitted.

His glasses contained no sulphate or other refiner, whereas the glasses of this work were refined with 0.35 mol % sodium sulphate.

5.1.2. The aims of the study on Fe-doped glasses

The aims are:

- To fit accurately the absorbance spectra of Fe^{2+} and Fe^{3+} ions in soda-lime-silica glass, including their tetrahedral and octahedral sites and UV-peaks.
- To calibrate as accurately as possible the concentration multipliers for the summed peak heights, i.e. linear absorption coefficients, for each kind of ion and site, by using the data from the literature and by using the measured concentrations of iron in the test glasses as references.
- To study the application of the fitting to the background correction caused by iron contamination at concentrations below 0,1 mol %.
- To verify the range of iron concentrations, within which the fitted spectra scales linearly (if such exist) and can be reliably used.
- To verify the reproducibility, precision and accuracy of the "measurement" of the Fe-ion and site concentrations by this method.
- To test the applicability of the fitted Fe spectra to the analysis of singly iron doped and doubly doped glasses in combination with $NaSO_4$, CuO or CeO_2.

5.2 Literature study on Fe-doped glasses

Questions to be answered by the following literature study concern the numbers of absorbance peaks for each kind of iron ion and site, fitting parameters (heights, i.e. extinction coefficients or optical densities, peak positions and widths), redox ratios, coexistence of tetrahedral and octahedral sites for both ions in soda-lime-silica glasses, concentration proportions for octahedral/tetrahedral sites, as well as the effects of glass host composition, melting conditions and annealing.

According to the Tanabe-Sugano ligand field theory (Bates, 1962; Kurkjian, 1968, 1970; Paul, 1982), octahedral and tetrahedral configurations of the surrounding oxygen ligands should give similar absorbance spectra for Fe^{3+} ions, because the five 3d electrons lie in a similar set of energy orbitals, provided that the surroundings have similar dimensions so that the host glass would provide a similar ligand field strength. In practice in silicate glasses, sets of four absorbance peaks are usually found for both configurations (Kurkjian et al, 1968; and Bates, 1964, to whose PhD thesis work they also refer), but the octahedral configuration peak positions

are found to be spread over a wider energy range, from 13000 to 27000 cm^{-1}, whereas the four peaks for tetrahedral sites are found within a narrower range from 18000 to 26300 cm^{-1}.

The peaks at the highest energy for both types of sites in the mentioned glasses lay almost on top of each other at 26200 cm^{-1} (at 370 - 380 nm) for both configurations and have therefore never been resolved in the same glass (Ades et al, 1990, Traverse et al, 1992, Bingham 2000). Some authors purposely fit the two spectra together (Bingham, 2000; Ades, 1990), thus assuming a constant proportion for their concentrations and constant positions, heights and widths of the peaks. Other differences and weaknesses are also found within the published data.

5.2.1. Early studies on iron absorbance spectra

Bamford (1961 and 1977, p. 36 – 38 and 63 - 64) studied iron doped glasses and absorption spectra of iron and sulphur in sodium silicate glasses. His conclusions are as follows: " 1. The proportion of iron in the ferric state in sodium silicate glasses has been shown to increase with the sodium oxide concentration of the glass. 2. The absorption band at 1.2 μm in the optical transmission curves of the glasses containing iron is associated with ferrous ions in a ligand field of octahedral symmetry, i.e. $Fe^{2+}O_6$ complexes. The pale blue coloration of reduced iron glasses is due to the extension of this absorption band into the visible region. 3. The absorption bands at 0.38, 0.425 and 0.44 μm together with the shift in the ultra-violet cut-off from 0.25 to 0.34 μm, are associated with ferric ions in a ligand field of octahedral symmetry in sodium silicate glasses, i.e. $Fe^{3+}O_6$ complexes. 4. Small quantities of sulphur in sodium silicate glasses melted under reducing conditions have been shown to produce two types of colouring centre. One centre associated with an absorption band at 0.41 μm, is favoured by the lower concentrations of sulphur. It is suggested that this absorption band arises from sulphide formation. The other centre, associated with absorption bands at 0.36 and 0.29 μm, is favoured by higher concentrations of sulphur. It is suggested that this absorption arises from polysulphide formation. The presence of iron is necessary for the coloration, the normal impurity (0.05 % by weight) being sufficient.

A few years later Steele and Douglas (1965) studied iron absorption spectra in sodium silicate and sodium borate glasses. They showed four absorption peaks for each Fe^{3+} octahedral and tetrahedral sites (Table 5.2.1), predicted from the known ligand field theory. The molar extinction coefficients of ferric ions at 380 nm was found to be 1,2 l $mol^{-1}cm^{-1}$. UV-peaks were found at 230 nm with an extinction coefficient of 7000 l $mol^{-1}cm^{-1}$ and at about 210 nm with an ext. coefficient of 3000 litre $mole^{-1}cm^{-1}$ and were assigned to Fe^{3+} and Fe^{2+} ions respectively. They are caused by charge transfer. They pointed out in their discussions that there were no ferric peaks at 735 and 570 nm in borate glasses, which they thought was because there were no Fe^{3+} octahedral sites in borate glasses. In silicate glass a broad absorption band at 1050 nm with

a molar extinction coefficient of 28,9 l $mol^{-1}cm^{-1}$ is reported, whereas in borate glasses the coefficient is only a tenth of it and the band was seen to shift to 980 nm. Fe^{2+} ions were suggested to be in octahedral sites.

Table 5.2.2 Ligand field predictions for ferric iron by Steele and Douglas (1965)

Band No	Ion	Transitions	Symmetry	Peak position λ, nm	Peak position ν, cm^{-1}
1	Fe^{3+}	${}^6\Gamma_1(s)\rightarrow{}^4\Gamma_5(D)$	Octa	380	26316
2	Fe^{3+}	${}^6\Gamma_1(s)\rightarrow{}^4\Gamma_1(G)$ ${}^6\Gamma_1(s)\rightarrow{}^4\Gamma_3(G)$	Octa	427	23410
3	Fe^{3+}	${}^6\Gamma_1(s)\rightarrow{}^4\Gamma_5(G)$	Octa	570	17544
4	Fe^{3+}	${}^6\Gamma_1(s)\rightarrow{}^4\Gamma_4(G)$	Octa	735	13600
5	Fe^{3+}	${}^6\Gamma_1(s)\rightarrow{}^4\Gamma_5(D)$	Tetra	380	26316
6	Fe^{3+}	${}^6\Gamma_1(s)\rightarrow{}^4\Gamma_1(G)$ ${}^6\Gamma_1(s)\rightarrow{}^4\Gamma_3(G)$	Tetra	427	23410
7	Fe^{3+}	${}^6\Gamma_1(s)\rightarrow{}^4\Gamma_5(G)$	Tetra	446	22422
8	Fe^{3+}	${}^6\Gamma_1(s)\rightarrow{}^4\Gamma_4(G)$	Tetra	500	20000

One of the most interesting studies on co-ordination of Fe^{3+} in glass for this work was done by Kurkjian et al (1968), who reported Mössbauer, optical and electron magnetic resonance spectra for Fe^{3+} in phosphate and silicate glasses. They studied special glasses that had Fe^{3+} ions predominantly either in tetrahedral or octahedral sites.

The Fe^{3+} ions were predominantly in octahedral sites in *phosphate glasses* (Fig. 5.2.1) for which three peaks ($^6A_1(S) \rightarrow {}^4T_1(G)$, $^6A_1(S) \rightarrow {}^4T_2(G)$ and $^6A_1(S) \rightarrow {}^4E^4A_1(D)$) at 13500 – 13600 cm^{-1}, 18800 – 19250 cm^{-1} and at 23800 – 24400 cm^{-1} respectively, were obtained. The fourth peak ($^6A_1(S) \rightarrow {}^4T_2(D)$) at about 26000 – 27000 cm^{-1} was obscured in most of the cases by the intense UV-edge.

They mention that analysis of the Fe^{3+} spectra for *silicate glasses* was much more difficult, because the Fe^{3+} ions were in both octahedral and tetrahedral sites, the absorbance spectra of which overlapped each other and contained four absorption peaks each. For a 40soda-60silica glass (Fig.5.2.2) doped with 0.1 mol % Fe_2O_3 (0.088 moles/litre) they reported $^6A_1(S) \rightarrow {}^4T_2(D)$ at 370 nm (27000 cm^{-1}) with optical density a = 1.6. The $^6A_1(S) \rightarrow {}^4T_1(G)$, $^6A_1(S) \rightarrow {}^4T_2(G)$ and $^6A_1(S) \rightarrow {}^4E^4A_1(G)$ were obtained at 480 nm (20800 cm^{-1}) with a = 0.28, at 448 nm

(22300 cm^{-1}) with density 0.75 and at 425 nm (23550 cm^{-1}) with a = 0.59, respectively. These values are for the tetrahedral sites, which were found to be dominant.

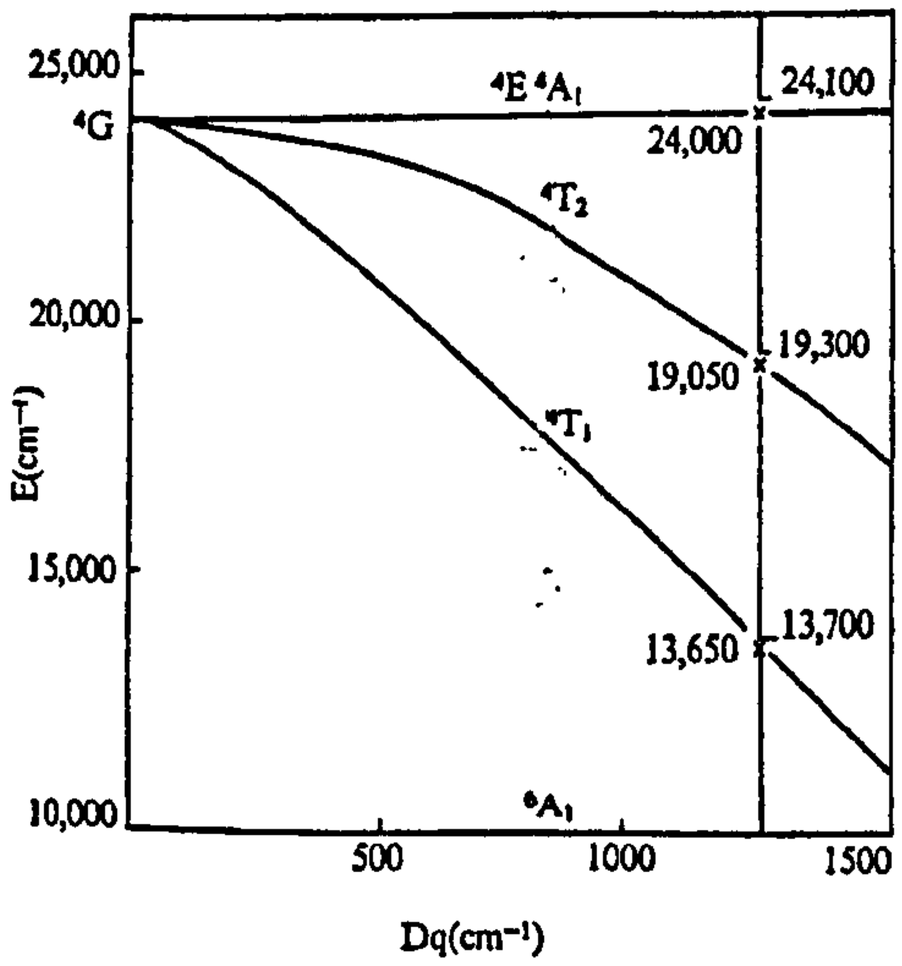

Fig.5.2.1 Energy level diagram for Fe^{3+} ($3d^5$, octahedral) with B = 900 and C = 3600 (C/B = 4.0). The calculated energies and those observed in a potassium-zinc-phosphate glass are shown for Dq = 1250 cm^{-1}. x calculated, - observed. (Kurkjian et al, 1968)

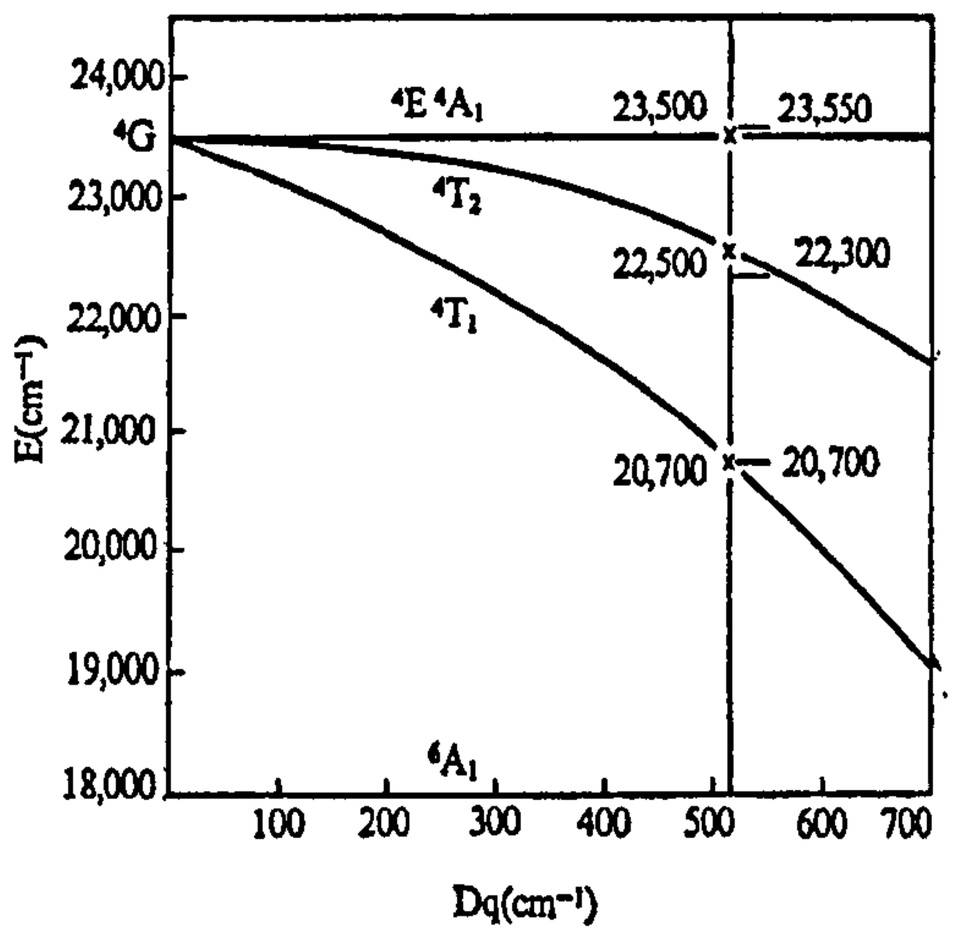

Fig. 5.2.2 Energy level diagram for Fe^{3+} ($3d^5$, tetrahedral) with B = 550, C = 3600 (C/B = 6.55). The calculated energies and those observed in a 40soda-60silica glass are shown for Dq = 515 cm^{-1}. The values for $^4T_2(D)$ are not shown. x calculated, - observed. Kurkjian et al, 1968).

The absorptivity of tetrahedral Fe^{3+} sites is usually an order of magnitude more than for octahedral sites. Kurkjian at el (1968) reported the ratios of absorptivities to be 7.5 for $^4T_2$ transitions, 3 for $^4T_1$ transitions and unity for $^4E^4A_1$ transitions. The percentage of octahedral sites in their sodium silicate glasses varied with iron concentration from 17 % at the added concentration of 0.1 mol % Fe_2O_3, to 9 % at 1.0 mol % Fe_2O_3, and to 30 % at 5.0 mol % Fe_2O_3. The amount of Fe_{oct}^{3+} was determined from the optical density at 650 nm (15400 cm^{-1}), assuming the octahedral sites in their 40soda-60silica glass had an almost similar size and ligand field strength to the octahedral sites of their phosphate glasses, an assumption that can be questioned. The optical basicity of the phosphate glasses is much lower than for the 40soda-60silica glass.

The 15soda-15lime-70silica glasses of this work are between the glasses of Kurkjian et al in optical basicity and other properties, and thus a slightly differing set of peak positions within a narrower wavenumber range for octahedral sites and an almost identical set for tetrahedral sites may fit for the test glasses of this work. (See next Chaps. 5.3 to 5.5).

In their discussions on tetrahedral sites, Kurkjian et al (1968) referred to Bates's thesis (1964) which concluded that for Fe^{3+} in tetrahedral sites in *potassium silicate glass* the peak assignments and positions were: $^6A_1(S) \rightarrow {}^4T_1(G)$ at ca. 19500 cm^{-1} (510 nm), $^6A_1(S) \rightarrow {}^4T_2(G)$

at 23000 cm^{-1} (435 nm), $^6A_1(S) \rightarrow {}^4E^4A_1(G)$ at 23800 cm^{-1} (420 nm), $^6A_1(S) \rightarrow {}^4T_2$ (D) at 26300 cm^{-1} (380 nm) with an unidentified broad band at 14000 – 20000 cm^{-1}.

Two broad absorption maxima have been obtained for Fe^{2+} ions at 9000 – 12000 cm^{-1} nm and at 4500 - 5000 cm^{-1}. Kurkjian (1970) discussed the splitting of the energy levels of Fe^{2+} ion ($3d^6$) in his Mössbauer study on iron doped glasses. Since his discussions, most researchers have attributed the Fe^{2+} band at 10000 cm^{-1} to octahedral sites. Burns (1993) described the energy levels of Fe^{2+} and other $3d^6$ ions, with the Orgel diagram (Fig. 5.2.3). He explained that the energy levels also split with a Jahn–Teller type of distortion, thus providing two absorbance peaks for octahedral sites, seen as a broadening of the band. Bates (1962, 1964), and later Ades et al (1990) and Bingham (2000), concluded that the band at 4500 cm^{-1} represented tetrahedral sites.

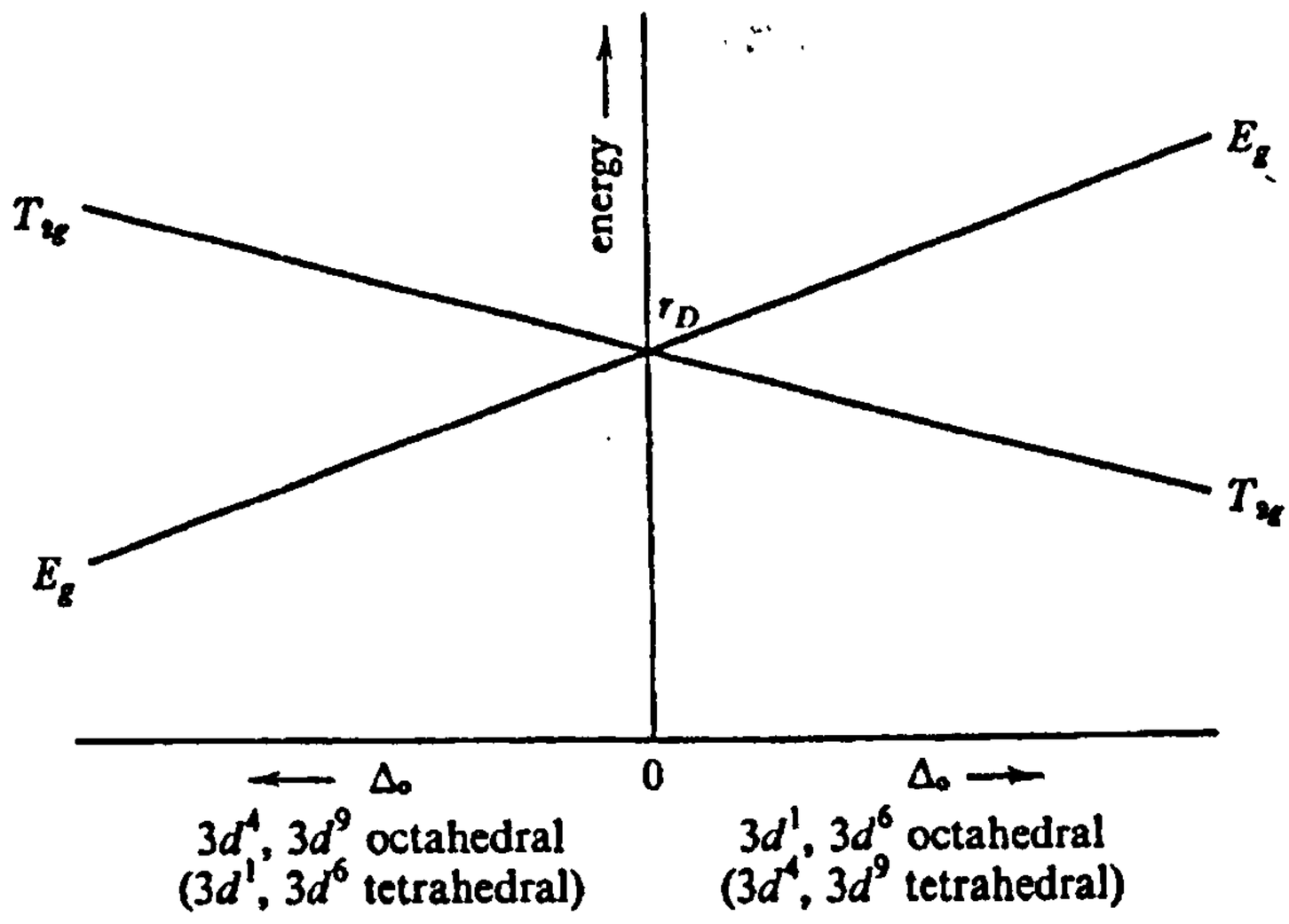

Fig. 5.2.3 Splitting of the energy levels of Fe^{2+} ($3d^6$, Orgel diagram), and similar energy level ions by symmetric cubic (in the middle) and non-symmetric octahedral and tetrahedral ligand fields (Burns, 1993, p. 60). A Jahn-Teller distortion, when applicable, will further split these energy levels.

5.2.2. Later studies on iron doped glasses

Fox et al (1982) suggested there are two kinds of tetrahedral sites of Fe^{3+} in high sodium glasses, for which they demonstrated a luminescence band consisting of two peaks at 16200 cm^{-1}, which was seen to move to 14600 cm^{-1} in low sodium glasses. They did not observe a luminescence band around 11500 cm^{-1} that would indicate the presence of Fe^{3+} in octahedral sites. They also suggested slightly different assignments for the Fe^{3+} absorption bands, but they did not fit Gaussian peaks to the data. Their background correction methods for either the UV-edge or IR edge are not described. From their data it can be deduced that they used some UV-

edge subtraction but did not subtract any IR-edge. Their absorptivity data at 10000 cm^{-1} (1,2 cm^{-1} for 0.5 mol % Fe_2O_3 added) and at 26000 cm^{-1} (0,8 cm^{-1}, for 0.5 mol % Fe_2O_3 added)), as well as the Fe^{3+} peaks seen in the spectra graphs at 15 mol % soda, agree with our results, see Chap. 5.4. The fitting of the spectra, however shows slightly, but systematically shifted peak positions.

Interestingly, Fox et al show a Tanabe-Sugano graph (Fig. 5.2.4, Fox et al, 1982), calculated with parameters B = 469 and C = 3689, and C/B = 7.87 for the bands of Fe^{3+}, that differs from the graphs of Kurkjian et al (1968, reproduced as Fig. 5.2.1 and 5.2.2 of this chapter). Fox has calculated the bands for a glass containing 15 weight % soda (close to the soda-lime-silica glass of this work), whereas Kurkjian et al did it for a disilicate glass with 40 % soda. The positions of the $^4T_2(G)$ and $^4T_1(G)$ bands are closer to each other at each Dq. This graph might fit better to the results of this work than Kurkjian's graph, even though the assignments of the observed bands in our data will differ from Fox's assignments, in common with Bingham's conclusions.

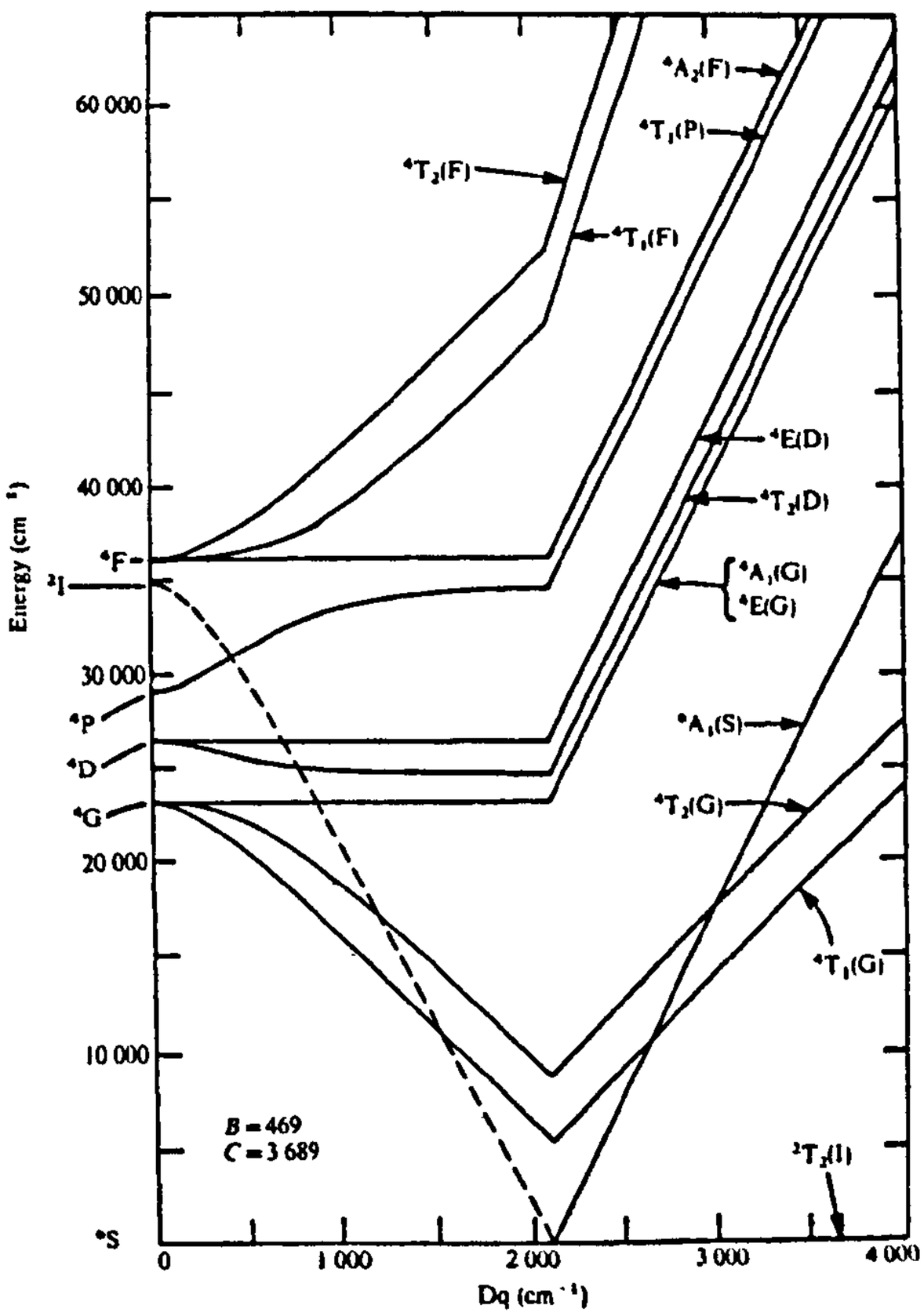

Fig. 5.2.4 Tanabe-Sugano diagram for Fe^{3+} ions in a Na_2O-5,67SiO_2 glass, according to Fox et al (1982).

Ades et al (1990) analysed the absorbance spectra in iron doped soda-lime-silica glasses at ambient temperature and at high temperatures. Actually the glasses also contained other species, such as MgO and Al_2O_3 as later reported by Traverse et al (1992). They fitted nine Gaussian peaks to the Fe^{2+} and Fe^{3+} spectra (Figs. 5.2.5 a and b and Table 5.2.1). They do not explain the origin of the Fe^{2+} peak No. 8 at about 7500 cm^{-1}, but give some hypotheses for it. Their peaks No 1 and 2 are common to both Fe^{3+} octahedral and tetrahedral sites. Thus they have four peaks for each of these sites for Fe^{3+} ions, one peak for Fe^{2+} octahedral sites and one peak for Fe^{2+} tetrahedral sites. They thus assume both kinds of configurations are present simultaneously in the glass as indicated in the EPR and Mössbauer analysis of Levy et al (1976).

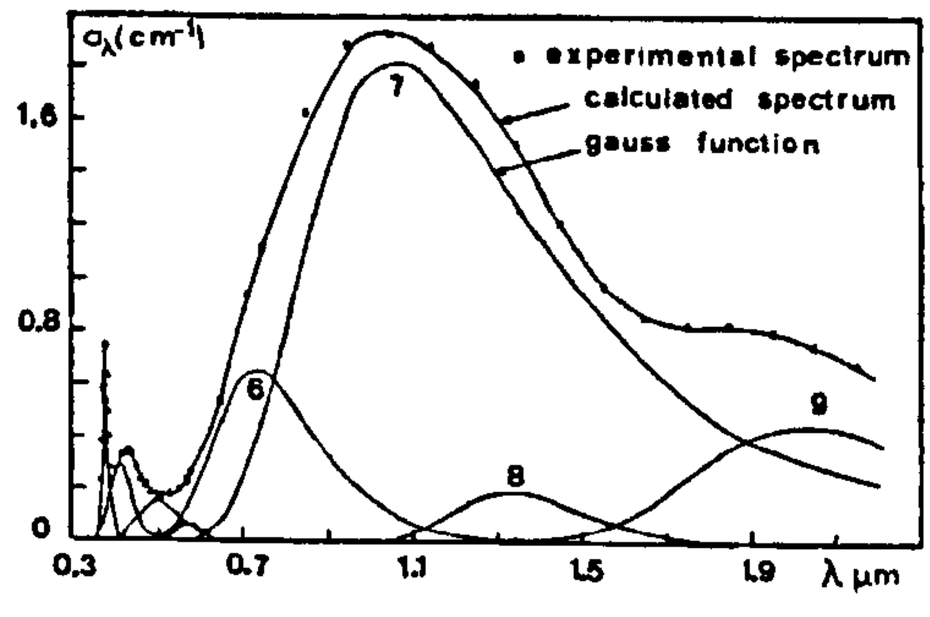

a

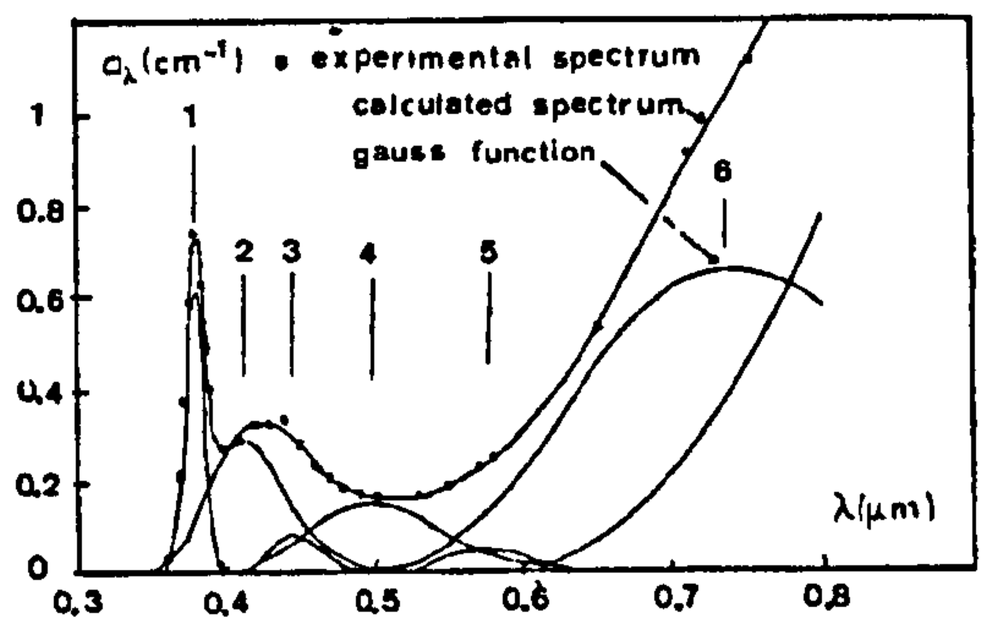

b

Fig. 5.2.5 a and b Fitted Gaussian peaks and their sum compared to the experimental iron absorption spectrum, according to Ades et al (1990).

Table 5.2.1. Assignment of the transitions to the absorption bands according to Ades et al (1990)

Band No	Ion	Transitions	Symmetry	Peak position λ, nm	Peak position ν, cm^{-1}
1	Fe^{3+}	${}^6\Gamma_1(s)\rightarrow{}^4\Gamma_5(D)$	octa-tetra	380.1	26307
2	Fe^{3+}	${}^6\Gamma_1(s)\rightarrow{}^4\Gamma_1(G)$	octa-tetra	412.5	24245
		${}^6\Gamma_1(s)\rightarrow{}^4\Gamma_3(G)$			
3	Fe^{3+}	${}^6\Gamma_1(s)\rightarrow{}^4\Gamma_5(G)$	Tetra	443.2	22563
4	Fe^{3+}	${}^6\Gamma_1(s)\rightarrow{}^4\Gamma_4(G)$	Tetra	496.6	20135
5	Fe^{3+}	${}^6\Gamma_1(s)\rightarrow{}^4\Gamma_5(G)$	Octa	574	17416
6	Fe^{3+}	${}^6\Gamma_1(s)\rightarrow{}^4\Gamma_4(G)$	Octa	737.2	13565
7	Fe^{2+}	${}^5\Gamma_5(D)\rightarrow{}^5\Gamma_3(D)$	Octa	1064	9396
8	Fe^{2+}	---	not identified	ca. 1330	ca. 7520
9	Fe^{2+}	${}^5\Gamma_3(D)\rightarrow{}^5\Gamma_5(D)$	Tetra	2040	4906

For Fe^{3+} Dq(octa) = 1370 cm^{-1}, Dq(tetra) = 672 cm^{-1}
For Fe^{2+} Dq(octa) = 941 cm^{-1}, Dq(tetra) = 491 cm^{-1}

They assumed that the proportion of [Fe^{3+} oct.]/[Fe^{3+} tet.] stays the same in all glasses independently of melting temperature. They studied low Fe concentrations (0,0202 – 0,179 mol/litre) and they quote the absorbance at 323 nm as a function of the total Fe concentration, and show a linear variation which gives an extinction coefficient 17,5 per (cm*mole*l^{-1}) (Ades, Fig. 3, p. 273). The absorbance at 323 is caused by the charge transfer bands of both Fe^{2+} and Fe^{3+} at 220 nm and 250 nm respectively. The concentration of Fe^{2+} ions in octahedral sites is plotted against the band height at 1060 nm, and a linear relationship is shown with a molar extinction coefficient 53,8 l $mol^{-1}cm^{-1}$ (corresponds to about 22 mol $\%^{-1}cm^{-1}$ with assuming the density of the glass is 2,5 kg/l). For Fe^{3+} in octahedral sites molar extinction coefficient 4,86 l $mol^{-1}cm^{-1}$ is obtained at 380 nm (corresponds to ca. 2,0 mol $\%^{-1}cm^{-1}$). The differences to Bamford 's (1977, p. 63 – 64) and Steele's (1965) values, e.g. 29 $mol^{-1}cm^{-1}$ at 1050 nm, are claimed to arise from the influence of the matrix, the charge transfer bands and the neighbouring bands, which they claim were not taken into account by Bamford. The errors associated with the measuring procedures and fitting statistics are discussed.

However, the fitting by Ades et al (1990) overlooked two issues. There is no evidence for their assumption that the proportion of [Fe^{3+} oct.]/[Fe^{3+} tet.] or [Fe^{2+} oct.]/[Fe^{2+} tet.] would not vary in the glasses with the melting temperature or oxygen pressure, because the content of Fe^{3+} is determined at 380 nm where both octahedral and tetrahedral Fe^{3+} have a peak, and the content of Fe^{2+} is determined at 1060 nm assuming only octahedral Fe^{2+} sites are present. There is no discussion or evidence that their fitted spectra scale with iron concentration. Also the analysis of the fitting of Fe^{2+} spectrum with three peaks at 9396, 4906 and 7000 cm^{-1} is not convincing. The Fe^{3+} peak at 13565 cm^{-1} is also questionable. It is a pity that Ades et al do not reveal the exact glass composition, melting or annealing conditions for their glasses; consequently our or other results cannot be compared to their data in detail.

In their later paper Traverse et al (1992) analysed further the same (Ades et al, 1990) and additional data. They explained better the inaccuracies in the determination of the [Fe], [Fe^{2+}] and [Fe^{3+}] concentrations by using the same methods as above. They claim a linear relationship between total iron content and concentration of both Fe^{2+} and Fe^{3+} ions by using simultaneous determination of them. A small error in one of them, however, can cause a problem for the other, because the sum, the total iron content is fixed. Actually, it is question of fitting of two parameters, both of which are uncertain.

They also claim consistency of the determined concentrations to better than 3 – 5 % accuracy for glasses doped with higher than 0.05 weight % Fe_2O_3, but do not reveal all the fitted Gaussian parameters used. They use the peak height at 380 nm as a measure for [Fe^{3+}]. The accuracy of this method is dependent on the quality and accuracy of the fitting of the UV peaks

(which is very challenging) and relies on the assumption that the proportion of Fe^{3+} ions in octahedral and tetrahedral sites is constant. As is later shown by Kukkadapu (2003) and this work (See Chap. 5 results), this may not be the case. Bingham (2000) used a similar fitting and background correction of optical spectra, and showed by Mössbauer spectroscopy and chemical analysis that the concentration of Fe^{2+} ions does not depend linearly on the concentration of added iron.

Bingham, 2000, 2001 and 2002 assumed that Fe^{3+} appeared in two states, but also assumed their proportion remained constant and fitted therefore both configurations together with a set of four common peaks. Furthermore, he suggested a shallow peak at 16000 cm^{-1} to be caused by intervalence charge transfer between Fe^{3+} and Fe^{2+} ions (Bingham 2000). He measured at very low absorbance level of about 0,2 either by using a low iron concentration or very thin samples, thus not necessarily having the best possible resolution in distinguishing the iron absorption data from the background or for fitting the data. He also used commercial SPSS software for fitting the peaks, and fitted the spectra in three sections, because the software does not resolve many peaks simultaneously. The same software was tried for fitting of the spectra of Cu-doped glasses of this work (Volotinen et al, 2004; Volotinen et al, 2005; Chap. 6), and was found to produce varying sets of data for overlapping peaks and could not resolve enough many peaks at one time. It can be, and needs to be, guided to find fitted peaks at proposed positions with proposed widths and heights, which makes it to an uncertain tool in fitting for multiple overlapping peaks.

Bingham showed that the fitted peak positions decrease linearly with increasing optical basicity of the host glass. He corrected for reflection losses by subtracting a constant absorbance (0.04) from the measured data over the wavelength scale 200 – 2500 nm. He corrected other background losses by subtracting the undoped host glass spectrum that was similarly reflection-loss-corrected and normalised to 1 cm thickness, thus assuming that the effect of the host glass and its contamination was stable. See further Chapters 5.4, 5.5 and 5.8 – 5.9 for the new fitted spectra and results of Bingham's soda-lime-silica glasses.

It is worthwhile mentioning that Hannoyer et al (1992) identified five absorbance peaks for Fe^{3+} in both tetrahedral and octahedral sites in their study on soda-lime-silica glasses. They however, did not fit the spectra. Bingham used the assignments of their paper as a guide for his conclusions.

5.2.3. Recent studies on iron doped glasses

Boulos etal (1997) and Glebov et al (1998) presented in many ways interesting results for iron and water absorption in a Na_2O-CaO-MgO-SiO_2 glasses. Their goals were identical to the goals of this work regarding the mathematical description of the iron absorbance spectra. In

their first paper on the study Boulos et al (1997) reported the Gaussian peak parameters for all water peaks at the wavenumbers below 4500 $cm^{-1}$and four peaks of ferrous iron at wavenumbers 3350 ± 50 cm^{-1}, 4934 ± 48 cm^{-1}, 7665 ± 100 cm^{-1} and 10785 ± 150 cm^{-1} for glasses melted in electric and gas furnaces. These numbers are close to the set of fitted peak positions obtained in this work, see Chaps. 5.4 – 5.9. They distinguished nicely the ferrous peak at 3350 cm^{-1} from the overlapping water peaks and IR-edge, but did not assign any of these peaks to any particular type of site, d-d transition or other meaning. They assumed a stable shape of the summed four ferrous peaks, thus assuming a linear scaling with iron concentration over the studied iron concentration range $5*10^{-4}$ – 0,9 weight % of added Fe_2O_3. The method to subtract the reflection and other surface losses is not described in detail.

In the later paper Glebov et al (1998) developed a mathematical description for the spectra of ferric ion and UV absorption peaks for both ferric and ferrous ions. Also in this study they started with an assumption that the shape of the Fe^{3+} spectrum including its UV-peaks, similarly as in their earlier study on the Fe^{2+} spectrum, is stable over the wavenumber range 3000 – 50000 cm^{-1}, meaning scale linearly with added Fe concentration over the wide range $8*10^{-4}$ – 0,9 weight % of Fe_2O_3 added to the glass. They used various sample thicknesses and fixed the data by an averaging calculation between the thicknesses, which method can be questioned. They also defined absorption coefficients at certain wavenumbers for both Fe^{2+} and Fe^{3+} spectra by comparison the data of two samples with different iron concentrations. They did not compare or calibrate their data with any other analysis method. Their obtained peak parameters and findings are further compared with the results of this work in Chap. 5.9.

Schirmer et al (2003) reported recently a high-temperature spectroscopic study of redox reactions in iron- and arsenic-doped soda-lime-silica glass melts. Increasing melting temperatures shift the UV absorption edge to longer wavelengths. All other bands, especially the Fe^{2+} band near 1100 nm, decreased in intensity at higher temperatures. For glasses, doped solely with iron, the temperature dependency of the extinction coefficient was quantitatively determined. Glasses doped with both arsenic and iron showed a different behaviour: the intensity of the bands decreased up to a temperature of 600 to 650 °C and then increased again. This can be described to a temperature dependent redox reaction: $2Fe^{3+} + As^{3+} \rightleftarrows 2Fe^{2+} + As^{5+}$. Increasing temperatures lead to a shift of the reaction to the right. This reaction is in equilibrium at temperatures > 650 °C and is frozen in at lower temperatures, depending on the respective iron and arsenic concentrations. The latter effects were explained by a numerical simulation assuming the redox reactions to be controlled by diffusion.

Schirmer et al (2003) also showed interesting absorption data for a 74 SiO_2 – 16 Na_2O – 10 CaO glass, which is reproduced in Fig. 5.2.6. They have not fitted or subtracted the IR edge or

the OH-peaks from the data for their fitting analysis, but their measured data looks similar to our data on iron doped glasses, and suggests there is an additional iron peak at wavelengths above 2000 nm, i.e. below the tetrahedral peak at 5000 cm^{-1}.

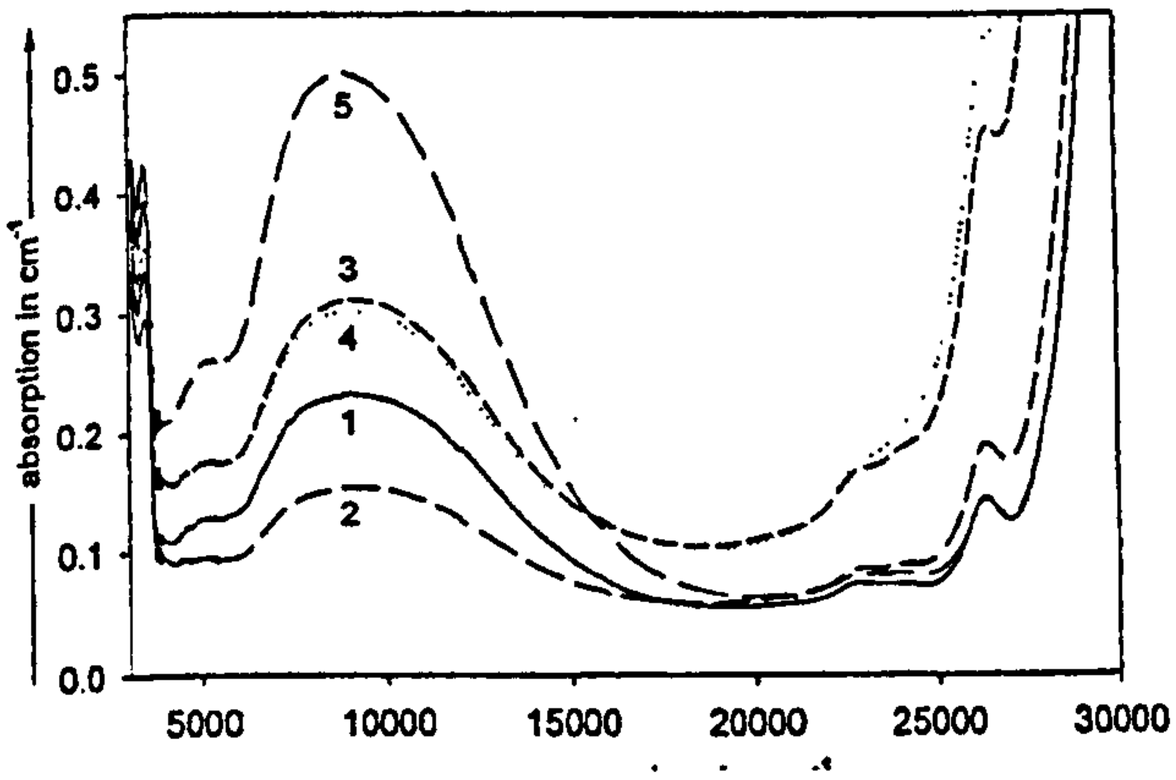

Fig. 5.2.6. Measured absorbance curves as presented by Shirmer et al.

The fitting analysis within the range 4000 – 19000 cm^{-1} is done in a similar way to that by Ades et al (1990) and Traverse et al (1992). They assume that the bands at 13000 and 17000 cm^{-1} belong to octahedral Fe^{3+} sites and the bands at 4000 and 9000 cm^{-1} to the Fe^{2+} tetrahedral and octahedral sites respectively. They do not, in common with Ades and Traverse, explain the fitted peak at 7500 cm^{-1}, even though they have included it in their fitting.

Kukkadapu et al (2003) also reported recently Mössbauer and optical spectroscopy studies of temperature and redox effects on iron local environments in Fe-doped (0.5 mol % Fe_2O_3) doped silicate glass (Fig. 5.2.7). The glass was a 18soda-72silica type of Owens-Illinois glass, containing about 10 % of other oxides. The intensities of both the Fe^{2+} bands at 1200 and 2020 nm (Fig. 5.2.7) increased with temperature in the samples melted in air. The intensity ratio between the peaks remained constant. However, a small difference is seen between the glass melted at the lowest (1300 °C) and highest (1600 °C) temperatures. Similarly, the peak heights depended on the melting conditions, being lowest for 12CO:88CO_2 conditions and highest for the most reducing 50CO/50CO_2 condition at 1500 °C. The ratio between the bands changed slightly.

However, they did not comment on the absorption above 2500 nm which also seemed to vary together with the intensity at 2020 nm Furthermore, a non-linearly varying Fe^{3+} level is reported for glasses melted at varied, reducing, CO/CO_2 conditions. A difference resulting from a Fe^{3+} site configuration change could be an explanation. There might also be some uncertainty in their UV-edge subtraction and no IR-edge background correction was made. They do not mention subtracting any reflection losses before normalising to thickness and they used non-

iron containing base glass absorption spectrum as a background. -It is difficult to make a suitable base glass under laboratory conditions. It is probable that a minor amount of iron was included in the base glasses as contamination, and their Fe^{2+} and Fe^{3+} UV-peaks therefore might have been included in the baseline data.

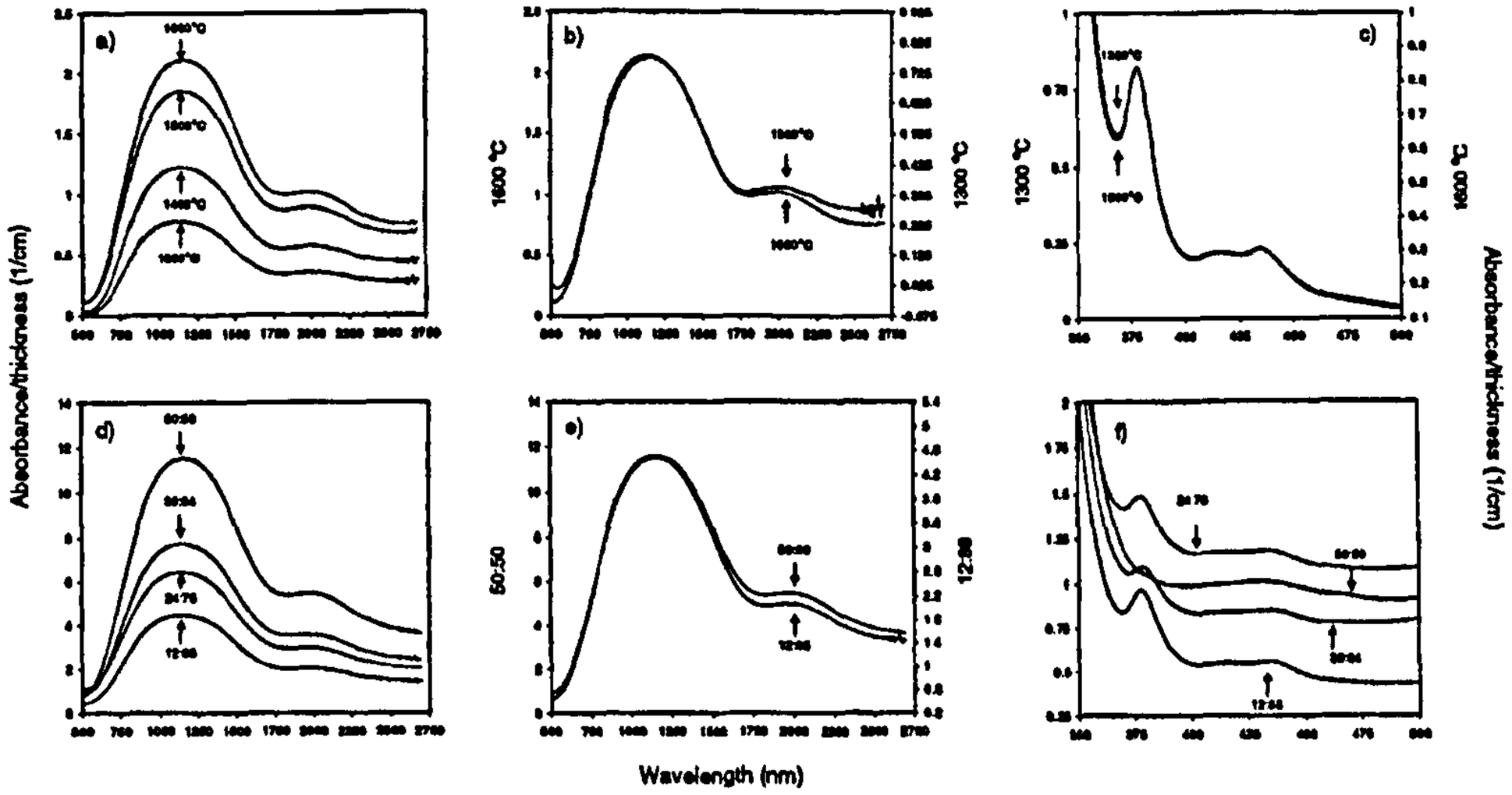

Fig. 1. UV–VIS–NIR spectra: (a) temperature effects on 1120- and 2020-nm band intensities for glasses melted between 1300 and 1600 °C in air, (b) little independent temperature effect on 1120- and 2020-nm band intensities for glasses melted between 1300 and 1600 °C (with two extreme cases), (c) no effect on UV absorption bands (with two extreme cases), (d) oxygen partial pressure effect on the 1120- and 2020-nm band intensities for the reduced glasses melted at 1500 °C under 12.3 ($12CO/88CO_2$) to 0.27×10^{-7} ($50CO/50CO_2$) atmosphere, (e) little independent temperature effect on 1120- and 2020-nm band intensities for the reduced glasses (with two extreme cases), (f) oxygen partial pressure effect on UV bands for the reduced glasses.

Fíg. 5.2.7. Kukkadapu's results (2003).

A more significant problem for the analysis, however, is the fact that there are intense Fe^{2+} and Fe^{3+} UV- peaks included in the Fe^{3+} data, and only a minor portion of the UV absorbance has been included in the baseline data. Apparently they did not fit the background loss or the iron spectra. So their findings, especially concerning variation of the Fe^{3+} spectrum, can be affected by the redox between Fe^{2+} and Fe^{3+} ions, i.e. can be questioned. The Mössbauer data of Kukkadapu et al (2003) do not prove or disprove the possibility that Fe^{2+} would appear in two kinds of sites. However, they prove that Fe^{3+} appears in both octahedral and tetrahedral sites.

Their conclusions support thus the coexistence of Fe_{oct}^{2+}, Fe_{tet}^{3+} and Fe_{oct}^{3+} environments in the glass samples. Specifically, the Mössbauer Fe^{3+} sextet represents isolated octahedral ferric ions (with a wide distribution), and the feature is related to the 375 nm optical band. The Mössbauer doublet primarily represents tetrahedral ferric ions, which is related to 415, 435 and 485 nm optical bands (that is similar to Kurkjian's data). Finally, the Fe^{2+} doublet represents octahedral ferrous ions with varying distortions, which is claimed to be related to the optical bands near 1120 and 2020 nm. It was also concluded from the study that ca. 10 % of the Fe^{3+}

exists in tetrahedral coordination in all the samples, a fraction that appears to be stable over the changes of melting temperature and oxygen partial pressure. The increase in the Fe_{oct}^{2+} content in the reduced samples was concluded to be solely due to reduction of the Fe^{3+} ions in octahedral sites. - These three latter inconsistent statements can be questioned. They are mentioned here as examples of the variation of statements and findings reported even in the recently published literature. For a more detailed discussion see Kukkadapu et al (2003).

Very recently Zawada et al (2005) reported that both Fe^{2+} and Fe^{3+} ions occurred in tetrahedral configuration in soda-lime-silica glasses melted in oxidising conditions, whereas also in octahedral configuration in the glasses melted in reducing conditions. They found also that the properties: density, microhardness, glass transition temperature and thermal expansion coefficient of the glass are dependent on the iron concentration and redox equilibrium.

An additional absorption peak at around 4000 – 3000 cm^{-1} (above 2500 nm) can be deduced from Zawada's absorption spectrum data for Fe^{2+} (Zawada et al, 2005). A slight difference in the peak heights of the Fe^{2+} peaks at 1000 and 2000 nm (at about 10000 and 5000 cm^{-1}) between reduced and oxidized glasses is seen. They conclude that this is evidence of a change in coordination number, i.e. in the structure of Fe^{2+} ion surrounding.

It can be summarised from the presented literature study that the absorbance spectrum of iron ions vary with glass composition, melting and annealing conditions. In addition to a redox ratio change between Fe^{2+} and Fe^{3+} ions, also the fractions of octahedral and tetrahedral sites may change. The separation and subtraction of the background losses from the iron absorbance spectrum seems to be very difficult, because many different ways have been used. No such fitting parameter sets are proposed that had been shown to scale with iron concentration.

The fitting parameter set originally presented by Ades et al (1990) have been used by many authors but only one fitted spectrum for per glass composition has been shown in each paper. Their fitting method does not separate the spectra of the octahedral and tetrahedral Fe^{3+} or Fe^{2+} sites. Many more conclusions could be drawn from the previous studies. – However, the most important conclusions for this work are: the fitting method to be developed should separate properly and accurately the iron absorbance from the significant background and surface losses and the spectrum parts for each Fe ion and each type of site should be separable. The summed fitted spectrum should scale with iron concentration.

5.3 Experiments of Fe-doped glasses

Iron has been studied as a single dopant at concentrations 0,05 – 1,5 mol % in soda-lime-silica glass, refined with 0,35 mol % sodium sulphate and melted at 1450 °C in both electric and gas-fired furnaces.

In order to test the fitting and in particular the scaling with concentration, absorption spectra were measured and fitted for a selected series of Fe - doped soda-lime-silica glasses melted in electric (Annex 1, glasses marked with "NCS/Ew" or "NCS/Es", such as Glasses 145, 193, 245, 246, 247 and 248) and gas-fired furnaces (Annex 1, glasses marked with "NCS/G" and "NCS/Gw", such as Glasses 81, 82, 83, 130, 141, 242, 225 and 228). The undoped Glasses 97 and 181 and a few others were also studied.

A selected series of Fe-doped soda-lime glasses were studied by Bingham in his PhD thesis (2000): PAB2ash, PAB35a, PAB16a and PAB24a. These glasses have the same composition as the soda-lime-silica (NCS) glasses of this work, but were prepared without sodium sulphate. The Fe-concentration varies from 0,2 to 2 mol %. The absorbance spectra were re-measured on the samples studied by Bingham in his thesis (2000). These spectra were re-fitted, in particular, to find out the effect of the thinner sample thickness, and whether the fitted spectra apply to his type of NCS glasses and scale similarly with Fe concentration.

The effects of the refiner Na_2SO_4 with varying sulphate content were also studied to fit the peaks of Fe-S chromophores appearing in sulphate- refined reduced glasses (Annex1, Table A2, Glasses 181, 225, 226, 227, 228, 229 and 242). Iron absorbance at a contamination level (below 0,1 mol % Fe ions) was studied with undoped glasses prepared at various purity levels of iron and at low iron doping concentrations with Glasses 1, 2, 9, 26, 97, 235, 196, 225 – 229, 242 and 245 (Annex 1, Table A2).

Iron was also doubly doped with all other transition metal colorants studied, and the glasses were melted in an electric furnace and had the same 15soda-15calcia-silica matrix (NCS). The study with Cu is reported in Chap. 6. The purpose is to prove the applicability of the iron fitting for the analysis of a doubly doped glass and to study the mutual redox between Fe and Cu.

The details of experimental procedures, sample preparation and analysis methods are given in Chaps. 2 and 3. The glass compositions calculated from the batch composition as well as the melting conditions and annealing procedures are given for each glass in Annex 1.

Diffuse reflection spectra were measured at wavelengths 180 – 800 nm on the Fe-doped samples of this work and Bingham's in order to find out roughly the positions, widths, shapes and relative height proportion of the charge transfer peaks of Fe^{2+} and Fe^{3+} ions.

The received glass compositions and Fe-concentrations were measured by SEM EDAX by P. Bingham for the some of the Fe-containing glasses (Annex 3). The glass compositions and contamination levels of iron received in gas furnace melted and electric melted samples were studied by XRF analysis for a few samples (Annex 3). The fitted results on Fe^{2+} and Fe^{3+} ion concentrations were also compared with the results of the wet chemical analysis, carried out on the Bingham's glasses (Bingham, 2000, p. 101). The calibration method used for the fitted spectrum is described in Chap. 5.4.

5.4 Fitting of Fe absorbance spectrum

5.4.1. Fe absorbance spectrum and fitting method

The first goal of this study of iron doped glasses is to find an accurate fit to the spectrum, which scales linearly, or at least systematically, with iron concentration for the absorbance spectrum at iron concentrations below 0,5 mol % (= roughly 0,7 weight %) Fe_2O_3 in the studied glasses. The fitting will be used for background correction of iron contamination and for mutual redox studies with other colouring ions. Even though there was a considerable guidance from the available literature data (Chap. 5.2), fitting the 42 parameters required to describe the 14 peaks (1 + 1 UV-peaks, 2 + 2 Fe^{2+} peaks and 4 + 4 Fe^{3+} peaks) was a great challenge, particularly so that the absorbance spectra of the same host glass doped with various iron concentrations could be fitted by adjusting the concentration multipliers for both ions and possibly the proportions of the octahedral and tetrahedral sites for both Fe^{2+} and Fe^{3+} ions. The scaling with iron concentration is not linear over a wider concentration scale, as can be concluded from the literature survey in Chap 5.2, but is shown in the following to be so over a limited concentration range. A few more fitting functions would be needed to describe how the sets of peaks are linked to redox reactions of the ions and sites in a soda-lime silica glasses prepared in various ways.

At first "the best fit so far" is presented for the low Fe concentration Glasses 245 and 246 doped with 0,1 and 0,2 mol % Fe_2O_3 (See Annex 1 for the compositions and preparation information) respectively (Figs. 5.4.1, 5.4.3 and 5.4.4). These 15soda-15calcia-70silica-0.35sulphate glasses were melted in an electric furnace at 1450 °C for 5 hours, stirred for four hours, subsequently annealed for one hour at 540 °C and cooled at a rate of 1°C/min to room temperature. Sample preparation and measurement are described in Chaps. 2 and 3.

The absorbance spectra of these glasses, from which the reflection loss has been subtracted and the data have been normalised to 1,00 cm thickness, are shown in Figs. 5.4.1 and 5.4.2. The received absorbance of Fe in Glass 246 is twice the Fe absorbance in Glass 245 (Fig. 5.4.1), except for the area of the water peaks and IR-edge at wavelengths above 2200 nm. So the iron absorbance scales perfectly with the iron concentration.

The reason for the difference above 2200 nm is an almost similar amount of the bound water of the glasses, independent of the iron content. The slight variation of the water content is a typical feature of these kinds of glasses melted in normal laboratory conditions in an open crucible in the open air electric furnace. The water content, which has diffused into the glass batch and during melting into the glass, is dependent on the humidity of the ambient air.

On the other hand, Glasses 247 and 248 doped with 1,0 and 2,0 mol % Fe_2O_3 (Fig. 5.4.2), prepared similarly to Glasses 245 and 246, do not show linear scaling with Fe concentration. Clearly Glass 248 has a lower Fe^{2+} band near 1100 nm indicating a different redox ratio $[Fe^{2+}]/[Fe^{3+}]$ compared to Glass 247 containing half of the iron concentration of Glass 248. The fitting of Glasses 247 and 248 and other high iron concentration glasses are described in Chap. 5.4.5.

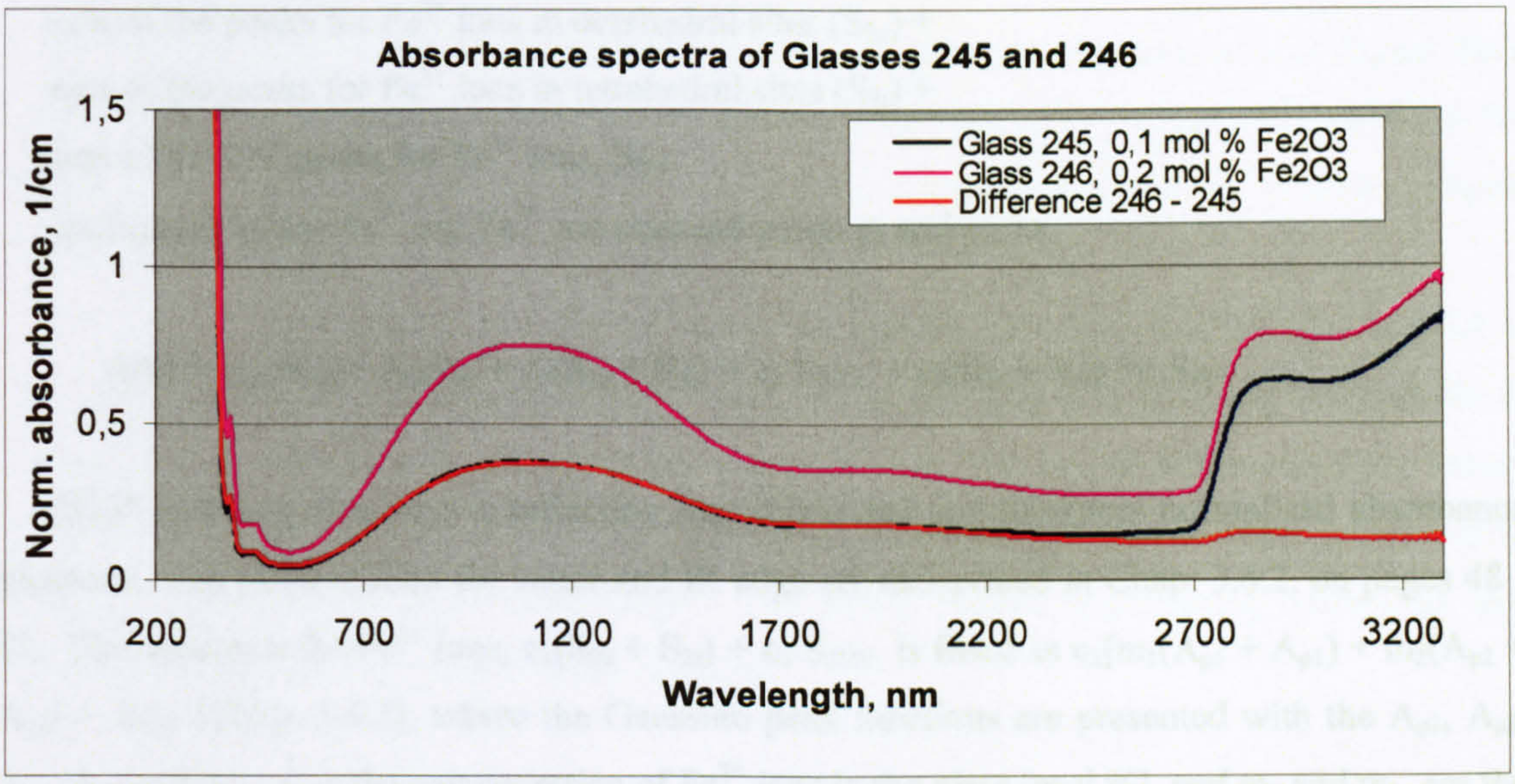

Fig. 5.4.1 Reflection loss corrected and thickness-normalised absorbance spectra of Glasses 245 and 246, doped with 0,1 and 0,2 mol % Fe_2O_3 respectively.

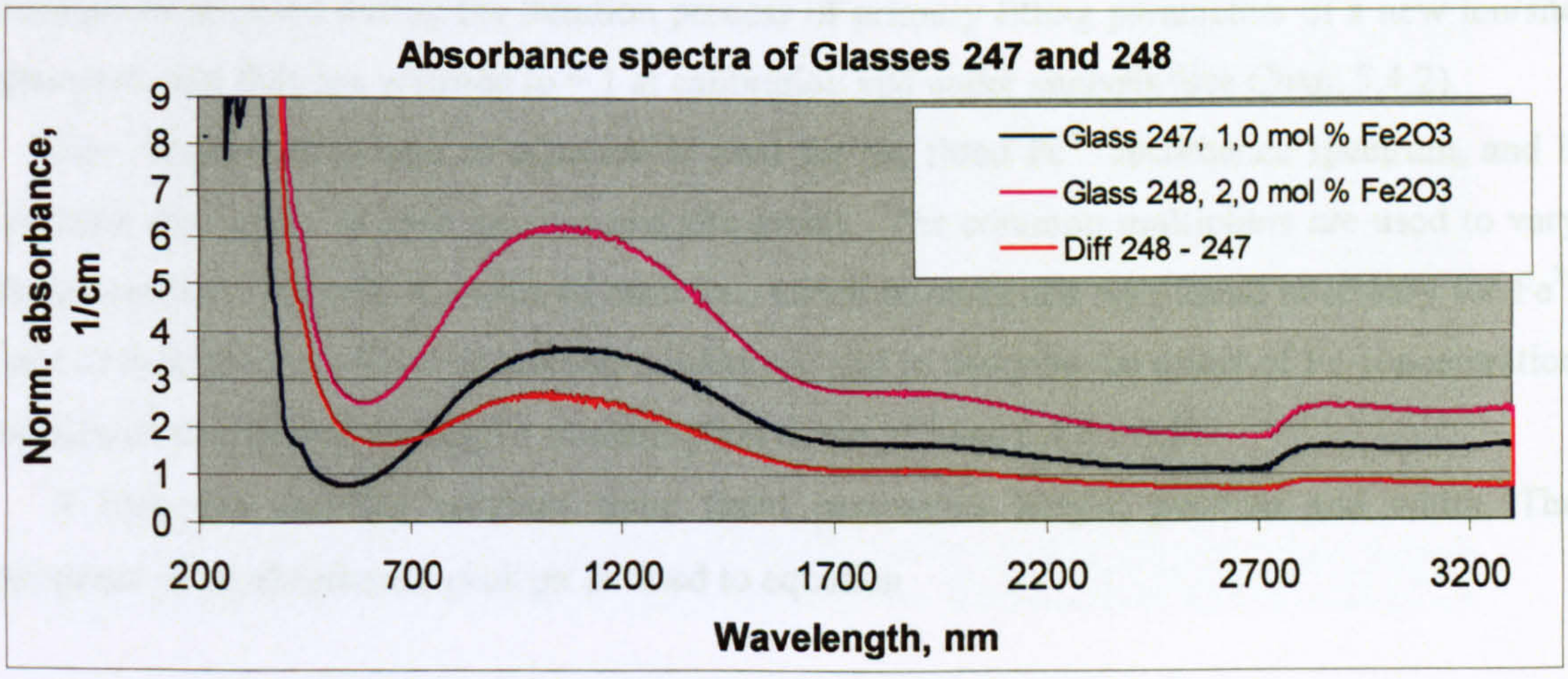

Fig. 5.4.2 Reflection loss corrected, normalised absorption spectra of Glasses 247 and 248, doped with 1,0 and 2,0 mol % Fe_2O_3.

The optical absorbance spectrum A(λ)* of a Fe doped soda-lime-silica glass can be accurately described mathematically on a wavenumber scale, i.e. on an energy scale, as A(ν), where $\nu = 1/\lambda$. The spectrum A(ν) is fitted as a sum of the parts of the spectrum:

OH-related absorbance (called water) and IR-edge ($c_{OH}S_{OH} + c_{IR}S_{IR}$) +

sum of the peaks for Fe^{2+} ions in octahedral sites (S_{2o}) +

sum of the peaks for Fe^{2+} ions in tetrahedral sites (S_{2t}) +

sum of the UV-peaks for Fe^{2+} ions, S_{2UV}

sum of the peaks for Fe^{3+} ions in octahedral sites (S_{3o}) +

sum of the peaks for Fe^{3+} ions in tetrahedral sites (S_{3t}) +

sum of the UV-peaks for Fe^{3+} ions, S_{UV}

multiplied by the Fe^{2+} and Fe^{3+} ion concentrations c_2 and c_3, i.e.

$$A(\nu) = c_{OH}S_{OH} + c_{IR}S_{IR} + c_2(S_{20} + S_{2t}) + c_2 S_{2UV} + c_3(S_{30} + S_{3t}) + c_3 S_{3UV}.$$

A(λ)* and thus also A(ν) is reflection loss subtracted and thickness normalised absorbance spectrum. The fitted spectra for water and IR edge are de3scribed in Chap. 3.6.2, on pages 48 - 51. The spectrum for Fe^{2+} ions, $c_2(S_{20} + S_{2t}) + c_2 S_{2UV}$, is fitted as $c_2[m_1(A_{p5} + A_{p1}) + m_2(A_{p2} + A_{p3}) + A_{p4}]$ (Chap. 5.4.3), where the Gaussian peak functions are presented with the A_{p1}, A_{p2}, A_{p3}, A_{p4} and A_{p5}, c_2 is the concentration of Fe^{2+} ions in the glass [mol %], and m_1 and m_2, are the common multipliers for the peak heights of each valence and type of site within Vis- Near IR range (Table 5.4.1, Fig. 5.4.5, p. 85). The peak p4 represents the UV-peak. The common multipliers are used during the iteration process of primary fitting parameters of a new ion/site spectrum, and they are adjusted to = 1 at calibration and under analysis (see Chap. 5.4.2).

The corresponding type of equation is used for the fitted Fe^{3+} absorbance spectrum, and it contains four peaks in each valence and site group. The common multipliers are used to vary the proportions between the sites of each ion, which in particular was found necessary for Fe^{3+} ions to describe the effects of melting conditions, and to describe the effect of Fe concentration outside of the linearly scaling Fe concentration range. (Chaps 5.4.4 – 5.8)

A Gaussian function contains three fitted parameters height, position and width. The spectrum of an absorbance peak px is fitted to equation

$$A_{px}(\nu) = \alpha_{px} * \exp\left(\frac{(-1*(\nu - \nu_{0px})^2)}{2*\Delta\nu_{px}^2}\right),$$

where ν is the wavenumber in cm^{-1}, α_{px} is the peak height at unit concentration, in 1/(cm*mol %), ν_{0px} is the peak position in cm^{-1} and $\Delta\nu_{px}$ is the peak width (= √2 * half width at half maximum) in cm^{-1}. The frequency scale of wavenumbers (1/wavelength) is used instead of wavelengths, because the transition energy distribution is considered.

Gaussian peaks are used, because they fit well, and because a normal distribution of ligand field strengths are assumed within the sites of the same type, due to thermal, dimensional and structural inhomogeneity of the glass structure. The widths of the peaks describe the distribution of the variation of the transition energies (caused by the site dimensional and ligand field strength variation in the glass), are seen in the following results to correspond roughly to the slopes of the ligand field theory (e.g. Fig. 5.2.1 and 5.2.2 (from Kurkjian et al, 1962) and Figure 22 of Fox et al, 1982).

Examples of the fitted spectra of iron doped NCS glasses are given in Figs 5.4.3 and 5.4.4. The fitted sum spectra of Glasses 245 (Fig. 5.4.3) and 246 (Fig. 5.4.4) agree almost perfectly to the measured, normalised and reflection loss corrected data. The overall differences (also shown in the graphs) are of the size of the measuring repeatability, i.e. less than ± 0,005 absorbance in a 3000 – 29000 cm^{-1} wavenumber range. The fitting method, parameters, calibration and accuracy are discussed in the next three chapters.

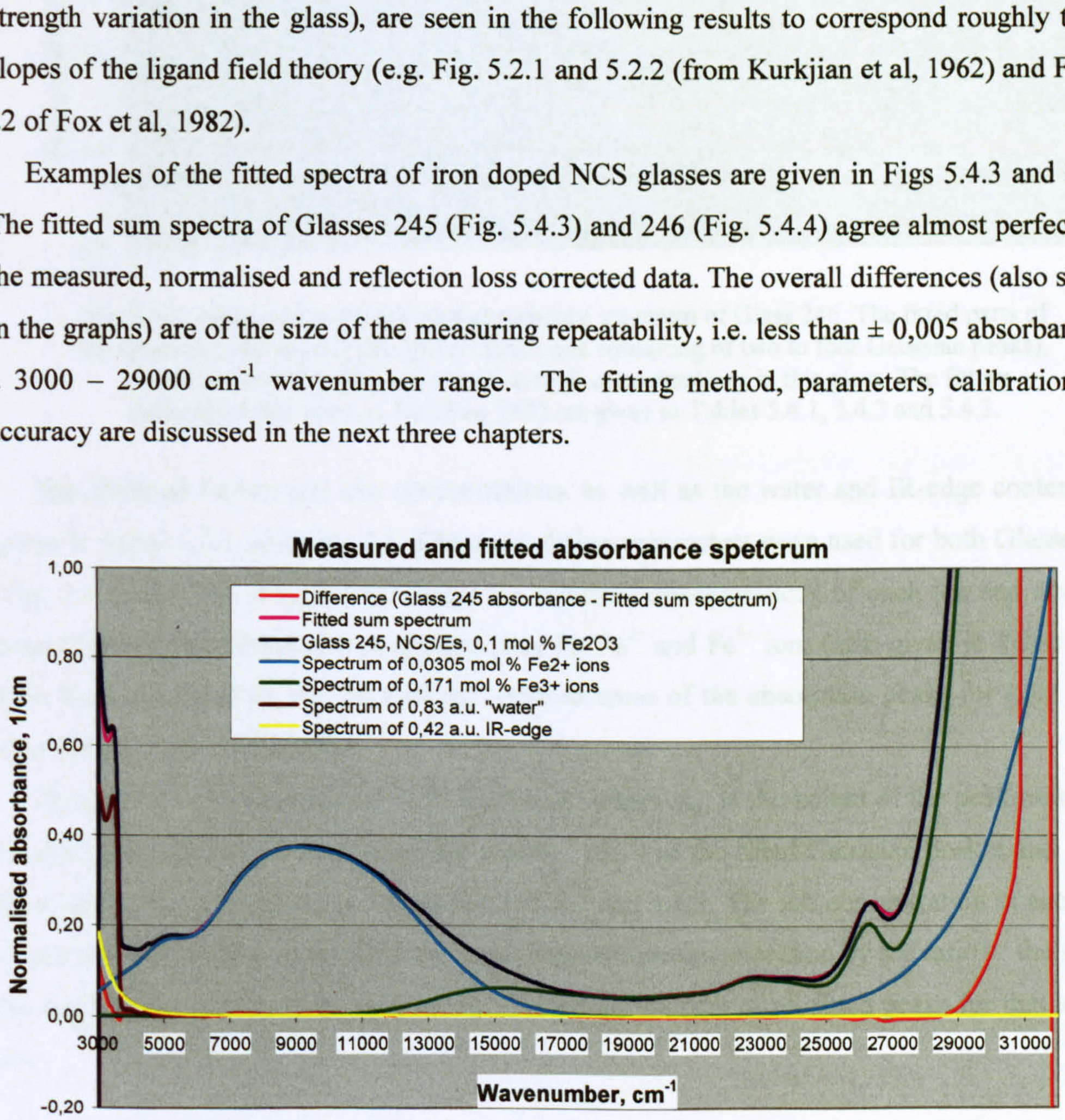

Fig. 5.4.3 Measured and fitted absorbance spectrum of Glass 245 and the difference curve are shown for NCS Glass 245 doped with 0,1 mol % Fe_2O_3. The summed, fitted parts of the spectrum, i.e. the spectra of Fe^{2+} ions, Fe^{3+} ions, water and IR-edge are shown. The fitting parameters are given in Tables 5.4.1, 5.4.2 and 5.4.3 and the fitted ion and site concentrations in Table 5.5.1.

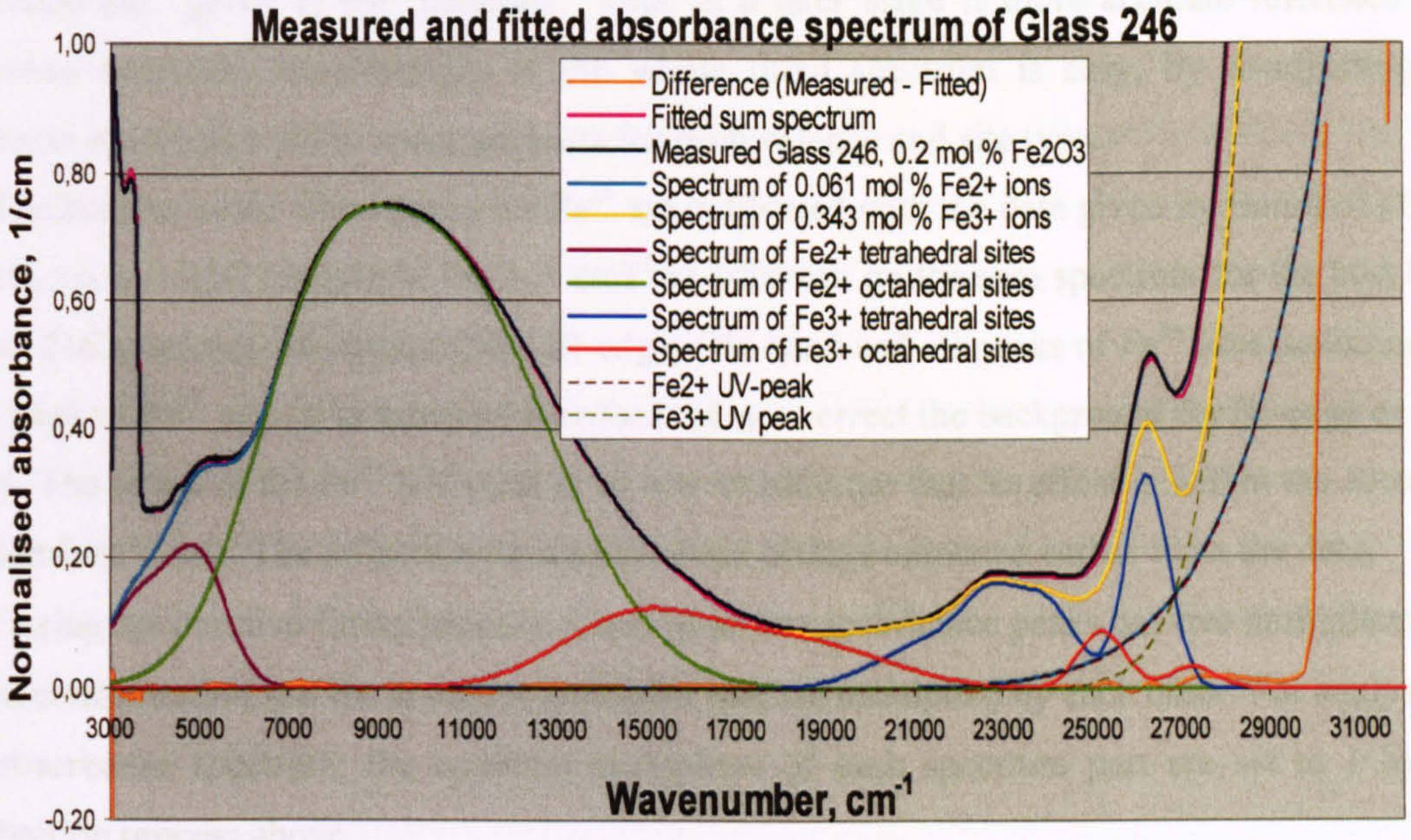

Fig. 5.4.4 Measured and fitted sum absorbance spectrum of Glass 246. The fitted parts of the spectrum, the ion and site spectra (each one consisting of two to four Gaussian peaks), as well as the UV-peaks, are shown at their concentrations in this glass. The fitting parameters (the same as for Glass 245) are given in Tables 5.4.1, 5.4.2 and 5.4.3.

The obtained Fe-ion and site concentrations, as well as the water and IR-edge contents are given in Table 5.5.1, in Chap. 5.5. The same fitting parameters were used for both Glasses 245 (Fig. 5.4.3) and 246 (Fig. 5.4.4), except the obtained concentrations of each ion and site. The proportions of tetrahedral and octahedral sites for Fe^{2+} and Fe^{3+} ions (also given in Table 5.5.1) have been estimated on the basis of the summed areas of the absorption peaks for each of the sites (Chaps. 5.4.2 and 5.4.3).

The peak area is proportional to ($\approx \alpha_{px} * {}_{\Delta}\nu_{px}$), where α_{px} is the height of the peak number x, i.e. the linear absorption coefficient (as mol $\%^{-1}$ cm^{-1}) of the fitted Gaussian peak x and ${}_{\Delta}\nu_{px}$ is the width of the peak given in Tables 5.4.1, 5.4.2 and 5.4.3. The ion concentration in each type of site is calculated by multiplying the total obtained ion concentration by the ratio = the sum of the areas of the peaks of that kind of site divided by the sum of all fitted peaks for that kind of ion.

5.4.2. Calibration of the fitted peak heights

The calibration procedure for the peak heights and multipliers for the combined fitted spectrum (Figs. 5.4.3 and 5.4.4) was complex and was done iteratively searching for a fit that would apply at least to glasses with three different iron concentrations. Because wet chemical analysis results on the glasses of this work were not available, the peak heights, i.e. linear

absorption coefficients [1/(mol % * cm)], are calibrated to agree to a single optical density value at 10000 cm^{-1} given in the literature. Thus in a later stage if more accurate reference data becomes available, re-calibration of the whole fitted spectrum is easy, by re-adjusting the common multipliers of the spectrum parts for each valence and site type.

The heights of the fitted peaks for Fe^{2+} are calibrated with the data given by Bamford (1977, p. 64), i.e. a = 9,00 (weight % Fe_2O_3 * cm)$^{-1}$ at 1000 nm on the sum spectrum for the best fit to Glass 246 spectrum consisting of the IR-edge, OH-band and all peaks of Fe^{2+} ions including the UV-peak of Fe^{2+} ions. It is assumed Bamford did not correct the background for IR-edge or OH-band. The effect of the Fe^{2+} UV-peak is so low at 1000 nm that its effect is within the accuracy of Bamford's data. The reflection losses have been always extracted earlier from the data.

During the iterative fitting process, a sum of an ion absorbance peaks has two multipliers, the fitted concentration and the common multiplier that are multiplied by each other. For analysis of an absorbance spectrum, the common multipliers of each spectrum part are set to 1 by the calibration process above.

The calibration of the iron absorbance spectrum is done in the following steps:

1. The sum of Fe^{2+} peaks that fits well to three Glasses 245, 246 and 145 is adjusted to have a common multiplier = 1.
2. The concentration multiplier of the Fe^{3+} ions (including Fe^{3+} UV-peak) is given the value zero (= 0,000).
3. The concentration multiplier of the Fe^{2+} spectrum is given the value 0,7556 mol % of Fe^{2+} ions, corresponding to 1 weight % of Fe_2O_3 added to these glasses.
4. Then the common multiplier of the Fe^{2+} ions is re-adjusted so that the sum absorbance A of the whole synthesized spectrum at 1000 nm (10000 cm^{-1}) becomes A = 9,000. The IR-edge, OH-band and Fe^{2+} spectra are included.
5. The common multiplier of Fe^{2+} spectrum is then re-re adjusted to = 1, by multiplying the fitted peak heights by a common factor, such that the synthesised spectrum absorbance A at 10000 cm^{-1} remains as 9,000.
6. The Fe^{3+} spectrum, including its UV-peak is then calibrated by iterative fitting to Glasses 245 and 246, so that the concentration multiplier of Fe^{3+} ions takes the value = [added Fe-ions] – [the received Fe^{2+} ions] + 0,015 mol %. The 0,015 mol % is an average addition of Fe ions received from the raw materials to a NCS glass melted in Pt crucible in an electric furnace (Annex 3). For NCS glasses melted in mullite crucibles in gas furnace 0,07 mol % Fe ions are added, and some variation between glasses is found (Annex 3). The common multiplier of Fe^{3+} ions is re-adjusted to 1 by re-adjusting the final peak heights to give the best fit to the data.

For the Fe doped NCS glasses of this work (Chap. 5.4.3) the fitted sum absorbance of the d-d transition peaks of Fe^{3+} ions at 380 nm is 0,746 (cm*weight % Fe_2O_3)$^{-1}$, and the sum of full Fe^{3+} ions spectrum including the UV-peak (i.e. the optical density) is 0,900 (cm*weight % Fe_2O_3)$^{-1}$, which is significantly less than 1,27 (cm*weight % Fe_2O_3)$^{-1}$ as given by Bamford (1977, p. 63). It suggests that the UV-peaks and reflection loss may have been subtracted differently. The corresponding Fe^{3+} sum absorbance at 380 nm, i.e. the linear absorption coefficient, a_1(380 nm) = 1,19 (cm*mol %)$^{-1}$ with the UV-peak included and 0,94 (cm*mol %)$^{-1}$ without the UV-peak (Chap. 5.4.4, Fig. 5.4.6). The UV-peaks and background losses have been subtracted in various ways in the literature, and various numbers for the absorption coefficient at this wavelength are thus reported (Chap. 5.2). The received extinction coefficients of Fe^{2+} defined at the band absorbance at 1000 nm are around 29 – 33 litre/(mol*cm), i.e. agree with the data of Bamford (Chap.5.5) as is expected.

Ades et al (1990) and Traverse et al (1992) reported much higher extinction coefficients in a different silicate glass. They report a molar extinction coefficient for Fe^{2+} ions at 1060 nm 53,8 l mol^{-1}cm^{-1}. For Fe^{3+} their molar extinction coefficient was 4,86 l mol^{-1}cm^{-1} at 380 nm. Also Bingham (2000) reported similar size of values for various silicate glasses. The differences are discussed in Chap.5.5.

5.4.3. Fitting of the spectrum of Fe^{2+} ions, octahedral and tetrahedral sites

Two pairs of absorbance peaks are obtained in the calibrated absorbance spectrum of 1 mol % Fe^{2+} ions (Fig. 5.4.5), one representing the octahedral and one the tetrahedral sites of Fe^{2+} ions. The two absorbance peaks of octahedral sites (Fig. 5.4.5, Table 5.4.1) in low iron concentration glasses 245, 246 and 145 are found at 10380 cm^{-1} and at 7490 cm^{-1} and are assigned to the transitions $^5T_2(D) \rightarrow {}^5E(D)$ (Fig. 5.2.3, designation T_{2g} corresponds to $^5T(D)$ and E_g to $^5E(D)$). The peak positions differ slightly from the data (10010 and 7650 cm^{-1}) reported in Bingham's thesis (2000, p.88) for an almost similar glass to this work (probably PAB2ash discussed in Chap. 5.5). The band is split into two peaks due to the Jahn-Teller distortion of an octahedral site elongated along the z-axis, that splits both the ground level $^5T_2(D)$ and the upper level $^5E(D)$, similar to the case of Cu^{2+} presented in Chap. 6. The peak at a higher energy is twice as tall and twice as broad as the peak at the lower energy as can expected for this kind of distortion. The peak position energies of the pairs differ almost exactly by factor 4/9 (Table 5.4.3.1), confirming that the Fe^{2+} ions are in tetrahedral and octahedral sites of the same glass host and there is thus a size difference of these sites.

The main assignments of the two pairs of fitted peaks agree with Bingham's data (2000, p. 87) and the reports of Ades et al (1990) and Traverse et al (1992). The octahedral Fe^{2+} peak positions and heights differ from the fitting of Ades et al, because the glass is slightly different (does not contain MgO) and the fitting has been made by another method. The estimated basicity difference between their (ca. 0,573) and our glass (0,583) explains at least a part of the difference in the fitted octahedral peaks of Fe^{3+}, meaning that the peak corresponding to their peak 6 is shifted towards higher energies in our glasses, and therefore our two main peaks of Fe^{2+} octahedral sites (corresponding roughly to their peaks 7 and 8) are easier to fit correctly to our glasses.

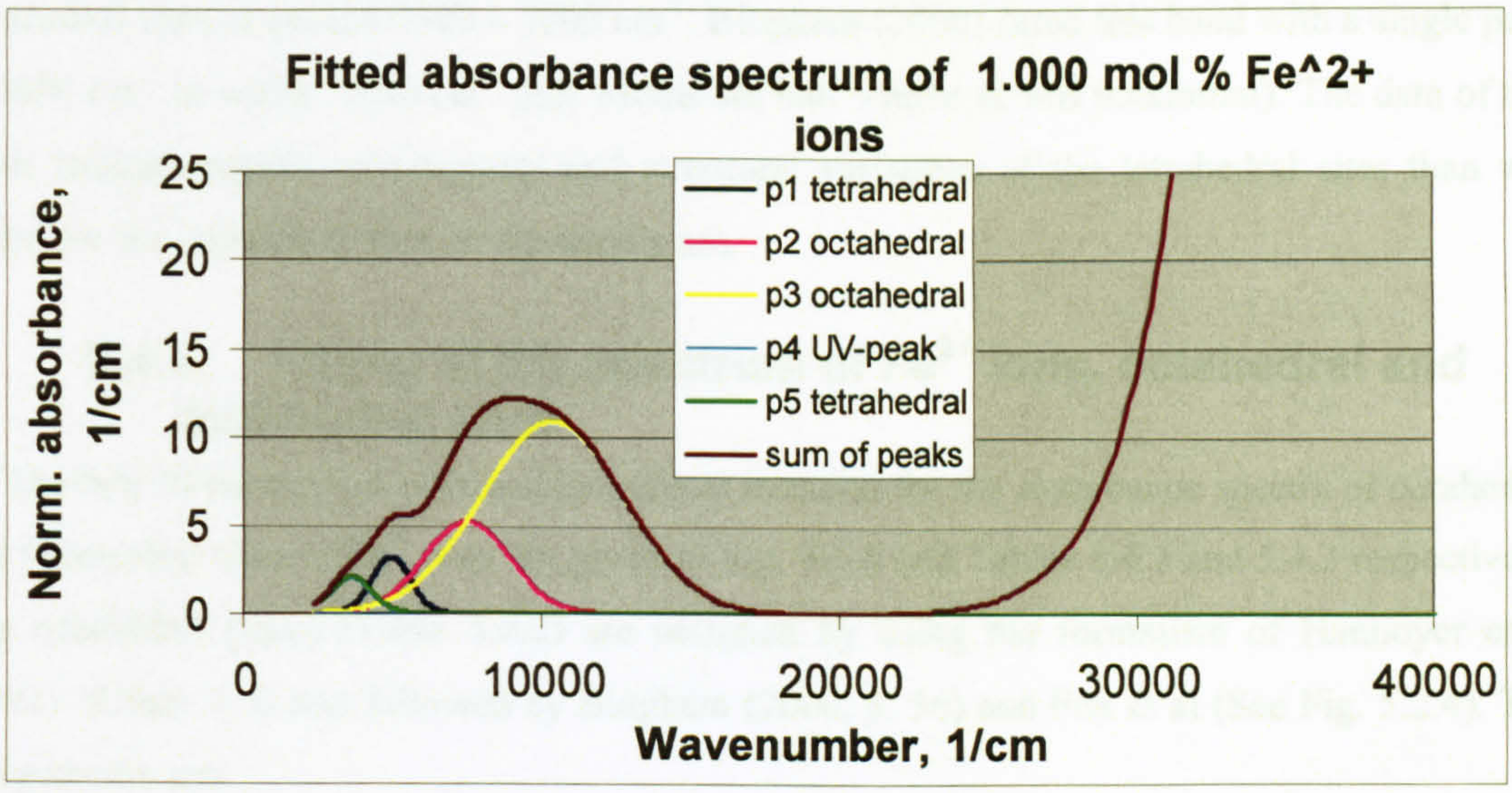

Fig. 5.4.5 Fitted absorbance spectrum of Fe^{2+} ions in 15soda-15lime-70silica glass doped with iron at low concentrations up to 0,5 mol % Fe_2O_3 added to the glass.

Table 5.4.1 Fitting parameters for Fig. 5.4.5, corresponding 1,0 mol % concentration level of Fe^{2+} ions in Glasses 245 and 246.

Fitted Gaussian peak parameters	**p5, tetrahedral**	**p1, tetrahedral**	**p2, octahedral**	**p3, octahedral**	**p4, UV-peak of Fe^{2+}**
ν_{0px}, peak position, cm^{-1}	3590 ± 20	4950 ± 10	7490 ± 10	10380 ± 10	46700 ± 40
$\Delta\nu_{px}$, peak width, cm^{-1}	700 ± 10	660 ± 10	1430 ± 10	2390 ± 10	5700 ± 20
α_{px}, peak height, mol $\%^{-1}cm^{-1}$	2,065 ± 0,001	3,183 ± 0,001	5,198 ± 0,001	10,944 ± 0,001	1000 ± 50

Note 1. 4/9 of 10380 cm^{-1} is 4613 $cm^{-1} \approx$ 4950 cm^{-1} and 4/9 of 7490 cm^{-1} is 3329 $cm^{-1} \approx$ 3590 cm^{-1}. The difference 10380 – 7490 cm^{-1} = 2890 cm^{-1}.

Two peaks are found to fit the tetrahedral sites of Fe^{2+} ions (Fig. 5.4.5, Table 5.4.1), positioned at 4950 and 3590 cm^{-1}, corresponding the transition $^5E(D) \rightarrow {}^5T_2(D)$ between the Jahn-Teller split energy levels of the tetrahedral sites (Fig. 5.2.3). These energies are approximately 4/9 of the energies of the octahedral site. The tetrahedral sites are slightly less Jahn-Teller distorted than the octahedral sites (peak at 3590 cm^{-1} is at a more higher energy compared to the 4/9 of the octahedral peak than the peak at 4590 cm^{-1}), and the average distance between the Fe^{2+} and oxygen ions are slightly smaller, giving slightly higher energies than the 4/9 of the octahedral sites. The height difference of the tetrahedral peaks is smaller and the widths of these peaks (660 and 700 cm^{-1}) are much smaller than the widths of the octahedral peaks, and also much smaller than usually is claimed for a single overall fitted peak for the tetrahedral sites at around 4500 – 5000 cm^{-1}. Bingham (2000) fitted this band with a single peak at 4800 cm^{-1} of width 1000 cm^{-1} (his widths are half widths at half maximum). The data of this work indicate smaller dimensional and structural variations of the tetrahedral sites than was found for the octahedral sites in the same glass.

5.4.4. Fitting of the spectrum of Fe^{3+} ions, octahedral and tetrahedral sites

The best fit parameters obtained by manual iteration for the absorbance spectra of octahedral and tetrahedral sites of Fe^{3+} ions are given in Fig. 5.4.6 and Tables 5.4.2 and 5.4.3 respectively. The octahedral peaks (Table 5.4.2) are assigned by using the formalism of Hannoyer et al (1992) (Chap. 5.2) and followed by Bingham (2000, p. 56) and Fox et al (See Fig. 5.2.4). The assignments are:

- Peak p1 at 14700 cm^{-1} is the transition $^6A_1(S) \rightarrow {}^4T_2(G)$;
- Peak p2 at 18350 cm^{-1} is $^6A_1(S) \rightarrow {}^4E{}^4A_1(D)$;
- Peak p3 at 25190 cm^{-1} is $^6A_1(S) \rightarrow {}^4T_2(D)$.
- Peak p9 at 27250 cm^{-1} is the transition $^6A_1(S) \rightarrow {}^4E(D)$.

The shallow peak for the transition $^6A_1(S) \rightarrow {}^4T_1(G)$ at the lowest energy was not found, similarly to the findings of Bingham (2000, p. 57).

The tetrahedral Fe^{3+} peaks (Table 5.4.3, Fig. 5.4.6) are assigned:

- Peak p4 at 21550 cm^{-1} is the $^6A_1(S) \rightarrow {}^4T_2(G)$,
- Peak p5 at 22740 cm^{-1} is the $^6A_1(S) \rightarrow {}^4E{}^4A_1(D)$,
- Peak p6 at 24020 cm^{-1} is $^6A_1(S) \rightarrow {}^4T_2(D)$.
- Peak p7 at 26220 cm^{-1} is the transition $^6A_1(S) \rightarrow {}^4E(D)$.

As for the octahedral sites, the peak of $^6A_1(S) \rightarrow {}^4T_1(G)$ transition was not found, however, one more broad peak might exist at 16000 – 18000 cm^{-1} in the high iron glasses, i.e. those with 1 mol % or more Fe_2O_3.

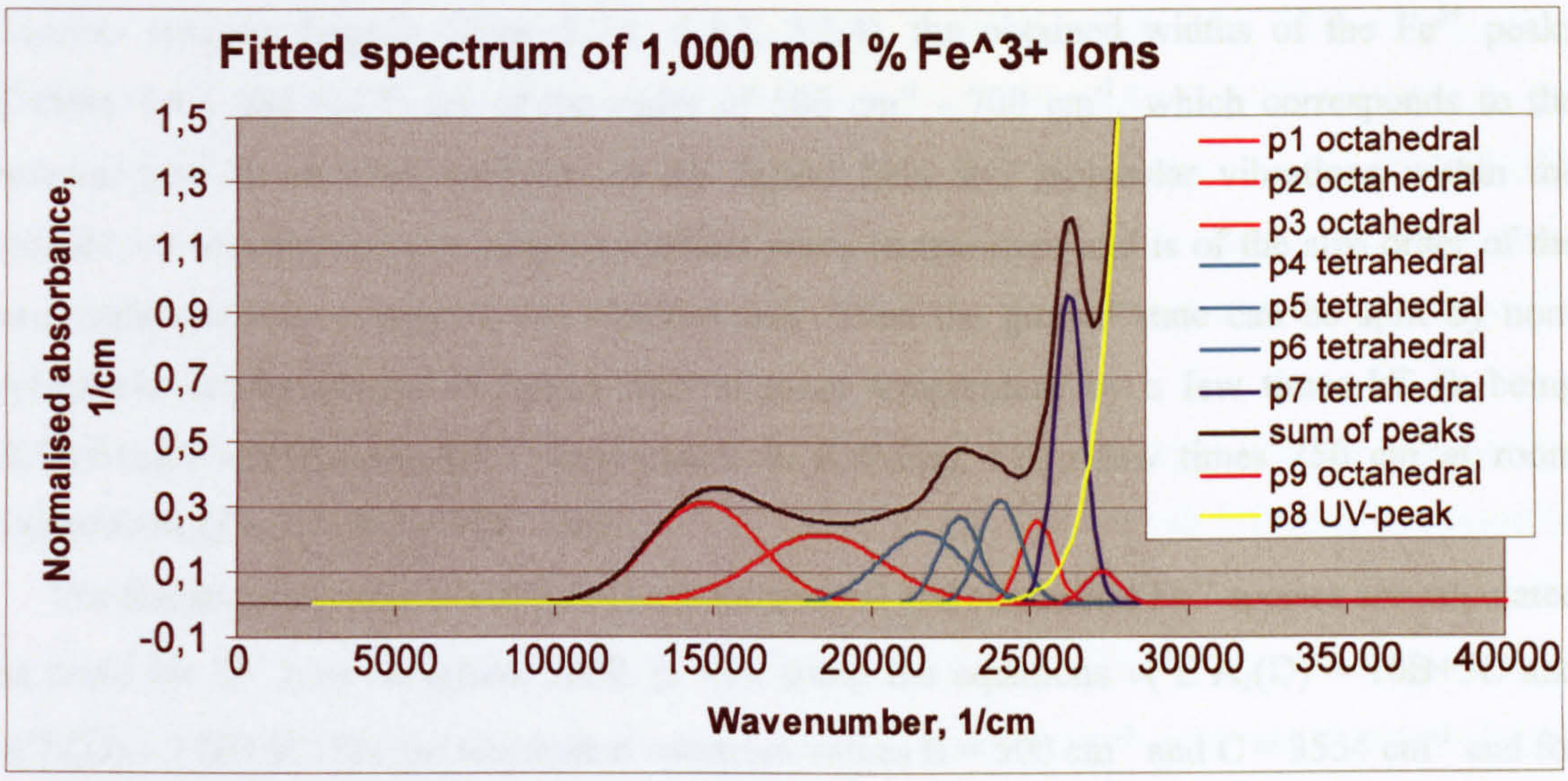

Fig. 5.4.6 Fitted absorbance spectrum of Fe^{3+} ions corresponding to 1 mol % concentration level in low iron glasses (doped with < 0,5 mol % Fe_2O_3).

Table 5.4.2 Fitted parameters of the absorbance spectrum of Fe^{3+} octahedral sites (Fig. 5.4.6)

Fitted parameters of Fe^{3+} octahedral peaks	**p1, octahedral**	**p2, octahedral**	**P3, octahedral**	**p9, octahedral**
ν_{0px}, peak position, cm^{-1}	14700 ± 50	18350 ± 20	25190 ± 10	27250 ± 10
$\Delta\nu_{px}$, peak width, cm^{-1}	1700 ± 20	2000 ± 30	530 ± 10	530 ± 10
α_{px}, peak height, mol $\%^{-1}cm^{-1}$	0,310 ± 0,001	0,210 ± 0,001	0,255 ± 0,001	0,098 ± 0,001

Table 5.4.3 Fitted parameters of the absorbance spectrum of Fe3+ tetrahedral sites (Fig. 5.4.6)

Fitted parameters of Fe^{3+} tetrahedral peaks	**p4, tetrahedral**	**p5, tetrahedral**	**p6, tetrahedral**	**p7, tetrahedral**	**p8, UV-peak of Fe^{3+}**
ν_{0px}, peak position, cm^{-1}	21550 ± 10	22740 ± 10	24020 ± 10	26220 ± 10	39360 ± 30
$\Delta\nu_{px}$, Peak width, cm^{-1}	1350 ± 20	650 ± 10	650 ± 10	480 ± 10	3050 ± 20
α_{px}, peak height, mol $\%^{-1}cm^{-1}$	0,218 ± 0,001	0,270 ± 0,001	0,323 ± 0,001	0,959 ± 0,001	1900 ± 50

For the peaks, whose corresponding transition energies are constant within a Dq range in a Tanabe- Sugano diagram (Figs. 5.2.1, 5.2.2, 5.2.4), the obtained widths of the Fe^{3+} peaks (Tables 5.4.2 and 5.4.3) are of the order of 500 cm^{-1} - 700 cm^{-1}, which corresponds to the thermal and dimensional variation of the ligand field and molecular vibrations within the studied wavenumber/energy range at ambient room temperature and is of the size order of the spin-orbit coupling energy of one electron pair. Even the ground state can be split by non-symmetric configurations of ligand field at room temperature by a few times kT (k being Boltzmann's coefficient and T temperature in Kelvins), i.e. a few times 250 cm^{-1}at room temperature (Paul, 1990, p. 304 – 305).

The Racah parameters B and C for both tetrahedral and octahedral Fe^{3+} spectra are calculated as usual for $3d^5$ ions (Bingham 2000, p. 49), using the equations $\nu(^4E^4A_1(D) = 10B+5C$ and $\nu(^4E(D) = 17B+5C$. For the tetrahedral spectrum values B = 500 cm^{-1} and C = 3554 cm^{-1} and for the octahedral spectrum values B = 1271 cm^{-1} and C = 1128 cm^{-1} were obtained. The tetrahedral parameters are close to the literature values, but the B-value for the octahedral spectrum is double the usual value (Bingham, 2000, p. 56). The reason for this is the assignment of the broad fitted (width = 2000 cm^{-1}) peak at 18350 cm^{-1} in this work as the transition $^6A_1(S) \rightarrow {}^4E^4A_1(D)$ for the octahedral spectrum. The peak may actually consist of two about similar height peaks, of which the lower energy one would be $^6A_1(S) \rightarrow {}^4T_2(G)$ and the higher one (around 19000 cm^{-1}) the transition $^6A_1(S) \rightarrow {}^4E^4A_1(D)$. In this case the lowest energy peak would be the transition $^6A_1(S) \rightarrow {}^4T_1(G)$ and the B of the octahedral spectrum would be well below 1000 cm^{-1}. This would make sense, because the photoluminescence band pointing out the transition $^6A_1(S) \rightarrow {}^4T_1(G)$ in low sodium soda-lime-silica glass is at around 14500 - 16600 cm^{-1} depending strongly on the iron concentration, according to Fox (1982). Bingham (2000, p. 109) measured and fitted a Gaussian peak to the data for his 0.5 mol % Fe_2O_3 containing soda-lime-silica glass (analysed in this work as Glass PAB35a) to be at 14230 cm^{-1} with width of 1880 cm^{-1} (half width at half maximum).

The obtained Racah parameters differ significantly from the glasses represented by Figs. 5.2.1 (phosphate glass with very low optical density) and 5.2.2 (40soda-60 silica glass with very high optical density), because the glass compositions differ greatly from the glass of this work.

5.4.5. Fitting of the UV- peaks of Fe^{2+} and Fe^{3+} ions

The literature (Chap. 5.2) gives a limited guidance for fitting the UV-peaks of the iron absorption spectrum. Much confusing data, in addition to those mentioned in Chap. 5.2, have been published for the positions of the UV-peaks (e.g. Ehrt, 2002). The glass compositions used, preparation methods, measurement methods and interpretation of the results all vary. Many researchers present results obtained for concentration levels of a few ppm, at which level

many kinds of contaminants (such as Cu, Cr, Ti, etc.) also show an UV-absorption; and thus it is difficult to separate shallow overlapping peaks from each other and from the background of such a pure glass. Various differing measurement results are shown for the UV edge that do not seem to scale either to the peak height at 380 nm, usually quoted as a measure for the Fe^{3+} content. Therefore diffused reflection measurements were carried on some of the powdered samples of iron containing glasses (Figs. 5.4.7 and 5.4.8). The method and calculation of the Kubelka-Munk function results are described in Chap. 3.

The reflectance peak heights or their positions do not directly correspond to the transmission absorbance spectra. At high absorbance (over 100) the reflectance peak UV-edge is moved to lower energies (as seen in Fig. 5.4.8). This occurs because at high absorption, according to the well-known Kramers-Kronig relationship (Wong et al, 1976, p. 153 – 154), refractive index is raised and thus also the reflectance in proportion to the absorbance is greater. However, the overall shape of the diffuse reflectance band indicates roughly the shape of the combined absorbance band and positions of the two main UV-peaks at about 39000 and 47000 cm^{-1}. The UV-peaks of the Fe-S complexes in a reduced Glass 228 are clearly seen, and the whole absorbance spectrum differ greatly from a similar Glass 225 not reduced by adding carbon (Fig. 5.4.7)

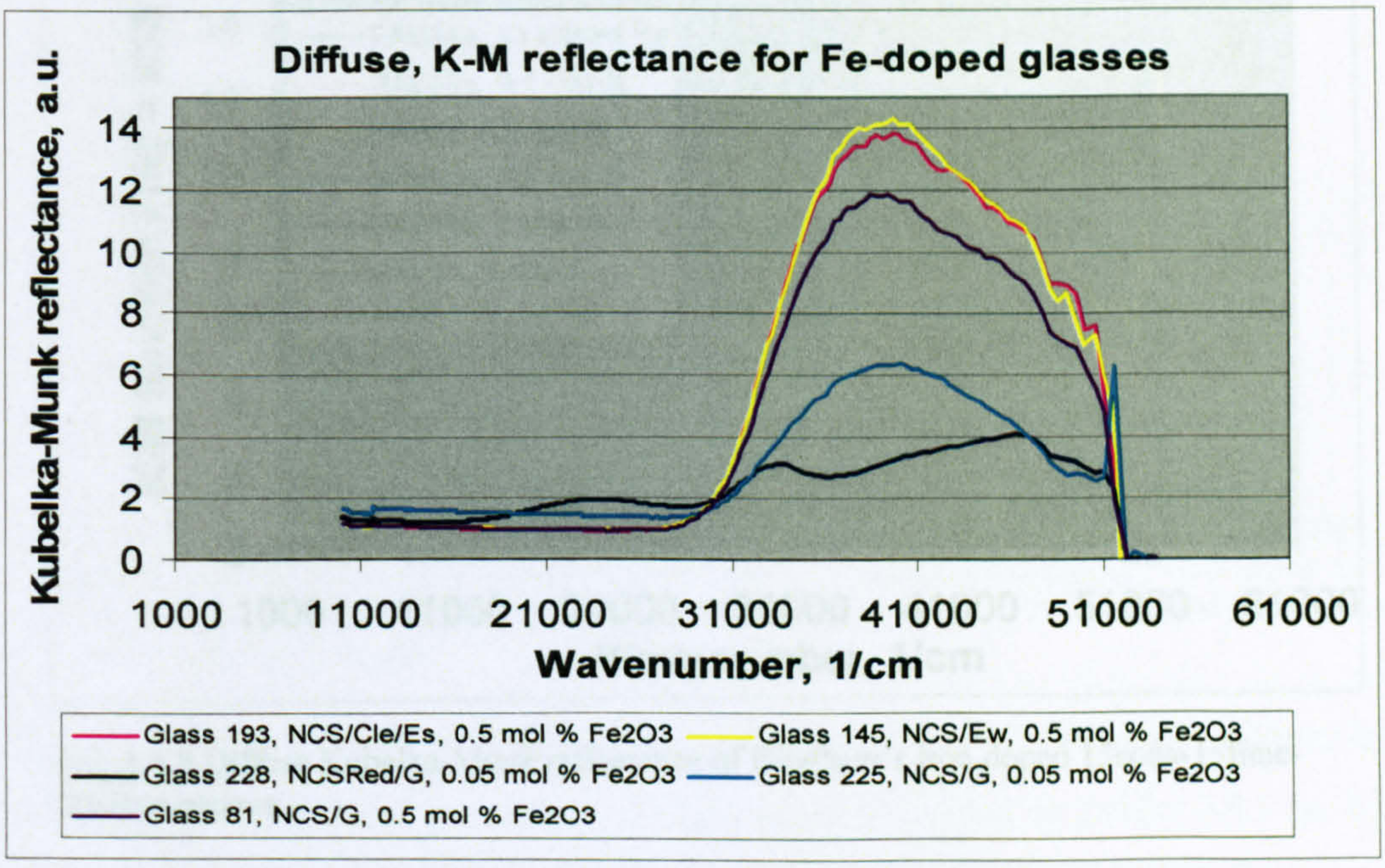

Fig. 5.4.7 Diffuse Kubelka-Munk reflectance for iron-doped 15soda-15lime-70silica-0,35sulphate glasses melted and prepared in various ways (see Annex 1 for details).

Glass 81, melted under reducing conditions in a gas-furnace, shows a significantly lower UV-band than Glasses 145 and 193 melted in an electric furnace. The most reduced Glass 228

shows typical Fe-S absorption peaks at ca. 24000 and 36000 cm^{-1}. By trial fitting to the Kubelka-Munk reflectance data and to the absorbance data of the other studied iron doped samples of Figs. 5.4.7 and 5.4.8, it was found that the absorbance bands could be fitted by two Gaussian peaks, one very broad peak at 46700 cm^{-1} and another taller and narrower at 39000 cm^{-1} (Fig. 5.4.9). The peak at 46700 cm^{-1} is assigned to Fe^{2+} and has a width of 5700 cm^{-1} and a linear absorption coefficient 1000 cm^{-1} mol $\%^{-1}$. The peak at 39360 cm^{-1} is assigned to Fe^{3+} ions, and has a width of 3050 cm^{-1} and a height of 1900 cm^{-1} mol $\%^{-1}$.

The assignment of the peaks is in agreement with Ades et al (1990), Traverse et al (1992) and Paul (1992). The peak heights (and areas) scale accurately with the concentrations of the Fe^{2+} and Fe^{3+} ions, validating the fitting also over the longer wavelength parts of the d-d transition spectra at wavenumbers 3000 – 27000 cm^{-1} for Glasses 245, 246, 145, PAB2ash and PAB35 a with low iron concentration. The scaling is good even for analysis of the other studied Fe-doped and undoped contaminated glasses with minor adjustments (See Chaps 5.5. – 5.8, and Chap. 6).

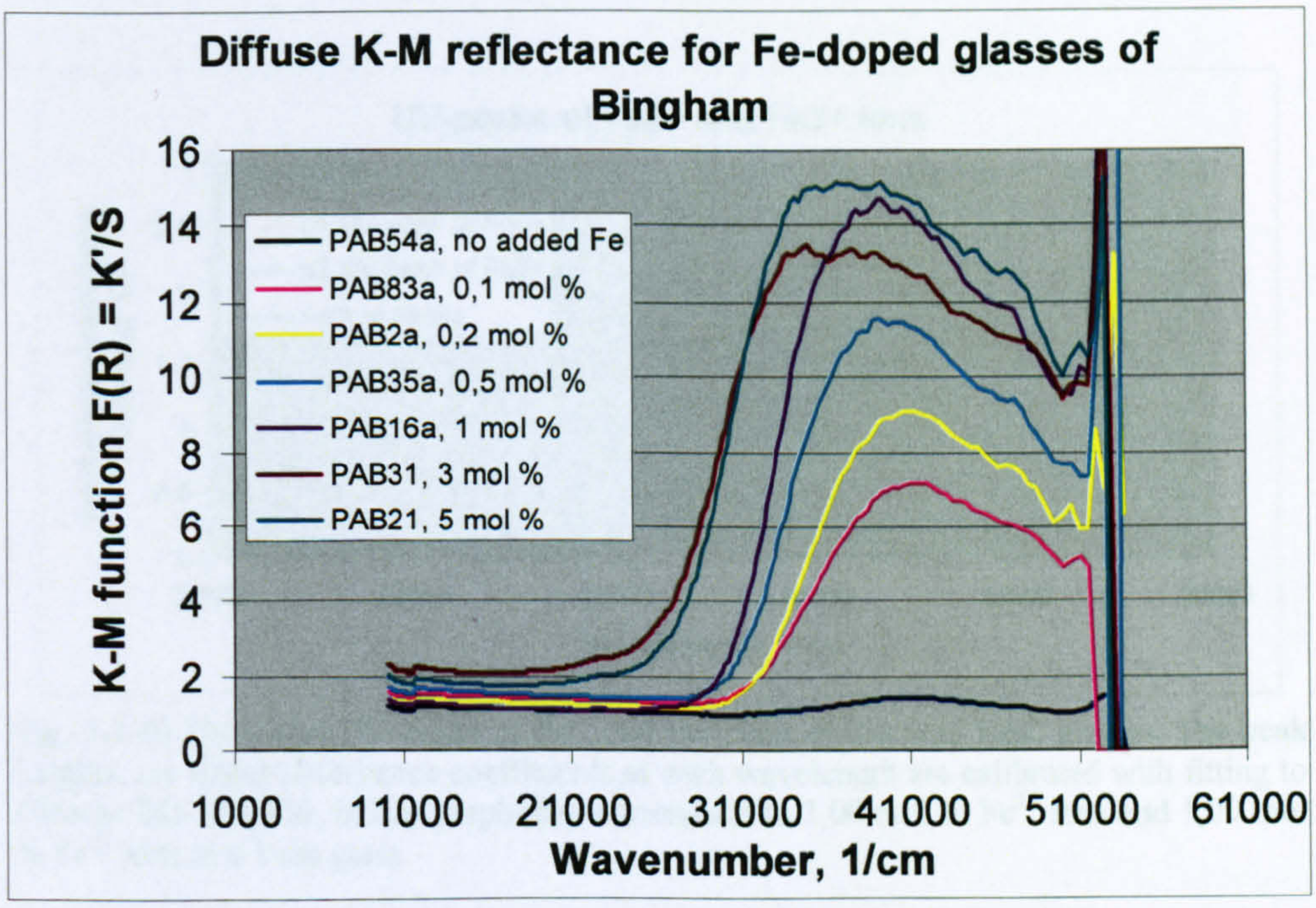

Fig. 5.4.8 Diffuse Kubelka-Munk reflectance of Bingham's iron doped 15soda-15lime-70silica glasses.

The K-M reflectance curves of Bingham's glasses, the absorbance spectra of which were also fitted in this work, show a variation with iron concentration seen also in the UV-edges of absorbance curves (Fig. 5.4.8). The UV-band becomes broader and has a shallower edge with increasing iron concentration, in particular for the glasses with more than 1 mol % Fe-

concentration. Those below 1 mol % seem to have an almost linear increase with Fe-concentration, which is confirmed by the fitting analysis of the absorption spectra.

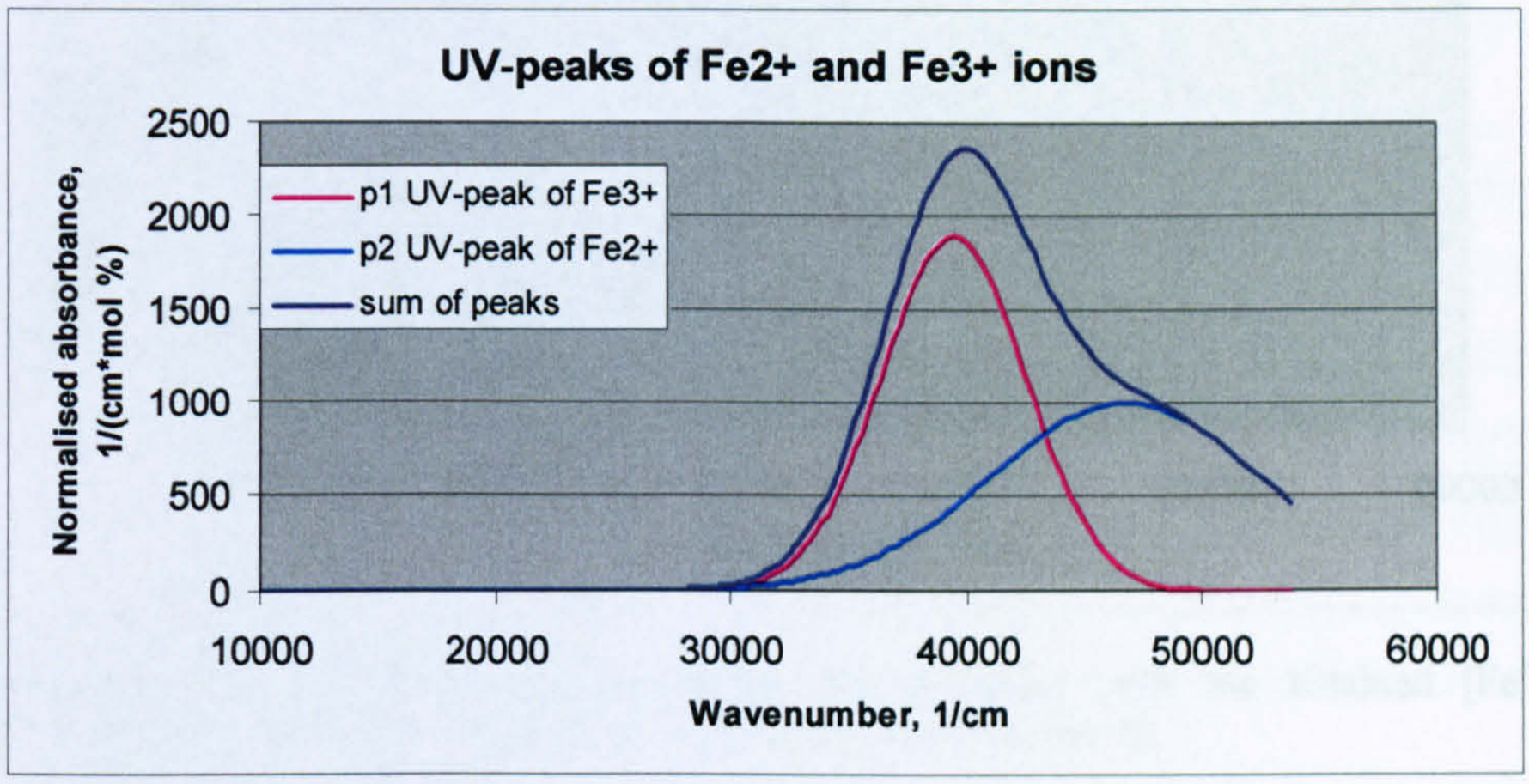

Fig. 5.4.9 The fitted UV-peaks of Fe^{2+} and Fe^{3+} ions in 15natria-15calcia-70silica glass corresponding to 1,00 mol % Fe^{2+} and 1,00 mol % Fe^{3+} ions in Glasses 245 and 246, at low concentration of iron (0 – 0,5 mol % Fe_2O_3).

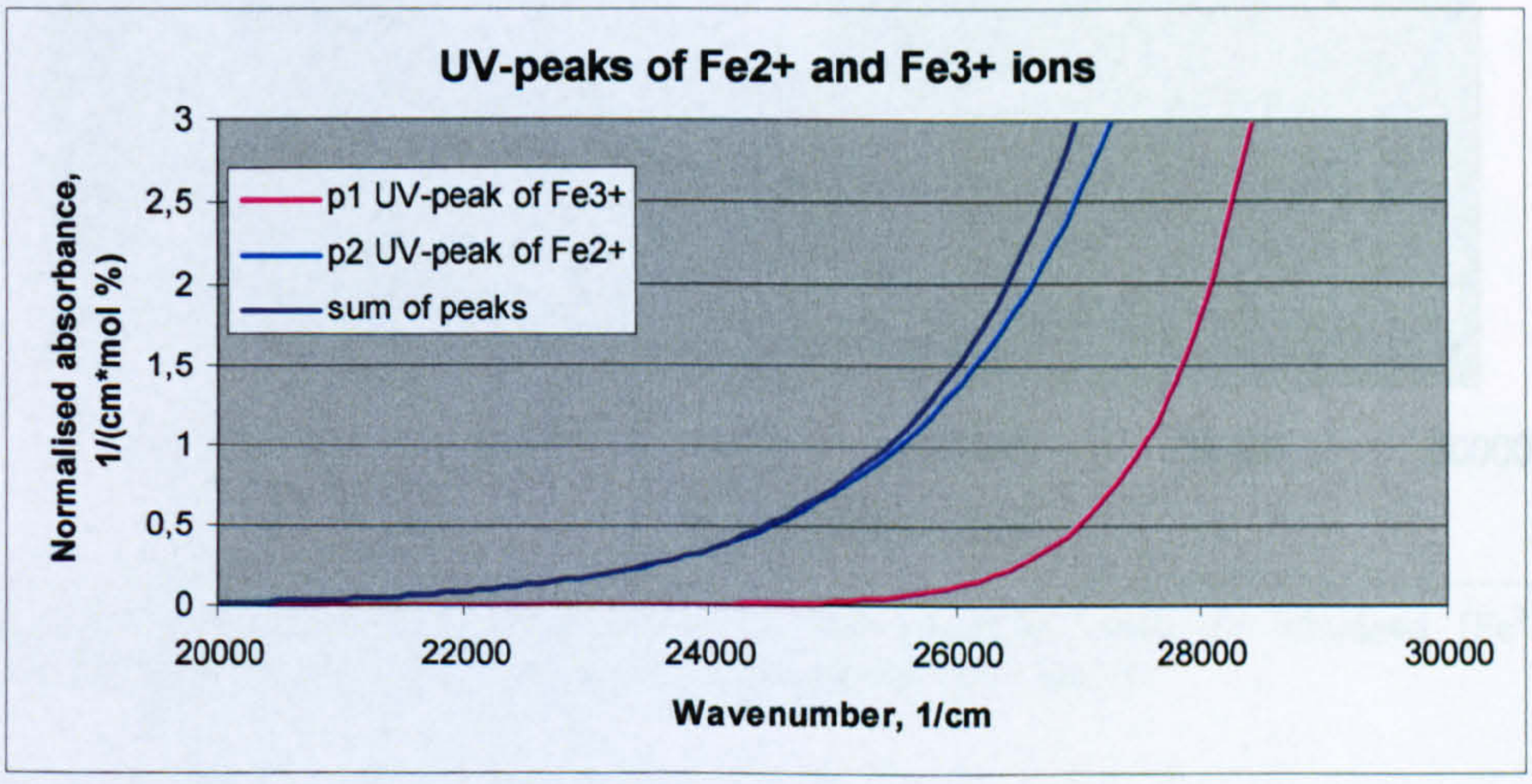

Fig. 5.4.10 The Fitted UV-peaks of Fe^{2+} and Fe^{3+} ions in low iron NSC glasses. The peak heights, i.e. linear absorbance coefficients at each wavelength are calibrated with fitting to Glasses 245 and 246. In this graph they correspond to 1,00 mol % Fe^{2+} ions and 1,00 mol % Fe^{3+} ions in a 1 cm glass.

The UV-absorbance spectra of the Fe^{2+} and Fe^{3+} were fitted with two peaks shown in Figs. 5.4.9 and 5.4.10. The fitted parameters of these peaks are given in Tables 5.4.1 (p. 85) and 5.4.3 (p. 87). These peaks are also included to the graphs of Fe^{2+} spectrum (Fig. 5.4.5) and Fe^{3+} spectrum (Fig. 5.4.6).

Normally only about 15 % of the iron ions are ferrous, so the effect of the ferric and ferrous ions on the UV-edge are of similar order of magnitude, and the peak tails cross each other at wavenumbers below 28000 cm^{-1} as is shown in Figs. 5.4.11 and 5.4.12.

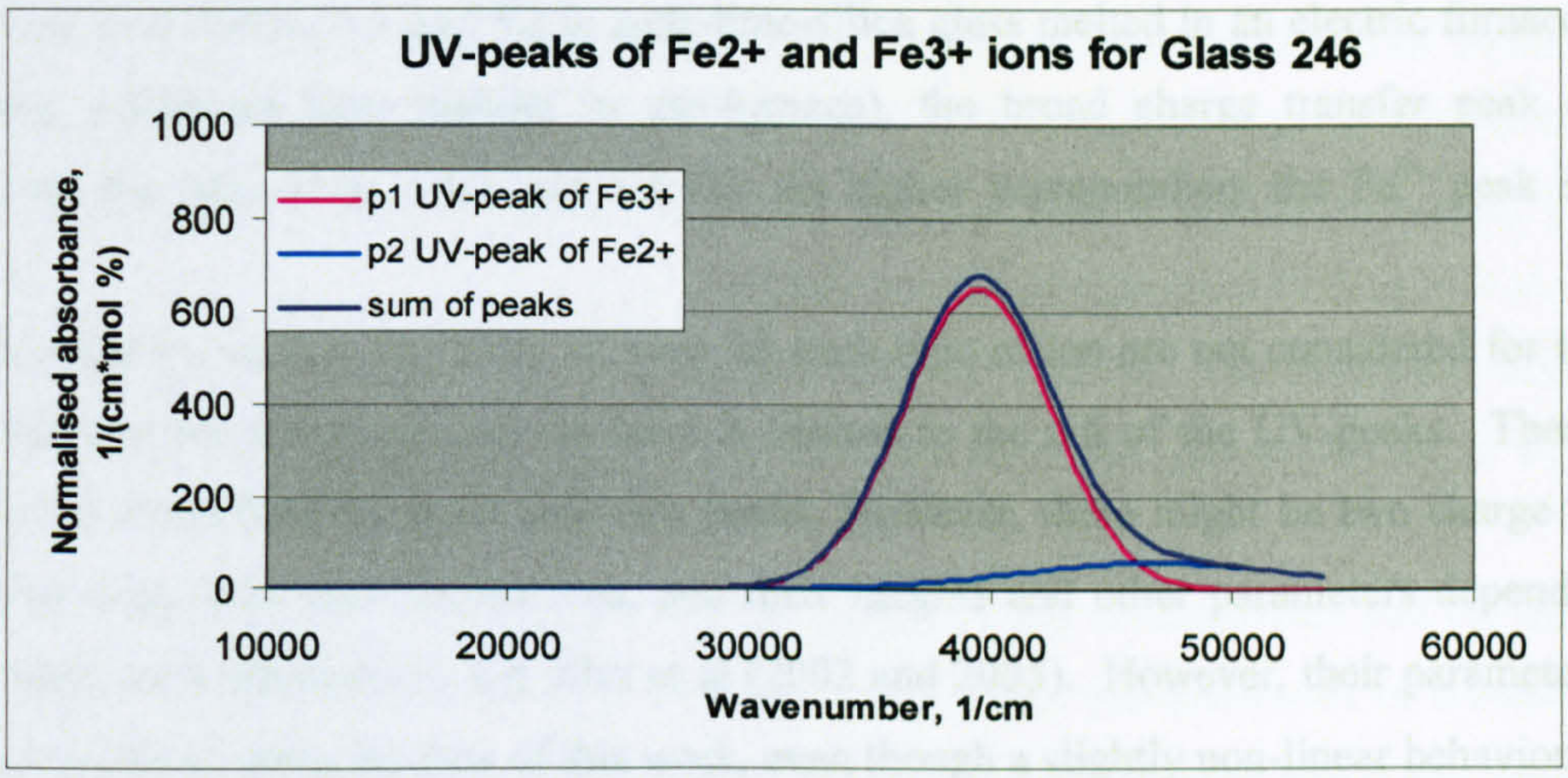

Fig.5.4.11 The UV-peaks fitted to Glass 246 spectrum, with the obtained [Fe^{3+}] concentration = 0,343 mol % and [Fe^{2+}] concentration 0,061 mol %.

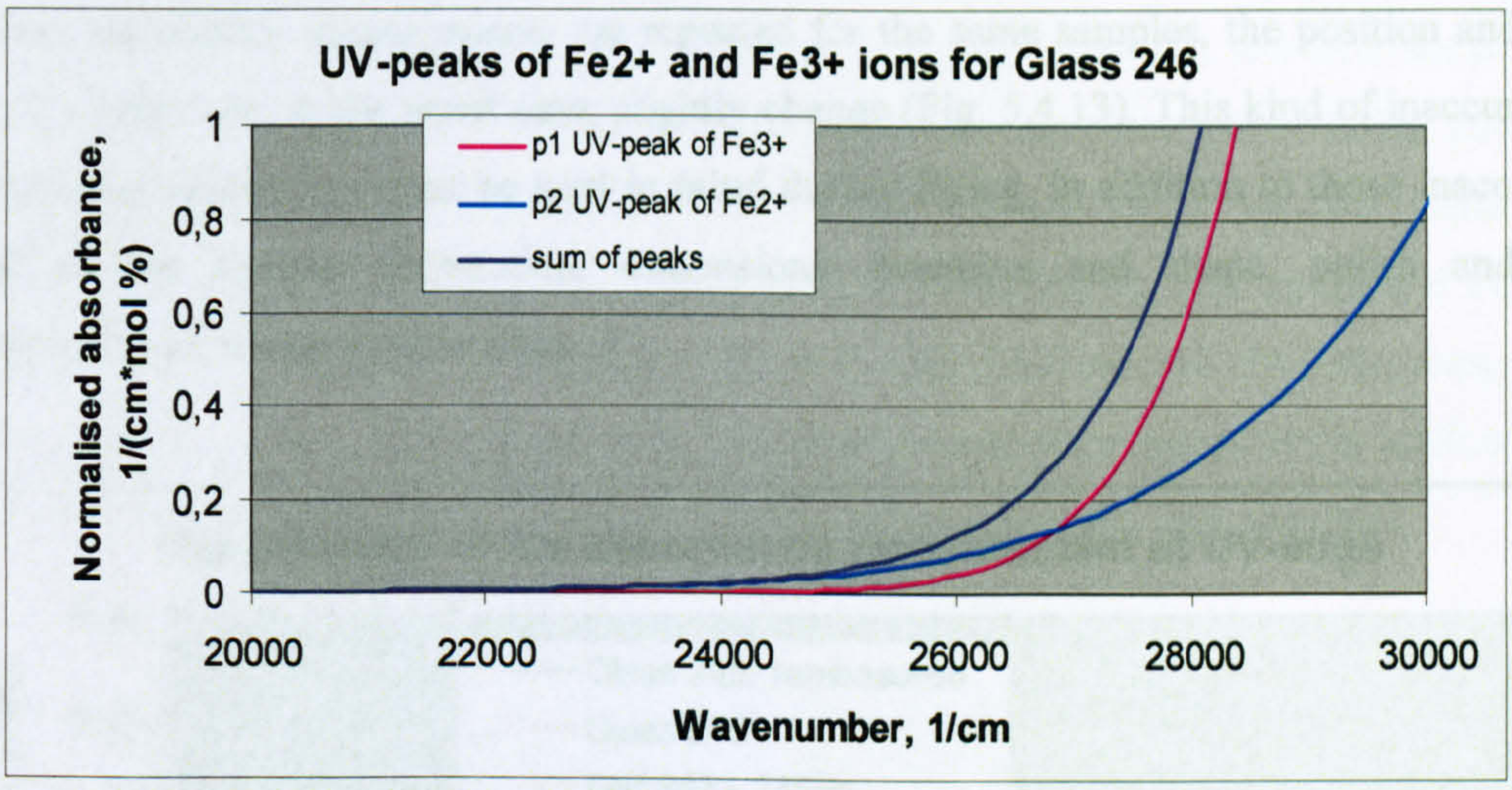

Fig.5.4.12 The UV edge fitted to Glass 246 spectrum, with the obtained [Fe^{3+}] concentration = 0,343 mol % and [Fe^{2+}] concentration 0,061 mol %.

The linear absorbance coefficients, i.e. peak heights of the UV-peaks were calibrated by a trial-and- error iteration fitting to Glasses 245 and 246, so that below 28000 cm^{-1} the sum of the peaks, multiplied by the concentrations of Fe^{2+} and Fe^{3+} ions (received from the fitting of the d-d transition spectra as described in Chaps 5.4.3 and 5.4.4), would give the smallest difference between the synthesized absorbance spectrum and the measured, normalised absorbance spectrum. The peak positions agree closely with what Traverse et al (1992) also suggested. Above 28000 cm^{-1} the absorbance data is not usually accurate. The shape of the fitted sum resembles the shape of the measured diffuse reflection spectra of these and other iron doped glasses, studied by the diffuse reflection method (See Fig. 5.4.7 and 5.4.8).

It is important to realise that when we look at the UV-absorption below wavenumbers 27000 of the low iron (below 0.5 mol %) in soda-lime-silica glass melted in an electric furnace (more oxidising conditions than melting in gas-furnace), the broad charge transfer peak of Fe^{2+} dominates the edge (Fig. 5.4.5 and 5.4.12). At higher wavenumbers the Fe^{3+} peak is more intense.

Other factors, such as the kinds of sites for each type of ion are not considered for the UV-band, because the measured data we have is limited to the tail of the UV-peaks. There is no evidence in these data for more than two peaks. However, there might be two charge transfer peaks for both ferric and ferrous ions, and their heights and other parameters depend on the actual sites, as is indicated by e.g. Ehrt et al (2002 and 2005). However, their parameters have not been resolved using the data of this work, even though a slightly non-linear behaviour of the absorption spectra obtained on high- iron glasses might suggest it (Chap. 5.5.). The fitting by two UV-peaks gives a sufficiently accurate fit for the purposes of this work.

When absorbance measurements are repeated for the same samples, the position and shape of the UV-edge can, in the worst case, slightly change (Fig. 5.4.13). This kind of inaccuracy on the measured absorbance must be kept in mind during fitting, in addition to those inaccuracies related to the sample preparation, dimensions, evenness and shape, polish and glass homogeneity, as is described in Chap. 3.

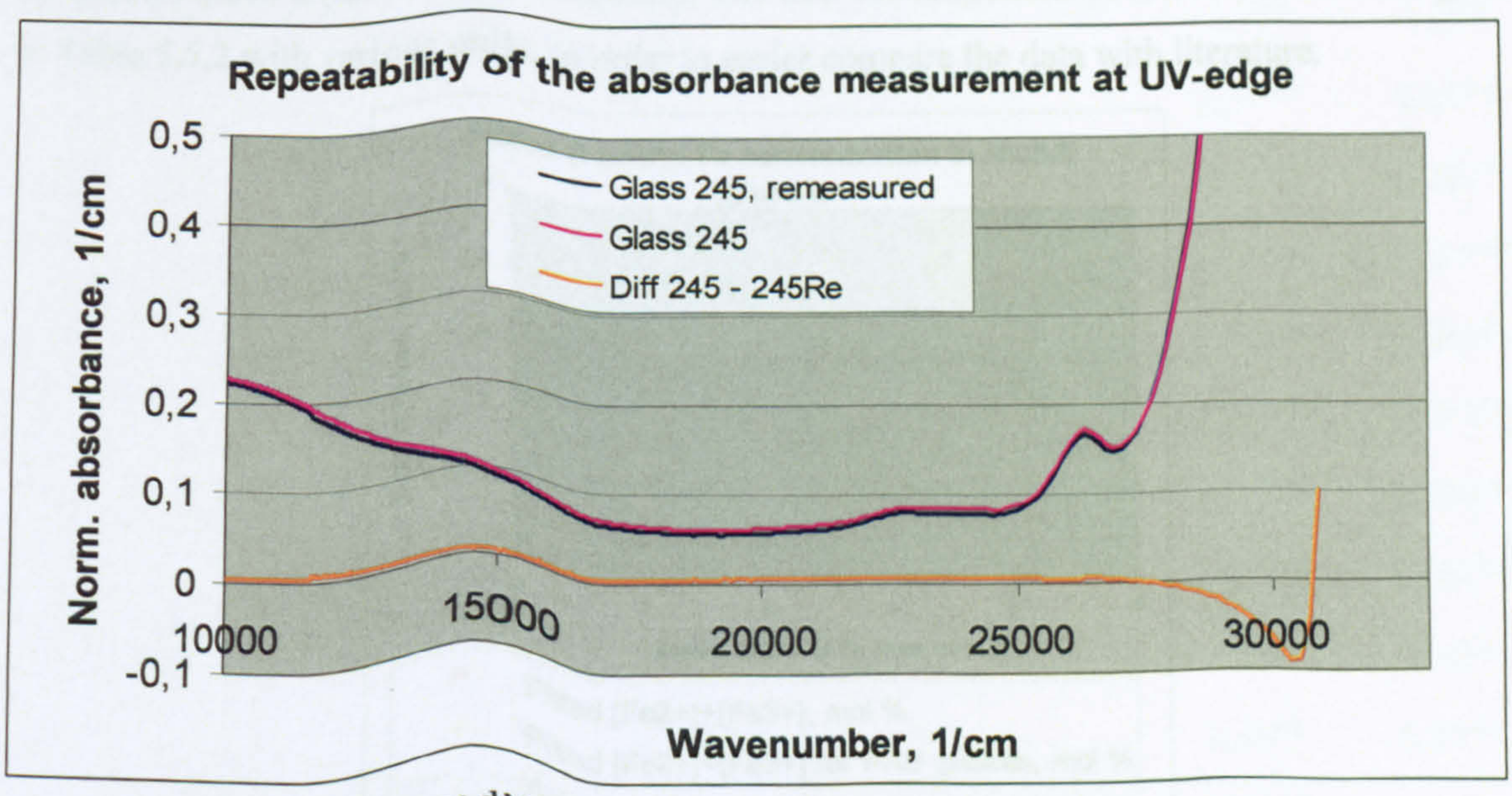

Fig. 5.4.13 A worst case difference between repeated measurements on the same sample.

5.5 Scaling of the fitted spectrum with Fe-concentration

The set of fitting parameters was developed as described in Chap. 5.4. The measured and fitted absorbance spectra for NCS glasses with various Fe-concentrations, as well as the fitted parameters of Glasses 145, 193, 247 and 248 and Bingham's Glasses PAB2ash, PAB35a, PAB16a and PAB24a are given in Annex 6. The spectra of Glasses 245 (Fig. 5.4.3) and 246 (Fig. 5.4.4) are presented in Chap. 5.4. The received Fe^{2+} and Fe^{3+} concentrations, obtained by the fitting analysis, are given in Table 5.5.1 for these Fe doped glasses melted in an electric furnace.

There is a very good agreement between the added Fe ion concentration and the sum of the obtained [Fe^{2+}] and [Fe^{3+}] concentrations (Fig. 5.5.1). The concentrations of tetrahedral and octahedral sites (Table 5.5.1) are estimated as the sum area of the fitted absorption peaks of the site (Chaps. 5.4.2 and 5.4.3).

All these glasses (Tables 5.5.1 and 5.5.2) have the same host glass composition, except PAB-glasses (Bingham, 2000) do not contain any sulphate. Glasses with a low iron concentration (245, 246, 145, PAB2ash and PAB35a) are all fitted with the same set of fitting parameters given in Chaps. 5.4.3 – 5.4.4 (Tables 5.4.1, 5.4.2, 5.4.2 and 5.4.3), by only adjusting the concentrations and, when needed, also the proportion of octahedral and tetrahedral Fe^{3+} ions' sites. The fitting parameters for Glasses 193, 247, 248, PAB16a and PAB24a were slightly modified, Annex 6 (the fitting parameters). The iron concentrations added to the batch are given in Table 5.5.2 with various units, in order to easier compare the data with literature.

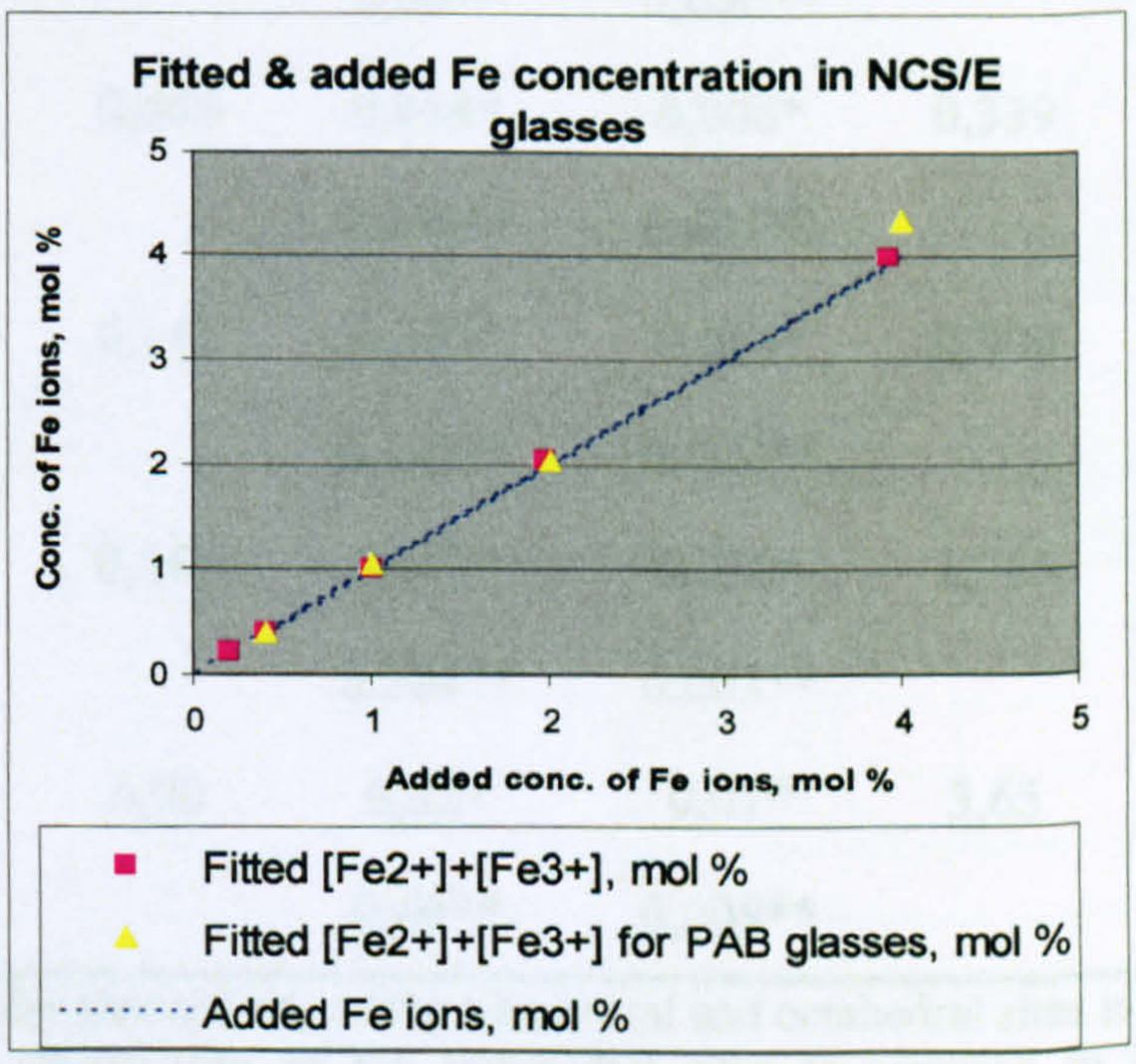

Fig. 5.5.1 Comparison between the added and fitted Fe ion concentrations of NCS glasses melted in an electric furnace (Tables 5.5.1 and 5.5.2).

The glasses contain a slightly varying amount of water, seen from the multipliers for the bound OH-band and IR-edge (Table 5.5.1)

Table 5.5.1. The fitted concentrations of Fe^{2+} and Fe^{3+} ions, fitted OH-content and IR-edge and the calculated portions of Fe^{2+} and Fe^{3+} ions in octahedral and tetrahedral sites, for Fe doped NCG glasses melted in an electric furnace.

Glass	OH-cont. a.u.	IR-edge, a.u.	[Fe^{2+}], mol %	[Fe^{2+} octa], mol %	[Fe^{2+} tetra], mol %	[Fe^{3+}], mol %	[Fe^{3+} octa], mol %	[Fe^{3+} tetra], mol %
245	0,86	0,42	0,0305	0,0276*	0,0029*	0,171	0,0852*	0,0858*
				0,0302**	0,00032**		0,155**	0,016**
246	0,89	0,72	0,061	0,0552*	0,0058*	0,343	0,171*	0,172*
				0,0604*	0,0006**		0,3116**	0,0314**
145	1,25	0,78	0,122	0,110*	0,0116*	0,88	0,439*	0,441*
				0,121**	0,00127**		0,799**	0,0805**
193	0,89	0,82	0,130	0,117*	0,013*	0,87	0,418*	0,451*
				0,129**	0,001**		0,785**	0,085**
247	0,90	0,80	0,295	0,264*	0,031*	1,755	0,880*	0,875*
				0,292**	0,003**		1,596**	0,159**
248	1,35	0,90	0,51	0,46*	0,053*	3,50	1,78*	1,73*
				0,50**	0,006**		3,19**	0,31**
PAB 2ash	1,2	0,72	0,060	0,054*	0,006*	0,339	0,157*	0,181*
				0,059**	0,001**		0,304**	0,035**
PAB	1,2	0,9	0,147	0,133*	0,014*	0,900	0,436*	0,464*
35a				0,145**	0,002**		0,813**	0,087**
PAB	0,90	0,80	0,287	0,257*	0,030*	1,765	0,872*	0,894*
16a				0,284**	0,003**		1,601**	0,164**
PAB	1,35	0,90	0,70	0,62*	0,07*	3,65	2,05*	1,61*
24a				0,69**	0,008**		3,38**	0,27**

Note * = The similar absorptivity of the tetrahedral and octahedral sites is assumed.
Note ** = The absorptivity of the tetrahedral sites is assumed to be 10 times the absorptivity of the octahedral sites.

The difference curves between the fitted and measured absorbance spectrum are shown in the absorbance graphs in Chap. 5.4.1 (Glasses 245 and 246) and in Annex 6 (the other glasses). The overall differences for Glasses 193, 247 and PAB16a are very small and of a similar size as for the low iron glasses 245 and 246, i.e. within the ± 0,005 variation limits of the measurement repeatability, and within ± 0,01 for the high iron glasses, that is within the glass and sample preparation repeatability. The low iron fitting does not agree completely to the spectrum of Glass 145, which is purposely shown to demonstrate how certain areas of the fitted spectrum show the kinds of the differences that are adjusted by the modifications of the fitting parameters for the high iron glasses (Tables A6.1, 2, 3).

Table 5.5.2 The added Fe concentrations in various units for the NCS glasses melted in an electric furnace. *Glass density = 2,5 kg/litre is assumed.

Fe concentration, calculated from the batch composition				
Glass	Fe_2O_3, mol %	Fe_2O_3, weight %	Fe ions, mol %	* Fe ions, mol/l
245	0,1	0,266	0,2	0,0834
246	0,2	0,532	0,4	0,1664
145	0,5	1,329	1	0,412
193	0,5	1,329	1	0,412
247	0,99	2,6	1,98	0,814
248	1,96	5,07	3,92	1,588
PAB2ash	0,2	0,27	0,4	0,166
PAB35a	0,5	1,33	1	0,413
PAB16a	1	2,6	2	0,815
PAB24a	2	5	4	1,588

Table 5.5.3 The received Fe-concentrations and fractions of Fe^{2+} ions, obtained with the fitting analysis * from the summed d-d transition peak areas and ** from the UV-peak peak areas.

	Fitted Fe ion concentrations and Fe^{2+} fractions		
Glass	Fitted $[Fe^{2+}]+[Fe^{3+}]$, mol %	Fitted $[Fe^{2+}]/[Fe\ ions]$	Fitted $[Fe^{2+}]/[Fe\ ions]$*, from UV-peaks
245	0,2015	0,151	0,149
246	0,404	0,151	0,149
145	1,002	0,122	0,120
193	1,000	0,129	0,142
247	2,050	0,144	0,15
248	4,010	0,127	0,16
PAB2ash	0,399	0,15	0,148
PAB35a	1,047	0,14	0,155
PAB16a	2,052	0,14	0,15
PAB24a	4,35	0,16	0,18

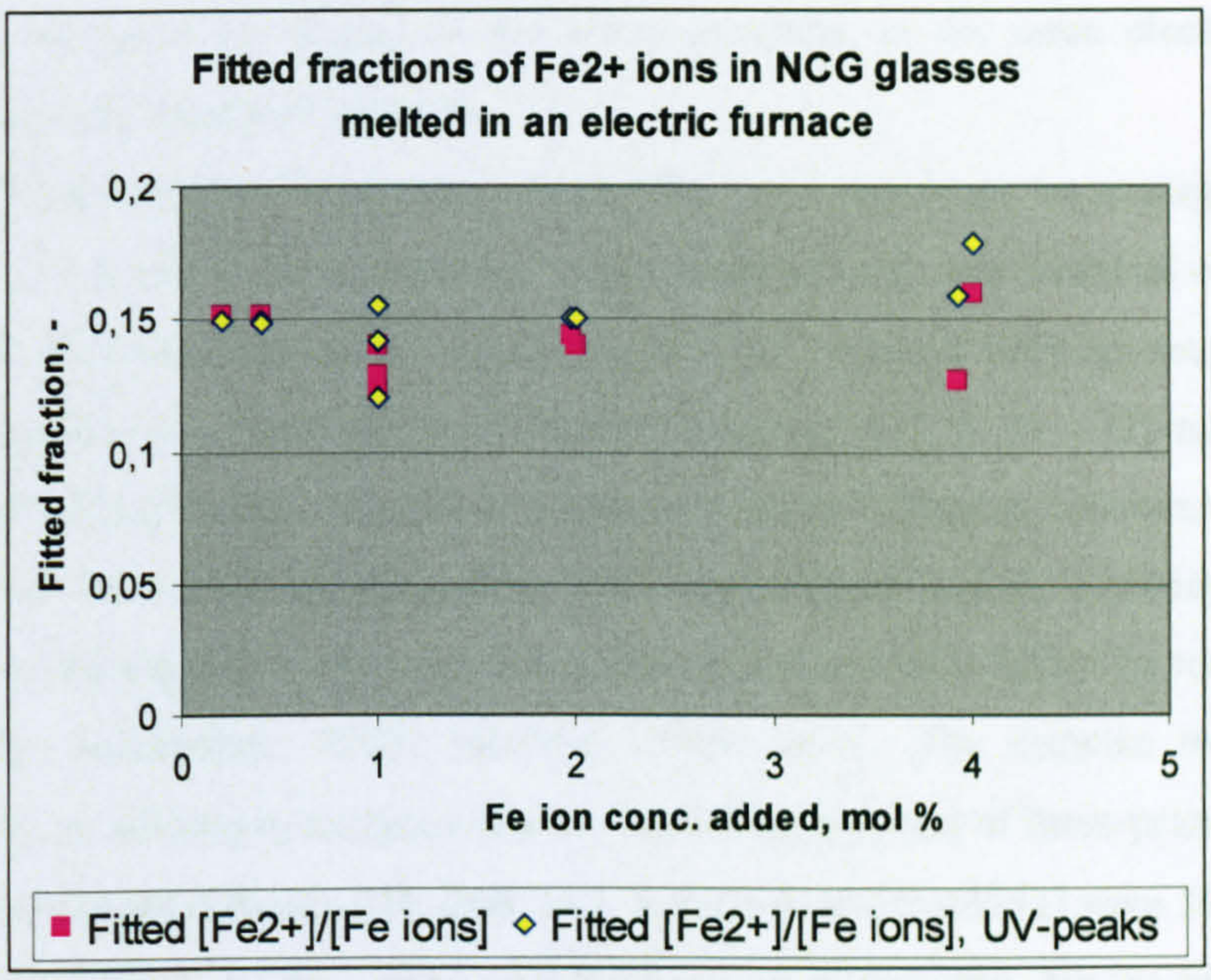

Fig. 5.5.2 Fractions of Fe^{2+} ions $[Fe^{2+}]/([Fe^{2+}]+[Fe^{3+}])$, obtained with the fitting analysis. Wet chemical data of Bingham (2000, p. 101) shows the fraction 0,16 ± 0,1 at 0 - 3 mol % Fe ions and 0,21 ± 0,2 at 4 mol % Fe ions.

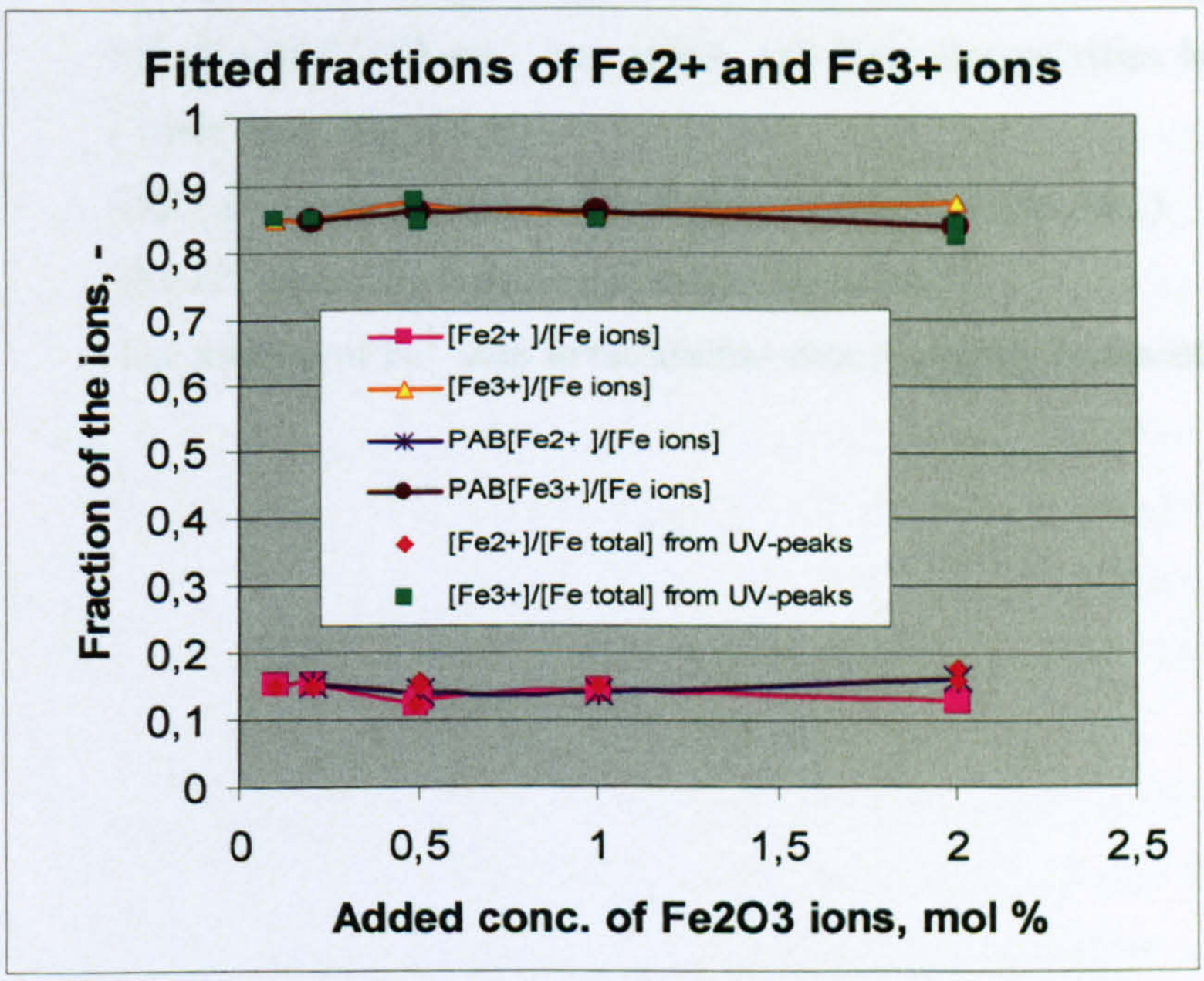

Fig. 5.5.3 Fractions of Fe^{2+} and Fe^{3+} ions in electric melted 15natria-15calcia-70silica glasses of this work and Bingham's (Table 5.5.1.), obtained by fitting analysis.

The average fraction of Fe^{2+} ions stays almost constant, 14 – 15 % (Table 5.5.3, Fig. 5.5.2), within the studied iron concentration range of 0,1 – 2,0 mol % added Fe_2O_3 in these glasses with

the same host composition, melted in the same crucibles, in the same electric furnaces, in similar conditions and annealed similarly.

The fitted fractions of Fe^{2+} ions (Table 5.5.2, Fig. 5.5.2 and 3) are on average slightly lower than expected (0,16 ± 0,01) from Bingham's data obtained with wet chemical method (2000, p. 101). The calibration absorbance 9,0 1/(cm*weight % Fe^{2+} ions) at 1064 nm may be slightly too high for these glasses (the composition of Bamford's glass (1977, p. 35 – 37) may differ slightly from the glasses of this work). There is a variation of the Fe^{2+} fraction between the glasses (Fig. 5.5.2), which has been probably caused by small temperature and air humidity differences in their melting, annealing and cooling processes that all are known to affect Fe redox (Chap. 5.2.; Beerkens, 2003; Kukkadapu, 2003; Johnston, 1964; etc.). The samples were melted and annealed in various laboratory furnaces one by one during a period of three years.

The low iron glasses (Glasses 245, 246, 145, PAB2ash and PAB35a) were fitted by the same set of parameters (Annex 6), but some modifications were necessary for the high iron glasses. The modifications made to the fitting parameters for the high iron glasses are:

- Fe^{3+} octahedral peaks move to a narrower energy scale. The furthest peaks at the lowest energies 14700 and 18350 cm^{-1} move to higher wavenumbers (Table A6.2 and Fig.5.5.3), while the peak positions at the highest energies 25190 and 27250 cm^{-1} stay stable and their absorptivities become higher (Table A6.2, Fig. 5.5.3),
- The Fe^{2+} tetrahedral peaks are slightly modified (Table A6.1).
- The UV-peaks are broader and taller (Table A6.3).
- The fraction of Fe^{3+} ions in tetrahedral sites is slightly increased (Fig. 5.5.4) .

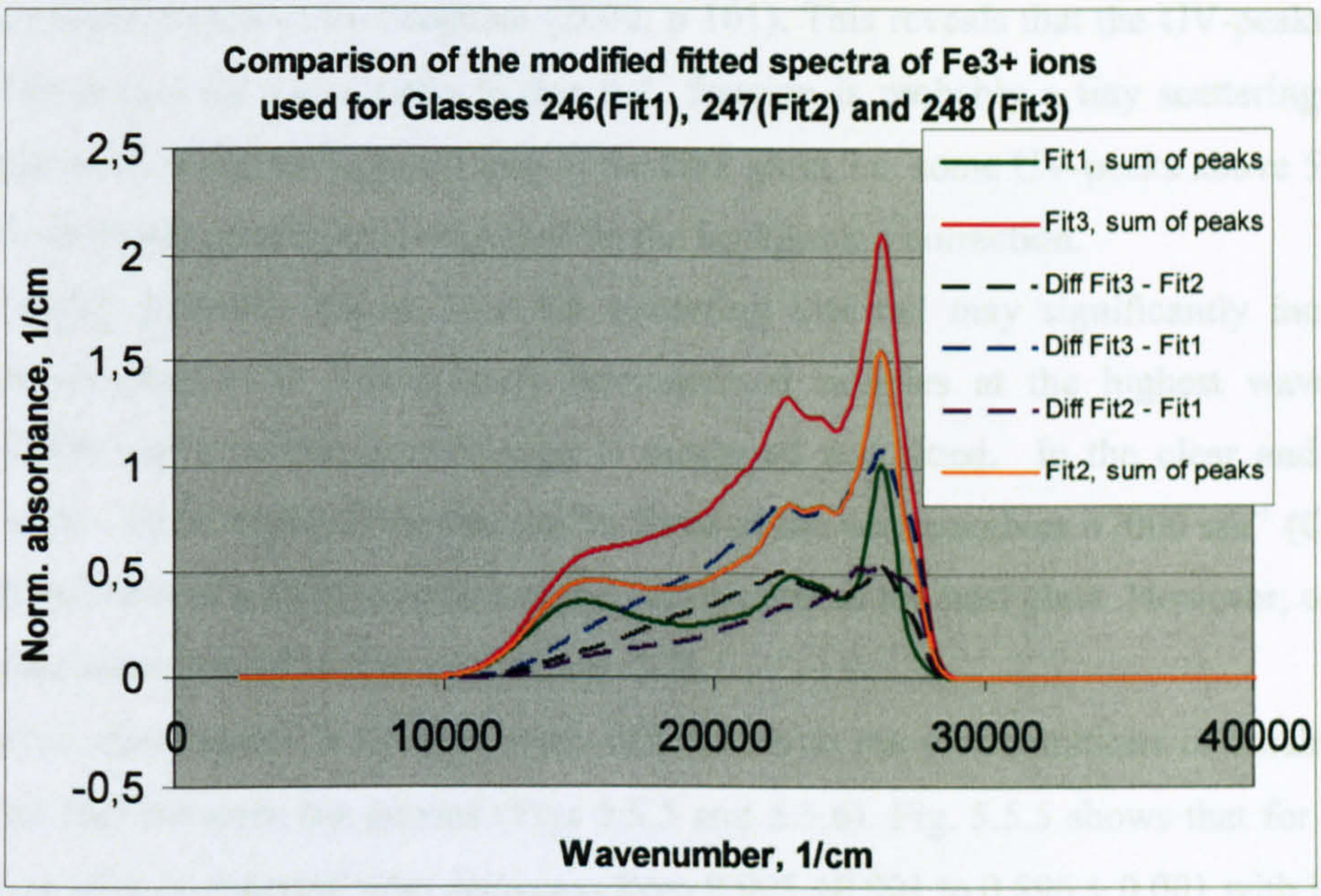

Fig. 5.5.4 The comparison of the modified fitted spectra for the Fe^{3+} ion concentration level 1.00 mol % fitted to Glass 246(Fit1), Glass 247(Fit2) and Glass 248(Fit3).

The most significant modifications with increasing iron concentration are made to the spectrum of Fe^{3+} ions (Fig. 5.5.4). The heights of the peaks around 25000 – 27000 cm^{-1} and for the peak at 22400 cm^{-1} increase, particularly for the peaks at the highest wavenumbers, whose positions are independent on the ligand field strength. The reason for that modification is either a systematic error in the fitting of the UV-peaks, or an increasing *intensity stealing* due to the overlapping of these peaks at 22000 – 27300 cm^{-1} with the increasingly intense charge-transfer UV-peaks of Fe^{3+} and Fe^{2+} (Paul, 1982, p. 303). Third possible reason could be distorted tetrahedral or octahedral sites (Paul, given on the same page), where the radiation polarised in the xy-plane of the complex is preferred for absorption compared to that in the xz or yz planes. Fox et al (1982) claimed that there are two kinds of tetrahedral sites in Fe-doped sodiumsilicate glasses. The data of this work does not support or deny of this possibility. Fitting with more sets of overlapping peaks would not improve anything.

The repeatability of the fitted total Fe ion concentration is very good, ± 0,001 mol %, for Fe concentrations 0,05 - 0,5 mol % of added Fe_2O_3, and about ± 0,3 at 2,0 mol % level (Tables 5.5.2 and 5.5.3). The obtained increase in Fe concentration compared with the input concentration is due to contamination from the raw materials and during the melting, and from the measurement and fitting accuracy.

Interestingly, the fractions of Fe^{2+} and Fe^{3+} ions (Table 5.5.1 and 3, Fig. 5.5.3), calculated from the areas of the fitted Fe^{2+} and Fe^{3+} UV-peaks, show very similar, although slightly higher, fractions of these ions compared to the main results (Table 5.5.1), i.e. slightly closer to the wet

chemical results measured by Bingham (2000, p 101). This reveals that the UV-peaks are well fitted. The reason for the slightly higher Fe^{2+} fraction is probably a tiny scattering loss and maybe also a tail of the background loss of the host glass, i.e. some UV-peaks above 52000 cm^{-1}, that are not fitted separately or excluded by the background correction.

It is highly probable that at least the scattering loss tail may significantly increase the measured absorbance for inadequately homogenised samples at the highest wavenumbers (above 28000 cm^{-1}), where the UV-edge is measured and fitted. In the clear and undoped glasses, a 20 – 30 % higher UV-peak can be fitted at the wavenumbers 47000 cm^{-1} (Glass 196, Annex 8), because of a stronger effect of the background of the host glass. However, only a few such glasses were studied in this work (Chap. 5.8).

However, there seems to be systematic differences in the concentrations of octahedral and tetrahedral sites between the glasses (Figs 5.5.5 and 5.5.6). Fig. 5.5.5 shows that for Fe^{2+} ions the fraction of the octahedral sites decreases from 0,905 ±0,001 to 0,896 ± 0,001 with increasing iron concentration, while the fraction on the tetrahedral sites slightly increases from 0,097 to 0,105 ±0,001. The fitted fraction of octahedral Fe^{3+} ion sites increases with increasing iron concentration (Fig. 5.5.6), in particular, for PAB glasses made without the sulphate addition. It must be remembered that these calculations are based on the modified fitting parameters, and only the sum of the fitted peaks for both types of sites has been calibrated, as given in Chap. 5.4.2. The results for Glass 193 agree with the results from PAB Glasses. The peak heights are not calibrated, because the linear absorption coefficients of the different types of sites are not known. However, a linear calibration would only change the level of site concentrations, not the trends. Only an error in assignments or fitting parameters of the site peaks, or of the UV-peaks, could change the trends. For further discussions of these findings, see Chap. 5.7.

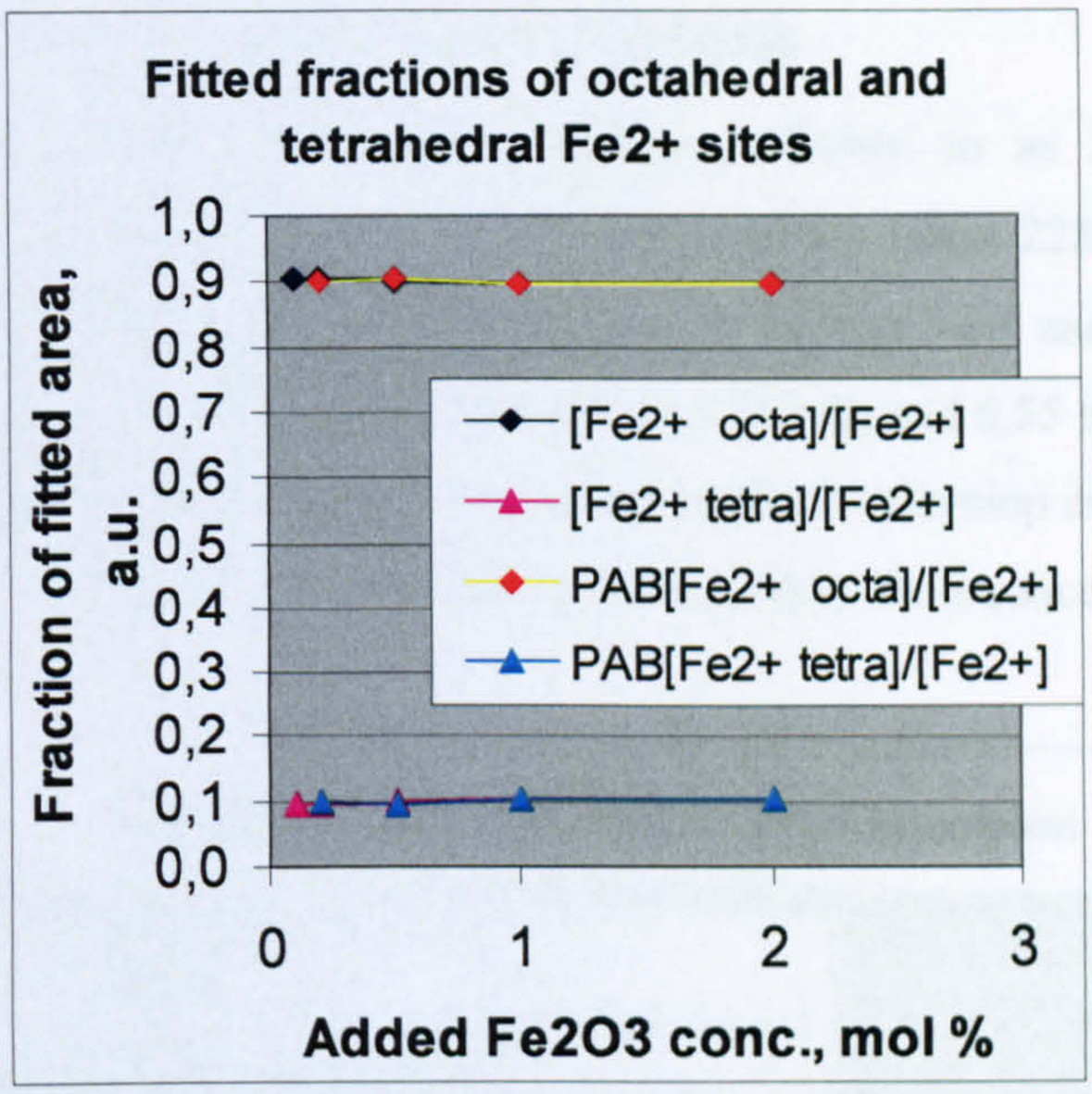

Fig. 5.5.5 Fractions of octahedral and tetrahedral sites of Fe^{2+} ions in electric melted 15natria-15calcia-70silica glasses, obtained by fitting analysis (Table 5.5.1). A similar absorptivity for both sites is assumed.

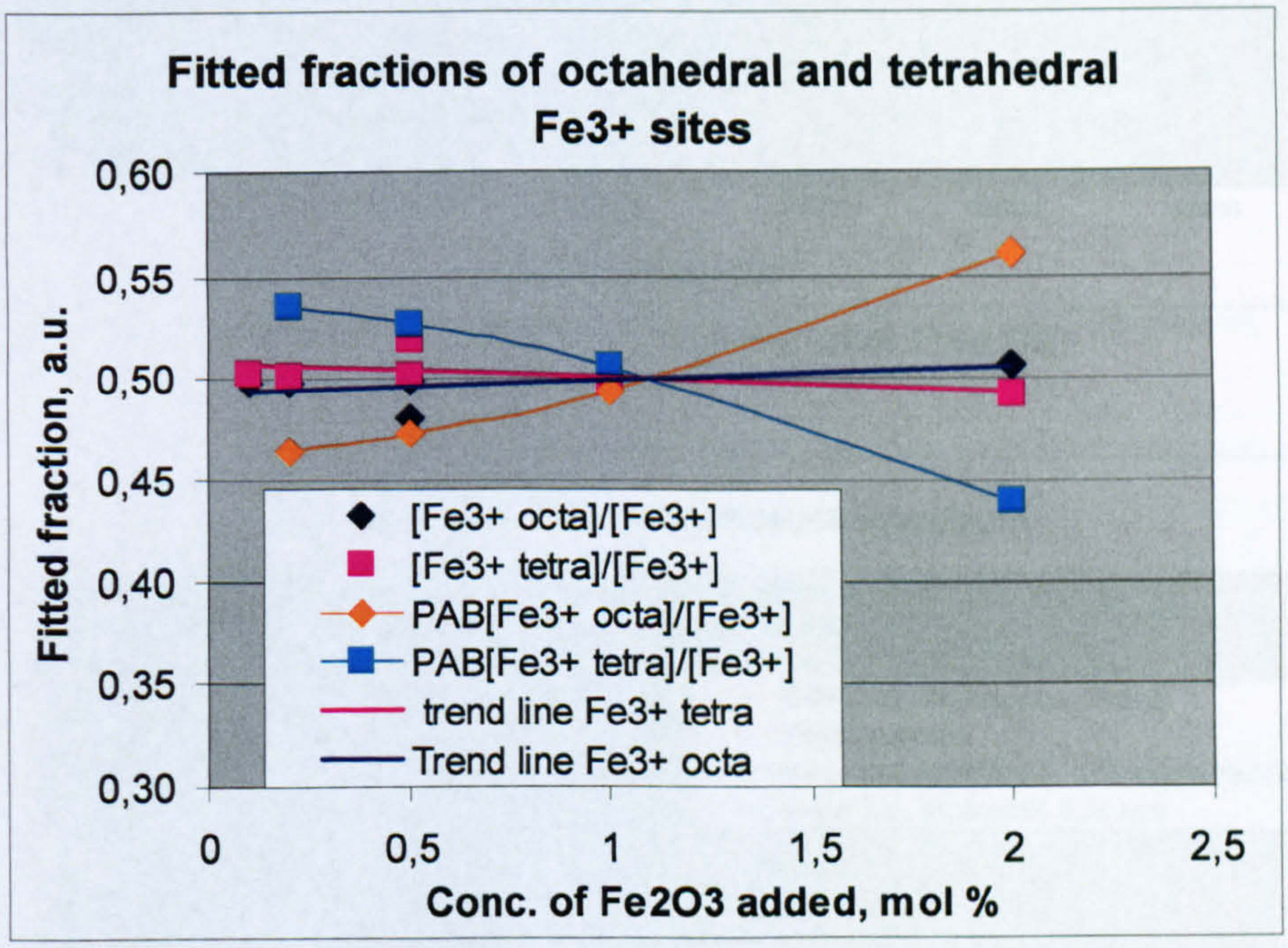

Fig. 5.5.6 Fractions of octahedral and tetrahedral sites of Fe^{3+} ions in electric melted 15natria-15calcia-70silica, obtained by fitting analysis (Table 5.5.1). A similar absorptivity of both sites is assumed.

The sulphate addition into this work glasses may have stabilised the redox of the Fe ions, in particular, the proportion of octahedral and tetrahedral Fe^{3+} sites, as reported for oxidising melting conditions by Müller-Simon (1994).

5.6 Fitting of Fe-S absorbance peaks

The absorbance spectrum of $Fe^{3+}[SO_3]$ species, referred to as Fe-S chromophores, was developed by fitting the spectrum of a low Fe concentration Glass 228 that was melted in a gas furnace and further reduced by adding 1,96 mol % carbon (Figs 5.6.1 and 2). The glass was doped with 0,05 mol % Fe_2O_3. Two samples of thicknesses 1,20 mm and 6,55 mm were prepared in order to obtain a fitted spectrum over a wide wavenumber scale. To develop an accurate fit, scaling with Fe-S concentration would require several glasses with various Fe-S concentrations.

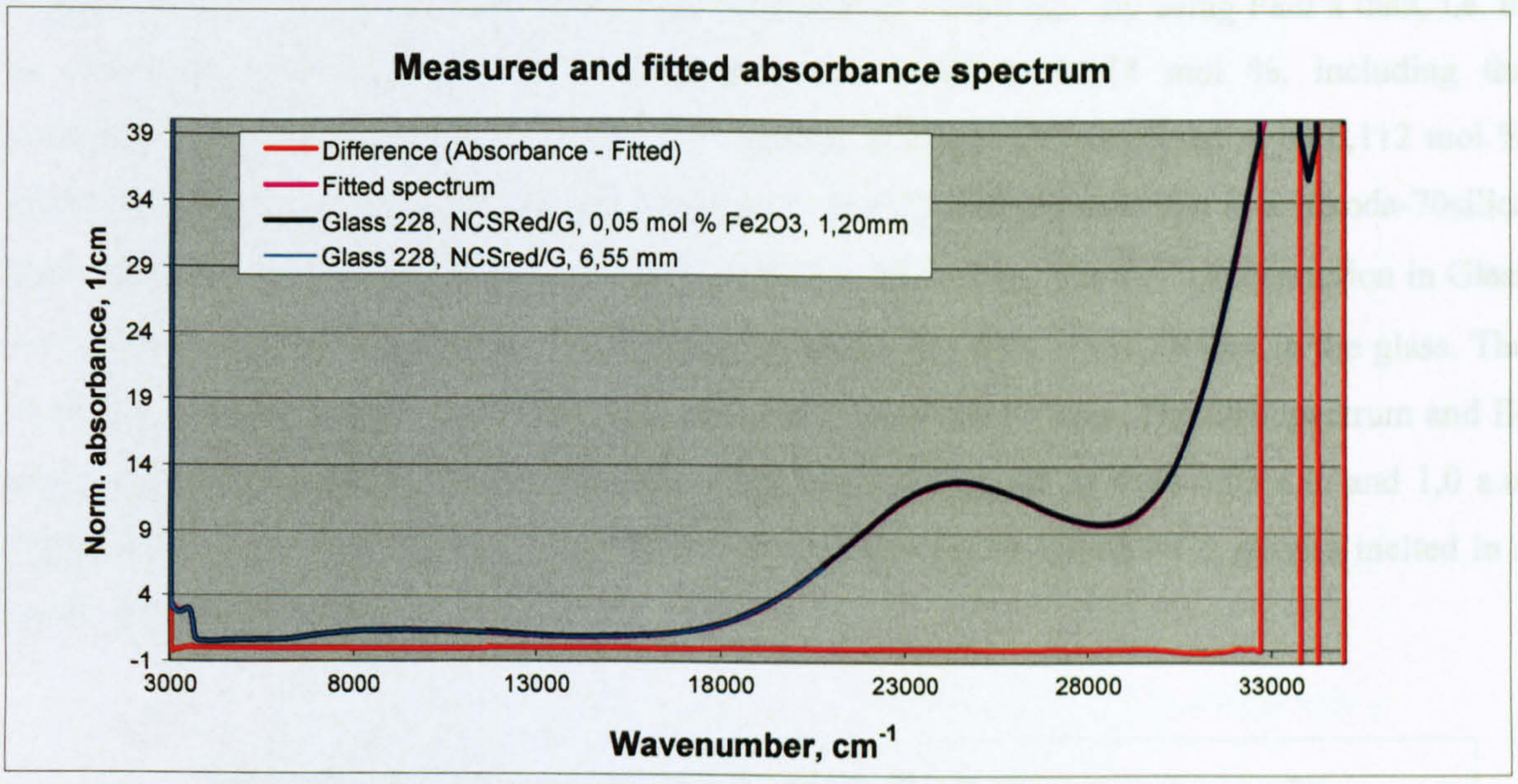

Fig. 5.6.1 Fitted absorbance spectrum of Fe-S containing amber Glass 288.

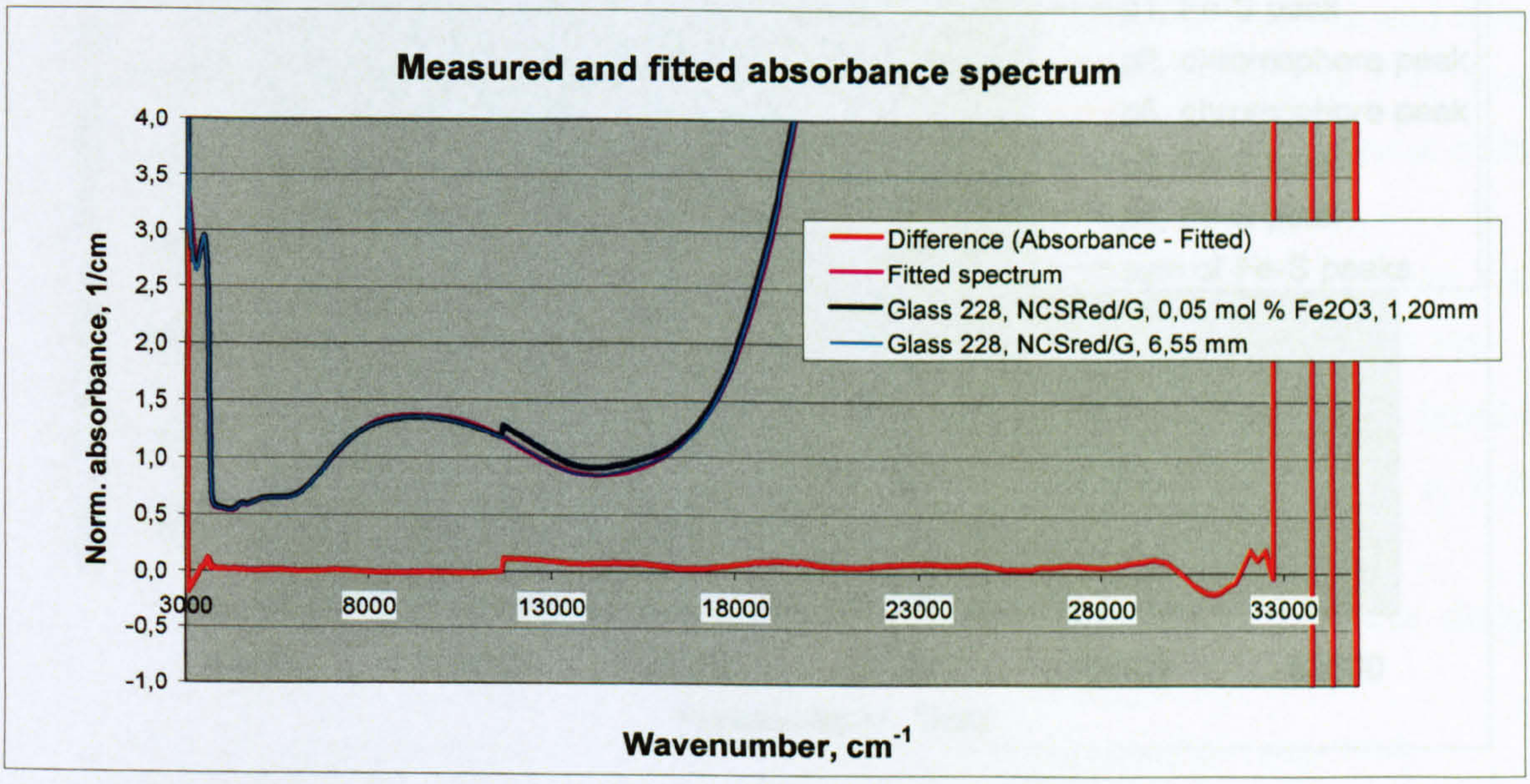

Fig. 5.6.2 Fitted absorbance spectrum of Fe-S containing amber Glass 288, shown with a more sensitive absorbance scale.

The fitting of the main two peaks was developed and calibrated using Paul's data (Paul, 1990, p. 329 - 330) as a guide. The Fe-S spectrum was found to contain three main peaks, of which usually only two highest ones at around 33900 cm^{-1} and 23500 cm^{-1} (Paul, 1990, p. 329) are reported. The extinction coefficient of the 23500 cm^{-1} band was reported by Paul as 9000 l mol^{-1} cm^{-1}, corresponding to about 3700 (mol % * cm)$^{-1}$ for the $Fe^{3+}[SO_3]$ species in the NCS glasses of this work. The linear absorption coefficient 26000 l mol^{-1} cm^{-1} for the peak at around 33900 cm^{-1} would be about 10700 (mol %*cm)$^{-1}$.

These bands were found at 34790 cm^{-1} and 24460 cm^{-1} in Glass 228 by fitting. The summed Fe-S spectrum for 1,0 mol % concentration was calibrated at 24460 cm^{-1} by using Paul's data, i.e. to be 3648 cm^{-1}. The total Fe ion concentration was fitted to 0,118 mol %, including the contamination from the mullite crucible. Fe^{2+} content in Glass 228 was fitted to be 0,112 mol % that is of the order of 94,5 % of the Fe ions present. Paul (1990) reported that in a 30soda-70silica glass melted at 1400 °C only 2.8 % of iron remained as ferric ions. The Fe^{3+} concentration in Glass 228 melted at 1450 °C was fitted to 0,003 mol %, which is 2.8 % of the Fe ions in the glass. The Fe-S concentration became to 0,00345 mol %, i.e. 2,9 % of the Fe ions. The OH-spectrum and IR edge concentration multipliers fitted to Glass 228 (Figs. 5.6.1 and 2) were 4,05 a.u. and 1,0 a.u. respectively. These are typical fitted OH and IR contents for Fe-doped NCS glasses melted in a gas furnace (Chap.5.7).

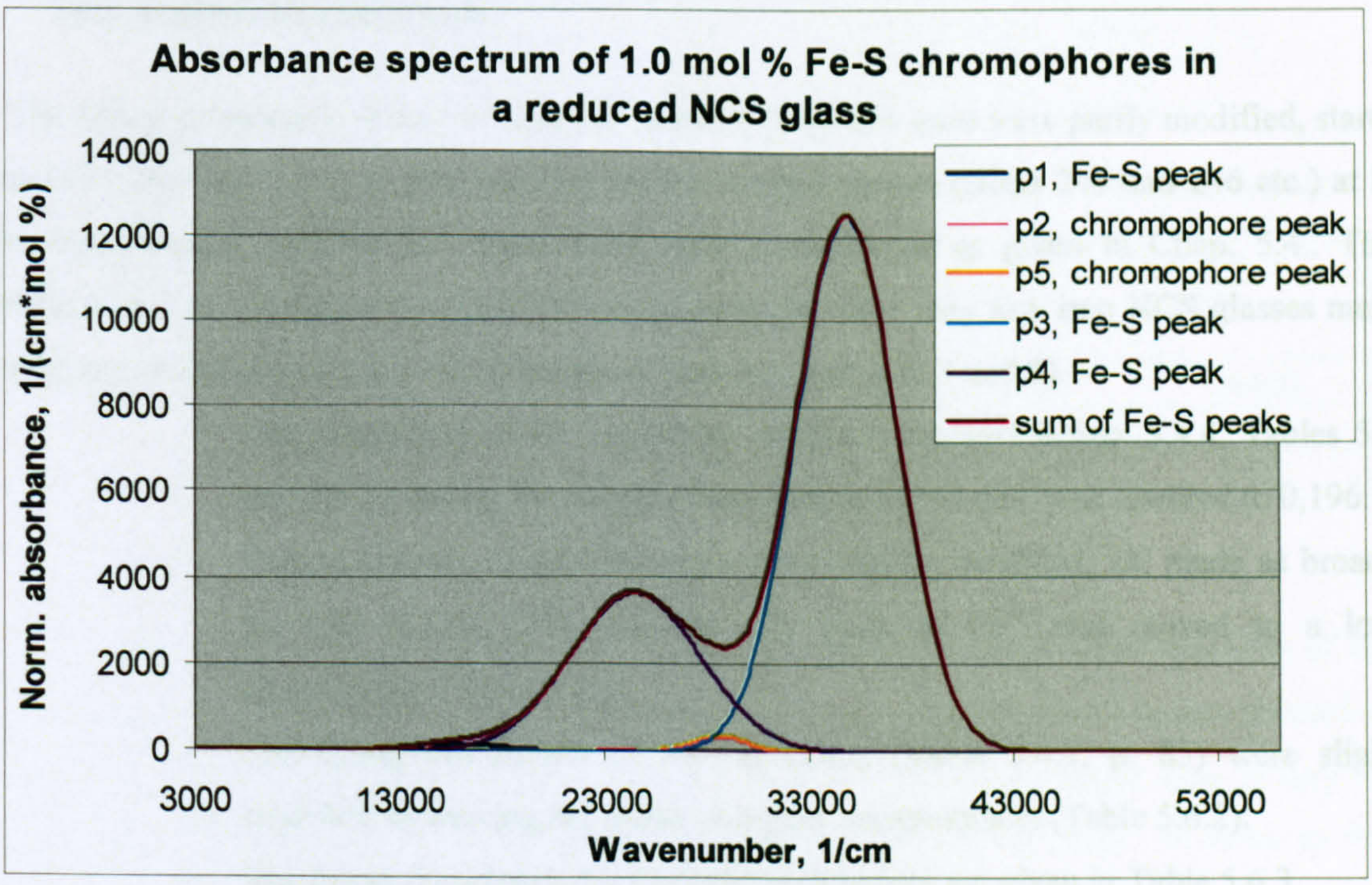

Fig. 5.6.3 Fitted and calibrated absorbance spectrum of 1,0 mol % Fe-S ions, used for fitting Glass 228.

A third peak at 15720 cm^{-1} has been obtained and also assigned to [Fe-S] because, it seems to scale with the Fe-S concentration. In addition, the Fe-S chromophore seems to have two other peaks between the high peaks, and they are suggested to be other absorption peaks of the same chromophores. The positions and widths of these mid-peaks resemble an absorbance spectrum of Fe^{3+} ions in octahedral sites (Ades et al, 1990).

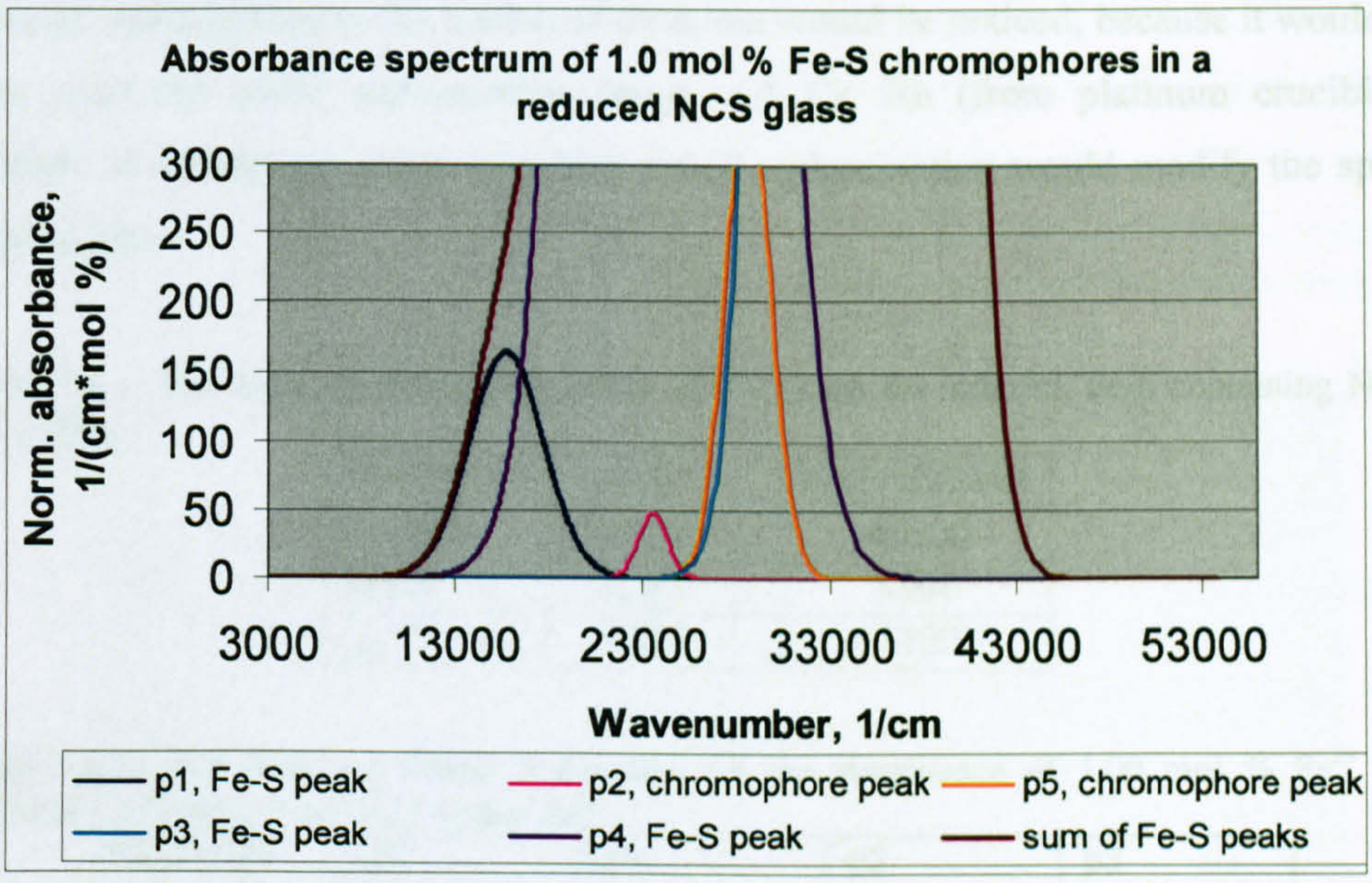

Fig. 5.6.4 Fitted absorbance spectrum of Fe-S ions as shown in Fig. 5.6.3, though with a more sensitive absorbance scale.

The fitting parameters of the Fe^{2+} and Fe^{3+} ions in Glass 288 used were partly modified, starting from FIT1 (see Fig. 5.5.4, p. 99) used for electric melted glasses (Glass 245 and 246 etc.) at low iron concentration, and the Fe^{2+} parameters were re-calibrated as given in Chap. 5.4.. These modifications are similar to the modifications needed for other very low iron NCS glasses melted in reducing conditions of a gas–fired furnace (Chap. 5.7, Annexes 7 and 8).

- The parameters of Fe^{3+} spectrum were not changed (Chap. 5.4.4, Tables 5.4.2 and 5.4.3), except the height of the peak at 25190 cm^{-1} was lowered to 0,196.
- The parameters of the UV-peaks were slightly modified, i.e. made as broad as for Fit2 (Glass 247), and the UV peak of Fe^{2+} was moved to a lower wavenumber (Table 5.6.1).
- The fitting parameters of Fe^{2+} spectrum (Table 5.4.1, p. 85) were slightly modified by moving the peaks to higher wavenumbers (Table 5.6.2).
- The fitting parameters for Fe-S chromophopres are given in Table 5.6.3.

It needs practise to be able to notice which glasses have any Fe-S peaks. The only hint is that the absorbance difference between the wavenumbers 22400 cm^{-1} and 26200 cm^{-1} is smaller in the glasses containing Fe-S chromophores than those that doesn't have Fe-S. The strong, shallow Fe-S peak at 24500 cm^{-1} raises the absorbance around 22000 – 24000 cm^{-1}, when Fe-S is present (Fig. 6.5.1). The Fe-S absorbance at around 26000 – 28000 cm^{-1} is much lower than at 23500 cm^{-1}, and thus the absorbance at 26200 cm^{-1} is raised much less. An unusually high constant background may cause a similar modification to the measured data, but would be noticed, because it would raise the absorbance over the entire wavenumber range. A Cr, Rh (from platinum crucible) or Cu contamination, or almost any other transition metal contamination would modify the spectrum at these wavelengths.

Table 5.6.1. The obtained fitting parameters of UV peaks for reduced, Fe-S containing NCS Glass 288.

Parameter	Fe3+UV		Fe2+UVpeak
position	39360		46500
width	3150		5990
α_p	1900		1100

Table 5.6.2. The obtained fitting parameters for the absorbance of 1,00 mol % Fe^{2+} for reduced, Fe-S containing NCS Glass 288.

Parameter	p5 tetrahedral	P1 tetrahedral	p2 octahedral	p3 octahedral
position	3590	4950	7450	10450
width	700	660	1430	2380
α_p	2,033	3,133	5,316	11,03

Table 5.6.3. The obtained fitting parameters for the absorbance of 1,00 mol % Fe-S complexes for reduced NCS Glass 288.

Parameter	p1, Fe-S peak	p2, chromophore peak	p5, chromophore peak	p3, Fe-S peak	p4, Fe-S peak
position	15720	23470	28600	34800	24460
Width	1990	800	1220	2460	3170
α_p	164	48	350	12550	3648

A clear indication of the presence of Fe-S complexes was also found in the spectrum of Glass 181 (Figs 5.6.5 and A8.1), an undoped NCS glass, melted in a gas furnace and further reduced with 0,49 mol % carbon. The UV-edge of Glass 181 is at wavenumbers lower than in any other undoped glass (Fig. A8.2) due to the lower content of Fe^{3+} ions in the glass. In order to fit the spectrum as shown in Fig. 5.6.5, the UV- peak parameters of Fe^{2+} and Fe^{3+} ions were slightly modified and the highest Fe-S was fitted at a higher wavenumber and with a narrower width (Fig.

5.6.6). The received fitting parameters are unsure, and thus not presented. Thus the dependency of all mentioned charge transfer peaks on the ion concentration, as well as on melting & annealing parameters should be studied carefully.

The total fitted iron content 0,026 mol % Fe ions of Glass 181 (0,0205 mol % as Fe^{2+}, 0,0059 mol % as Fe^{3+} and 0,000026 mol % as Fe-S chromophores) was lower than for other in mullite crucible melted undoped glasses. Maybe the sulphite or carbon somehow prevents the iron leaching from the crucible into the glass, or the calibration extinction coefficient used for the calibration of the Fe-S spectrum is not right. The fitted fraction of the Fe^{3+} ions in octahedral sites was unusually high, i.e. 0,77.

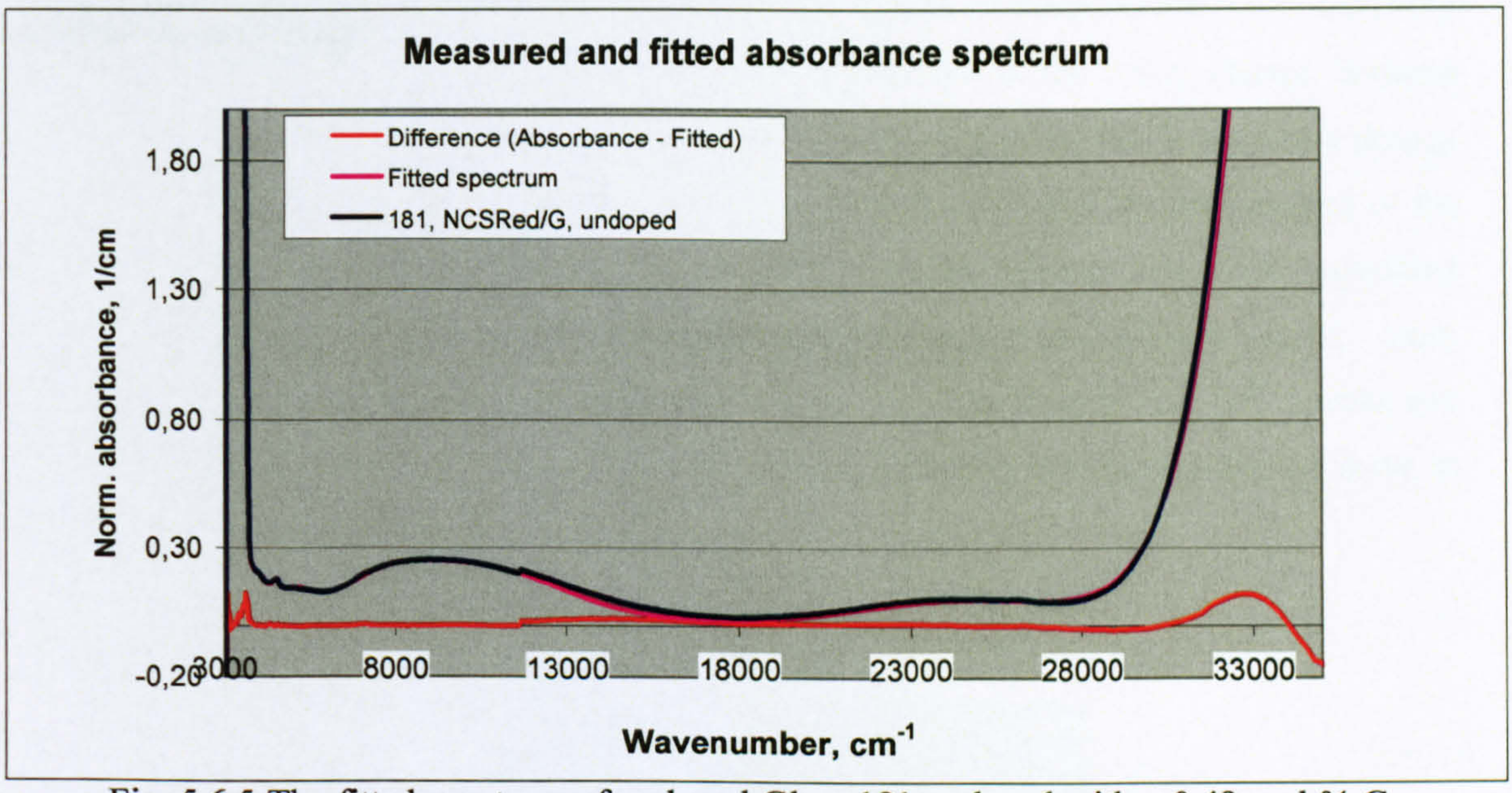

Fig. 5.6.5 The fitted spectrum of undoped Glass 181, reduced with a 0,49 mol % C and melted in a gas furnace. A peak of Fe-S chromophore around 24000 cm^{-1} is clearly noticed.

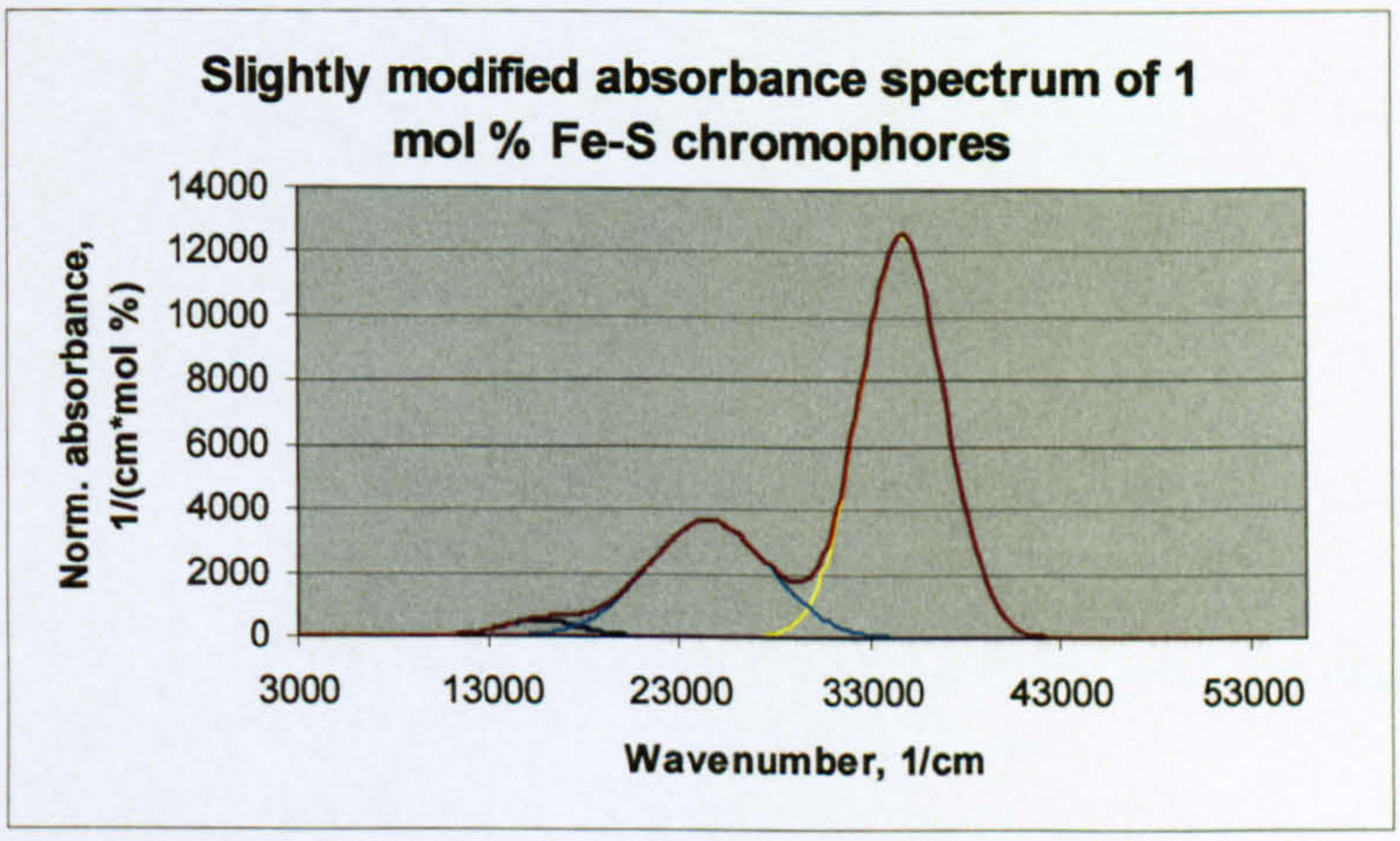

Fig. 5.6.6 The slightly modified absorbance spectrum of Fe-S chromophores for Glass 181.

The dependency of the absorbance spectrum of Fe - S chomophores on the concentration of sulphate and melting conditions was studied briefly. In Annex 8, Fig. A8.2, the spectra of the Glasses 225 – 227 and 229 with varying sulphate concentration from 0,25 to 0,45 mol % and doped with 0,05 mol % added Fe_2O_3 show normal behaviour, i.e. they have a UV-edge defined by the Fe-content and the UV-peaks of Fe^{3+} and Fe^{2+} ions. Sulphate can be concluded to have a reducing effect on iron (Fig. A8.2), resulting in a higher Fe^{2+} absorbance at around 1000 cm^{-1} and a lower absorbance over wavenumber range 15000 – 28000 cm^{-1} (Fig. A8.2). However, no Fe-S chromophores were found in Glasses 225, 226, 227 and 229 by fitting analysis. Glass 229 was oxidised by adding 2,0 mol % $NaNO_3$, thus containing more Fe^{3+} ions and less Fe^{2+} ions than Glasses 225, 226 and 227 (Annex 8, Fig. A8.2). A quantitative analysis of these glasses will be reported in a later stage.

5.7 Effect of melting conditions and redox

5.7.1. Results for Fe-doped NCS glasses melted in a gas furnace

The absorbance spectra and fitting parameters for the iron doped NCS glasses melted in a gas furnace are shown in Annex 7 and Table 5.71.

Development of the fitting parameters and calibration of ion concentrations for Fe^{2+} and Fe^{3+} ions spectra for the glasses melted under reducing conditions of a gas furnace was done in a similar way as for the glasses melted in an electric furnace, described in Chaps. 5.4 and 5.5. The Fe absorbance spectra of the glasses melted under reducing conditions (Annex 7, Figs. A7.1 – A7.6) differ, however, slightly from the absorbance spectra of those melted under oxidising conditions (Chaps. 5.4 and 5.5; and Annex 6). In addition to the redox change between concentrations of Fe^{2+} and Fe^{3+} ions, the main modification needed for the fitting was a change to the peak heights of the octahedral Fe^{3+} sites, that were raised, while the peak heights of the tetrahedral Fe^{3+} sites were decreased. This causes a similar change into their calculated concentrations (Table 5.7.1). The calculation suggests that these glasses contain more octahedral Fe^{3+} sites than tetrahedral (Table 5.7.1, Fig. 5.7.1). The behaviour of Fe^{2+} spectra and site concentrations were also different from the electric glasses, as is explained further down in this chapter.

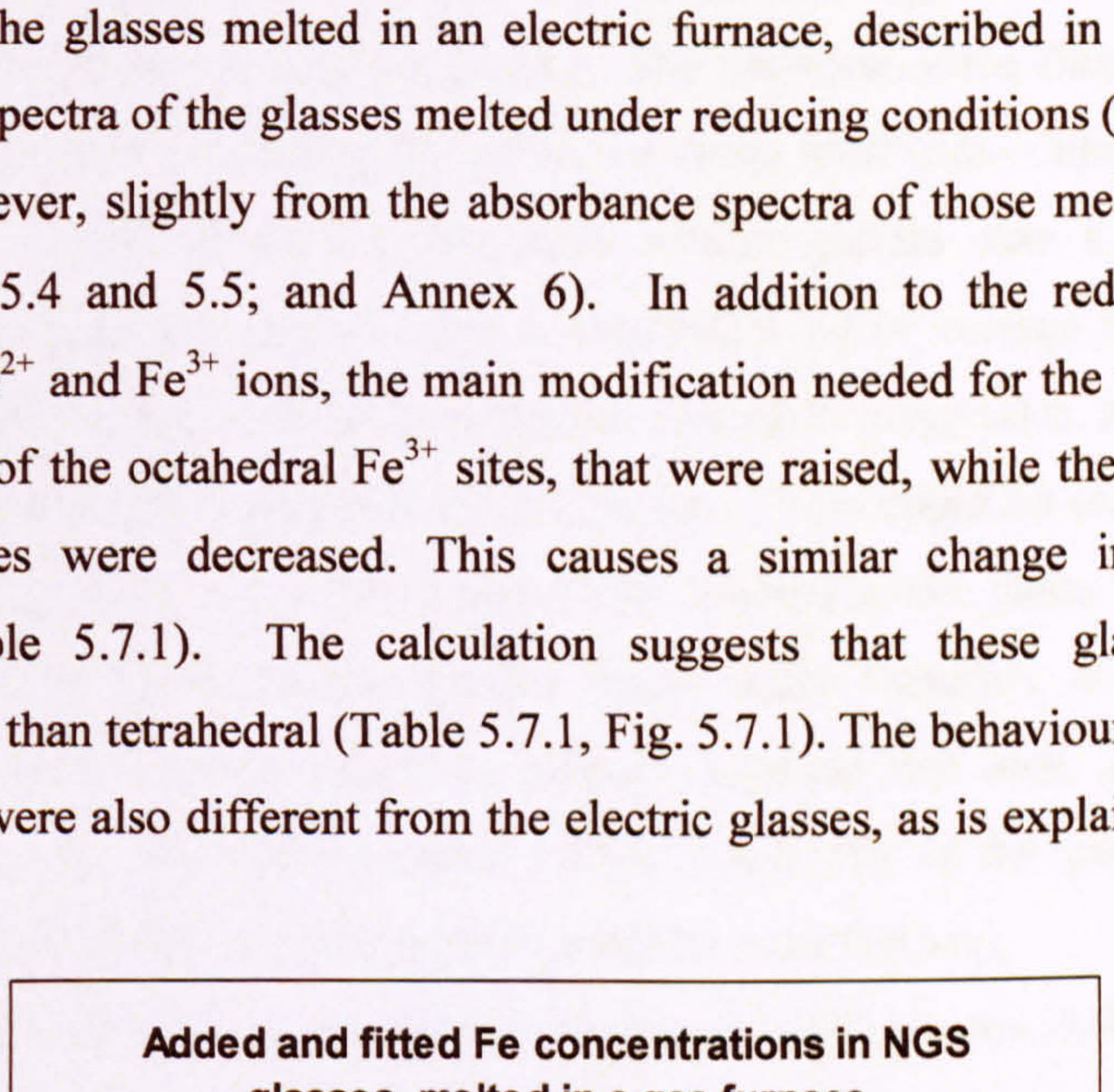

Fig. 5.7.1 Comparison between the fitted and added Fe concentrations in Fe doped NCS glasses melted in a gas furnace.

There is a linear correlation and agreement between the fitted and added iron concentration also in the NCS glasses melted in a gas furnace in mullite crucibles (Fig. 5.7.1, Table 5.7.1,

Annex 7). However, the total fitted concentration of Fe ions in these glasses is slightly higher than in the similar glasses melted in an electric furnace (Fig. 5.7.1, Table 5.7.1 and Chap. 5.5). Also the variation from a glass to another is slightly greater. The reason is the varying Fe contamination content leached into the melts from the mullite crucibles and tongs used to move the crucibles for re-filling.

The fitting parameters (Annex 7, Tables A7.1 – 4) of Fe^{2+} and Fe^{3+} ions spectra vary only a little from glass to glass and from the fitting parameters used for the glasses melted in electric furnace. The material is slightly too limited to establish one single fit that would scale linearly with Fe-concentration for the gas melted glasses. The variation of the fitting parameters can be assumed to correspond to the uncertainty of the received total iron content and other species, and inhomogeneity of the glasses. A few more similar glasses over a slightly wider Fe—concentration range would give a possibility to establish a list of average fitting parameters and their variation ranges for this melting environment and glass preparation method. The greatest uncertainty is involved to the parameters of UV-peaks. There might be some other background loss involved, raising either from other species also leached to the melts from the crucibles or light scattering loss raised from the greater micro scale variation of the glass structure, compared to the similar glasses melted in electric furnaces that were also homogenised by casting to frit into the water and re-melted. Only Glass 242 of the gas melted glasses was treated in this way and melted in a platinum crucible in a gas furnace.

The results of the fitting analysis on the Fe-doped NCG glasses melted in a gas furnace (Annex 7, Table 5.7.1) show the following findings:

- A small fraction of the Fe^{3+} ions are found in Fe-S bond containing chromophores (Chap. 5.6, Table 5.7.1, Annexes 7 and 8), which increases the absorbance at wavenumbers 15000 – 28000 cm^{-1}, in particular around 23000 cm^{-1} and around 15500 cm^{-1}.
- A significantly higher average fraction of Fe^{2+} ions, about 19 % (compared to 15 % in an electric furnace melted glasses) and a greater variation from a glass to another, i.e. ± 3 %, for the glasses within 0,25 – 0,74 mol % added Fe_2O_3 iron concentration range were found, as was expected from the literature survey (Chap. 5.2.).
- An additional strong reducing effect was caused by a 0,49 mol % carbon addition (Glass 130), which raised the Fe^{2+} fraction to the level of 30,4 % and Fe-S concentration to $6*10^{-5}$ mol %, whereas a decrease of the fraction down to 15,3 % was found in Glass 141, oxidised by a nitrate addition of 1 mol %, as was also expected from the literature Chap. 5.2.

- Slightly higher fractions of Fe^{2+} ions were found in tetrahedral sites (Table 5.7.1 and Fig. 5.7.3) in undoped and low-iron glasses, compared to the similar glasses melted in oxidising conditions.
- An increased overall absorbance level over the visible range 400 – 700 nm due was found to fit with higher concentrations of Fe^{3+} ions in octahedral sites (agrees to the findings in recent literature Chap. 5.2.), compared to the similar glasses melted in oxidising conditions of an electric furnace (Table 5.7.1, Annex 7).
- The fitted heights of the Fe^{2+} and Fe^{3+} UV-peaks (Table A7.3), are slightly lower than in electric melted glasses, as was also suggested by the diffuse reflection spectra analysis for these glasses (Fig. 5.4.7, p. 89).

Table 5.7.1 The fitted concentrations of the spectrum parts and the calculated portions of Fe^{2+} and Fe^{3+} ions in octahedral and tetrahedral sites.

Glass	OH-cont. a.u.	IR-edge, a.u.	[Fe-S], a.u.	$[Fe^{2+}]$, mol %	$[Fe^{2+}$ octa], a.u*.	$[Fe^{2+}$ tetra], a.u.*	$[Fe^{3+}]$, mol %	$[Fe^{3+}$ octa], a.u.*	$[Fe^{3+}$ tetra], a.u.*
97	4,0	0,7	-	0,0090	0,0077	0,0013	0,062	0,036	0,025
242**	3,45	0,7	-	0,0214	0,0023	0,0191	0,079	0,0449	0,0341
225	4,1	0,7	-	0,0297	0,0038	0,0252	0,087	0,0417	0,0393
82	4,1	0,7	$5*10^{-6}$	0,100	0,089	0,011	0,405	0,221	0,184
81	3,7	0,5	$1*10^{-5}$	0,160	0,143	0,017	0,855	0,428	0,427
83	4,5	0,5	$5*10^{-5}$	0,321	0,287	0,033	1,18	0,676	0,504
130	4,9	0,5	$5,6*10^{-5}$	0,337	0,301	0,036	0,790	0,511	0,278
141	3,7	0,5	$2*10^{-5}$	0,150	0,134	0,016	0,830	0,428	0,427

Note * = estimated by multiplying the ion concentration by the fraction of the site peaks area divided by the total fitted area of the ion peaks. Similar absorptivities of the tetrahedral and octahedral sites are assumed.
Note ** = made of purified ingredients, melted in Pt crucible.

The undoped Glass 97 shows a high fitted iron concentration (0,07 mol %, Table 5.7.1), which is of the order the XRF analysis result for the mullite crucible melted glasses Glasses 97 and 28 (Annex 3), but above the contamination level of the raw materials, ca. 0,015 weight % ≈ 0,01 mol % Fe_2O_3, as was measured for Glasses 86 and 41 melted in a platinum crucible (Annex 3). The extra iron in Glass 97, about 0,06 mol %, has leached out to the melt from the mullite crucible. It is also noticed that the additional leached iron fraction is highest in the undoped glass, and decreases with the added iron concentration (Tables 5.7.1 and A7.1). This is

understandable, because the chemical leaching reaction tries to reach an equilibrium iron concentration of a similar order in the glass melt as in the mullite. For the glasses with an added iron concentration of the order of mullite level or higher, the iron leaching from the mullite reduces.

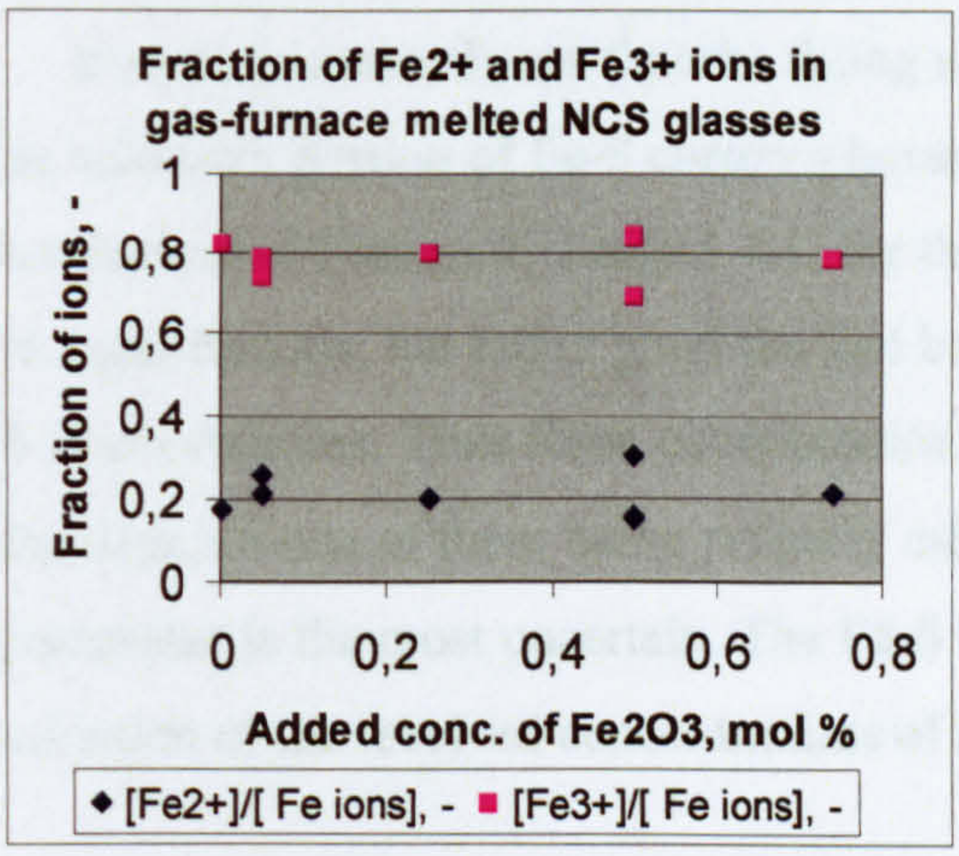

Fig. 5.7.2 Fractions of Fe^{2+} and Fe^{3+} ions in NCS glasses melted in a gas furnace, obtained by the fitting analysis. The concentration of Fe^{3+} ions in Fe-S chromophores is included to the total Fe concentrations. The results of the reduced Glass 130 and oxidised Glass 141 are included (Table 5.7.1).

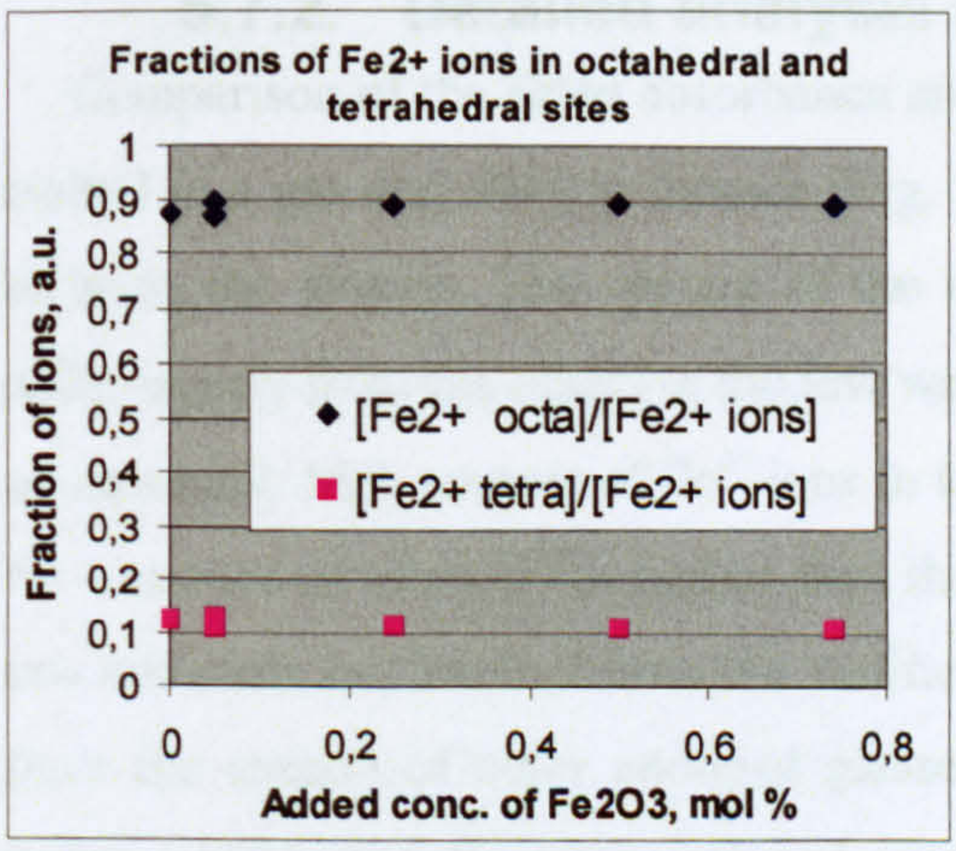

Fig. 5.7.3 Fractions of Fe^{2+} ions in octahedral and tetrahedral sites in gas furnace melted NCS glasses (Table 5.7.1).

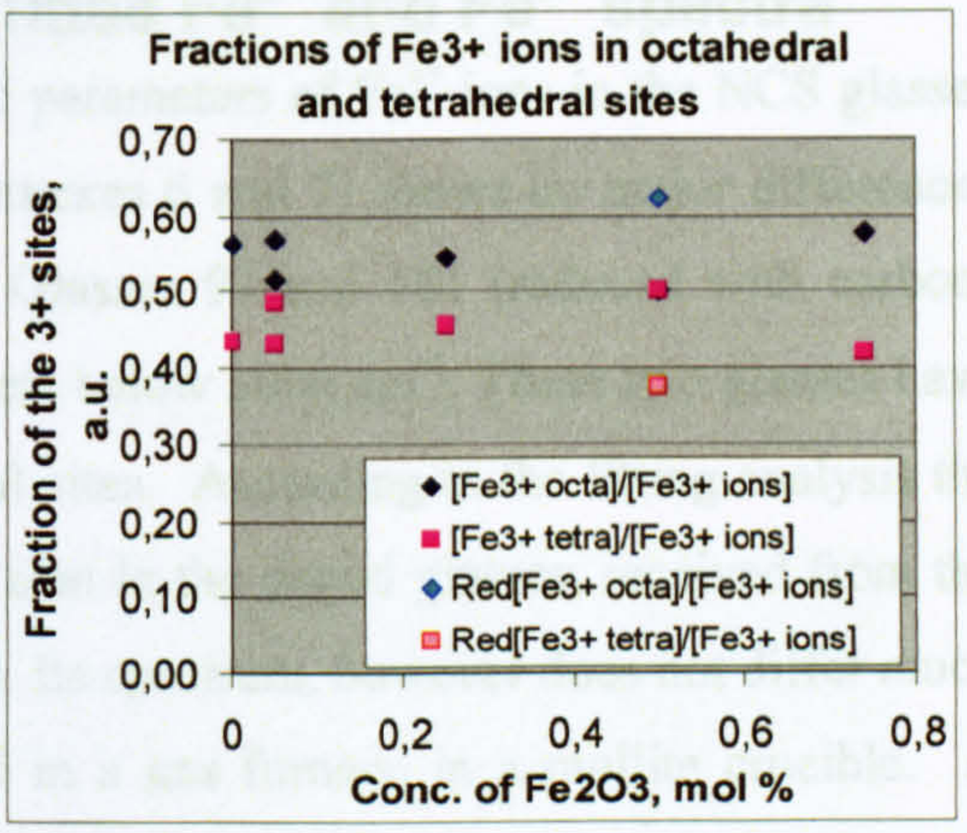

Fig. 5.7.4 Fractions of octahedral and tetrahedral sites in gas furnace melted NCS glasses (Table 5.7.1).

The obtained fractions of Fe^{2+} ions in octahedral and tetrahedral sites stay at the same, slightly with iron concentration increasing and decreasing level respectively (Fig. 5.7.3, data of Glasses 130 and 141 are included), in spite of the redox ratio $[Fe^{2+}]/[Fe^{3+}]$ changes caused by addition of carbon or nitrate (Figs, 5.7.2).

The obtained fractions of Fe^{3+} ions in octahedral and tetrahedral sites are changed in the reduced Glass 130, i.e. seem to change with a major change in redox. The balance between the Fe^{3+} sites seems to be sensitive to the melting conditions and glass preparation. Glasses 81, 82 and 83 were melted in separate crucibles in the same furnace and annealed simultaneously in the

same electric furnace, together with four other glasses. There are differences in the ion and site fractions between these glasses, as can be obtained from the data of Table 5.7.1. The glasses were not stirred and they might have experienced a few degrees difference in a melting and/or annealing temperature. These glasses probably have not achieved an equilibrium state for the chemical reactions or complete homogeneity of oxygen concentration.

It must be remembered that the fitting analysis might not be so accurate quantitatively, when an unknown portion of Fe-S chromophores may, or may not, be involved. The "best fits so far" are presented (Annex 7, Table 5.7.1) for the Fe-doped and sulphate refined NCS glasses melted in a gas furnace, but rather good fits had been received also without including the spectra of Fe-S chromophores. Thus three concentration parameters ([Fe^{2+}], [Fe^{3+}] and [Fe-S]) were fitted to the data, no-one of them being properly calibrated, and the calibration of the Fe-S concentration parameter is the most uncertain. The Fe-S concentrations received are small, of the order of the variation of the received concentrations of Fe^{2+} and Fe^{3+} ions.

5.7.2. Detailed analysis of the fitted Fe^{2+} and Fe^{3+} spectra

Comparison of the fitted absorbance spectra and parameters of Fe^{2+} ions in the NCS glasses melted in a gas and electric furnace (Fig. 5.7.4, Annexes 6 and 7) shows no major differences between the glasses. The spectra of the undoped Glasses 97 and 181 (reduced with carbon) differ mostly from the others at the low wavenumbers below 5000 cm^{-1}. These two glasses have an unusually high content of Fe^{2+} ions in tetrahedral sites. According to the fitting analysis the Fe – content of Glass 97 is higher than the excess iron in the doped glasses, received from the raw materials and leached from the mullite crucible. Its spectrum, however does not differ much from the spectra of other undoped glasses melted in a gas furnace in a mullite crucible. A tentative fitting of the other undoped, very low iron glasses (Glasses, 1, 9, 26, 235, Annex 8) suggested a slightly higher fraction of the tetrahedral Fe^{2+} sites in very low iron glasses than in average in the studied Fe-doped glasses. However, this kind of statement should be confirmed by a careful analysis by another method.

The Fe^{2+} absorbance spectrum can be seen be affected by melting conditions (Figs. 5.7.4 and 5). Glass 130 that was reduced with adding 0,49 mol % carbon, has highest octahedral Fe^{2+} band and is fitted with broader peaks at the positions closer to each others, compared to other of other glasses. Correspondingly its tetrahedral band is smallest.

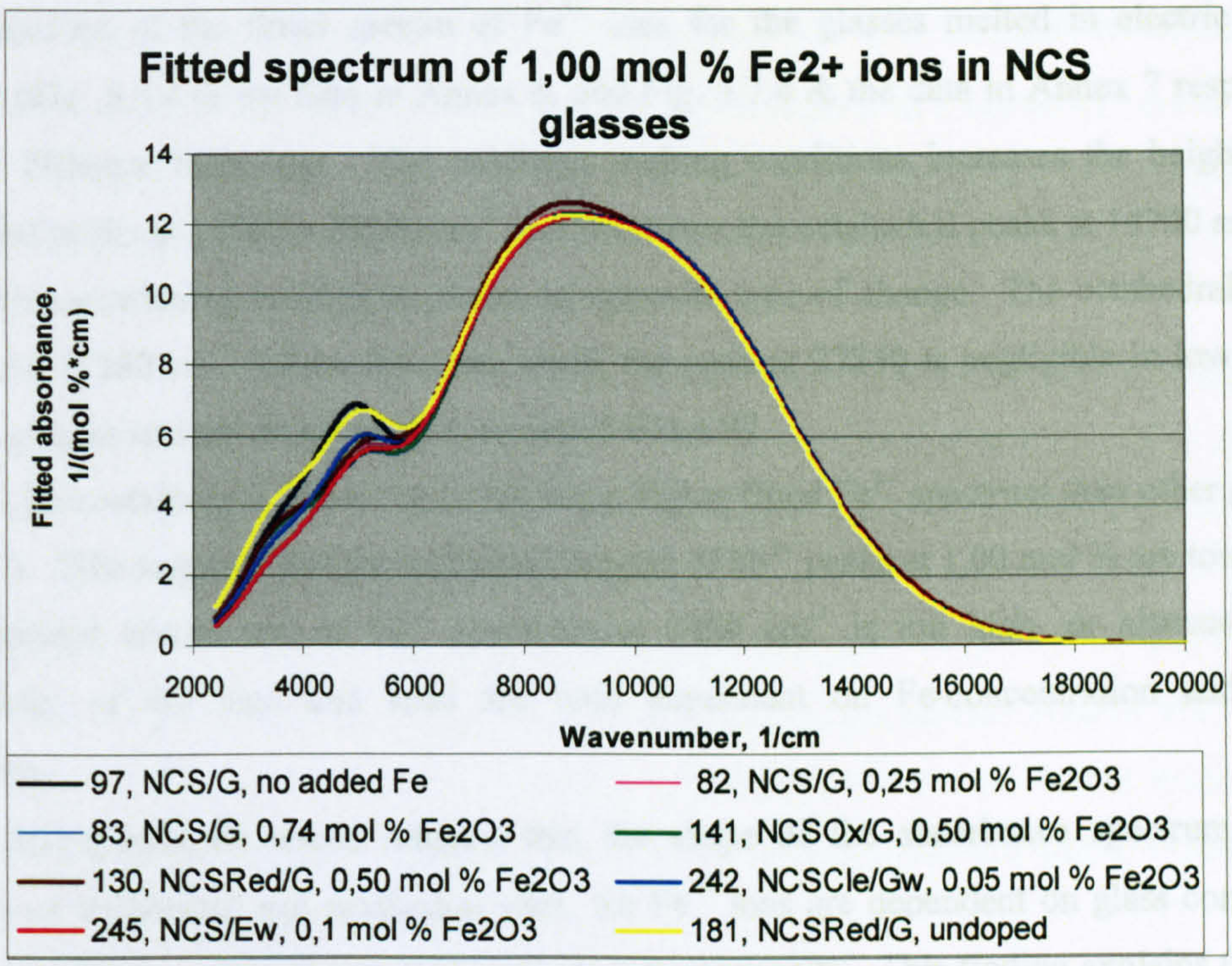

Fig. 5.7.4 The fitted spectrum of Fe^{2+} ions in NCS glasses melted in gas and electric furnaces, showing the changes in the whole spectrum caused by iron concentration and effect of reducing and oxidising agents.

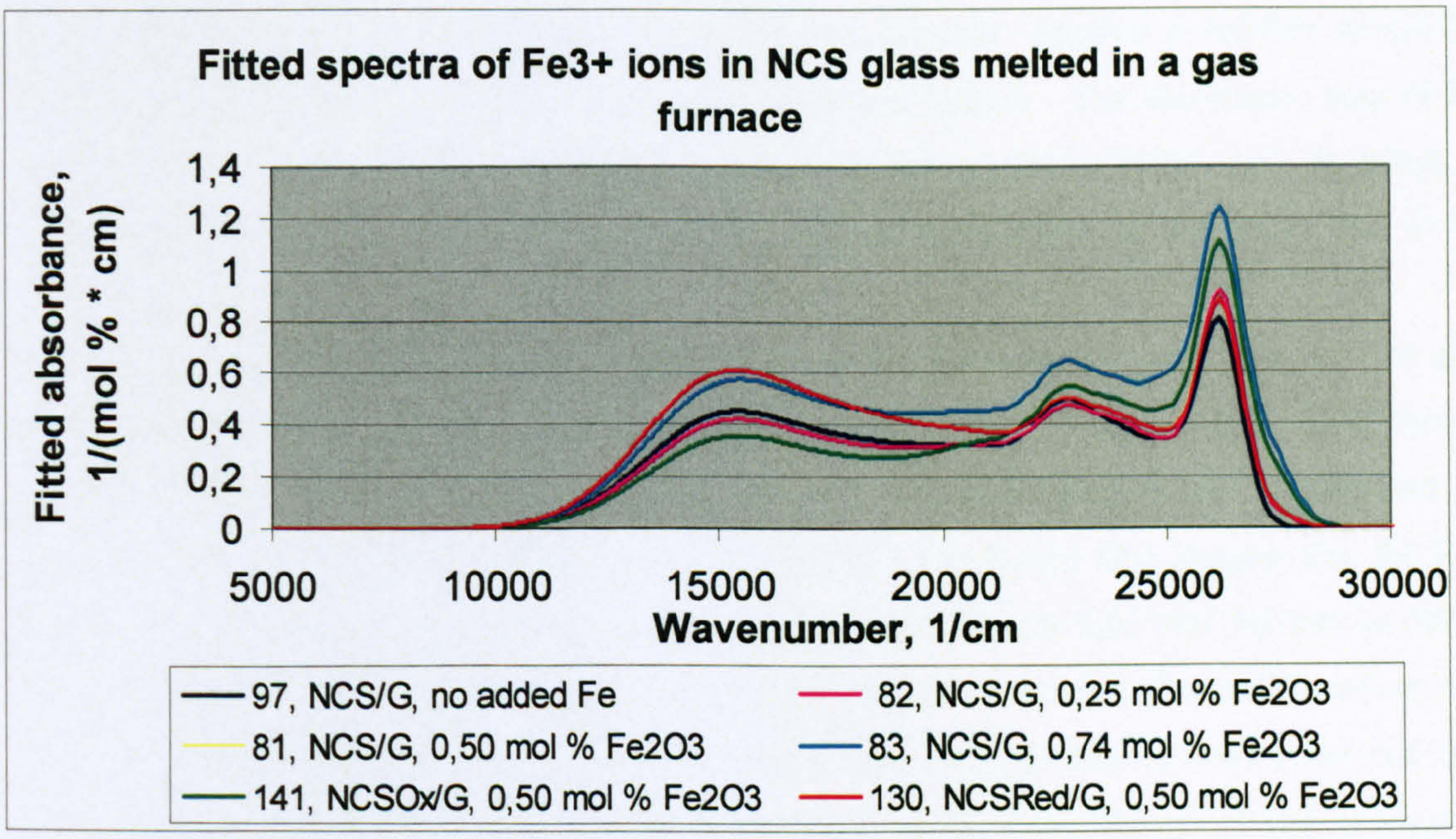

Fig. 5.7.5 The fitted spectrum of Fe^{3+} ions in NCS glasses melted in a gas furnace, showing the changes caused by varying of the Fe concentration, as well as reducing and oxidising agents.

Comparison of the fitted spectra of Fe^{3+} ions for the glasses melted in electric and gas furnaces (Fig. 5.5.4 & the data in Annex 6, and Fig. 5.7.4 & the data in Annex 7 respectively) shows a different behaviour. The oxidising melting conditions increases the heights of the tetrahedral peaks at 22000 – 26200 cm^{-1} and decreases the octahedral peaks at 14700 and 18350 cm^{-1}, whereas reducing conditions causes an opposite type of change. The octahedral peaks at 25190 and 27250 cm^{-1} follow the same trend, the peak at 27250 is negligible in low iron and reduced glasses and not found at all in undoped Glass 97.

Glass 83 containing 0,74 mol % Fe_2O_3 has a higher fitted Fe^{3+} spectrum than other glasses in Fig. 5.7.5. This suggests that the calibrated heights of Fe^{3+} peaks at 1,00 mol % are too low, and the calibrated absorbance of Fe^{2+} spectrum at 1000 cm^{-1} is too high, or alternatively the absorbtivity of the ions and sites are both dependent on Fe-concentration and melting conditions.

The fitting analysis results suggest that the shape of the absorbance spectrum, and the fractions of tetrahedral and octahedral sites, for Fe^{3+} ions are dependent on glass composition, melting conditions, iron concentration and glass homogeneity. This finding explains the variety of conclusions and results found in literature for similar kind of glasses (Chap.5.2).

5.8 Fitting of absorbance spectrum for Fe contamination

The Figs. A8.2, A8.3 and A8.4 (Annex 8) show the measured absorbance curves for undoped and low iron glasses melted in both gas and electric furnaces. The fitting and results for most of these glasses are discussed in previous chapters: Glasses 97, 242 and 225 in Chap. 7.5, Glasses 181 and 228 in Chap. 5.6 and Glass 245 in Chap. 5.4.

Glass 97 (fitted in Chap.5.7) and the other fitted glasses, can be reliably analysed by fitting, because they had a well prepared sample (the curve has no step at 860 nm, (11655 cm^{-1}) between the detectors) and they show a significant iron absorbance (Table 5.7.1, Glass 97: 0,07 mol % Fe ions) compared to all other issues causing absorption.

The absorbance curves for Glasses 9, 26, 200, 186, 188, 226 – 229, 235, 33 and 196, shown in Annex 8, were fitted tentatively. It was found that the UV-edge, not the shallow absorbance peaks within visible and Near IR range, is the most accurate indicator for the dopant levels at very low concentrations, provided that all contamination species are identified and their UV-peak parameters at low concentration level are known.

The undoped Glasses 235, 196 and 33 melted in an electric furnace (Fig. A8.4) contain obviously both Cu (Chap. 6) and Fe as contamination, because there is an shallow band below 23000 cm^{-1} and another around 13000 cm^{-1} similarly to the Glass 197 that is slightly (0,004 mol %) doped with Cu. Both Cu^{2+} and Cu^{1+} have strong absorbance peaks at UV, so Cu contaminated glasses can not be correctly fitted without Cu absorption peaks. Another possibility would be Pt dissolved into the glass from the crucible used in electric furnace. The absorbance step of Glass 197 curve at 11655 cm^{-1} reveals that the absorbance over 15000 – 28000 cm^{-1} is raised. The absorbance should be at the same level as the shown absorbance for the glass 188 at these wavenumbers.

The conclusions are that singly Fe doped glasses at low Fe concentrations down to 0,05 mol % can be analysed by the fitting method developed by using 0,1 - 1 cm samples, as is shown in previous chapters. Most probably by using thicker, well homogenised and equilibrated glass samples, much lower Fe concentrations can be studied. The results also suggest that the Fe ion redox ratios and the fractions of sites for very low Fe glasses (below 0,05 mol %) may be different and vary more from sample to another compared to more Fe containing glasses. However, this is only an indication, not properly proved. No thicker than 10 mm samples were measured in this work. The larger variation seen in the fitted parameters at low iron glasses can also be caused by the variation in contamination species, sample preparation and melting conditions.

5.9 Discussion and conclusions of the fitting method and results for the Fe-doped glasses

5.9.1. Suitability, accuracy and repeatability of the fitting method

Summed Gaussian peaks are shown to be suitable for fitting the UV-Vis-Near IR absorbance spectrum of iron in soda-lime-silica glass at low iron concentrations. A mathematical description for a full 200 – 3300 nm UV-Vis-Near IR absorbance spectrum of iron has thus been developed and tested for analysis of two series of NCS glass samples melted in oxidising conditions in an electric furnace and in reducing conditions in a gas furnace. The respective charge transfer UV peaks are also included to the fitted spectra and they are shown to scale linearly with the Fe^{2+} and Fe^{3+} ion concentrations within a limited iron concentration range up to 0,5 mol %. The fitted spectrum can be used for quantitative valence, redox and structural analysis of iron contamination and iron doping for sulphate refined 15natria-15calcia-70silica glasses at iron concentrations 0,02 – 1 mol % and melted in various conditions.

It is demonstrated, for first time, that the absorbance spectra of octahedral and tethedral sites for both Fe^{2+} and Fe^{3+} can be fitted separately. The concentrations: [Fe], [Fe^{2+}], [Fe^{3+}] can be obtained with ±0,001 repeatability. For the first time, also the measures for the site concentrations: [Fe^{2+}, octa], [Fe^{2+}, tetra], [Fe^{3+}octa] and [Fe^{3+}, tetra] can be simultaneously established, as the summed areas of their fitted absorbance peaks, from a measured absorbance spectrum with the developed wide (200 – 3200 nm) range optical absorbance spectroscopy method, provided that the glass samples are carefully melted and prepared and the measurement is done accurately. The site concentrations are given in arbitrary units, because no suitable calibration method was available within this project.

It is a requirement for accurate fitting and calculation of the correct concentrations that all significant background losses are also fitted with the same order of precision and repeatability as the iron spectrum itself. The background losses, quoted with the fitted concentration parameters, for the "water" peaks and the "IR-edge" are demonstrated to depend on the glass melting conditions, redox and crucible material and to vary slightly from sample to sample. The accurate separation of the water and IR-edge spectra from the Fe spectrum is essential for the accurate fitting of the Fe^{2+} spectrum (on which the calibration of the concentrations of the whole method are based). The water and IR edge are seen to vary significantly from sample to sample, and particularly the water level is higher for the glasses melted in gas furnace compared to electric melting, which condition increases three – fourfold the absorbance of the fitted OH-peaks. The reasons are probably: The significantly higher concentration of dissolved water originating from

the combustion of the hydrocarbon gas fuel, and from the mullite crucibles dissolved Al_2O_3 to the melt, which leads to more intense Al-OH peaks.

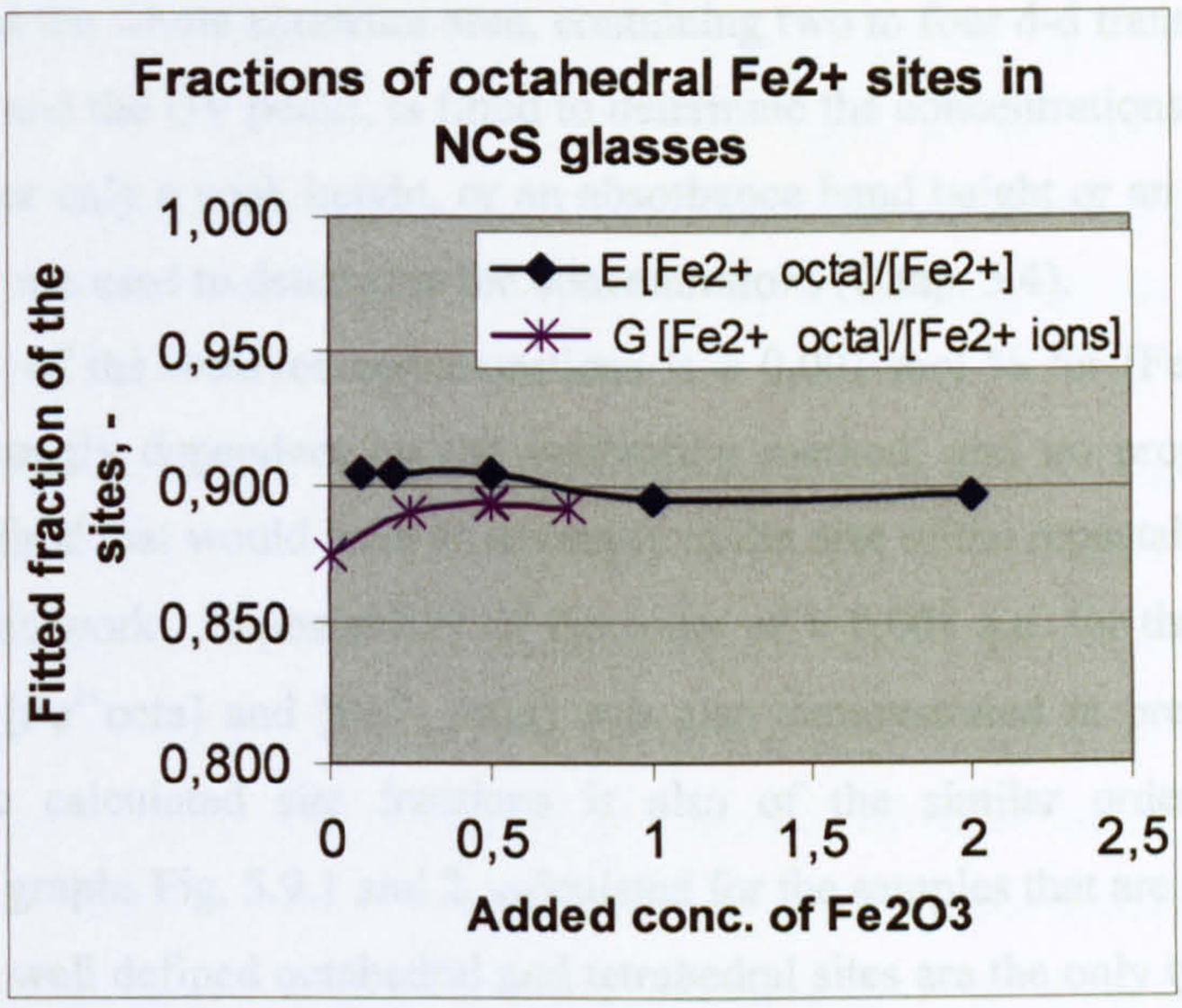

Fig. 5.9.1 Comparison of the fitted fractions for octahedral sites of Fe^{2+} ions, as calculated from the fitted results in Chaps. 5.5 and 5.7. Only the glasses with similar host composition is included. The results for those glasses that were melted differently or made of ultra pure chemicals or reduced/oxidised by adding of carbon/nitrate are excluded.

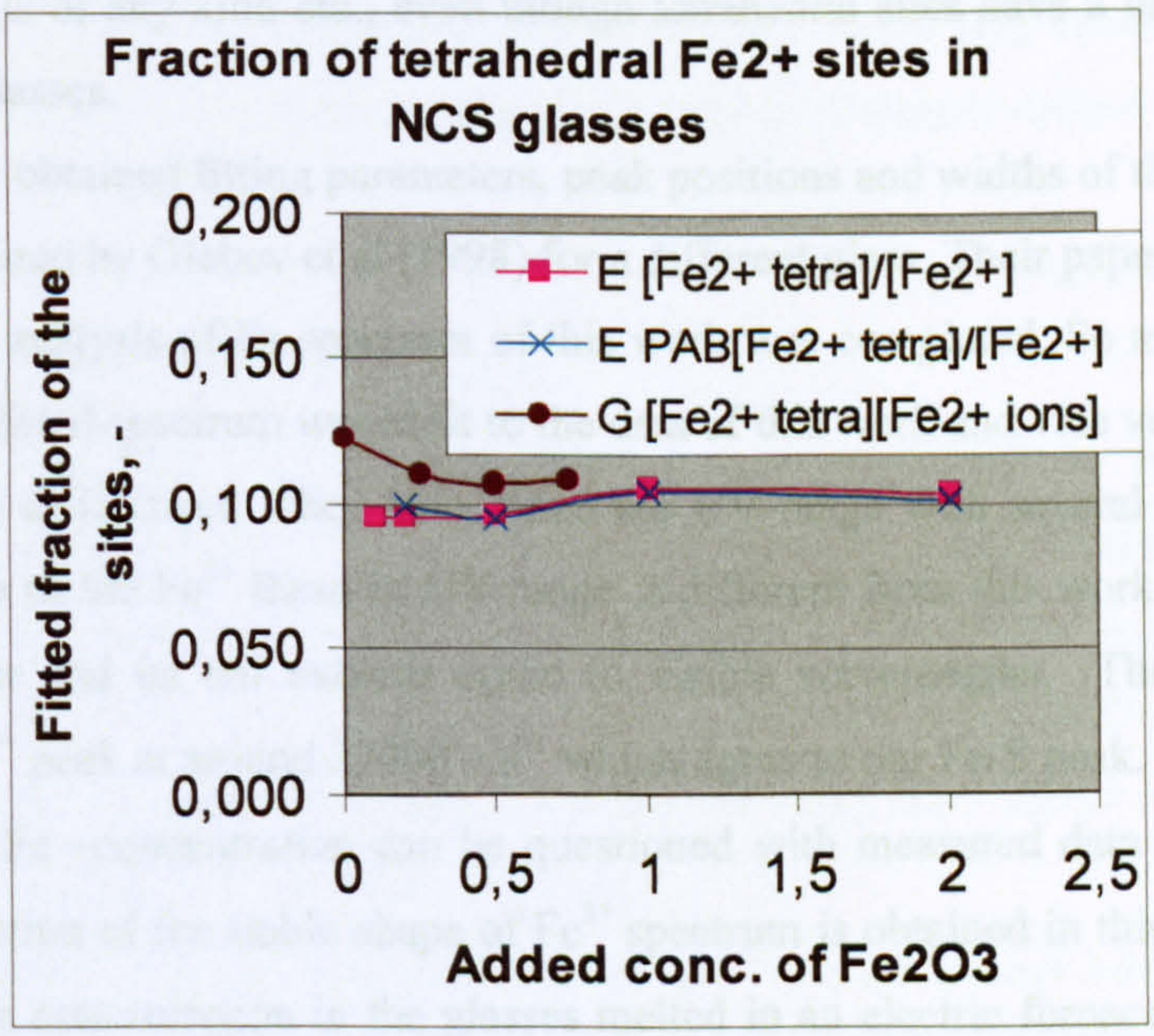

Fig. 5.9.2 Comparison of the fitted fractions for octahedral sites of Fe^{2+} ions, as calculated from the fitted results in Chaps. 5.5 and 5.7. Only the glasses with similar host composition is included. The results for those glasses that were melted differently or made of ultra pure chemicals or reduced/oxidised by adding of carbon/nitrate are excluded.

The method provides, as demonstrated, the ion and site concentrations with very high precision. In Figs, 5.9.1 and 2, the precision is demonstrated buy showing only those results, which are made of exactly similar host glass composition and melted by the two main melting methods studied. The reason for this is that the whole spectrum area, containing two to four d-d transition peaks for each kind of ion and site and the UV peaks, is fitted to determine the concentrations and fractions of the ions and sites. Earlier only a peak height, or an absorbance band height or an absorbance value at certain wavenumber are used to determine the concentrations (Chap. 5.4).

The repeatability of the received concentrations is ± 0,001 mol % for [Fe], [Fe^{2+}] and [Fe^{3+}]. The accuracy is strongly dependent on the calibration method, and no proper calibration with another analysis method that would have an accuracy of the size of the repeatability of this method, was available for this work. Repeatability of the order of ± 0,001 a.u. for the measures of [Fe^{2+}, octa], [Fe^{2+}, tetra], [Fe^{3+}octa] and [Fe^{3+}, tetra] was also demonstrated in previous chapters. The repeatability of the calculated site fractions is also of the similar order of magnitude, as demonstrated in the graphs Fig. 5.9.1 and 2, calculated for the samples that are strictly comparable.

In the case these well defined octahedral and tetrahedral sites are the only types of sites for iron ions in these glasses, and their concentrations could be measured by any other way accurately from a glass, these concentrations could also be calibrated and determined with the similar order of accuracy as the ions concentrations. The developed fitting method is based on an assumption that iron ions at these low concentration levels are found in separate octahedral and tetrahedral sites, not in clusters or crystals of any kind etc., even though tetrahedral sites have a network forming role for iron in silicate glasses.

Interestingly, the obtained fitting parameters, peak positions and widths of this work are close to the parameters obtained by Glebov et al (1998) for a different glass. Their paper was actually found after the fitting and analysis of Fe spectrum of this work was completed. So more work should be done to test if their fitted spectrum would fit to the data of this work and vice versa. However, there are also remarkable differences. They have fitted the UV-range with several peaks for both Fe^{2+} and Fe^{3+}. The shape of the Fe^{2+} Band in UV range is different from this work. Here the Fe^{2+} UV peak is much wider and its tail extends down to visible wavelengths. They have fitted there another shallow Fe^{2+} peak at around 23000 cm^{-1} which agree to our Fe-S peak. Their assumption of linear scaling with Fe –concentration can be questioned with measured data of this work (Chap. 5.4.). Their assumption of the stable shape of Fe^{3+} spectrum is obtained in this work only within a narrow scale of iron concentration in the glasses melted in an electric furnace. Their Fe^{2+} peak at 400 nm is also questioned. No similar peak has been assigned to Fe^{2+} in this work, however, the noticed variation of the shape of Fe^{3+} spectrum, fitted as the change in the fraction of the octahedral and tetrahedral sites could explain their finding.

5.9.2. Application range of fitting analysis

The fitting method is most repeatable and scales nicely with Fe concentration for the samples melted in electric furnace and homogenised with casting to frit in the middle of melting (Chaps. 5.4 and 5). For these kinds of glasses at Fe concentration range 0,05 – 0,5 mol % added Fe_2O_3 one set of fitting parameters is defined in Chap. 5.4. They apply to the used type of host glass composition. No other composition was tested, but the set of parameters may easily be modified to apply to the glasses having similar optical basicity or for those made of the same ingredients by varying their concentrations.

The fitting method works also for the tested glasses melted in reducing conditions of a gas furnace. The obtained variation of the fitting parameters (given in Annex 7) and ion and site concentrations are assumed to araise from the variation of the melting method of the samples, not from the reducing as such. Inert crucibles and homogenising of the glass by at least casting to frit is a requirement to make comparable glass samples of the size of 100 – 300 g.

It can be concluded that the fitting analysis can work even at lower concentrations of iron than 0,05 mol % added Fe_2O_3 in well prepared samples (Chap. 5.8) . The lower the concentration, the harder it is to separate the received Fe absorbance from various other reasons causing absorbance. More work is recommended with properly melted and thicker samples. The fitting parameters for the UV-peaks are easier to find and fit, when the Fe^{2+} and Fe^{3+} concentrations can be accurately determined at first from the relevant data in the visible and Near IR range.

The high iron concentrations, higher than 0,5 mol % of added Fe_2O_3 cause very intensive UV-peaks, and were only studied a little for a couple of samples of electric melted glasses in this work. Moore work is thus recommended.

5.9.3. Other new findings

The new absorbance peak earlier found by Boulos et al (1998), but not reported by Bingham (2000), has been obtained for Fe^{2+} ions at 3560 cm^{-1} in the NCS glasses studied, and it is assigned to a second absorbance peak for elongated tetrahedral sites (a Jahn-Teller type of distortion). The peak is involved to the measured data published by e.g. Shrimer et al (2003) and Kukkadapu et al (2003), but not fitted or recognised by them. Bingham and many other earlier researchers have seen only one tetrahedral peak of Fe^{2+}, at 4500 - 5000 cm^{-1}.

The probable reasons why the new peak at 3600 cm^{-1} has not always been discovered, are: a) most researchers have measured the spectra up to 2500 nm (i.e. above 4000 cm^{-1}) and b) because there have not been any accurate fitting available, until recently (Navarro et al, 2005), to resolve anything under the overlapping OH-peaks in the range between 2000 – 4000 cm^{-1}. c) Only a careful comparison of absorbance spectra for similar glasses doped with various transition metal

ions can show that there is an extra peak in iron doped glasses in this region, as was reported by Boulos et al (1997) and as has been also done in this work.

The absorbance spectrum of Fe^{3+}-S chromophores was fitted (Chap. 5.6.) with three main peaks Gaussian peaks and two tiny side peaks. It is for first time the shallow band at around 15000 cm^{-1} is fitted and assigned to these chromophores. The fitted spectrum have been used for analysis of Fe-S concentration received in the Fe doped NGS glasses melted in a gas furnace. However, the calibration of the absorption coefficients and the accuracy and validity of the obtained parameters should be tested in a wider test series of several samples, with varying sulphate and carbon contents, as well as melting conditions and glass composition.

5.9.4. Weaknesses and recommendation for future work

The most significant weakness of this work is the absence of quantitative ion and site concentration measurements obtained by another reliable method in the same glasses, which would validate the method and prove the results and accuracies. Wet chemical analysis is the only well-known method for the ions concentrations, but its accuracy is of the order of ± 0,1 - 0,3 mol %, and would not thus be sufficient to fully confirm the accuracies reported here. It is strongly recommended that wet chemical analysis, or any other more accurate method be used for a series of well prepared and fitted samples to calibrate the absolute ion concentration accuracy as well as possible. Another method that would equally accurately establish the structures of iron sites and measure the concentrations there is also recommended. Only such results could finally validate the results and usefulness of the developed method, indicated and suggested by the comparison of the results between the two series of the glasses shown in Figs. 5.9.1 and 2.

The fitting parameter sets of the Fe^{2+} and Fe^{3+} spectra for the glasses melted in a gas furnace should be tested with many more samples, or with a new set of samples melted in inert crucibles and homogenised. For Bingham's glasses thicker samples should be used, in order to test if that would decrease the variation between the samples. Variation of the spectra (the shapes, redox and fractions of the types of sites) with host glass composition are expected, based on the results obtained by Bingham. The work could be done by using this work's fitting analysis method on Bingham's samples.

The main difference between this work and the fitting analyses of iron absorbance spectra previously reported in literature is that any earlier data on peak positions or other fitted parameters has not been used as fixed parameters, only as a guide. The peaks for octahedral sites and tetrahedral sites are re-fitted by multiple iteration by using several glasses containing different iron concentrations and searching systematically for a set of data that would fit several glasses without any change other than concentrations and, when necessary, the proportion of the tetrahedral and

octahedral sites. Such a set of 42 fitting parameters has been found for the series of NCS glasses melted in electric furnace at iron concentration levels of 0,05 – 0,5 mol % of added Fe_2O_3 (Chap. 5.4 and 5.5). The changes that were necessary to fit also the glasses containing 1 – 2 mol % Fe_2O_3 (the octahedral peak positions moved to higher energies, Fig. 5.5.4) are suggested to be caused by the small decrease of the optical basicity, i.e. the decrease of the ligand field strength caused by the higher iron addition.

More literature and experimental studies, than were done in this work, should be carried out to find out how much the Fe-S or S ion spectra is modified by a glass composition, melting conditions and other preparation parameters. From J. Duffy's various publications, it is known that peak position of charge transfer peaks for Pb, Bi, etc. ions doped in very low concentrations can be used to "measure" the optical basicity and fictive temperature of a glass. Fictive temperature is the temperature at which the structure of the glass freezes during cooling. According to Bamford (1977, p. 108) the Fe – S peaks are found at 425 nm (at 23500 cm^{-1}, with an extinction coefficient 9000 l mol^{-1} cm^{-1}) and at 290 nm (at 34500 cm^{-1} 26000 l mol^{-1}) in potassium silicate glass and at 410 nm (24400 cm^{-1}) & 290 nm in soda-lime-silica glass.

The suitability and sensitivity of the fitted iron spectrum to redox analysis on doubly doped glasses is demonstrated with an analysis on Cu and Fe co-doped NCS glasses presented in Chap. 6.

6. The mathematical description of absorbance spectra for copper doped glasses

6.1 The aims of the study on Cu-doped glasses

In this chapter, the questions that needs to be addressed for mathematical fitting of the d-d transition and charge transfer absorbance spectra of Cu^{2+} and Cu^{1+} ions are examined further from the conclusions reported in the Annex 9 and 10 (Volotinen et al, 2004 and 2005), conference presentations based on preliminary results of this work. Mathematical descriptions of these spectra are developed for the 200 – 3200 nm wavelength range, in a similar way to the fitting of the Fe spectrum described in Chap. 5. The spectra are fitted as a sum of Gaussian peaks for Cu-doped 15soda-15calcia-70silica glasses melted in electric and gas furnaces. The complete version of the fitted spectra for Cu^{1+} and Cu^{2+} ions together with the fitted spectra of Fe^{2+} and Fe^{3+} ions given in Chaps. 5.4.3 – 5, is applied to the analysis of glasses doubly doped with Cu and Fe (Chap. 6.8).

The effect of Cu concentration and melting conditions of the redox of Cu^{1+} and Cu^{2+} ions with Fe present as a contaminant and as co-dopant. Electron paramagnetic spectroscopy has been performed on some of the glasses to confirm the analysis of the optical spectroscopy results.

Background loss corrections including Fe contamination were made, as described in Chaps. 3 – 5. The glasses and samples were prepared and measured as is described in Chap. 2. In this chapter analysis is a development and deepening of the analysis of the Cu^{2+} ion spectra and corrects the energy level diagram of Annex 10 for Cu^{2+} ions and provides more accurate fitting parameters than those presented by Volotinen et al (2004).

The following questions are answered in this study: Can the Cu^{2+} absorption band at 12700 cm^{-1} be accurately fitted with two Gaussian peaks, and if so, which two? Can other sets of Gaussian peaks also be fitted to the same data? How can the right set of peaks be identified? Can the background be corrected for the mutual redox between Cu and Fe ions at normal Fe-contamination levels (shown in Fig. 3.1.1.1, Chap. 3.1.1) and on co-doping with Fe? What effect does the fitted background correction have on the analysis results? Do the positions, heights, splitting and widths of the Cu^{2+} ion peaks vary systematically with Cu-concentration, melting conditions, host glass optical basicity etc.? A tetragonal elongation distortion of the octahedral configuration of the closest neighbouring oxygen ions causes the splitting of the absorption band according to Halcrow's literature review (2003) of Cu^{2+} in chemical compounds, including oxide glasses. This conclusion is shown to agree with the fitting analysis

and with the electron paramagnetic resonance analysis made on the glasses of this project (the next chapters and also Volotinen ,2005, Annex 9 of this thesis).

6.2 Literature study of Cu-doped glasses

Copper forms colours in silicate glasses ranging from sky blue to green (Cu^{2+} -ions, intraionic d^9 transitions), colourless (Cu^{+}-ions, no intraionic transitions; Weyl, 1951; Bates, 1962; Bamford, 1977; Paul, 1982; Scholze, 1991) and intense red, i.e. copper ruby caused by either metallic Cu-atoms, plasmon oscillations of free electrons (Bae et al, 1994; Nakai et al, 1999) or by clustered particles of crystallised Cu_2O (Murase et al, 2001; Habib, 2003). Paramagnetic Cu^{2+} ions show a broad, asymmetric absorption band at around 780 – 800 nm wavelength (12700 cm^{-1}) and a weak band at 450 nm (22000 cm^{-1}) in a soda-lime-silica glass, according to Bamford (1977, p. 48). Cable et al (1989 b) showed that the Cu^{2+} band was centred at 12800 cm^{-1} (780 nm), with an extinction coefficient ranging from 20,8 to 25,8 $(cm*mol/l)^{-1}$ in soda lime silica glasses, and that both the extinction coefficient and $[Cu^{+}]/[Cu^{2+}]$ ratio increase with increasing glass basicity. Cable et al (1989 a) also reported the Cu^{2+} extinction coefficient for $17{,}6Na_2O$-12CaO-$70{,}4SiO_2$ glass to be 21,7 $(cm*mol/l)^{-1}$ which corresponds to 9,16 $(cm*mol\ \%)^{-1}$ and 6,90 $(cm*weight\ \%)^{-1}$, more than double of the optical density 3,0 $(cm*weight\ \%)^{-1}$ given by Bamford (1977, p. 66). In addition, Cable et al (1989 a) showed that $\log[Cu^{1+}]/[Cu^{2+}]$ linearly depended on the melting temperature. The ratio $[Cu^{1+}]/[Cu^{2+}]$ varied from 0,318 (1400 °C) to 0,626 (1503 °C), being 0,439 for the glass melted at 1450 °C, while the enthalpy, ΔH, for the reaction was found to be 154 kJ $mole^{-1}$. Later (1992) they also showed that the value of the extinction coefficient $\varepsilon(Cu^{2+})$ decreases in the case of an increase of basicity, made by replacing a smaller alkali ion by a larger alkali ion.

It is worthwhile pointing out that copper has three valence states in soda-lime-silica glasses, Cu^{2+}, Cu^{1+} and metallic Cu. Durán et al (1985 a) showed by atomic absorption spectroscopy (total copper content) and volumetric (cerimetry) and electron paramagnetic resonance techniques (the Cu^{+} and Cu^{2+} concentrations) that 73 - 93 % of the Cu added, turned to Cu^{2+} ions in $16Na_2O$-10CaO-$74SiO_2$ glass when it was melted under oxidising conditions and 1,6 – 40 % when melted under reducing conditions (Fig. 6.2.1). The accuracy was reported to be 7 % and the added CuO concentrations were 0,5 – 2,0 weight %. They also measured Cu^{1+} concentrations by atomic absorption spectroscopy and concluded that 0,01 – 0,15 weight % (= 1 – 7 %) of the CuO added might have turned to metallic Cu.

Zhou et al (1993) showed for a lead borate glass, that the band is centred at 13800 cm^{-1} with an extinction coefficient of 48 $(cm*mol/l)^{-1}$. The glasses melted in reducing conditions were colourless, while those melted in oxidising conditions were yellow or yellow-brown. The UV cut-off was at the shortest wavelengths for the reduced glass and longest for the oxidised

glasses, similar to the behaviour of the Cu-doped glasses in this work, shown in the next chapters.

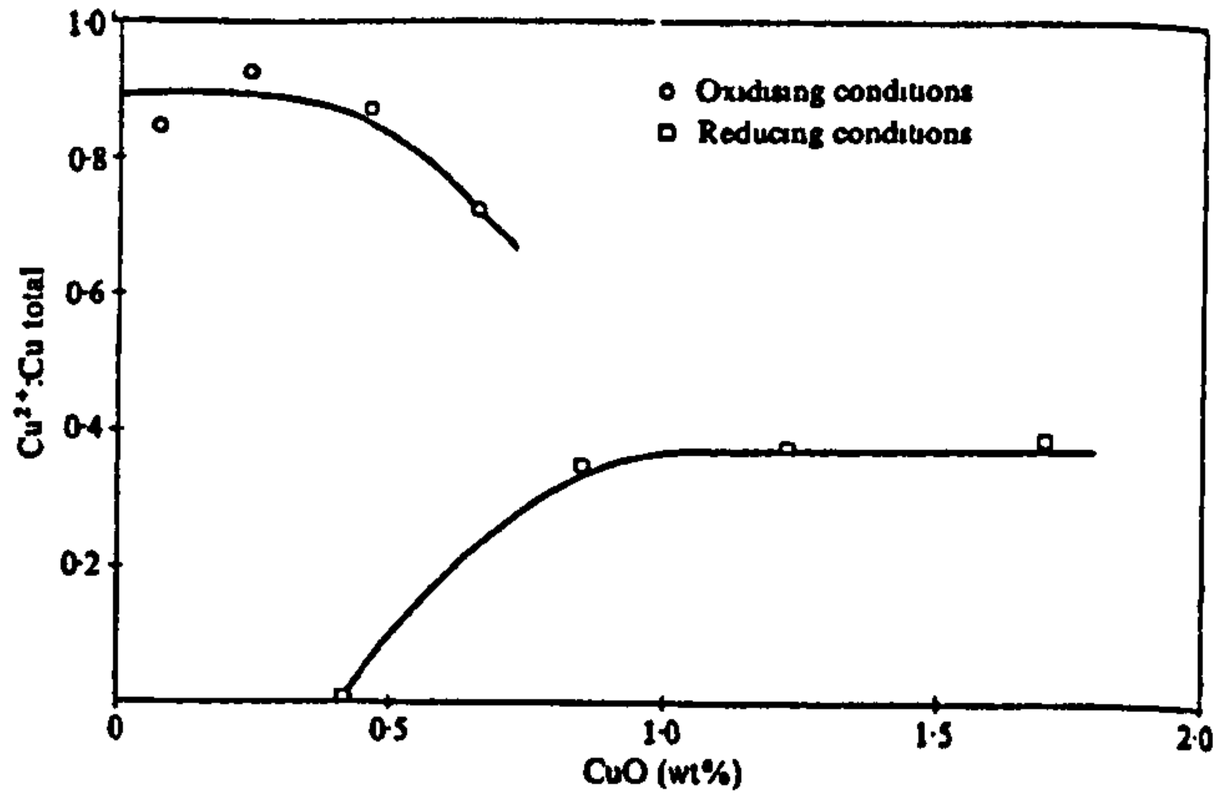

Fig. 6.2.1 The fraction of Cu turned to Cu^{2+} ions in a 16 Na_2O-10CaO-74SiO_2 glass melted under oxidising and reducing conditions (Duran, 1985 a).

Less well known are the absorbance bands in the UV range. The intense and narrow charge transfer band of Cu^{2+} (an allowed intrinsic 3d-4s transition) is positioned around 33000 cm^{-1} (see the following chapters), while Cu^{1+} ions only have a broad charge transfer band (from the Cu^{1+} ion to oxygen ions) at UV wavenumbers around 43000 cm^{-1} in soda-lime-silica glasses (Xiang, 1988, p. 4) and at 45000 cm^{-1} in borate glasses (Zhang et al, 1990). The tails of these bands extend to the visible wavelengths, and they together define the UV-edge of solely Cu-doped silicate glasses (Zhang et al, 1990). Bae et al (1994, referring to their earlier paper 1991) have shown that both Cu^{2+} and Cu^{1+} ions have intense absorption bands at UV-region for copper phosphate glasses. The tails of both these bands extend into the visible region and the colour as well as the wavenumber of minimum absorbance are dependent on the redox ratio $[Cu^{1+}]/[Cu^{2+}]$. In their copper phosphate glasses the wavenumber for minimum absorbance moved from 16100 cm^{-1} to 18000 cm^{-1} with a change of ratio $[Cu^{2+}]/(Cu]$ from 20 % to 100 % (Bae et al, 1994).

The Cu^{2+} absorbance band position and height have been studied by fitting it with two (Duran, 1983 and 1985a) or three (Bae et al, 1994) Gaussian peaks in various kinds of glasses, as a function of host glass composition, melting conditions and refining agents. Gaskell (1992) reported that the oxygen ions surrounding Cu^{2+}-ions are well structured as a distorted octahedron in copper sodium phosphate glass. Halcrow (2003 a and b) reviewed the structures of the closest ligands for Cu^{2+} (Fig. 6.2.1) in various chemical compounds. He concluded that isolated Cu(II) ions doped into MgO and CaO show EPR spectra that are apparently isotropic to very low temperatures, and which show only small g-splittings even at 1,2 K, referring to Reynolds (1974). The data have been interpreted on the basis of Cu^{2+} sites showing unusually small Jahn-Teller distortions, which are dynamically disordered over all three axes of the cubic

unit cell. However, Halcrow's main conclusion is that in most of the inorganic solid hosts examined the structure is a normal elongated Jahn-Teller distorted octahedron, together with structural disorder that varies from site to site in all dimensions.

Thus the absorbance band of Cu^{2+} ions at 12700 cm^{-1} can be expected to be a sum of two broad peaks, of which the one at higher energy should be more intense and the one at a lower energy only about half of the height of the more intense one (Fig. 6.2.1). The reason is that only one electron from the d_{xy} level can be excited to the upper half filled d_{x2-y2} level creating the weaker absorption peak at a lower energy, whereas two electrons can be excited from the lowest d_{xz} and d_{yz} levels to the vacancy, creating a double intensity peak at a higher energy. The splitting of the peaks equals the energy difference between d_{xy} and d_{xz}, d_{yz} levels. The third possible transition to fill the vacancy at the highest level is a transition between the two top levels, but its energy would be small, of the order of the splitting of the lower levels, thus locating it at infrared wavenumbers.

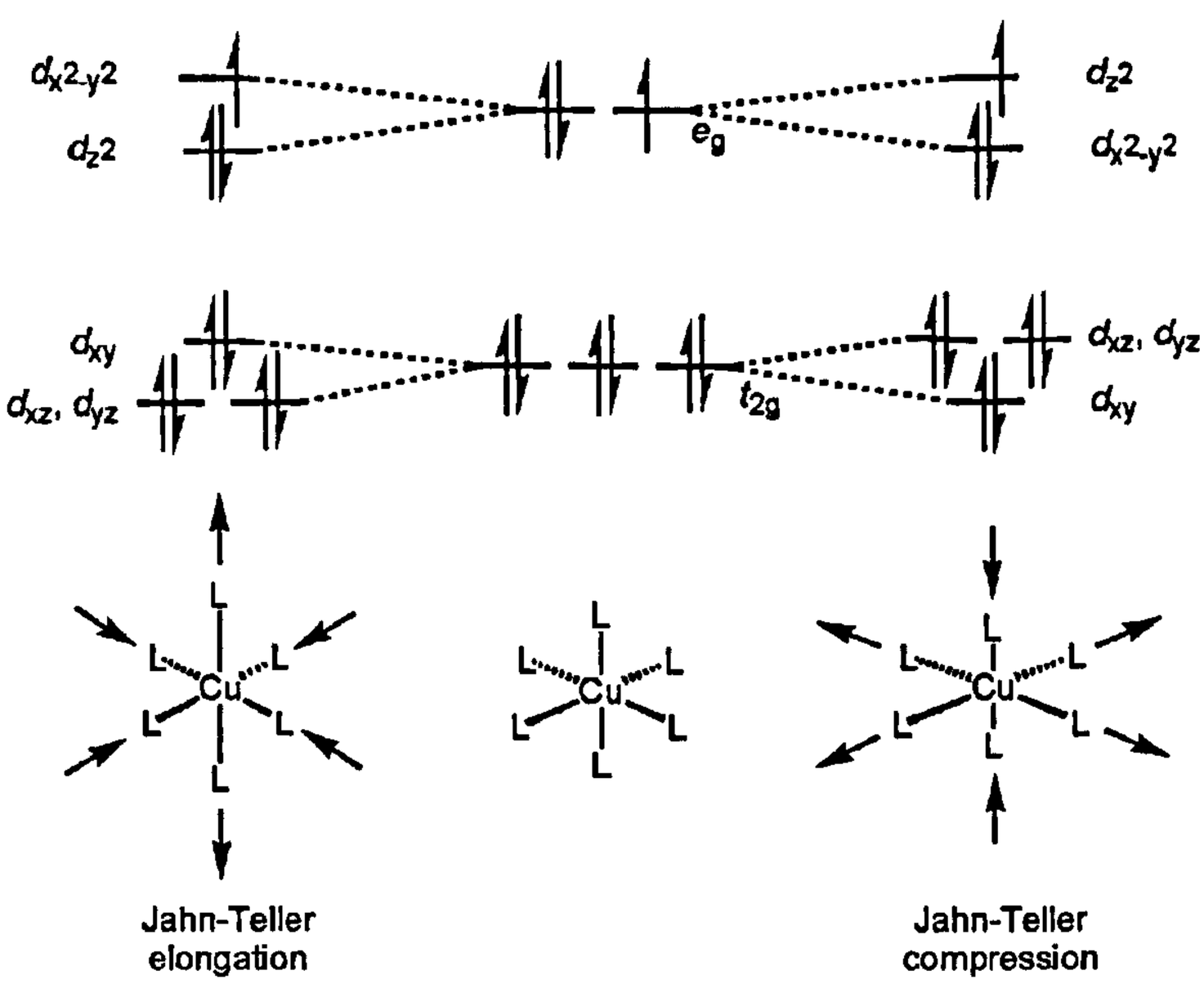

Fig. 6.2.1 Diagram shows two (elongation along z-axis and flattening along z-axis) Jahn-Teller splittings of the d-energy levels in an octahedral $[CuL_6]^{2+}$ complexes, where L is the ligand anion, as well as the structural distortions that result from them (Halcrow, 2003 b).

It is concluded by most of the above mentioned authors that the asymmetric Cu^{2+} band at 12700 cm^{-1} in soda-lime-silica glasses is caused by splitting of this band due to a Jahn-Teller elongated tetragonal distortion of the oxygen anion octahedral, as described above. However, there is confusion in the literature concerning whether the distortion is large or small, fixed or varying, whether it creates two or three split peaks and their separation, etc. The broad band has been fitted using two peaks at a large separation of 3000 – 4000 cm^{-1} by Durán et al (1983,

1985) suggesting a large, square planar distortion, and by three peaks (a main peak with satellites at ± 2000 cm^{-1}) by Bae et al (1994) suggesting an even more extreme distortion which causes the d_z^2 to become lower than d_{xy}.

6.3 Experiments of Cu-doped glasses

In order to determine a set of accurate fitting parameters 15soda-15calcia-70silica glasses (referred as NCS glasses) with 0,2 – 1,5 mol % CuO added were melted in electric and gas-fired furnaces. The glasses were refined with 0,35 mol % sulphate and some of the glasses were further reduced with 0,5 mol % carbon, or oxidised with 1 mol % $NaNO_3$. The details of the glass melting and annealing process are described in Chap. 2 and also given together with the glass composition information in Annex 1.

In order to examine the effect of host glass basicity, silicate glasses containing 60 – 70 mol % silica and 5 – 15 mol % of three or four of the following glass network formers and modifiers (Li_2O, Na_2O, K_2O, CaO, BaO, MgO, B_2O_3, Al_2O_3) and doped with 0.2 - 1.0 mol% CuO, were melted in a gas-fired furnace. The optical basicity values were calculated from batch compositions using the equation and partial Λ(oxide) basicity values of the ingredients given by Duffy (2002), as described in Chap. 1.4.7. The results of these studies are only reported in Annexes 9 and 10. The new set of fitting parameters remains to be applied to these glasses. It is planned as a future work.

The samples were prepared and the optical absorbance spectra were measured as described in Chap. 2. The optical spectra were normalised and the background corrected according to the procedures given in Chaps. 3.5 – 3.7. Fe-contamination was assumed to be of the order of 0,07 mol % of Fe ions (≈ 0,07 – 0,109 weight % Fe_2O_3) for the glasses melted in a gas-fired furnace and ca. 0,012 mol % Fe ions (≈ 0,015 weight % Fe_2O_3) for the glasses melted in electric furnaces, as was measured for a few glasses (Annex 3). For analysis of the effect of host glass basicity, the spectra were further normalised to 1 mol % CuO concentration.

The set of fitting parameters for Cu^{1+} and Cu^{2+} spectra were developed in the following three stages:

1. In a similar way to Bingham's study on Fe-doped glasses (2000, 2001, 2002), the non-linear regression analysis of software SPSS 12.0.1 for Windows was used to fit the normalised and background corrected absorption spectrum over the wavenumber range 20600 - 4170 cm^{-1}. These results are given in Annex 10. Two Gaussian peaks with six freely varying parameters (peak height1, position1, width1, height2, position2 and width2) were used. The background correction was done by subtracting the normalised absorption spectrum of a similar undoped host glass. For fitting with SPSS a narrower

wavenumber range was used for glasses with a narrower Cu^{2+} band. The same starting values of the six fitting parameters were used for all glasses. Fitting with different numbers (one, two and three) of peaks was also investigated.

2. Dr. Klement at Alexsander Dubček University of Trencin (Annex 9), used PeakFit-v4.12 an other software to fit the same data used (Annex 10) with sets of two and three Gaussian peaks. The results are given in Annex 5. Background correction of the raw data was achieved by subtracting the thickness normalised spectrum of a similar undoped glass, not by fitting the background and taking into account the mutual Fe-Cu cross redox.
3. Thirdly, Excel software was used manually, in a similar way to that described in Chap. 5, to improve the background correction by applying the fitted Fe-absorbance spectra and the fitting parameters of the Cu^{1+} and Cu^{2+} absorbance peaks over the wide 3000 – 50000 cm^{-1} wavenumber range.

An EPR analysis on the selected Cu-doped glasses of this work was made by Dr. Klement at The University of Alexander Dubček, Trencin, Slovak Republic. The purpose of these studies was to find out detailed information on the Cu^{2+} ion sites in the glasses studied; i.e. whether they are teragonally distorted, elongated or flattened octahedral sites.

6.4 Results of Cu-doped glasses

6.4.1. Observations at glass casting

The Cu-doped glasses showed a particular colour sequence during casting, not seen for other transition metal dopants studied. At first the hottest Cu-doped glass melt was intensely orange, as all glass melts do. At a slightly lower temperature the melt turns transparent reddish and then to greenish/brownish or bluish, but for the copper containing glasses the red colour intensified becoming intense opaque red (enamel type of appearance), after that a transparent dark green and green light shining colour was seen for about 10 – 20 seconds, which after a while changed to the final blue colour. These colour shifts and, in particular, the enamel like intense red and the green light seen at high temperatures are probably caused by metallic Cu or Cu_2O nano-sized particles (the intense opaque red) and by fluorescence from the Cu^+ ions (the green light) (Dúran et al, 1985) that are present in the copper doped glass at high temperatures and at low Cu concentrations even at room temperature (Mekki et al, 1997).

6.4.2. Absorbance spectra of Cu-doped NCS glasses melted in electric and gas furnace

The Cu^{2+} absorbance band is centred at 12750 cm^{-1} for all Cu-doped NCS glasses (15soda-15calcia-70silica-0,35sulphate) studied. On the next two pages the absorption spectra of Cu-doped soda lime-silica glasses, melted in electric (Fig. 6.4.1 a and b) and gas-fired furnaces (Fig. 6.4.3 a and b) are shown. The reflection loss correction curve (developed in Chap. 3.5, Fig. 3.5.5 and 3.5.6) was seen to be at a slightly too high level for Cu-doped glasses made of purified ingredients (marked as NCSCle/..) melted in an electric furnace. Thus for the undoped Glass 196 and for the glasses doped with less than 0,2 mol % CuO a function $A_{ref2}(\lambda) = A_{ref}(\lambda) - 0{,}0014$ was used as the reflection loss correction (Chap. 3.5, p. 40).

All these glasses and other solely Cu-doped glasses melted in this work were turquoise blue with a slightly different hue depending on host glass. No other colours were seen, even though a shallow band at 450 nm is seen in Glasses 197S, 197O and 75 (Fig. 6.4.1 b) that have a low Cu-concentration. Its position agrees with Bamford's (1977, p. 48) results, but its height decreases with increasing Cu and Cu^{2+} concentrations. Thus it is fitted with a separate peak (See Chap. 6.6). The tail of the Cu^{1+} UV band at 43000 – 45000 cm^{-1} is seen at the wavenumbers 20000 – 26000 cm^{-1} and the UV peak of Cu^{2+} ions dominates the absorbance at wavenumbers above 26000 - 35000 cm^{-1} (Figs. 6.4.1 b and 6.4.3 b). The shape and position of the broad Cu^{2+} band at 12700 cm^{-1} is very much the same at all ion concentrations (6.4.2) in all

NCS glasses melted in both electric and gas furnaces. The behaviour of the absorbance spectra in the gas melted Cu-doped NCS glasses is shown in Figs. 6.4.3 a and b and 6.4.4.

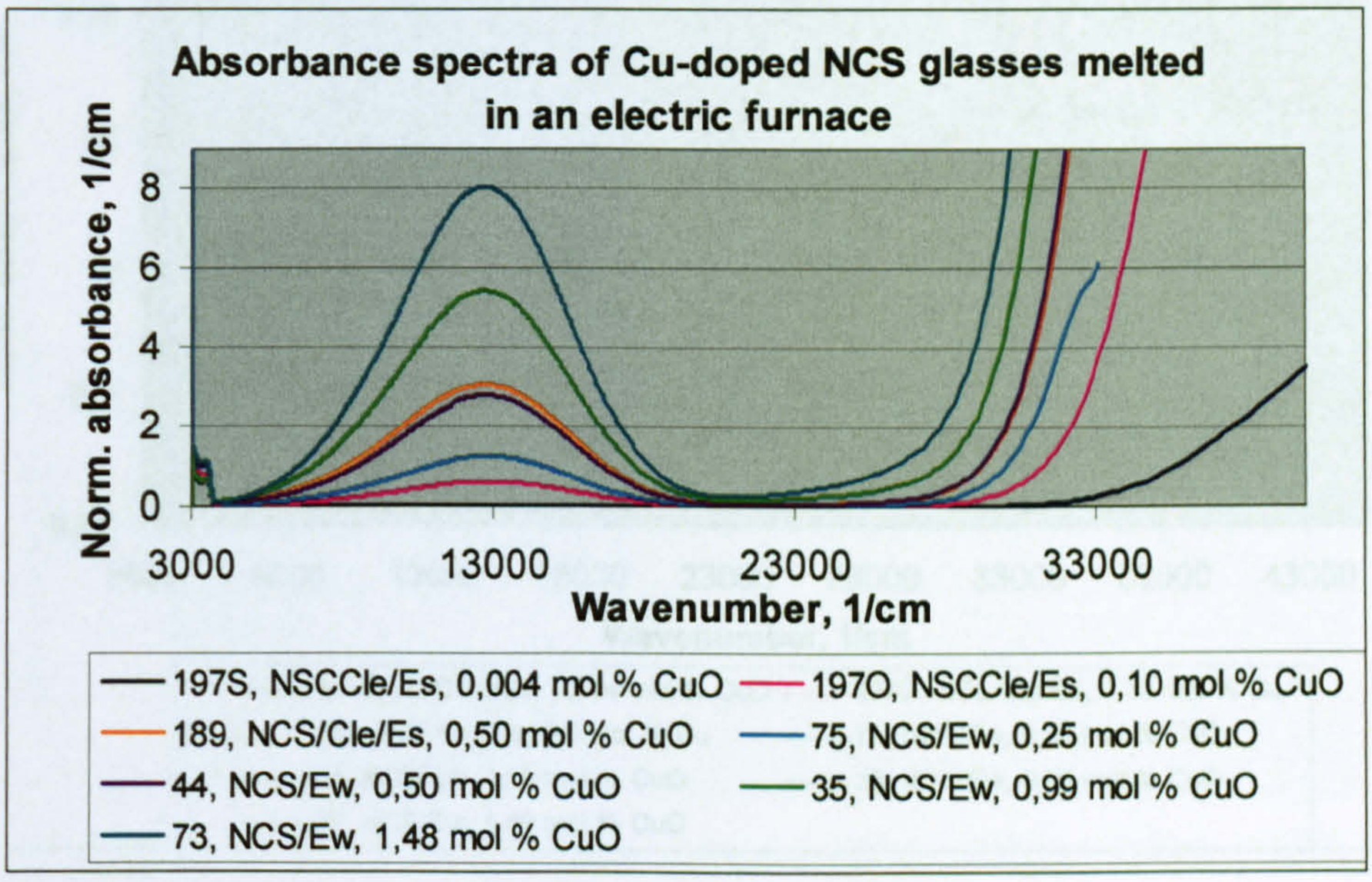

Fig. 6.4.1 a Absorbance spectra of Cu-doped NCS glasses melted in an electric furnace. The reflection losses are subtracted as described above.

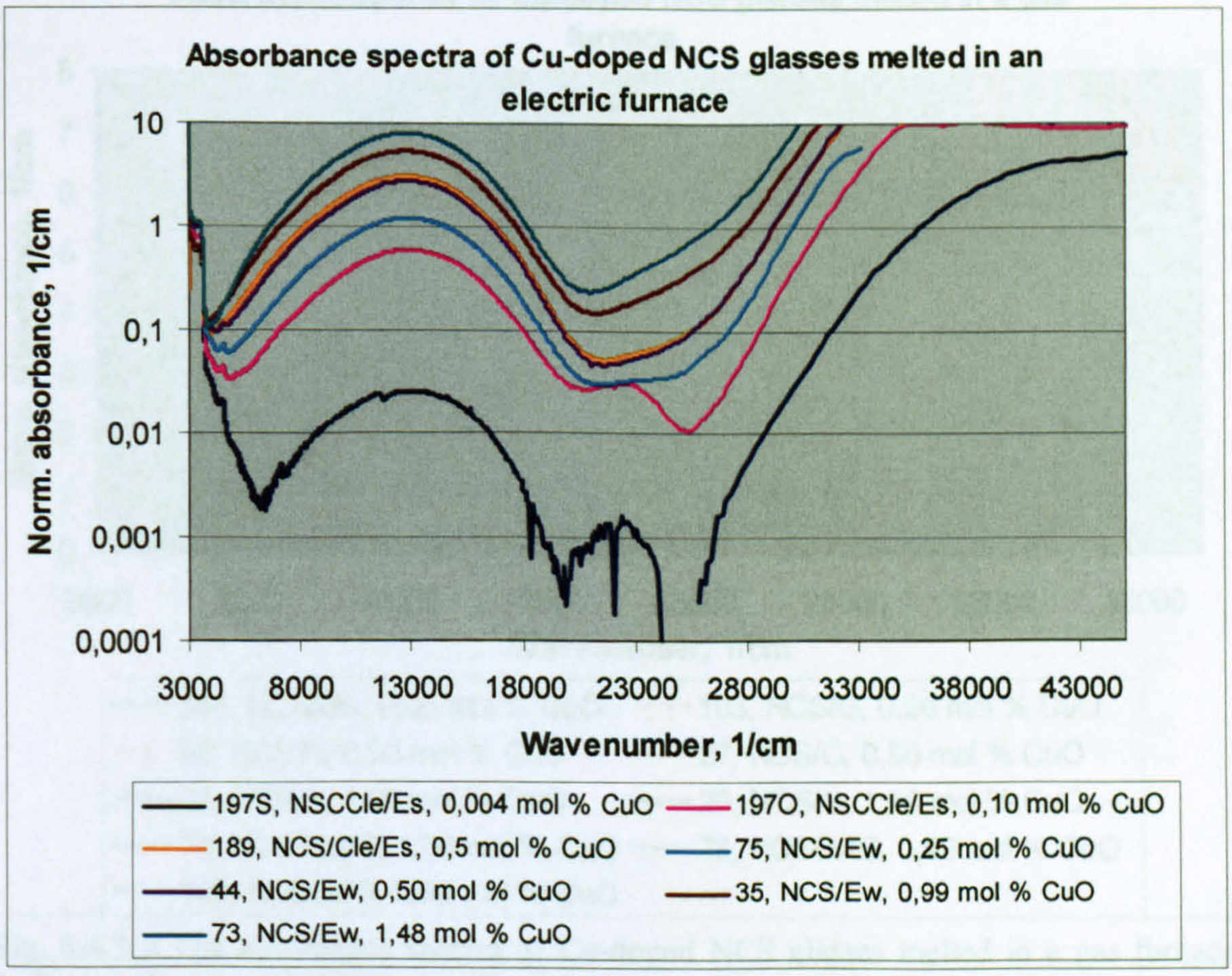

Fig, 6.4.1 b The absorbance spectra of Cu-doped NCS glasses melted in an electric furnace, shown as a function of wavenumber on a logarithmic absorbance scale. The same data as in Fig. 6.4.1 a.

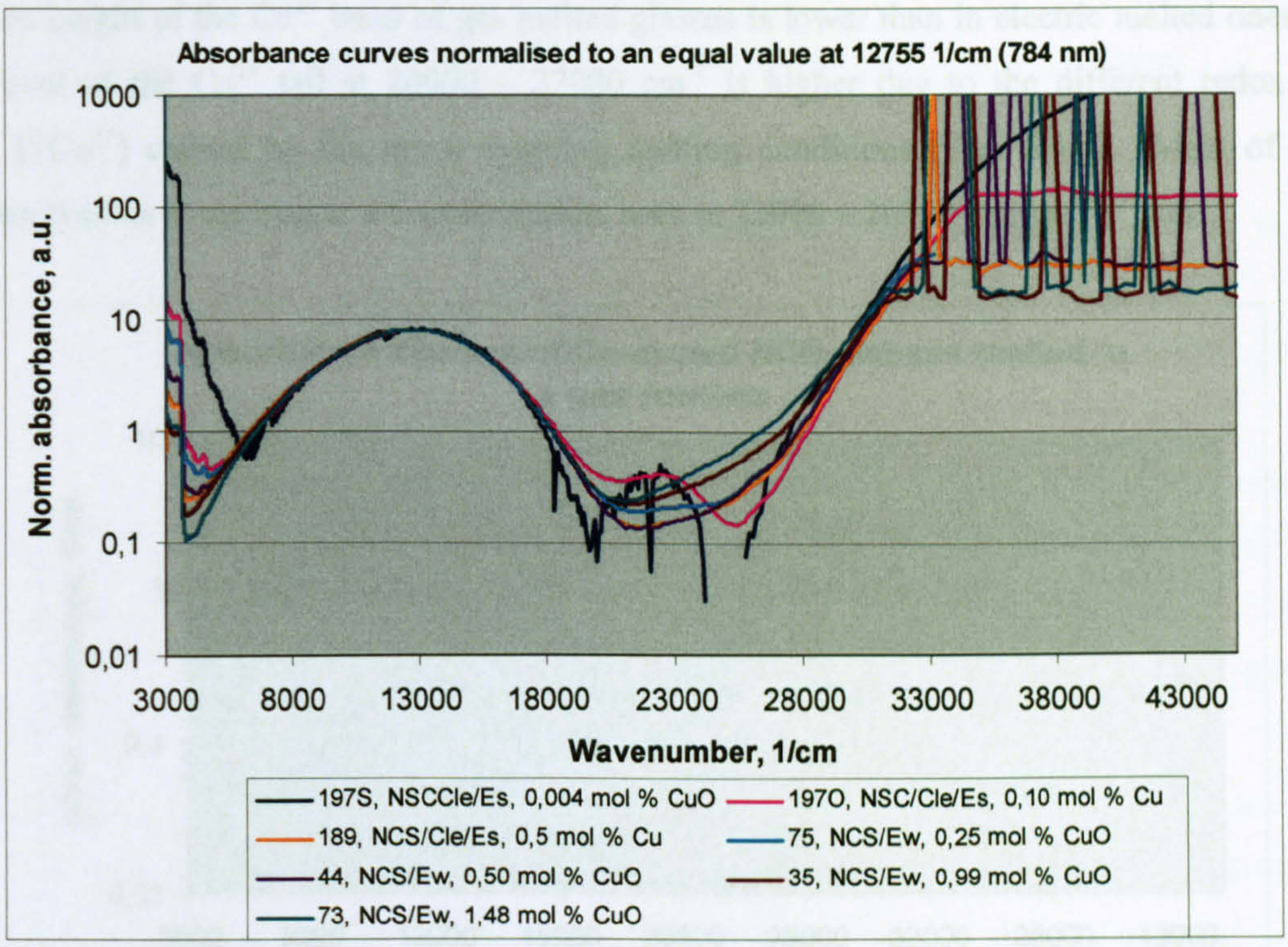

Fig. 6.4.2 The absorbance curves of Fig. 6.4.1 normalised to an equal absorbance value (8,0325 1/cm) at the top of the Cu^{2+} band of the Glass 73.

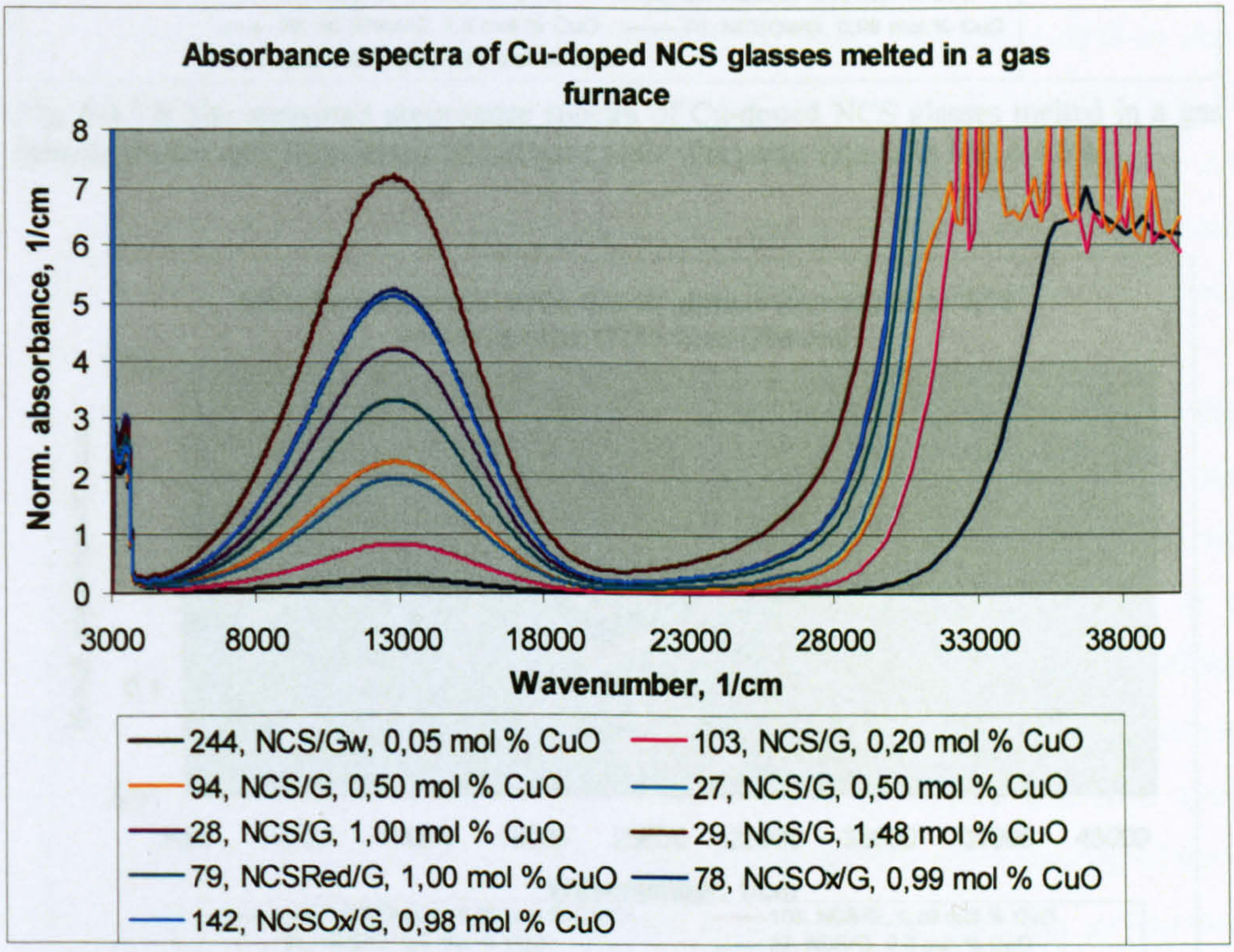

Fig. 6.4.3 a The absorbance spectra of Cu-doped NCS glasses melted in a gas furnace. Reflection losses are subtracted as described above. Glass 79 is further reduced with 0,49 mol % carbon and Glasses 78 and 142 are oxidised with 0,45 and 0,99 mol % $NaNO_3$ resp.. Glass 244 is made of purified ingredients and melted in a platinum crucible. Glass 94 was melted in as 1 kg in a larger crucible, whereas the others are melted as 300 g.

The height of the Cu^{2+} band of gas melted glasses is lower than in electric melted ones, and the level of the Cu^{1+} tail at 20000 – 27000 cm^{-1} is higher due to the different redox ratio $[Cu^{1+}]/[Cu^{2+}]$ caused by the more reducing melting conditions (Fig. 6.4.4). Most of these glasses contain some iron as a contamination, seen at 22000 – 26300 cm^{-1} as Fe^{3+} ions.

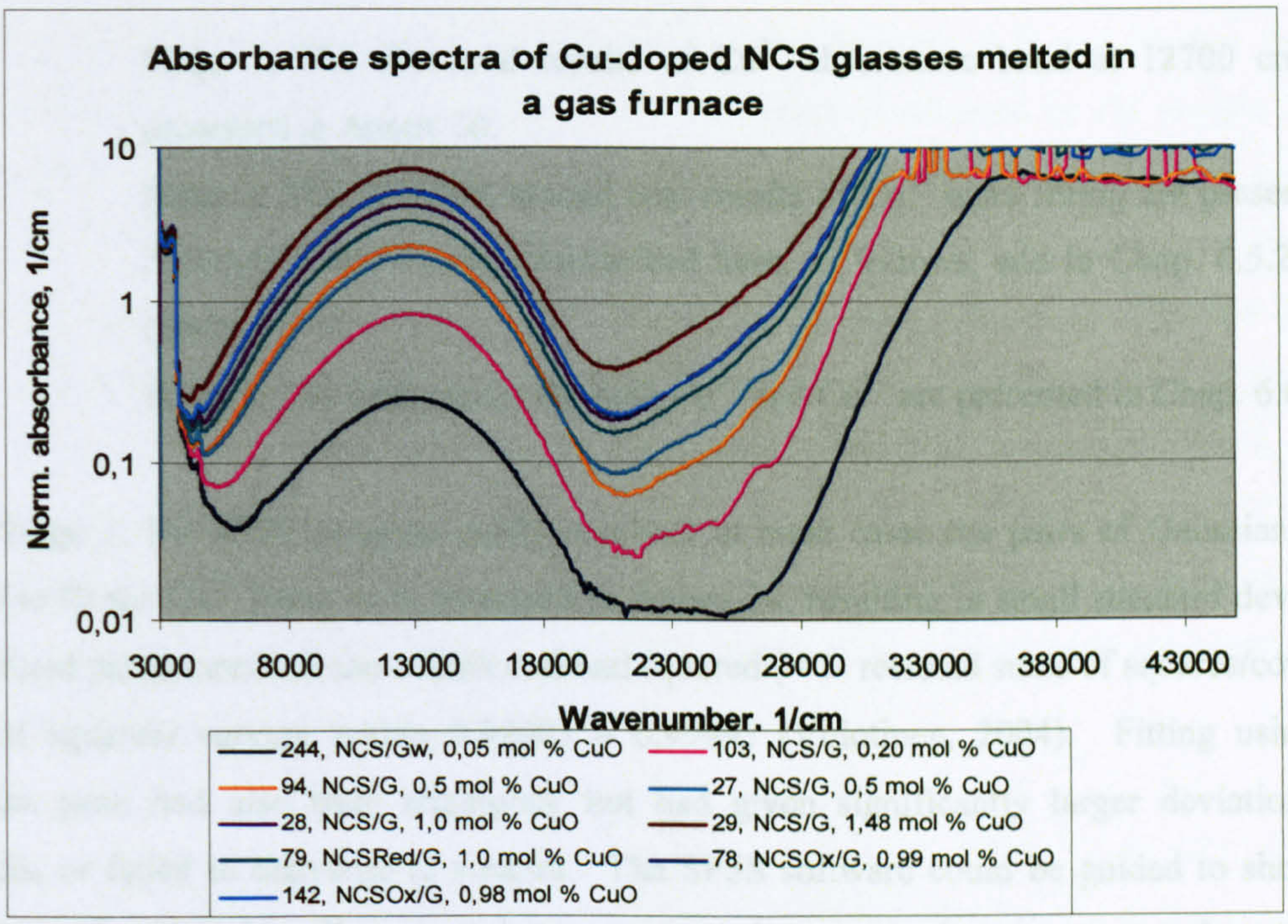

Fig. 6.4.3.b The measured absorbance spectra of Cu-doped NCS glasses melted in a gas furnace shown with logarithmic absorbance scale (the same data as in Fig. 6.4.3 a).

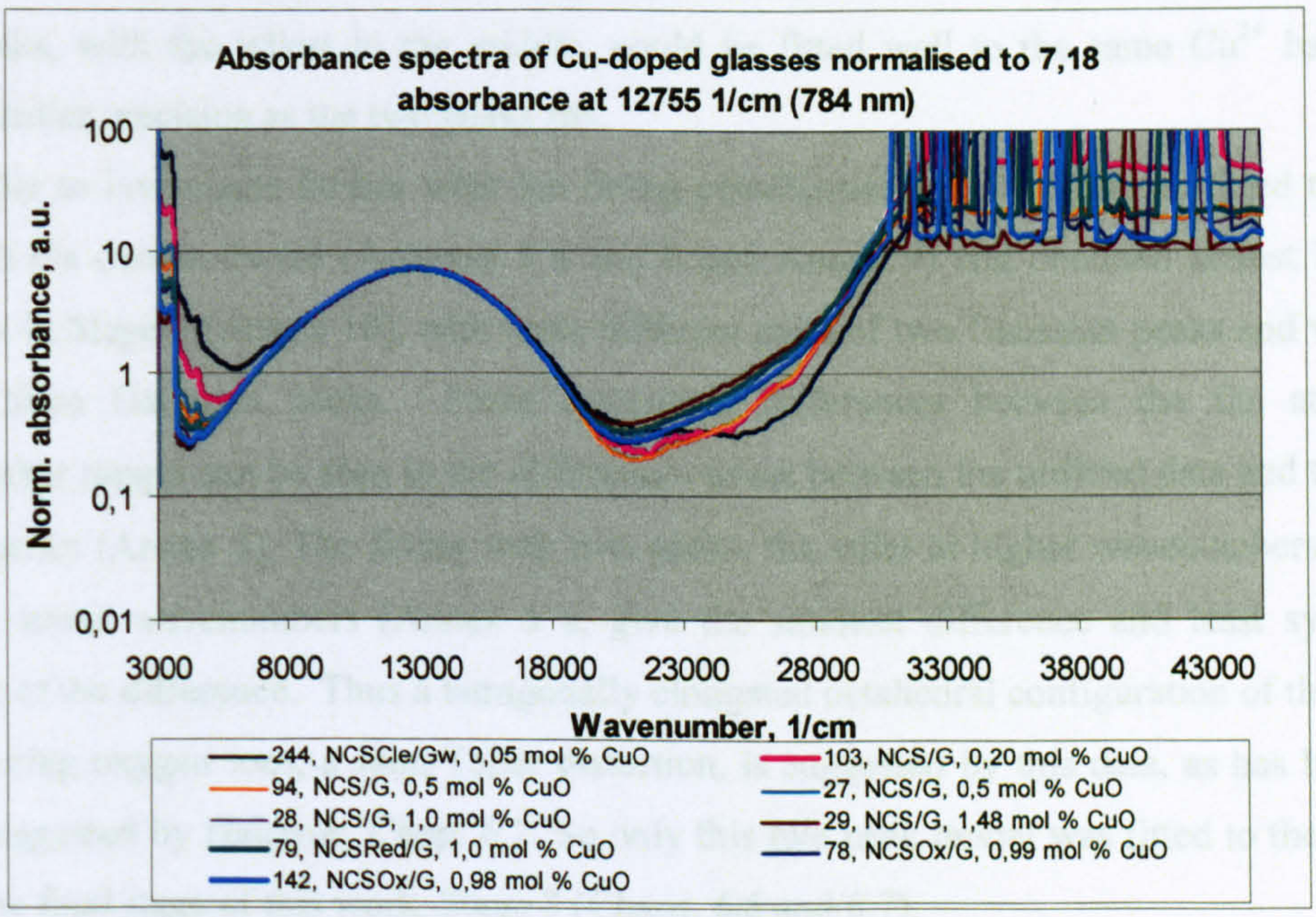

Fig. 6.4.4 The absorbance curves of the gas melted data (Fig. 6.4.3) normalised to the same height at the Cu^{2+} band at 12755 cm^{-1}.

6.5 Development of the fitting parameters for Cu ions

6.5.1. Results of Stages 1 and 2

The fitting parameters for Cu^{2+} and Cu^{1+} ion absorbance spectra were developed in three stages:

- Stage 1. The first trial results of Cu^{2+} absorbance band at 12700 cm^{-1} are presented in Annex 10.
- Stage 2. The EPR and second trial results of Cu^{2+} band fitting are presented in Annexes 5 and 9, and summarized here, as follows, and in Chap. 6.5.2 (EPR results).
- Stage 3. The final results for both Cu^{2+} and Cu^{1+} are presented in Chap. 6.6.

At Stage 1, the SPSS program easily resolved in most cases the pairs of Gaussian peaks needed to fit the Cu^{2+} band, as is presented in Annex 10, resulting in small standard deviations of the fitted parameters and the overall residual squared (= 1- residual sums of squares/corrected sums of squares) varying within 0.99983 – 0.99995 (Volotinen, 2004). Fitting using one Gaussian peak had also been attempted, but had given significantly larger deviations and residuals, or failed to converge to a result. The SPSS software could be guided to show two peak fits with either the taller one at lower wavenumber or at a longer wavenumber; the two models had similar overall residuals and standard deviations for the fitted parameters. At Stage 2 it was also noticed, that for some of the glasses (with particular host glass compositions) also three peaks, with the tallest in the middle, could be fitted well to the same Cu^{2+} band with almost similar precision as the two peaks fits.

In order to investigate further what the fitting possibilities are, Dr. Klement fitted the same data with his own software (Annexes 5 a and b and Annex 9) and obtained almost identical results as in Stage 1 (Annex 10), with three different pairs of two Gaussian peaks and with two sets of three Gaussian peaks. Some systematic differences between the fits at certain wavenumber ranges can be seen in the difference curves between the unfitted data and the fitted sum of peaks (Annex 5). The fitting with two peaks, the taller at higher wavenumbers and the lower at lower wavenumbers (Annex 5 a, give the smallest difference and least systematic variation of the difference. Thus a tetragonally elongated octahedral configuration of the closest neighbouring oxygen ions, a Jahn-Teller distortion, is suggested by this data, as has been also earlier suggested by Halcrow, Chap. 6.2. So only this two peak model was fitted to the Cu data during the final stage of this work, Stage 3 (Chaps. 6.6 and 6.7).

6.5.2. EPR results on Cu-doped glasses

EPR analysis of the selected Cu-doped glasses of this work was made by Dr. Klement at the University of Alexander Dubcek, Trencin, Slovak Republic. According to him (Volotinen et al, 2005 = Annex 9), the EPR spectra of all Cu^{2+}-doped (0,5 and 1;0 mol % CuO) silicate glasses studied exhibit axial symmetry with three of four $^{63}Cu(I=3/2)$ hyperfine transitions in the parallel region resolved (Fig. 6.5.1). His conclusions (Annexes 5 b and 9) that the spin Hamiltonian (SH) parameters are typical for the Cu^{2+} ions coordinated by six oxygen ions in tetragonally distorted, elongated octahedral environment were obtained from the EPR analysis, referring to (Andronenko et al, 2004) and Kivelson et al (1961). The estimated MO parameters (Annex 5b) indicate partial covalency of the σ-bond and in plane π-bonding. The low level of Fe contamination compared to Cu^{2+} content had no influence on the EPR spectra of the Cu^{2+}-doped glasses. In the low magnetic field region a signal of very low intensity at $g \approx 4$, due to Fe^{3+} ions, was observed.

– A further analysis of his data (Annex 5 b) and re-fitting of the properly background corrected absorbance spectra for the Cu-doped glasses with various host compositions, in comparison with each other, is recommended.

6.6 Fitting parameters of Cu^{2+} and Cu^{1+} ions spectra

The absorbance spectrum of Cu ions is fitted with two Gaussian peaks assigned to Cu^{2+} d-d transitions around 12700 cm^{-1} and one or two UV-peaks assigned to 3d – 4s allowed transitions at 33000 and 35000 cm^{-1} (Chaps. 6.7 and 6.8, Annex 11). The Cu^{1+} spectrum is fitted with one broad UV-peak at 43000 – 45000 cm^{-1} assigned to a metal-to-ligand charge transfer. In addition, a shallow, unknown peak at 22200 cm^{-1} is fitted. The tentative fitting parameters of all these peaks for all singly Cu-doped NCS glasses studied are given in Annex 11 (Tables A11.1 and 2). The fitting parameters for glasses doubly doped with the Cu and Fe are given in Annex 11 (Tables A11.3 and 4).

6.6.1. Fitted spectrum of Cu^{1+} ions and other species

The fitted spectrum for Cu^{1+} ions consists of two peaks. The main broad charge transfer peak is found at 45000 cm^{-1} in singly doped glasses and at 43000 – 44000 cm^{-1} in the glasses co-doped with Fe. The unknown shallow peak at 22200 cm^{-1} that appears in those glasses containing 0,2 mol % or less Cu, are shown in Figs. 6.6.1 a and b. The graphs are drawn with the set of parameters fitting Glass 35 (Table 6.6.1) that have been used for most singly and doubly doped glasses (Annex 11, Chaps 6.7 and 6.8). At least one more iteration stage would be needed to find the one fixed set of Cu^{1+} peak parameters that would fit all studied glasses presented in Annex 11 and Chap. 6.8.

Table 6.6.1. The obtained fitting parameters for the absorbance of 1 mol % Cu^{1+} ions in Cu doped Glass 35, melted in an electric furnace.

Parameter	Peak5, unknown peak	Peak6, UV peak of Cu^{1+}
Position, cm^{-1}	22200	45000
Width, cm^{-1}	2000	7700
Height, a.u. $(\sim cm*mol\ \%)^{-1}$	0,2	40

The dimension of the unit concentration for the graphs (Figs. 6.6.1 and b) is given as "a.u.", even though it is meant to be 1 mol %. The reason is that there was no real calibration with a wet chemical or other analysis method available for the unit. The estimation of the extinction coefficients, i.e. the peak heights, was done assuming the peaks heights are linearly dependent on the Cu^{1+} concentration with Glass 73, by difference, assuming all its Cu ions are either Cu^{2+} or Cu^{1+} ions, as is described in Chap. 6.7. This estimation, as well as all the presented fitting parameters (Tables A11.1 and A11.3) are tentative, in particular, because the width and position

of the peaks varied slightly between the glasses (Tables A11.1 and A11.3). The tentative assumption, that the Cu^{1+} absorbance spectrum (Figs. 6.6.1 a and b) represents 1 mol % of Cu^{1+} ions is used for the calculations of Cu^{+1} ion concentrations in Chaps. 6.7 and 6.8.

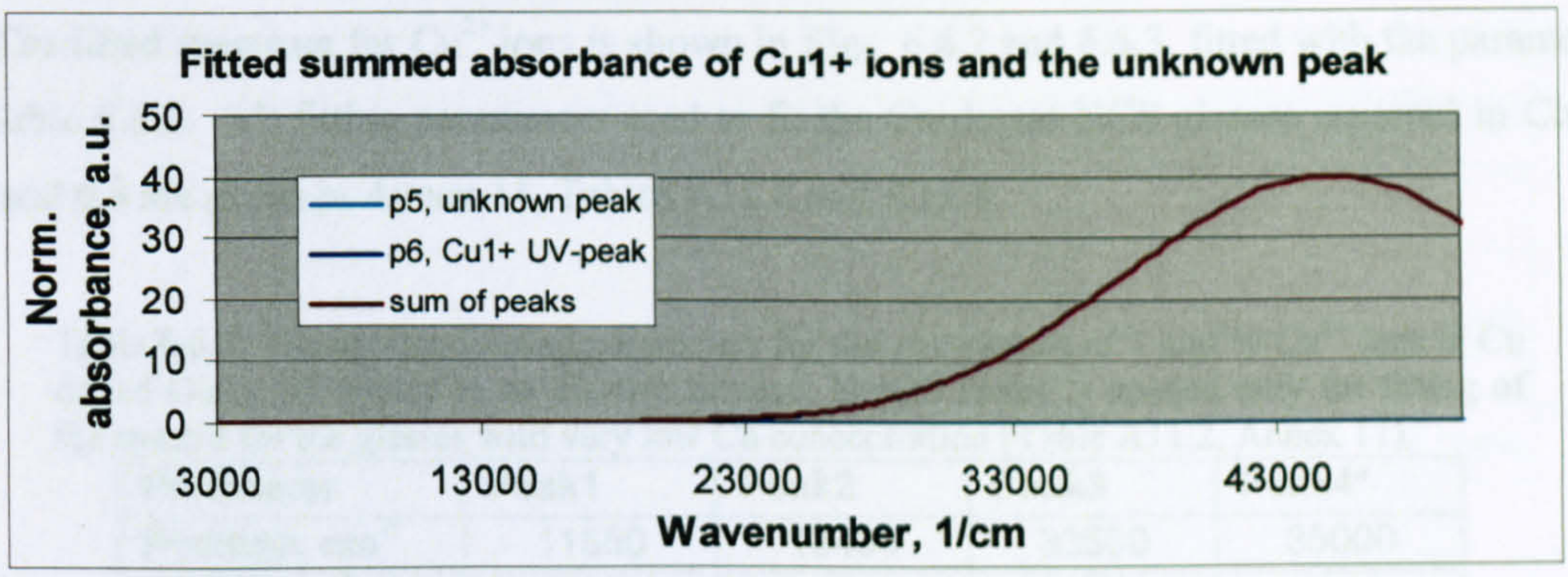

Fig. 6.6.1 a The fitted absorbance spectrum of Cu^{1+} ions in Cu-doped NCS glasses, summed with the shallow unknown peak at 22200 cm^{-1}. The fitting parameters of Glass 35 are used (Table 6.6.1). The tentative assumption is that this absorbance spectrum represents 1 mol % of Cu^{1+} ions.

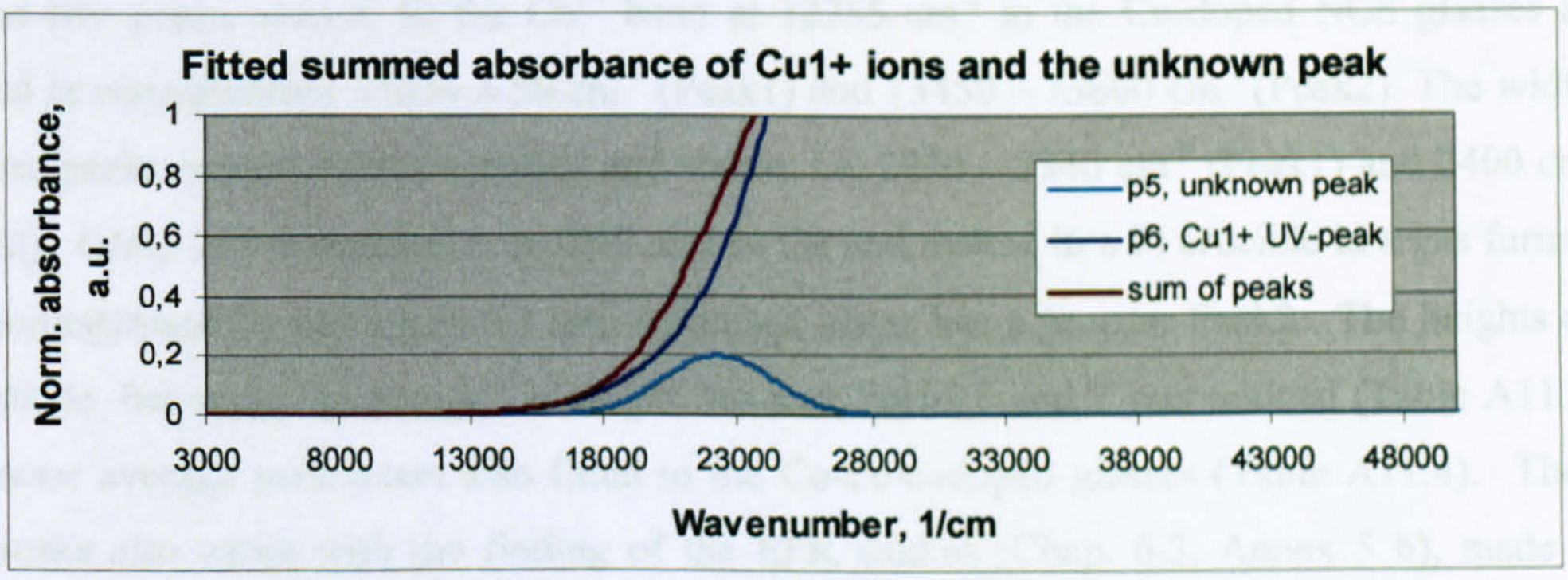

Fig. 6.6.1 b The same data as in Fig. 6.6.1 a, shown with a more sensitive absorbance scale, representing the fitted absorbance spectrum of Cu^{1+} ions in Cu-doped NCS glasses, summed with the shallow unknown peak at 22200 cm^{-1}. The fitting parameters of Glass 35 are used (Table 6.6.1).

No fitted peak for Fe ions or Fe-S chromophpres (shown in Chap. 5.6) can explain the origin of the unknown Peak5. It is believed to be 1) either S_2^- – ions remaining in the glass from the refiner sulphide, i.e. S^{2-} ions that may have reacted with Fe^{3+} or Cu^{2+} ions reducing them to Fe^{2+} and Cu^{1+} (Bach et al, 1995, p.363); 2) or nano-sized metallic Cu particles, 3) or nano-sized Cu_2O particles. Metallic Cu and Cu_2O particle peaks are, however, usually obtained at 550 nm (18000 cm^{-1}) (Duran et al, 1984; Manikandan et al, 2003; Cattaruzza et al, 2005). Residual SO_3 exists in the studied glasses, as is shown by XRF and EDX analyses (Annex 3). The unknown peak is also seen in the undoped Glass 196 (Annex 8, and Fig. 6.4.1 b) made of purified

chemicals. Thus it is concluded that Glass 196 is contaminated by a very small amount of Cu (Table 6.7.1), obviously received from the electric furnace.

6.6.2. *Fitted spectrum of Cu^{2+} ions*

The fitted spectrum for Cu^{2+} ions is shown in Figs. 6.6.2 and 6.6.3, fitted with the parameters in Table 6.6.2. All fitting parameters used to fit the Cu-doped NCS glasses reported in Chaps. 6.7 and 6.8 are given in Annex 11, Tables A11.2 and A11.4.

Table 6.6.2. The obtained fitting parameters for the absorbance of 1 mol % Cu^{2+} ions in Cu doped Glass, 35 melted in an electric furnace. Note*: Peak4 is needed only for fitting of the spectra for the glasses with very low Cu concentration (Table A11.2, Annex 11).

Parameter	Peak1	Peak2	Peak3	Peak4*
Position, cm^{-1}	11550	13400	33500	35000
Width, cm^{-1}	2940	2400	2000	1000
Height, a.u. $(\sim cm*mol\ \%)^{-1}$	3,88	4,21	20,4	61,2

The two peaks used to fit the Cu^{2+} band at 12755 cm^{-1} in the Cu-doped NCS glasses are centred at wavenumbers 11600 ± 50 cm^{-1} (Peak1) and 13450 – 13600 cm^{-1} (Peak2). The widths of these peaks remain almost constant and stable, i.e. 2930 – 2940 cm^{-1} (Peak1) and 2400 cm^{-1} (Peak2). Glass 244 containing only 0,05 mol % Cu and melted in a Pt crucible in a gas furnace and homogenised by casting to frit into deionised water has a broader Peak2. The heights are also stable, but some "exchange" in height between Peaks 1 and 2 was noticed (Table A11.2). The same average parameters also fitted to the Cu-Fe-codoped glasses (Table A11.4). These two peaks also agree with the finding of the EPR studies (Chap. 6.3, Annex 5 b), made on several of these glasses (Table 6.7.1) melted in both environments, that the configuration of the surrounding oxygen ions to the Cu^{2+} ions is octahedral with an elongated tetragonal Jahn – Teller distortion, that separates the d-d energy orbitals of the ion in an octahedral site. The separation is 1800 cm^{-1} – 1850 cm^{-1}. The peaks are further apart from each other and at slightly higher wavenumbers in glasses containing the least Cu. Reducing melting conditions, however, seems to move the peaks to lower wavenumbers.

The UV band of Cu^{2+} ions, representing an allowed transition from the 3d orbitals to 4s orbital, is fitted in most cases by one peak at 33300 – 33600 cm^{-1}, with a 1810 – 2060 cm^{-1} width and height of 20,4 $(cm*mol\ \%)^{-1}$ (Tables A11.2 and 11.4), calibrated with Glass 73, as described in Chap. 6.7. Actually, there are probably two of these peaks, the second one at around 35000 cm^{-1}. The fitted UV-band with these two peaks (Fig. 6.6.3) shows actually similar shape to an excitation spectra at around 280 nm for a photoluminescence at 500 nm, assigned to

Cu_2O nanocrystals or Cu^+ ions, reported by Manikandan et al (2003) for a Cu-doped soda-lime-silica glass.

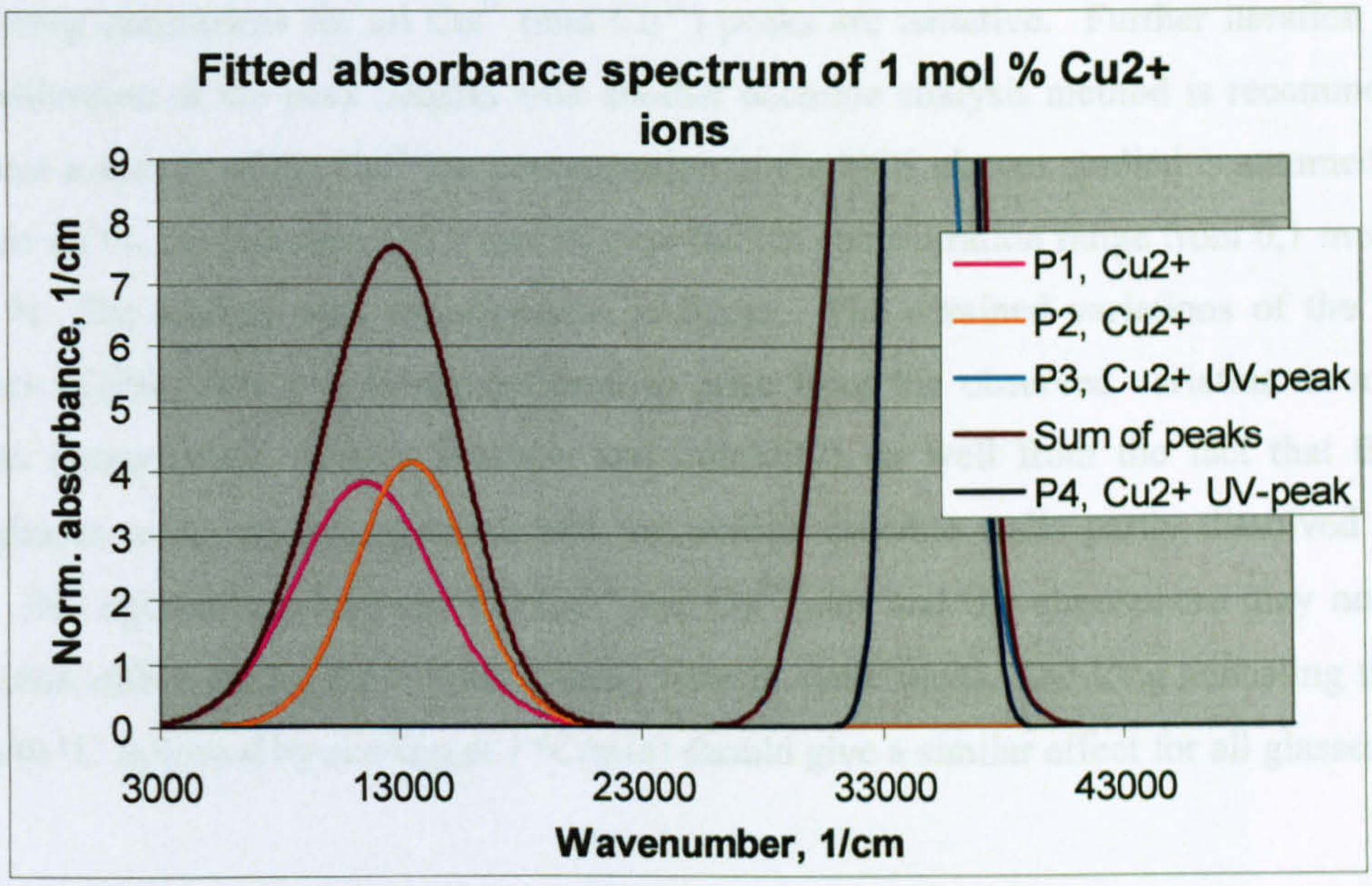

Fig. 6.6.2 Fitted absorbance spectrum of Cu^{2+} ions in NCS glasses. The fitting parameters (Tables 6.6.2 and A11.2) of Glass 35 are used, except the Peak 4 that is added. A calibration accuracy ± 0,1 mol % is assumed.

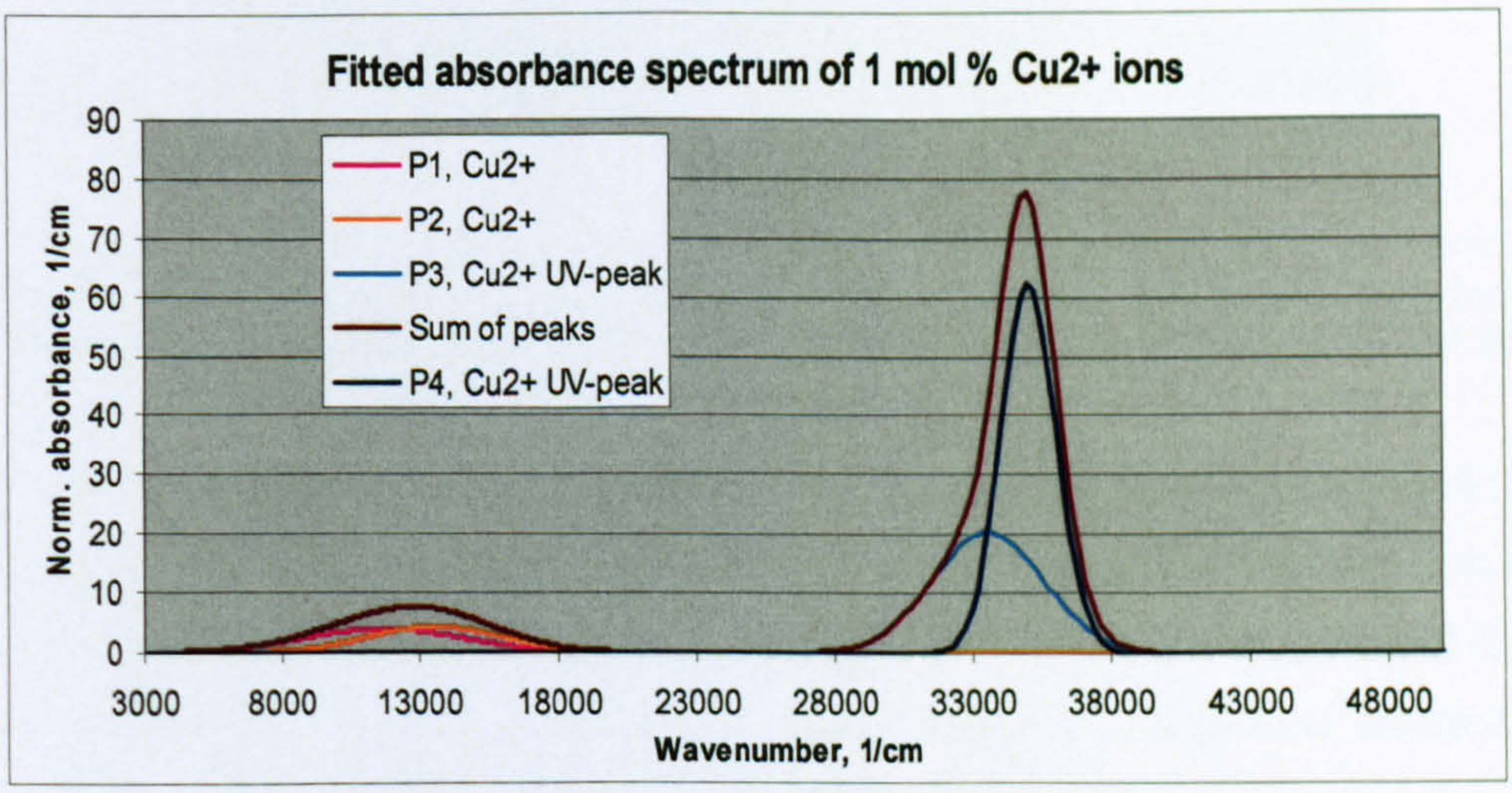

Fig. 6.6.3 Fitted absorbance spectrum of Cu^{2+} ions in NCS glasses. The fitting parameters (Table 6.6.2 and Table A11.2) of Glass 35 are used, except the Peak 4 that is added.

However, the measured data is limited to the tail of this double band at the wavenumbers below 30000 cm^{-1}, where only the tail of the band at 33300 cm^{-1} is significant. The fitting of the second band was necessary only for the cases where both Cu and Fe concentrations were low: Glasses 197O, 197S, 196 and 244 made of purified chemicals (Table A11.2). In most cases the

100 times more intense Fe^{3+} UV-band at 39360 cm^{-1} is so high that its absorbance at wavenumbers above 28000 cm^{-1} is of the same order of magnitude as the Cu^{2+} UV band, even though the Fe^{3+} is only present in these glasses as a contamination.

The fitting parameters for all Cu^{2+} (and Cu^{1+}) peaks are tentative. Further iteration and a proper calibration of the peak heights with another accurate analysis method is recommended. The present accuracy of the Cu^{2+} ion concentration in the NCS glasses studied is assumed to be better than 10 %, i.e. less than ± 0,1 mol % over the Cu concentration range from 0,1 mol % to 1,5 mol %. The scaling with concentration is linear. The obtained variations of the fitting parameters (Tables A11.1 – 4) are believed to arise from the observed variation in melting conditions (temperature, oxygen pressure and humidity), as well from the fact that the gas melted glasses were not homogenised and the mullite crucible walls partly dissolved to the glasses. The equilibrium between the Cu^{1+} and Cu^{2+} ions and the atmosphere may not have been reached either during the 5 hour melting time in static melts. The long annealing time (1 hour at 540 °C followed by cooling at 1 °C/min) should give a similar effect for all glasses.

6.7 Fitted spectra of Cu absorbance in the sulphate-refined NCS glasses

A typical example of the measured and fitted spectrum of a Cu-doped NCS glass is shown in Fig. 6.7.1. The glasses contain some iron contamination at a similar concentration as the Fe-doped glasses (Chaps. 5.4 – 5.8), and the contamination iron spectra are fitted by using the Fit1 presented in Chap. 5.5, p. 99. The fitted and measured spectra of the Cu-doped glasses melted in an electric furnace are shown in Fig. 6.7.2. and in Fig. A11.1 for those melted in a gas furnace. The fitting parameters used for the Cu^{2+} and Cu^{1+} peaks are presented in Tables A11.1 and A11.2.

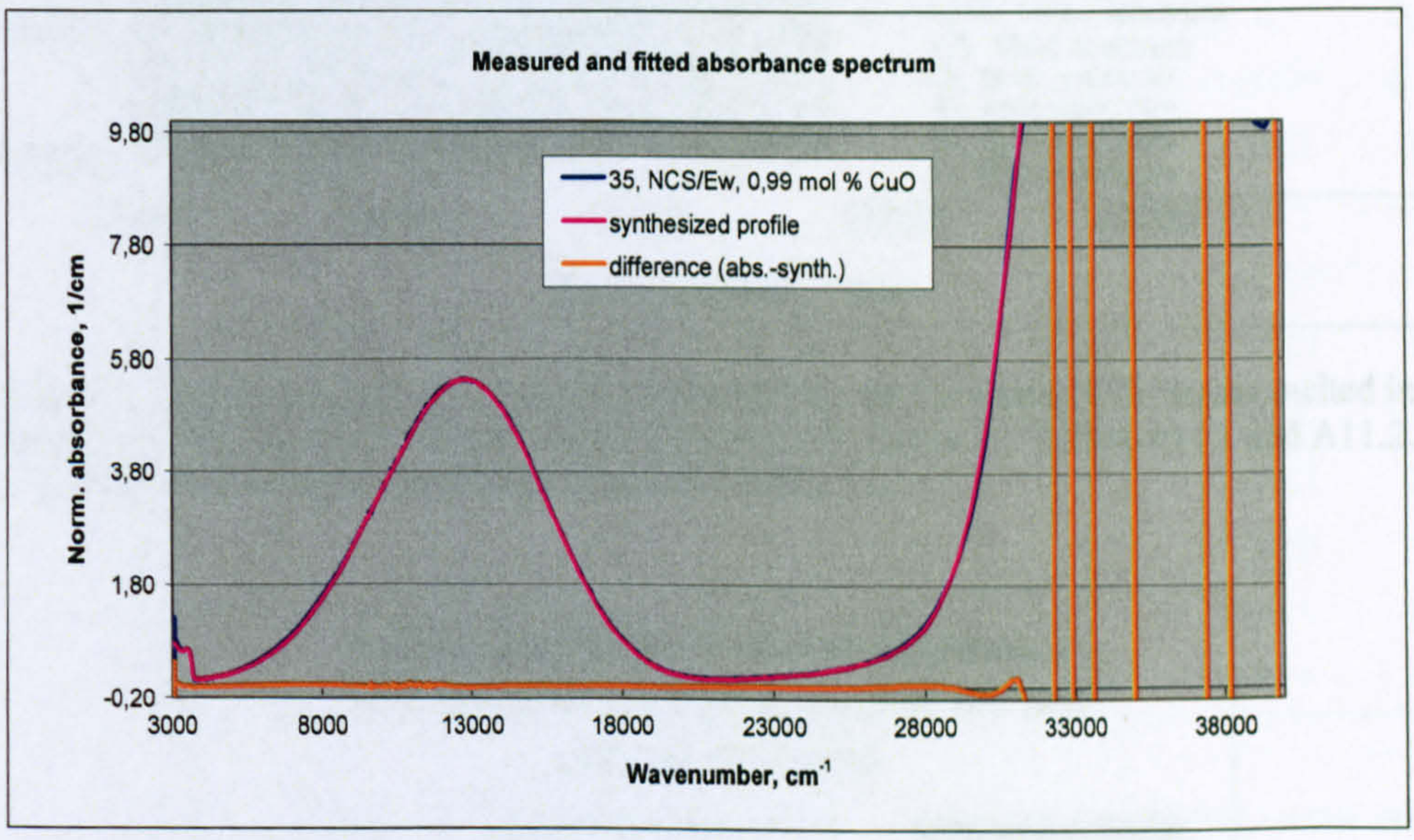

Fig. 6.7.1 The measured and fitted absorbance curves of Glass 35 a Cu-doped NCS glass, melted in an electric furnace. The fitted concentrations are given in Table 6.7.1 and the fitting parameters in Annex 11.

The fitted concentration factors of water and IR-edge, the fitted concentrations of Cu^{2+} and Cu^{1+} ions as well as the concentrations of Fe^{2+} and Fe^{3+} ion contaminations are given in Table 6.7.1. The concentration of Cu^{2+} ions was tentatively calibrated, so that the summed Cu^{2+} band height at 12755 cm^{-1} was adjusted to be slightly below the extinction coefficient 21,7 $(cm*mol/l)^{-1}$ reported by Cable et al (1987 and 1992) at 12755 cm^{-1}, because the optical basicity for the NCS glass is slightly higher than for their glass. The concentration of Cu^{1+} was tentatively adjusted so that the sum concentration of Cu ions $[Cu^{2+}] + [Cu^{+1}]$ of Cu in Glass 73 doped with 1,48 mol % CuO, would be 1,48 mol %. Later it was seen in analysis of the Fe and Cu codoped glasses that the calibration of both concentrations should be re-adjusted. Most probably the assumed extinction coefficients of both ions are slightly too low (See Chap. 6.6), giving slightly too high concentrations (Table 6.7.1).

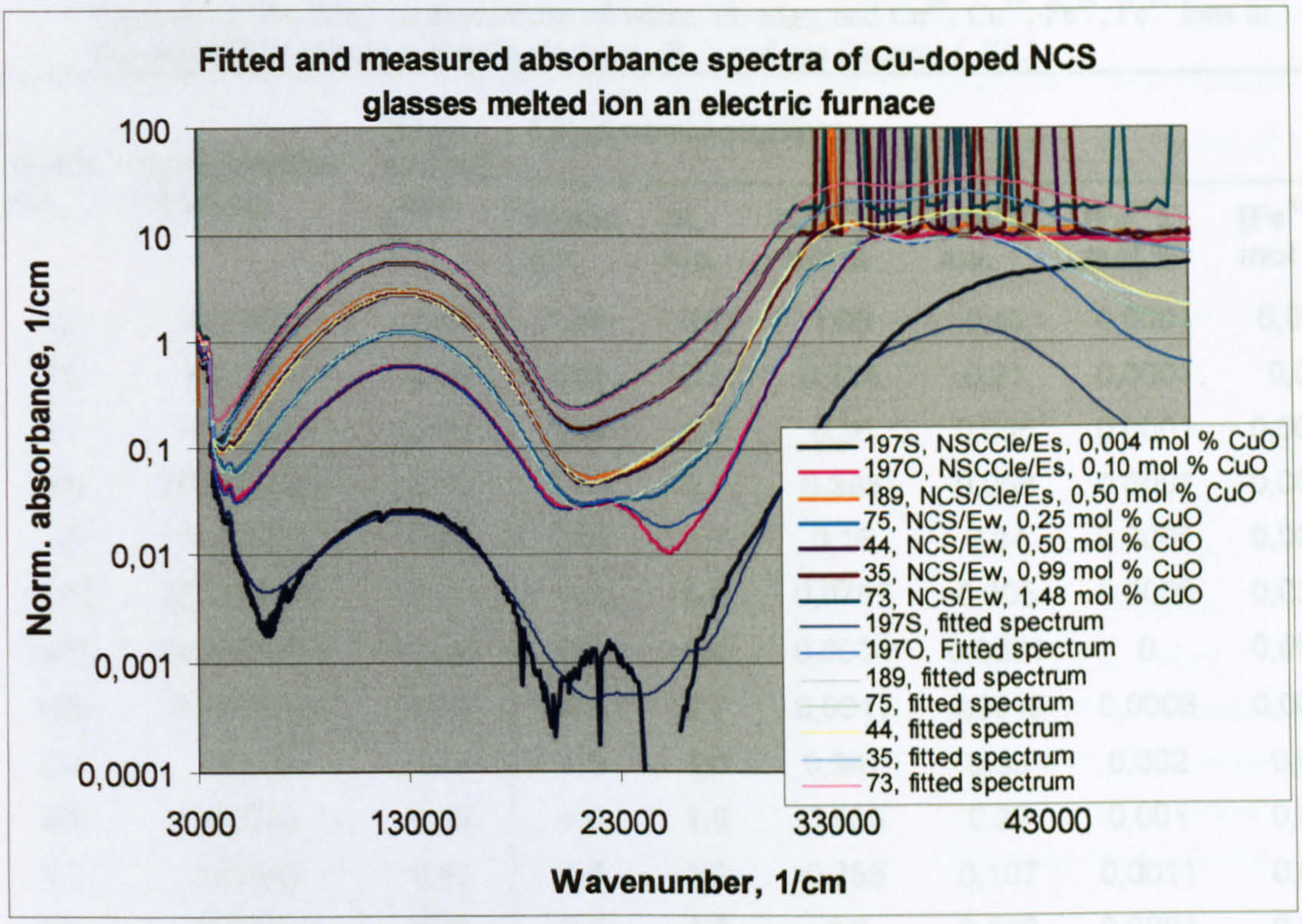

Fig. 6.7.2 The measured and fitted absorbance spectra for Cu doped NCS glasses melted in an electric furnace. The fitting parameters are given in Annex 11, Tables A11.1 and A11.2. The obtained ion concentrations are given in Table 6.7.1.

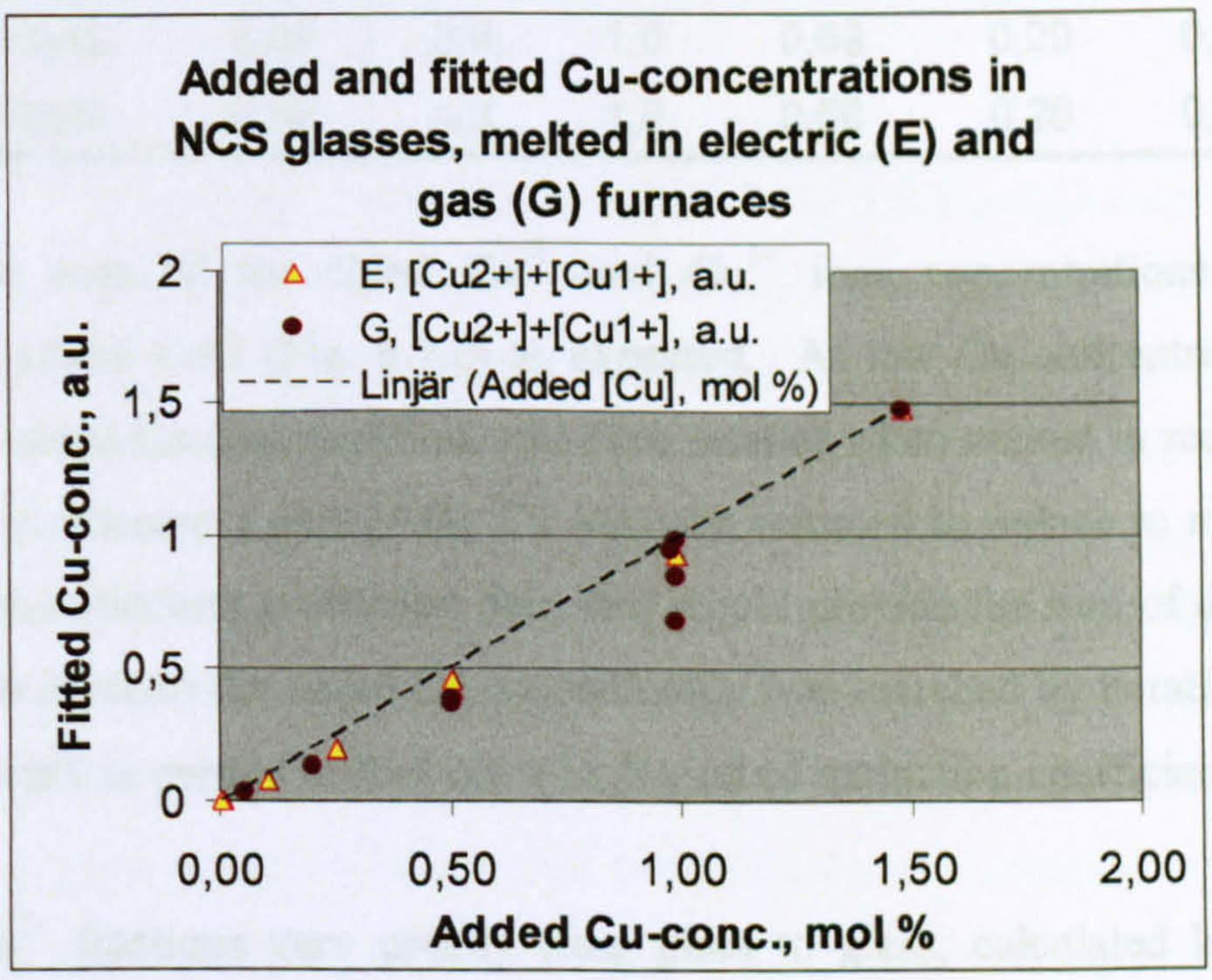

Fig. 6.7.3 Comparison of the fitted sum $[Cu^{2+}]+[Cu^{1+}]$ with the added Cu-concentration, for Cu-doped NCS glasses melted in electric (E) and gas (G) furnaces (Table 6.7.1). The differing point at 1,00 mol % represents Glass 79 that was further reduced with 0,49 mol % carbon.

Table 6.7.1 The fitted concentrations of water, IR-edge, and Cu^{2+}, Cu^{1+}, Fe^{2+}, Fe^{3+} ions in Cu-doped NGS glasses melted in electric (../E..) and gas furnaces (../G..) .

Glass No	Composition /melting	[CuO, added], mol %	Fitted concentrations					
			Water, a.u.	IR, a.u.	$[Cu^{2+}]$, mol %	$[Cu^{1+}]$, a.u.	$[Fe^{2+}]$, mol %	$[Fe^{3+}]$, mol %
73	NCS/Ew	1,48	1,46	0,7	1,05	0,43	0,0001	0,011
35	NCS/Ew	0,99	0,9	0,4	0,715	0,21	0,0001	0,01
44	NCS/Ew	0,50	1,46	0,7	0,36	0,055	0,0001	0,0081
189	NCSCle/Es	0,50	1,46	0,7	0,395	0,058	0,0001	0,0041
75	NCS/Ew	0,25	1,46	0,7	0,16	0,04	0,0001	0,0081
197O	NCSCle/Es	0,10	1,2	0,5	0,0767	0,005	0,0005	0,0051
197S	NCSCle/Es	0,004	0,9	0,4	0,0034	0,0001	0	0,0006
196	NCSCle/Es	0,00	0,9	0,7	0,0017	0,0015	0,0008	0,0029
29	NCS/G	1,48	4,5	1,0	0,947	0,53	0,002	0,08
28	NCS/G	0,99	4,5	1,0	0,555	0,29	0,001	0,08
27	NCS/G	0,50	4,5	1,2	0,255	0,107	0,0011	0,08
94	NCS/G	0,50	3,5	1,2	0,3	0,082	0,0001	0,04
103	NCS/G	0,20	3,7	1,5	0,111	0,02	0,0001	0,04
244	NCSCle/Gw	0,05	3,2	1,6	0,0331	0,005	0,0001	0,004
79	NCSRed/G	0,99	4,2	1,0	0,44	0,24	0,001	0,05
78	NCSOx/G	0,99	3,9	1,0	0,69	0,29	0,001	0,07
142	NCSOx/G	0,98	4,2	1,0	0,68	0,26	0,001	0,08

However, the sum of the fitted Cu^{2+} and Cu^{1+} ions concentrations scale with the concentration of added CuO (Fig. 6.7.2) as expected. At low Cu concentrations the sum is smaller than the added Cu concentration, and even smaller when melted in reducing conditions or further reduced, because a part of the Cu ions are assumed to reduce to metallic Cu atoms (Fig. 6.7.2). Such extinction coefficient pair, that would provide the sum of the concentrations $[Cu^{2+}] + [Cu^{1+}]$ to agree to the added Cu concentration was searched by iteration, but not found so far. Further work is needed to find out which kind of extinction coefficients would provide this, if any.

The fitted Cu^{2+} fractions vary greatly from glass to glass, calculated by comparing the obtained $[Cu^{2+}]$ and $[Cu^{1+}]$ with the added Cu concentration (Fig. 6.7.3), while the Cu^{1+} fractions show clearer trends for both electric and gas melted glasses. The Cu^{2+} concentrations of the glasses melted in electric furnace are higher than for glasses melted in a gas furnace, while the Cu^{1+} concentrations are higher for gas melted glasses, as is expected. The results differ slightly from the results (Fig. 6.2.1, p.124) presented by Durán et al (1985 a). However, their

data for glasses melted in oxidising conditions are obtained at different added Cu concentration range than the data for the reducing conditions. They present only Cu^{2+} concentration data, because they did not fit or measure the $[Cu^{1+}]$ data and assumed that the $[Cu^{1+}]$ is equal to the [added Cu] – $[Cu^{2+}]$.

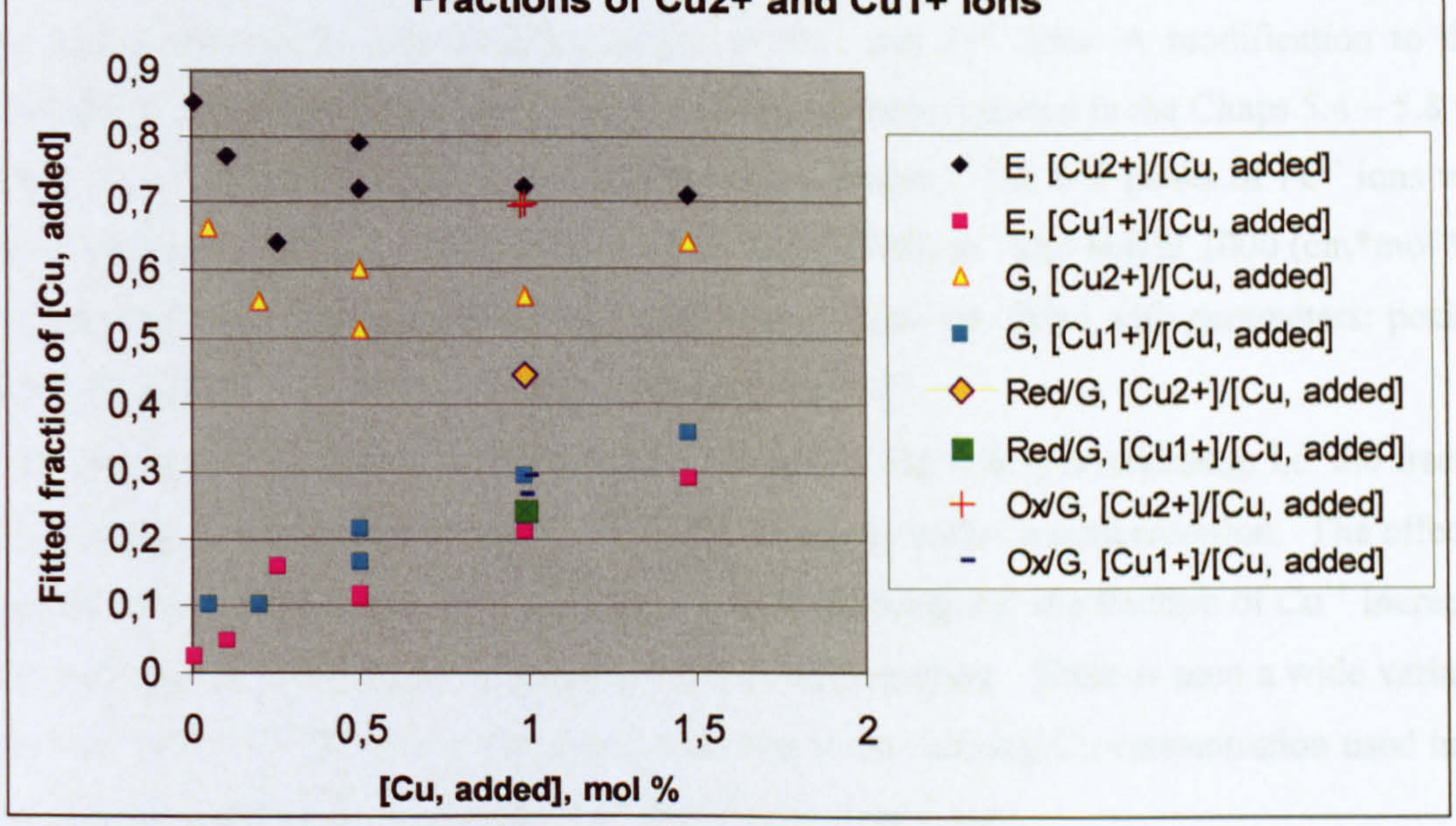

Fig. 6.7.4 Fitted fractions of Cu^{2+} and Cu^{1+} ions in Cu doped NCS glasses melted in electric (E) and gas (G) furnaces (Table 6.7.1).

The reason for the larger Cu^{2+} variation obtained can be the assumed error of the calibration of the band height. Smaller Cu^{2+} concentrations obtained with a higher extinction coefficient, would vary less. Various other reasons can be imagined. Another uncertainty is the reflection loss correction method, in particular at the lowest Cu-concentrations studied. A third reason is uncertainty in the fitting parameters of the UV peaks for both ions (See the next chapter). A fourth reason is an uncertainty in the redox ratio of the contaminating Fe ions. However, the most probable reason is the preparation differences between the individual glasses (melting temperature, annealing temperature, purity of the deionised water into which the electric melted glasses were homogenised, and for the gas melted glasses the total missing of homogenising and dissolution of the mullite to the glass melt, which might have been slightly different for each glass, as was seen from the crucible. As mentioned in the literature study, Cu redox is very sensitive to the melting conditions, temperature, etc.

6.8 Fitting of spectra for Cu and Fe codoped NCS glasses

The fitted and measured absorbance spectra of the NCS glasses doubly doped with Fe and Cu are shown in Figs. 6.8.1 and 2. The fitted concentrations are shown in Table 6.8.1 and the fitting parameters of Cu ions are given in Annex 11, Tables A11.3 and 4. The fitting parameters for Fe^{2+} and Fe^{3+} are given in Chapters 5.4 and 5 (electric melted glasses) and 5.7 (gas melted glasses). The sets of parameters fitted for a similar iron concentration in a singly Fe-doped glass were used for the d-d transition peaks of Fe^{2+} and Fe^{3+} ions. A modification to their octahedral and tetrahedral site fractions and peak parameters reported in the Chaps 5.4 – 5.8 was needed, i.e. to obtain a fit also to the doubly doped glasses. The UV peaks of Fe^{2+} ions were fitted with the parameters: position 46700 cm^{1}, width 5990 cm^{-1} and height 1000 $(cm*mol\ \%)^{-1}$ for all the doubly doped glasses. The UV peak of Fe^{3+} ions was fitted with parameters: position 39360 cm^{1}, width 3150 cm^{-1} and height 1900 $(cm*mol\ \%)^{-1}$.

The effect of Cu addition on the Fe redox, shown in Fig. 6.8.3, is oxidising, i.e. the fraction of Fe^{3+} increases while the fraction of Fe^{2+} ions decreases with Cu-concentration. The effect of Fe addition on the Cu redox, shown in Fig. 6.8.4, is reducing, i.e. the fraction of Cu^{1+} increases, while the fraction of Cu^{2+} ions decreases with Fe concentration. There is seen a wide variation in the Cu^{2+} and Cu^{1+} fractions (Fig. 6.8.4). It is due to the varying Cu concentration used in the tested glasses (Table 6.8.1). However, the trends are clearly seen.

The Glass 94 spectrum differs from the other doubly doped glasses (Figs. 6.8.1 and 2), showing a UV-edge at lower wavenumbers than expected. The fitted amount of Cu ions $[Cu^{2+}]$ + $[Cu^{1+}]$ is actually 1,47 mol %, while only 0,99 mol % CuO should have been added (Table 6.8.1). A weighing error, or a significant precipitation of Cu^{1+} containing nanoparticles (Cattaruzza et al, 2005, Manikandan et al, 2003), might be the reason. Another glass with similar composition should be melted.

The analysis of these results is planned to continue with a quantitative analysis on the seen trends. i.e. does the actual number of moles of Fe^{2+} oxidised correspond with the proportion of reduced Cu^{2+}. It would also be interesting to examine the concentrations of both ions during annealing. Preliminary results obtained by Mr. Andrew Wilkinson, who in his MSc project tested some of these glasses at various annealing temperature, suggested such a change.

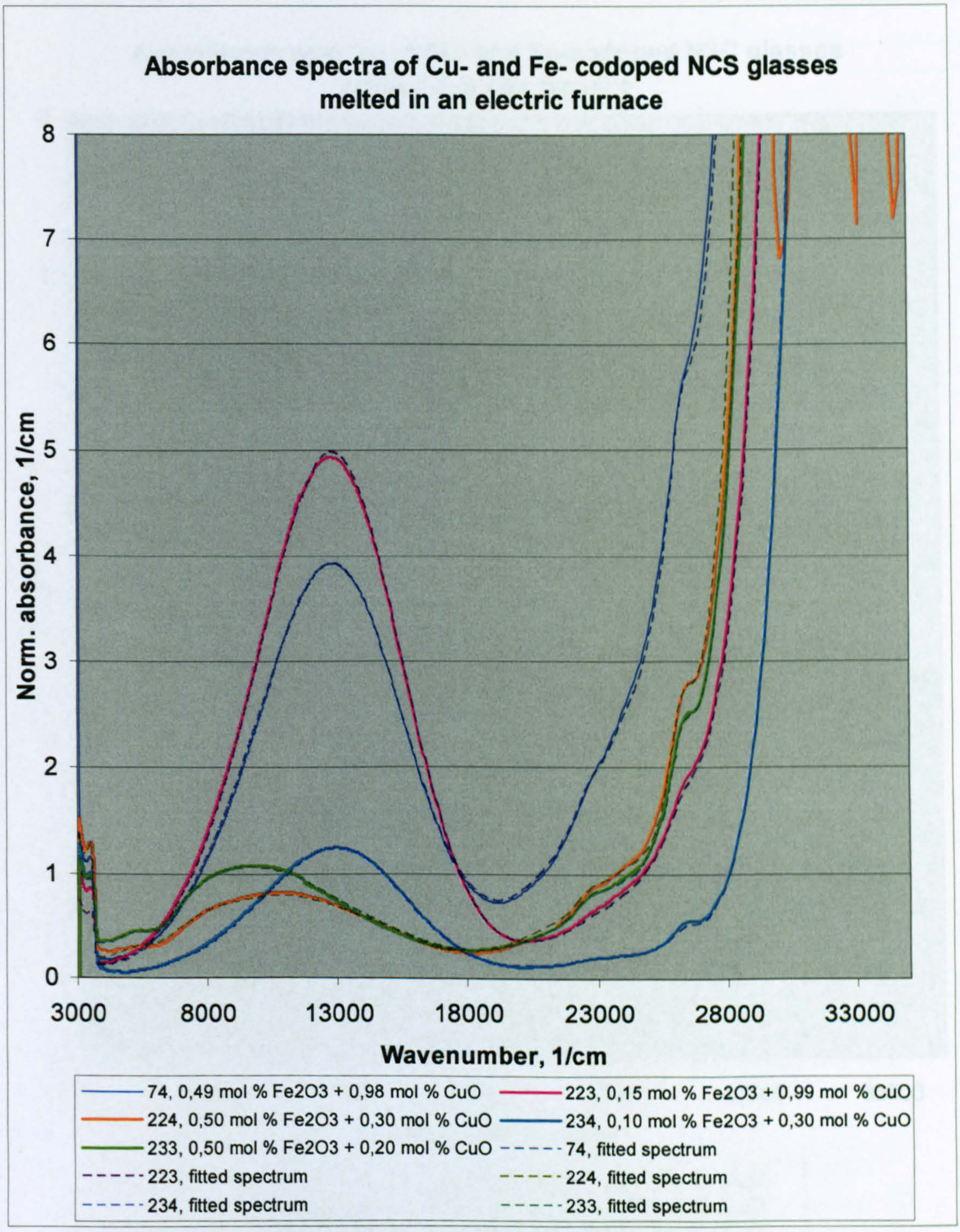

Fig. 6.8.1 Measured and fitted spectra of doubly with Cu and Fe doped NCS glasses melted in an electric furnace. The fitted concentrations are given in Table 6.8.1 and the fitting parameters of Cu ions in Table A11.3 and A11.4. Fe fitting parameters (FIT1) are given in Chaps. 5.3 and 5.4, and in Chap5.5. p. 99.

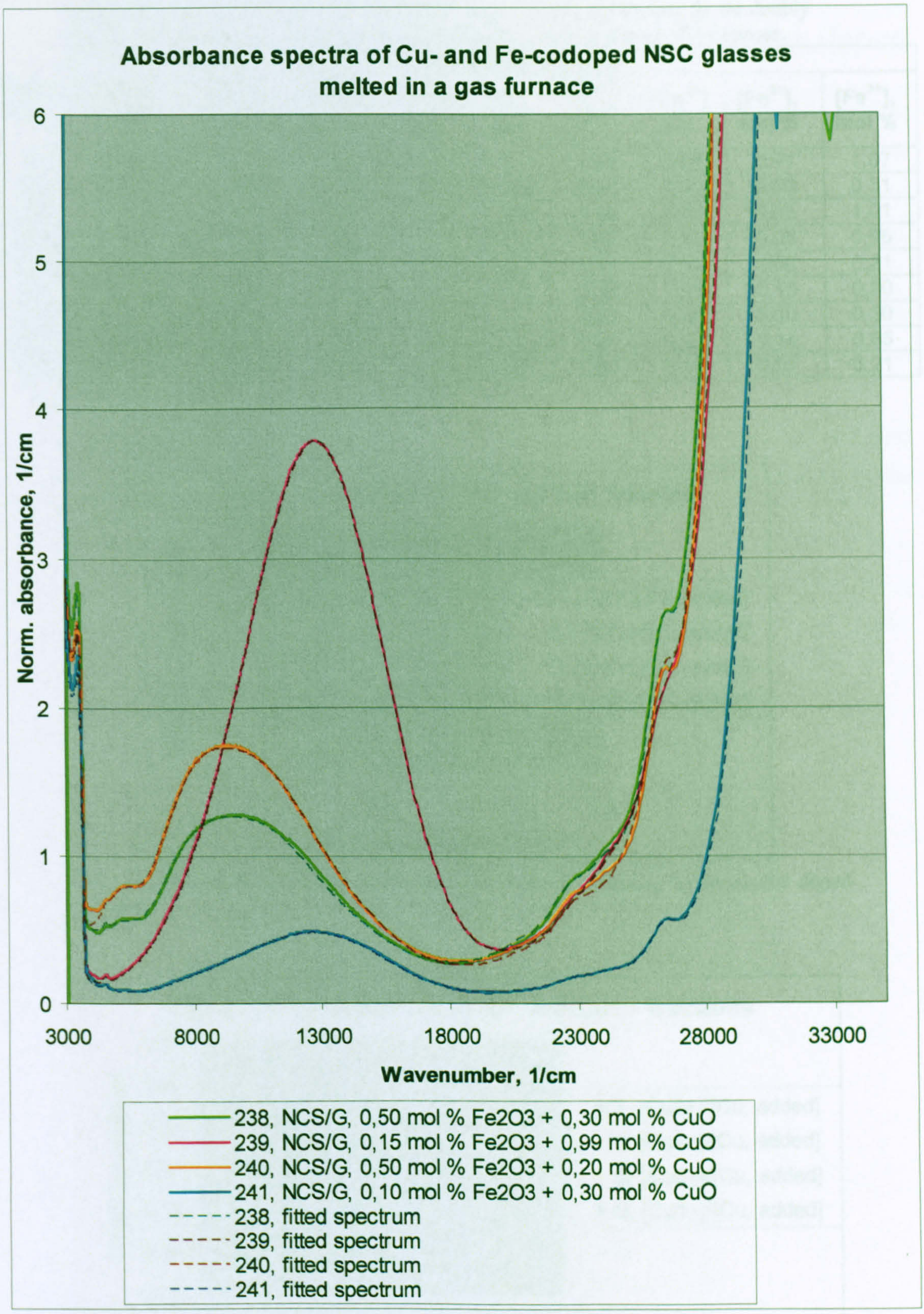

Fig. 6.8.2 Measured and fitted spectra of doubly with Cu and Fe doped NCS glasses melted in an electric furnace. The fitted concentrations are given in Table 6.8.1, the fitting parameters of Cu ions in Table A11.3 and A11.4. Fe ion fitting parameters are given in Chap. 5.7.

Table 6.8.1 Fitted concentrations of water, IR-edge, Cu ions and Fe ions for the doubly with Cu and Fe doped NCS glasses melted in electric (../Ew) and gas (../G) furnaces.

Glass No	Comp. / melting	[CuO, added], mol %	[Fe_2O_3, added], mol %	Fitted concentrations					
				Water, a.u.	IR, a.u.	[Cu^{2+}], mol %	[Cu^{1+}], a.u.	[Fe^{2+}], mol %	[Fe^{3+}], mol %
74	NCS/Ew	0,98	0,49	1,72	0,7	0,49	0,98	0,01	1,07
223	NCS/Ew	0,99	0,15	0,9	0,4	0,65	0,60	0,00	0,31
224	NCS/Ew	0,30	0,50	1,9	0,4	0,04	0,26	0,05	1,01
233	NCS/Ew	0,20	0,50	1,0	1,0	0,02	0,19	0,08	0,95
234	NCS/Ew	0,30	0,10	1,46	0,7	0,16	0,14	0,00	0,21
238	NCS/G	0,30	0,50	3,8	1,2	0,02	0,28	0,10	0,90
239	NCS/G	0,99	0,15	3,9	1	0,50	0,50	0,00	0,30
240	NCS/G	0,20	0,50	3,5	1	0,01	0,20	0,14	0,85
241	NCS/G	0,30	0,10	3,5	0,7	0,05	0,14	0,01	0,21

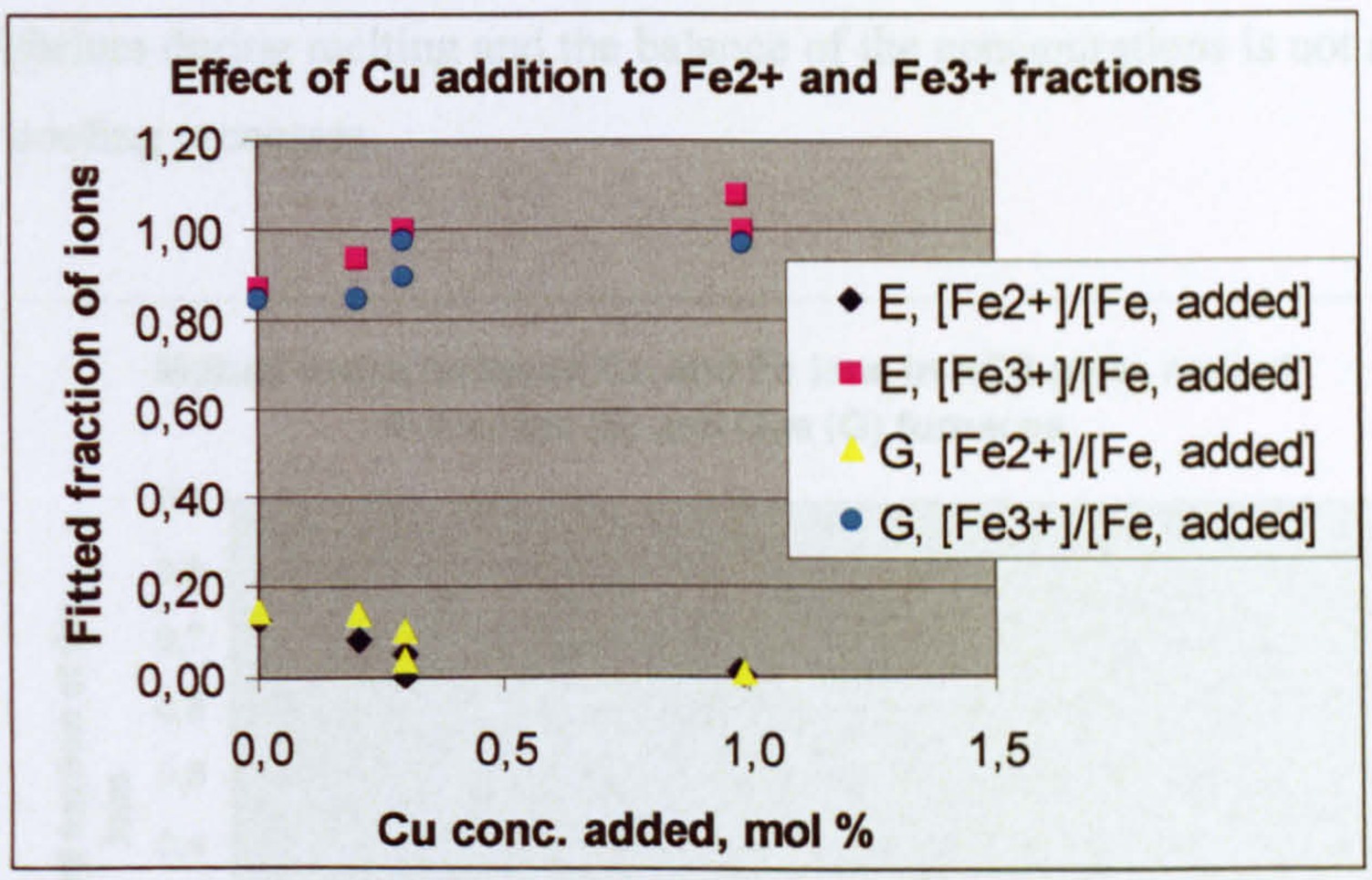

Fig. 6.8.3 The effect of Cu addition to the Fe^{2+} and Fe^{3+} fractions in the doubly doped glasses.

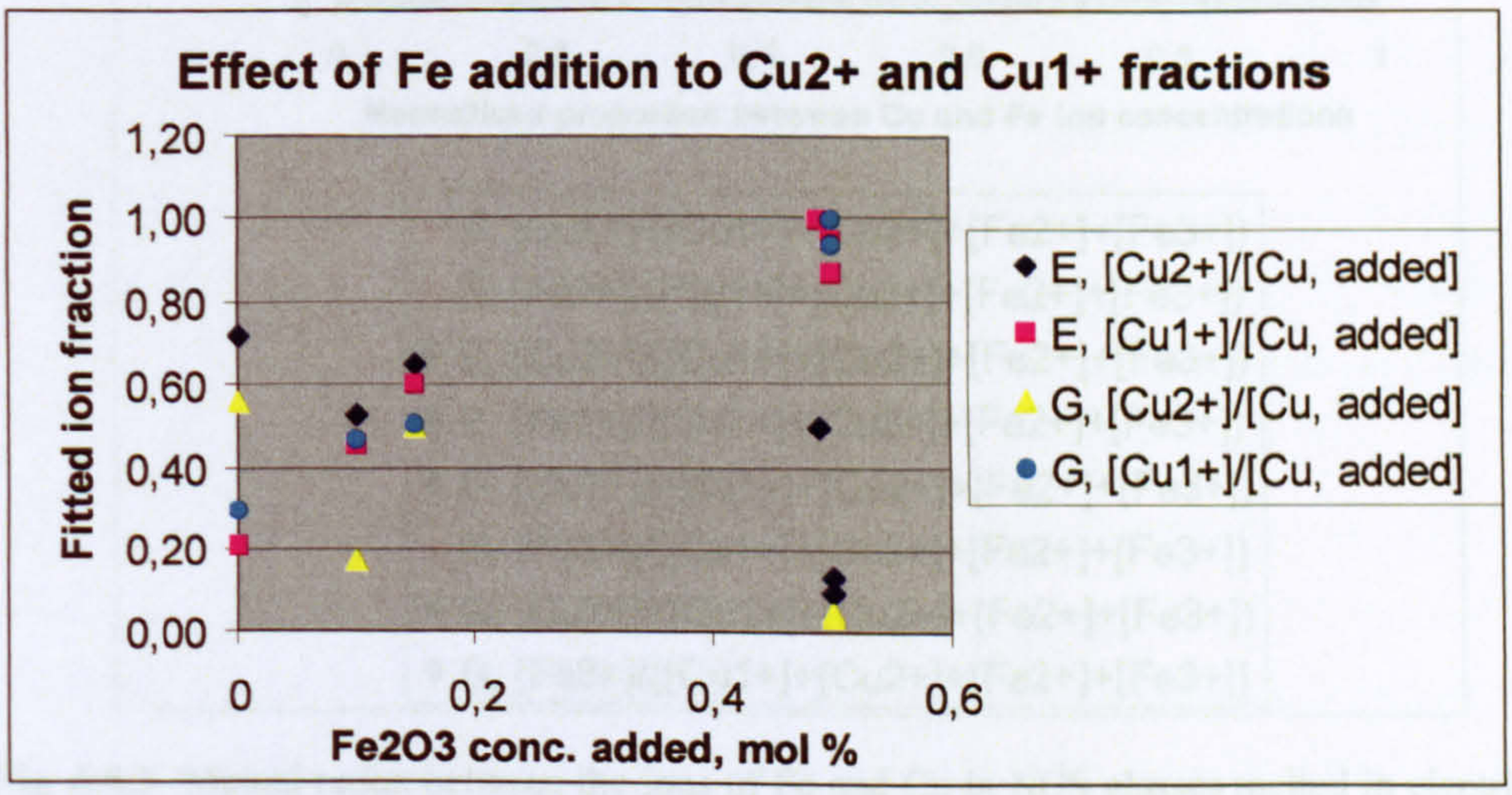

Fig. 6.8.4 The effect of Fe addition to the Cu^{2+} and Cu^{1+} fractions in the doubly doped glasses.

6.8.2. Meaning of the fitted results for the doubly doped glasses

The obtained fitted concentrations of the doubly doped NCS glasses can be calculated in another way to look at the mutual redox, for which the ratio of Fe and Cu concentrations matter most. The obtained concentration fractions (normalised by the sum of the ions) are shown as a function of the normalised proportion ratio of the concentrations ([Cu, fitted]/[Fe, fitted])/([Cu, fitted]+[Fe, fitted]), as shown in Fig. 6.8.5. At the left hand axis, all colorants are copper ([Fe, fitted] = 0, at the right hand side all colorants are iron [Cu, fitted] = 0, and the concentration proportion varies between these axis, being equal in the middle, i.e. at the normalised proportion ratio = 0,5.

It is assumed that the chemical mutual redox reactions between the copper and iron ions reach the equilibrium during melting and the balance of the concentrations is not affected by the annealing and cooling processes.

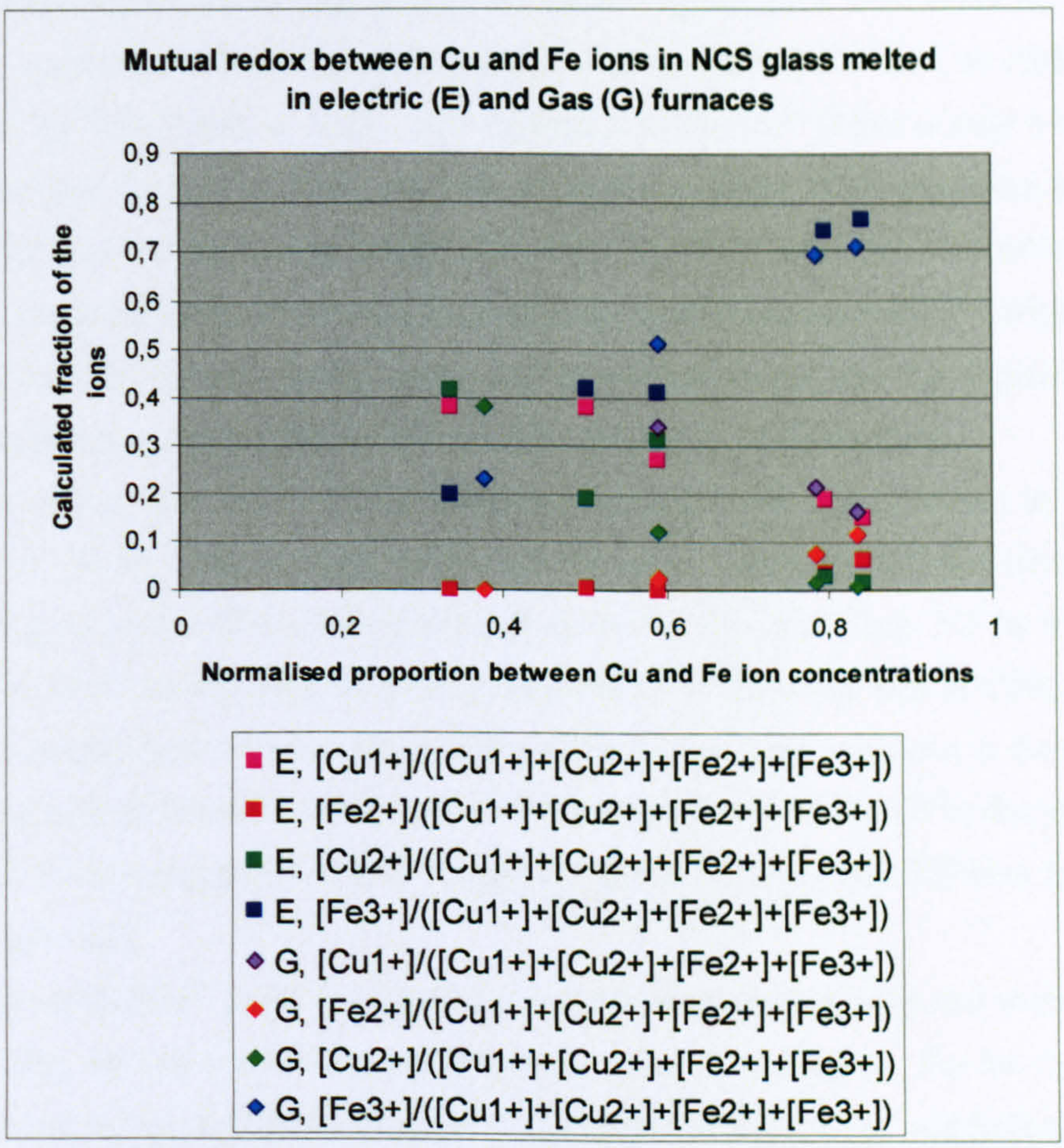

Fig. 6.8.5 Mutual redox between the ions of Fe and Cu in NCS glasses melted in electric and gas furnaces. The same data is shown in previous graphs, 'Figs. 6.8.2 and 6.8.3 and in Table 6.8.1.

Clear trends are obtained for all four ions, and a clear difference in the redox is seen to be caused by the melting conditions. It can be concluded that a small proportion of copper can oxidise all Fe^{2+} ions to Fe^{3+}. But it would not help to make the glass transparent in the visible range, because instead we would have a lot of Cu^{1+} ions (40 %) that absorb also visible light and still a remarkable concentration of Cu^{2+} ions left. However, the hue of the glass would change, because the absorption spectra of Fe^{2+} and Cu^{2+} ions have different shape. It is seldom realised that there is a significant proportion and concentration of Cu^{1+} present in these kinds of glasses, even though the iron concentration would be much higher than Cu concentration. At high iron proportion all Cu^{2+} ions disappear.

The data will be further analysed in near future.

6.9 Discussion and conclusions of the fitting analysis of Cu absorbance spectra

6.9.1. Fitted Cu^{2+} absorbance band at 12750 cm^{-1}

Two Gaussian peaks centred at 11600 ± 50 cm^{-1} and at 13500 ± 100 cm^{-1} fit accurately to the absorbance band centred 12755 cm^{-1} of Cu^{2+} ions in the NCS glasses studied in this work. The separation of the peaks is 1800 ± 150 cm^{-1}. The fitted peak at the lower energy 11600 cm^{-1} is slightly broader and has a little lower height than the peak at 13500 cm^{-1}. The peak widths are broader (2940 and 2400 cm^{-1} respectively) than for the fitted peaks of Fe^{2+} ions at 7500 and 10400 cm^{-1} in octahedral sites (with the widths 1430 and 2390 cm^{-1}; Chap. 5.4 – 5.8), both are obtained in the same host glass melted in the similar conditions. Thus the ligand field strength caused by the host glass (≈ optical basicity) is the same. The obtained configurations of the sites in both cases are elongated octahedra. But there is a difference in the length of elongation and in the variation distribution of the elongation.

The obtained separation of the fitted Cu^{2+} peaks agrees to a few times kT (k being Boltzmann's constant) at room temperature, i.e. is of the order of 2000 cm^{-1}, as earlier told for the Cu^{2+} ions by Paul (1990, p. 305). The separation of the Cu^{2+} peaks is only a half of the separation obtained for the Fe^{2+} ions. Thus the average elongation of the octahedra of the Cu^{2+} ions is smaller than the elongation for the Fe^{2+} sites. The Fe^{2+} ions have six electrons and d_6 structure of energy orbitals and Cu^{2+} ions have nine electrons on d_9 structure of orbitals and both orbital structures are splitted to two upper and two lower levels, and the separation of the absorbance peak top energies represent the average elongation of the octahedra.

The lower energy peak of Cu^{2+} ions is centred at almost the same position as the higher energy peak of the Fe^{2+}ions and their widths are the same, within the fitting tolerance of 10^{-1} cm. According to the Tanabe-Sugano graphs for d_9 and d_6, shown in Chap. 5.2 for a symmetric octahedra, the curves representing the fitted peak positions of these two ions as a function of the ligand field strength have the same slope at the same energy (peak position) in the same host. Thus when we look at the octahedral peaks of two species the width should be the same for the peaks located at the same position, even though the peaks represent two different ions Cu^{2+} or Fe^{2+}, in the same host.

The heights of the Cu^{2+} peaks (representing or one unit of concentration and amount of Cu^{2+} ions) are similar, whereas for Fe^{2+} the estimated proportion ½ is obtained. For the Cu^{2+} ions the peak at the lower energy is twice as broad as it should be (as it is for Fe^{2+} octahedral), and even broader than the peak at the higher energy. If the elongation variation distribution of the Cu^{2+}

octahedra would be as narrow as it is for the Fe^{2+} octahedral, the proportion of the peak heights and peak widths should be about equal.

The nature of Gaussian peak, i.e. of the normal distribution calculated for one unit number of population, is such that if the variation distribution within the population becomes twice so broad, the height (the probability to find the studied "thing" at the average value) of the distribution decreases to a half. So the height of the Cu^{2+}peak at the lower energy is almost four times as high as it would be if the elongation variation would be the only reason for the broad breath and the height of the peak. Thus the explanation for the peak width and height is the almost square planar structure of the very large elongation of Cu^{2+} sites. In such a case the lower of the upper levels lies at the same energy as the upper of the lower levels. Thus there are in practise only three levels of energy and at both of the lower levels 4 electrons, i.e. en equal amount of electrons to get excited to the upper level of the electron vacancy. Thus it can be concluded that the sites of Cu^{2+} ions are elongated octahedra, but the elongation varies from site to site and in average is of the order extent representing a square planar structure. These conclusions agree to the conclusions of Durán et al (1985 b) for Cu doped silicate glasses and to Bae et al (1994) conclusions for Cu^{2+} sites in copper phosphate glasses ($50CuO - 50P_2O_5$).

Another possible explanation for the unexpected wide peak at the lower energy could be that a small fraction of the Cu^{2+} ions are in tetrahedral sites. Such a peak would locate at 4/9 of 13400 cm^{-1}, which is 5950 cm^{-1}, as was actually fitted by Bae at al (1994). However, Mekki et al (1997) showed that CuO is a glass network modifier, not a former. – Further studies would be needed to find out whether or not Cu^{2+} ions appear in any other kinds of sites in addition to the elongated octahedral sites confirmed with the EPR studies of this work (Chap. 6.4).

The fitted peak parameters differ from the earlier published results of Duran et al (1985 b) who fitted two peaks near 12500 cm^{-1} and 8500 cm^{-1} and from Bae et al (1994), who fitted three peaks at 12600 cm^{-1}, 10600 cm^{-1} and 8500 cm^{-1}. In both cases the peak at 8000 – 9000 cm^{-1} is very shallow, and might thus in both cases be associated with Fe^{2+}-contamination, or the IR-edge tail that were not corrected from their data.

Our results of Stage 2 (Chap. 6.4) showed that the same data can be fitted with almost the same precision with various sets of two and three Gaussian peaks. In addition, Bae's glass contained 40 to 55 mol % copper oxide, i.e. as a glass former rather than a dopant, which would modify the optical basicity. Durán's disilicate and diborate glasses differed from our NCS glass as well.

The measured absorbance bands are also in accord with absorption curves measured for free Cu^{2+}-ions in aqueous liquid and crystal by Bates (1962, p. 251), for which a symmetric octahedral configuration of neighbouring oxygen anions is agreed. These absorption peaks are

at the same position as our measured absorption bands for Cu^{2+} in glass. In addition, the band width (FWHM) is similar, thus indicating that the Cu^{2+} bands in glass are not significantly wider than in a symmetric octahedral configuration. Thus the tetragonal distortion associated with the splitting of the fitted peaks should be small, significantly less than the FWHM width of the original band, as is the case for the results presented in Chaps. 6.5 – 6.8 in this work. Gaskell et al (1992) have shown, by neutron diffraction measurements, that the configuration of oxygen ions around an Cu^{2+} ion is clearly a distorted octahedron in a copper sodium phosphate glass, where four oxygens locate at 1,96 Å distance and two at 2,51 Å. They also suggest that the distance of these two might vary from site to site around the average value. Furthermore, the next neighbouring cations (Na^{+}) were also well defined, and conclusions were that the Cu^{2+} ions environment is ruled by that, and is clearly not random.

So the final conclusion is that the Cu^{2+} band can be fitted accurately as suggested in Chaps. 6.5 – 6.7, but the fitting of the band can be done also by various other sets of two and three Gaussian peaks (Chap 6.4). Thus the fitting results of optical absorbance spectroscopy can not alone be used to determine the configuration of the sites of Cu^{2+} ions in the kind of 15soda-15lime-70silica-0,35sulphate glass studied. However, the fitting results agree with what Burns (1993, p. 235) says: "All Cu(II) compounds contain Cu^{2+} ions in low-symmetry environments, ranging from tetragonally distorted (elongated) octahedral to square planar coordination sites".

6.9.2. *Fitting of absorbance spectra of Cu ions in singly and doubly doped NCS glasses*

The absorbance spectra of Cu^{1+} and Cu^{2+} ions are successfully fitted with summed Gaussian peaks. The fitted spectra of both ions scale with Cu concentration linearly. However, in some cases adjustments are needed because there is an unknown peak at 450 nm involved in the spectra of low Cu and low iron glasses. In addition there might be some metallic Cu particles involved especially for those Cu- doped glasses melted in reducing conditions and in those doubly doped glasses containing a lot of iron. The concentrations of both ions are calibrated only tentatively, and an analysis with another accurate and reliable method should be carried out on the same samples to find out more accurate extinction coefficients for all fitted absorbance peaks.

The UV-peaks are fitted only at the wavenumbers, where the UV-edge is measured reliably. There might be more UV-peaks involved in the absorbance spectra of both Cu and Fe ions at the wavenumbers above 30000 cm, but their tails are either summed together to the fitted peaks or do not extend to the reliably measured wavenumber range.

7. Summary of conclusions

7.1 Introduction

Colour design of silicate glasses can be computerised. The results of this work suggest that absorbance spectra for coloured, decolorised and filtering glasses can be predicted from a batch composition and melting & annealing conditions; and conversely: the concentrations for each colorant ion and site can be identified from a measured absorbance spectrum.

The necessary accurate mathematical descriptions for the absorbance spectra of the two most common colorants and contaminants, Cu and Fe, have been developed over the wavenumber range extending from UV to Near IR (40000 – 3000 cm^{-1}, i.e. 250 – 3300 nm) in a soda-lime-silica glass. The obtained fitted spectra have been used to analyse the mutual redox ratios and concentrations of the Fe and Cu ions and sites for a number of contaminated, singly and doubly doped glasses at varied concentration levels, melted in reducing and oxidising conditions.

No doubt, the absorbance spectra of other ionic colorants can also be fitted; using the measured absorbance spectra of the TM and Re doped glasses, also prepared within this work, and earlier reported in the interim progress reports to the Dept. of Eng. Materials and in the conference presentations (T Volotinen et al, 2004 a and b, 2005 a and b, 2006). The fitted spectra of the Ce and Fe codoped glasses of this work will be presented in July 2007 at the 21st ICG in Strasbourg.

7.1 Fitting of the absorbance spectra Fe and Cu ions

In this thesis, answers have been found for many of the relevant questions regarding the mathematical description of the absorbance spectra of two ionic colorants and concerning the application of the fitting analysis to the various glasses. However, some more questions need further work.

Accurate fitting parameters of the absorbance spectra of Cu and Fe ions have been obtained for summed Gaussian peaks for each valence (Cu^{1+}, Cu^{2+}, Fe^{2+} and Fe^{3+}) and site (Fe^{2+} octahedral and tetrahedral, Fe^{3+} octahedral and tetrahedral) in NCS glasses melted in oxidising and reducing conditions. The fitting parameters (peak heights, i.e. extinction coefficients in $(cm*mol\ \%)^{-1}$ units, peak positions and peak widths) have been defined for all five peaks of Fe^{2+} ions, nine peaks of Fe^{3+} ions, four peaks of Cu^{2+} ions and one peak for Cu^{1+} ions, including the UV peaks of all these ions that define the UV-edge of the absorbance spectra and in most cases extend far into the visible range.

The extinction coefficients (peak heights) of all fitted Fe peaks have been calibrated through an iterative process. At first the heights of the fitted Fe^{2+} peaks (including the UV-peak of Fe^{2+}

ions) are calibrated on the summed absorbance at 1000 nm (not at the band top) for a 1,000 mol % concentration and 1,00 cm thickness of glass with the literature data from the well-known source (Bamford, 1977). Then the height of the summed band of the fitted d-d transition Fe^{3+} peaks (without the UV-peak) for the octahedral and tetrahedral sites, is calibrated using the difference between the concentrations of Fe^{2+} ions and the added & contamination Fe. After that, the height of the UV peak of Fe^{3+} ions was adjusted so that it fits the measured absorbance data. Furthermore, this procedure was repeated many times for the set of five measured spectra at various Fe-concentrations, in order to get all fitting parameters (heights, positions and widths) of all Fe peaks well established so that the measured absorbance spectra over a 0,05 – 0,50 mol % added Fe_2O_3 concentration range could be fitted with the same set of parameters by changing only the fitted concentrations of the ions, each valence and site, with the smallest possible residual over the entire wavelength range.

In addition, five Gaussian peaks are fitted to the absorbance spectrum of Fe-S chromophores, which are necessary to fit the Fe-doped NCS glasses melted in reduced conditions, and the heights of these peaks are calibrated according to the literature data (Paul, 1981). The fitting parameters are identified for one unknown peak at 22200 cm^{-1} found in the glasses that are Fe and Cu contaminated or codoped with low concentrations of these ions. This peak might be caused by some chemical specie containing S or Fe-S-Cu (such as Fe-Cu-sulphide), or by disproportionated metallic Cu particles, or by Fe ions containing particles (Burns, 1993).

It was realised in the beginning of the work that all significant factors affecting the measured data should be deeply understood and all possible errors and uncertainties kept to a minimum. The signal-to-noise ratios and ion absorbance-to-background loss ratios had to be kept as high as possible. Because the glasses were made of a commercial grade of ingredients, the first task was to develop reliable fitting parameters for iron, the most common contaminant in the prepared glass samples. Sufficiently accurate fitting parameters that would have scaled with Fe-concentration were not found from the literature. The non-purified ingredients provided a realistic case to develop such mathematical descriptions that could hopefully be used for commercial glass making, i.e. to analyse the colour changes caused by mutual redox between the contaminant iron and added colorants, and to design decolorising batches for glass making from contaminated raw materials.

One of the major challenges was to fit correctly the reflection losses at the UV-edge. In the beginning, it was thought that the UV edge would be mainly caused by the spectrum of Fe^{3+} ions and reflection losses. Because that didn't fit well to the measured data, all possibilities other than the absorbance of the colorants and reflection loss had to be either excluded, or accurately fitted. Therefore the various measurements of reflection and scattering spectra were

carried out. It was concluded from the measurements that the main factors for the UV-edge for singly iron doped and contaminated glasses are the iron absorbance and reflection loss, provided that the samples were properly melted, homogenised, annealed and prepared. Later on analysis of the codoped data for the Fe and Cu, as well as recently for the Ce and Fe, finally proved that the Fe^{2+} absorbance spectrum extends from the UV to the Near IR, i.e. over the entire 200 – 3300 nm wavelength range, even at very low concentration level of Fe contamination. Both Cu (shown in this report) and Ce (Volotinen et al, ICG 2007) can through a mutual redox with the Fe ions oxidise the Fe^{2+} ions, whilst themselves being reduced from Cu^{2+} to Cu^{1+} (or from Ce^{4+} to Ce^{3+}). Thus it was understood that the third significant absorbance at the UV edge in iron doped glasses is caused by the Fe^{2+} ions. So the absorbance spectrum of Fe^{2+} ions extends over the entire wavelength range used in this work. However, its significance was not pointed out within the results of those earlier researcher's, whose fitting data was used as a guidance in the beginning of this work (Chap. 5.2). Only Glebov et al (1997) and Boulos et al (2002) have, to my present knowledge, reported similar conclusions for the Fe^{2+} spectra, predicted from a fitting analysis of absorbance spectra on iron doped glasses.

A reflection loss curve $A_{ref}(\lambda)$ over the wavelength range 200 – 3300 nm was developed, because such was not found from literature. The effects of the colorants on the glass refractive index or on the reflection loss at the ends of the wavelength scale were not known. The obtained reflection loss correction curve was estimated from the average refractive index data measured for a set of undoped and doped NCS glasses, and on direct reflectance measurements made on similar NCS glass doped with Mn and Cr, that has very high absorbance over the entire visible range by fitting Cauchy equation to the data over the wavelength range 200 – 3300 nm and using the known shape of refractive index curve for pure silica as a quidance.

Fitting of the tail of the IR-edge, present in all glasses in addition to the OH- peaks at wavenumbers below 4500 cm^{-1}, with an exponential function was found necessary. The OH^- band below 3800 cm^{-1} was fitted using the parameters recently presented by Navarro et al (2005). Two additional peaks at longer wavenumbers were also identified as OH^- peaks with the help of literature and fitted with Gaussian peaks and summed together under one concentration multiplier fitted at an analysis to each measured absorbance curve according to its OH^- (water) concentration. Neither the IR edge or the water concentration were calibrated for real concentration units, though a.u. units were used. The results obtained suggest that the concentration of water could be measured accurately by calibrating the extinction coefficients (the heights) of the obtained fitted peaks.

The repeatability of the ion and site concentrations obtained by the fitting method of Fe^{2+} and Fe^{3+} ions and their sites was found to be of the order of 0,001 mol %, i.e. better than for any

other known method. The accuracy might be of the same order of magnitude. The calibration needs, however, to be confirmed by another analysis method. A similar order of accuracy magnitude is expected for the fitting analysis of Cu ions. The extinction coefficients need to be calibrated by another method also for Cu^{2+} and Cu^{1+} ions.

7.2 Fitting analyses results of Fe doped glasses

The Fe^{2+} and Fe^{3+} fitted absorbance spectra were for first time shown to scale with Fe concentration over the range 0,1 – 0,5 mol % of Fe_2O_3 added and with minor modification also over the wider range from 0,01 – 2 mol % of Fe_2O_3. Furthermore, the fractions of tetrahedral and octahedral Fe^{3+} sites were also for first time shown by fitting analysis to change slightly with Fe concentration. The melting environment was shown to have on significant effect on the redox ratio of the ion concentrations and on the fractions of sites. Host glass composition, temperature during melting, annealing and cooling processes might also change the ratios of the redox and site concentrations. These remain to be investigated in future, and can be done with a greater resolution by the developed fitting analysis than with other methods.

It was also shown that Fe-S chromophores exist in the Fe doped glasses melted under reducing conditions. A significant error would be caused in the prediction of absorbance values, if the absorbance of Fe-S chromophores is neglected. The extinction coefficients are 3 – 20 times higher than for UV peaks of Fe^{3+} and Fe^{2+}, and the only reason that they do not dominate the absorption spectrum is that their concentration is very low.

The new peak at 3590 cm^{-1} for Fe^{2+} ions in tetrahedral sites was confirmed by the consistent fitting analysis of numerous measured spectra, and also was confirmed after the analysis in references by Glebov and Boulos (1997, 2002) who fitted the spectrum of a slightly different soda-lime-silica-magnesia commercial container glass.

During fitting, consistent trends were obtained in the ratios of the site concentrations. The reported numbers might not be absolutely right, because the relationship of the absorptivities is not known or calibrated. However, the ratio might be significantly closer to 1 (that is used) than to the figure of 10 mentioned in several literature sources, because the changes in relative peak heights are of a similar size. If the number were ten, the absorbance of the tetrahedral sites would increase by a factor of ten when one unit of octahedral sites is decreased; provided that the oxidation or reduction states of the ions is independent of the site distribution. It would be interesting to study, whether it is or is not. The fitting method would be a suitable analysis tool to do that.

Fitting of the absorbance spectrum of Fe^{3+} ions was most complex. Also the behaviour as a function of Fe-concentration under at different melting conditions was complex. Similar

behaviour had been seen by Glebov and Boulos (1997, 2002) and they had therefore fitted only the spectra for glasses melted at oxidising conditions in the Fe concentration range where the spectrum is stable, i.e. the behaviour can be described by one parameter, the Fe^{3+} concentration. In this work, the complex variation between the octahedral and tetrahedral sites is fitted for both kinds of melting conditions, and clear trends are demonstrated.

The most interesting confirmation, however for the fitted parameters of the Fe absorbance spectrum and for the usefulness of the developed fitting method, were the results obtained from the analysis of the glasses doubly doped with Cu and Fe at various concentration relationships. The mutual redox reaction trends were clearly shown and which were also clearly different for the oxidising and reducing conditions. Even the fractions of tetrahedral and octahedral sites are slightly affected by the presence and concentration of Cu ions. These results are so recent that they are only briefly presented here, but will be reported at a later stage in detail.

The fitting method and parameters should urgently be tested for Fe doped glasses made with varied host glass compositions resembling commercial glasses. Even though there is a comprehensive understanding how the Fe absorbance spectrum changes with optical basicity of the glass (= ligand field) (Bingham et al, 2001 and 2002; Duffyet al numerous papers) this test would finally validate the fitting method and the fitting parameters; and further develop the mathematical description of the absorbance spectra. Another recommended continuation is to fit all relevant mutual redox pairs, including the chemical refiners, reducing and oxidicing agents, not tested here. With these mathematical developments the applicability and feasibility of the fitting method to computerised colour design and analysis of glass compositions from measured absorbance curves would further improve.

7.3 Conclusions for the analysis of Cu doped glasses

The absorbance spectra of both Cu^{2+} and Cu^{1+} ions were determined for singly and doubly NCS glasses, melted in oxidising and reducing conditions within Cu concentration range extending from the contamination level to 1,5 mol % of added CuO. The absorbance spectra of both ions have been also fitted with summed Gaussian peaks, three (four) peaks for Cu^{2+} spectrum and one peak for Cu^{1+} spectrum, including those UV peaks that significantly affect the absorbance data within the range 3000 – ca. 35000 cm^{-1}. For first time, to my present knowledge, the absorbance peak tail, extending down to visible range, was fitted and used to quantify the concentration of Cu^{1+} ions in NCS glass.

The sets of fitting parameters are established and the peak heights, are tentatively calibrated through a similar three stage process as the fitted spectra of the Fe ions. The calibration was started by adjusting the heights of the Cu^{2+} peaks at the summed band top at 784 nm (12755 cm^{-}

[1]) to lie slightly under the data determined by Cable et al (1989) for a slightly different glass. Cable et al did not correct for the background caused by the IR-edge tail or for the OH bands and subtracted a slightly different, constant reflection loss over the wavelength range. The height of the Cu^{1+} peak was calibrated by relying on an advanced guess, close to literature data for other glasses. The iterative repeating with fitting of the data at several Cu concentrations was repeated only a couple of times, and some of the peak parameters were still necessary to be varied in fitting of the glasses (Annex 11).

There is an uncertainty in the obtained concentration levels of Cu^{1+} ions. The obtained results show that the sum [Cu^{2+} fitted]+[Cu^{1+} fitted] is smaller than the [Cu added] at low Cu concentrations. This finding agree with Duráns analysis, suggesting that below 0,5 mol % of added CuO, a few per cents of Cu end up to a non-absorbing form, i.e. metallic Cu atoms or very small nanoparticles of metallic Cu or crystalline Cu_2O. A lower extinction coefficient of Cu^{1+} ion peak would give the fitted sum concentration of Cu^{2+} and Cu^{1+} ions to exceed the added concentration of Cu ions, and a higher one would show a larger difference between the fitted sum and added concentration. At least a couple of iterative processes and further adjustment of both Cu^{2+} and Cu^{+1} peak heights might help. The best would be, however, to have accurate second analysis for the concentrations of all Cu containing species in these glasses. The redox reactions between the three Cu species, Cu^{2+}, Cu^{1+} and metallic Cu concentration should be further investigated for the similar glasses as analysed here.

The origin for the unknown peak at 22200 cm^{-1} and the effect and possible mutual redox reactions between various valence states of S and Cu ions in presence of Fe ions should be further investigated to determine the fitting parameters and the conditions under which these reaction affect absorbance spectra of Cu-doped glasses.

Differently from the constant Fe ion fractions at oxidising and reducing melting conditions, t he obtained ion fractions of Cu^{2+} and Cu^{1+}, compared to the added Cu concentration vary with Cu concentration for both melting conditions. The equilibrium of the redox reactions between Cu^{2+}, Cu^{1+}, the assumed metallic atoms and the oxygen of environment was maybe not achieved during the still 5 hours melting time, or was significantly changed during the cooling and/or annealing. Further investigations are needed to find out the reasons for the behaviour of the ion fractions with increasing Cu concentration.

Interestingly, the presented sets of fitting parameters provided for the glasses doubly doped with Fe and Cu, however, the concentrations of Cu and Fe ions that follow the simple mutual redox theory, as is shown and discussed in the last chapter of the results. Thus the established fitting parameters of both Cu ions might be right. More samples on various Fe/Cu concentration ratios would provide the basis to fit the redox reaction curves accurately. Such data could be

then used to design colours and predict ion concentration in Fe and Cu doped glasses. The data would maybe help to develop Cu ruby glasses reduced by iron and sulphate. Such glasses are desired by tableware industry, who manufacture harmful CdS ruby glasses and who might not want to replace them with expensive Au ruby glasses either.

In addition to the mentioned recommendations the effects of host glass should be studied by re-fitting the data available in this work and fitted during the stage 1 of the Cu analysis. The reasons for the changing of the ion fractions with Cu concentration need to be searched by melting similar glasses as used here and stirring the melts during 4 hours of the melting time, at both reducing and oxidising conditions. The effects of melting temperature, cooling process and annealing should be tested. The mutual redox with iron, sulphate and other colourants should be tested.

Bibliography

1. Adams, R V, 1961, *Infra-Red Absorption due to Water in Glass*, Physics and Chemistry of Glasses, Vol. 2, No. 2, p. 39 - 49.
2. Ades, C, Toganidis, T, Traverse, J P, 1990, *High temperature optical spectra of soda-lime-silica glasses and modelization in view of energetic applications,* Jour. of Non-Cryst. Sol. Vol. 122, p. 272 – 279.
3. Andronenko, S I, Andronenko, R R, Vasil'ev A V and Zagrebel'nyi, O A, 2004, Glass Phys. Chem. Vol. 30, p. 230 -, and the references cited therein.
4. Bach, H, Neuroth, N, 1995, *The Properties of Optical Glass*, Springer-Verlag, Berlin Heidelberg.
5. Bae, B-S and Weinberg, M C, 1994, *Optical Absorption of copper phosphate glasses in the visible spectrum,* Jour. of Non-Cryst. Sol., Vol. 168, p. 223 - 231.
6. Bae, B-S and Weinberg, M C,1991, J. Am. Ceram. Soc., Vol. 74, p. 3039 -.
7. Bamford, C R, 1977, *Colour generation and control in glass*, Elsevier Scientific publ. company, Amsterdam, Netherlands.
8. Bass M, 1995, *Handbook of Optics, Optical Society of America*, 2nd Ed. McGraw-Hill Inc, USA, Vol II.
9. Bates, T, 1962, *Ligand field theory and absorption spectra of transition-metal ions in glasses,* Chap. 5 of *Modern aspects of the vitreous state*, Vol. 2. Ed. by J. D. Mackenzie, Butterworth & Co. Ltd., p. 195 – 254.
10. Baumeister, P, 2002, *Bandpass filters for wavelength division multiplexing WDM,* OFC2002, Short course notes, No: SC126.
11. Beerkens, R C G, 2003, *Amber chromophore formation in sulphur- and iron-containing soda-lime-silica glasses,* Glass Sci. Technol., Vol. 76, No.4. p. 166 – 175.
12. Bingham P A, 2000, *The Environment of Iron in Silicate Glasses*, PhD-Thesis, The Department of Engineering Materials, Sheffield University, UK.
13. Bingham P A, Parker, J M, 2001, *Novel Structural behaviour of iron in alkali-alkaline earth-silica glasses*, Proc. Int. Congr. Glass, Vol. 2., Extended Abstracts, p. 14 – 15.
14. Bingham, P A, Parker, J M, Searle, T, Williams, J M, Smith I, 2002, *Novel structural behaviour of iron in alkali-alkaline-earth-silica glasses*, C.R. Chimie, Vol. 5, p. 787 – 796.
15. Bishay, A M and Makar l, 1969, *Iron in calcium phosphate glasses*, J. of the Am. Ceram. Soc. Vol 52, No. 11, p. 605 -609.

16. Boulos, E N, Glebov L P, Smirnova T V, (1997), *Absorption of iron and water in the Na_2O-CaO-MgO-SiO_2 glasses I. Separation of ferrous and hydroxyl spectra in the near IR region,* Jour. of Non-Cryst. Sol. Vol. 221, p. 213 – 221.
17. Bray, C, 2000, *Ceramic and Glass: a basic technology*, Society of Glass Technology, Sheffield, UK.
18. Bray, C, 2003, *Glass Blowing from the furnace*, Society of Glass Technology, Sheffield, UK
19. Brockman, W et al, *Glass Production – Glass Refinement Processes and Technology*, Ed. II, 2002, VDMA, Messe Dusseldorf GmbH.
20. Burns, R C, 1993, *Mineralogical Applications of Crystal Field Theory*, 2nd Ed., Cambridge University press, UK.
21. Cable, M, Hulme, R, 1985, *Measurement of the Ferrous:ferric ratio in flint glasses and its uses*, Glass Technology, Vol. 26, No 4, p. 170 - 175.
22. Cable, M, Xiang, Z, 1989 a, *Cuprous-Cupric equilibrium in soda-lime-silica glasses melted in air,* Phys. Chem. Glasses, Vol. 30, No. 6, p. 237 – 242.
23. Cable, M, Xiang, Z, 1989 b, *Extinction coefficient of the cupric ion in soda-lime-silica glasses*, Glastech. Ber., Vol. 62, No. 11, p. 382 – 388.
24. Cable, M, Xiang, Z, 1992, *The optical spectra of copper ions in alkali-lime-silica glasses,* Phys. Chem. Glasses, Vol. 33, No. 4, p. 154 - 160.
25. Cable, M, 1996, *Physics and Chemistry of Glass Making, Lecture notes for third year B. Eng., Module 322*, University of Sheffield, Department of Engineering Materials
26. Cable, M, 1996 b, *The Calculation of Glass and Glass Batch Compositions*, 5th ed. Dept. of Eng. Mat., Univ. of Sheffield.
27. Cattaruzza, E, Battaglin, G, Canton P, Sada C, 2005, *Some structural and optical properties of copper and copper oxide nanoparticles in silica films formed by co-deposition of copper and silica*, Jour. of Non-Cryst. Sol. Vol. 351, p. 1932 – 1936.
28. Chandrasekhar, V et al, *Distorted octahedral sites of Cr^{3+} doped sodium phosphate glasses,* Glass Techn., Vol. 43 No.1, 2002.
29. Clark-Monks C, Parker J M, *Stones and Cord in Glass*, 1980, Society of Glass Technology, Sheffield, UK.
30. Corning 1969, Ref. index data
31. Cotton, F A, Wilkinson, G, 1988, *Advanced Inorganic Chemistry*, 5th Ed., John Wiley & Sons, Inc., USA.
32. Doremus, R H, *Glass Science*, 2nd ed. 1994, John Wiley & Sons Inc. New York, USA.

33. Duffy, J A, Ingram, M D, Fong, S, 2000, *Effect of basicity on chemical bonding of metal ions in glass and its relevance to their stability,* Phys. Chem. Chem. Phys., Vol. 2, p. 1829 – 1833.
34. Duffy, J A, Ingram M D, 2002, *Solvent properties of glass melts: resemblance to aqueous solutions,* C. R. Chimie, Vol. 5, 797 - 804.
35. Duffy, J A, 2004 A, *Relationship between optical basicity and thermochemistry of silicates,* J. Phys. Chem. B, Vol. 108, p. 7641 – 7645.
36. Duffy, J A, 2004 B, *Relationship between Cationic Charge, Coordination Number, and polarizability in Oxidic Materials,* J. Phys. Chem. B, Vol. 108, p. 14137 – 14141.
37. Durán, A, 1983, *Influencia de la incorporacion de oxido de cobre en vidrios*, PhD-Thesis, Universidad Autonoma De Madrid, Spain.
38. Durán, A, Fernández Navarro, J M, 1984, *Study of the colouring process in copper ruby glasses by optical and EPR spectroscopy,* Jour. of Mat. Sci., Vol. 19, p. 1468 – 1475.
39. Durán, A, Valle F J, 1985 a, *Analysis of the different states of oxidation of copper in glasses: redox equilibrium,* Glass technology, Vol. 26, No. 4, p. 179 – 185.
40. Durán, A, Fernández Navarro, J M, 1985 b, *The colouring of glass by Cu^{2+} ions*, Phys. Chem. Glasses, Vol. 26, No. 4, p. 126 - 131.
41. Ehrt, D, 2002, *UV-absorption and radiation effects in different glasses doped with iron and tin in the ppm range*, Comptes Rendus Chimie, Vol. 5, Issue 11, P. 679 – 692.
42. Ehrt, D, Leister M, Matthai, A, 2001, *Polyvalent elements iron, tin and titanium in silicate, phosphate and fluoride glasses and melts*, Phys. Chem. Glasses, Vol. 42, No.3, p. 231 – 239.
43. Fanderlik, I, 1983, *Optical properties of glass*, Elsevier Science Publ. Company, Czechoslovakia.
44. Flygt, E et al, *Boken om glas, Glafo*, 2005, Allkopia i Växjö AB.
45. France, P W, 1991, *Optical Fibre Lasers & Amplifiers,* Blackie and Son Ltd, Glasgow, UK.
46. Fuxi, G, 1992, *Optical and spectroscopic properties of glasses*, Springer-Verlag, USA, 1992.
47. Fox, K E, Furukawa, T, White, W B, 1982, *Transition metal ions in silicate melts. Part2. Iron in sodium silicate glasses,* Phys. and Chem. Glasses, Vol. 23, No. 5, p. 169 – 178.
48. Gaskell, P H, 1992, *Structure of a copper sodium phosphate glass by neutron scattering with isotopic substitution,* J Non-Cryst. Solids, Vol. 150, p. 80 - 86.
49. Gaber, M, Harder, U, Hahnert M and Geissler N, 1995, *Water release behaviour of soda-lime-silica glass melts*, Glastech. Ber. Glass Sci Technol. Vol. 68, No. 11, p. 339 -345.

50. Geotti-Bianchini F and De Riu, L, 1995, *Infrared spectroscopic analysis of water incorporated in the structure of industrial soda-lime-silica glasses*, Glastech. Ber. Glass Sci. Technol. Vol. 68, No. 7, p. 228 – 240.
51. Goldman, D S, 1983, *Oxidation Equilibrium of Iron in Borosilicate Glass*, J. Amer. Ceram. Soc., Vol. 66 p. 205 – 209.
52. Gerlach, S, Claussen, O and Russel, C, 1998 a, *Self-diffusion of iron in alkali-magnesia-silica glass melts*, Jour. of Non-Cryst. Sol. Vol. 226, p. 11 – 18.
53. Gerlach, S, Claussen, O and Russel, C, 1998 b, *Thermodynamics of iron in alkali-magnesia-silica glasses*, J. of Non-Cryst. Sol., Vol. 238, p. 75 - 82.
54. Glebov, L B, Boulos E N, 2002, *Absorption of iron and water in the Na_2O-CaO-MgO-SiO_2 glasses. II. Selection of intrinsic, ferric, and ferrous spectra in the visible and UV regions,* Jour. of Non-Cryst. Sol., Vol. 242, p. 49 – 62.
55. Hannoyer, B, Lenglet, M, Durr, J, Cortes, R, 1992, *Spectroscopic evidence of octahedral iron (III) in soda-lime-silicate glasses*, Non-Cryst. Sol., Vol. 151 p. 209 – 216.
56. Halcrow, M A, 2003 a, *Interpreting and controlling the structures of six-coordinate copper (II) centres – When is a compression really a compression?*, Dalton Trans., p. 4375 – 4384.
57. Halcrow, M A, 2003 b, Dalton Trans., p. 4463 -, at website: www.rsc.org/dalton
58. Hecht E, *Optics*, International 4th Ed., Addison Wesley, 2002.
59. Hunt, R W G, 1987, *Measuring Colour*, Ellis Horwood Limited, Chichester, England.
60. Izawa T and Sudo S, 1987, *Optical Materials: Materials and fabrication*, KTK Scientific Publiches, Tokyo,.
61. Johnston, W, D, 1964, *Oxidation-reduction equilibria in iron-containing glass*, Jour. Amer. Ceram. Soc., Vol 4, p.198 - 204.
62. Judd, D B, Wyszecki, G, 1975, *Color in Business Science and Industry*, 3rd ed, Wiley, New York.
63. Karlsson, K, 1969, Glasteknisk Tidskrift, Vol. 24, No. 13.
64. Kido L, Muller M, Russel, C, 2004, *Redox reactions occuring during temperature change in soda-lime-silicate melts doped with copper and antimony or copper and tin,* Phys. Chem. Glasses, Vol. 45, No.1, p. 21 – 26.
65. Kivelson D and Neiman, R, 1961, *J. Chem. Phys.* Vol. *35*, p. 145-.
66. Klein, M V and Furtak, T E, *Optics,* 2nd Ed. John Wiley et Sons Inc. 1986, p. 71.
67. Kukkadapu, R K, Li, H, Smith, G L, Crum, j D, Jeoung, J-S, Poisl, W H, Weinberg, M C, 2003, *Mössbauer and optical spectroscopic study of temperature and redox effects on*

iron local environments in a Fe-doped (0.5 mol % Fe_2O_3) 18Na_2O-72SiO_2 glass, Jour. Non-Cryst. Sol., Vol. 317, p. 301 – 318.

68. Kurkjian C R and Sigety E A, 1968, *Co-Ordination of Fe^{3+} in glass*, Phys. and Chem. of Glasses, Vol. 9, No. 3, p. 73 – 83.
69. Lever, A B P, 1968, *Inorganic Electronic Spectroscopy,* Elsevier Publishing Company, Amsterdam, The Netherlands.
70. Levy, R A, Lupis, C H P, Flinn, P A, 1976, *Mössbauer analysis of the valence and coordination of iron cations in $SiO_2 - Na_2O - CaO$ glasses*, Phys. and Chem. of Glass., Vol. 17, No. 4, p. 94 – 103.
71. Manikandan, D, Mohan S, Nair, K G M, 2003, *Photoluminescence of embedded copper nanoclusters in soda-lime glass,* Materials Letters, Vol. 57, p. 1391 – 1394.
72. McKenzie, H W & Hand, R J, 1999, *Basic Optical Stress Measurements in Glass*, Society of Glass Technology, Sheffield, UK.
73. Mekki, A, Holland D and McConville, 1997, C F, *X-ray photoelectron Spectroscopy study of copper sodium silicate glass surfaces*, Jour. of Non-Crystalline Solids, Vol. 215, p. 271 – 282.
74. Muller-Simon, H, 1994, *On the interaction between oxygen, iron and sulfurin industrial glass melts*, Glastech. Ber. Glass Sci. Technol., Vol. 67, No. 11, p. 297 – 303.
75. Muller-Simon, H, 1996, *Electron exchange reactions between polyvalent elements in soda-lime-silica and sodium borate glasses*, Glastech. Ber. Glass Sci. Technol., Vol. 69, No. 12, p. 387 – 395.
76. Musikant, S, *Optical materials*, Marcel Dekker, Inc. New York, 1986.
77. Lever, A B P, 1968, *Inorganic Electronic Spectroscopy*, Elsevier Publishing Company, Amsterdam NL.
78. Navarra, G, 2005, *OH-related infrared absorption bands in oxide glasses*, J. of Non-Cryst. Sol., Vol. 351, p. 1796 – 1800.
79. Parkash, P G, Rao, J L, 2004, *Cu^{2+} ions in sodium fluoride-sodium borate glasses studied by EPR and optical absorption technigues,* Jour. of Mat. Sci., Vol. 39, p. 193 – 200.
80. Parker, J M, 2004, *Inorganic glasses and their interactions with light*, Rev. Prog. Color., Vol. 34, p. 26 - 38.
81. Paul, A, 1982, *Chemistry of glasses*, 2nd Ed. Chapman and Hall, London.
82. Rao, C N R, Raveau, B, 1995, *Transition Metal Oxides*, VCH Publishers, Inc, New York USA.
83. Rawson, H, 1991, *Glasses and Their Applications*, The Institute of Metals, Brookfield, USA.

84. *Refractories in the Glass Industry*, SGT Refractories Committee, Society of Glass Technology, Sheffield, UK.
85. Reynolds, R W, et al 1974, ????, Phys. Rev. B, Vol. 10, p. 3802-.
86. Schirmer, H, et al, 2003, *High-temperature spectroscopic study of redox reactions in iron-and arsenic-doped melts*, Glass Sci. Technol. Vol. 76, No.2, 49 – 55.
87. Scholze, H, 1991, *Glass, Nature, Structure and Properties*, Translated by Lakin, M J, Springer-Verlag, New York Inc.
88. Simmingsköld, B, *Raw Materials for Glass Melting*, Edited by K.H. Teisen and R.D. Wright, 1997, Society of Glass Technology, Sheffield, UK
89. Sudo, S, 1999, *Optical amplifiers: materials, devices and applications*, Artec House Inc. New York.
90. *The Science of Color, 1973,* published by Committee of Colorimetry of The Optical Society of America, Edwards Brothers Inc, Ann Arbor, Michigan, USA.
91. Traverse, J-P, Toganidis, T, Adés C, 1992, *Spectrophotometric analysis of ferrous, ferric and total iron content in soda-lime-silica glass,* Glastech. Ber. Vol. 65. No. 8, p. 201 - 205.
92. Trier, W, *Glass Furnaces Design Construction and Operation*, Translated by K.L. Loewenstein, 2000, Society of Glass Technology, Sheffield, UK
93. Turpin 1965, Corning 1969
94. Varshneya, A K, *Fundamentals of Inorganic Glasses*, 1994, Academic Press, San Diego.
95. Vogel, E, private discussion at Bellcore, Morristown, New Jersey.
96. Vogel, W, 1994, *Glass Chemistry*, 2nd English Ed. Springer-Verlag, Berlin Heidelberg.
97. Volotinen, T T and Parker, J M, 2004 a, *Absorption spectrum addition of transition metal pairs in silicate glasses*, presented at The New Researchers Forum at The SGT conference in Liverpool, U.K.
98. Volotinen, T T, Parker, J M, 2004 b, *Analysis of absorption peak widths of Cu^{2+}-ions in silicate glasses,* Presentation at XX ICG in Tokyo, Sept. 2004. (= ANNEX 10 of this thesis).
99. Volotinen, T T, Klement, R and Parker, J M, 2005 a, *The Coordination Environment of Cu2+ –Ions in Silicate Glasses, Studied by Optical Absorption and EPR Spectroscopy: An Effect of Composition on Spectral Parameters and Structure*, a poster presentation at Slovakian Glass Society conference in Herlany, June 2005.
100. Volotinen, T T, Parker, J M, Wilkinson, A P and Hollis, D, 2005 b, *Accurate background loss correction for optical absorption spectroscopy of coloured silicate glasses*, a presentation at SGT conference Glass: Past, Present and Future, Sheffield, U.K..

101. Volotinen, T T, Parker,J M, Bingham,P A, Wilkinson A P and Kirk, N, 2006, *Computer modelling of optical absorption spectra*, a conference presentation at ESG2006/Glass: The Art of Science, Sunderland, U.K.

102. Weast R C, 1987, *Handbook of Chemistry and Physics*, 67th Edition, CRC Press, Inc. Boca Raton, Florida.

103. Wells, A, F, 1984, *Structural Inorganic Chemistry*, 5th Ed., Oxford, UK.

104. West, A, R, 2004, *Basic Solid State Chemistry*, 2nd Ed., John Wiley & Sons , LTD, Wiltshire, Great Britain.

105. West, M, 2001, *A quality system for the production and determination of the elemental composition of two coloured soda-lime-silica glass reference materials,* Glass Techn. Vol. 42, No 415, p. 109 - 112 and website: www.uniquant.com.

106. Weyl, W A, 1951, reprinted 1999, *Coloured Glasses*, The Society of Glass Technology, Sheffield, UK.

107. Wolfe, W L and Zissis, G J, *The Infrared Handbook*, Environmental Research Institute of Michigan, Ann Arbor Mi, 1978.

108. Wong J and Angell, C A, 1976, *Glass Structure by Spectroscopy*, Marcel Dekker, Inc. New York, USA.

109. Xiang, Z, 1988, *Oxidation-reduction equilibrium of copper in silicate glasses*, PhD-Thesis, University of Sheffield, UK.

110. Zarzycki J, 1982, *Glasses and the vitreous state*, Cambridge Solid State Science Series, UK.

111. Zawada, A; Hessenkemper, H; Höhne, D and Bieniarz, P, 2005, *Influence of redox equilibrium on the properties of glasses with a high iron concentration,* Glass Sci. Technol. Vol. 78, No. 3, p. 106 – 110.

112. Zhang J C, Moine, B, Pedrini, C, Parent C, Flem, G, 1990, *Optical spectroscopy of monovalent copper-doped borate glasses,* J. Phys. Chem. Solids, Vol. 51, No. 8, p. 933 – 939.

113. Zhou, Z, Navrotsky, A, McClure, D S, 1993, *Oxidation states of copper in lead borate glass,* Phys. Chem. Glasses, Vol. 34, No. 6, p. 251 – 254.

ANNEX 1

Information of the prepared glass samples

The following codes are used in the following tables to describe the glass composition, melting conditions and annealing process. These compositions are calculated from the batch. The received final glass compositions differ slightly due to dissolution of contaminants from mullite crucibles used for melting in gas-fired furnaces and due to evaporation during melting of the volatile components, such as soda, boric oxide, potash and zinc oxide. See Chap. 2.1 and 2.2.

Codes used for the glass composition:

- N = soda (natria), Na_2O
- C = lime (calcia), CaO
- S = silica, SiO_2
- M = magnesia, MgO
- A = aluminium oxide, Al_2O_3
- K = potash (kalia), K_2O
- B = boric oxide, B_2O_3
- Ba = baria, BaO
- Li = lithia, Li_2O
- P = phosphorus pentoxide, P_2O_5
- Zn = zinc oxide, ZnO
- Pb = lead oxide, PbO
- cle = the batch is made of ultra pure ingredients
- Ox = An oxidation agent, $NaNO_3$, was added
- Red = A reducing agent, carbon, was added

Melting conditions:

- G = gas furnace, 1450 °C, melting time 5 h;
- Es = electric furnace, stirred, 1450 °C, melting time 5 h;
- Ew = electric furnace, cast to frit into deionised water at 3 h melting at 1450 °C then re-melted for 2 h
- Gw = gas furnace, cast to frit into deionised water at 3 h melting at 1450 °C then re-melted for 2 h

Annealing process:

- An = normal annealing conditions, 540 °C 1 h and cooling with 1 °C/min down to 25 °C

Table A1 Composition of the trial test samples, calculated from the batch composition

No	Type of glass, melting / annealing	Colorant/ mol %	Silica mol %	Na_2O mol %	CaO mol %	K_2O mol %	MgO mol %	Al_2O_3 mol %	Refiner Na_2SO_4 mol %	Red/oxid. agent/ mol %
ttv1	NCSKMA /G/An	-	71.64	13.01	11.68	0.25	2.22	1.17	0.69	-
ttv2	NCSKMA /G/An	Cr_2O_3/ 0.039	71.64	13.01	11.68	0.25	2.22	1.17	0.69	-
ttv3	NCSKMA /G/An	Cr_2O_3/ 0.020	71.65	13.01	11.68	0.25	2.22	1.17	0.69	-
ttv4	NCSKMA /G/An	Fe_3O_4/ 0.026	71.65	13.01	11.68	0.25	2.22	1.17	0.69	-
ttv5	NCSKMA /G/An	Fe_3O_4/ 0.013	71.66	13.01	11.68	0.25	2.22	1.17	0.69	-
ttv6	NLSKMA /G/An	Fe_3O_4/ 0.023	65.16	11.83	10.62	0.23	2.01	1.06	0.63	Carbon 9.06
ttv7	NCSKMA /G/An	Fe_3O_4/ 0.026	71.82	13.13	11.71	0.25	2.22	1.17	0.69	$NaNO_3$ 0.51

Table A2 Glass composition of the ordinary test samples, calculated from the batch composition

No	Host glass/ melting/ annealing	Colorant/ mol %	Silica, mol %	Na_2O, mol %	CaO, mol %	Other/ mol %	Refiner Na_2SO_4 mol %	Red/oxid. agent/ mol %
1	NCS/G/An	-	69.57	14.45	15.97	-	0.72	-
2	NCS/G/An	Fe_3O_4/0.08	69.52	14.94	15.96	-	0.72	-
3	NCS/G/An	Fe_3O_4/1.02	68.86	14.31	15.81	-	0.72	-
4	NCS/G/An	Fe_3O_4/1.10	68.81	14.30	15.80	-	0.72	-
5	NCS/G/An	NiO/0.48	69.24	14.38	15.90	-	0.72	-
6	NCS/G/An	Fe_3O_4/0.21	69.43	14.41	15.94	-	0.72	-
7	NCS/G/An	NiO/0.95	68.91	14.32	15.82	-	0.72	-
8	NCS/G/An	NiO/0.48 Fe_2O_3/0.30	68.91	14.31	15.82	-	0.72	-
9	NCS/G/An	-	71.00	15.00	14.00	-	0.45	-
10	NCS/G/An	Cr_2O_3/0.30	70.79	14.95	13.96	-	0.45	-
11	KCS/G/An	-	70.93	0.55	13.99	K_2O/14.54	0.55	-
12	KCS/G/An	Cr_2O_3/0.30	70.72	0.55	13.94	K_2O/14.49	0.55	-
13	NMS/G/An	-	71.00	15.00	-	MgO/14.00	0.45	-
14	NMS/G/An	Cr_2O_3/0.30	70.79	14.95	-	MgO/13.96	0.45	-
15	NCSB/G/An	-	64.33	15.63	14.77	B_2O_3/5.27	0.37	-
16	NCSB/G/An	Cr_2O_3/0.31	64.13	15.58	14.72	B_2O_3/5.26	0.37	-
17	NCSA/G/An	-	61.00	15.00	14.00	Al_2O_3/10.00	0.35	-
18	NCSA/G/An	Cr_2O_3/0.30	60.82	14.96	13.96	Al_2O_3/9.97	0.35	-
19	NCSP/G---	--	65.36	14.28	15.00	P_2O_5/5.36	0.37	lost in f.
20	NCSP/G/An	Cr_2O_3/0.28	65.18	14.24	14.96	P_2O_5/5.34	0.37	lost in f.
21	NCS/G/An	NiO/0.59	70.58	14.91	13.92	-	0.45	-
22	KCS/G/An	NiO/0.55	70.54	0.55	13.91	K_2O/14.46	0.55	-
23	NMS/G/An	NiO/0.66	76.09	16.07	-	MgO/7.17	0.48	-
24	NCSB/G/An	NiO/0.62	63.93	15.53	14.67	B_2O_3/5.24	0.37	-
25	NCSA/G/An	NiO/0.59	60.64	14.91	13.92	Al_2O_3/9.94	0.35	-
26	NCS/G/An	-	70.00	15.00	15.00	-	0.45	-
27	NCS/G/An	CuO/0.50	69.65	14.93	14.93	-	0.45	-
28	NCS/G/An	CuO/0.99	69.31	14.85	14.85	-	0.45	-
29	NCS/G/An	CuO1.48	68.96	14.78	14.78	-	0.44	-
30	NCS/G/An	CoO/0.17	69.88	14.98	14.98	-	0.45	-
31	NCS/G/An	CoO/0.33	69.77	14.95	14.95	-	0.45	-
32	NCS/G/An	CoO/0.50	69.65	14.93	14.93	-	0.45	-
33	NCS/Es/An	---	70.00	15.00	15.00	-	0.45	-
34	NCS/Es/An	NiO/0.74	69.48	14.89	14.89	-	0.45	-

No	Host glass/ melting/ annealing	Colorant/ mol %	Silica, mol %	Na_2O, mol %	CaO, mol %	Other/ mol %	Refiner Na_2SO_4 mol %	Red/oxid. agent/ mol %
35	NCS/Ew/An	CuO/0.99	69.31	14.85	14.85	-	0.35	-
36	NCS/Ew/An	CoO/0.99	69.31	14.85	14.85	-	0.35	-
37	NCS/Ew/An	CoO/0.33	69.77	14.95	14.95	-	0.35	-
38	NCS/Ew/An	Cr_2O_3/0.11	69.86	14.87	14.97	-	0.35	-
39	NCS/Ew/An	CoO/0.10	69.93	14.99	14.99	-	0.35	-
40	NCS/Ew/An	Cr_2O_3/0.99	69.31	14.85	14.85	-	0.35	-
41	NCS/Ew/An	---	70.00	15.00	15.00	-	0.35	-
42	KCS/Ew/An	Cr_2O_3/0.50	69.65	0.35	14.93	K_2O/ 14.58	0.35	-
43	NMS/Ew/An	Cr_2O_3/0.30	70.49	15.11	-	MgO/ 14.10	0.35	lost in f.
44	NCS/Ew/An	CuO/0.50	69.65	14.93	14.93	-	0.35	-
45	NCS/G/An	V_2O_5/0.50	69.65	14.93	14.93	-	0.35	-
46	NCS/G/An	V_2O_5/0.99	69.31	14.85	14.85	-	0.35	-
47	NCS/G/An	MnO_2/0.50	69.65	14.93	14.93	-	0.35	-
48	NCS/G/An	MnO_2/0.99	69.31	14.85	14.85	-	0.35	-
49	NCS/G/An	V_2O_5/0.94	69.96	14.13	14.13	-	0.35	C, Red./ 4.83
50	NCS/G/An	V_2O_5/0.99	69.48	14.89	14.59	-	0.35	$NaNO_3$ Ox./ 0.50
51	NCS/G/An	MnO_2/0.98	69.06	14.56	14.80	-	0.35	$NaNO_3$ Ox./ 0.49
52	NCS/Ew/An	MnO_2/0.99	69.31	14.85	14.85	-	0.35	-
53	NCS/Ew/An	MnO_2/0.50	69.65	14.93	14.93	-	0.35	-
54	NCS/Ew/An	V_2O_5/0.99	69.31	14.85	14.85	-	0.35	-
55	NCS/Ew/An	V_2O_5/0.50	69.65	14.93	14.93	-	0.35	-
56	NCS/Ew/An	CuO/0.50 CoO/0.10	69.58	14.91	14.91	-	0.35	-
57	NCS/Ew/An	CuO/0.49 NiO/0.74	69.14	14.81	14.81	-	0.35	-
58	NCS/Ew/An	CoO/0.10 NiO/0.74	69.41	14.87	14.87	-	0.35	-
59	BaCS/G/An	CuO/0.99	69.31	0.35	14.85	BaO/ 14.51	0.35	-
60	KCS/G/An	CuO/0.99	69.31	0.35	14.85	K_2O/ 14.50	0.35	-
61	NCSA/G/An	CuO/0.99	64.36	14.85	14.85	Al_2O_3/ 4.95	0.35	-
62	NCSB/G/An	CuO/0.99	59.41	14.85	14.85	B_2O_3/ 9.90	0.35	lost in f.
63	NCSLi/G/An	CuO/1.05	68.06	7.33	15.71	Li_2O/ 7.85	0.35	-
64	NBaS/G/An	CuO/0.99	69.31	14.85	-	BaO/ 14.85	0.35	-

No	Host glass/ melting/ annealing	Colorant/ mol %	Silica, mol %	Na_2O, mol %	CaO, mol %	Other/ mol %	Refiner Na_2SO_4 mol %	Red/oxid. agent/ mol %
65	KACS/G/An	CuO/0.99	64.36	0.35	14.85	Al_2O_3/ 4.95 K_2O/ 14.50	0.35	-
66	NCS/Ew/An	V_2O_5/0.50 NiO/0.50	69.31	14.85	14.85	-	0.35	-
67	NCS/Ew/An	V_2O_5/0.50 CoO/0.10	69.58	14.91	14.91	-	0.35	-
68	NCS/Ew/An	Cr_2O_3/0.30 CuO/0.99	69.10	14.81	14.81	-	0.35	-
69	NCS/Ew/An	Cr_2O_3/0.30 NiO/0.74	69.27	14.84	14.84	-	0.35	-
70	NCS/Ew/An	Cr_2O_3/0.30 CoO/0.10	69.72	14.94	14.94	-	0.35	-
71	NCS/Ew/An	NiO/0.74 Fe_2O_3/0.30	69.27	14.84	14.84	-	0.35	-
72	NCS/Ew/An	Cr_2O_3/0.30 Fe_2O_3/0.50	69.44	14.88	14.88	-	0.35	-
73	NCS/Ew/An	CuO/1.48	68.97	14.78	14.78	-	0.34	-
74	NCS/Ew/An	CuO/0.98 Fe_2O_3/0.49	68.97	14.78	14.78	-	0.34	-
75	NCS/Ew/An	CuO/0.25	69.83	14.96	14.96	-	0.35	-
76	NCS/Ew/An	CuO/0.98 MnO_2/0.98	68.63	14.71	14.71	-	0.34	-
77	NCSB/G/An	CuO/0.99	64.36	14.85	14.85	B_2O_3/4.95	0.35	-
78	NCS/G/An	CuO/0.99	69.46	14.66	14.88	-	0.35	$NaNO_3$/0.45
79	NCS/G/An	CuO/0.99	69.17	14.53	14.82	-	0.35	C/ 0.49
80	NCS/G/An	CuO/0.20	69.86	14.97	14.97	-	0.35	-
81	NCS/G/An	Fe_2O_3/0.50	69.65	14.93	14.92	-	0.35	-
82	NCS/G/An	Fe_2O_3/0.25	69.83	14.96	14.96	-	0.35	-
83	NCS/G/An	Fe_2O_3/ 0.74	69.48	14.89	14.89	-	0.35	-
84	NCS/Ew/An	CuO/ 0.99 V_2O_5/ 0.49	68.97	14.78	14.78	-	0.35	-
85	NCS/Ew/An	V_2O_5/ 0.5 Cr_2O_3/ 0.3	69.44	14.88	14.88	-	0.35	
86	NCS/Ew/An	MnO_2/ 1.0 Cr_2O_3/ 0.3	69.10	14.81	14.81	-	0.35	

No	Host glass/ melting/ annealing	Colorant/ mol %	Silica, mol %	Na_2O, mol %	CaO, mol %	Other/ mol %	Refiner Na_2SO_4 mol %	Red/oxid. agent/ mol %
87	NCS/Ew/An	Fe_2O_3/ 0.50 CoO/ 0.033	69.27	14.84	14.84	-	0.35	
88	BaCS/G/An	CuO/ 1.00	69.76	0.35	14.95	BaO/13.95	0.35	
89	NCSLi/G/An	CuO/ 0.20	69.83	7.53	14.96	Li_2O/7.48	0.35	
90	NKCSA/G/An	CuO/ 0.99	64.13	5.28	14.80	K_2O/ 9.87 Al_2O_3/ 4.93	0.35	
91	MCS/G/An	CuO/ 0.20	69.82	0.35	14.81	MgO/ 14.81	0.35	Lost in f.
92	MCS/G/An	CuO/ 1.00	69.68	0.35	14.56	MgO/ 14.42	0.35	Lost in f.
93	MCS/G/An	CuO/ 1.00	69.49	-	14.58	MgO/ 14.58	0.35	Sn/0.33,lost
94	NCS/G/An	CuO/ 0.50	69.91	14.93	14.93	-	0.35	
95	NCSLi/Ew/An	CuO/ 0.99	69.14	7.46	14.82	Li_2O/ 7.60	0.35	
96	NCSLi/Ew/An	CuO/ 0.20	69.83	7.53	14.96	Li_2O/ 7.48	0.35	
97	NCS/G/An	-	70.00	15.00	15.00	-	0.35	
98	BaCS/G/An	-	70.46	0.35	15.10	BaO/14.09	0.35	
99	NCSLi/G/An	-	69.96	7.55	14.99	Li_2O/7.50	0.35	
100	NKCSA/G/An	-	64.77	5.33	14.95	K_2O/9.96 Al_2O_3/ 4.99	0.35	
101	NCSB/G/An	-	65.00	15.00	15.00	B_2O_3/5.00	0.35	
102	PCS	-	70.00	0.35	15.00	K_2O/14.65	0.35	
103	NCS/G/An big	CuO/ 0.20	69.86	14.97	14.97	-	0.35	-
104	NCS/G/An big	Cr_2O_3/ 0.15	69.90	14.98	14.98	-	0.35	-
105	NCMS/G/An	CuO/ 0.53	68.73	10.94	9.90	MgO/9.90	0.37	-
106	KCSM/G/An	CuO/ 0.53	68.73	0.37	9.90	MgO/9.90 K_2O/10.57	0.37	-
107	NCSA/G/An	-	61.90	14.29	14.29	Al_2O_3/9.52	0.33	-
108	KCSA/G/An	-	61.90	0.33	14.29	K_2O/13.95 Al_2O_3/9.52	0.33	-
109	NBaS/G/An	-	70.00	15.00	-	BaO/15.00	0.35	-
110	NCMS/G/An	-	68.95	10.98	9.93	MgO/9.93	0.37	-
111	NCMS/G/An	CuO/1.05	68.37	10.89	9.85	MgO/9.85	0.37	-
112	NCMB/G/An	CuO/1.05	68.36	0.37	9.85	MgO/9.85 B_2O_3/10.52	0.37	Lost in furnace
113	KCMS/G/An	-	69.09	0.37	9.95	MgO/9.95 K_2O/10.63	0.37	-
114	NCSLi/Ew/An	-	69.97	7.55	14.99	Li_2O/7.50	0.35	-

No	Host glass/ melting/ annealing	Colorant/ mol %	Silica, mol %	Na_2O, mol %	CaO, mol %	Other/ mol %	Refiner Na_2SO_4 mol %	Red/oxid. agent/ mol %
115	NCS/Ew/An	MnO_2/0.99 Fe_2O_3/0.49	68.97	14.78	14.78	-	0.34	-
116	NCS/Ew/An	V_2O_5/0.49 Fe_2O_5/0.50	69.31	14.85	14.85	-	0.35	-
117	NCS/Ew/An	V_2O_5/0.49 MnO_2/0.99	68.95	14.78	14.78	-	0.34	-
118	NCS/Ew/An	MnO_2/0.99 CoO/0.033	69.28	14.85	14.85	-	0.35	-
119	NCS/Ew/An	MnO_2/0.99 NiO/0.49	68.97	14.78	14.78	-	0.34	-
120	NCS/G/An	TiO_2/0.50	69.65	14.93	14.93	-	0.35	-
121	NCS/G/An	TiO_2/0.99	69.31	14.85	14.85	-	0.35	-
122	NCS/G/An	TiO_2/1.48	68.97	14.78	14.78	-	0.35	-
123	NCS/G/An	TiO_2/0.99	69.48	14.64	14.89	-	0.35	$NaNO_3$/0.50
124	NCS/G/An	TiO_2/0.99	68.87	14.78	14.78	-	0.35	C/0.49
125	NCS/G/An	MnO_2/0.98	68.63	14.71	14.71	-	0.34	C/0.98
126	NCS/G/An	V_2O_5/0.49	68.97	14.78	14.78	-	0.34	C/0.99
127	NCS/G/An	MnO_2/0.98	68.63	14.71	14.71	-	0.34	C/0.98
128	NCS/G/An	Cr_2O_3/0.30	69.37	14.87	14.87	-	0.35	C/0.60
129	NCS/G/An	NiO/0.73	68.98	14.78	14.78	-	0.34	C/0.73, lost
130	NCS/G/An	Fe_2O_3/0.50	69.31	14.85	14.85	-	0.35	C/0.49
131	NCS/G/An	CuO/0.98	68.63	14.71	14.71	-	0.34	C/0.98, lost
132	NCS/G/An	CoO/0.033	69.77	14.95	14.95	-	0.35	C/0.30
133	NCS/Ew/An	MnO_2/0.98 NiO/0.73	68.80	14.74	14.74	-	0.34	-
134	NCS/Ew/An	MnO_2/0.81 NiO/0.61	69.01	14.79	14.79	-	0.35	-
135	NCS/Ew/An	MnO_2/0.82 Cr_2O_3/0.25	68.97	15.00	14.96	-	0.35	-
136	NCS/Ew/An	Fe_2O_3/0.25 NiO/0.61	69.40	14.87	14.87	-	0.35	-
137	NCS/G/An	V_2O_5/0.50	70.00	14.50	15.00	-	0.35	$NaNO_3$/0.99

No	Host glass/ melting/ annealing	Colorant/ mol %	Silica, mol %	Na_2O, mol %	CaO, mol %	Other/ mol %	Refiner Na_2SO_4 mol %	Red/oxid. agent/ mol %
138	NCS/G/An	MnO_2/0.99	69.65	14.43	14.93	-	0.35	$NaNO_3$/0.99
139	NCS/G/An	Cr_2O_3/0.30	70.00	14.70	15.00	-	0.35	$NaNO_3$/0.60
140	NCS/G/An	NiO/0.73	69.74	14.58	14.94	-	0.35	$NaNO_3$/0.73
141	NCS/G/An	Fe_2O_3/0.50	70.00	14.50	15.00	-	0.35	$NaNO_3$/1.00
142	NCS/G/An	CuO/0.98	69.65	14.43	14.93	-	0.35	$NaNO_3$/0.99
143	NCS/G/An	CoO/0.066	70.16	14.73	15.04	-	0.35	$NaNO_3$/0.60
144	NCS/Es/An	Er_2O_3/0.33	69.77	14.95	14.95	-	0.35	-
145	NCS/Ew/An	Fe_2O_3/0.50	69.65	14.92	14.92	-	0.35	-
146	NCS/Ew/An	NiO/0.50	69.65	14.93	14.93	-	0.35	-
147	NCS/Ew/An	Cr_2O_3/0.05	69.96	14.99	14.99	-	0.35	-
148	NCS/Ew/An	Cr_2O_3/0.15 CuO/0,49	69.13	14.81	15.41	-	0.35	-
149	NCS/Ew/An	Fe_2O_3/0.50 Cr_2O_3/0.30	69.44	14.88	14.88	-	0.35	-
150	NCS/Ew/An	Fe_2O_3/0.50 CoO/0.033	69.63	14.92	14.92	-	0.35	-
151	NCS/Ew/An	MnO_2/0.50 Cr_2O_3/0.15	69.52	14.92	14.92	-	0.35	-
152	NCS/Es/An	Er_2O_3/0.5	69.65	14.92	14.93	-	0.35	-
153	NCS/Es/An	Ce_2O_3/0.47	69.63	14.92	14.95	-	0.35	-
154	NCS/Es/An	Sm_2O_3/0.36	69.73	14.95	14.97	-	0.35	-
155	NCS/Es/An	Ho_2O_3/0.50	69.65	14.93	14.93	-	0.35	-
156	NCS/Es/An	TlO_2/0.81	69.63	14.92	14.92	-	0.35	-
157	NCS/Es/An	Nd_2O_3/0.50	69.65	14.93	14.93	-	0.35	-
158	NCS/Es/An	Pr_2O_3/0.50	69.65	14.93	14.93	-	0.35	-
159	NCS/Es/An	Eu_2O_3/0.56	69.80	14.96	14.98	-	0.35	-
160	NCS/Es/An	Tb_2O_3/0.50	69.65	14.92	14.93	-	0.35	-
161	NCS/Es/An	Dy_2O_3/0.50	69.65	14.93	14.93	-	0.35	-
162	NCS/ES/An	Nd_2O_3/0.50 Pr_2O_3/0.50	69.31	14.85	14.85	-	0.35	-

No	Host glass/ melting/ annealing	Colorant/ mol %	Silica, mol %	Na_2O, mol %	CaO, mol %	Other/ mol %	Refiner Na_2SO_4 mol %	Red/oxid. agent/ mol %
163	NCS/Ew/An	Nd_2O_3/0.50 TiO_2/2.10	68.19	14.61	14.61	-	0.35	-
164	NCS/Es/An	Ce_2O_3/0.49 TiO_2/0.99	68.97	14.78	14.78	-	0.35	-
165	NCS/G/An	TiO_2/0.99 V_2O_5/0.50	69.38	14.27	14.87	-	0.35	-
166	NCS/G/An	TiO_2/0.99 MnO_2/0.99	69.03	14.20	14.79	-	0.35	-
167	NCS/G/An	TiO_2/0.99 Cr_2O_3/0.50	69.38	14.27	14.87	-	0.35	-
168	NCS/G/An	TiO_2/0.99 Fe_2O_3/0.50	69.51	14.11	14.89	-	0.35	-
169	NCS/G/An	TiO_2/1.0 CoO/0.022	69.71	14.34	14.94	-	0.35	-
170	NCS/G/An	TiO_2/0.99 NiO/0.50	69.38	14.27	14.87	-	0.35	-
171	NCS/G/An	TiO_2/0.99 CuO/0.99	69.03	14.20	14.79	-	0.35	-
172	NCS/G/An	CeO_2/0.99 V_2O_5/0.49	68.97	14.78	14.78	-	0.35	
173	NCS/G/An	CeO_2/0.98 MnO_2/0.98	68.63	14.71	14.71	-	0.35	-
174	NCS/G/An	CeO_2/0.99 Cr_2O_3/0.49	68.96	14.78	14.78	-	0.35	-
175	NCS/G/An	CeO_2/0.98 Fe_2O_3/0.49	68.97	14.78	14.78	-	0.35	-
176	NCS/G/An	CeO_2/0.99 CoO/0.033	69.28	14.85	14.85	-	0.35	-
177	NCS/G/An	CeO_2/0.97 NiO/0.97	67.91	14.55	14.55	-	0.35	OBs Too much NiO.
178	NCS/G/An	CeO_2/0.98 CuO/0.98	68.63	14.71	14.71	-	0.35	-
179	NCSLi/G/An	CuO/0.20	69.86	7.49	14.97	Li_2O/7.48	0.35	-

No	Host glass/ melting/ annealing	Colorant/ mol %	Silica, mol %	Na_2O, mol %	CaO, mol %	Other/ mol %	Refiner Na_2SO_4 mol %	Red/oxid. agent/ mol %
180	NCSOx/G/An	-base-	69.65	15.44	14.92	-	0.35	$NaNO_3$/0.99 contamin.
181	NCSRed/G/An	-base-	69.31	14.85	14.85	-	0.35	Carbon/0.99
182	NCSLi/G/An	CuO/0.50	69.65	7.46	14.93	Li_2O/7.46	0.35	-
183	NCS/G/An	MnO_2/0.99 Fe_2O_3/0.49	68.97	14.78	14.78	-	0.35	-
184	NCS/G/An	MnO_2/0.99 Cr_2O_3/0.30	69.10	14.81	14.81	-	0.35	-
185	NCS/G/An	MnO_2/0.98 CuO/0.98	68.63	14.71	14.71	-	0.35	-
186	NCSOx/G/An	-base-	69.30	15.84	14.85	-	0.35	$NaNO_3$/0.99 too much Na
187	NCS/G/An	NiO/0.49 CeO_2/1.09	68.89	14.77	14.76	-	0.35	-
188	NCScle/Es/An	-base-	70.00	15.00	15.00	-	0.35	Cu-cont.
189	NCScle/Es/An	CuO/0.50	69.67	14.91	14.91	-	0.35	-
190	NCScle/Es/An	MnO_2/0.99 Cr_2O_3/0.33	69.77	14.95	14.95	-	0.35	-
191	NCScle/Es/An	Cr_2O_3/0.33	69.77	14.95	14.95	-	0.35	-
192	NCScle/Es/An	MnO_2/0.99	69.31	14.85	14.85	-	0.35	-
193	NCScle/Es/An	Fe_2O_3/0.49	68.86	14.76	14.76	-	0.35	-
194	NCSCle/EH/An	-	70.00	15.00	15.00	-	0.35	-
195	NCScle/Ew/An	-	70.00	15.00	15.00	-	0.35	Cu-cont.-
196	NCScle/Es/An	-	70.00	15.00	15.00	-	0.35	purest
197S	NCScle/Es/An	CuO/0.10	69.93	14.99	14.98	-	0.35	-
197O		CuO/0.004						
198	NCS/Ew/An	CeO_2/0.99	69.65	14.93	14.93	-	0.35	-
199	NCS/Ew/An	CeO_2/0.98 CuO/0.99	68.97	14.78	14.78	-	0.34	-
200	NCSOx/G/An	base	70.00	15.00	15.00	-	0.35	$NaNO_3$/1.00
201	NCSCl/Ew/An	Clear Ew base	70.00	15.00	15.00	-	0.35	Replaces 195

No	Host glass/ melting/ annealing	Colorant/ mol %	Silica, mol %	Na_2O, mol %	CaO, mol %	Other/ mol %	Refiner Na_2SO_4 mol %	Red/oxid. agent/ mol %
202	NCS/G/An	CeO_2/0.99 CoO/0.033	69.28	14.85	14.85	-	0.35	-
203	NCS/G/An	CeO_2/0.99 NiO/0.39	69.03	14.79	14.79	-	0.35	-
204	NCS/G/An	CeO_2/0.98 CuO/0.98	68.63	14.71	14.71	-	0.35	-
205	NCS/G/An	CeO_2/0.99 V_2O_5/0.49	69.97	14.78	14.78	-	0.35	-
206	NCS/G/An	CeO_2/0.99 Cr_2O_3/0.30	69.10	14.81	14.81	-	0.35	-
207	NCS/G/An	CeO_2/0.98 MnO_2/0.99	68.63	14.71	14.71	-	0.35	-
208	NCS/G/An	CeO_2/0.99 Fe_2O_3/0.49	68.97	14.78	14.78	-	0.35	-
209	NCS/Ew/An	MnO_2/1.95 Cr_2O_3/0.59	68.26	14.58	14.63	-	0.35	-
210	NCS/Ew/An	Cr_2O_3/0.30 CeO_2/0.94	69.13	14.81	14.81	-	0.35	-
211	NCS/Ew/An	NiO/0.30 CeO_2/0.94	69.13	14.81	14.81	-	0.35	-
212	NCS/Ew/An	CuO/0.20 Sm_2O_3/0.50	69.51	14.90	14.90	-	0.35	-
213	NCS/Ew/An	Cr_2O_3/0.30 Sm_2O_3/0.50	69.44	14.88	14.88	-	0.35	-
214	NCS/Ew/An	NiO/0.30 Sm_2O_3/0.50	69.44	14.88	14.88	-	0.35	-
215	NCS/Ew/An	MnO_2/0.1 Cr_2O_3/0.03	69.91	14.89	14.98	-	0.35	-
216	NCS/Ew/An	MnO_2/0.30 Cr_2O_3/0.09	69.73	14.94	14.94	-	0.35	-
217	NCS/Ew/An	MnO_2/0.99 Cr_2O_3/0.15	69.90	14.83	14.83	-	0.35	-
218	NCS/Ew/An	MnO_2/0.98 Cr_2O_3/0.59	68.90	14.76	14.76	-	0.35	-
219	NCS/Ew/An	MnO_2/1.96 Cr_2O_3/0.29	68.42	14.66	14.66	-	0.35	-

No	Host glass/ melting/ annealing	Colorant/ mol %	Silica, mol %	Na_2O, mol %	CaO, mol %	Other/ mol %	Refiner Na_2SO_4 mol %	Red/oxid. agent/ mol %
220	NCS/Ew/An	MnO_2/0.30 Cr_2O_3/0.30	69.58	14.91	14.91	-	0.35	-
221	NCS/Ew/An	MnO_2/0.1 Cr_2O_3/0.03	69.91	14.98	14.98	-	0.35	-
222	NCS/Ew/An	MnO_2/0.02 Cr_2O_3/0.006	69.98	15.00	15.00	-	0.35	-
223	NCS/Ew/An	Fe_2O_3/0.15 CuO/0.99	69.20	14.83	14.83	-	0.35	-
224	NCS/Ew/An	Fe_2O_3/0.50 CuO/0.30	69.44	14.88	14.88	-	0.35	-
225	NCS/G/An	Fe_2O_3/0.05	69.96	14.99	14.99	-	0.35	-
226	NCS/G/An	Fe_2O_3/0.05	69.96	14.99	14.99	-	0.25	-
227	NCS/G/An	Fe_2O_3/0.05	69.96	14.99	14.99	-	0.45	-
228	NCS/G/An	Fe_2O_3/0.05	68.59	14.70	14.70	-	0.34	Carbon/1.96
229	NCS/G/An	Fe_2O_3/0.05	68.59	14.99	14.99	-	0.34	$NaNO_3$/2.00
230	NCS/G/An	CeO_2/0.99	69.31	14.85	14.85	-	0.35	-
231	NCS/G/An	Fe_2O_3/0.10/ CeO_2/0.99	69.24	14.84	14.84	-	0.35	-
232	NCS/Ew/An	Fe_2O_3/0.10/ CeO_2/0.98	68.50	14.68	14.68	-	0.34	$NaNO_3$/1.07
233	NCS/Ew/An	Fe_2O_3/0.50 CuO/0.20	69.5	14.90	14.90	-	0.35	-
234	NCS/Ew/An	Fe_2O_3/0.10 CuO/0.30	69.72	14.94	14.94	-	0.35	-
235	NCS/Ew/An	Base (=41)	70.00	15.00	15.00	-	0.35	-
236	NPbS/G/An	base	74.69	9.30	-	PbO/16.00	0.16	Too little sulfate
237	NZnS/GAn	base	70.00	15.00	15.00	ZnO/15.00	0.35	-
238	NCS/G/An	Fe_2O_3/0.50 CuO/0.30	69.44	14.88	14.88	-	0.35	-
239	NCS/G/An	Fe_2O_3/0.15 CuO/0.99	69.20	14.83	14.83	-	0.35	-
240	NCS/G/An	Fe_2O_3/0.50 CuO/0.20	69.51	14.90	14.90	-	0.35	-

No	Host glass/ melting/ annealing	Colorant/ mol %	Silica, mol %	Na_2O, mol %	CaO, mol %	Other/ mol %	Refiner Na_2SO_4 mol %	Red/oxid. agent/ mol %
241	NCS/G/An	Fe_2O_3/0.10 CuO/0.30	69.72	14.94	14.94	-	0.35	-
242	NCScle/Gw/An	Fe_2O_3/0.05	69.96	14.99	14.99	-	0.35	-
243	NCScle/Gw/An	Cr_2O_3/0.033	69.98	15.00	15.00	-	0.35	-
244	NCScle/Gw/An	CuO/0.05	69.97	14.99	14.99	-	0.35	-
245	NCS/Ew/An	Fe_2O_3/0.10	69.93	14.98	14.98	-	0.35	-
246	NCS/Ew/An	Fe_2O_3/0.20	69.86	14.97	14.97	-	0.35	-
247	NCS/Ew/An	Fe_2O_3/0.99	69.31	14.85	14.85	-	0.35	-
248	NCS/Ew/An	Fe_2O_3/1.96	68.63	14.71	14.71	-	0.35	-

ANNEX 2

Measured refractive indexes of glass samples

The refractive indexes were measured with Metricon Model 2010 Prism Coupler Thin Film Thickness/Refractive Index Measurement System, by using bulk measuring arrangement, as described in Chap. 2. 7.

Sample	n at 632.8 nm	n at 1300 nm	n at 1550 nm
SiO_2 reference	1.45730	1.44764	1.44445
11	1.5213	1.51071	1.50771
13	1.49766	1.48681	1.48414
15, average	1.532495	1.52065	1.51774
15	1.53266	1.52065	1.51782
15	1.53233	1.52065	1.51766
16	1.53478	1.52292	1.52008
17	1.52938	1.51789	1.51522
26, average	1.527243	1.51545	1.51261
26	1.52691		
26	1.52741		
26	1.52741		
27	1.52905	1.51854	1.51538
34	1.52757	1.5161	1.51327
35	1.52954	1.51887	1.51571
36	1.52987	1.51773	1.51538
39	1.52691	1.51529	1.51261
40	1.53902	1.52647	1.52396
52	1.52954	1.51789	1.51522
54	1.53609	1.52405	1.52105
59	1.58151	1.56898	1.56584
63	1.54453	1.53193	1.52909

Sample	n at 632.8 nm	n at 1300 nm	n at 1550 nm
68	1.5356	1.52389	1.52089
81	1.53364	1.52179	1.51928
86	1.53527	1.52243	1.52008
94, average	1.53025	1.51879	1.51587
94V	1.53004	1.51871	1.51587
94A	1.5304	1.51887	1.51587
94X	1.5302	1.51887	1.51587
94T	1.53036	1.51871	1.51587
122	1.53788	1.5255	1.52283
130	1.53331	1.52146	1.51847
135	1.53544	1.52324	1.51992
141	1.53446	1.52243	1.51992
145	1.53266	1.52082	1.51798
151	1.532	1.52017	1.51733
152	1.53184	1.52049	1.51749
153	1.53429	1.52243	1.51976
154	1.52989	1.51822	1.51538
155	1.53184	1.52049	1.51749
156	1.53036	1.51806	1.51587
157	1.53348	1.52195	1.51911
158	1.53086	1.51822	1.51587
159	1.53118	1.52017	1.51733
160	1.532	1.52049	1.51749
161	1.5302	1.51838	1.51554
162	1.53805	1.52566	1.52331
163	1.54663	1.53305	1.53037
183	1.53674	1.5247	1.52235

Sample	n at 632.8 nm	n at 1300 nm	n at 1550 nm
194	1.52797	1.5161	1.51343
197	1.52757	1.51643	1.51343
198	1.53364	1.52163	1.51895
199	1.53739	1.52466	1.52267
201	1.52691	1.51512	1.51261
208	1.53837	1.52663	1.52347
209	1.54291	1.53001	1.52749
210	1.53951	1.52727	1.52444
216	1.53118	1.51919	1.51668

ANNEX 3

XRF composition analysis results, compared with the batch composition

Sample	Oxide	Meas. Conc. Weight %	Std. Error, Weight %	Cons. calc. from batch, Weight %	Cons. calc. from batch Mol %
Glass 28	SiO_2	69.80	0.09	69.45	69.31
NCS, gas-melted,	CaO	12.79	0.17	13.89	14.85
doped with Cu	Na_2O	13.34	0.37	15.35	14.85
	SO_3	0.285	0.041	0.46	0.45
	CuO	0.949	0.019	1.31	0.99
	Al_2O_3	2.28	0.07		
	K_2O	0.380	0.051		
	Fe_2O_3	0.0740	0.0054		
	MgO	0.0727	0.0059		
	TiO_2	0.0189	0.0017		
	P	0.0072	0.0009		
Glass 97	SiO_2	69.70	0.09	70.37	70.00
NCS, gas-melted,	CaO	17.61	0.19	14.07	15.00
non-doped	Na_2O	10.37	0.33	15.56	15.00
	SO_3	0.406	0.054	0.36	0.35
	Al_2O_3	1.18	0.05		
	K_2O	0.405	0.053		
	Fe_2O_3	0.109	0.008		
	BaO	0.077	0.012		
	MgO	0.0602	0.0050		
	TiO_2	0.0218	0.0019		
	SrO	0.0106	0.0016		
	P	0.0094	0.0009		
	Cr_2O_3	0.0062	0.0018		
	CuO	0.0054	0.0008		
Glass 86	SiO_2	70.08	0.09	68.84	69.10
NCS, electric melted,	CaO	12.91	0.17	13.77	14.81
doped with Cr and Mn	Na_2O	14.84	0.39	15.22	14.81
	SO_3	0.389	0.052	0.36	0.35
	MnO	0.985	0.015	1.42 (MnO_2)	1.00 (MnO_2)
	Cr_2O_3	0.675	0.011	0.75	0.30
	Fe_2O_3	0.0143	0.0023		
	MgO	0.0375	0.0032		
	TiO_2	0.0120	0.0015		
	SrO	0.0082	0.0033		
	K_2O	0.0072	0.0014		
	CuO	0.0121	0.0012		
Glass 41	SiO_2	70.77	0.09	70.37	70.00
NCS, electric melted,	CaO	13.28	0.17	14.07	15.00
non-doped	Na_2O	15.38	0.40	15.56	15.00
	SO_3	0.470	0.059	0.36	0.35
	MgO	0.0396	0.0034		
	Fe_2O_3	0.0162	0.0022		
	TiO_2	0.0137	0.0015		
	ZnO	0.0066	0.0009		

Composition of two iron doped glasses, analysed by EDX, P. Bingham

Sample	Oxide	Conc. mol %
Glass 246	SiO_2	69,8
NCS/Ew	CaO	15,4
0,2 mol % Fe_2O_3	Na_2O	15,0
	SO_3	0,3
	Al_2O_3	0,3
	Fe_2O_3	0,2
Glass 247	SiO_2	68,8
NCS/Ew	CaO	15,0
1,0 mol % Fe_2O_3	Na_2O	14,6
	SO_3	0,3
	Al_2O_3	0,3
	Fe_2O_3	1,1

Annex 4

Information of raw materials and mullite crucibles, including impurity contents

Oxide received	Source material	Supplier/ product code	Residues, maximum content, m% Impurities: (multiplication factor), concentration, % (w %)
Al-, Si-, Na-oxides leaching	mullite crucible (corrosion at gas furnace melting)	SU/ internal product	Information not available, to be analysed later. Expected: relatively high contents of Si, Al and Na (raw materials of crucible) and high impurity contents: Fe, Mn, Ti and Ni , etc.
SiO_2	LA Sand	Tilcon/L30A	SiO2: 99.8 %, Al2O3: 0.05%, Fe2O3: 0.009%, Na2O>0.05%, K2O<0.01%, CaO<0.02%, MgO<0.05%, loss on ignition 0.07%
Na_2O	Na_2CO_3		Under investigation, to be added later
CaO	$CaCO_3$	Omya UK/ MINFIL L220	CaCO3: 99.3 %, SiO2: 0.3%, Fe2O3: 0.02%, HCL: 0.4%,
K_2O	K_2CO_3		Under investigation
MgO	$MgCO_3$		Under investigation
Al_2O_3	$Al(OH)_3$		Under investigation
B_2O_3	B_2O_3		Under investigation
P_2O_5+ Na_2O	$Na_5P_3O_{10}$		Under investigation
Na_2O	Na_2SO_4, refiner of bubbles	Fisons 14204 or S/6640/ anhydrous	Residues: SO_2, S_2, SO_3, ^{-}S, $^{-2}SO_4$, < 0.3 - 0.7 m% Impurities: (factor: 0.003- 0.007m%*) Cl 0.01%, Fe< 0.002%, Pb< 0.0015%, Moisture: 2.0 %, NO_3<0.01%, K<0.1%
Na_2O	$NaNO_3$, oxidising agent	?	Residues: , N_2, SiON, SiN_3, SiHN Impurities: (factor: 0.003- 0.007m%*)
--	Graphite [C], reducing agent	Not known	Residues: SiC, SiOC Impurities: (factor: 0.01- 0.1 m%*), not available, to be analysed, if needed
Fe^{2+}, Fe^{3+}	Fe_2O_3, Fe_3O_4	Not known	Residues: - Impurities: (factor: 0.001- 0.02m%*), not available, to be analysed, if needed
Ni^{2+}, Ni^{3+}	NiO	Hopkin& Williams 6063	Residues: - Impurities: (factor: 0.001- 0.02m%*)
Cr^{2+}, Cr^{3+}	Cr_2O_3, Cr_3O_4	BDH 27757	Residues: - Impurities: (factor: 0.001- 0.02m%*)
Cu^{2+}	CuO	Fisons C/8360/50	Residues: - Impurities: (factor: 0.005-0.02m%*) Si< 0.02%, P<0.01 %, S<0.01%, Zn<0.02%,Mg<0.005%, Pb<0.02%, Na<0.02%, K<0.005%, N<0.005%, Fe<0.05%, Cl<0.005%, Ca<0.02%
Co^{2+}, Co^{3+}	$CoCO_3$	BDH 27789	Residues: - Impurities: (factor: 0.001- 0.02m%*)

ANNEX 5 a

Fitting Cu^{2+} band of Glass 111 with two, three and four peaks, using the program PeakFit-v4.12, by Dr. R. Klement, The University of Aleksander Dubcek, Trencin, 2005

A5.1 Fitting the Cu^{2+} band of Glass 111 using two peaks

Fitting function: Gauss Amplitude: $$y = a_0 \exp\left[-\frac{1}{2}\left(\frac{x-a_1}{a_2}\right)^2\right]$$

Case 1, Background correction of the data: YES

Note: Various starting positions, amplitudes and widths of the peak fitted led to the same final result showed below.

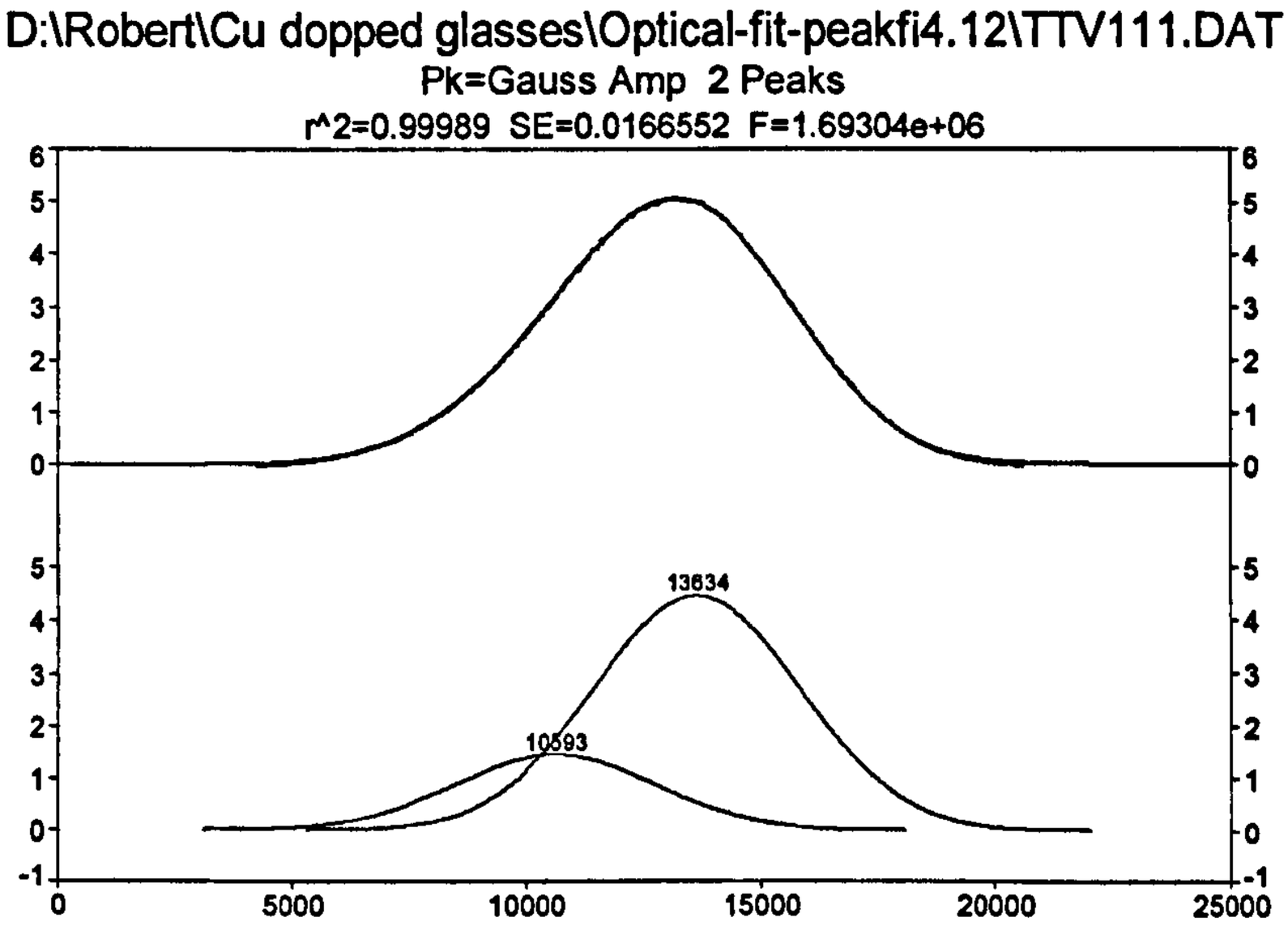

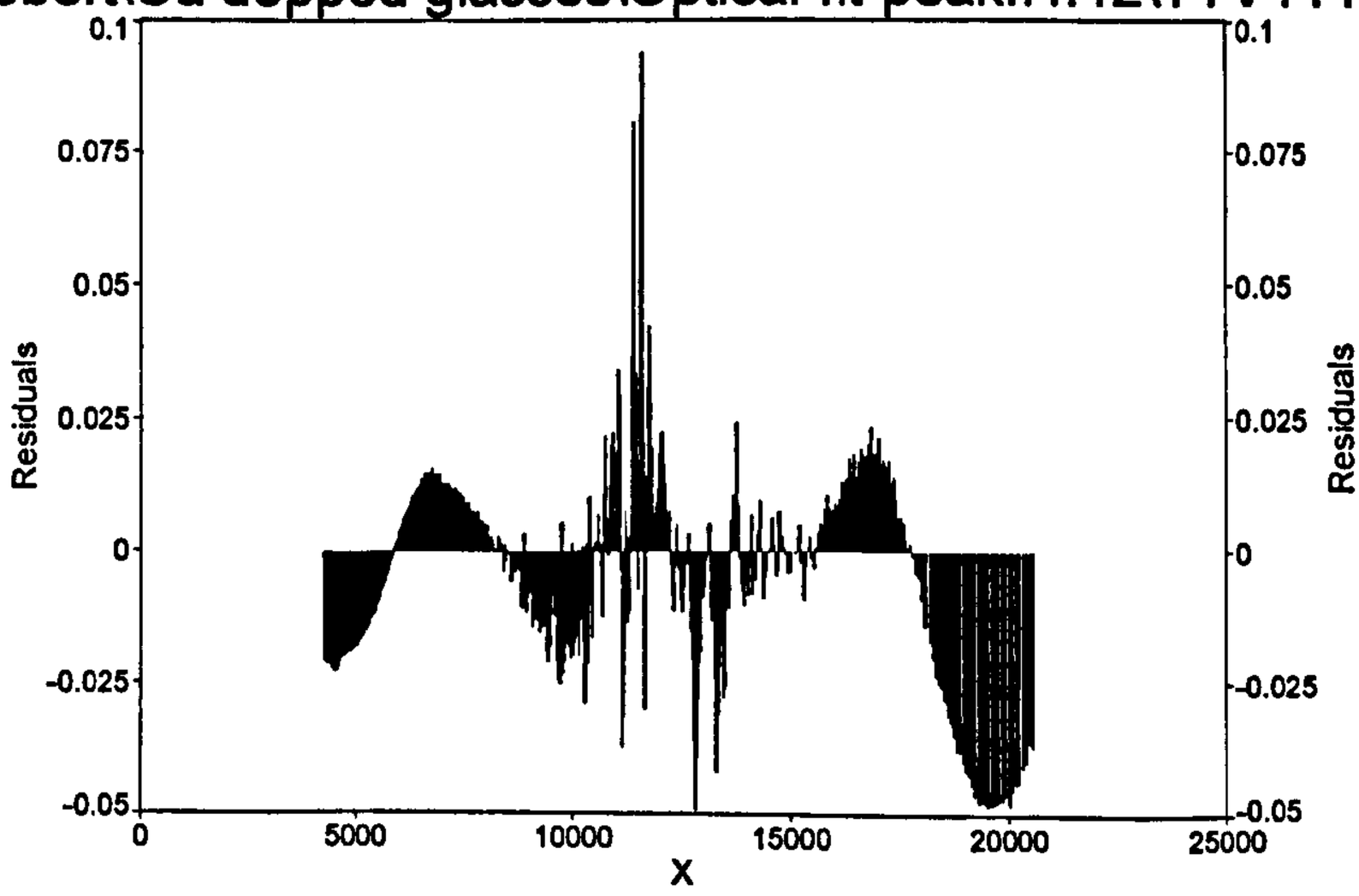

Fitted Parameters

r^2 Coef Det	DF Adj r^2	Fit Std Err	F-value
0.99988968	0.99988897	0.01665520	1.693e+06

Peak	Type	a0	a1	a2
1	Gauss Amp	1.44998171	10592.7041	2174.99411
2	Gauss Amp	4.45583166	13634.3488	2221.31553

Measured Values

Peak	Type	Amplitude	Center	FWHM	Asym50	FW Base Asym10
1	Gauss Amp	1.44998171	10592.7041	5121.71974	1.00000000	10252.1885 1.00000000
2	Gauss Amp	4.45583166	13634.3488	5230.79833	1.00000000	10470.5321 1.00000000

Peak	Type	Anlytc Area	% Area	Int Area	% Area	Centroid Moment2
1	Gauss Amp	7905.15779	24.1635009	7891.54001	24.1484149	10604.7275 4.6536e+06
2	Gauss Amp	24810.1255	75.8364991	24787.7892	75.8515851	13627.7447 4.8865e+06
	Total	32715.2833	100.000000	32679.3292	100.000000	

Parameter Statistics

Peak 1 Gauss Amp

Parm	Value	Std Error	t-value	95Confidence Limits	
Amp	1.44998171	0.08106291	17.8871169	1.29089517	1.60906824
Ctr	10592.7041	90.2301291	117.396531	10415.6269	10769.7814
Wid	2174.99411	21.9479548	99.0978035	2131.92110	2218.06713

Peak 2 Gauss Amp

Parm	Value	Std Error	t-value	95Confidence Limits	
Amp	4.45583166	0.07317618	60.8918343	4.31222289	4.59944043
Ctr	13634.3488	33.8646543	402.612963	13567.8892	13700.8084
Wid	2221.31553	10.5910157	209.735835	2200.53058	2242.10047

Analysis of Variance

r^2 Coef Det	DF Adj r^2	Fit Std Err
0.99988968	0.99988897	0.01665520

Source	Sum of Squares	DF	Mean Square	F
Regr	2348.2077	5	469.64153	1693039
Error	0.25908748	934	0.00027739558	
Total	2348.4667	939		

Details of Fit

Set Convergence	State	Iterations	Minimization	Extent
1E-7	Converged	7	Least Squares	1/1

Curvature Matrix	Constraints	Violated
Sparse-Roots	20.0000-5.00000-20.0000- None - None	0

Case 2, Background correction of the data: NO

Note: Various starting positions, amplitudes and widths of the peak fitted led to the final results showed below. In this case, there are two possibilities how to fit the absorption data.

D:\Robo\Cooperation\Parker-Volotinen-Sheffield\Cu dopped glasses\Optical-fit-pea

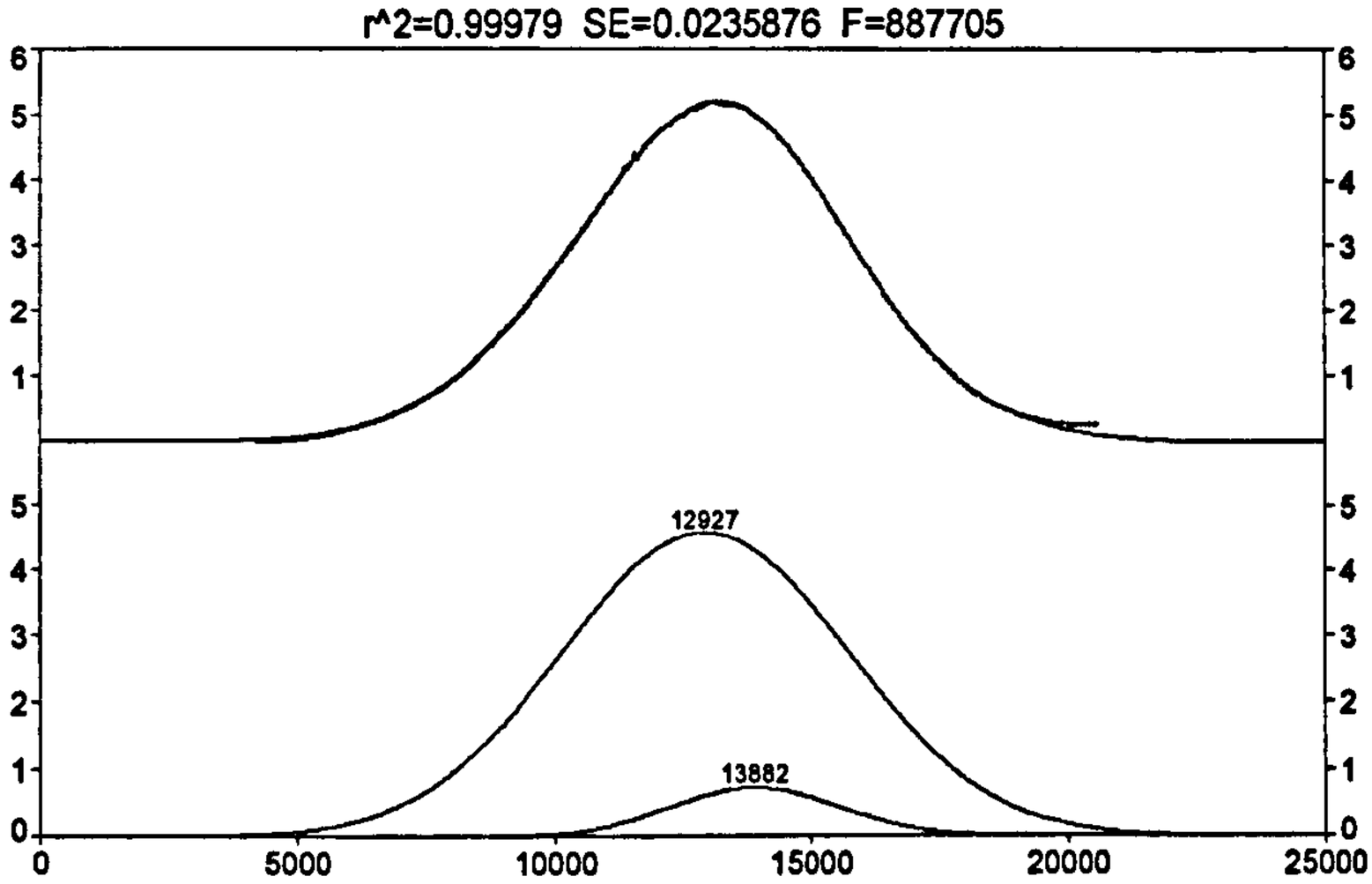

D:\Robo\Cooperation\Parker-Volotinen-Sheffield\Cu dopped glasses\Optical-fit-pea

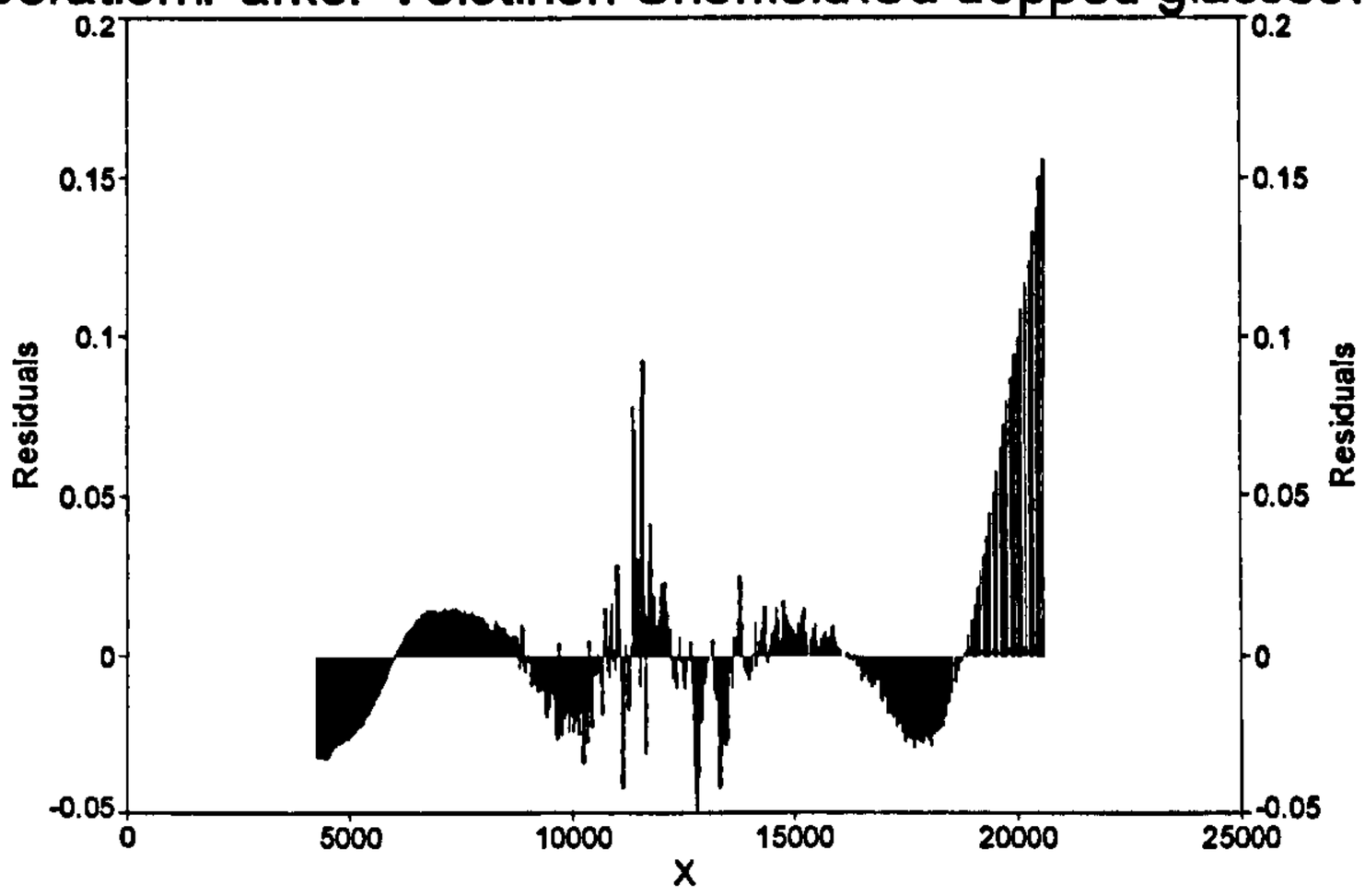

Fitted Parameters

r^2 Coef Det	DF Adj r^2	Fit Std Err	F-value
0.99978961	0.99978826	0.02358761	8.877e+05

Peak	Type	a0	a1	a2
1	Gauss Amp	4.57506742	12927.0923	2772.92421
2	Gauss Amp	0.73131751	13882.1734	1622.19243

Measured Values

Peak	Type	Amplitude	Center	FWHM	Asym50	FW Base	Asym10
1	Gauss Amp	4.57506742	12927.0923	6529.73750	1.00000000	13070.6293	1.00000000
2	Gauss Amp	0.73131751	13882.1734	3819.97124	1.00000000	7646.46786	1.00000000

Peak	Type	Anlytc Area	% Area	Int Area	% Area	Centroid	Moment2
1	Gauss Amp	31799.8763	91.4483716	31680.3469	91.4190197	12910.4827	7.4291e+06

2	Gauss Amp	2973.70768	8.55162838	2973.65291	8.58098033	13882.0435
	2.6306e+06					
	Total	34773.5840	100.000000	34653.9998	100.000000	

Parameter Statistics

Peak 1 Gauss Amp

Parm	Value	Std Error	t-value	95	
Amp	4.57506742	0.02402870	190.400093	4.52791092	4.62222392
Ctr	12927.0923	6.44881019	2004.57013	12914.4364	12939.7481
Wid	2772.92421	2.98200828	929.884812	2767.07199	2778.77642

Peak 2 Gauss Amp

Parm	Value	Std Error	t-value	95	
Amp	0.73131751	0.02435857	30.0230122	0.68351365	0.77912137
Ctr	13882.1734	18.0853005	767.594288	13846.6809	13917.6659
Wid	1622.19243	26.6845897	60.7913572	1569.82373	1674.56112

Analysis of Variance

r^2 Coef Det	DF Adj r^2	Fit Std Err
0.99978961	0.99978826	0.02358761

Source	Sum of Squares	DF	Mean Square	F
Regr	2469.4855	5	493.8971	887705
Error	0.51965449	934	0.00055637526	
Total	2470.0051	939		

Details of Fit

Set Convergence	State	Iterations	Minimization	Extent
1E-7	Converged	7	Least Squares	1/1
Curvature Matrix	Constraints			Violated
Sparse-Roots	20.0000-5.00000-20.0000-	None	- None	0

Case 3: Another variation of Case 2

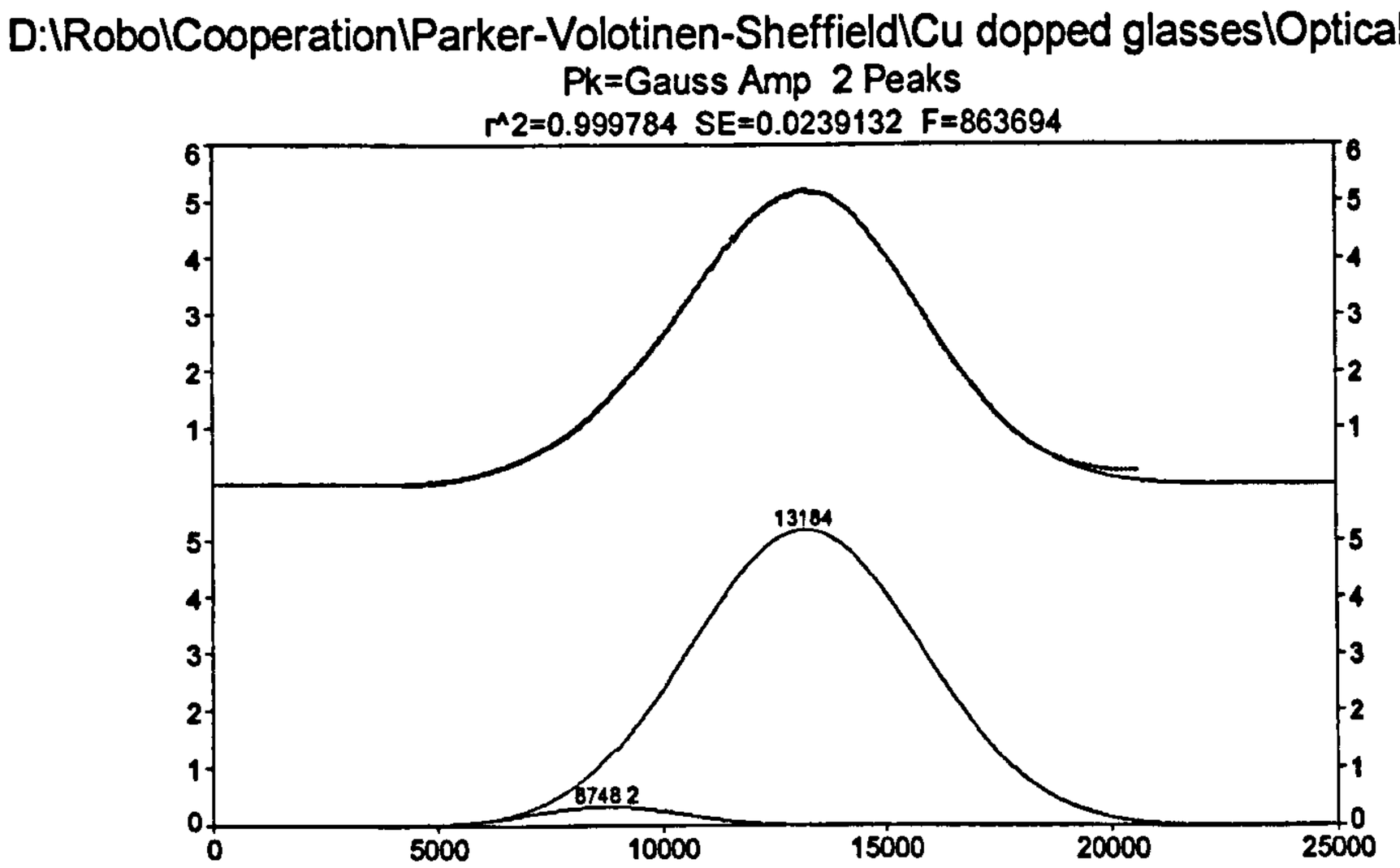

Fitted Parameters

r^2 Coef Det	DF Adj r^2	Fit Std Err	F-value
0.99978377	0.99978238	0.02391316	8.6369e+05

Peak	Type	a0	a1	a2
1	Gauss Amp	0.34181148	8748.24771	1715.50325
2	Gauss Amp	5.20128916	13183.7817	2545.29788

D:\Robo\Cooperation\Parker-Volotinen-Sheffield\Cu dopped glasses\Optical-fit-pea

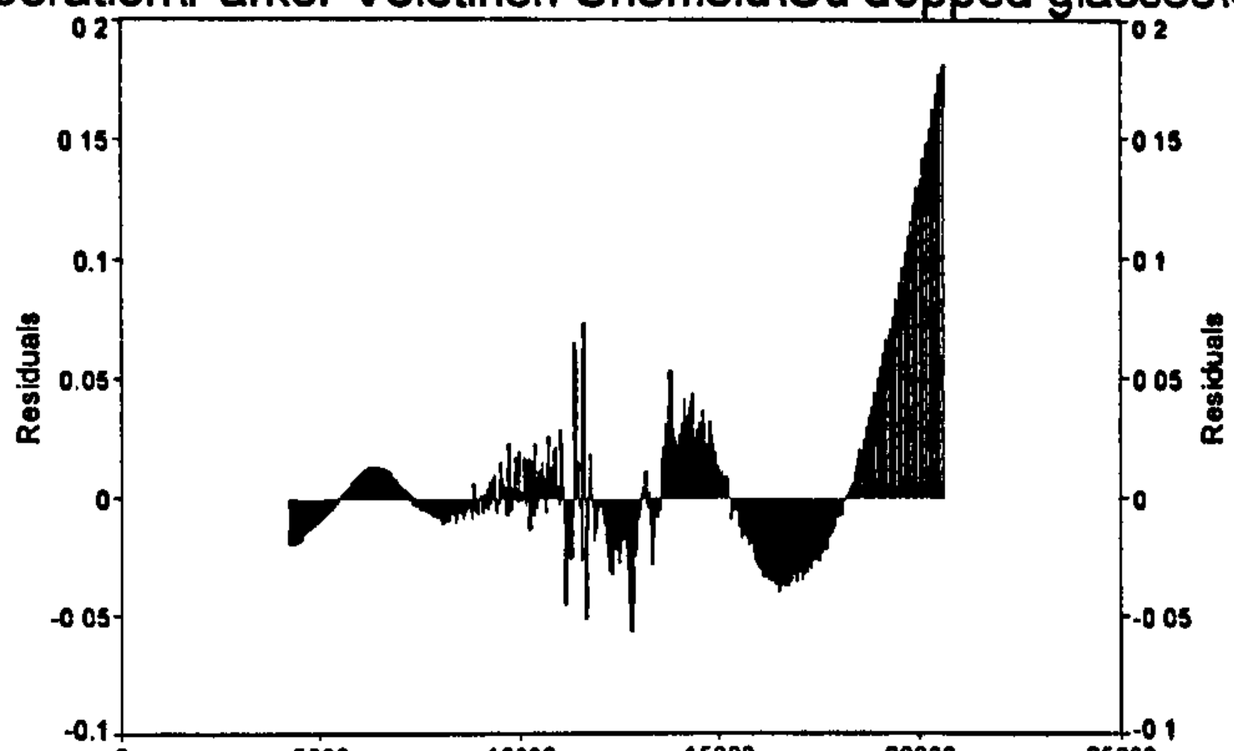

Measured Values

Peak	Type	Amplitude	Center	FWHM	Asym50	FW Base	Asym10
1	Gauss Amp	0.34181148	8748.24771	4039.70145	1.00000000	8086.30363	1.00000000
2	Gauss Amp	5.20128916	13183.7817	5993.71847	1.00000000	11997.6756	1.00000000

Peak	Type	Anlytc Area	% Area	Int Area	% Area	Centroid	Moment2
1	Gauss Amp	1469.83346	4.24137321	1463.62643	4.23256103	8769.67262	2.8457e+06
2	Gauss Amp	33184.8263	95.7586268	33116.5349	95.7674390	13170.8800	6.3488e+06
	Total	34654.6597	100.000000	34580.1613	100.000000		

Parameter Statistics

Peak 1 Gauss Amp

Parm	Value	Std Error	t-value	95	
Amp	0.34181148	0.01237868	27.6129164	0.31751823	0.36610473
Ctr	8748.24771	49.4610060	176.871609	8651.18013	8845.31528
Wid	1715.50325	26.5170221	64.6944159	1663.46341	1767.54310

Peak 2 Gauss Amp

Parm	Value	Std Error	t-value	95	
Amp	5.20128916	0.00394402	1318.77772	5.19354899	5.20902933
Ctr	13183.7817	6.52191472	2021.45877	13170.9824	13196.5810
Wid	2545.29788	4.99927476	509.133425	2535.48677	2555.10899

Analysis of Variance

r^2 Coef Det	DF Adj r^2	Fit Std Err
0.99978377	0.99978238	0.02391316

Source	Sum of Squares	DF	Mean Square	F
Regr	2469.471	5	493.89421	863693.99
Error	0.53409795	934	0.00057183935	
Total	2470.0051	939		

Details of Fit

Set Convergence	State	Iterations	Minimization	Extent
1E-7	Converged	7	Least Squares	1/1

Curvature Matrix	Constraints				Violated
Sparse-Roots	20.0000	-5.00000	-20.0000	- None - None	0

A5.2 Fitting the Cu^{2+} band of Glass 111 using three peaks

Case 2.1 A fitting with three peaks

Background correction of the data: YES

Note: Various starting positions, amplitudes and widths of the peak fitted led to the same final result showed below.

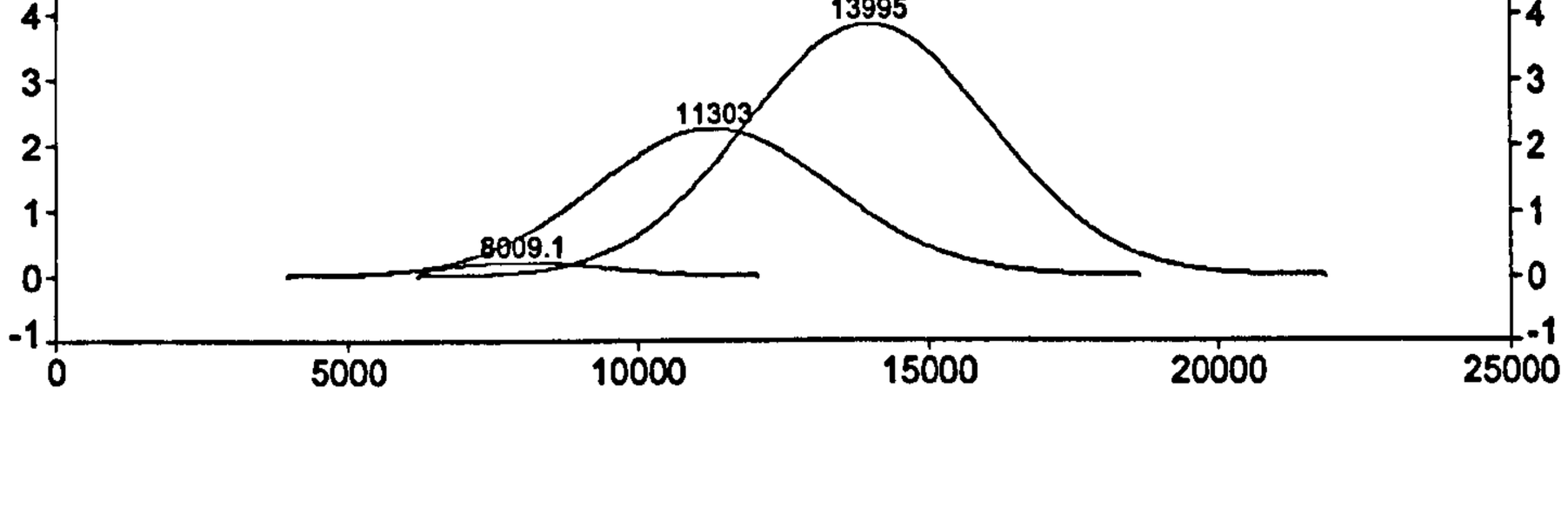

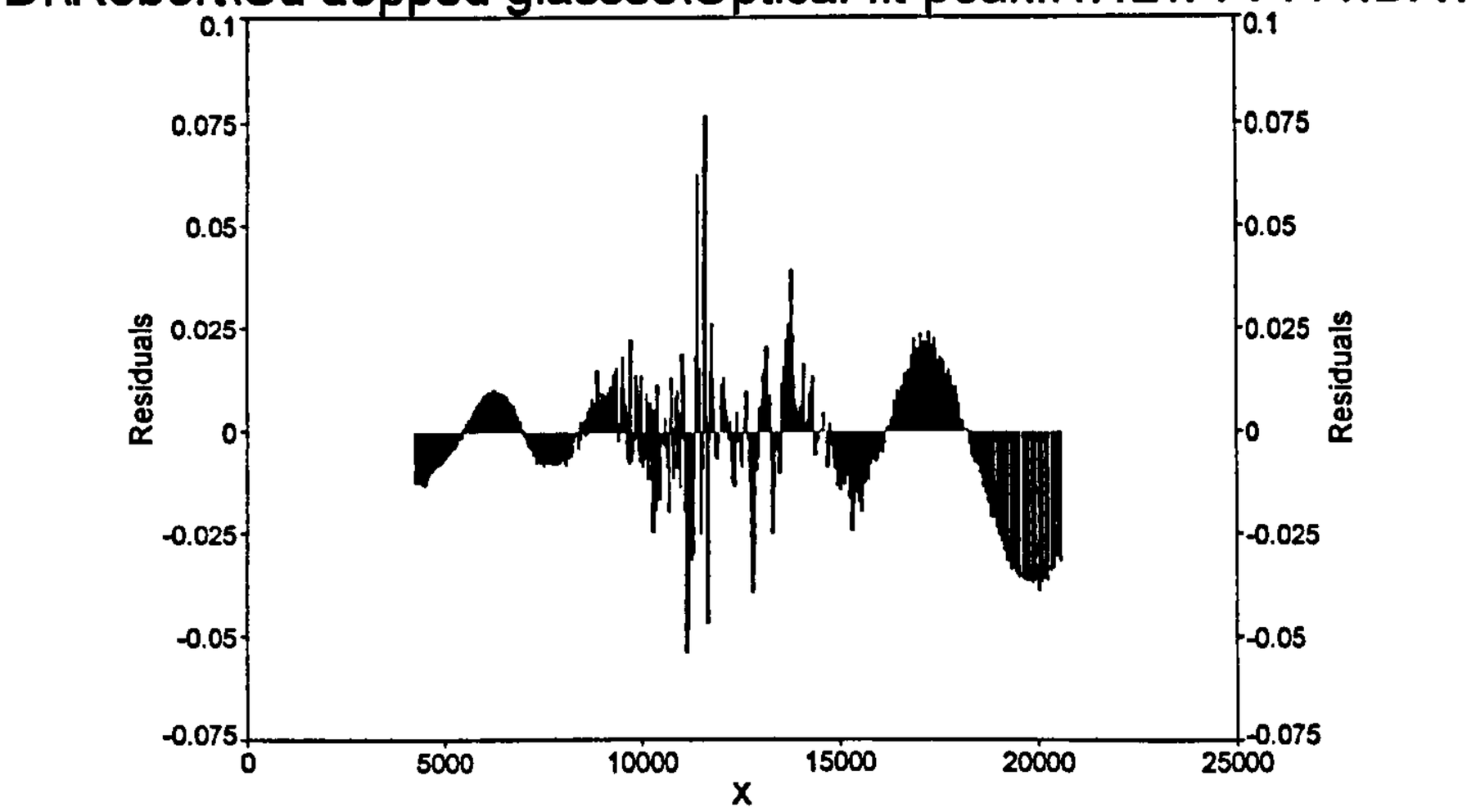

Fitted Parameters

r^2 Coef Det	DF Adj r^2	Fit Std Err	F-value
0.99994517	0.99994464	0.01176044	2.1224e+06

Peak	Type	a0	a1	a2
1	Gauss Amp	0.21657150	8009.10879	1430.71714
2	Gauss Amp	2.25448718	11303.1288	2055.36362
3	Gauss Amp	3.85646487	13995.2216	2097.27314

Measured Values

Peak	Type	Amplitude	Center	FWHM	Asym50	FW Base	Asym10
1	Gauss Amp	0.21657150	8009.10879	3369.08140	1.00000000	6743.91795	1.00000000
2	Gauss Amp	2.25448718	11303.1288	4840.01144	1.00000000	9688.29072	1.00000000
3	Gauss Amp	3.85646487	13995.2216	4938.70084	1.00000000	9885.83810	1.00000000

Peak	Type	Anlytc Area	% Area	Int Area	% Area	Centroid	Moment2
1	Gauss Amp	776.685193	2.37768268	773.478174	2.36959816	8026.61978	1.9805e+06
2	Gauss Amp	11615.1913	35.5578290	11611.7911	35.5734393	11305.2977	4.2087e+06
3	Gauss Amp	20273.7604	62.0644883	20256.4751	62.0569626	13989.1441	4.3583e+06
	Total	32665.6369	100.000000	32641.7444	100.000000		

Parameter Statistics

Peak 1 Gauss Amp

Parm	Value	Std Error	t-value	95	
Amp	0.21657150	0.09618653	2.25157821	0.02780396	0.40533905
Ctr	8009.10879	192.977395	41.5028341	7630.38770	8387.82989
Wid	1430.71714	110.333563	12.9671979	1214.18583	1647.24845

Peak 2 Gauss Amp

Parm	Value	Std Error	t-value	95	
Amp	2.25448718	0.56516018	3.98911189	1.14535167	3.36362269
Ctr	11303.1288	349.797017	32.3133940	10616.6468	11989.6108
Wid	2055.36362	189.671963	10.8364124	1683.12948	2427.59775

Peak 3 Gauss Amp

Parm	Value	Std Error	t-value	95	
Amp	3.85646487	0.60278721	6.39772182	2.67348574	5.03944401
Ctr	13995.2216	219.079170	63.8820275	13565.2753	14425.1678
Wid	2097.27314	43.9034819	47.7700869	2011.11189	2183.43440

Analysis of Variance

r^2 Coef Det	DF Adj r^2	Fit Std Err
0.99994517	0.99994464	0.01176044

Source	Sum of Squares	DF	Mean Square	F
Regr	2348.338	8	293.54225	2122382.7
Error	0.12876463	931	0.00013830788	
Total	2348.4667	939		

Details of Fit

Set Convergence	State	Iterations	Minimization	Extent
1E-7	Converged	7	Least Squares	1/1

Curvature Matrix	Constraints				Violated
Sparse-Roots	20.0000	-5.00000	-20.0000	- None - None	0

Case 2.2, Another fitting with three peaks

Background correction of the data: NO

Note: Various starting positions, amplitudes and widths of the peak fitted led to the final results showed below. When the only three peaks are used in fitting procedure, one peak seems to simulate the background.

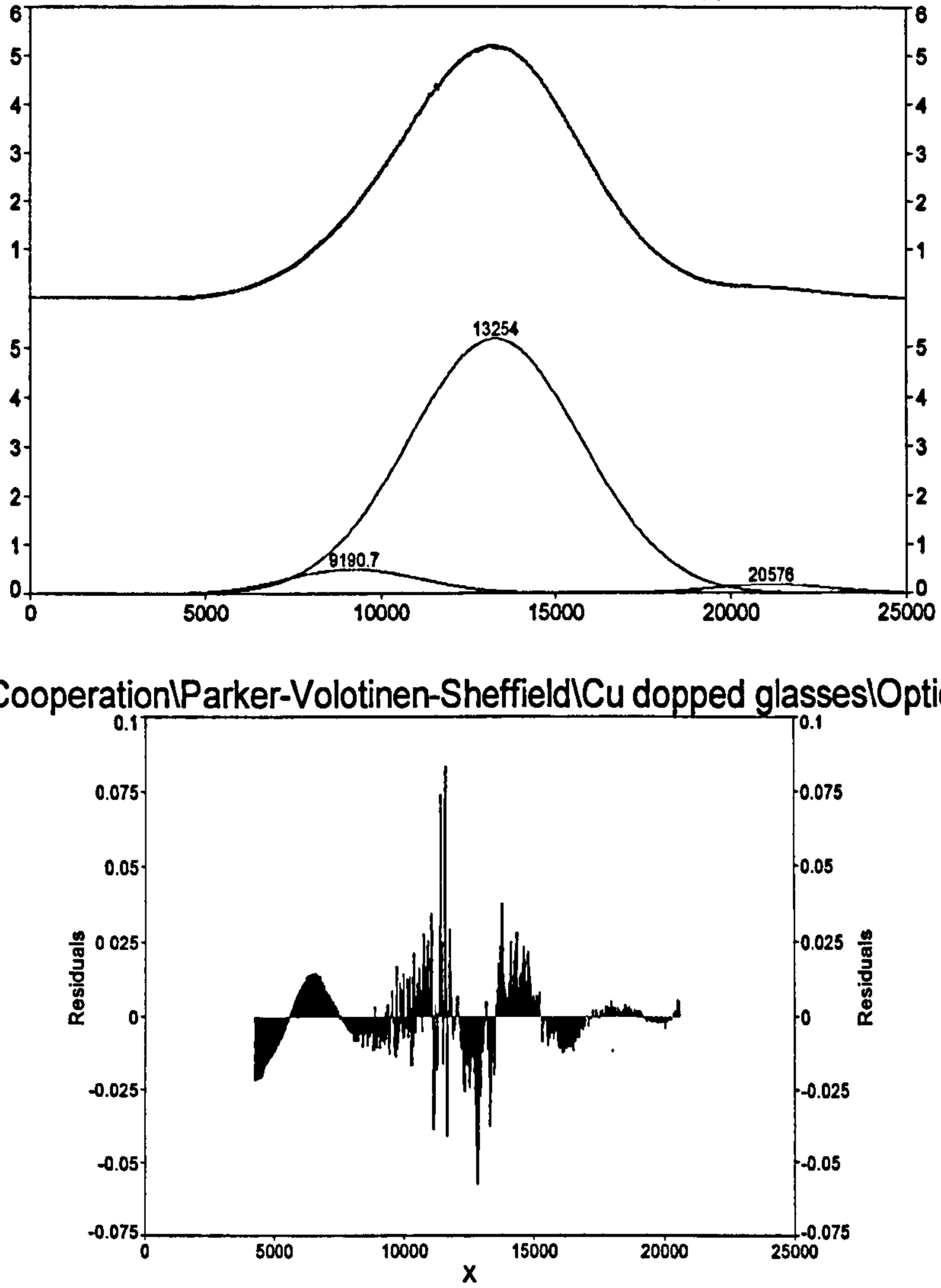

Case 2.3 A fitting with four peaks

The fit with four peaks (one simulating the background – on right side of spectrum) leads to the following result.

Fitted Parameters

r^2 Coef Det	DF Adj r^2	Fit Std Err	F-value
0.99996289	0.99996253	0.00992209	3.1361e+06

Peak	Type	a0	a1	a2
1	Gauss Amp	0.09599321	6980.90218	1071.55620
2	Gauss Amp	0.51372319	9456.96078	1698.87493
3	Gauss Amp	5.17403899	13261.9816	2471.19510
4	Gauss Amp	0.19896466	21158.9520	1627.14210

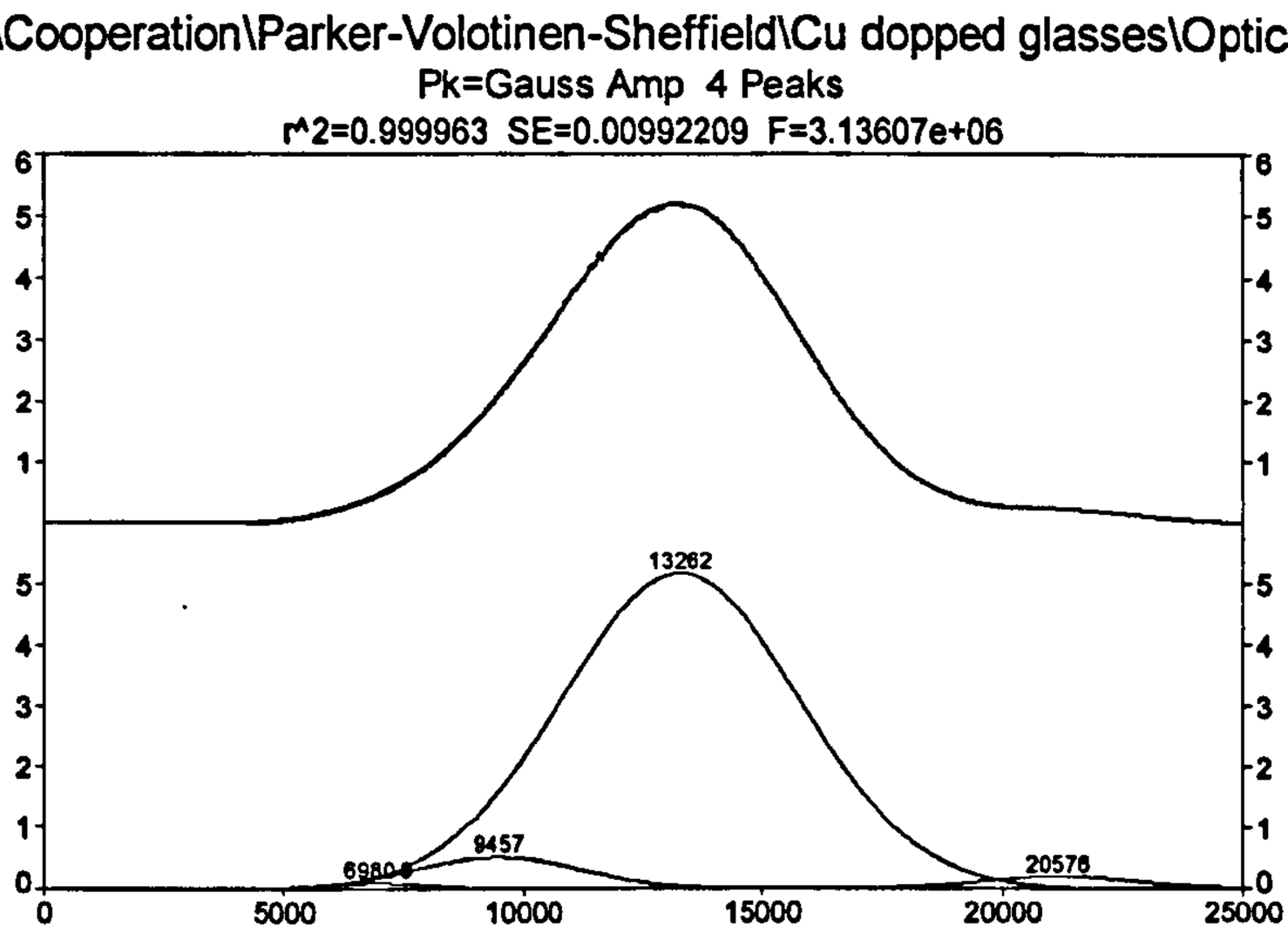

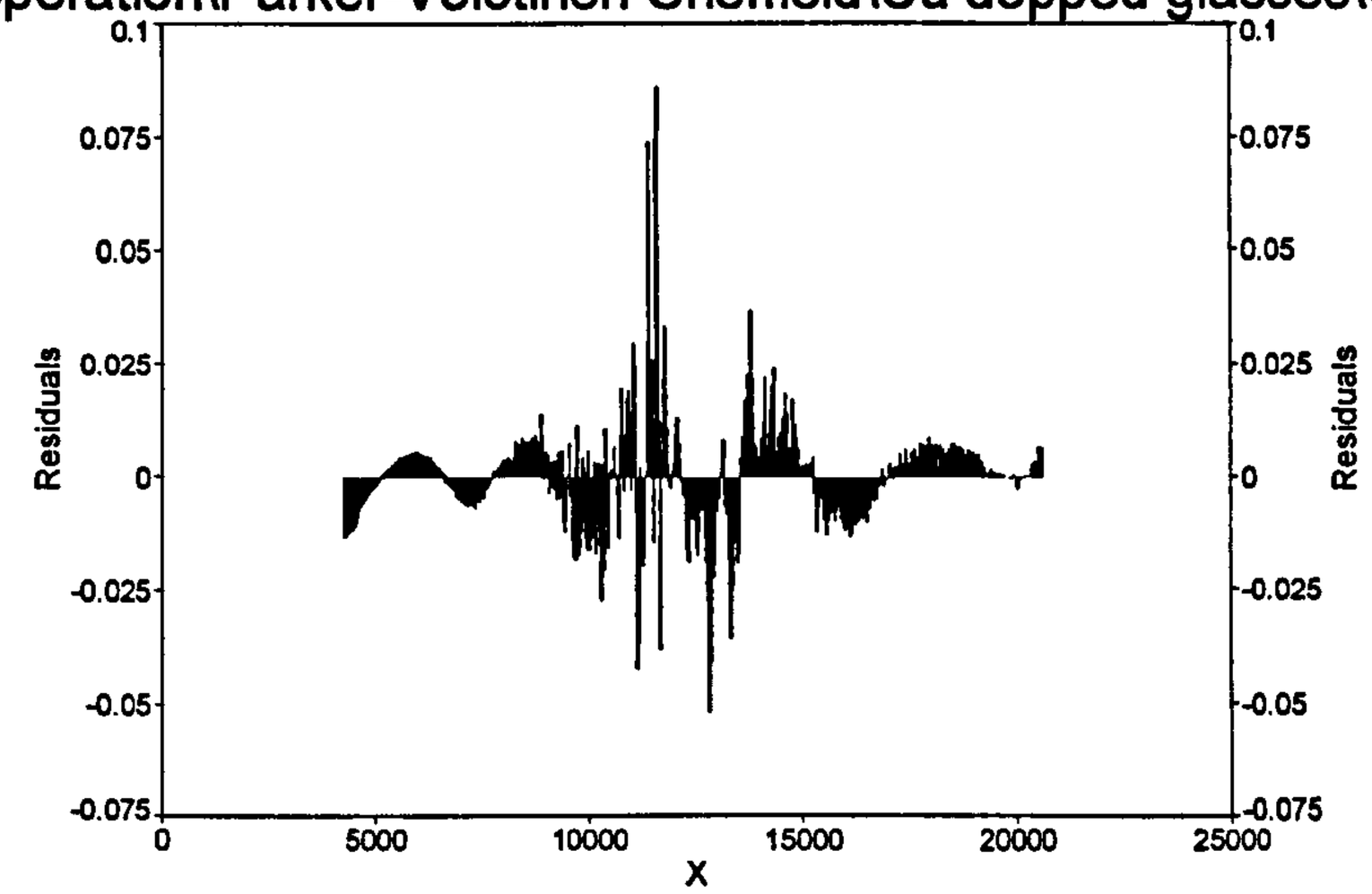

Measured Values

Peak	Type	Amplitude	Center	FWHM	Asym50	FW Base Asym10
1	Gauss Amp	0.09599321	6980.90218	2523.32201	1.00000000	5050.95443 1.00000000
2	Gauss Amp	0.51372319	9456.96078	4000.54475	1.00000000	8007.92334 1.00000000
3	Gauss Amp	5.17403899	13261.9816	5819.21975	1.00000000	11648.3801 1.00000000
4	Gauss Amp	0.18660206	20576.1313	4005.00738	1.82105756	7728.36680 1.39416044

Peak	Type	Anlytc Area	% Area	Int Area	% Area	Centroid Moment2
1	Gauss Amp	257.837098	0.73027387	256.514971	0.73858594	6996.83033 1.1042e+06
2	Gauss Amp	2187.66346	6.19613493	2185.37362	6.29236660	9462.93196 2.8549e+06
3	Gauss Amp	32049.8990	90.7751589	31996.4383	92.1276425	13250.8552 6.005e+06
4	Gauss Amp	811.505299	2.29843229	292.224584	0.84140496	19468.3137 7.7467e+05

Total	35306.9048	100.000000	34730.5514	100.000000	

Parameter Statistics

Peak 1 Gauss Amp

Parm	Value	Std Error	t-value	95	
Amp	0.09599321	0.02180464	4.40242037	0.05320126	0.13878516
Ctr	6980.90218	80.2426184	86.9974375	6823.42481	7138.37955
Wid	1071.55620	67.3800457	15.9031681	939.321823	1203.79057

Peak 2 Gauss Amp

Parm	Value	Std Error	t-value	95	
Amp	0.51372319	0.02329841	22.0497140	0.46799971	0.55944667
Ctr	9456.96078	37.0579238	255.194027	9384.23404	9529.68753
Wid	1698.87493	67.6988763	25.0945810	1566.01485	1831.73502

Peak 3 Gauss Amp

Parm	Value	Std Error	t-value	95	
Amp	5.17403899	0.01019099	507.707064	5.15403901	5.19403897
Ctr	13261.9816	9.70453165	1366.57616	13242.9363	13281.0269
Wid	2471.19510	4.66411262	529.831781	2462.04170	2480.34849

Peak 4 Gauss Amp

Parm	Value	Std Error	t-value	95
Amp	0.19896466			
Ctr	21158.9520			
Wid	1627.14210			

Analysis of Variance

r^2 Coef Det	DF Adj r^2	Fit Std Err
0.99996289	0.99996253	0.00992209

Source	Sum of Squares	DF	Mean Square	F
Regr	2469.9135	8	308.73918	3136065.6
Error	0.091655029	931	9.8447936e-05	
Total	2470.0051	939		

Details of Fit

Set Convergence	State	Iterations	Minimization	Extent
1E-7	Not Fitted	0	Least Squares	1/1

Curvature Matrix	Constraints				Violated
Sparse-Roots	20.0000	-5.00000	-20.0000	- None - None	0

ANNEX 5 b

The results of EPR analysis on the selected Cu-doped silicate glasses, by Dr. R. Klement, The University of Aleksander Dubcek, Trencin

Table A5b.1 Composition of the Cu-doped glasses analysed with EPR method

Glass	Composition					Refiner Na_2SO_4 mol %
	CuO mol %	SiO_2 mol %	Na_2O Mol %	CaO mol %	Other mol %	
TTV 27	0.50	69.65	14.93	14.93	–	0.45
TTV 28	0.99	69.31	14.85	14.85	–	0.45
TTV 35	0.99	69.31	14.85	14.85	–	0.35
TTV 44	0.50	69.65	14.93	14.93	–	0.35
TTV 60	0.99	69.31	0.35	14.85	K_2O / 14.50	0.35
TTV 61	0.99	64.36	14.85	14.85	Al_2O_3 / 4.95	0.35
TTV 63	1.05	68.06	7.33	15.71	Li_2O / 7.85	0.35
TTV 64	0.99	69.31	14.85	–	BaO / 14.85	0.35
TTV 65	0.99	64.36	0.35	14.85	Al_2O_3 / 4.95 K_2O / 14.50	0.35
TTV 77	0.99	64.36	14.85	14.85	B_2O_3 / 4.95	0.35
TTV 88	1.00	69.76	0.35	14.95	BaO / 13.95	0.35
TTV 90	0.99	64.13	5.28	14.80	K_2O / 9.87 Al_2O_3 / 4.93	0.35
TTV 95	0.99	69.14	7.46	14.82	Li_2O / 7.60	0.35
TTV 105	0.53	68.73	10.94	9.90	MgO / 9.90	0.37
TTV 106	0.53	68.73	0.37	9.90	MgO / 9.90 K_2O / 10.57	0.37
TTV 111	1.05	68.37	10.89	9.85	MgO / 9.85	0.37

Table A5.2 Spectral parameters of selected glass samples doped with CuO

Sample name	EPR Spectral (Spin Hamiltonian) Parameters #				Optical Absorption		
	$g_{//}$	$g_{\perp}$	$A_{//}$ (MHz)	$A_{\perp}$ (MHz)	d-d transition (cm^{-1})	Fitted Peak 1 position (cm^{-1})	Fitted Peak 2 position (cm^{-1})
TTV 27	2.383	2.0674	411	42	12887	12585	13711
TTV 28	2.381	2.0687	421	43	12887	12450	13560
TTV 35	2.382	2.0695	425	42	12658	12126	13516
TTV 44	2.382	2.0683	418	48	12722	11962	13523
TTV 60	2.379	2.0688	423	44	12165	11794	12929
TTV 61	2.375	2.0667	425	41	12853	12605	13886
TTV 63	2.378	2.0678	422	41	12953	12767	14007
TTV 64	2.386	2.0684	416	43	12594	12542	13063
TTV 65	2.376	2.0668	416	45	12407	12043	12553
TTV 77	2.379	2.0673	420	41	12887	12392	13185
TTV 88	2.377	2.0672	418	40	12626	12667	-
TTV 90	2.374	2.0670	426	45	12563	12251	13248
TTV 95	2.377	2.0670	428	39	13123	12569	13954
TTV 105	2.374	2.0670	428	43	13404	12892	14003
TTV 106	2.370	2.0685	435	46	13123	12801	13557
TTV 111	2.375	2.0685	429	39	13123	12926	13886

 # The hyperfine splitting constants are given in MHz (for conversion to cm^{-1}, divide values by 3×10^4).

Table A5.3 MO coefficients calculated from EPR data and energy of optical d–d transitions for selected glass samples doped with CuO

Sample name	MO coefficients					
	Calculated from the energy of d–d transition (broad band)		Calculated from the energy of peak 2 position ($^2B_{1g}\rightarrow{}^2B_{2g}$)		Calculated from the energy of peak 2 position ($^2B_{1g}\rightarrow{}^2B_{2g}$)	
	α^2	β_1^2	α^2	β_1^2	Γ_σ (%)	Γ_π (%)
TTV 27	0.829	0.893	0.829	0.950	37.2	10.0
TTV 28	0.837	0.880	0.837	0.926	35.5	14.8
TTV 35	0.842	0.861	0.842	0.920	34.4	16.0
TTV 44	0.835	0.873	0.835	0.928	35.9	14.4
TTV 60	0.837	0.826	0.837	0.878	35.5	24.3
TTV 61	0.834	0.867	0.834	0.937	36.2	12.7
TTV 63	0.835	0.880	0.835	0.952	36.0	9.7
TTV 64	0.837	0.871	0.837	0.904	35.4	19.3
TTV 65	0.827	0.847	0.827	0.857	37.7	28.7
TTV 77	0.834	0.879	0.834	0.899	36.2	20.1
TTV 88	0.830	0.861	0.830	0.920	37.1	15.9
TTV 90	0.834	0.845	0.834	0.891	36.1	21.8
TTV 95	0.839	0.885	0.839	0.941	35.1	11.8
TTV 105	0.836	0.900	0.836	0.940	35.7	12.0
TTV 106	0.839	0.868	0.839	0.897	35.1	20.6
TTV 111	0.839	0.881	0.839	0.932	35.2	13.7

Note: The possible optical transitions in order of increasing energy: $^2B_{1g}\rightarrow{}^2E_g$ > $^2B_{1g}\rightarrow{}^2B_{2g}$ > $^2B_{1g}\rightarrow{}^2A_{1g}$. The transition $^2B_{1g}\rightarrow{}^2E_g$ is usually not observed due to its overlapping with intense charge transfer band in UV region of the spectra. The other two transitions are usually observed as one broad band, which can be fitted by two peaks attributable to $^2B_{1g}\rightarrow{}^2B_{2g}$ and $^2B_{1g}\rightarrow{}^2A_{1g}$ transitions.

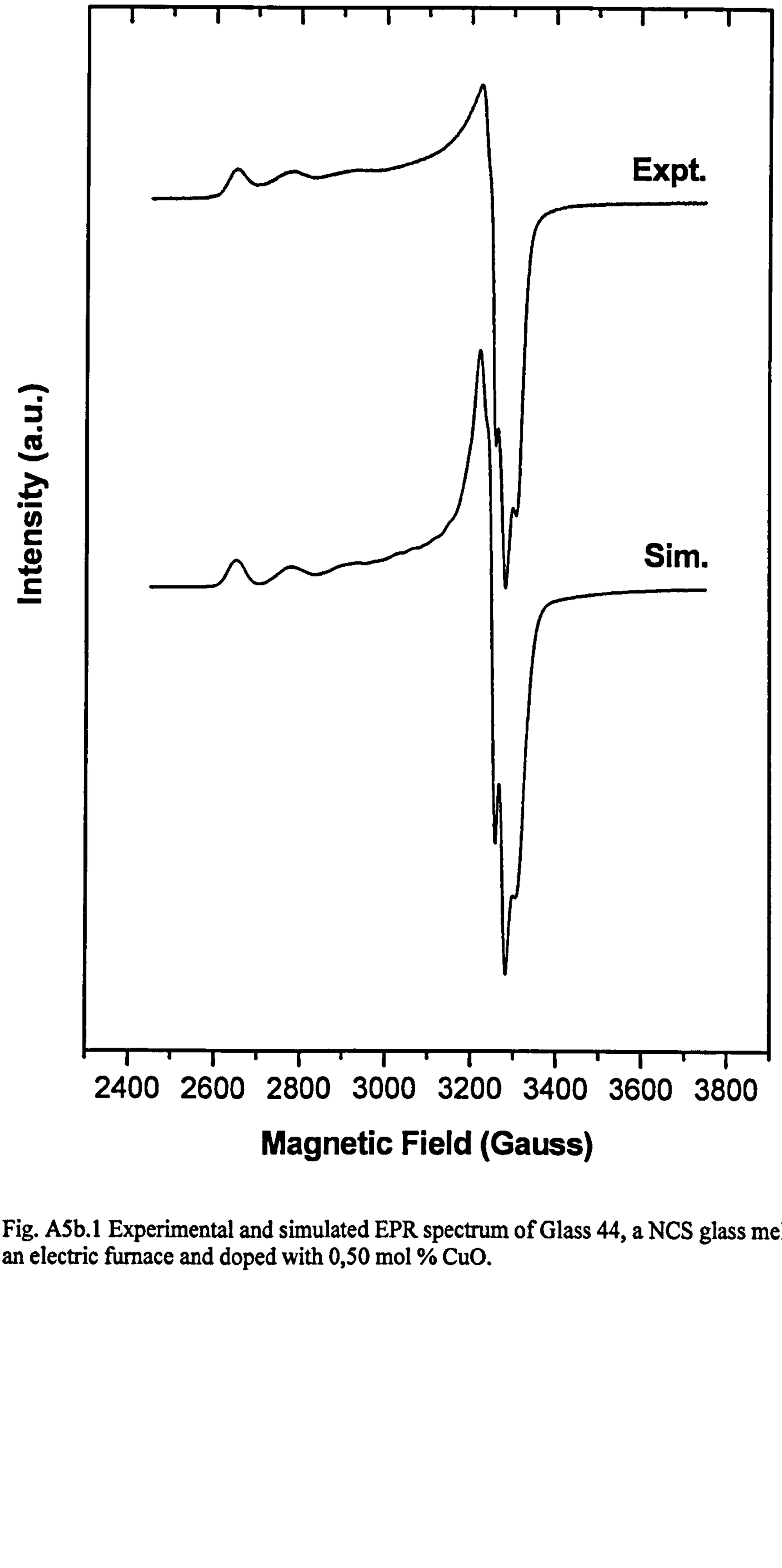

Fig. A5b.1 Experimental and simulated EPR spectrum of Glass 44, a NCS glass melted in an electric furnace and doped with 0,50 mol % CuO.

Annex 6

The fitted spectra and parameters for the Fe-doped NCS glasses melted in an electric furnace

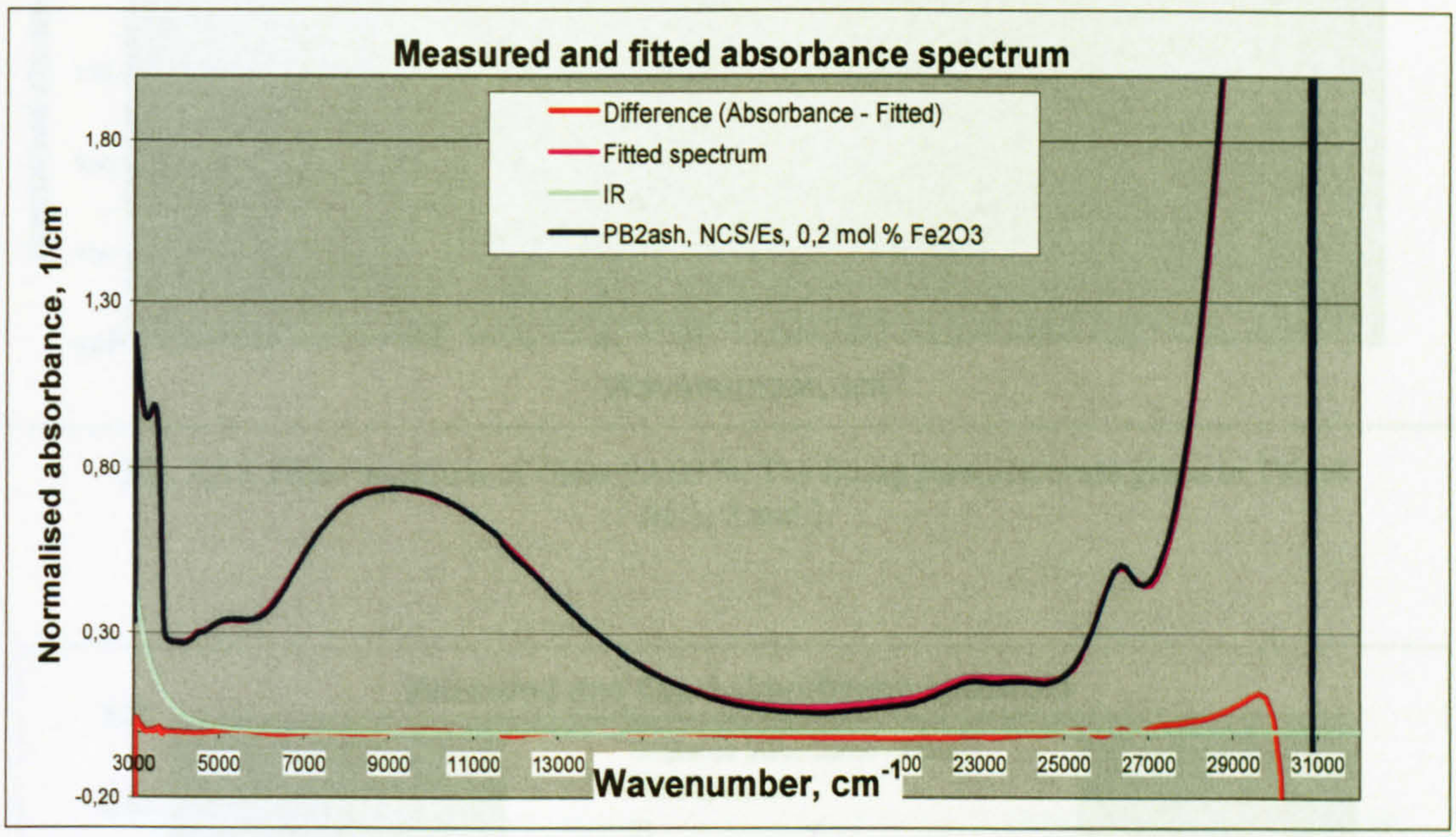

Fig. A6.1 Fitted spectrum of Glass PAB2ash. The fitting parameters as for Glass 246.

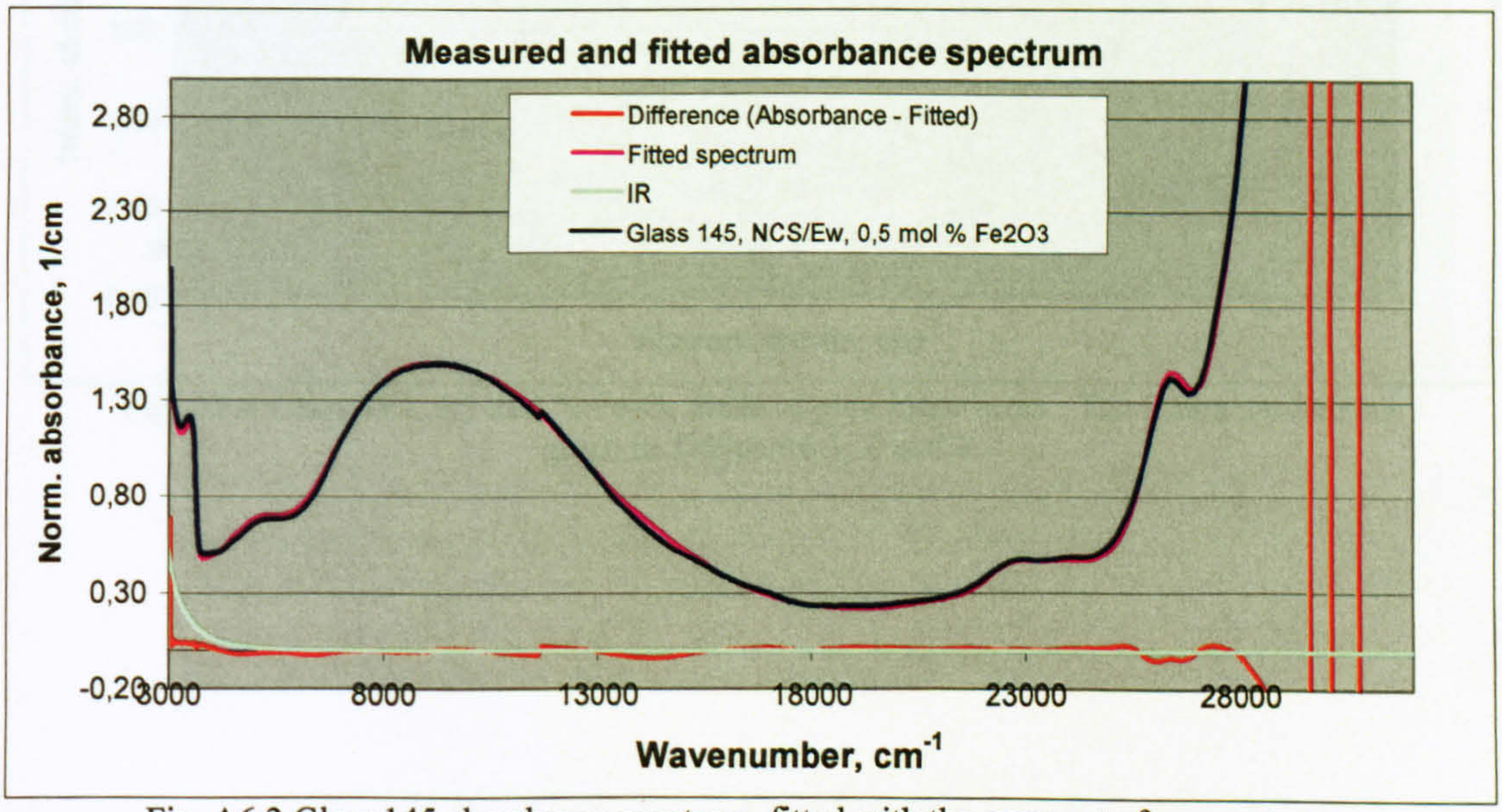

Fig. A6.2 Glass 145 absorbance spectrum, fitted with the same set of parameters as Glasses 245 and 246.

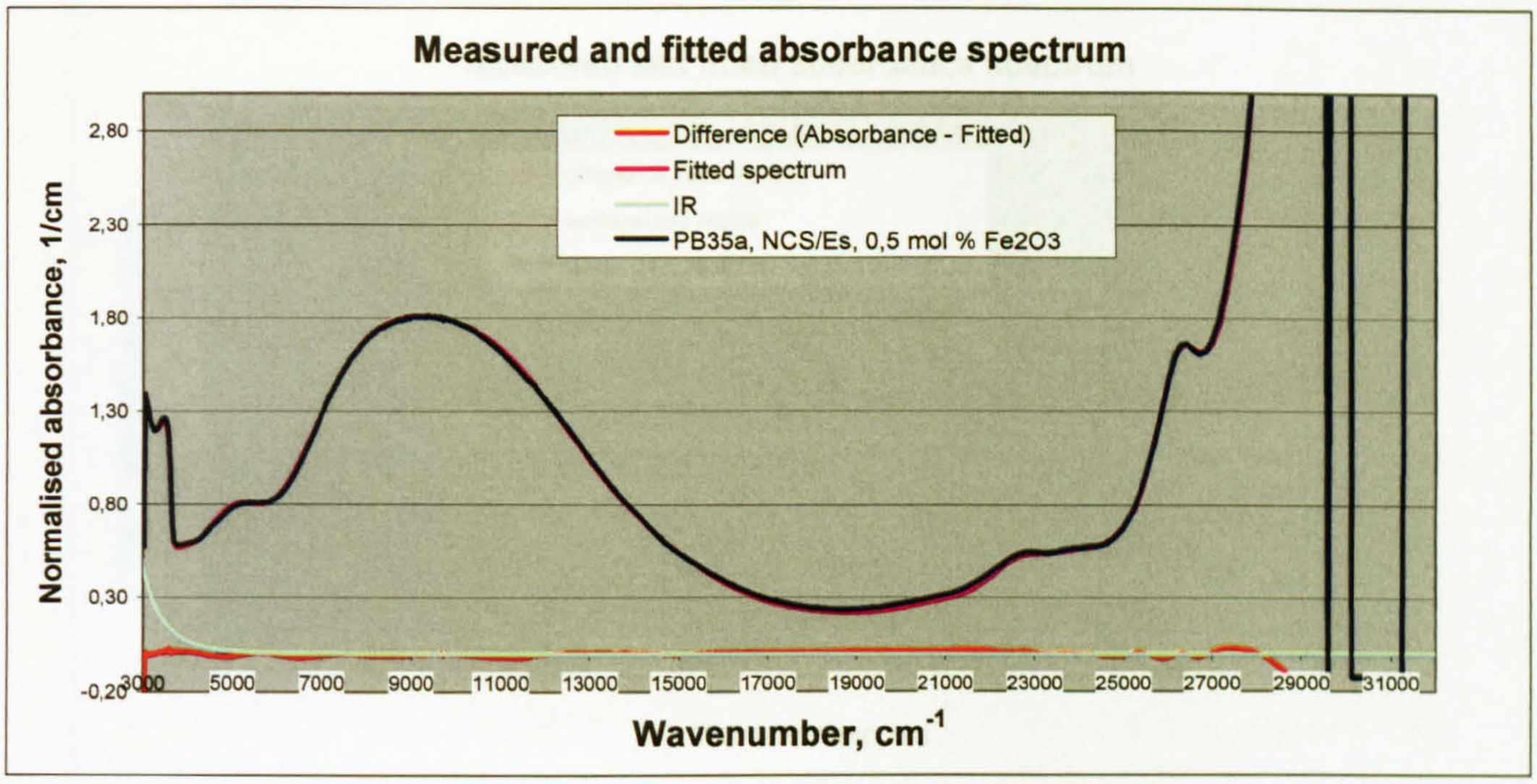

Fig. A6.3 Fitted spectrum of Glass PAB35a. The fitting parameters are given in Tables A6.1, 2 and 3.

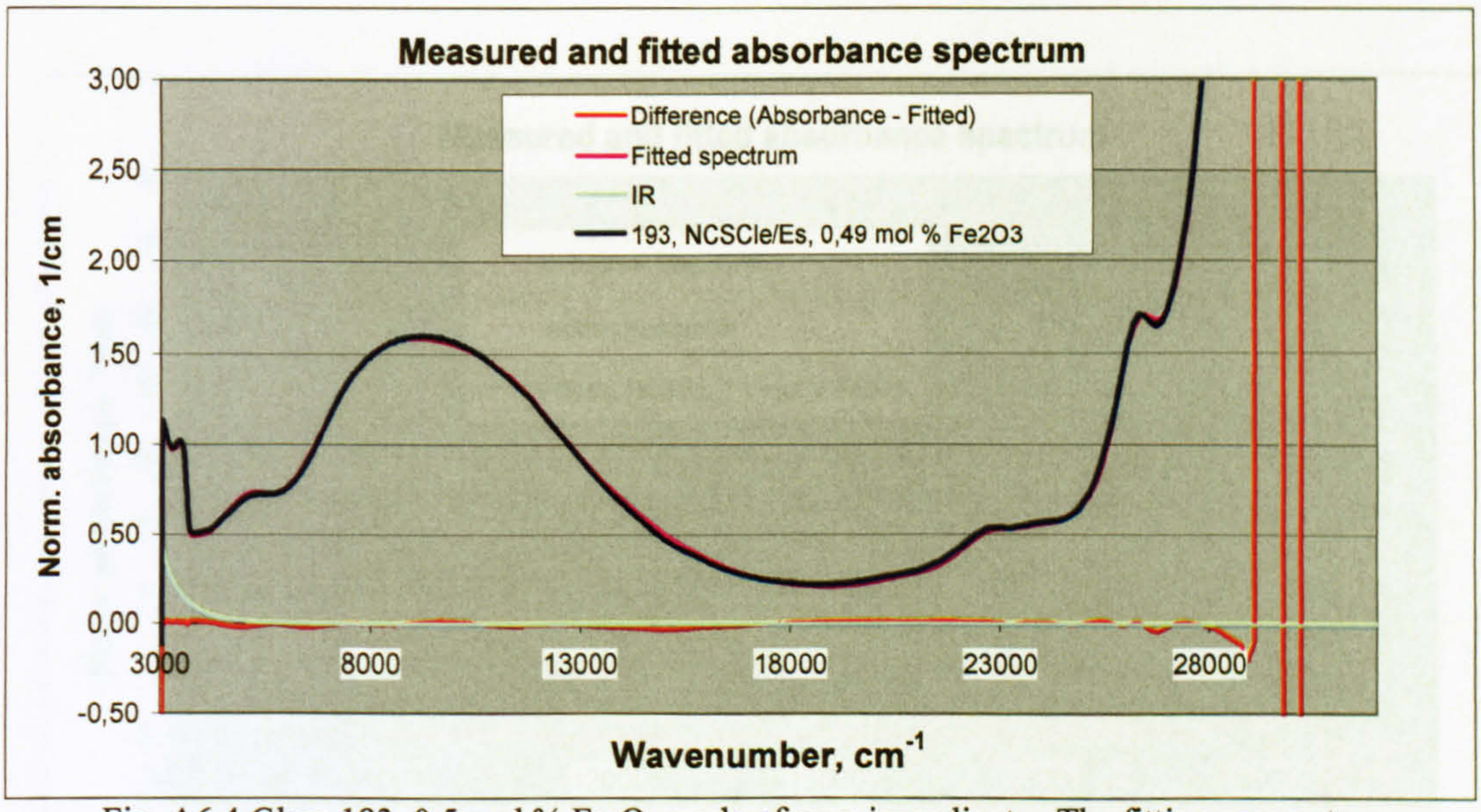

Fig. A6.4 Glass 193, 0.5 mol % Fe_2O_3 made of pure ingredients. The fitting parameters given in Tables A6.1, 2 and 3.

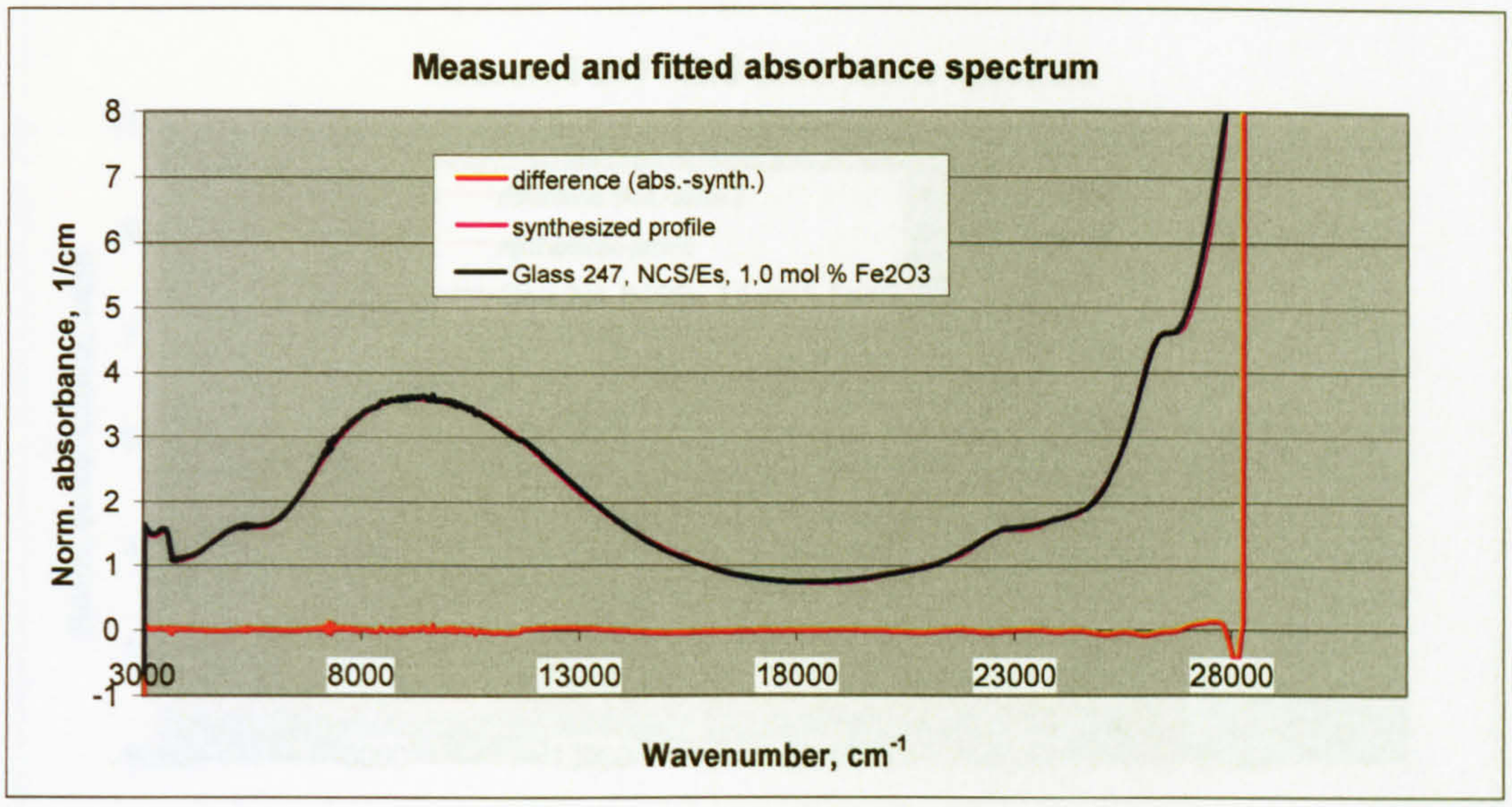

Fig. A6.5 Fitted spectrum of Glass 247. The fitting parameters given in Tables A6.1, 2 and 3.

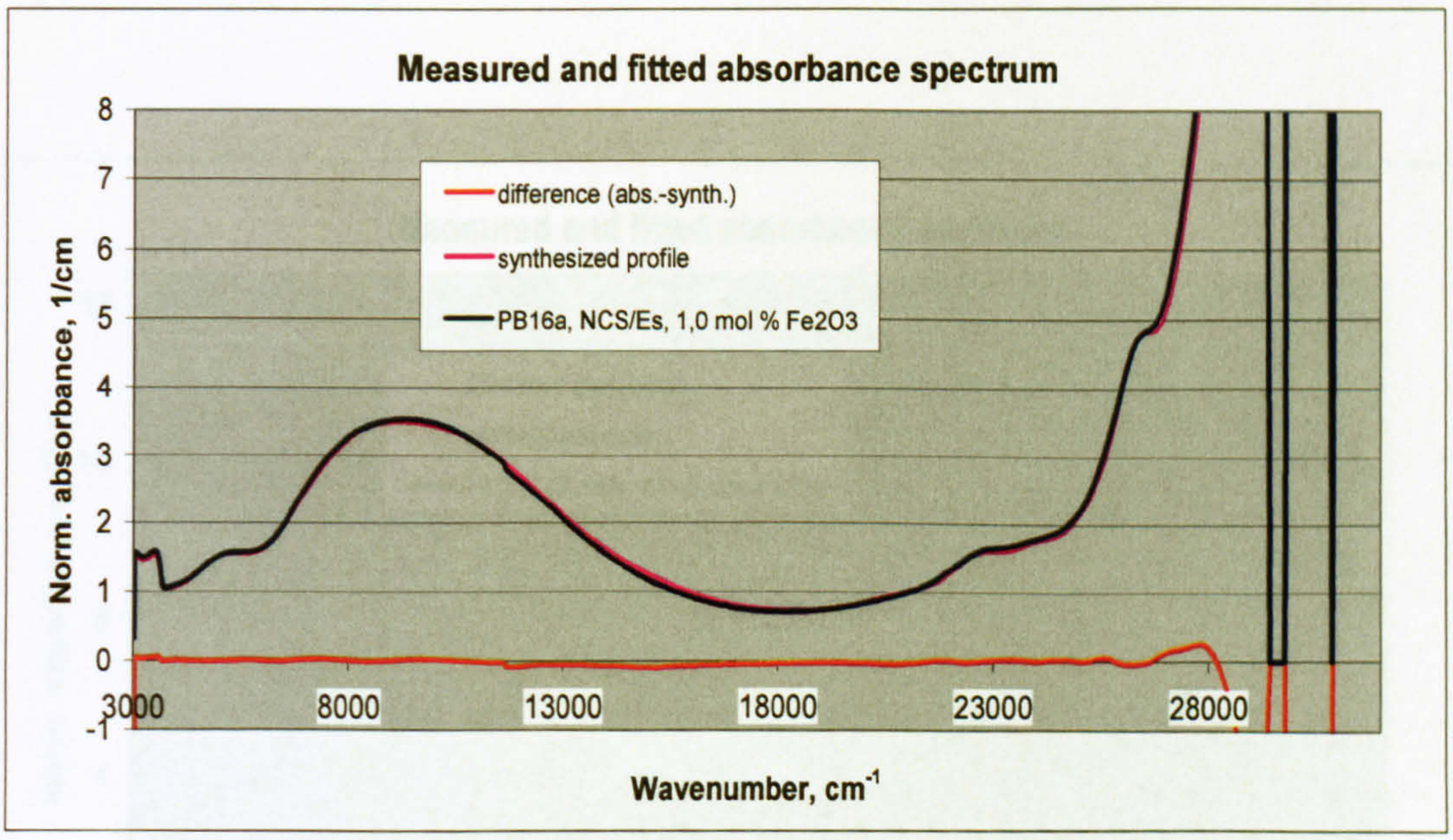

Fig. A6.6 Fitted spectrum of Glass PAB16a. The fitting parameters are given in Tables A6.1, 2 and 3.

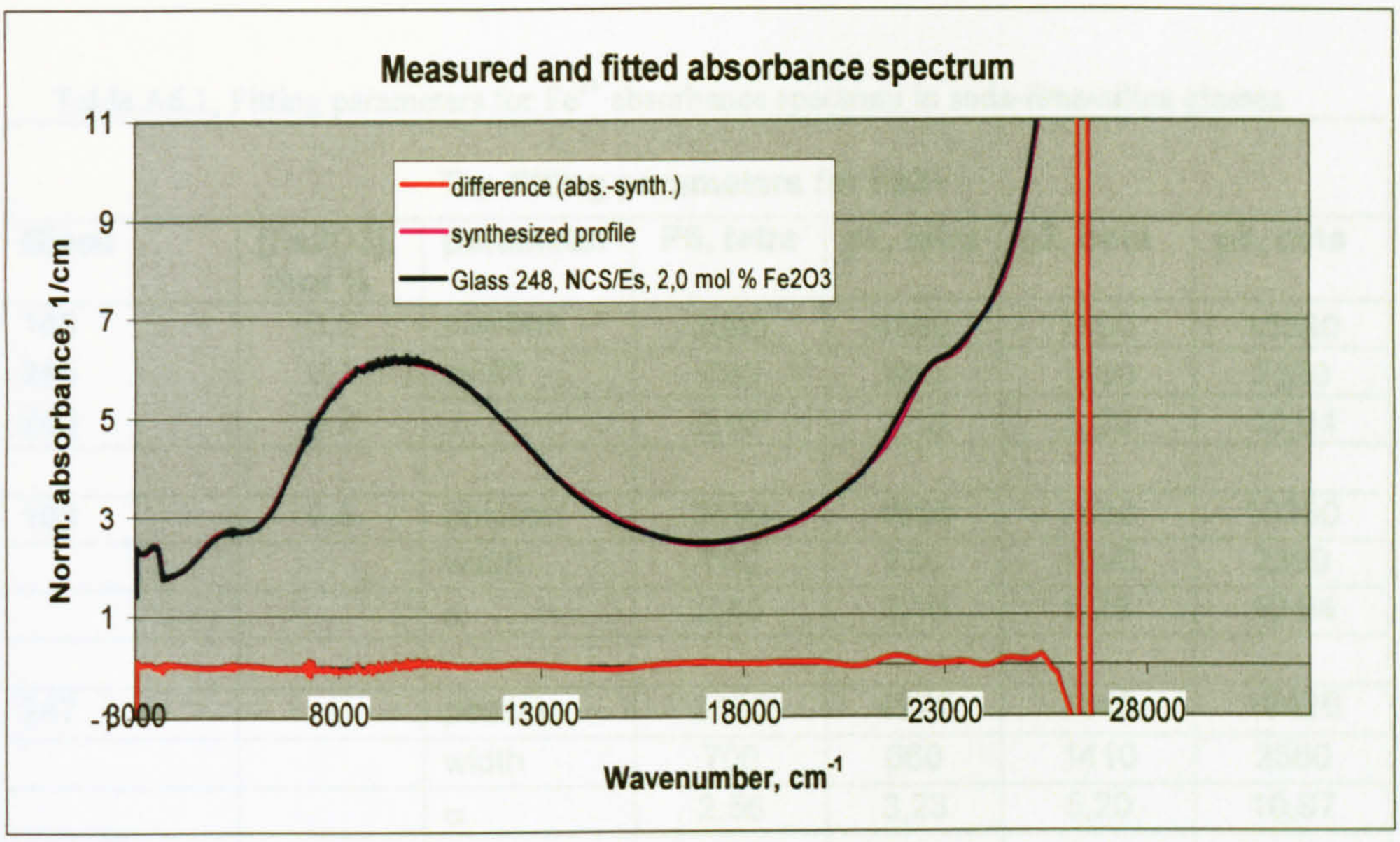

Fig. A6.7 Fitted spectrum of Glass 248. The fitting parameters are given in Tables A6.1, 2 and 3.

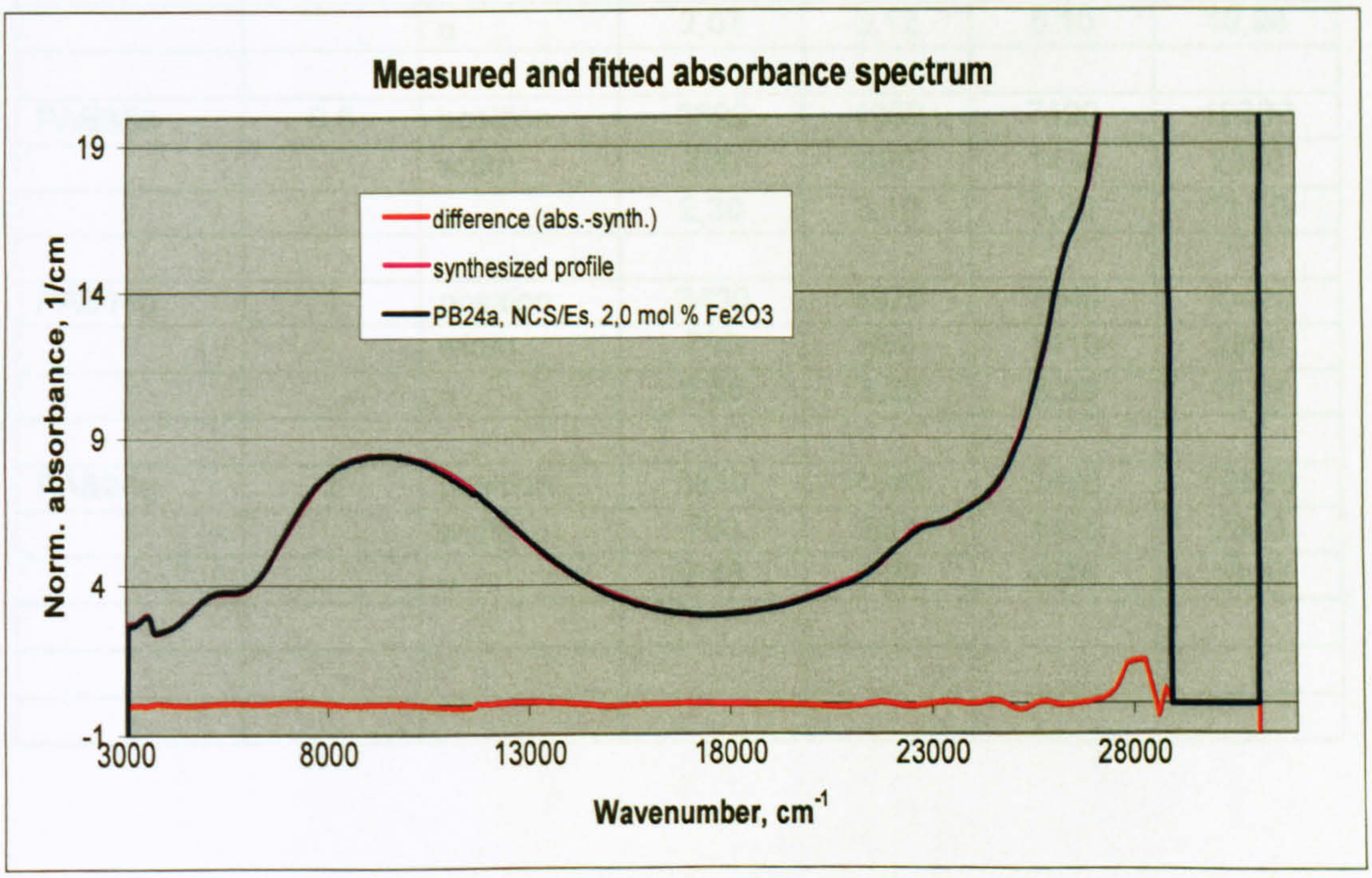

Fig. A6.8 Fitted spectrum of Glass PAB24a. The fitting parameters are given in Tables A6.1, 2 and 3.

Table A6.1, Fitting parameters for Fe^{2+} absorbance spectrum in soda-lime-silica glasses

The fitting parameters for Fe2+						
Glass	**[Fe2O3], mol %**	**parameter**	**P5, tetra**	**p1, tetra**	**p2, octa**	**p3, octa**
145	0,5	position	3590	4950	7490	10380
245	0,1	width	700	660	1430	2390
246	0,2	α	2,07	3,18	5,20	10,94
193	0,5	position	3590	4980	7530	10380
		width	700	630	1390	2390
		α	2,40	3,16	5,20	10,94
247	1	position	3490	4970	7540	10420
		width	700	660	1410	2350
		α	2,56	3,23	5,20	10,97
248	2	position	3510	4990	7590	10520
		width	700	660	1410	2350
		α	2,48	3,19	5,20	10,97
PAB2ash	0,2	position	3540	4920	7490	10300
		width	700	660	1400	2390
		α	2,07	3,12	5,10	10,94
PAB35a	0,5	position	3590	4960	7490	10380
		width	700	620	1430	2350
		α	2,30	3,10	5,20	11,10
PAB16a	1	position	3490	4970	7540	10420
		width	700	660	1410	2350
		α	2,56	3,23	5,20	10,97
PAB24a	2	position	3510	4990	7590	10520
		width	700	680	1410	2350
		α	2,48	3,22	5,20	10,97

Table A6.2, Fitted parameters for Fe^{3+} in soda-lime-silica glasses

Glass	parameter	p1, octa	p2, octa	p3, octa	p9, octa		p4, tetra	p5, tetra	p6, tetra	p7, tetra
145	position	14700	18350	25190	27250		21550	22740	24020	26220
245, and	Width	1700	2000	530	530		1350	650	650	480
246	α	0,310	0,210	0,255	0,098		0,218	0,270	0,323	0,959
193	position	14800	18650	25190	27250		21550	22740	24020	26220
	Width	1700	2000	530	530		1350	650	650	480
	α	0,278	0,211	0,273	0,220		0,253	0,297	0,354	1,008
Fit2, 247	position	14850	18590	25250	27300		21550	22740	24090	26240
	Width	1700	2000	500	480		1300	650	650	480
	α	0,379	0,355	0,657	0,502		0,406	0,442	0,645	1,413
Fit3, 248	position	14900	18790	25250	27300		21640	22740	24090	26240
	Width	1700	2000	500	480		1280	650	650	480
	α	0,464	0,628	0,956	0,773		0,690	0,649	0,947	1,893
PAB2ash	position	14700	18350	25190	27250		21550	22740	24020	26220
Fit1	Width	1700	2000	530	530		1350	650	650	480
	α	0,262	0,177	0,215	0,083		0,208	0,258	0,308	0,948
PAB35a	position	14700	18350	25190	27250		21550	22740	24020	26220
	Width	1700	2000	530	530		1350	650	650	480
	α	0,291	0,196	0,285	0,092		0,231	0,286	0,342	0,918
PAB16a	position	14850	18590	25250	27300		21550	22740	24090	26240
	Width	1700	2000	500	480		1300	650	650	480
	α	0,372	0,350	0,646	0,494		0,412	0,448	0,654	1,433
PAB24a	position	15080	18900	25250	27300		21640	22740	24090	26240
	Width	1700	2000	480	480		1280	650	650	480
	α	0,564	0,720	0,940	0,835		0,675	0,636	0,927	1,589

Table A6.3 Fitted parameters for The UV-peaks of Fe^{3+} and Fe^{2+} ions

Glass	parameter	Fe^{3+} UV-peak	Fe^{2+} UV-peak
145	position	39360	46700
245	width	3050	5700
246	α	190	100
193	position	39360	46100
	width	3080	5960
	α	180	110
247	position	39290	46400
	width	3150	5990
	α	200	110
248	position	39380	46400
	width	3300	6800
	α	190	120
PAB2ash	position	39340	46700
	width	3050	5700
	α	190	100
PAB35a	position	39380	46300
	width	3080	5960
	α	190	110
PAB16a	position	39260	46400
	width	3190	5990
	α	190	110
PAB24a	position	39220	46400
	width	3160	6550
	α	210	115

Annex 7

The fitted spectra and parameters for the Fe-doped NCS glasses, melted in a gas furnace

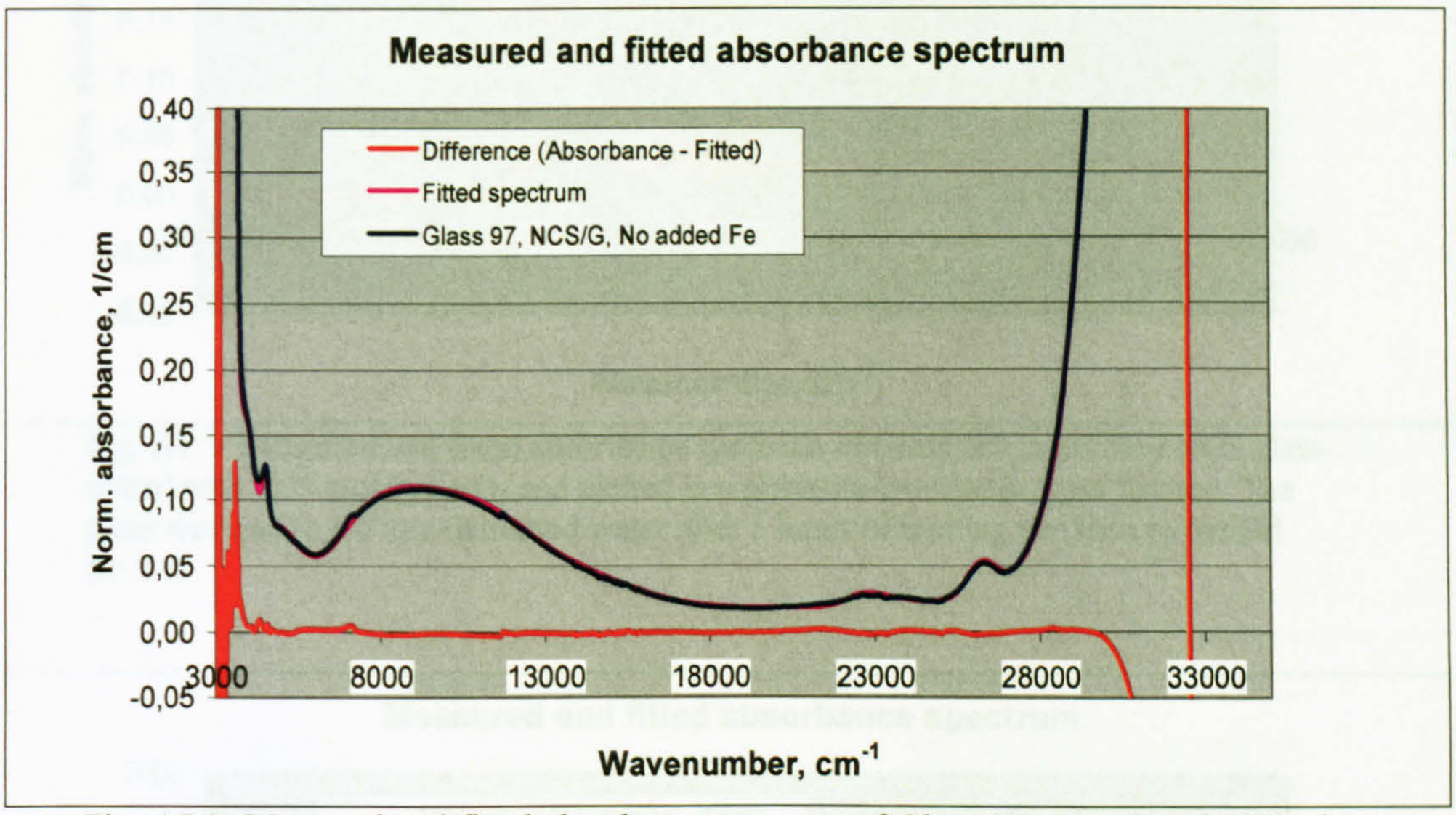

Fig. A7.1 Measured and fitted absorbance spectrum of Glass 97, an undoped NCS glass melted in a gas furnace.

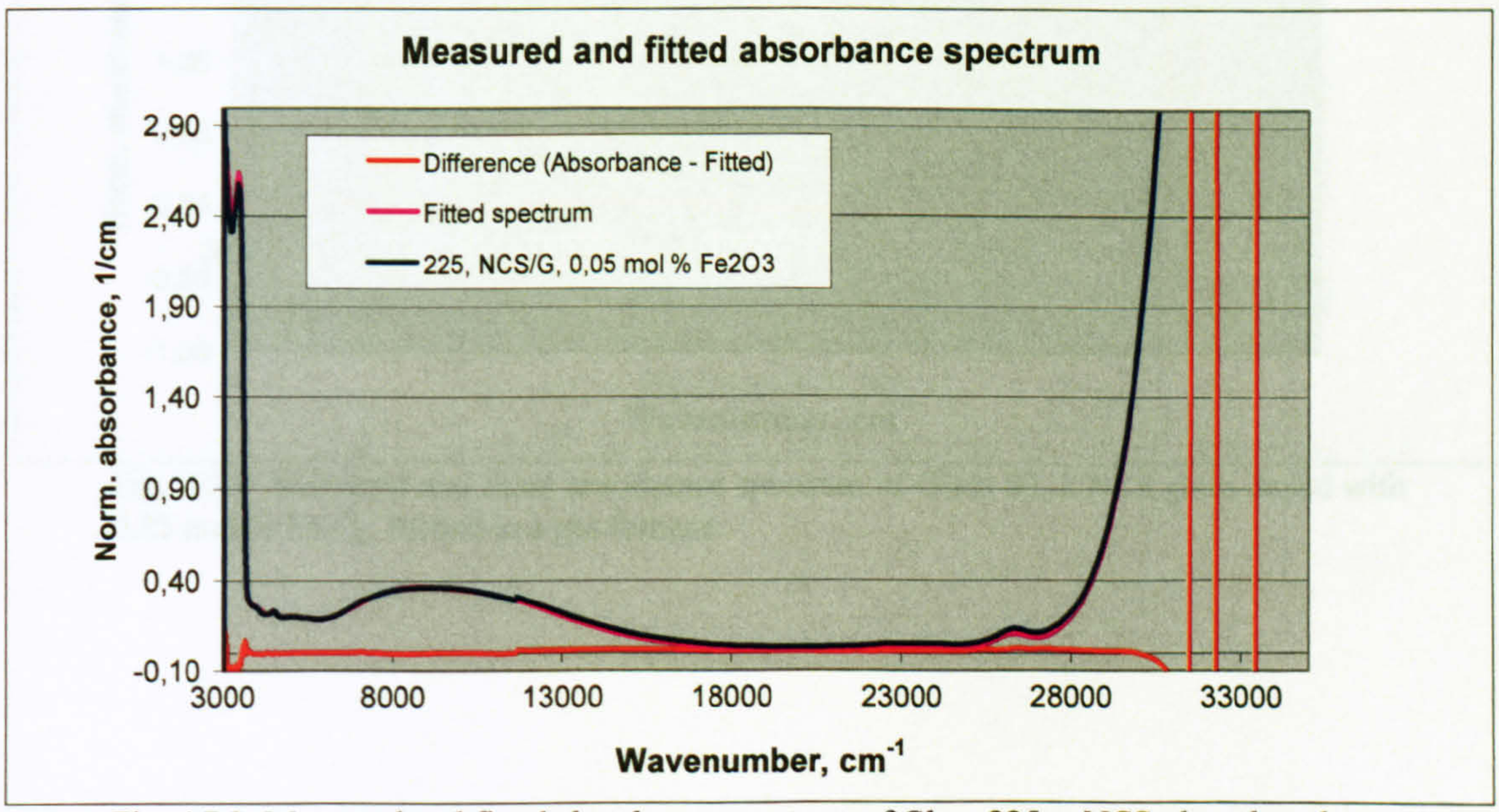

Fig. A7.2 Measured and fitted absorbance spectrum of Glass 225, a NCS glass doped with 0,05 mol % Fe_2O_3 and melted in a gas furnace.

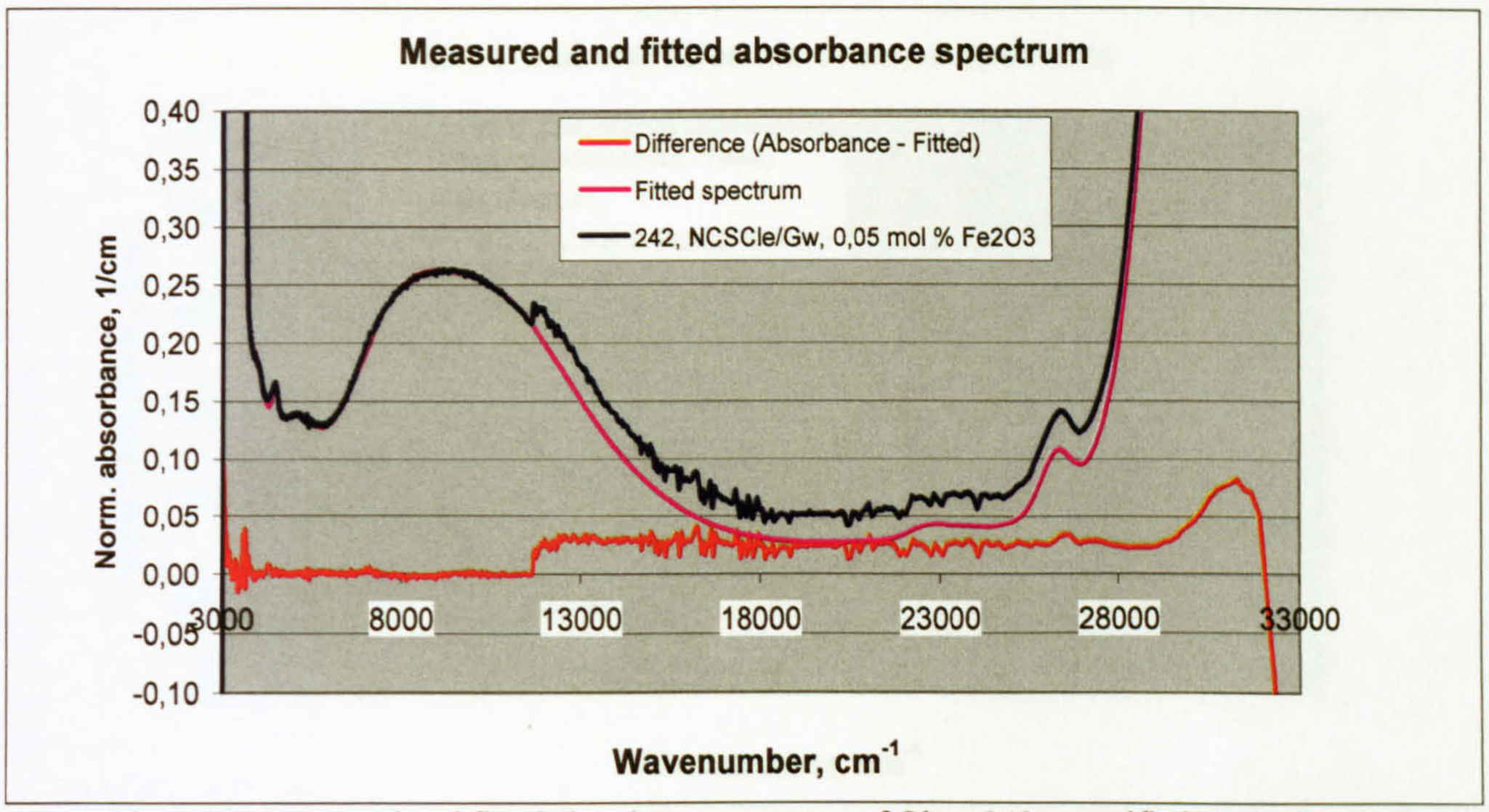

Fig. A7.3 Measured and fitted absorbance spectrum of Glass 242, a purified NCS glass doped with 0,05 mol % Fe_2O_3 and melted in a platinum crucible in a gas furnace. The glass was cast to frit into deionised water after 3 hours of melting and then re-melted for 2 h.

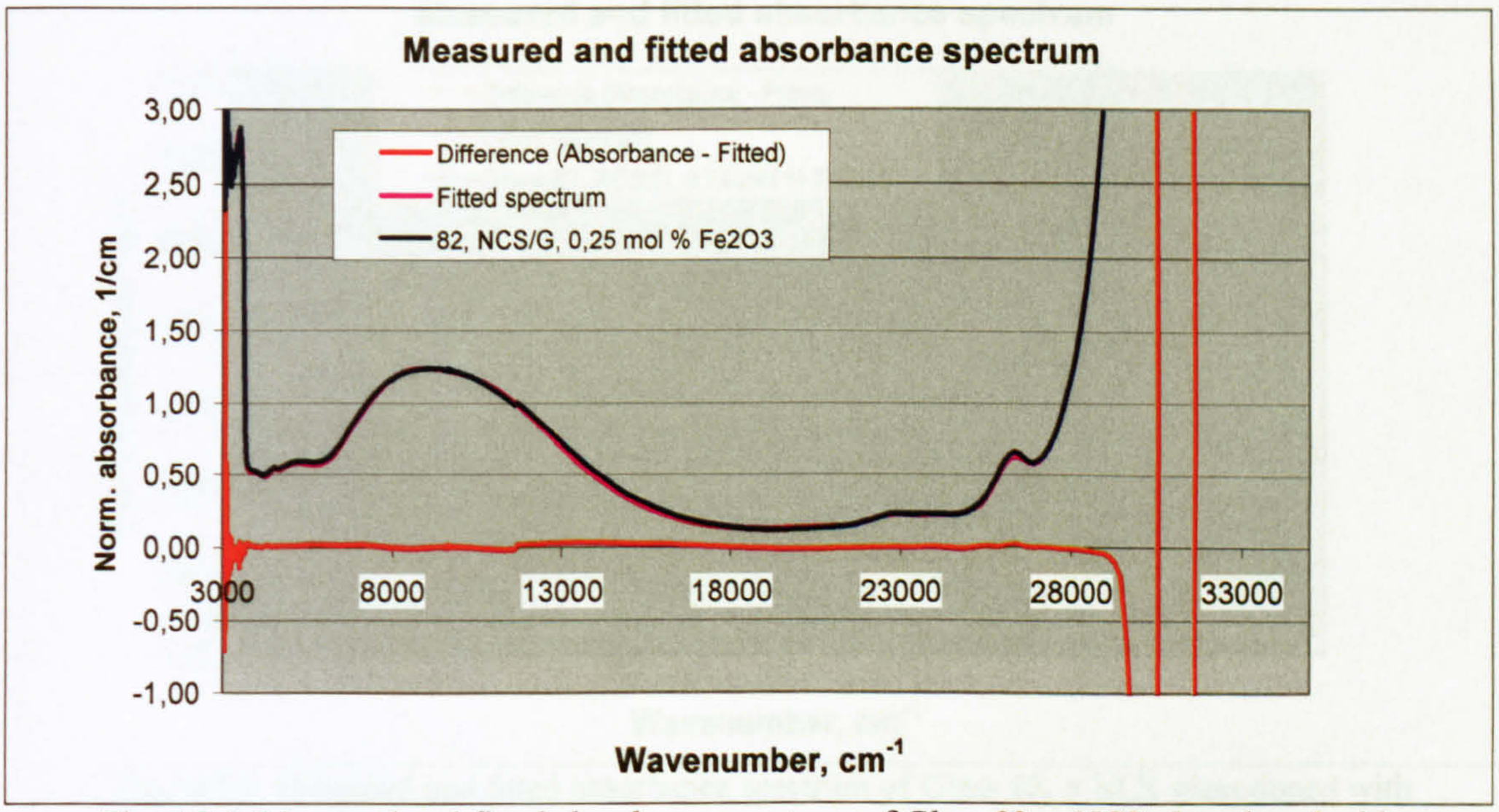

Fig. A7.4 Measured and fitted absorbance spectrum of Glass 82, a NCS glass doped with 0,25 mol % Fe_2O_3, melted in a gas furnace.

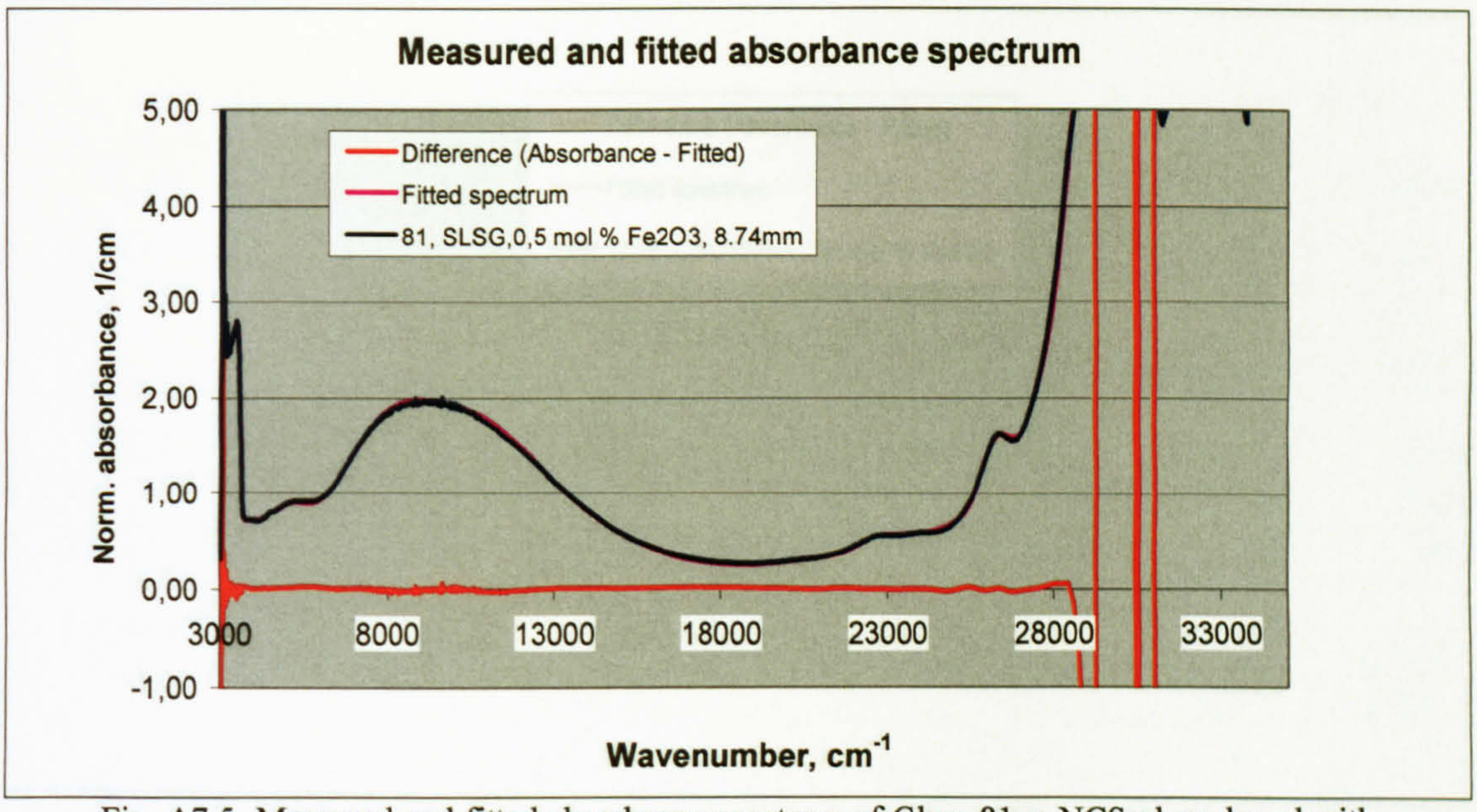

Fig. A7.5 Measured and fitted absorbance spectrum of Glass 81, a NCS glass doped with 0,50 mol % Fe_2O_3, melted in a gas furnace.

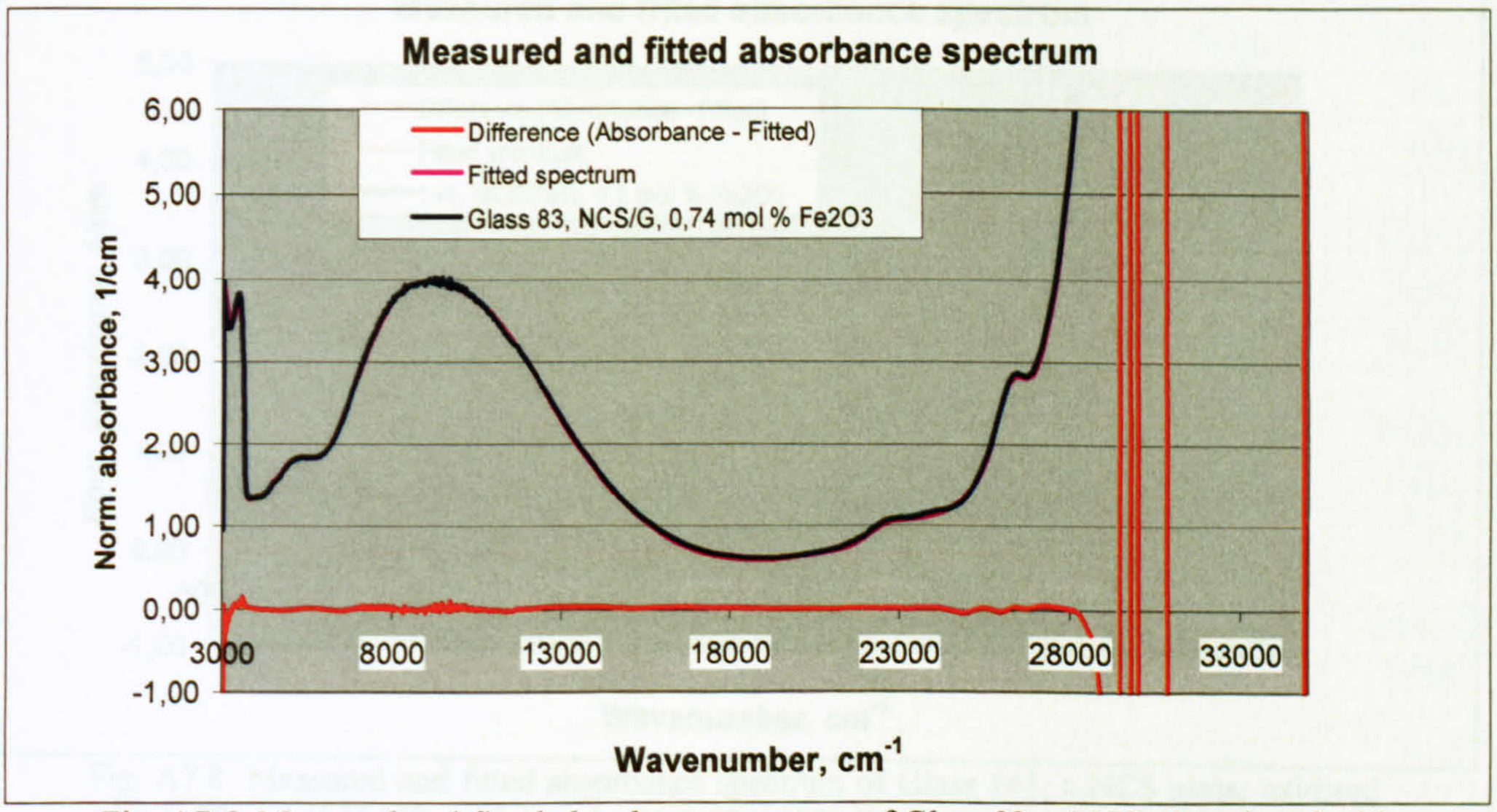

Fig. A7.6 Measured and fitted absorbance spectrum of Glass 83, a NCS glass doped with 0,74 mol % Fe_2O_3, melted in a gas furnace.

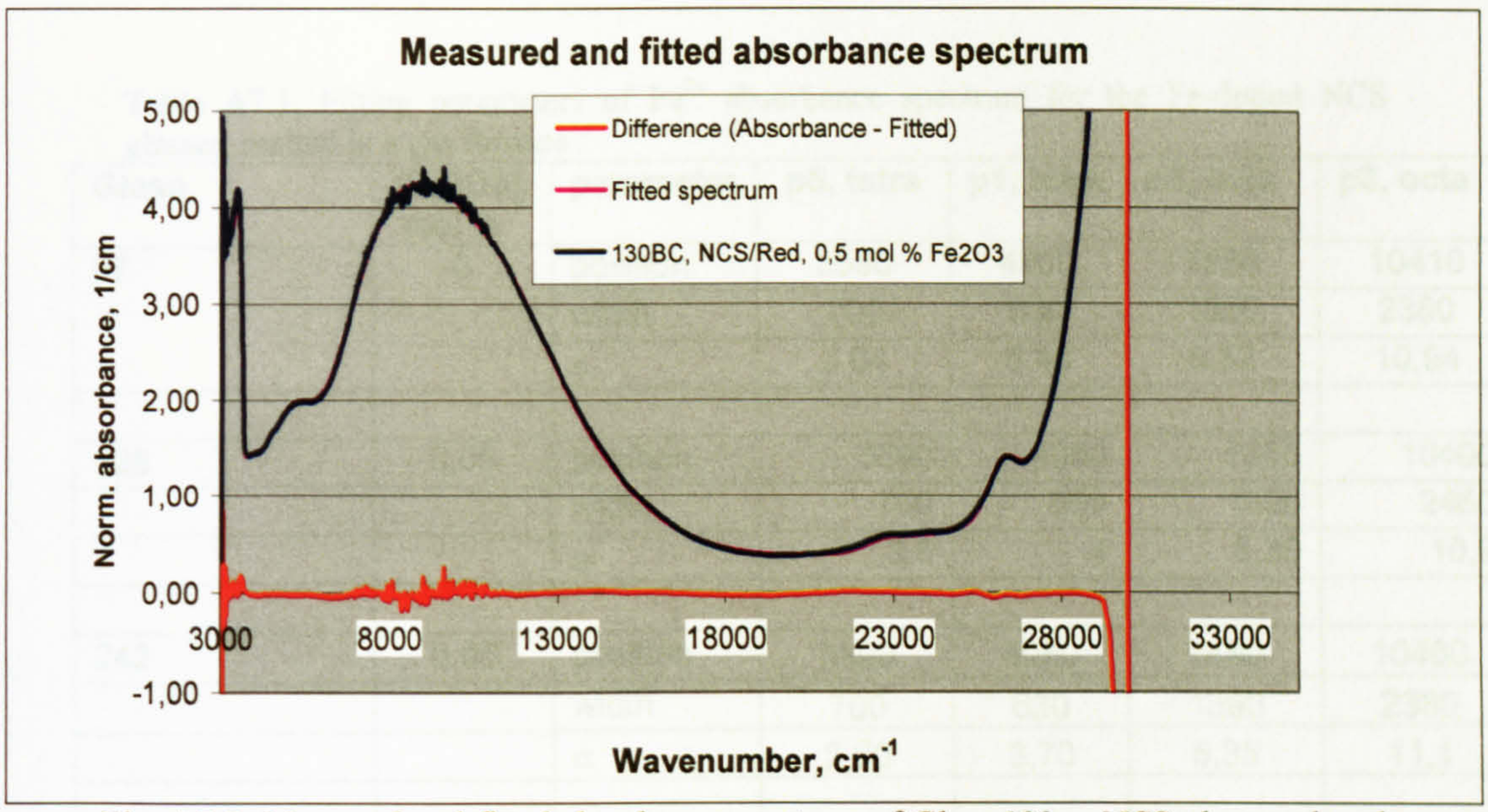

Fig. A7.7 Measured and fitted absorbance spectrum of Glass 130, a NCS glass, reduced with 0,49 mol % carbon and doped with 0,50 mol % Fe_2O_3, melted in a gas furnace.

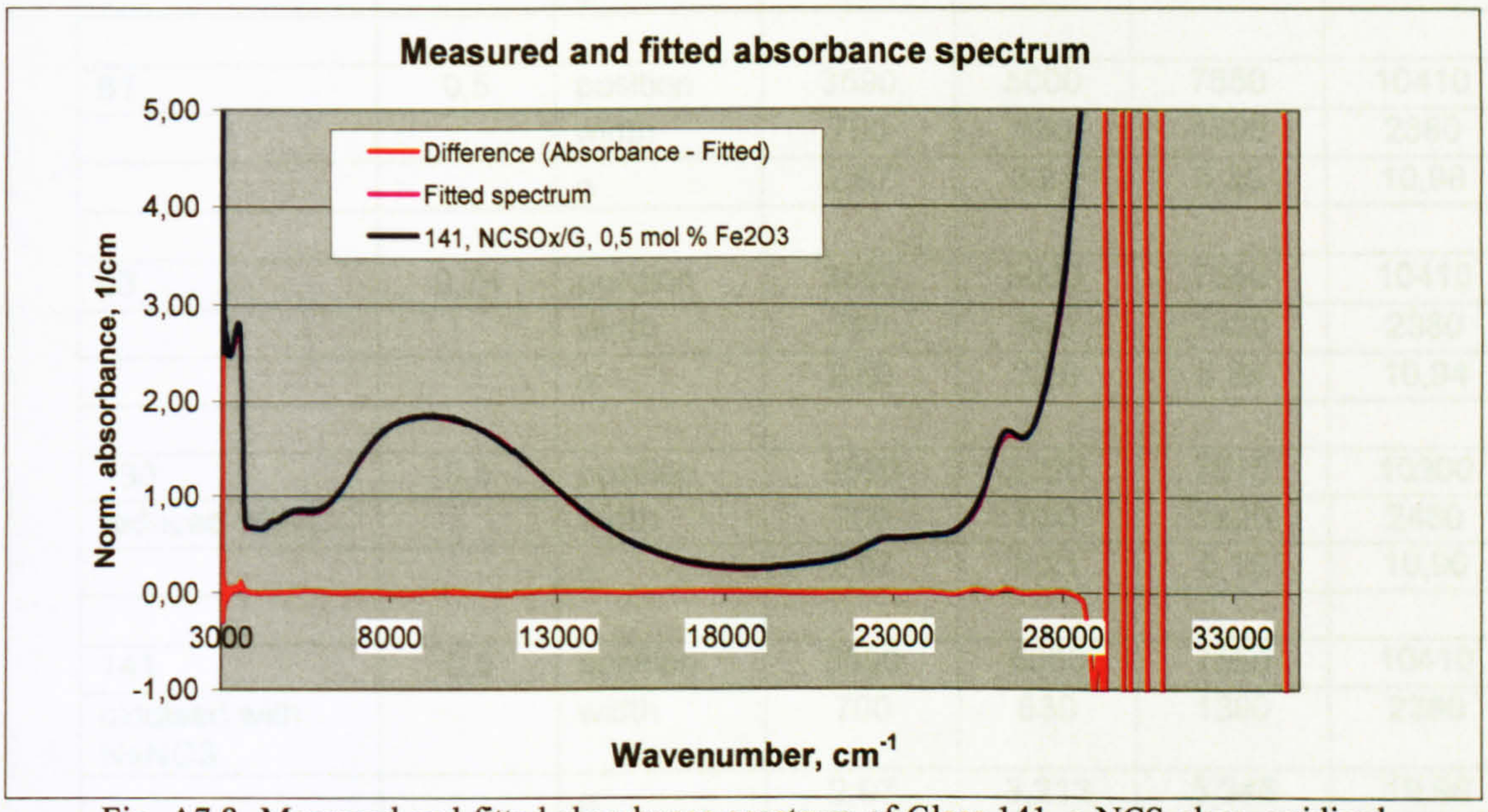

Fig. A7.8 Measured and fitted absorbance spectrum of Glass 141, a NCS glass, oxidised with 1, 00 mol % $NaNO_3$ and doped with 0,50 mol % Fe_2O_3, melted in a gas furnace.

Table A7.1, Fitting parameters of Fe^{2+} absorbance spectrum for the Fe-doped NCS glasses, melted in a gas furnace

Glass	[Fe2O3], mol %	parameter	p5, tetra	p1, tetra	p2, octa	p3, octa
97	0	position	3590	4900	7550	10410
		width	700	630	1390	2380
		α	3,04	5,48	5,32	10,94
225	0,05	position	3590	4950	7530	10400
		width	700	660	1390	2460
		α	3,5	4	5,39	10,9
242	0,05	position	3590	4950	7480	10400
		width	700	630	1390	2380
		α	2,60	3,70	5,35	11,1
82	0,25	position	3590	5000	7550	10400
		width	700	630	1390	2360
		α	3,05	3,4	5,46	10,96
81	0,5	position	3590	5000	7550	10410
		width	700	630	1390	2380
		α	2,97	3,21	5,35	10,98
83	0,74	position	3590	5000	7550	10410
		width	700	640	1420	2380
		α	2,60	3,20	5,33	10,94
130	0,5	position	3590	5020	7570	10300
reduced with C		width	700	630	1420	2480
		α	2,97	3,21	5,15	10,90
141	0,5	position	3590	5000	7550	10410
oxidised with NaNO3		width	700	630	1390	2380
		α	2,97	3,213	5,346	10,98

Table A7.2, Fitted parameters of the Fe^{3+} absorbance spectra for the Fe-doped NCS glasses, melted in a gas furnace

Glass	parameter	p1, octa	p2, octa	p3, octa	p9, octa		P4, tetra	p5, tetra	p6, tetra	p7, tetra
97	position	14900	18540	25140	27250		21510	22750	24020	26200
	width	1700	2000	530	530		1350	650	650	470
	α	0,381	0,280	0,224	0,112		0,198	0,308	0,286	0,660
225	position	14700	18040	25100	27230		21510	22750	24020	26210
	width	1700	2000	530	530		1350	650	650	470
	α	0,375	0,25	0,2	0		0,25	0,28	0,325	0,94
242	position	14800	18340	25140	27250		21510	22750	24020	26200
	width	1700	2000	530	530		1350	650	650	470
	α	0,408	0,3024	0,288	0,096		0,234	0,2912	0,338	0,884
82	position	14800	18540	25140	27250		21510	22750	24020	26200
	width	1700	2000	530	530		1350	650	650	470
	α	0,3536	0,26	0,26	0,104		0,216	0,2688	0,312	0,9024
81	position	14900	18540	25140	27250		21510	22750	24020	26200
	width	1700	2000	530	530		1350	650	650	470
	α	0,306	0,225	0,315	0,225		0,2475	0,308	0,3575	0,99
83	position	14850	18500	25140	27250		21610	22750	24020	26200
	width	1700	2000	530	530		1350	650	650	470
	α	0,477	0,393	0,421	0,211		0,329	0,335	0,419	1,076
130	position	14800	18340	25140	27250		21510	22750	24020	26200
reduced with C	width	1750	2000	530	530		1350	650	650	470
	α	0,4984	0,392	0,224	0,112		0,198	0,2464	0,286	0,8272
141	position	14900	18540	25140	27250		21510	22750	24020	26200
oxidised with NaNO3	width	1700	2000	530	530		1350	650	650	470
	α	0,306	0,225	0,315	0,225		0,2475	0,308	0,3575	1,034

Table A7.3 Fitted parameters for the UV-peaks of Fe^{3+} and Fe^{2+} ions

Glass	parameter	Fe^{3+} UV-peak	Fe^{2+} UV-peak
97	position	39470	46850
	width	2970	5660
	α	1500	900
225	position	38750	47400
	width	2900	5500
	α	1900	900
242	position	39000	47300
	width	2940	5700
	α	1900	1000
82	position	39350	46700
	width	3050	5700
	α	1900	950
81	position	39400	46700
	width	3090	5990
	α	1800	1050
83	position	39380	46700
	width	3130	6000
	α	1700	1000
130	position	39460	46900
reduced with C	width	3030	5700
	α	1700	950
141	position	39400	46700
oxidised with NaNO3	width	3140	5990
	α	1700	1000

Table A7.4 Fitting parameters for the Fe-S chromophore absorbance spectra in Fe- doped NCS glasses, melted in a gas furnace.

Glass		p1	p2	p3	p4	p5
97		15720	23470	28600	34790	24460
		1990	800	1220	2450	3170
		164	48	350	12550	3648
225		15720	23470	28600	34790	24460
		1990	800	1220	2450	3170
		164	48	350	12550	3648
242		15720	23470	28600	34790	24460
		1990	800	1220	2450	3170
		164	48	350	12550	3648
82		15720	23470	28600	34790	24460
		1990	800	1220	2450	3170
		164	48	350	12550	3648
81		15720	23470	28600	34790	24460
		1990	800	1220	2450	3170
		164	48	350	12550	3648
83		15720	23470	28600	34790	24460
		1990	800	1220	2450	3170
		164	48	350	12550	3648
130		15720	23470	28600	34790	24460
reduced with C		1990	800	1220	2450	3170
		1000	48	350	12550	3648
141		15720	23470	28600	34790	24460
oxidised with NaNO3		1990	800	1220	2450	3170
		164	48	350	12550	3648

Annex 8

Absorbance spectra of undoped and low iron NCS glasses

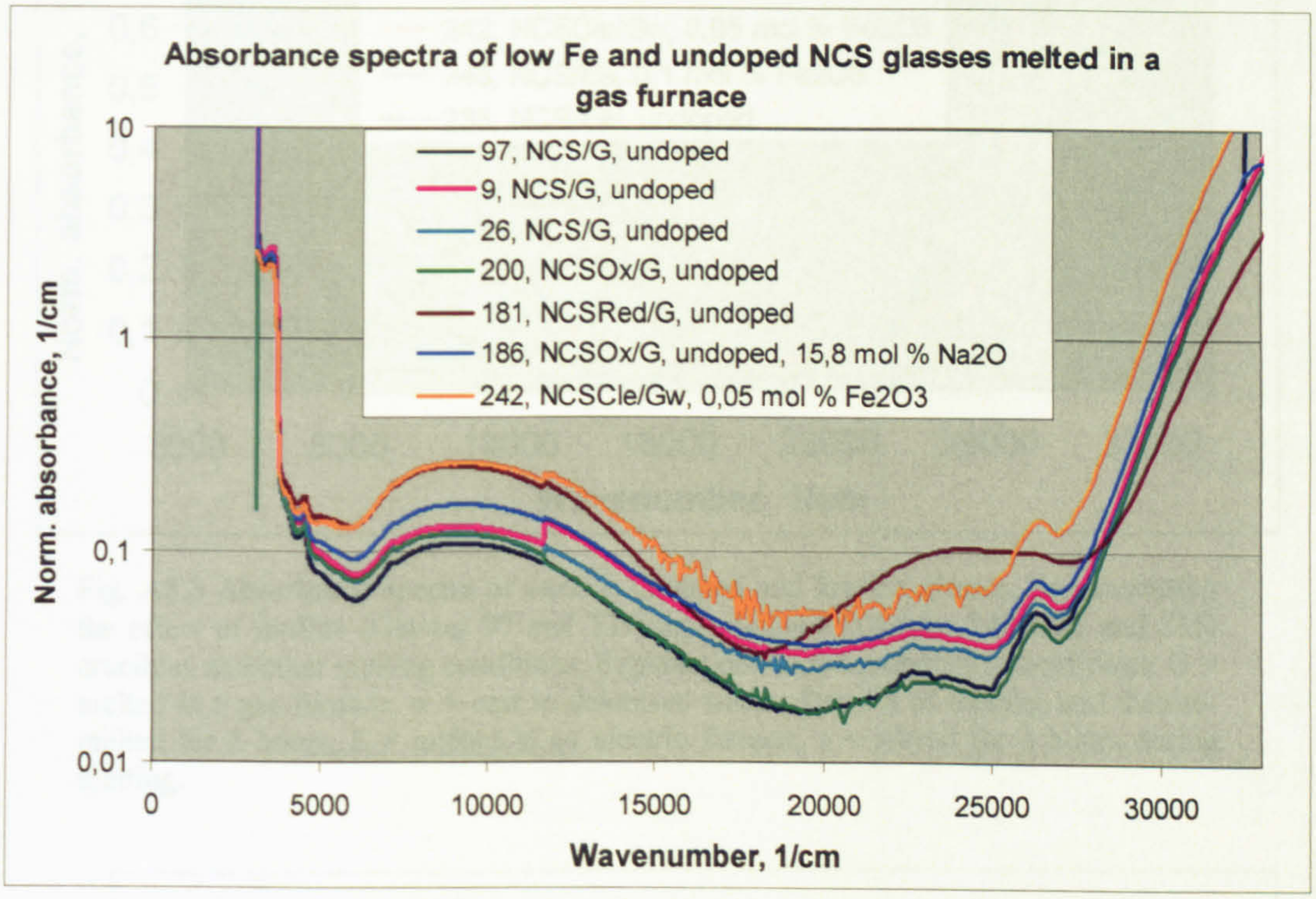

Fig. A8.1 Undoped and low Fe NCS glasses melted in a gas furnace. Glasses 9 and 26 contain more sulphate (0,45 mol %) than the other glasses (0,35 mol %).

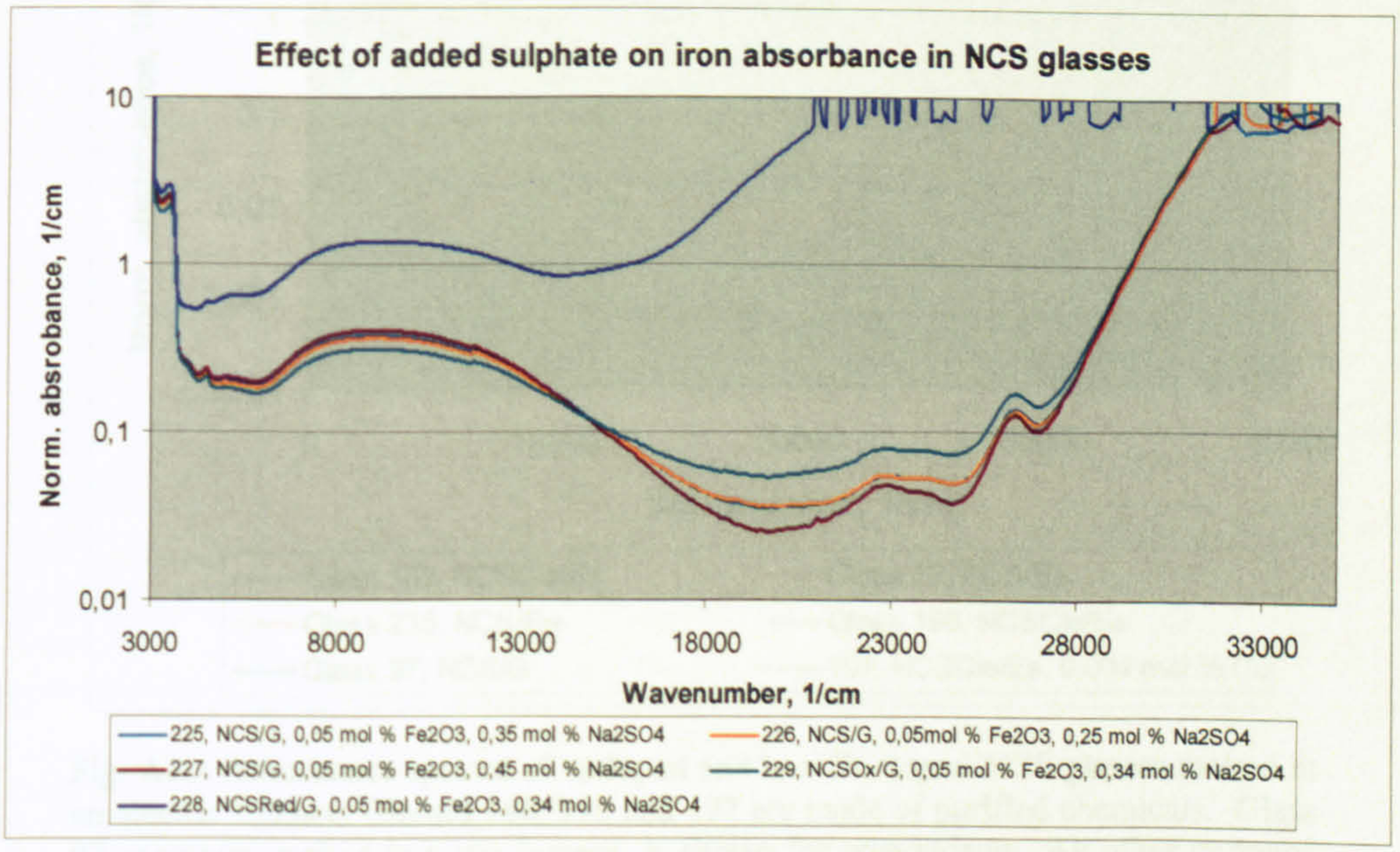

Fig. A8.2 Absorbance spectra of NCS/G glasses doped with 0,05 mol % Fe_2O_3 and various concentration of sulphate. Glass 228 is reduced with 1,96 mol % C and Glass 229 oxidised with 2,00 mol % $NaNO_3$.

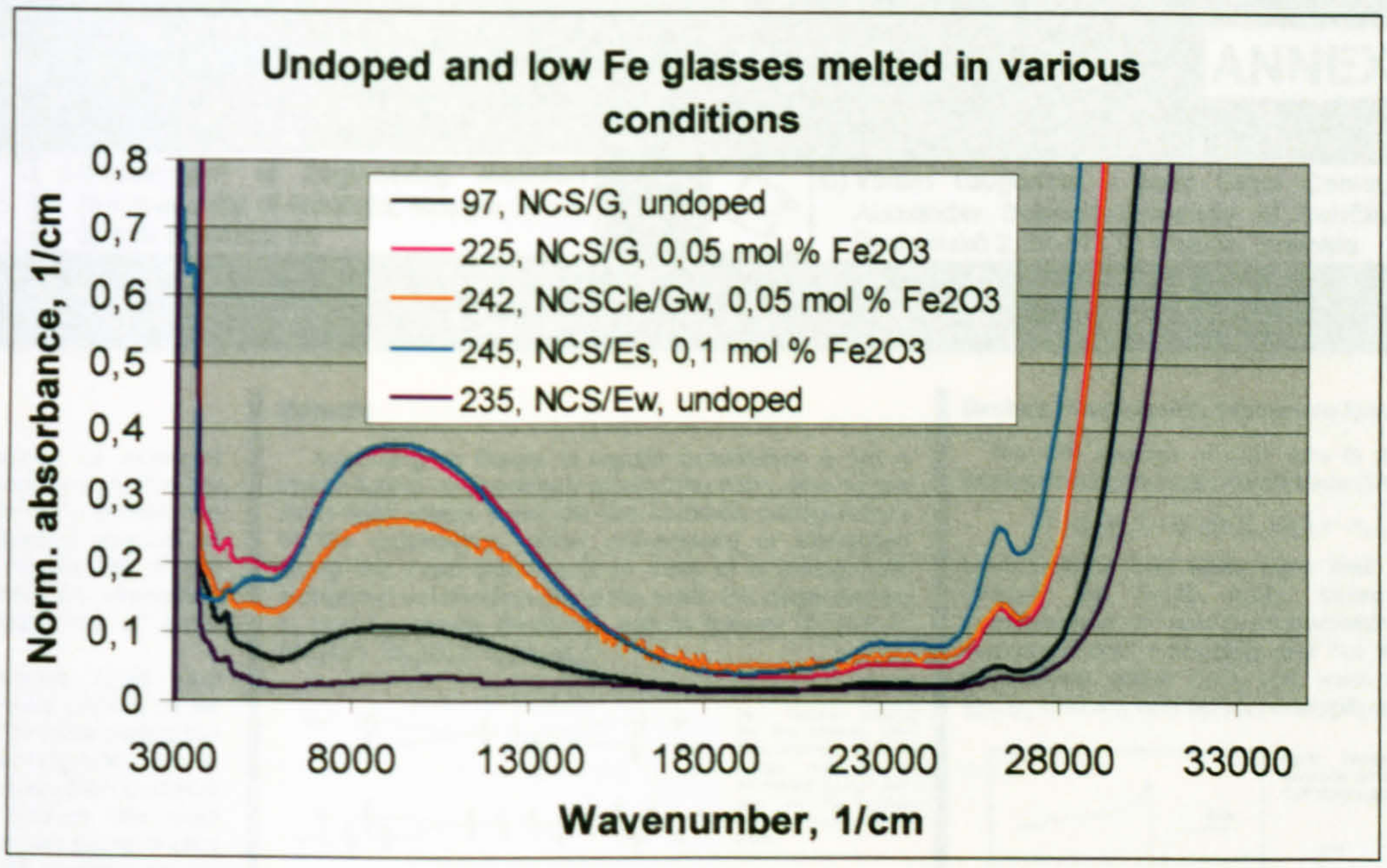

Fig. A8.3 Absorbance spectra of various undoped and low Fe glasses, demonstrating the effect of mullite (Glasses 97 and 225) and platinum (Glasses 242, 245 and 235) crucibles and other melting conditions. Explanations of the preparation conditions: G = melted in a gas furnace, w = cast to deionised water after 3 h of melting and then re-melted for 2 hours, E = melted in an electric furnace, s = stirred for 4 hours during melting.

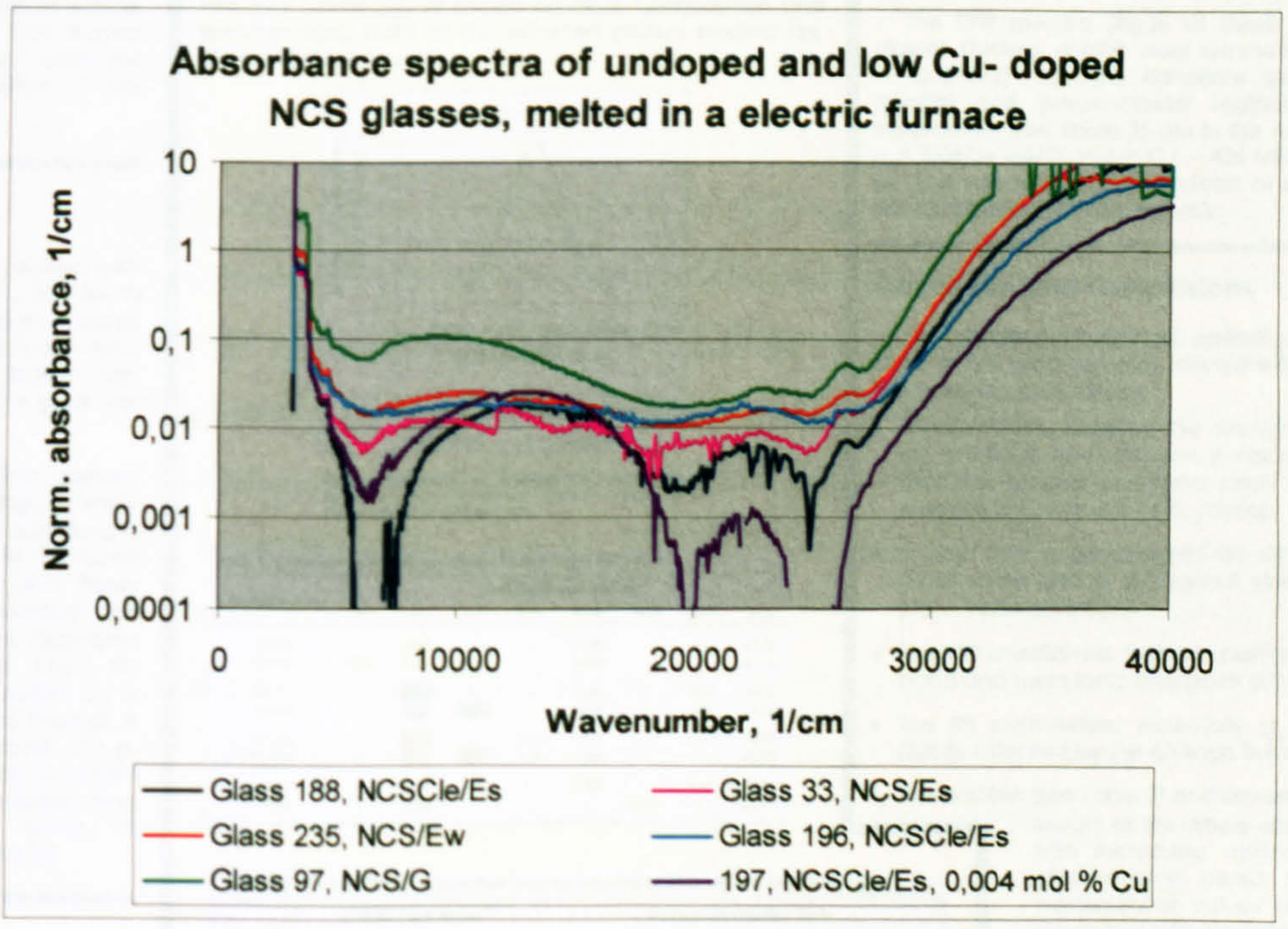

Fig. A8.4 Absorbance spectra of undoped and low Cu-doped NCS glasses melted in an electric furnace. Glasses 188, 196 and 197 are made of purified chemicals. Glass 97 spectrum, melted in a gas furnace, is shown for comparison. All other undoped glasses, except 97, are slightly Cu-contaminated. Fe-contamination is very low in Glasses 196 and 197.

The Coordination Environment of Cu^{2+} – Ions in Silicate Glasses, Studied by Optical Absorption and EPR Spectroscopy: An Effect of Composition on Spectral Parameters and Structure

Tarja T. Volotinen [a], Robert Klement [b] and John M. Parker [a]

ANNEX 9

[a] Department of Engineering Materials The University of Sheffield, Mappin Street, S1 3JD Sheffield, UK

[b] Vitrum Laugaricio – Joint Glass Center, Alexander Dubček University of Trenčín, Študentská 2, SK-911 50 Trenčín, Slovakia

Introduction

For the design and manufacture of coloured glasses, filters and glass optical fibres it is important to know and control optical properties of the glasses. The optical properties such as absorption spectra of different transition metals (dopant), linearity of the absorption on dopant ion concentration, absorption peak position, its width and height, are of great importance.

Electron paramagnetic resonance (EPR) and optical absorption spectroscopy have proved to be powerful experimental techniques for determining the coordination environment of paramagnetic ions in glasses [1]. The variation of glass composition (network formers and/or modifiers) may change the local environment of the transition metal ions incorporated into glasses, leading to ligand field changes usually reflected in the EPR and optical absorption spectra. Moreover, the information on nature of metal-ligand bond can be obtained by correlating EPR and optical data [2].

The properties of a glass can often be altered by the addition of a network modifiers to the network former (e.g. SiO_2) In this work alkali and alkaline earth oxides are varied. The gradual replacement of one kind of alkali oxide (alkaline earth oxide) by another, leads to non-linear change of properties of alkali (alkali-alkaline earth) glasses. This phenomenon is called mixed alkali (mixed oxide) effect [3].

In the present study we report the results of optical absorption and EPR spectroscopy of Cu^{2+}-doped soda-lime-silica and other silicate glasses, which are discussed with respect to the composition of the mixed alkali and alkali earth elements.

Experimental

Preparation of glasses: Silicate glasses, doped with 1 mol.% CuO, containing 60–70 mol.% SiO_2 and 30–40 mol.% of three or four of the following glass network formers or modifiers (Li_2O, Na_2O, K_2O, CaO, BaO, MgO, B_2O_3, Al_2O_3) were melted in mullite crucibles in gas-fired furnace at 1450 °C. Consequently, the glass was treated in a standard way [5].

Instrumentation: The optical absorption spectra were measured at room temperature using a Perkin-Elmer Launch 900 spectrometer over a wavelength range of 200 – 3200 nm. The spectra were corrected for reflection losses, base glass absorption and finally normalised to 1 cm thickness. The corrected and normalised data were fitted using non-linear regression analysis of mathematical software SPSS 12.0.1 for Windows [5]. The EPR spectra were recorded on a Bruker SRC-200D spectrometer, operating at X-band. A 100 kHz magnetic field modulation was used. The g-factors are quoted relative to reference standard marker (DPPH). The EPR spectra were simulated using the program QPOW developed by group of Prof. R.L. Belford (University of Illinois, Urbana) [4].

References

[1] H. Hosono, H. Kawazoe T. Kanawaza, *J. Non-Cryst. Solids* **1979**, 33, 103.
[2] D. Kivelson, R. Neiman, *J. Chem. Phys.* **1961**, *35*, 145.
[3] (a) D.E. Day, *J. Non-Cryst. Solids* **1976**, *21*, 372.; (b) A. H. Dietzel, *Phys. Chem. Glasses* **1983**, *24*, 172.
[4] (a) M.J. Nilges, PhD. Thesis, University of Illinois, Urbana, Illinois.; (b) R.L. Belford and M.J. Nilges, *Computer Simulation of Powder Spctra*, EPR Symposium, 21st Rocky Mountain Conference, Denver, Colorado, August **1979**.
[5] T.T. Volotinen, J.M. Parker, *Analysis of Absorption Peak widths of Cu2+ ions in Silicate Glasses*, XX. Glass Conference, Kyoto, Japan, **2004**.
[6] S.I. Andronenko, R.R. Andronenko, A.V. Vasilev, O.A. Zagrebelnyi, *Glass. Phys. Chem.* **2004**, *30*, 230 and references cited therein.

Results

According to theory, a regular octahedron is not a stable ligand arrangement around the Cu^{2+}. Due to the Jahn–Teller effect, there are two common configurations of the octahedron, either compressed or elongated along the z-axis (see Fig.1). In case of a tetragonally elongated octahedron along the z-axis, the degenerated E_g and T_{2g} energy levels are split as follows: $^2B_{1g}(d_{x^2-y^2})$, $^2A_{1g}(d_{z^2})$, $^2B_{2g}(d_{xy})$, $^2E_g(d_{xz},d_{yz})$.

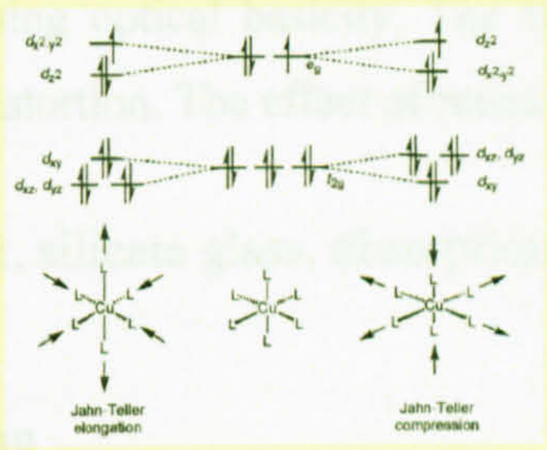

Fig.1: Diagram showing the two possible Jahn–Teller splittings of the d-energy levels in an octahedral $[CuL_6]^{2+}$ complex, and the structural distortions that results from them.

Optical Absorption Spectroscopy

In the VIS region of optical absorption spectra of all glasses studied, only a single asymmetric broad band (at about 12700 cm^{-1}) was observed. This was deconvoluted into two bands [5], as shown on Fig.2. Composition and spectroscopic data of the selected glasses studied are given in Tables 1 and 2.

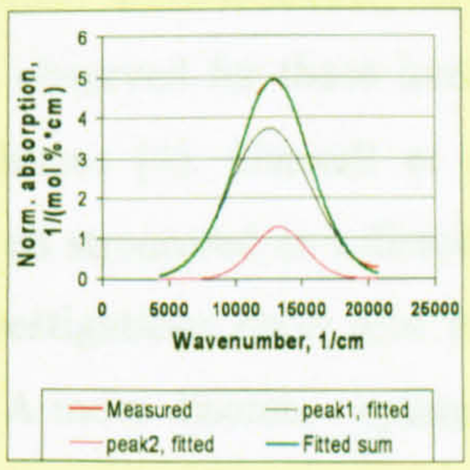

Fig.2.: Representative experimental absorption spectrum of Cu^{2+}-doped glasses and its deconvolution into two bands.

Table 1: Composition of the selected glasses studied doped with CuO

Sample name	Composition (in mol. %)							
	Li_2O	Na_2O	K_2O	MgO	CaO	BaO	Al_2O_3	SiO_2
TTV 28	–	15.05	–	–	14.85	–	–	69.31
TTV 95	7.60	7.61	–	–	14.82	–	–	69.14
TTV 61	–	15.00	–	–	14.85	–	4.95	64.36
TTV 65	–	0.50	14.50	–	14.85	–	4.95	64.36
TTV 105	–	11.10	–	9.90	9.90	–	–	68.73
TTV 106	–	0.53	10.57	9.90	9.90			68.73
TTV 61	–	15.00	–	–	14.85	–	4.95	64.36
TTV 64	–	15.00	–	–	–	14.85	–	69.31

Table 2: EPR and Optical Absorption Data for selected glasses studied doped with CuO

Sample name	EPR SH Parameters[#]				Optical Absorption Data		
	$g_{//}$	$g_\perp$	$\lvert A_{//}\rvert$ (MHz)	$\lvert A_\perp\rvert$ (MHz)	Peak top position, d-d transition (cm^{-1})	Fitted Peak 1 position (cm^{-1})	Fitted Peak 2 position (cm^{-1})
TTV 28	2.381	2.0687	421	43	12887	12450	13560
TTV 95	2.377	2.0670	428	39	13123	12569	13954
TTV 61	2.375	2.0667	425	41	12853	12605	13886
TTV 65	2.376	2.0668	416	45	12407	12043	12553
TTV 105	2.374	2.0670	428	43	13404	12892	14003
TTV 106	2.370	2.0685	435	46	13123	12801	13557
TTV 61	2.375	2.0667	425	41	12853	12605	13886
TTV 64	2.386	2.0684	416	43	12594	12542	13063

[#] The hyperfine splitting constants are given in MHz (for conversion to cm^{-1}, divide values by 3×10^4)

Electron Paramagnetic Resonance Spectroscopy

The EPR spectra of Cu^{2+} ions in silicate glasses were analysed using the spin Hamiltonian (SH)

$$\hat{H} = g_{//}\beta H_z \hat{S}_z + g_\perp \beta (H_x \hat{S}_x + H_y \hat{S}_y) + A_{//} \hat{I}_z \hat{S}_z + A_\perp (\hat{I}_x \hat{S}_x + \hat{I}_y \hat{S}_y)$$

were symbols and terms have their usual meaning; for $^{63,65}Cu^{2+}$ ion $S=1/2$, $I=3/2$. Molecular orbital (MO) coefficients α^2, β_1^2 and β characterizing the covalency of in-plane σ and π bonding and out of plane π bonding, respectively, within CuO_6 unit, were estimated from EPR ($g_{//}$, $g_\perp$ and $A_{//}$) and optical absorption data.

Fig.3.: Representative experimental and computer simulated X-band EPR spectrum of Cu^{2+} silicate glass.

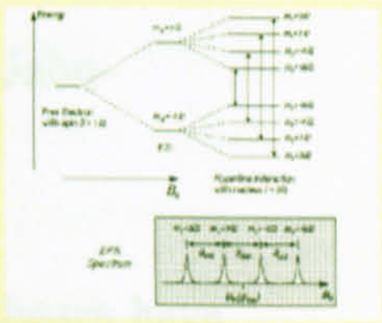

Scheme1: Instructive scheme showing the origin of the hyperfine splitting.

The EPR spectra (Fig.3) of these Cu^{2+}-doped silicate glasses studied, exhibit axial symmetry with three of four $^{63,65}Cu(I=3/2)$ hyperfine transitions (see Scheme1) in the parallel and perpendicular regions resolved. The SH parameters (see Table 2) are in the range: $g_{//}$ = 2.37–2.39, $g_\perp$ = 2.067 – 2.070, $|A_{//}|$ = 411 – 435 MHz, $|A_\perp|$ = 39 – 48 MHz [6]. The values of MO coefficients of α^2 and β_1^2 estimated are ≈ 0.83 and 0.92, respectively.

Discussion and Conclusions

The detailed analysis of optical absorption and EPR data of the glass samples, doped with Cu^{2+} ions, point to the following conclusions:

- The g-values, obeying the relationship $g_{//} > g_\perp > g_e$ (g_e = 2.0023, free electron g value) point to the fact, that the ground electronic state of a paramagnetic electron in Cu^{2+} is $d_{x^2-y^2}$ ($^2B_{1g}$ state).
- A Cu^{2+} ion is coordinated by six oxygen ions in an octahedron with a tetragonal elongation along z-axis (Jahn-Teller distortion).
- The MO coefficients indicate partial covalency of the σ-bond and more ionic character of in-plane π-bonding.
- The SH parameters, especially $g_{//}$ and $A_{//}$, are only slightly affected by the change in composition of glass.
- The position (see Table 2) and separation (≈ 1250 cm^{-1} or lower) of the fitted absorption peaks vary with increasing optical basicity (OB) of glasses; both peaks shift towards lower wavenumber values and their separation decreases with increasing OB of glasses [5]. These changes in spectral (absorption and EPR) parameters are most probably due to structural changes taking place with composition, which are reflected in change of ligand field strength around Cu^{2+} ion.
- Further work on both analysis of EPR data and fitting procedure of optical absorption data is still in progress. The final results will be reported at a later stage.

ANALYSIS OF ABSORPTION PEAK WIDTHS OF CU^{2+}-IONS IN SILICATE GLASSES

T. T. Volotinen and J. M. Parker*
The Department of Engineering Materials, The University of Sheffield, Sheffield S10 2FF, UK
mtp02ttv@shef.ac.uk

The width and splitting of the Cu^{2+} absorption peak at 12700 cm^{-1} in silicate glasses has been examined and systematic trends of the peak positions, heights, splitting and widths with optical basicity have been analysed using ligand field theory. The tetragonal distortion that causes the splitting is small, just 520 – 1250 cm^{-1}, and decreases with increasing optical basicity. The width and asymmetry of the principal peak arises from this splitting into two peaks that become broader with increasing optical basicity. The breadth of the individual peaks is attibuted to varying degrees of distortion. The effect of redox is also considered.

(Key words: copper, silicate glass, absorption peak width, ligand field theory, Jahn-Teller)

1. Introduction

The absorption peak positions and heights of transition metal ion colorants in glasses have been studied as a function of host glass composition [1,2,3,4] but their widths have been less thoroughly investigated. For many applications, e.g. designing coloured glasses and filters, it is important to be able to control simultaneously the peak widths, heights and positions. The relatively large peak widths observed for these ions have been assumed to be one indicator of the random structure of glasses [4]. Gaskell et al [5] has reported that the oxygen ions surrounding Cu^{2+}-ions are well structured as a distorted octahedron in copper sodium phosphate glass. In various recent investigations short and medium range structural ordering has been reported for certain glasses. A more discrete explanation for the absorption peak width of Cu^{2+}-ions as a function of host glass composition and redox is sought in this work.

The width of the asymmetric Cu^{2+} peak at 12700 cm^{-1} is caused by splitting of this peak due to a Jahn-Teller induced tetragonal distortion of the oxygen anion octahedra around this cation [1,6,7,8]. However, there is confusion about whether the distortion is large or small, fixed or varying, how many split peaks there should be, and their separation. The broadening has been attributed to a large separation (3000 – 4000 cm^{-1}) of two peaks [7], or three peaks (a main peak with satellites at ± 2000 cm^{-1}) [6]. Bingham et al [9,10] reported how the position (energy) of the Fe^{2+} absorption peak around 8500 cm^{-1} decreases with increasing optical basicity of the host glass. Cable and Xiang have shown a decrease of peak position and a broadening for the Cu^{2+} peak with basicity [11]. This suggests that the effect of the ligand field on the electron

transitions associated with the absorption, decreases with the basicity, which should mean a smaller distortion and a smaller separation. There is thus confusion within the earlier explanations for the width of this Cu^{2+} peak.

Here we report a systematic study of the Cu^{2+} absorption peak at 12700 cm^{-1} in a wide range of Cu-doped silicate glasses, examining the optimum fitting profile and the trends of these fitted peak positions, heights and widths with optical basicity of the host glass in relation to the composition and redox. The results will be interpreted in relation to ligand field theory.

2. Experimental

Silicate glasses, doped with 1 mol% CuO, containing 60 – 70 mol % silica (sand) and 5 – 15 mol % of three or four of the following glass network formers and modifiers (Li_2O, Na_2O, K_2O, CaO, BaO, MgO, B_2O_3, Al_2O_3) were melted in mullite crucibles in gas-fired furnace at 1450°C for five hours. The alkali and alkali earths were added as carbonates except that the melts were refined with 0.35 mol % Na_2SO_4 replacing the equivalent amount of Na_2CO_3. The samples were cast as 6-8 mm free plates on a warmed iron plate, annealed at 540 °C for one hour and subsequently cooled at a rate of 1°C/min to room temperature. To check the effect of redox on the absorption peak, soda(70)-lime(15)-silica(15) samples doped with 0.2 – 1.5 mol % CuO were also melted in both a gas-fired (oxygen content 1-3 %) and an electrically-heated (oxygen content 21 %) furnace with and without oxidising (1 mol % Na_2SO_4) or reducing agents (0.5 mol % carbon).

Glass samples (2 cm × 2 cm × 4 mm) were manually polished in six stages using silicon carbide powders (grit size 240, 400 and 600) and water; using silicon carbide metal polishing papers (800 and 1200) with water, and finished with CeO_2-powder of 2 μm particle size with water. The CeO_2-powder finish is a chemical corrosion process, enhanced by mechanically removing the reaction residues against the rotating wheel. The optical basicity values were calculated from batch compositions using the equation and partial Λ(oxide) basicity values of the ingredients given by Duffy [12].

The transmission absorption spectra of the prepared samples was measured over a 184 - 3200 nm range, using a Perkin-Elmer Launch 900 spectrometer with 2 nm scanning step. The measured absorption spectra were corrected by subtracting the reflection losses at both surfaces (assumed to be equivalent to an absorbance of 0.036) and after that by normalising to 1 cm thickness. The clear base glass absorption for each type of studied glass was also measured and normalised in a similar way, and then subtracted from the normalised coloured glass spectra. Thus the pure absorption spectra of the dopant ions was received. For fitting Gaussian peaks, the spectra were further normalised for 1 mol % concentration.

The corrected and normalised data were fitted over the wavenumber range 20600 - 4170 cm^{-1}, using two Gaussian peaks with six freely varying parameters (peak height1, position1, width1, height2, position2 and width2) using the non-linear regression analysis of the mathematical software SPSS 12.0.1 for Windows. For some glasses a narrower wavenumber range was used because the peak was narrower. The same starting values of the six fitting parameters were used for all results. Fits including different numbers of peaks were also investigated.

3. Results

Our Cu-doped glasses showed a particular colour sequence during casting, not seen for other transition metal dopants studied. At first the Cu-doped melt glass was intensely orange. Then the red colour intensified, becoming opaque red, after that a transparent dark green colour was seen for about 10 – 20 seconds, which after a while changed to the final blue colour. These colour shifts, in particular the green light, seen at high temperatures are probably caused by fluorescence of Cu^{+} ions [7], which are always present in Cu-doped glasses.

The absorption band for Cu^{2+} lay at 12000 – 13000 cm^{-1} for our blue glasses (Fig. 1). No other colours were seen. The program easily resolved most of the cases at the first trial resulting in small standard deviations and the overall residual squared (= 1- residual sums of squares/corrected sums of squares) varied within 0.99983 – 0.99995 (Fig. 2). Fitting using one Gaussian peak was attempted but gave significantly larger deviations and residuals, or failed to converge to a result. The two standard deviation error bars of the fitted parameters were 0.1 % or less, thus being smaller than the squares and dots shown on the Figs. 2 a, b, and c. The optical basicity values (Fig.2.), calculated from the batch, are only qualitative. An uncertainty of ± 0.05 might thus be involved. (See Discussions)

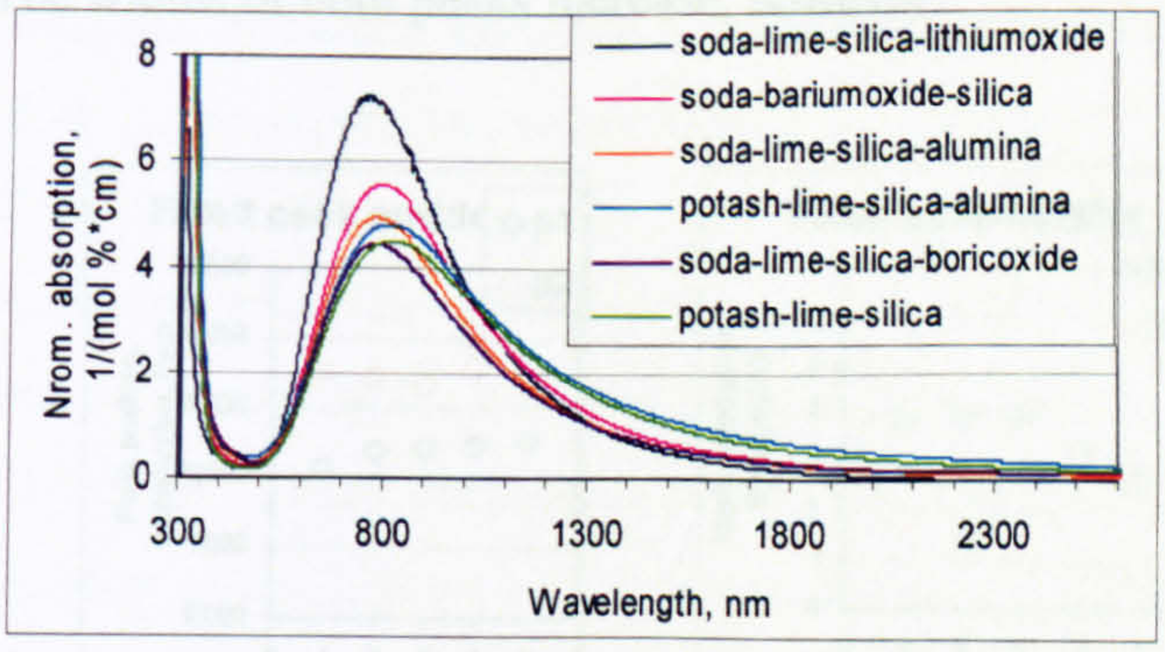

Fig. 1a Examples of the normalised absorption peaks of Cu^{2+}-ions in various silicate glasses, shown in height order from tallest down.

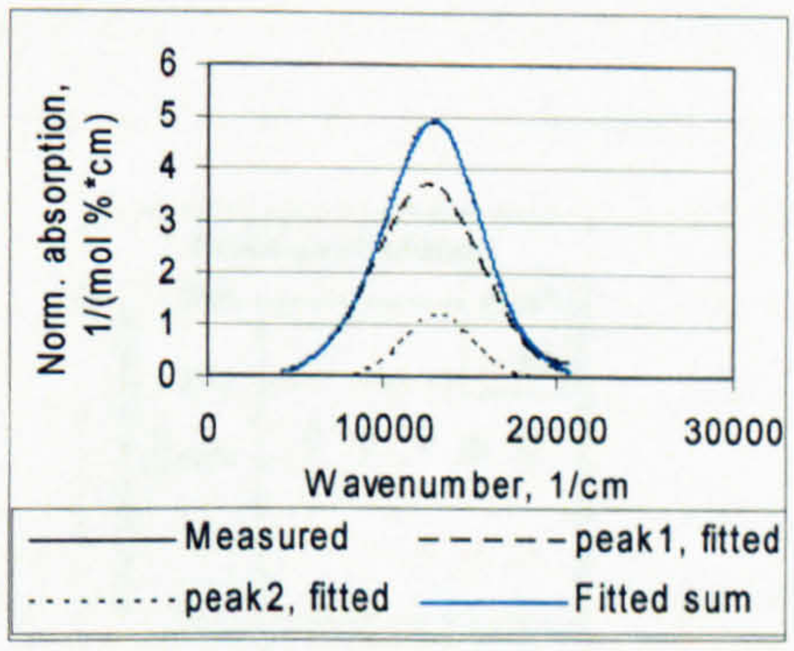

Fig. 1b Agreement of the measured and fitted data for Cu^{2+}-ion peak in the soda-lime-silica-alumina glass.

The fitting analysis clearly showed that two peaks, whose positions are separated by from 520 to 1250 cm^{-1}, fit accurately to the broad Cu^{2+} absorption band. The peak at the lower

absorbed energy of the transition is higher and wider. The ratio of the peak heights decreases from 5:1 to 3:2 with increase of optical basicity. The borosilicate glass differs from the trend, showing lower peak positions, more equal heights and smaller widths than the other glasses.

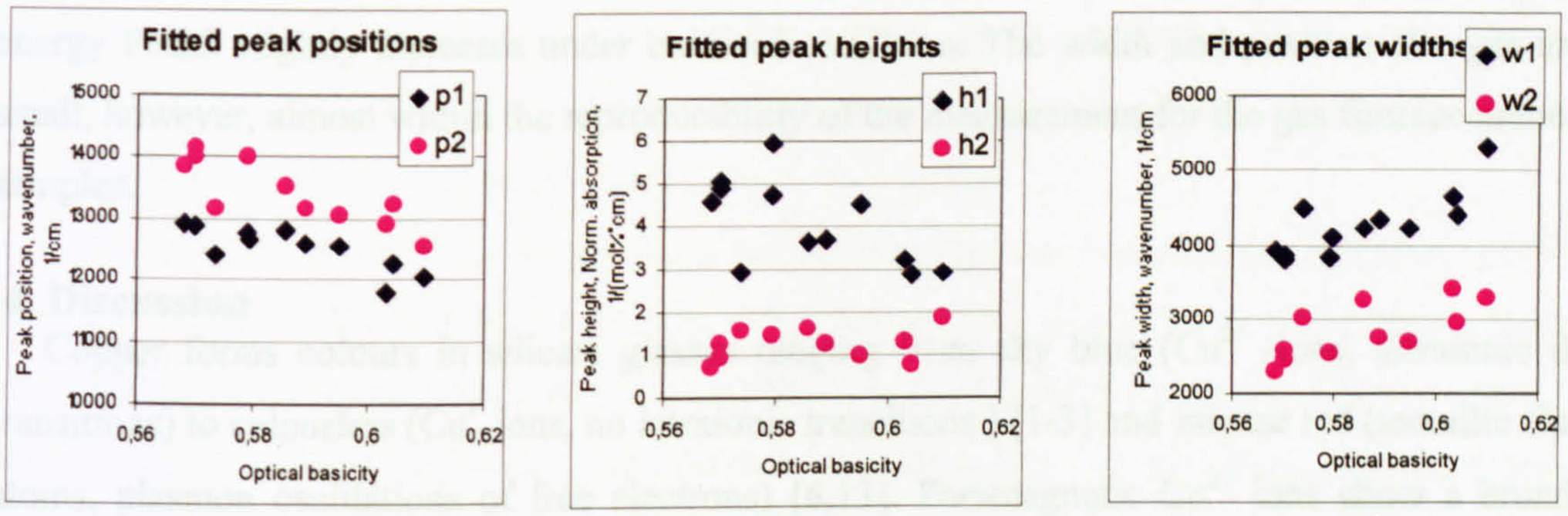

2a 2b 2c

Fig. 2 The positions, heights and widths of the two fitted Gaussian peaks for the normalised Cu^{2+} absorption peak at 12700 cm^{-1} in various silicate glasses, shown as a function of optical basicity of the host glass.

The separation of the fitted peak positions decreases from 1250 to 520 cm^{-1} with increasing optical basicity (Fig. 2a). Both peaks move towards lower wavenumber (lower energy) with increasing basicity. The height of Peak2 (higher energy) is independent of the optical basicity, lying around 1.0 $(mol\ \%*cm)^{-1}$ for all studied glasses, but the height of Peak1 (lower energy) shows a clear decreasing trend with optical basicity increase (Fig. 2b and 2a). The widths of these peaks differ significantly, Peak2 width increases from 2300 to 3500 cm^{-1} and Peak1 from 3800 to 5300 cm^{-1} with increasing basicity. The peak widths differ by 1000 – 1500 cm^{-1}. Thus the transitions with the higher energy are more strictly defined than those with the lower energy. The split peaks become more equal in height and position in glasses with high optical basicity. The widths of both peaks increase, however.

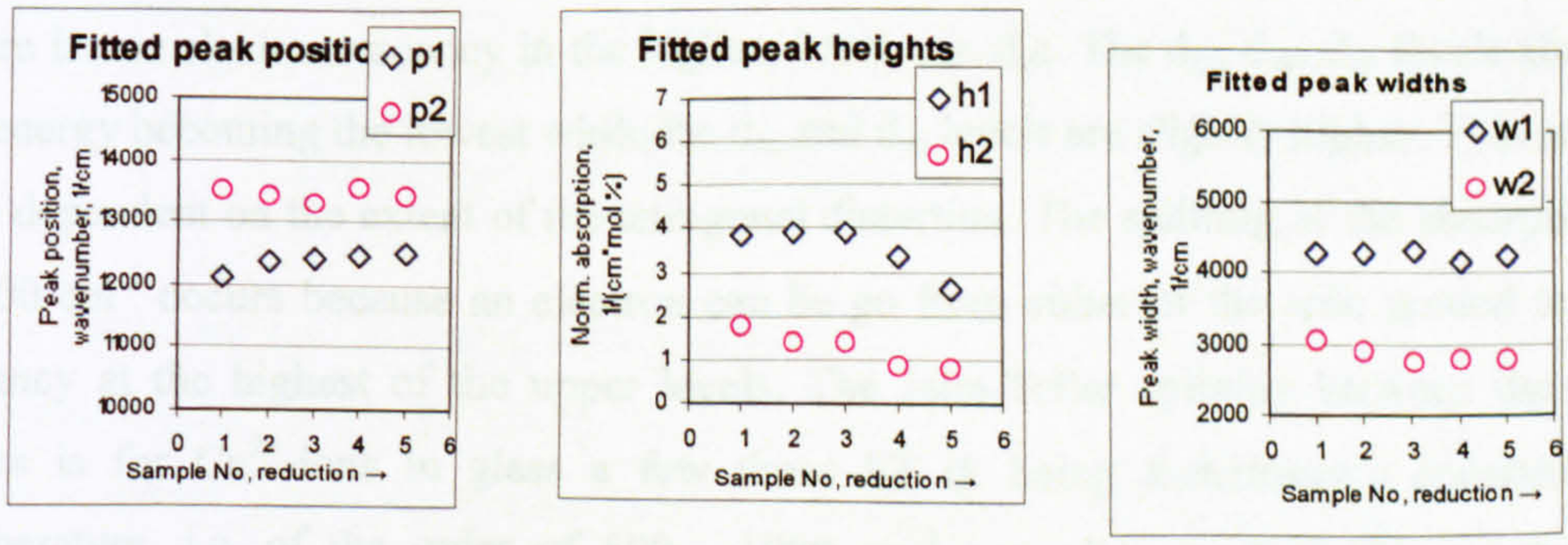

3a 3b 3c

Fig. 3 Effect of reducing and oxidising melting conditions on the Cu^{2+}-ion absorption in soda-lime-silica glass: Fitted peak positions, heights and widths shown with increasing reduction. The melting conditions: Sample No 1: electric furnace, free air, No 2 and 3: gas furnace with oxidising agent, No 4. gas furnace, no agent and No 5. gas furnace with reducing agent.

The results in Fig. 3 for the soda-lime-silica glass samples melted under oxidising and reducing conditions show that redox affects the peak heights, reducing conditions lowering the Cu^{2+} concentration. The peaks are also slightly closer and become more equal in height in the reduced glass compared to Sample 1, the most oxidised glass. The peak width of the higher energy Peak2 slightly increases under oxidised condition. The width and position changes are small, however, almost within the reproducibility of the measurement for the gas furnace melted samples.

4. Discussion

Copper forms colours in silicate glasses ranging from sky blue (Cu^{2+} -ions, intraionic d^9 transitions) to colourless (Cu^{+}-ions, no intraionic transitions) [1-3] and intense red (metallic Cu-atoms, plasmon oscillations of free electrons) [6,13]. Paramagnetic Cu^{2+} ions show a broad, asymmetric absorption peak of 300 – 400 nm full width at half maximum height (FWHM) (~ 4000 cm^{-1} width on an energy scale) at around 780 – 800 nm wavelength (12700 cm^{-1}) [1, 2]. Cable and Xiang [11] have shown that an increase in glass basicity favours a more symmetrical shape of the peak on an energy scale and suggested that the overall absorption band might be a combination of at least two Gaussian peaks. Ligand field theory, thoroughly analysed by Bates and Paul [1, 8], suggests a splitting to two closely positioned peaks for a slight tetragonal distortion of the octahedral sites. The position separation of these peaks is dependent on the extent of the distortion.

An octahedral coordination of nearest neighbouring anions causes separation of the Cu^{2+} d^9-electron energy levels, leaving six electrons (d_{xz}, d_{yz}, d_{xy}) in the three degenerate lower energy levels and three electrons in the two upper degenerate levels ($d_{x^2-y^2}$, d_{z^2}). The position of the absorption band at 12700 cm^{-1} measures the energy gap between these two levels. In glass a tetragonal distortion along the z-axis further splits the upper level to two new levels ($d_{x^2-y^2}$) and (d_{z^2}), whose separation, dependent on the glass host, is a measure of the extent of the distortion. There is one electron vacancy in the highest level, viz. d_{z^2}. The d_{xz}, d_{yz}, d_{xy} levels also split, the d_{xy} energy becoming the lowest while the d_{xz} and d_{yz} levels are slightly higher. This separation is also dependent on the extent of the tetragonal distortion. The splitting of the absorption band at 12700 cm^{-1} occurs because an electron can be go from either of the split ground levels to the vacancy at the highest of the upper levels. The Jahn-Teller splitting between the absorption peaks is for Cu^{2+}-ions in glass a few times kT (k being Boltzmann's constant) at room temperature, i.e. of the order of 500 - 1000 cm^{-1} according to Paul [8] and therefore the probability of the vacant energy level being the $d_{x^2-y^2}$ level is small. This theory agrees well with our results.

The height difference between the split peaks can be explained in the following way. At room temperature there are two pairs of electrons (spin-up and spin-down) at the upper (d_{xz}, d_{yz}) of the split ground levels and only one pair on the lowest energy level (d_{xy}). The upper $d_{x^2-y^2}$ level contains one pair while the d_{z^2} level has only one electron. It is thus more probable that an electron from the d_{yz}, d_{xy} pair of levels is lifted up to the d_{z^2} level (spin-allowed, Laporte-forbidden transition). Thus the split absorption peak at a lower energy is more probable, resulting in a more intense absorption peak.

Our results show that the absorption spectra can be fitted by two closely positioned (500 – 1000 cm^{-1}) peaks fitted with high precision and agree with the given theory, indicating a slight tetragonal distortion. This conclusion differs from the earlier published results of Duran et al [7] who fitted two peaks at 12700 cm^{-1} and 9000 cm^{-1} and from Bae and Weinberg who fitted three peaks at 12600 cm^{-1}, 10600 cm^{-1} and 8500 cm^{-1}. The peak at 8000 – 9000 cm^{-1} might in both cases be associated with Fe^{2+}-contamination. If three peaks are fitted to one peak data, it is likely that the positions will be different, compared to the case of a fit using just two peaks. In addition, Bae's glass contained copper oxide as a network former rather than dopant, which would increase optical basicity. Thus their peaks at lower energies are actually in accordance with our results.

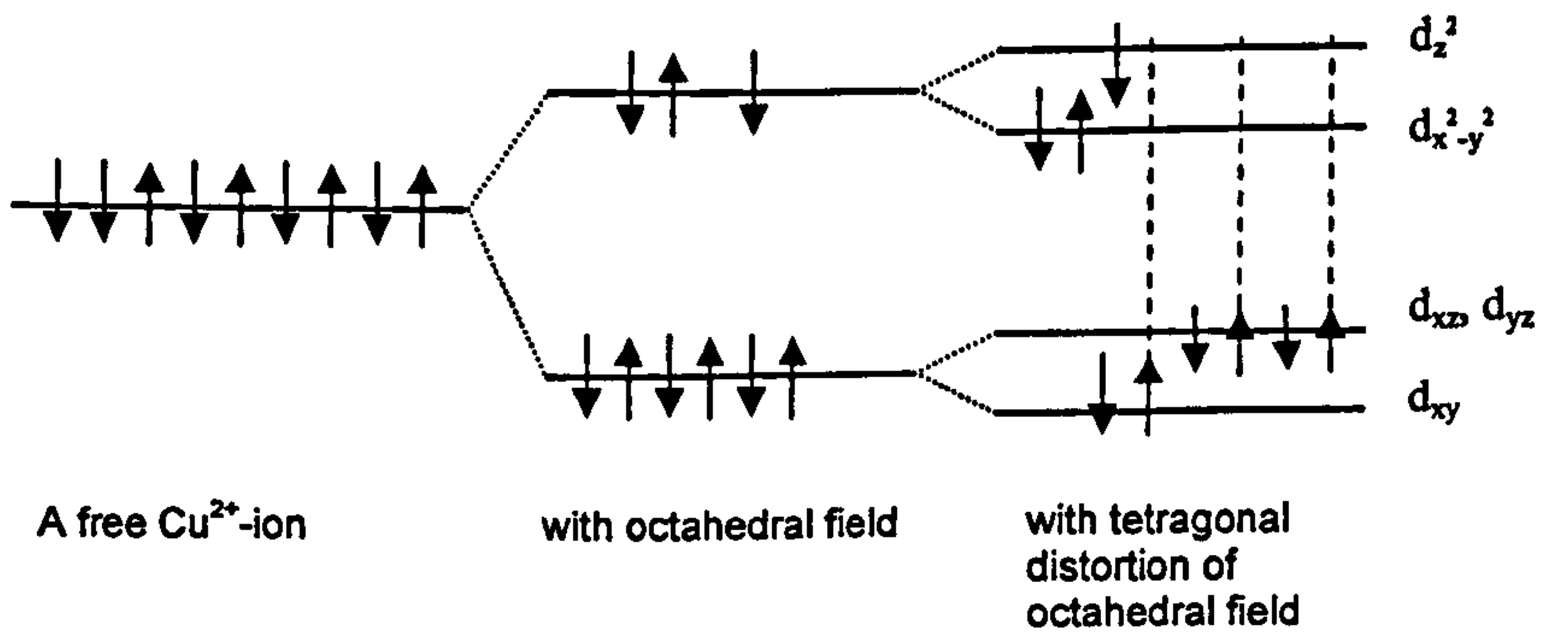

Fig. 4 Splitting of the d^9-energy levels in Cu^{2+} ion in glass. The separation of the upper energy levels is caused by an octahedral ligand field that has a slight tetragonal distortion, splitting the ground and excited energy levels. The most probable transitions are marked with dotted lines. The final split peak energies are not drawn accurately to scale

Our results are also in accord with absorption curves measured for free Cu^{2+}-ions in aqueous liquid and crystal [1, 8], for which the pure octahedral configuration of neighbouring oxygen anions is agreed. These absorption peaks are at the same position as our measured absorption bands for Cu^{2+} in glass. In addition, the band width (FWHM) is similar, thus indicating that the Cu^{2+} bands in glass are not significantly wider than in pure octahedral configuration. Thus the tetragonal distortion associated with the splitting should be slight and the splitting of the fitted

peaks should be small, significantly less than the FWHM width of the original band, as is the case for the results received in this work. Gaskell et al [5] have shown, by neutron diffraction measurements, that the surrounding of Cu^{2+} is clearly a distorted octahedron in copper sodium phosphate glass, where four oxygens locate at 1.96 Å distance and two at 2.51 Å. They also suggest that the distance of these two might vary from site to site around the average value. Furthermore the next neighbouring cations (Na^{+}) were also well defined, and conclusions were that the Cu^{2+} ions environment is ruled by that, and is clearly not random.

Our fitting resolved the two closely positioned Gaussian peaks for the Cu^{2+} absorption band precisely, because:

The subtraction of the reflection losses and base glass absorption were made carefully. The base glass correction is significant, because OH^{-}- and Fe^{2+}-ions were present as a contamination in our glasses. Fe^{2+} has it octahedral peak at 8000 – 9000 cm^{-1} and its tiny tetrahedral peak around 4000 cm^{-1}. The presence of OH^{-} increases the minimum absorption at all wavelengths, because it can be combined to various glass-modifier and glass-forming ingredients of these glasses e.g. when combined with Si- ions, as"-Si-OH", it has a broad absorption peak at 7200 cm^{-1}.

Bates claimed the peak at 4000 cm^{-1} is for Cu^{2+}. We do not see this peak after the subtraction of the base glass absorption, but we saw a peak at these wavelengths at the raw data, suggesting it is caused by the host glass and Fe contamination.

The mathematical fitting software used in this work is a very recent, improved version. A one year older version of the same software could not resolve the closely positioned Gaussian peaks properly. Many trials were needed to give a precise fit. Non-precise fitting results suggested some peaks at much greater separation (e.g. at 12700 cm^{-1} and 8000 – 9000 cm^{-1}) and with much greater height difference.

The large widths of the fitted peaks obtained and the width difference between the fitted peaks can be explained as follows: A general reason for the broad peaks is variation of the extent of the tetragonal distortion. Where the ligand ions are closer on average to the copper ions (higher energy transitions) less variability in position might be expected, as is in fact observed. Another possibility would be a transition from the higher low level to the lower upper-level. This transition may occur if the vacancy moves to the lower upper level due to an earlier transition or a vibrational interaction between the electrons of the upper levels (broadening by 1000 cm^{-1}), or due to paramagnetic nature of the non-paired electron. According to Paul this spin-orbit coupling transition is probable. This transition peak would be positioned at slightly lower energy than the popular low energy transition and cause broadening by 100 – 1000 cm^{-1}. In a similar way also the high energy peak might be broadened. There might also be

transitions between the upper levels and between the lower levels. Such transitions would appear at much lower energy (at much longer wavelengths), because for a slight distortion the energy gap is much smaller than the significant energy gap between the upper and lower levels.

5. Conclusions

The C^{2+}-ion in silicate glasses occupies well defined octahedral sites with a slight tetragonal distortion. Two overlapping Gaussian peaks separated by 500 - 1200 cm^{-1} have been fitted to a high precision to the measured, background corrected normalised peak at 12700 cm^{-1}. Clear trends of peak heights, positions and widths with optical basicity of the host glass are shown. The relatively large split peak widths originate from the variation of the tetragonal distortion and from vibration and spin-orbit coupling involving secondary transitions of non-paired electrons between closely sited split levels. Increasing theoptical basicity causes broadening of the split peaks.

References

[1] Bates T, Modern aspects of the vitreous state, Ed. by J. D. Mackenzie, Butterworth & Co., Vol. 2. p. 195-254 (1962).

[2] Weyl W A, Coloured Glasses, Soc. of Glass Tech. London (1959).

[3] Bamford C R, Colour generation and control in glass, Elsevier, Amsterdam (1977)

[4] Wong J and Angell C A, Glass structure by spectroscopy, Marcel Dekker, New York (1976).

[5] Gaskell P H, J Non-Cryst. Solids, Vol 150, 80-86 (1992).

[6] Bae B-S and Weinberg M C, J. Non-Cryst. Solids. Vol. 168, 223-231 (1994).

[7] Durán A et al, Phys. Chem Glasses, Vol 26, 126-131 (1985).

[8] Paul A, Chemistry of Glasses, Chapman and Hall, London, 204-270 (1982).

[9] Bingham P A et al, Proc. Int. Congr. Class Volume I, Invited Papers, 14-15 (2001).

[10] Bingham P A et al, C. R. Chimie, Vol 5, 787-796 (2002).

[11] Cable M et al, Phys. Chem. Glasses, Vol. 33, 154-160 (1992).

[12] Duffy J A et al, C. R. Chimie, Vol. 5, 797-804 (2002).

[13] Nakai I et al, J. Am. Ceram. Soc., Vol 82, 689-95, (1999).

ANNEX 11, Fitting results for Cu doped and co-doped glasses

Fitted spectra of Cu doped glasses melted in a gas furnace

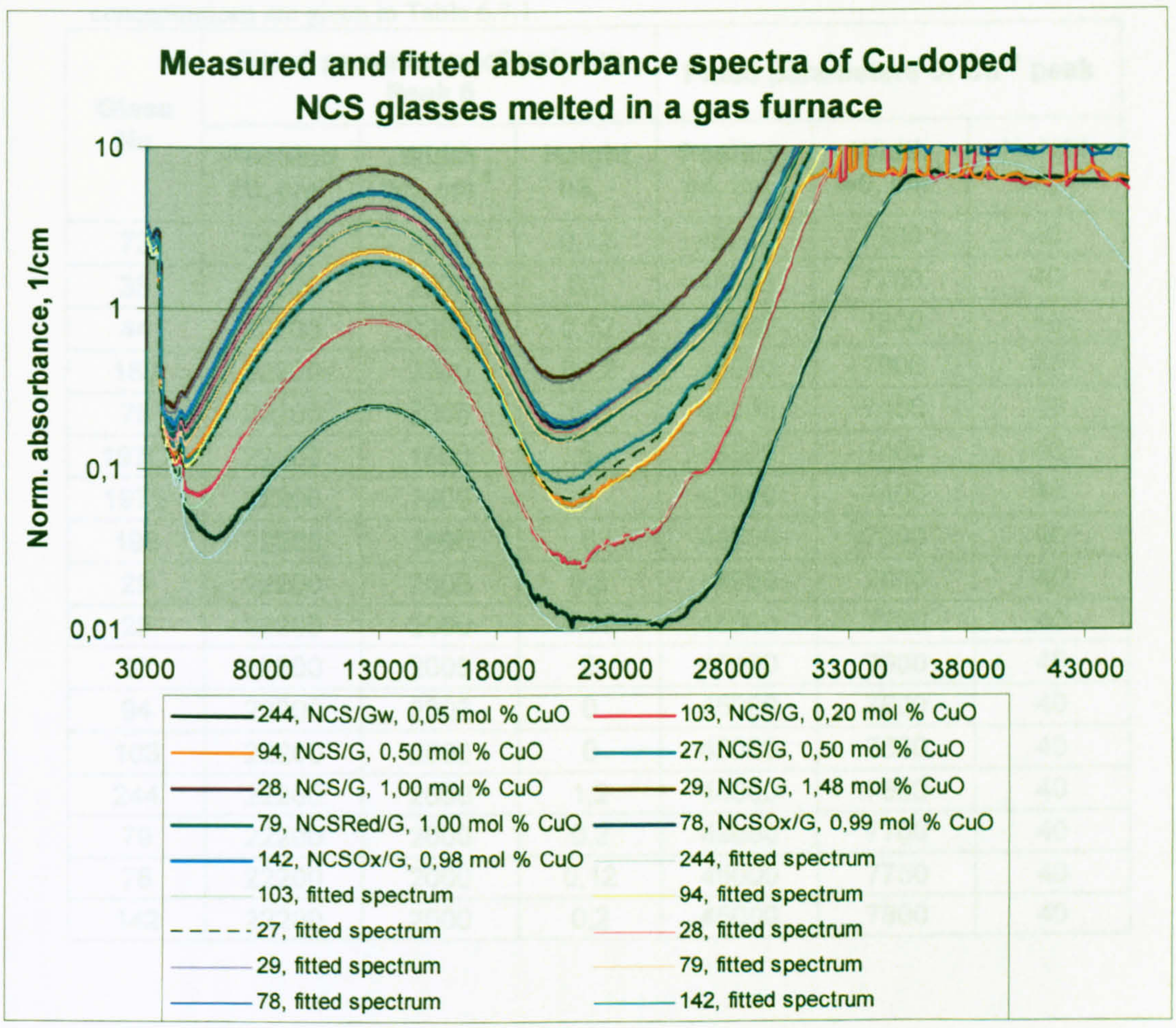

Fig. A11.1 The measured and fitted absorbance spectra for Cu doped NCS glasses melted in a gas furnace. The fitting parameters are given in Tables A11.1 and A11.2. The obtained ion concentrations are given in Table 6.7.1.

Fitting parameters of Cu^{2+} and Cu^{1+} ions in singly and doubly doped NCS glasses

Table A11.1 Fitting parameters of the Cu^{1+} UV-peak and the unknown peak in Cu doped NCS glasses melted in electric and gas furnaces. The melting conditions and added Cu concentrations are given in Table 6.7.1.

Glass No	Fitted parameters of unkown Peak 5			Fitted parameters of Cu^{1+} peak		
	Position P5, cm^{-1}	Width w5, cm^{-1}	Height h5, -	Position p6, cm^{-1}	Width w6, cm^{-1}	Height h6, -
73	22200	2000	0,12	45000	7700	40
35	22200	2000	0,2	45000	7700	40
44	22200	2000	0,12	45000	7800	45
189	22200	2000	0,12	45000	7800	45
75	22200	2000	0,2	45000	7400	39
197O	22200	1600	5	43800	7400	48
197S	22200	1600	1	43800	7400	40
196	22200	1600	6	44000	7000	40
29	22200	2000	0,2	44950	7800	40
28	22200	2000	0,12	45000	7700	40
27	22200	2000	0	45000	7600	40
94	22200	2000	0	45000	7800	40
103	22200	2000	0	45000	7800	40
244	22200	2000	1,2	45000	7850	40
79	22200	2000	0,2	45000	7700	40
78	22200	2000	0,12	45000	7750	40
142	22200	2000	0,2	45000	7800	40

Table A11.2 Fitting parameters of the Cu^{2+} d-d transitions (p1 and p2) and UV-peaks (p3 and p4) in singly with Cu doped NCS glasses melted in electric and gas furnaces. The melting conditions and added Cu concentrations are given in Table 6.7.1.

Glass No	Fitted parameters of Cu^{2+} peaks											
	Position p1, cm^{-1}	Width w1, cm^{-1}	Height h1, -	Position p2, cm^{-1}	Width w2, cm^{-1}	Height h2, -	Position p3, cm^{-1}	Width w3, cm^{-1}	Height h3, -	Position p4, cm^{-1}	Width w4, cm^{-1}	Height h4, -
73	11650	2930	3,876	13400	2400	4,213	33300	2030	20,4			
35	11550	2940	3,876	13470	2400	4,213	33500	2000	20,4			
44	11650	2930	3,876	13400	2400	4,213	33450	1850	25,5			
189	11600	2980	3,927	13450	2420	4,213	33450	1850	25,5			
75	11650	2930	3,876	13450	2400	4,213	33300	1810	25,5			
197O	11650	2930	3,876	13600	2400	4,213	33800	1900	23,46	35000	1000	61,2
197S	11650	2930	3,876	13600	2400	4,213	33300	2020	20,4	35000	1000	61,2
196	11650	2930	3,876	13800	2400	4,213	33300	2020	25,5	35100	1000	61,2
29	11550	2950	3,723	13460	2450	4,284	33520	2020	20,4			
28	11550	2940	3,723	13460	2400	4,284	33520	2020	20,4			
27	11550	2940	3,723	13460	2400	4,284	33520	2020	20,4			
94	11550	2940	3,672	13450	2400	4,294	33540	2000	20,4			
103	11550	2940	3,672	13450	2400	4,335	33560	1960	20,4			
244	11500	2940	3,672	13580	2450	4,335	33950	1800	20,4	35200	900	45,9
79	11550	2940	3,723	13460	2400	4,284	33400	2010	20,4			
78	11550	2940	3,723	13460	2400	4,284	33550	1960	20,4			
142	11550	2940	3,723	13440	2400	4,284	33610	2020	20,4			

Table A11.3 Fitting parameters of the Cu^{1+} UV-peak (Peak6) and the unknown Peak5 in NCS glasses doubly doped with Cu and Fe and melted in electric and gas furnaces. The melting conditions and added Cu and Fe concentrations are given in Table 6.8.1.

Glass No	Fitted parameters of the unkown Peak5			Fitted parameters of Cu^{1+} UV peak		
	Position p5, cm^{-1p}	Width w5, cm^{-1}	Height h5, -	Position p6, cm^{-1}	Width w6, cm^{-1}	Height h6, -
74				43300	7680	41
223				44500	7700	40
224				44700	7600	40
233	22200	2000	0,2	43500	7850	45
234				44500	7500	40
238				44500	7800	40
239				43800	7850	40
240	22200	2000	0,4	43400	7500	40
241				44600	7500	40

Table A11.4 Fitting parameters of the Cu^{2+} d-d transitions (Peak1 and Peak2) and UV-peaks (Peak3 and Peak4) in NCS glasses doubly doped with Cu and Fe and melted in electric and gas furnaces. The melting conditions and added Cu and Fe concentrations are given in Table 6.8.1.

Glass No	Fitted parameters of Cu^{2+} peaks											
	Position p1, cm^{-1}	Width w1, cm^{-1}	Height h1, -	Position p2, cm^{-1}	Width w2, cm^{-1}	Height h2, -	Position p3, cm^{-1}	Width w3, cm^{-1}	Height h3, -	Position p4, cm^{-1}	Width w4, cm^{-1}	Height h4, -
74	11550	2940	3,876	13400	2400	4,213	33250	2060	25,5			
223	11550	2940	3,876	13470	2400	4,213	33500	2000	20,4			
224	11550	2940	3,876	13470	2400	4,213	33900	2020	20,4			
233	11650	2930	3,876	13400	2400	4,213	33670	2050	20,4			
234	11650	2930	3,876	13450	2400	4,213	33500	1810	20,4			
238	11550	2940	3,723	13460	2400	4,284	33300	2020	20,4			
239	11550	2940	3,723	13460	2400	4,284	33550	2000	20,4			
240	11550	2940	3,723	13460	2400	4,284	33820	1800	20,4			
241	11550	2940	3,723	13200	2400	4,284	33100	2020	20,4			